

ORBITAL TRANSFER VEHICLE

CONCEPT DEFINITION AND SYSTEMS ANALYSIS STUDY

FINAL REPORT – PHASE I VOLUME II, BOOK 3

CONFIGURATION AND SUBSYSTEM TRADE STUDIES 1986

NASA/MSFC
NAS8-36107

(NASA-CR-183685-Vol-2-Bk-3) ORBITAL
TRANSFER VEHICLE CONCEPT DEFINITION AND
SYSTEMS ANALYSIS STUDY, VOLUME 2, BOOK 3
Final Report (Boeing Aerospace Co.) 559 p

BOEING

D180-29108-2-3

N89-71065

00/16 Unclass 0219863

**ORBITAL TRANSFER VEHICLE
CONCEPT DEFINITION
AND
SYSTEM ANALYSIS STUDY**

Final Report

Volume II, Book 3

CONFIGURATION AND SUBSYSTEM TRADE STUDIES

D180-29108-2-3

December 1986

DPD NUMBER - 637

DR NUMBER-4

CONTRACT NAS8-36107

Submitted to

The National Aeronautics and Space Administration

George C. Marshall Space Flight Center

By

Boeing Aerospace Company

Seattle, Washington 98124

This Page
Intentionally
Left
Blank

FOREWORD

This final report of the Orbital Transfer Vehicle (OTV) Concept Definition and System Analysis Study was prepared by Boeing Aerospace Company for the National Aeronautics and Space Administration's George C. Marshall Space Flight Center in accordance with Contract NAS8-36107. The study was conducted under the direction of the NASA OTV Study Manager, Mr. Donald Saxton and during the period from August 1984 to September 1986.

This final report is organized into the following nine documents:

- VOL. I Executive Summary (Rev. A)
- VOL. II OTV Concept Definition & Evaluation
 - Book 1 - Mission Analysis & System Requirements
 - Book 2 - Selected OTV Concept Definition - Phase I
 - Book 3 - Configuration and Subsystem Trade Studies
 - Book 4 - Operations and Propellant Logistics
- VOL. III System & Program Trades
- VOL. IV Space Station Accommodations
- VOL. V WBS & Dictionary
- VOL. VI Cost Estimates
- VOL. VII Integrated Technology Development Plan
- VOL. VIII Environmental Analysis
- VOL. IX Implications of Alternate Mission Models and Launch Vehicles

The following personnel were key contributors during the conduct of the study in the disciplines shown:

Study Manager	E. Davis (Phase I-3rd and 4th Quarters and Phase II)
	D. Andrews (Phase I-1st and 2nd Quarters)
Mission & System Analysis	J. Jordan, J. Hamilton
Configurations	D. Parkman, W. Sanders, D. MacWhirter
Propulsion	W. Patterson, L. Cooper, G. Schmidt
Structures	M. Musgrove, L. Duvall, D. Christianson, M. Wright
Thermal Control	T. Flynn, R. Savage

Avionics
Electrical Power
Mass Properties
Reliability
Aerothermodynamics
Aeroguidance
Aerodynamics
Performance
Launch Operations
Flight Operations
Propellant Logistics
Station Accommodations
Cost & Programmatics
Documentation Support

D. Johnson, T. Moser, R.J. Gewin, D. Norvell
R.J. Gewin
J. Cannon
J. Reh
R. Savage, P. Keller
J. Bradt
S. Ferguson
M. Martin
J. Hagen
J. Jordan, M. Martin
W. Patterson, L. Cooper, C. Wilkinson
D. Eder, C. Wilkinson
D. Hasstedt, J. Kuhn, W. Yukawa
T. Sanders, S. Becklund

For further information contact:

Don Saxton
NASA MSFC/PF20
MSFC, AL 35812
(205) 544-5035

Eldon E. Davis
Boeing Aerospace Company. M/S 8C-59
P.O. Box 3999
Seattle, WA 98124-2499
(206) 773-6012

TABLE OF CONTENTS

	<u>Page</u>
1.0 INTRODUCTION	1
1.1 Background	1
1.2 Objectives and Issues	1
1.3 Study/Report Organization	2
1.4 Document Content	2
2.0 CONFIGURATIONS	5
2.1 Top Level Requirements	5
2.2 Space Based OTV's	5
2.2.1 Ballute Brake OTV	5
2.2.2 Symmetrical Lifting Brake OTV	42
2.2.3 Shaped Brake OTV	65
2.3 Propellant Logistics Systems	84
2.3.1 Propellant Storage Tanks	84
2.3.2 Propellant Delivery Tanker	84
2.4 Ground Based OTV's	91
2.4.1 SCB Ballute Brake OTV	91
2.4.2 ACC Lifting Brake OTV	115
3.0 STRUCTURES	135
3.1 Structural Requirements	135
3.2 Structure Design Approach	141
3.3 Vehicle Structural Subsystems Analysis	154

TABLE OF CONTENTS (con't)		Page
4.0	PROPULSION	195
4.1	Main Propulsion System	195
4.2	Reaction Control System	212
5.0	THERMAL PROTECTION AND CONTROL	223
5.1	Top Level Requirements	223
5.2	Thermal Protection Systems	224
5.3	Analysis Approach	227
5.4	Ballute Brake OTV	243
5.5	Lifting Brake OTV	266
5.6	Shaped Brake OTV	276
5.7	Mission Impact and Aerothermal Uncertainties	281
5.8	Summary Comparison	289
5.9	Aerothermal Issues	294
5.10	Thermal Control	297
6.0	GUIDANCE AND NAVIGATION	299
6.1	Aeroassist Guidance and Navigation Considerations	299
6.2	Trades and Analyses	312
7.0	DATA MANAGEMENT SUBSYSTEM TRADES	377
7.1	System Architecture Trade	377
7.2	Fault Tolerance Technique Trade	379
7.3	Hardware Trades	379
7.4	Software Trades	379
8.0	ELECTRICAL POWER SUBSYSTEM	383
8.1	Power Source Definition	

TABLE OF CONTENTS (con't)	Page
8.2 Trades and Analyses	387
9.0 PERFORMANCE	410
9.1 Groundrules and Assumptions	410
9.2 Trajectory Analysis	411
9.3 Performance Analysis	421
9.4 Space Based Vehicle Trades	423
9.5 Ground Based Vehicle Trades	436
9.6 Evolutionary Vehicle Configuration	438
9.7 Vehicle Sensitivities	447
10.0 AERODYNAMIC DATA DEVELOPMENT	455
10.1 Ballute Brake OTV	455
10.2 Symmetrical Brake OTV	466
10.3 Shaped Brake OTV	466
11.0 OTV RELIABILITY ANALYSIS	475
11.1 Introduction	475
11.2 Reliability Model	475
11.3 OTV Missions	484
11.4 Redundancy Optimization	484
11.5 Maintenance Implications	497
11.6 LCC/Reliability Optimization	504
11.7 Conclusions and Recommendations	512
12.0 REFERENCES	515

TABLE OF CONTENTS (con't)

Page

Appendix

A.	Ascent to a 12 Hour Molniya Orbit	519
B.	OTV Phasing with Space Station	535
C.	Burn Losses for the OTV	544

ACRONYMS AND ABBREVIATIONS

A/A	Aeroassist
ACC	Aft Cargo Carrier
AFE	Aeroassist Flight Experiment
AGE	Aerospace Ground Equipment
AL	Aluminum
ASE	Airborne Support Equipment
A/T	Acceptance Test, Auxiliary Tank
AUX	Auxiliary
AVG	Average
B/B	Ballute Brake
B/W	Backwall
CDR	Critical Design Review
CLV	Cargo Launch Vehicle
CPU	Central Processing Unit
CUM	Cumulative
DAK	Double Aluminized Kapton
DDT&E	Design, Development, Test & Evaluation
DELIV	Delivery
DMS	Data Management System
DMU	Data Management Unit
DoD	Department of Defense
EOM	End of Mission
EPS	Electrical Power System
FACIL	Facility
FFC	First Flight Certification
FLTS	Flights
FOSR	Flexible Optical Surface Reflector
FRCI	Fiber Refractory Composite Insulation
FRS	Fully Reusable System
F.S.	Fail Safe

FSI	Flexible Surface Insulation
FTA	Facilities Test Article
GB	Ground Based
GEO	Geostationary Earth Orbit
GOCM	Ground Operations Cost Model
GPS	Global Positioning System
GRIEP	Graphite Epoxy
GRD	Ground
IOC	Initial Operational Capability
IMU	Inertial Measurement Unit
IRU	Inertial Reference Unit
IUS	Inertial Upper Stage
JSC	Johnson Space Center
KBS	Knowledge Base System
L/B	Lifting Brake
LCC	Life Cycle Cost
LCC	Launch Control Center
L/D	Lift to Drag
MCS	Mission Control System
MGSS	Mobile GEO Service Station
MLI	Multilayer Insulation
MPS	Main Propulsion System
MPTA	Main Propulsion Test Article
MSFC	Marshall Space Flight Center
OMV	Orbital Maneuvering Vehicle
OPS	Operations
OTV	Orbital Transfer Vehicle
P/A	Propulsion/Avionics
PAM	Payload Assist Module, Propulsion Avionics Module
PDR	Preliminary Design Review
PFC	Preliminary Flight Certification

P/L	Payload
PIP	Payload Integration Plan
PROD	Production
PROP	Propellant
PRS	Partially Reusable System
RCS	Reaction Control System
REF	Reference
RGB	Reusable Ground Based
R&R	Remove & Replace
RSB	Reusable Space Based
RSI	Reusable Surface Insulation
SB	Space Based
S/C	Spacecraft
SCB	Shuttle Cargo Bay
SIL	Systems Integration Laboratory
STA	Structural Test Article
STG	Stage
STS	Space Transportation System
T/D	Turndown
TDRS	Tracking Data Relay Satellite
TFU	Theoretical First Unit
TPS	Thermal Protection System
TT&C	Telemetry, Tracking and Control
WBS	Work Breakdown Structure

This Page
Intentionally
Left
Blank

1.0 INTRODUCTION

This section provides a description of the study in terms of background, objectives, issues, organization of study and report, and the content of this specific volume.

Use of trade names, names of manufacturers, or recommendations in this report does not constitute an official endorsement, either expressed or implied, by the National Aeronautics and Space Administration.

And finally, it should be recognized that this study was conducted prior to the STS safety review that resulted in an STS position of "no Centaur in Shuttle" and subsequently an indication of no plans to accommodate a cryo OTV or OTV propellant dump/vent. The implications of this decision are briefly addressed in section 2.2 of the Volume I and also in Volume IX reporting the Phase II effort which had the OTV launched by an unmanned cargo launch vehicle. A full assessment of a safety compatible cryo OTV launched by the Shuttle will require analysis in a future study.

1.1 BACKGROUND

Access to GEO and earth escape capability is currently achieved through the use of partially reusable and expendable launch systems and expendable upper stages. Projected mission requirements beyond the mid-1990's indicate durations and payload characteristics in terms of mass and nature (manned missions) that will exceed the capabilities of the existing upper stage fleet. Equally important as the physical shortfalls is the relatively high cost to the payload. Based on STS launch and existing upper stages, the cost of delivering payloads to GEO range from \$12,000 to \$24,000 per pound.

A significant step in overcoming the above factors would be the development of a new highly efficient upper stage. Numerous studies (ref. 1, 2, 3, 4) have been conducted during the past decade concerning the definition of such a stage and its program. The scope of these investigations have included a wide variety of system-level issues dealing with reusability, the type of propulsion to be used, benefits of aeroassist, ground- and space-basing, and impact of the launch system.

1.2 OBJECTIVES AND ISSUES

The overall objective of this study was to re-examine many of these same issues but within the framework of the most recent projections in technology readiness,

realization that a space station is a firm national commitment, and a refinement in mission projections out to 2010.

During the nineteen-month technical effort the specific issues addressed were:

- a. What are the driving missions?
- b. What are the preferred space-based OTV characteristics in terms of propulsion, aeroassist, staging, and operability features?
- c. What are the preferred ground-based OTV characteristics in terms of delivery mode, aeroassist, and ability to satisfy the most demanding missions?
- d. How extensive are the orbital support systems in terms of propellant logistics and space station accommodations?
- e. Where should the OTV be based?
- f. How cost effective is a reusable OTV program?
- g. What are the implications of using advanced launch vehicles?

1.3 STUDY AND REPORT ORGANIZATION

Accomplishment of the objectives and investigation of the issues was done considering two basic combinations of mission models and launch systems. Phase I concerned itself with a mission model having 145 OTV flights during the 1995-2010 timeframe (Revision 8 OTV mission model) and relied solely on the Space Shuttle for launching. Phase 2 considered a more ambitious model (Rev. 9) having 442 flights during the same time frame as well as use of a large unmanned cargo launch vehicle and an advanced Space Shuttle (STS II).

The study is reported in nine separate volumes. Volume I presents an overview of the results and findings for the entire study. Volume II through VIII contains material associated only with the Phase I activity. Volume IX presents material unique to the Phase II activity. Phase I involved five quarters of the technical effort and one quarter was associated with the Phase II analyses.

1.4 DOCUMENT CONTENT

This specific document reports the work associated with the systems analysis of the OTV, configurations, subsystems, and supporting technical areas. The key program groundrules influencing the analysis of these areas include use of the Rev 8 mission model involving 145 OTV flights beginning in 1994 and ending in 2010 and an STS launch system emphasizing 72K lbm capability and sensitivity to 65K lbm. In general, the trades, studies, and analyses that are discussed deal with each of these topics on an

individual basis. System level analysis dealing with multiple discipline trades are discussed in Volume III.

Unless otherwise stated, the units used in this document, and to be assumed if none are given, are as follows:

Length - feet or inches

Weight - pounds mass (lbm)

Force - pounds force (lbf)

Thrust - pounds force (lbf)

Temperature - degrees fahrenheit ($^{\circ}$ F)

Heating Rate - BTU/ft² sec

This Page
Intentionally
Left
Blank

2.0 CONFIGURATIONS

This section presents a chronological history of each of the OTV configurations developed during this study.

2.1 TOP LEVEL REQUIREMENTS

Table 2.1-1 shows the top level requirements used to guide the configuration definition of the OTVs.

2.2 SPACE BASED OTVS

This section discusses the configuration activity associated with the development of a ballute brake OTV, symmetrical lifting brake OTV, and shaped brake OTV. All concepts are based at a Space Station which is in a 270 nmi/28 $\frac{1}{2}$ ^o orbit. Servicing of the vehicle at the station includes maintenance, refueling, and payload integration.

The following subsections present the vehicle reference configurations and, chronologically, the trades and analyses performed to refine the configurations and finally a description of the selected baseline vehicle.

2.2.1 Space Based Ballute Braked OTV

2.2.1.1 Initial Reference Configuration

Figure 2.2.1-1 shows the initial reference configuration for the ballute braked Shuttle cargo bay (SCB) compatible OTV. The configuration was based upon our AOTV study which was ongoing at the start of this study.

Main propulsion is provided by two 6000 lb thrust advanced expander cycle engines. Two engines were selected to provide engine out capability for manned missions. Disconnect plates have been provided for the engines allowing them to be replaced on orbit.

The aerobrake is a 50 foot diameter, 60 degree half angle, 600 degree F backwall temperature ballute. The ballute was reusable. Subsequent analyses resulted in switching to a ballute concept that is used only once.

The LO₂ and LH₂ tanks have hemispherical domes to minimize the weight of the tanks. Both tanks have conformal meteoroid/debris shield as shown in figure 2.2.1-2; however, the section of shield covering the cylindrical section of the LH₂ tank (dashed lines in figure 2.2.1-2) is deployable to a standoff distance of 6 inches. This permitted

TABLE 2.1-1
OTV CONFIGURATION REQUIREMENTS

- o General
 - o Reusability--All vehicles to be designed to be retrieved and refurbished
 - o Airframe - 40 mission service life
 - o Tankage - 40 mission service life
 - o Avionics - 40 mission service life
 - o Aeroassist - 1 mission life for ballute
 - 5 mission life for lifting brake
 - 20 mission life for shaped brake
 - o Main Engine (ASE) - 10 hours, 20 flights
 - o On-Orbit Storage Tanks - 5 year service life
- o Satisfy Safety Requirements
 - o Shuttle/Space Station
 - o OTV Mission - No single credible failure shall preclude the safe return of the crew
 - o Any hardware jettisoned during a mission shall be disposed of through controlled deorbit or other acceptable non- interference mode
 - o OTV System shall be NASA STDN and TDRS compatible (communications and tracking)
 - o The OTV design shall include the following flight performance reserves:

TABLE 2.1-1 (continued)
OTV CONFIGURATION REQUIREMENTS

- o Main propulsion - 2% on each delta-V maneuver
- o Reaction control system - 10% of mission nominal RCS propellant
- o Electrical power system - 20% of mission nominal reactants
- o Mission Times - Use 12 hours at LEO for phasing
 - o GEO delivery - 1 day at GEO
 - o Manned GEO sortie - 18 days at GEO
- o Pre-Launch
- o Ground services (electrical, fluid, and gases) will be through orbiter service panels
- o Launch
- o The OTV and its payload will be launched to orbit by the STS, either in the Orbiter cargo bay or in the aft cargo compartment (ACC).
- o The sum of the masses of the OTV and its consumables, the airborne support equipment and its consumables, orbiter- furnished airborne support equipment, and payload shall not exceed the weight determined by the following:

Launch wt = 87,960 - 11 (altitude, in nm)
- o The OTV system shall provide for a structural adaptor and a deployment/release mechanism.
- o Satisfy the static and dynamic loads, thermal, contamination, physical envelope, CG, and other requirements of payload accommodations handbook, Vol XIV of JSC document 07700.
- o The OTV system shall provide for the dumping of propellants through the orbiter service panels in the event of an abort.

TABLE 2.1-1 (continued)
OTV CONFIGURATION REQUIREMENTS

- o Mission - Significant Payloads
 - o 20,000 lb delivery to GEO limited to 0.1 g max. acceleration
 - o 10,000 lb multiple-manifest payload to GEO
 - o 7500 lb GEO manned sortie with 7500 lb return
- o Recovery
 - o (Space-Based) retrieved by OMV from parking orbit - OTV to remain passive during docking and reberthing at space station
 - o (Ground Based) retrieved by shuttle RMS from parking orbit
 - o OTV to remain passive during docking and reberthing
 - o Reconnect umbilicals for purge and status monitoring prior to reentry

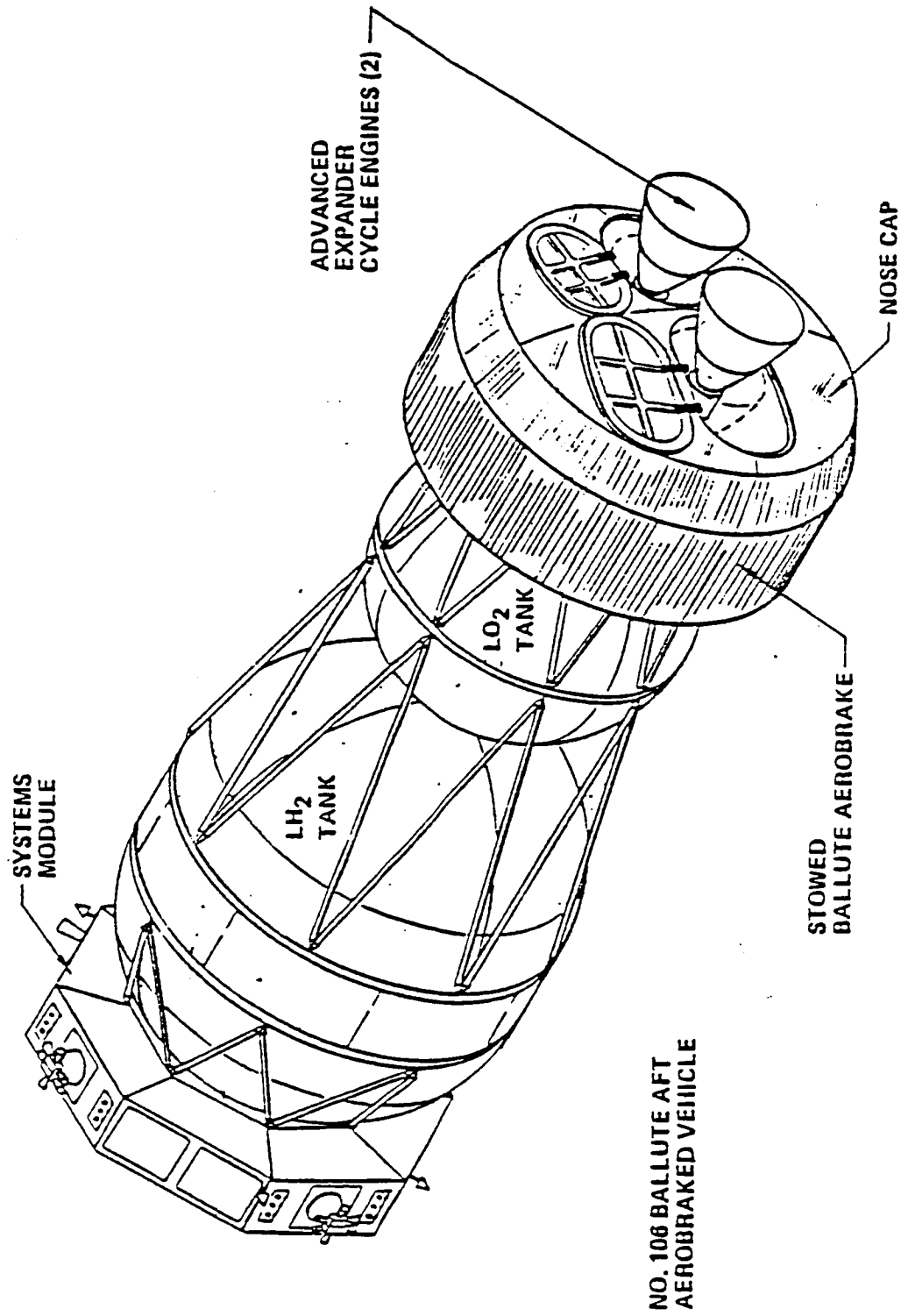
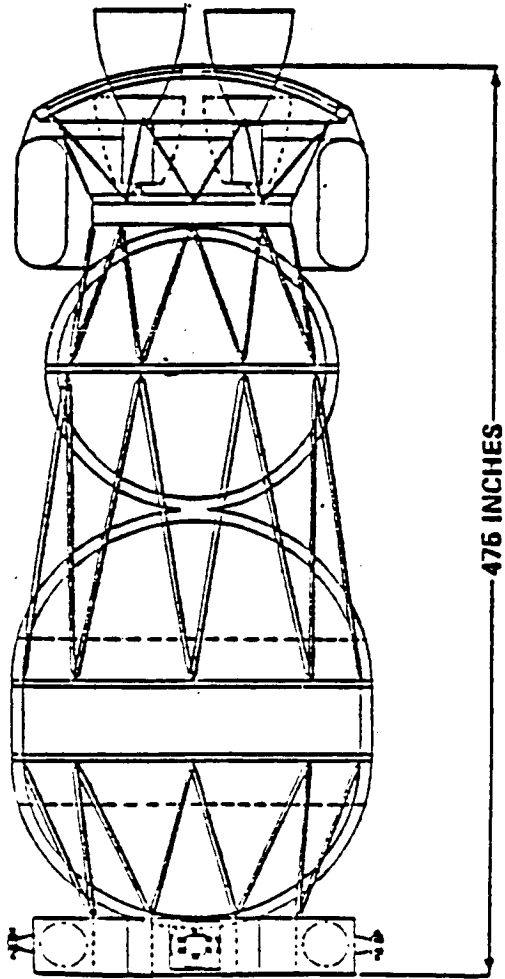


Figure 2.2.1-1 Reference Space Based Ballute Braked OTV



STRUCTURE	2579	MPS RESIDUAL	565
AEROBRAKE SYSTEM	2452	ACS RESIDUAL	31
AVIONICS	600	EPS RESIDUAL	23
ELECTRICAL POWER	650	(BURNOUT WEIGHT)	(9442)
MAIN PROPULSION	868	INFLIGHT LOSSES	212
ATTITUDE CONTROL	185	MPS PROPELLANT	55,000
SPACE MAINTENANCE	320	ACS PROPELLANT	545
WEIGHT GROWTH	1151	EPS REACTANT	62
(DRY WEIGHT)	(8823)	(GROSS WEIGHT)	(65,261)

Figure 2.2.1-2 Point Design SCB Aerobrake OTV Reference SpaceBased Concept No. 106A

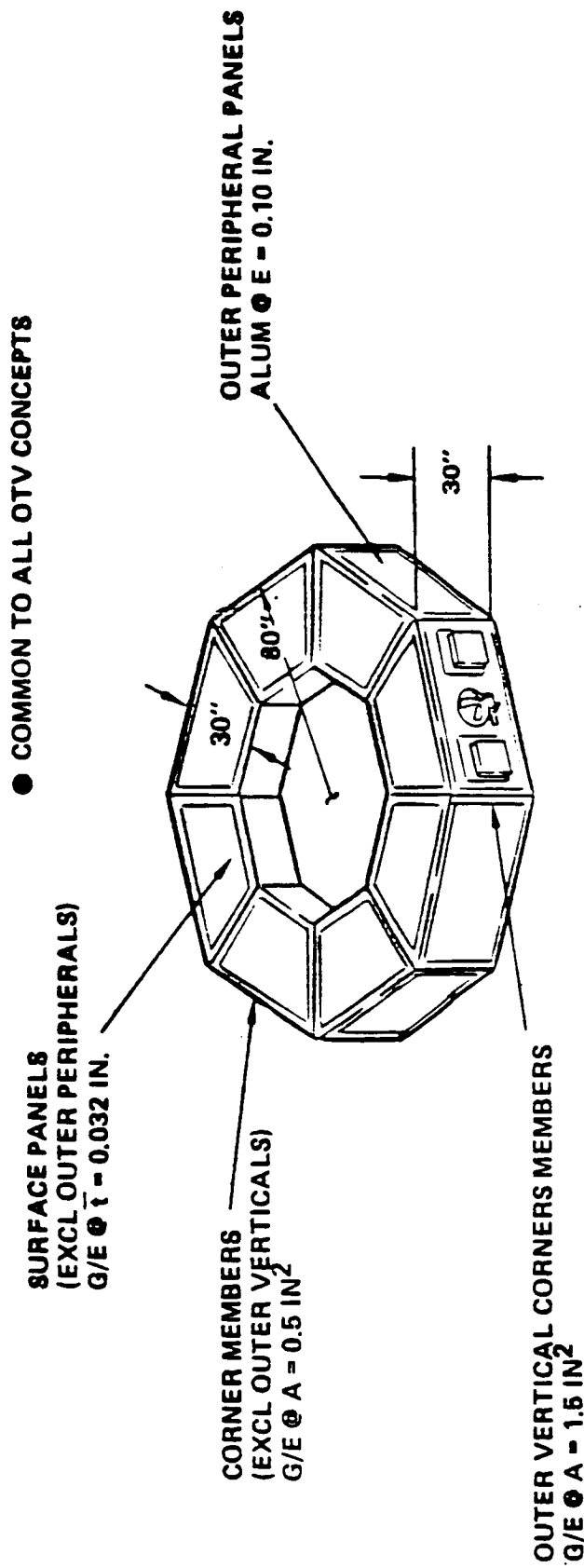
the LH2 tank to be 170 inches in diameter while optimizing the weight of the shield. The LO2 tank is located aft because its smaller diameter integrates well with the engine thrust structure and allows room for ballute stowage. Graphite/epoxy tubes with aluminum end fittings connect the tanks to the rest of the vehicle's primary structure. Support of the tanks in this manner minimized heat conduction into the tanks and helps control propellant boiloff losses. The use of a truss tube system to support the cryogenic tankage is used for all concepts of this study. The space based OTV will be initially transported to space empty. Since this results in low structural loads, the tank walls can be used as primary structure rather than having to have a structural shell around the tankage.

Figure 2.2.1-3 shows the systems module located on the forward end of the vehicle. The systems module houses the avionics, electrical power system, reaction control system, and payload interfaces. A 30 inch deep octagon structure was selected for the systems module based on an estimate of the total area required for the equipment and because it provides flat interface surfaces for the avionics. Flat surfaces simplifies the design of the doors and avionic support structure. Space maintenance provisions have been provided for the IRU, GPS, transponder, RF power amplifiers, and DMUs. The fuel cells are also replaceable on orbit. The RCS is a hydrazine system with 4 thruster modules which are installed and maintainable on orbit. Installation of the thruster modules on orbit allow them to be stood off from the vehicle body to reduce contamination and heating effects. The systems module is located at the forward end of the vehicle to minimize the view factor of the avionics radiators to the hot ballute during and after the aeromaneuver, keeps the RCS thrusters away from the deflated ballute, and provides both top and side access to the equipment for removal and installation.

Figure 2.2.1-2 shows a top level weight statement for this configuration.

2.2.1.2 Major Trades and Analyses on Initial Reference Concept

The following five top level trades and analyses were performed off this reference configuration; 1) ballute sizing analysis, 2) systems module location trade, 3) tankage shape trade, 4) engine type and sizing trade, and 5) reliability analysis. The first three trades and analyses are presented below. The engine type and sizing trade is presented in section 4.0 and the reliability analysis is presented in section 11.0. The engine sizing trade resulted in changing to 5000 lb thrust engines, and the engine selection trade verified continued use of advanced expander cycle engines. The reliability analysis



SURFACE PANELS (EXCL OUTER PERIPHERALS)	75
OUTER PERIPHERAL PANELS	151
CORNER MEMBERS (EXCL OUTER VERTICALS)	78
OUTER VERTICAL CORNER MEMBERS	22
ASSEMBLY PROVISIONS	50
EQUIPMENT INSTALLATION PROVISIONS	100
<hr/>	
TOTAL STRUCTURES WEIGHT	476 LB.

Figure 2.2.1-3 Equipment Module Structure

indicated that life cycle cost savings would occur with redundancy in the avionics and EPS equipment, RCS thrusters, and having a total of two main engines.

Ballute Sizing. Ballute diameter is affected by three controlling factors; 1) the design heating limit of the ballute fabric, 2) the required turn-down ratio, and 3) the required static stability control margin (cp-cg margin).

As discussed in the aerothermal documentation section 5.0, the fabric heating is a function of the ballistic coefficient (W/C_{DA}) of the vehicle during the aeromaneuver. For a constant reentry weight, if the ballute diameter is increased the ballistic coefficient and fabric peak temperature decrease. The design heating limit of the fabric, therefore, can be expressed approximately as a fixed ballistic coefficient. The ballute diameter must be sized to yield a ballistic coefficient less than this heating limit coefficient.

Ballute turn-down is accomplished by varying the internal pressure of the ballute during the aeromaneuver. As the pressure decreases, the C_{DA} of the ballute decreases and the ballistic coefficient increases. Varying the C_{DA} allows drag control and, thereby, delta-V control during the aeromaneuver. The maximum turn-down ratio ($(C_{DA})_{max}/(C_{DA})_{min}$) is limited; however, by the physical characteristics of the ballute.

The third diameter controlling factor is the static stability control margin or the distance between the center of pressure of the ballute at the maximum turned-down position and the center of gravity of the total vehicle and payload. A positive static margin is necessary because the aerodynamic moments are large relative to the RCS moments. The aerodynamic moment for a one degree change in angle of attack with a static margin of 5% of the length of the ballute is as large as 1070 ft-lb, as compared with an RCS moment of only 445 ft-lb. The aero stability limits usually size the ballute diameter. Since the ballute weight increases by the square of its diameter, a vehicle aft cg placement becomes important to reduce ballute diameter and; therefore, weight. The desirability of an aft cg during the aeromaneuver supports the aft placement of the LO2 tank.

In summary, ballute sizing is dependent on vehicle dimensions and center-of-gravity for a desired backwall temperature (1500°F) and turn-down ratio range. The SB ballute braked OTV resulting from our optimization studies for a stage diameter of 14.5 ft, a length of 35.2 ft, and a start burn weight of 74,140 lbs when sized for a GEO man sortie mission has a diameter of 50 ft. The aerobreaking provisions include a ballute

with a 1500°F backwall temperature and a turn-down ratio of 1.5 (max/min ratio of CDA).

Systems Module Location. To investigate the effects of moving the cg aft, a trade was performed on placing the systems module between the fuel and oxidizer tanks rather than forward on the vehicle. Figure 2.2.1-4 shows the reduction in ballute diameter and weight for a given usable propellant load. Mid body placement of the systems module was selected as a reference configuration concept for both the space based and ground based ballute braked vehicles based on this data.

Tank Shape. Alternate tank shapes were also investigated as a means of moving the vehicle cg aft. Figure 2.2.1-5 shows vehicle configurations with 0.707 elliptical domed LO₂/LH₂ tankage and a toroidal LO₂ tank with a 0.707 elliptical domed LH₂ tank used for this trade. Figure 2.2.1-6 shows the length and weight trends. Although the toroidal tank yields the smallest ballute diameter due to its short length, the tank itself increased in weight more than the ballute weight savings resulting in a higher vehicle inert weight than the elliptical domed tank vehicle. This data resulted in the selection of 0.707 elliptical domed tanks for both the space based and the ground based vehicles. Figure 2.2.1-7 shows the effect of the systems module placement and tank shape trade on the ballute sizing.

2.2.1.3 Revised Reference Configuration

Figure 2.2.1-8 shows the revised reference vehicle configuration resulting from the above trades and analyses.

2.2.1.4 Trades and Analyses on Revised Reference Configuration

Using the revised reference configuration further trades and analyses were conducted on the ballute, RCS, avionics and EPS, TPS, and meteoroid/debris protection.

Ballute. Ballute configuration trades regarding thermal protection, drag control and shape are presented in sections 5, 6, and 10 respectively of this document. These trades resulted in changing to a 70 degree half angle, 1500 degree F backwall temperature ballute which is jettisoned after each mission. Furthermore, the ballute has a turn down ratio (TDR) of 1.5 with a forward to aft attachment point distance of at least half the ballute radius. A detailed design of the ballute installation and jettisoning provisions is given below. The vehicle is originally transported to orbit empty and

- 1500° B/W TEMP, 1.5 TDR BALLUTE USED
- 7.5 K LB RETURN PAYLOAD

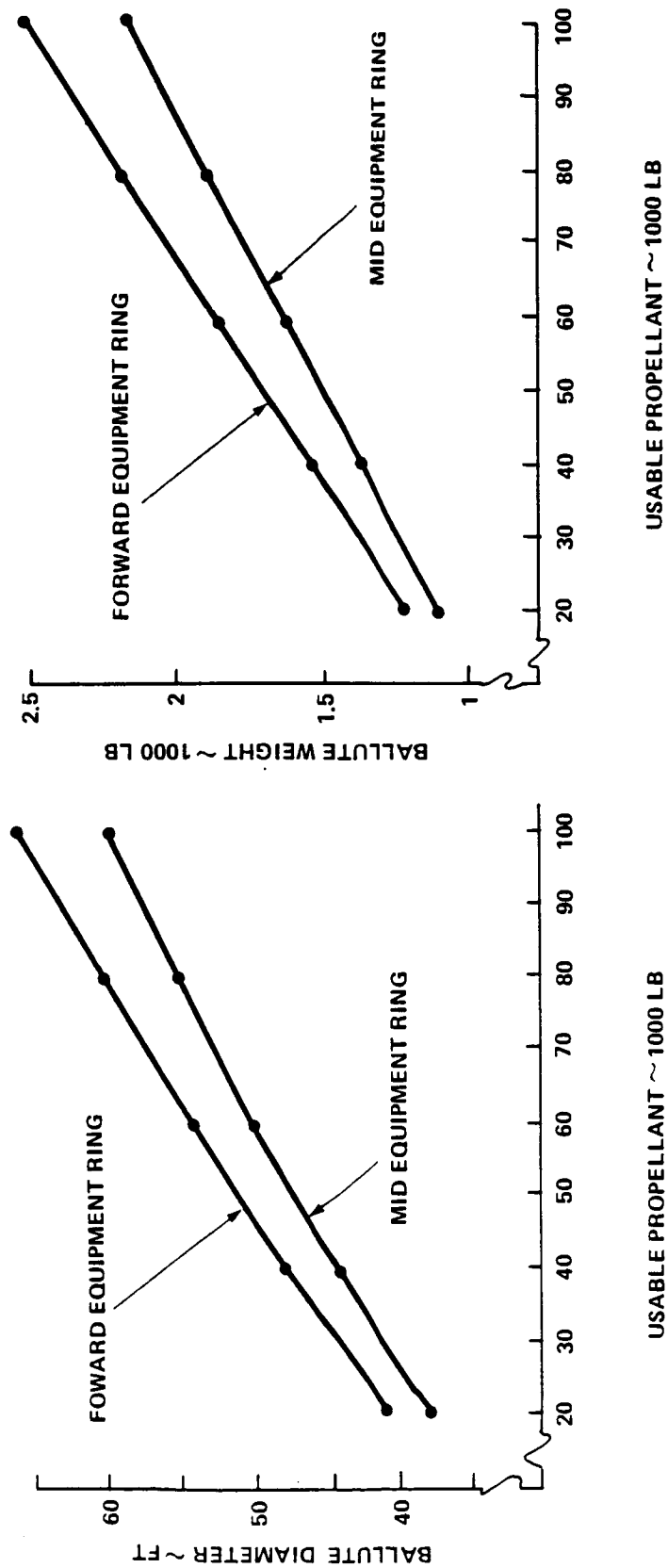


Figure 2.2.1.4 Equipment Ring Placement Trade Ballute Sizing Trends

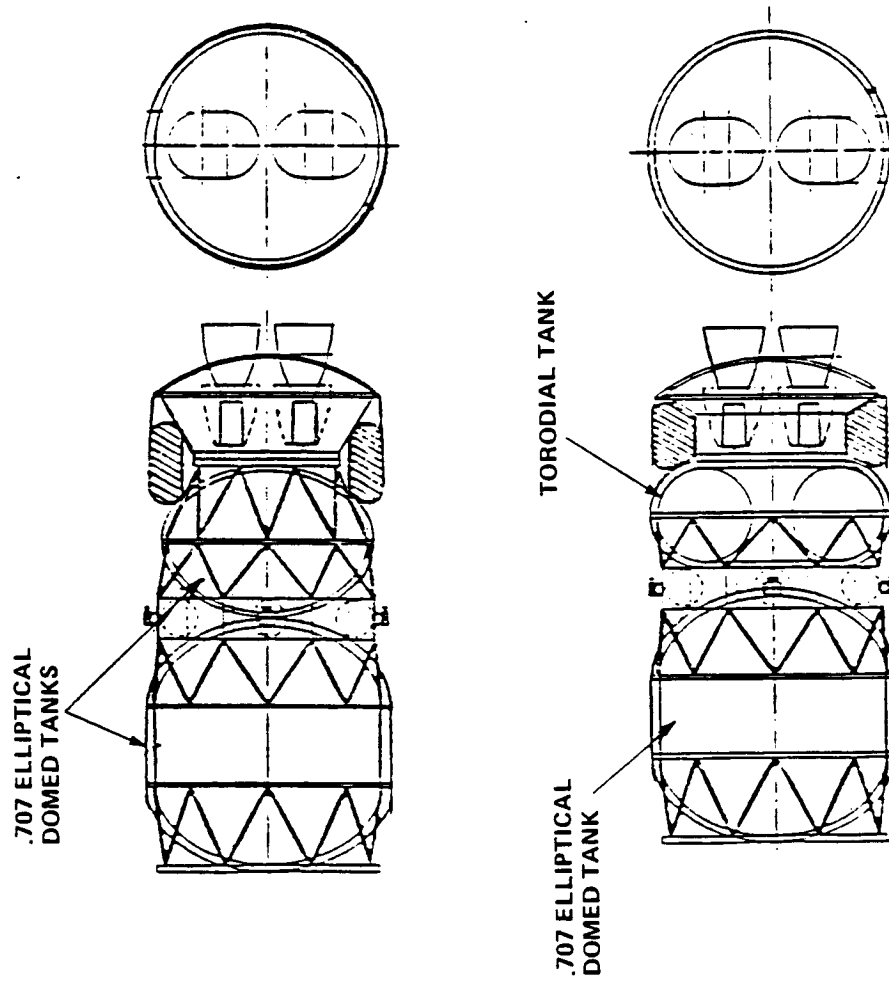


Figure 2.2.1-5 Tank Shape Trade

- MID AVIONICS RING, 55 K LB LO_2/LH_2 PROPELLANT CAPACITY
- BALLUTE SIZED TO PROVIDE STABILITY MARGIN FOR 5500 LB PAYLOAD RETURN
- SPACE-BASED CONFIGURATIONS

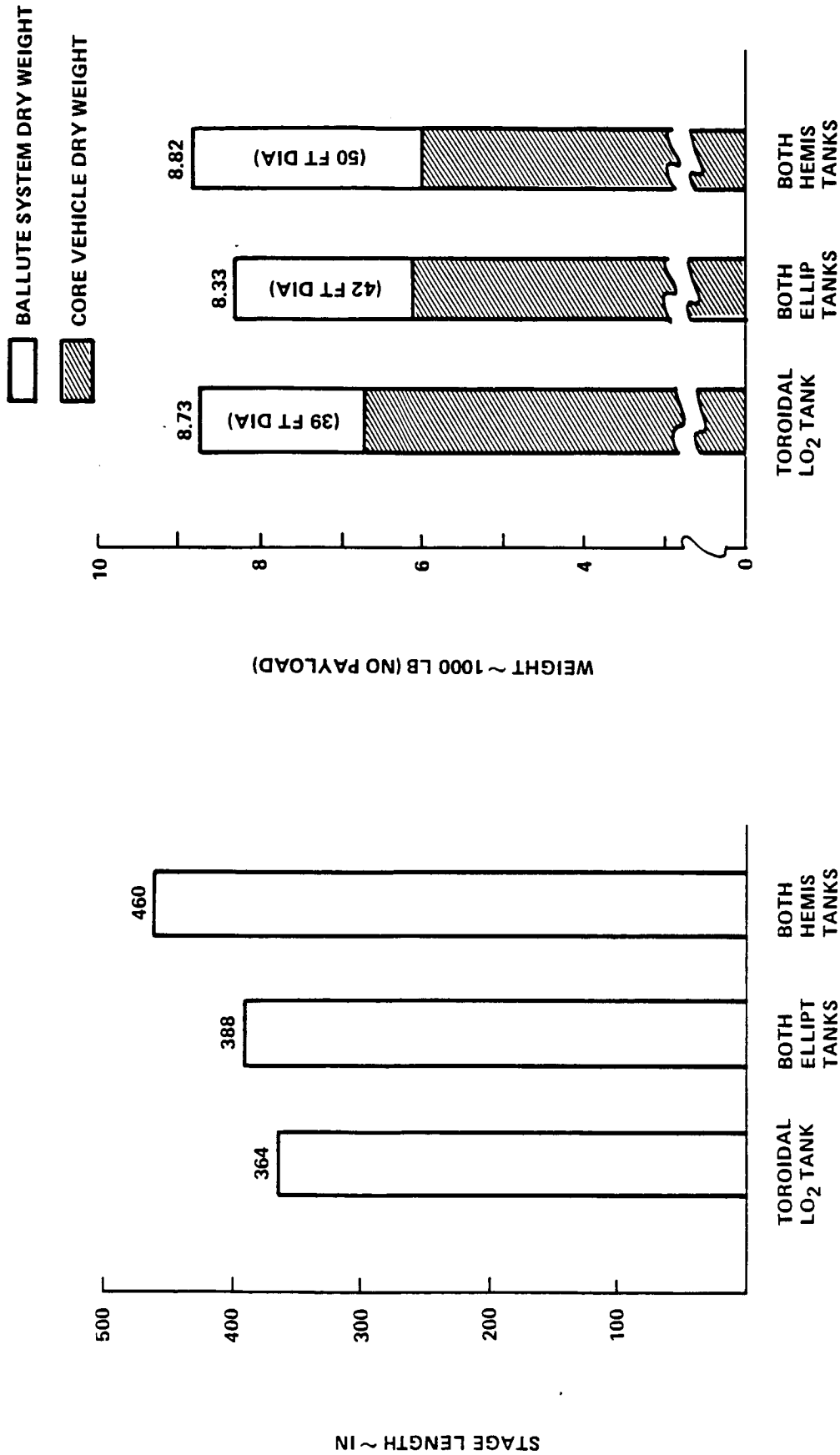


Figure 2.2.1-6 Tank Shape Trade Vehicle Weight and Length

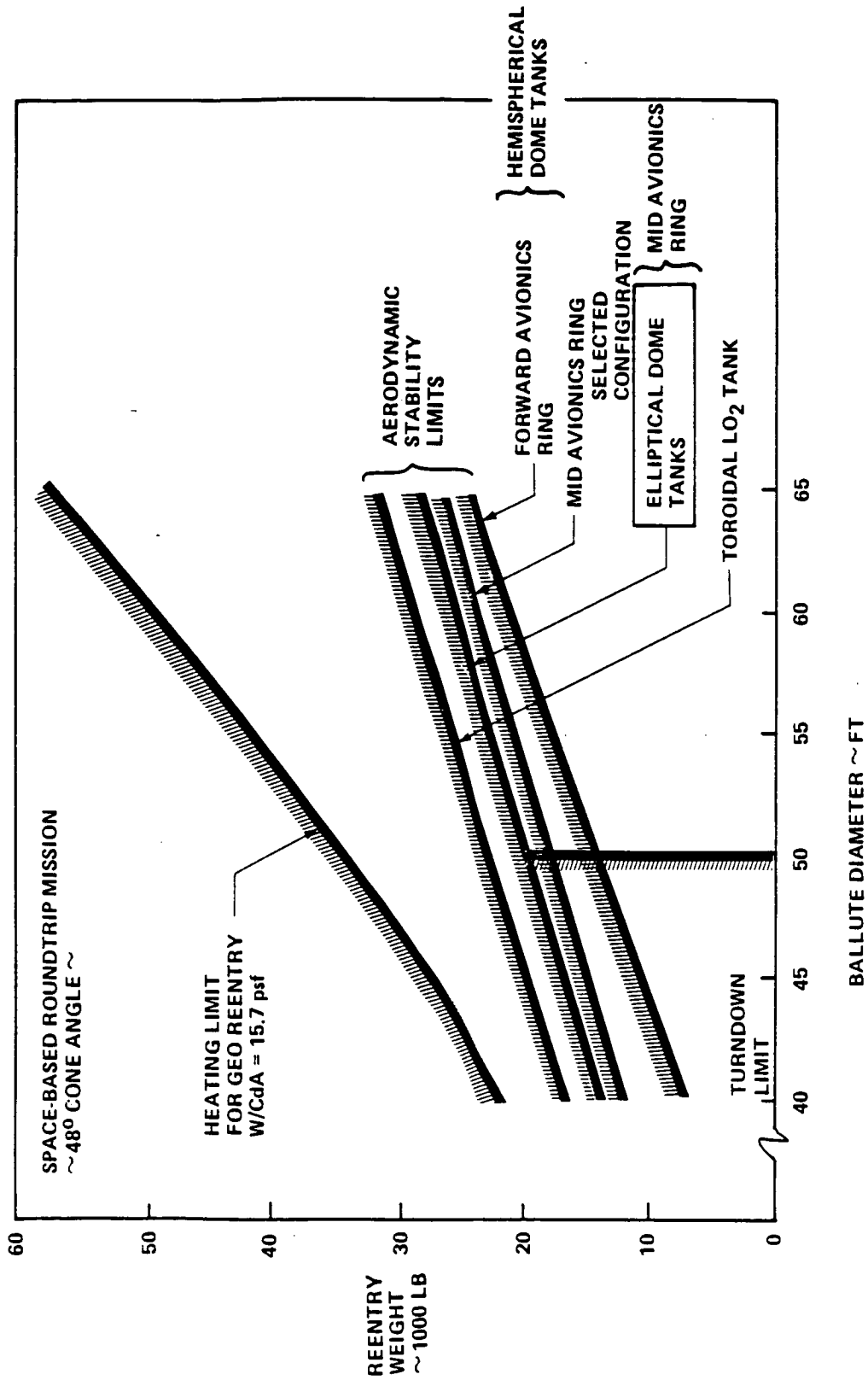


Figure 2.2.1-7 Ballute Sizing Criteria

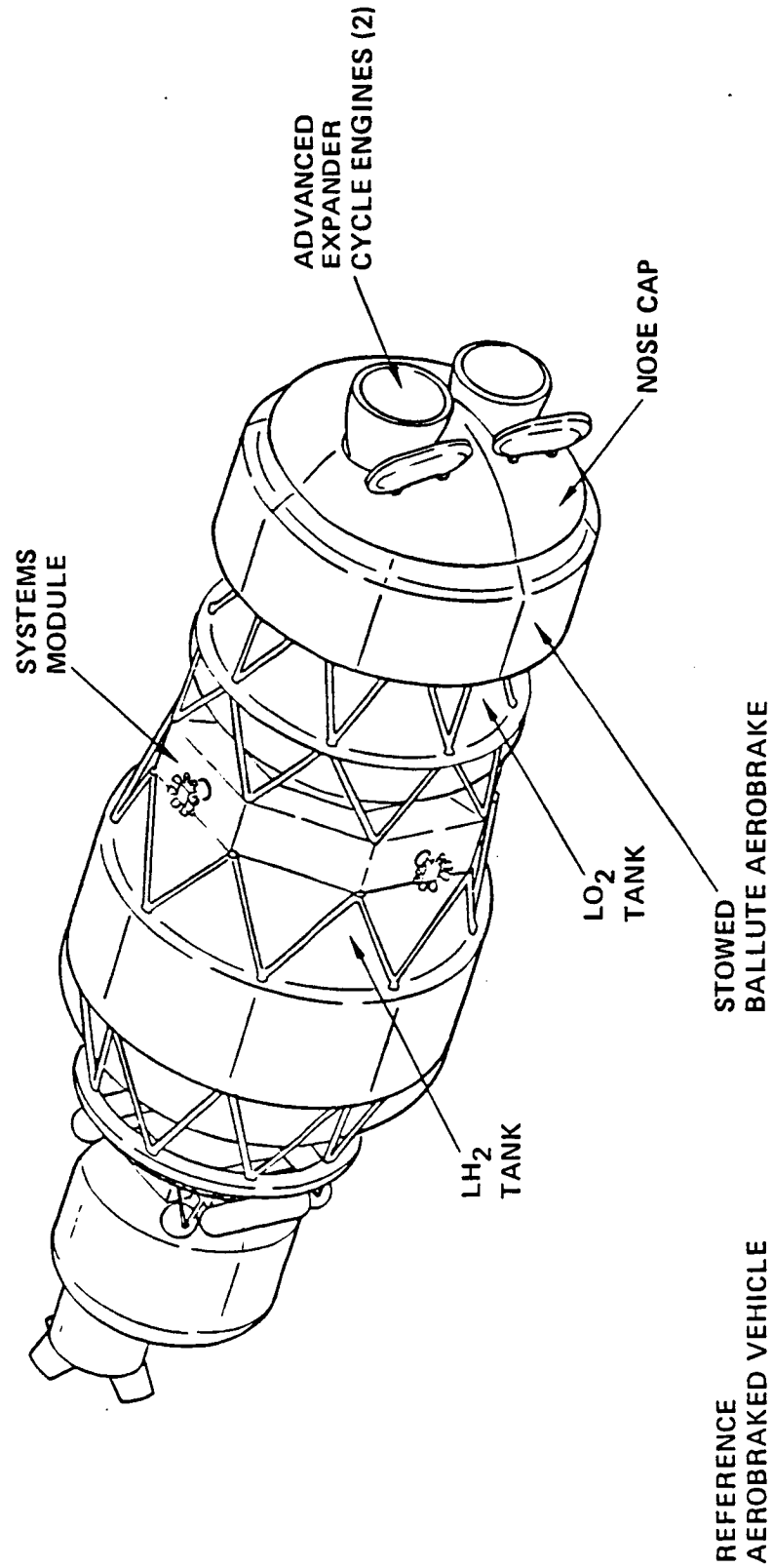


Figure 2.21-8 OTV Ballute-Braked Concept
— Revised Reference Configuration

without a ballute allowing ASE to be temporarily attached to the engine primary structure. ASE is also attached via the payload interface to complete the support of the vehicle for transport.

RCS. The RCS has been moved forward for three reasons; 1) eliminate thrusters heating avionic radiators, 2) eliminate contamination of avionic radiators, 3) reduce plume impact on ballute jettisoning, and 4) increase area for avionics in ring.

EPS Radiator. The EPS and avionic radiators were sized using nominal earth infrared, albedo and solar radiation heating on a vehicle performing a thermal roll. The EPS radiator is located adjacent to the avionics to allow assembly and checkout as a unit before integration into the vehicle. The EPS radiator is shown faceted since it conforms to the primary strut structure to which it is attached.

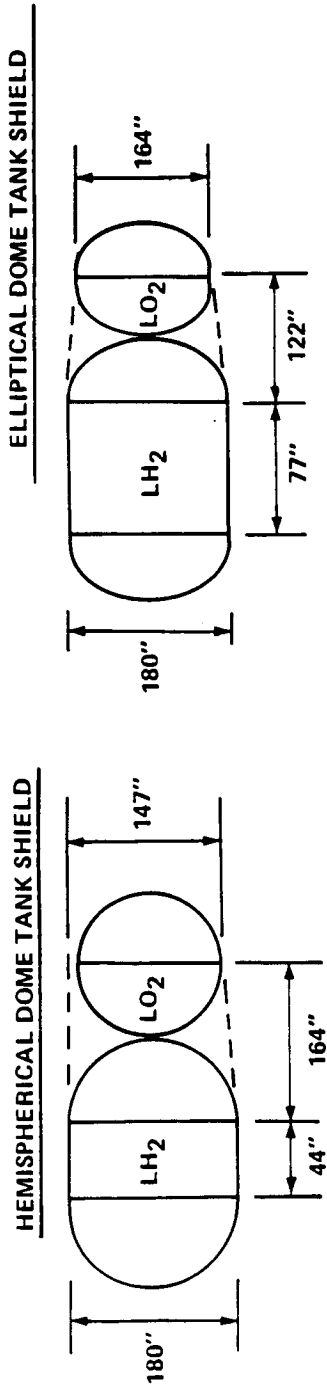
TPS. The 1500 degree ballute requires insulation external to the meteoroid/debris shield. Since the EPS and avionics' radiators cannot be insulated, the backwall of the ballute is insulated in this area to reduce the heat transfer; however, this insulation by itself will not keep the avionics below their design temperatures. As a reference concept, we have used phase change materiel (myrietic acid, a salt that melts at 136°F) around critical avionics to keep temperatures within limits.


Meteoroid/Debris Shielding. Figure 2.2.1-9 shows the results of a trade comparing meteoroid/debris shielding conformal to the tank dome heads versus shielding placed along the vehicle body lines. Placing the shield along the body lines and using the EPS radiator and avionics ring as part of the shield yields the least added shield area and; therefore, the least weight. Integrating the EPS radiator and avionics ring with the shield and considering the primary load path of the mid body avionics ring allows elimination of the box structure enclosing the avionics as in the systems module design. Furthermore, meteoroid/debris shield analysis presented in section 3.0 resulted in changing to a 3 inch standoff distance over the LH2 tank's cylindrical section and the elimination of the deployed shield. The tank was resized using a 3 inch static and dynamic clearance to a maximum diameter of 168 inches.

2.2.1.5 Selected Space Based Ballute OTV Configuration

Figure 2.2.1-10 shows the final configuration of the space based, ballute braked OTV. Table 2.2.1-1 shows a synopsis of the design features of this configuration.

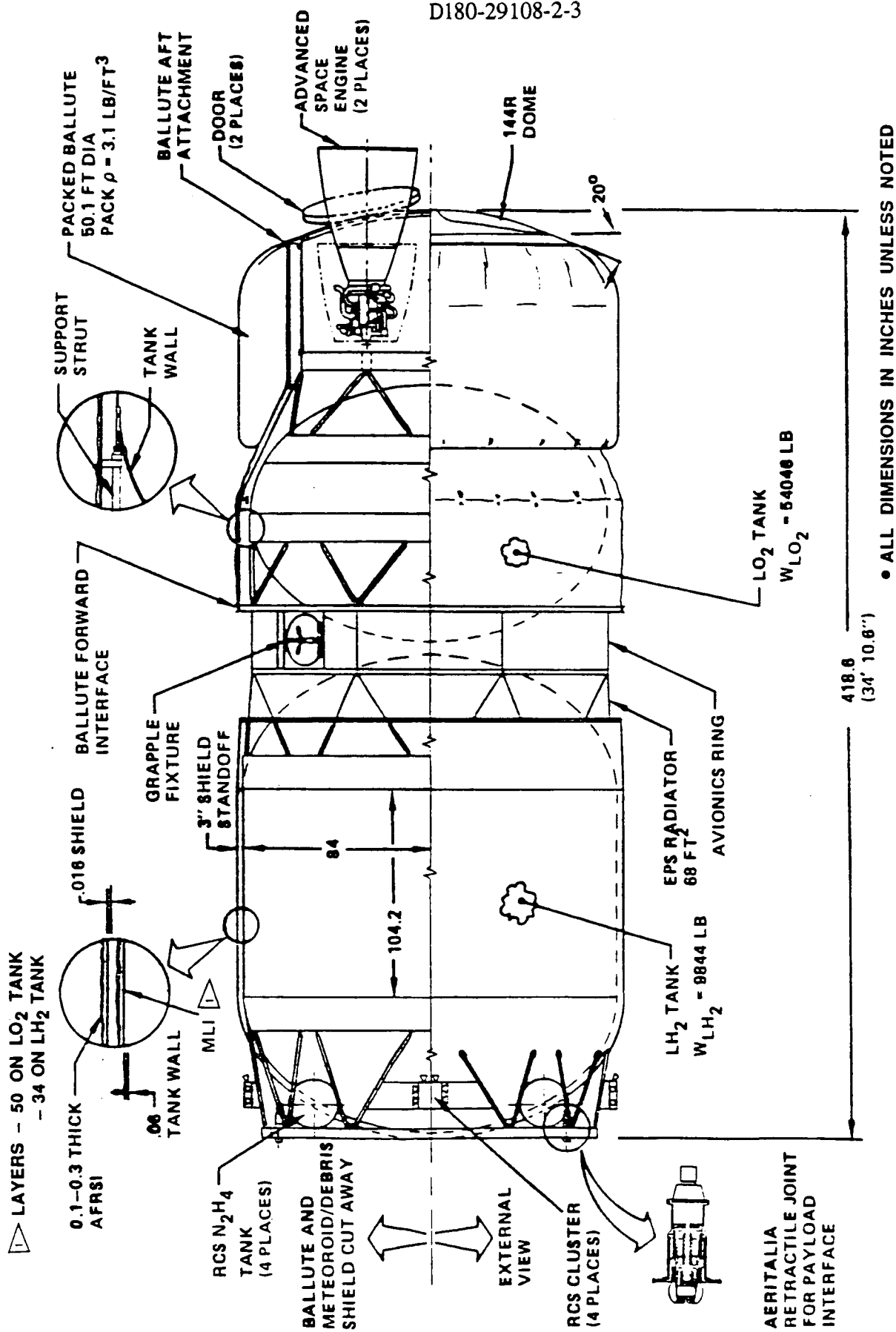
SIZED FOR 59 K LB LO₂/LH₂ PROPELLANT



TOTAL SURFACE AREA			
	CONFORMAL TO TANK HEADS	ALONG VEHICLE LINES (NO EQUIP RING)	ALONG VEHICLE LINES (WITH EQUIP RING) 
		1351 ft ²	1167 ft ²
HEMISPHERICAL DOME TANKS	1351 ft ²	1350 ft ²	1167 ft ²
ELLIPTICAL DOME TANKS	1351 ft ²	1286 ft ²	1121 ft ²

 ASSUME EQUIPMENT RING AND RADIATOR IS 168 IN DIA X 45 IN LONG AND PROTECTS AREA BETWEEN TANKS (165 ft²)

Figure 2.2.1-9 Meteoroid/Debris Shielding Area Trade



• ALL DIMENSIONS IN INCHES UNLESS NOTED

Figure 2.2.1-10 Final Configuration Space-Based Ballute-Braked OTV-Single Stage

Table 2.2.1-1 Configuration Features Space-Based Ballute Braked OTV

<u>FEATURE</u>	<u>RATIONALE</u>
● MID BODY AVIONICS RING	● AFT C.G. REDUCES BALLUTE DIAMETER SIZED FOR AERO-STABILITY
● **EPS RADIATOR LOCATED ADJACENT TO AVIONICS RING	● CO-LOCATES ALL RADIATORS ON VEHICLE ● EPS RADIATOR ADJACENT TO EPS
● RADIATORS SIZED ASSUMING OTV PERFORMS THERMAL ROLL	● RESULTS IN SMALLER RADIATOR AREA AND LESS WEIGHT ● PAYLOADS USUALLY REQUIRE ROLL FOR THERMAL CONTROL
● **EPS RADIATOR AND AVIONICS RING INTEGRATED WITH METEOROID/DEBRIS SHIELD	● ELIMINATE STRUCTURAL BOX AROUND AVIONICS ● LESS SHIELD AREA THAN CONFORMAL DOME DESIGN ● SHIELD SUPPORTED BY TANK SUPPORT STRUTS
● **RCS LOCATED FORWARD	● ELIMINATE CONTAMINATION AND HEATING OF RADIATORS ● REDUCE PLUME IMPINGEMENT ON BALLUTE
● AVIONICS, MAIN ENGINES, BALLUTE, RCS THRUSTERS ARE ORUs	● EVA REPLACEMENT POSSIBLE AND COSTS LESS THAN EARTH RETURN
● MAXIMUM DIAMETER 174"	● 3" STATIC AND DYNAMIC CLEARANCE IN STS PLB
● **NON-DEPLOYABLE SHIELD WITH 3" STANDOFF DISTANCE	● YIELDS MINIMUM GAGE SHIELD—LARGER SPACING DOES NOT REDUCE WEIGHT
● LO ₂ AND LH ₂ TANKS CARRY PRIMARY LOADS	● ENGINE LOADS ARE RELATIVELY LOW ● TANK PRESSURIZATION KEEPS TANKWALLS IN TENSION
● **70° JETTISONABLE BALLUTE WITH 1500° BACKWALL TEMPERATURE	● LEAST WEIGHT BALLUTE SYSTEM ● INSULATION REQUIRED AROUND TANKAGE
● **BALLUTE FORWARD ATTACHMENT POINT HALF BALLUTE RADIUS FROM AFT ATTACHMENT POINT	● PERMITS 1.5 TURN DOWN RATIO

* = CHANGES FROM MIDTERM CONCEPT

Major Elements. Figure 2.2.1-11 shows three major structural elements which are removable via EVA. The ballute is installed and jettisoned after each flight. The heat shield structure is removed only when a main engine must be replaced. Removal provides the EVA astronaut access to the engine interface since the nozzle doors are not large enough to admit an EVA astronaut.

Figure 2.2.1-12 shows our actuator and linkage design concept for opening the nozzle doors on the heat shield support structure. The doors open almost 180 degrees to reduce peak temperatures in the doors due to the engine radiation and recirculation environment. The door TPS closures are envisioned to be similar to the umbilical or gear door closures used on the Shuttle.

Ballute Attachment. Our reference design uses three marman type clamp bands to secure the ballute and heat shield to the vehicle core. The ballute clamp bands are automatically latched while the heat shield band is manually latched. Automatic latching could be pneumatic (as shown) or electrically driven.

The major hardware for the installation and jettisoning of the ballute is shown in figure 2.2.1-13. The system is designed to ease EVA installation of the ballute, keep the chance of damaging the tiles on the heat shield to a minimum during installation and assure jettisoning of the ballute after use. A structural assembly supports the ballute itself during transport and installation. The ASE used to transport the ballute to the Space Station and the fixture used to support the ballute at the station attaches to the marman clamp interface on the ballute support structure. During installation, rollers on the ballute structure engage guide tracks on the heat shield. The tracks are funnel shaped at the ends so the ballute only needs to be grossly positioned initially. As the ballute is drawn onto the tracks by the shuttle mechanism, the narrowing tracks precisely position the ballute.

The ballute installation sequence is shown in figure 2.2.1-14. The shuttle mechanism/spool system is used to winch the ballute onto the vehicle. After the second set of rollers is engaged, the tool used to initially position the ballute can be removed. After the ballute has been seated and clamped, the temporary transport corset is manually removed to free the end of the ballute which must be threaded under the forward attachment clamp. The clamp is then partially closed, the ballute edge bead is seated against the clamp and the clamp is fully closed finishing the installation.

Ballute inflation occurs just prior to the aeromaneuver. Jettisoning the main corset initiates the inflation sequence. Figure 2.2.1-15 shows the main corset

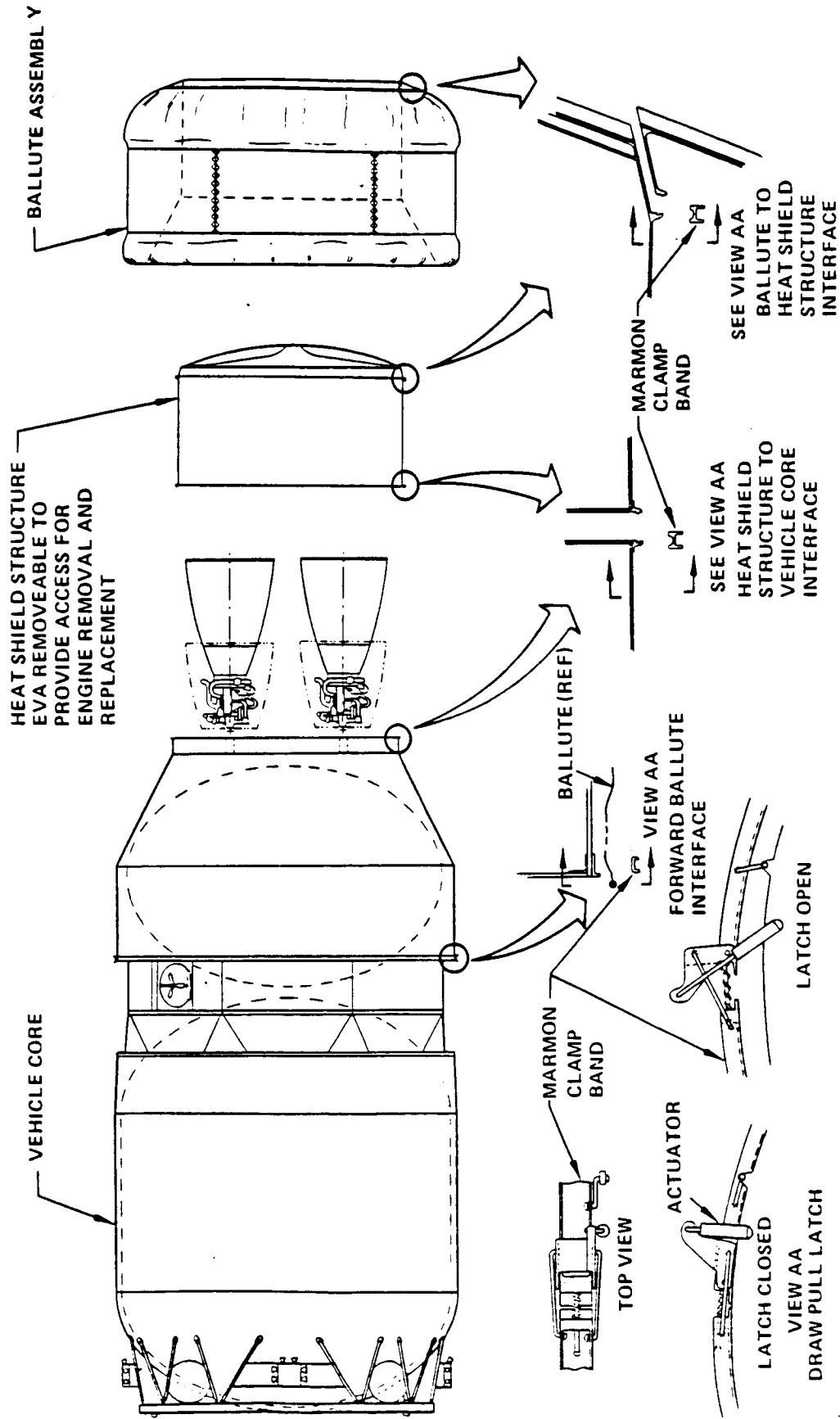


Figure 2.2.1-11 Vehicle Elements Space Based Ballute-Braked OTV—Single Stage

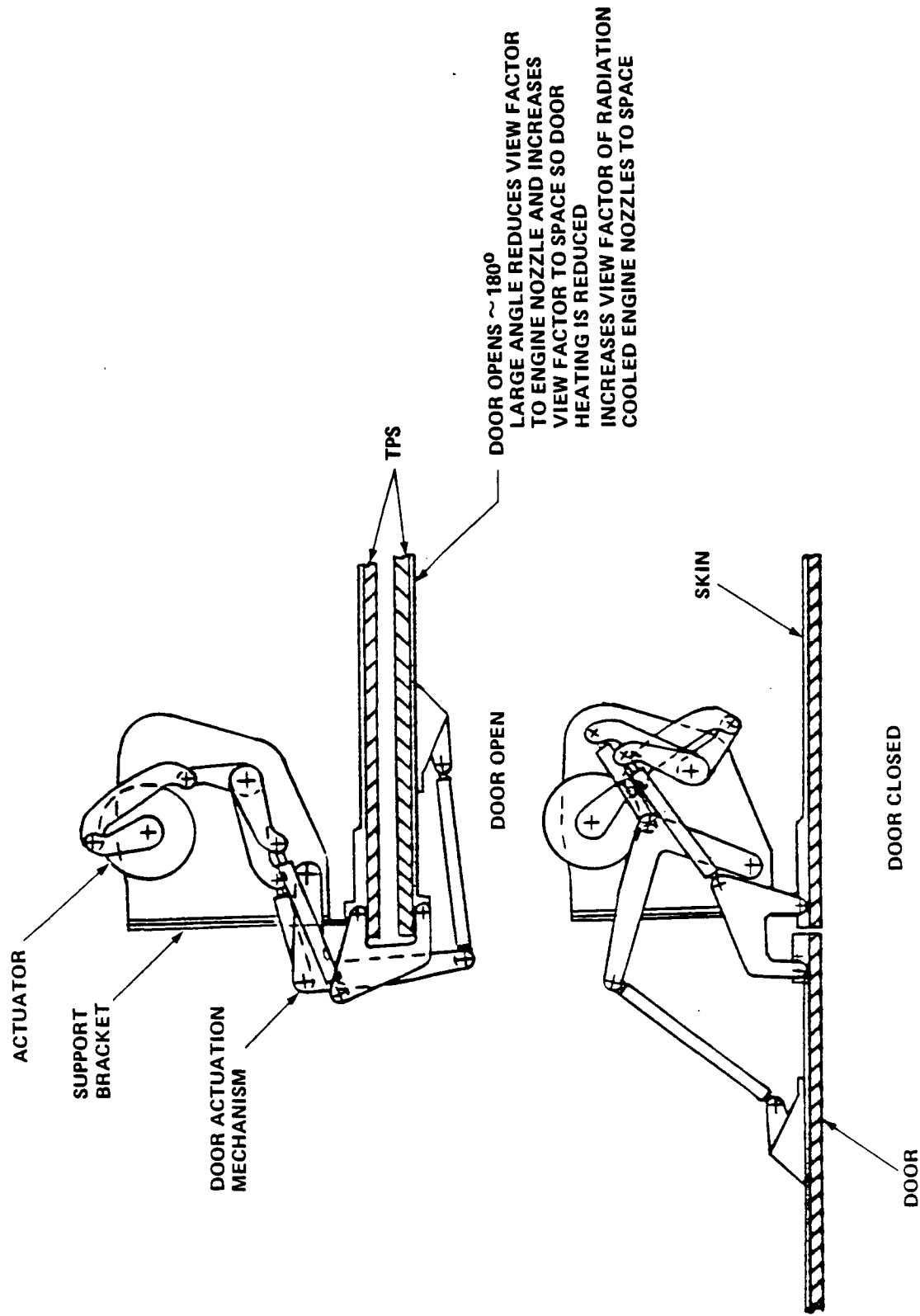


Figure 2.2.1-12 Engine Door Hinge/Actuation System Based on Orbiter/External Tank Umbilical Closeout Doors

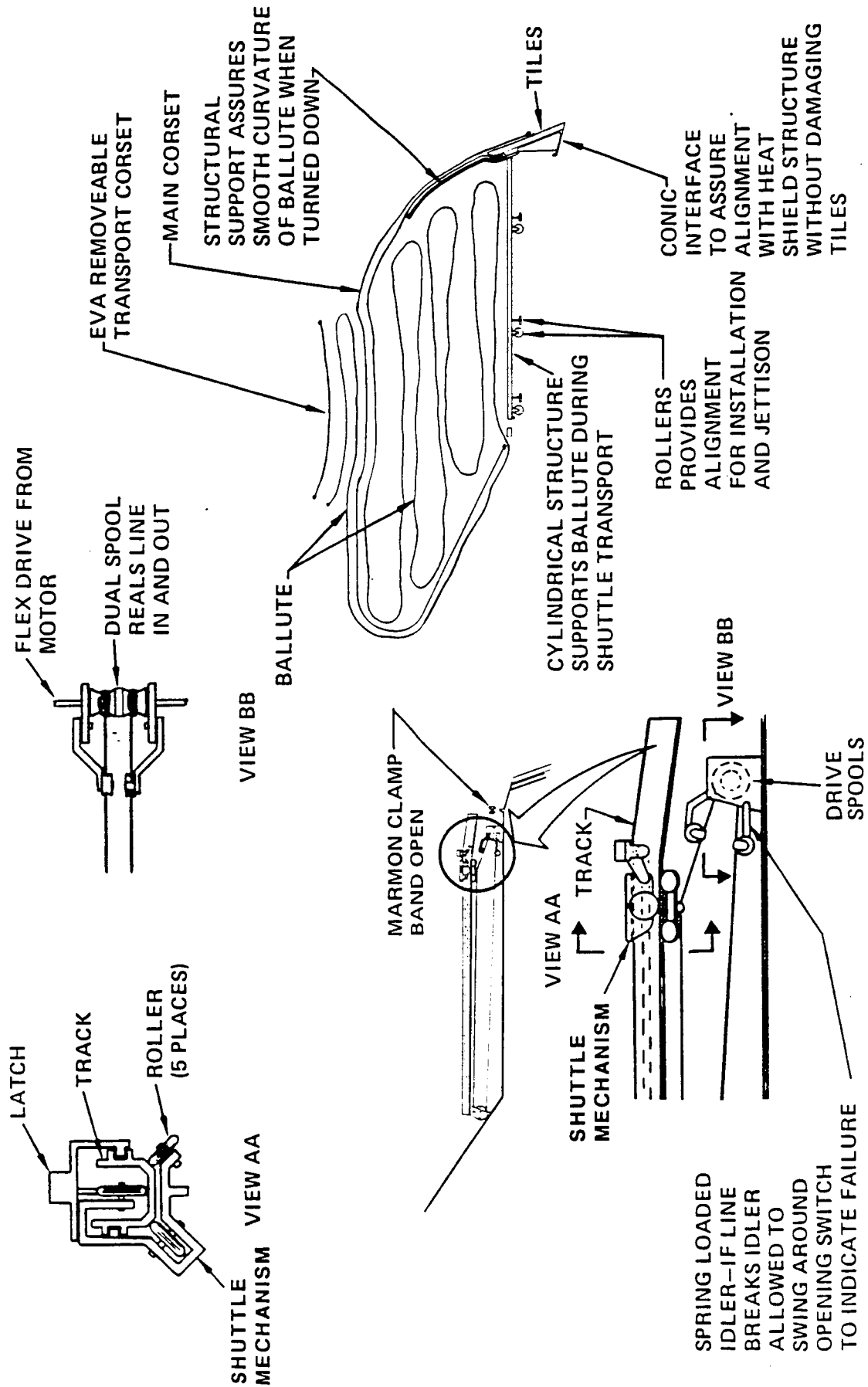
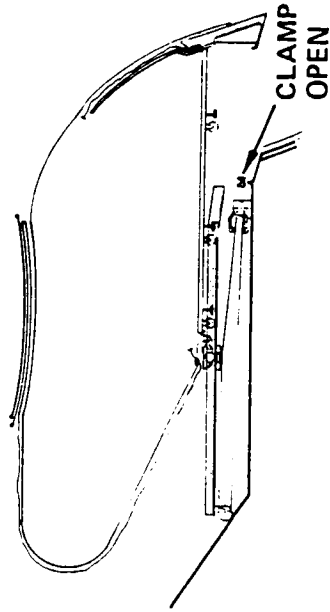
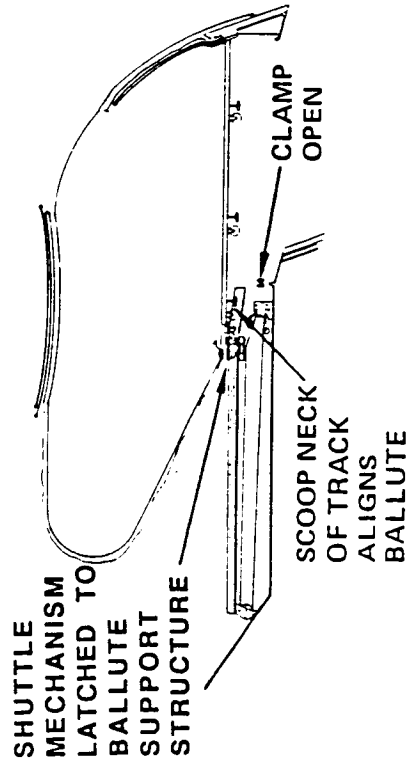


Figure 2.2.1-13 Ballute Installation/Jettison Provisions

SPOOL/SHUTTLE MECHANISM SYSTEM
PULLS BALLUTE ONTO VEHICLE



INITIAL ENGAGEMENT



MARMON CLAMP CLOSED TO
COMPLETE INSTALLATION

ASTRONAUT INSTALLS
BALLUTE UNDER
FORWARD CLAMP
BAND

TEMPORARY CORSET
REMOVED EVA

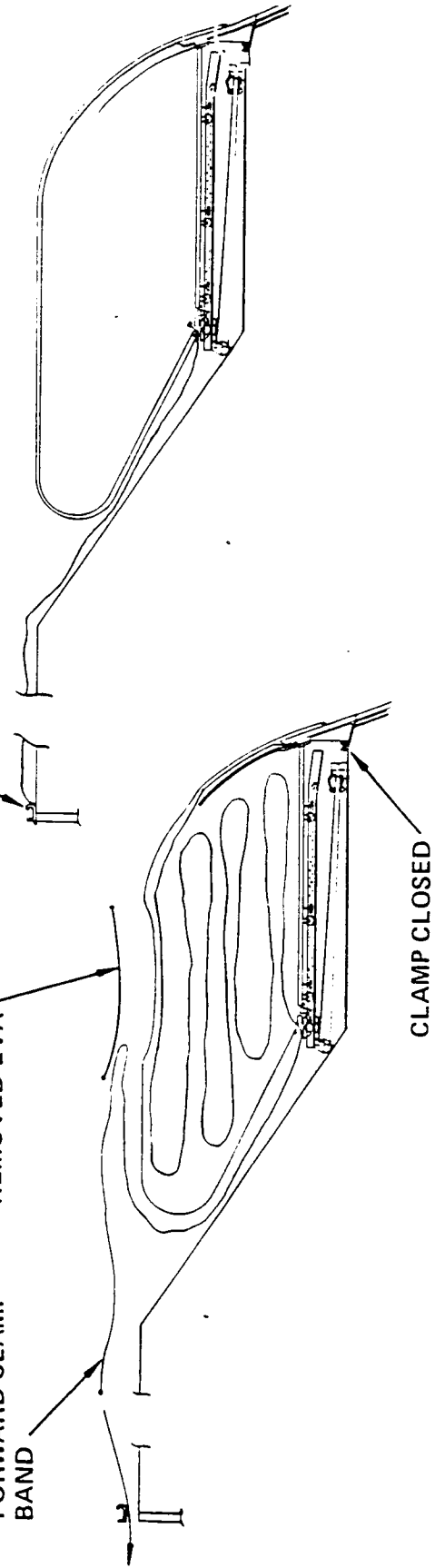


Figure 2.2.1-14 Ballute Installation Sequence

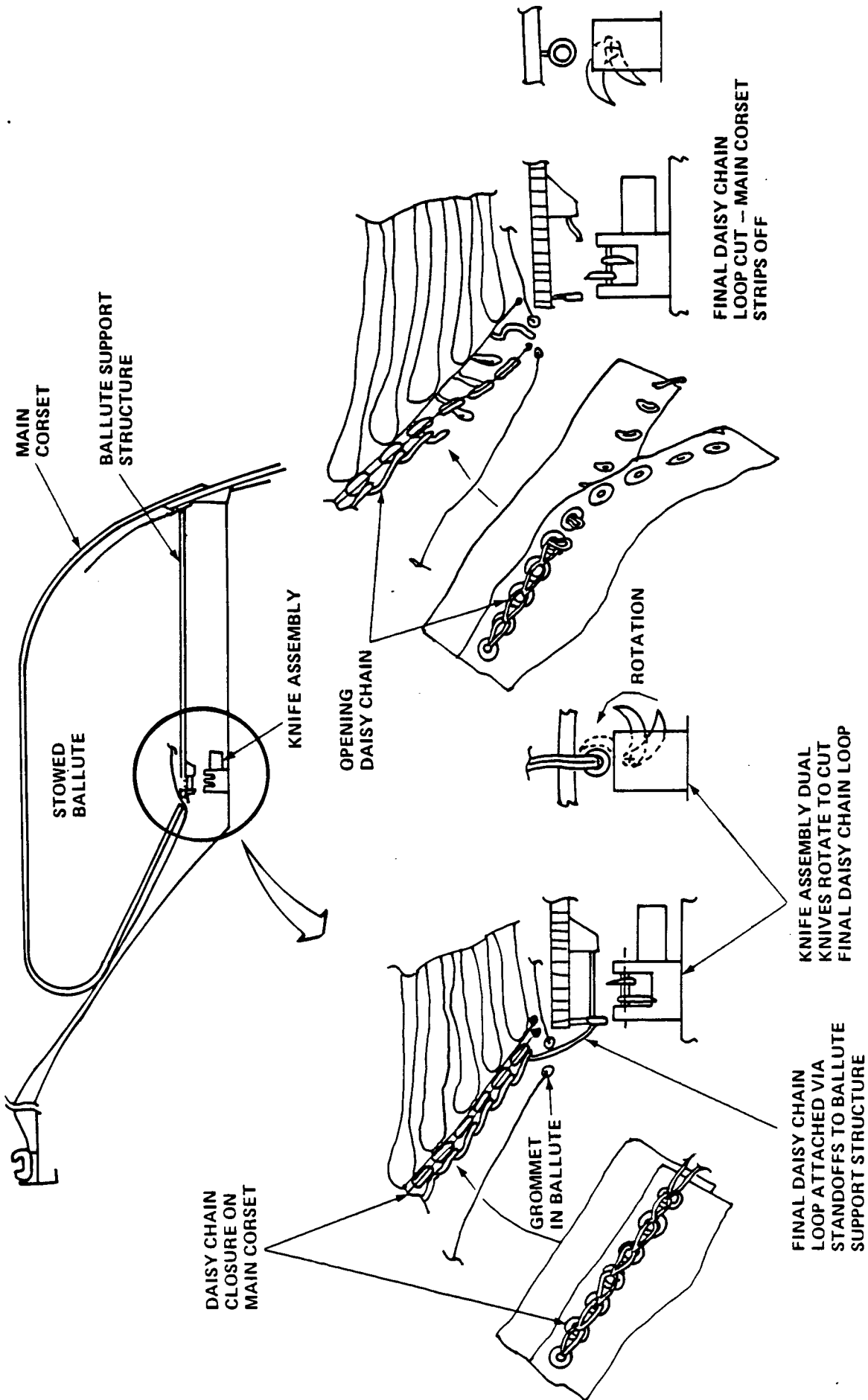


Figure 2.2.1-15 Jettisoning of Main Corset Prior to Ballute Inflation

jettisoning procedure. The corset is installed in segments held together by daisy chain closures. The final daisy chain loop is suspended between standoffs on the ballute support structure. Upon installation, the final loop is automatically properly positioned over a rotating knife assembly. To jettison the ballute, the knife assembly severs the final loop allowing the daisy chain to unchain and the corset is stripped away by the inflating ballute.

The ballute is inflated with GN2 before and during the aeromaneuver and therefore, provides the means for controlling drag. Figure 2.2.1-16 shows the ballute shape at several points in the aeromaneuver. Modulation of the internal pressure controls the location of the center of pressure (cp) of the ballute from fully inflated to a 1.5 turned down shape. A 5 percent stability margin between the cp of the turned down ballute and the cg of the vehicle sizes the ballute as shown in figure 2.2.1-17. The limits shown correspond to the ballute sizing factors discussed earlier. The 1.5 turn-down limit line in this figure shows that a 33 ft diameter ballute is the smallest ballute which can be attached to the 126 inch diameter aft attachment interface and still have a turn down ratio of 1.5.

After the aeromaneuver is complete, the ballute forms into a torus shape from internal pressure loads. The hot ballute is jettisoned as soon as possible to minimize its thermal impact on the vehicle. Jettisoning of the ballute is the opposite of the installation and is shown in figure 2.2.1-18. The shuttle mechanism/spool system winches the ballute off the vehicle while the RCS thrusters move the vehicle away from the ballute. Tapes connecting the forward edge of the ballute to its support structure ensure that the forward edge is pulled from under the open marmon clamp band.

Avionics Placement. An initial layout of the avionics installation is shown in figure 2.2.1-19. Equipment associated with particular subsystems have been located together. The first four bays and part of the fifth are dedicated to the electrical power subsystem. The fifth and sixth bays contain the TT&C subsystem. The seventh and part of the eighth contain the GN&C subsystem and the main propulsion subsystem occupies the remainder of the bay. Provisions for the equipment needed to man-rate the vehicle are initially installed; however, the avionics themselves are only installed the manned flights.

The GN2 bottles required for main engine seal purge and ballute inflation are located behind the EPS radiators.

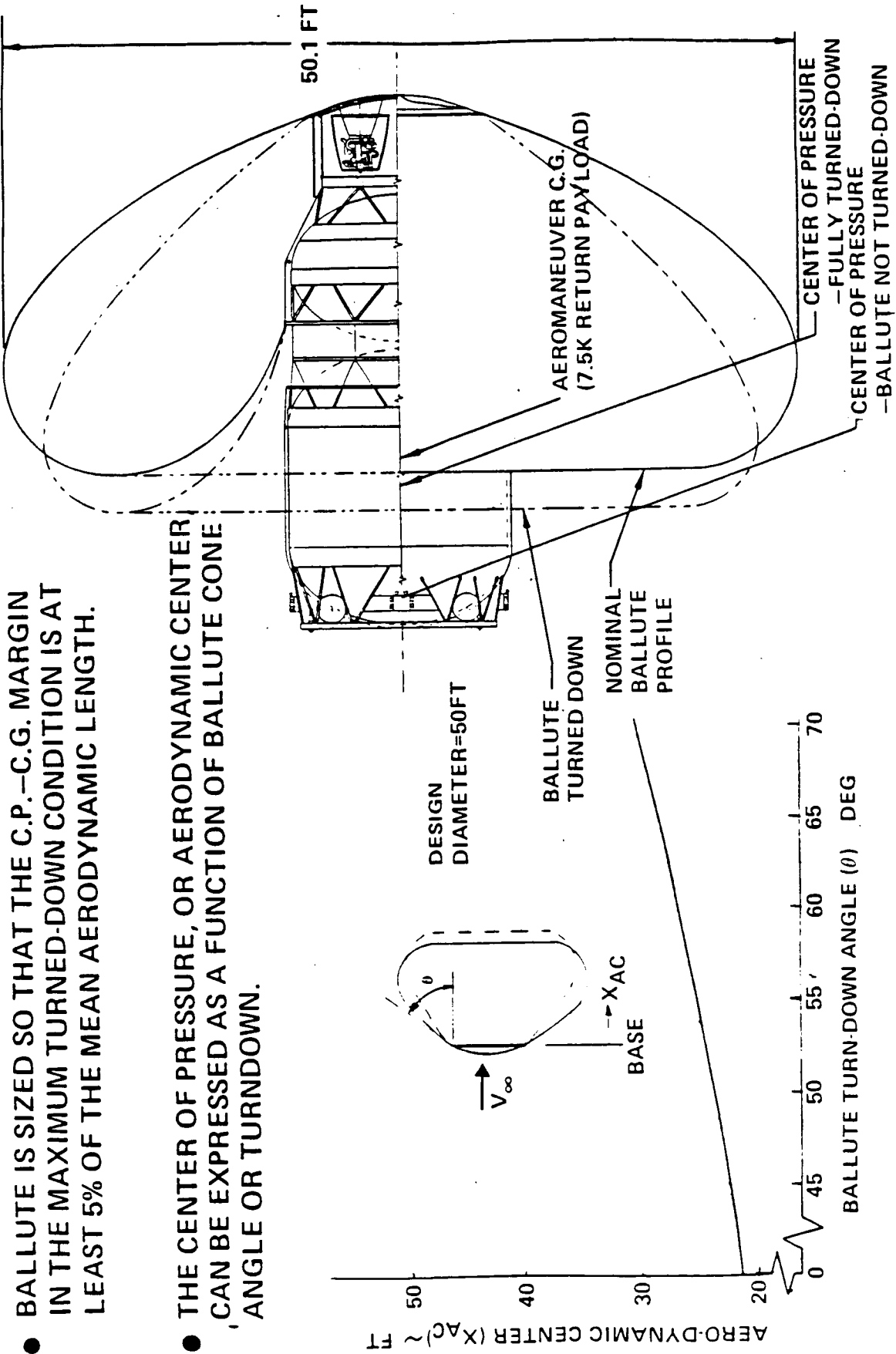


Figure 2.2.1-16 Ballute Inflated and Modulated During Aeromaneuver

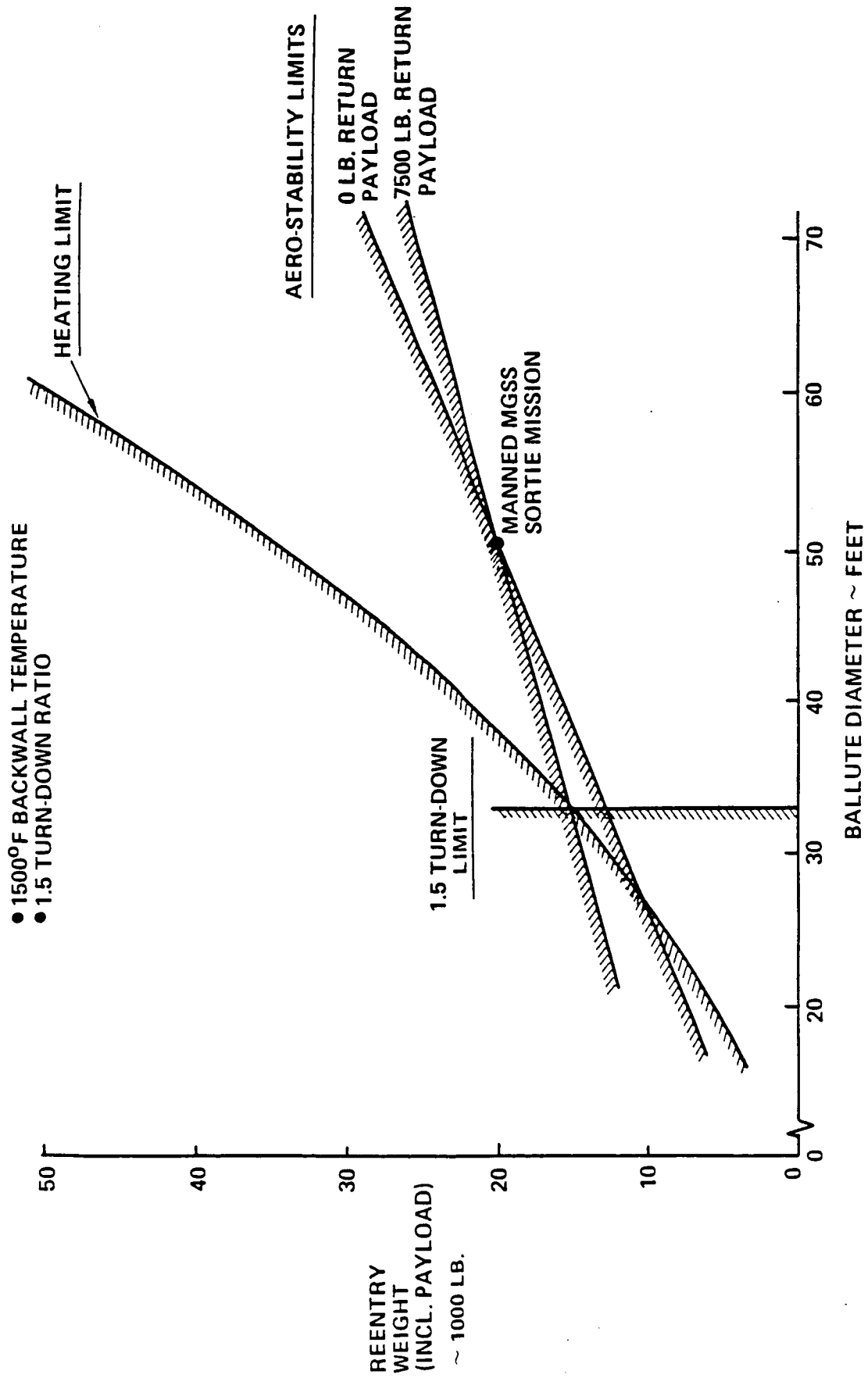


Figure 2.2.1-17 Brake Diameter Sizing Space-Based Ballute-Braked OTV—Single Stage

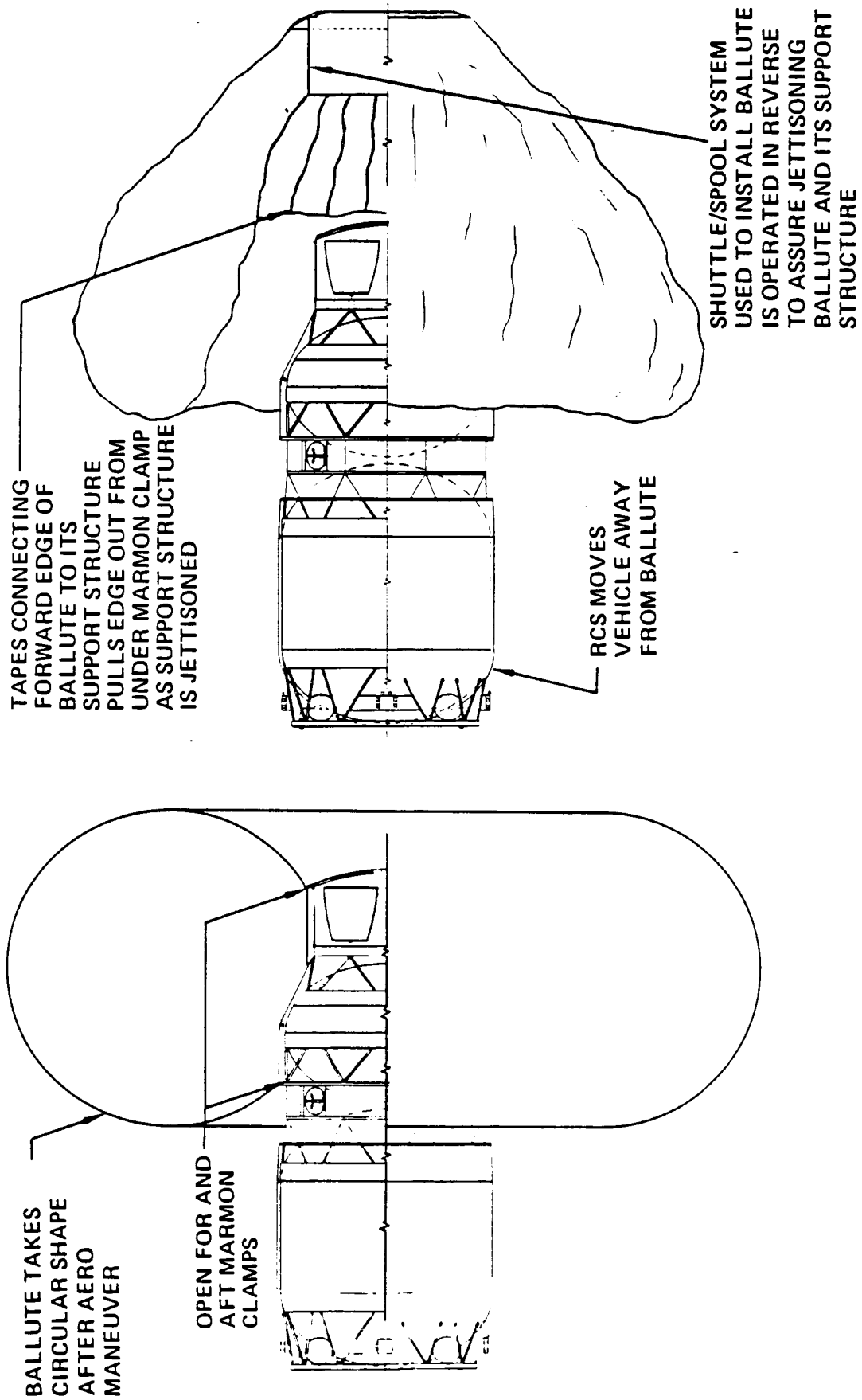
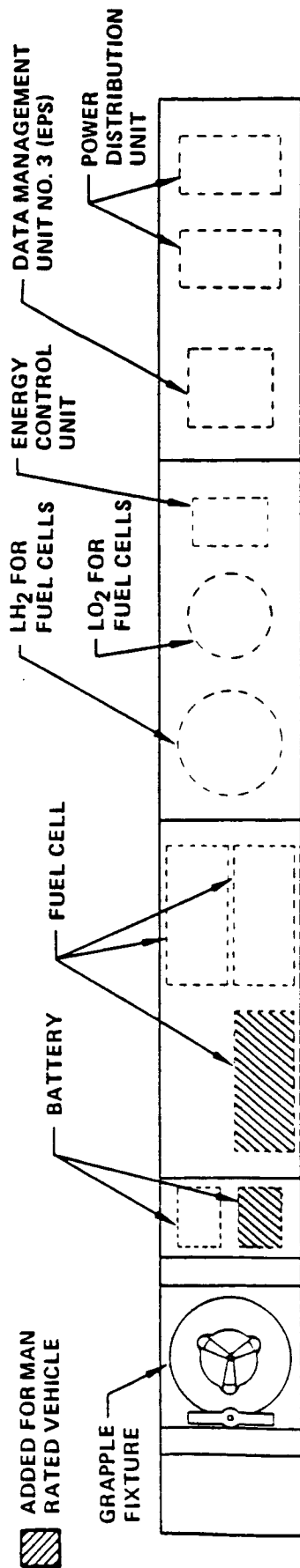


Figure 2.2.1-18 Ballute Jettisoning



D180-29108-2-3

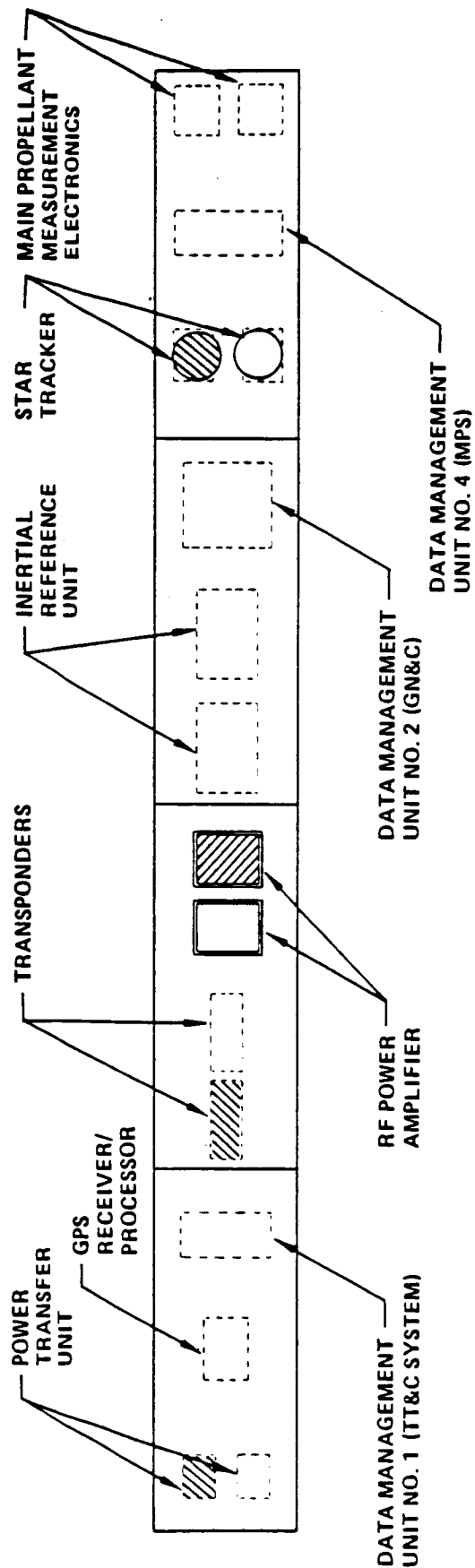


Figure 2.2.1-19 Avionic Ring

Weights. Figure 2.2.1-20 shows a top level weight summary for the manned sortie mission of the space based, ballute braked vehicle. The subsystems are man-rated. Included in structures are body and stiffening ring structures, thrust structure, equipment support structure, tankage and tankage support structure, as well as all structure associated with the ballute, both jettisonable and non-jettisonable. Propulsion systems include both main propulsion and reaction control systems. Thermal control and protection includes tank insulation, and active thermal protection during the aeromaneuver. Other systems are shown. Space maintenance provisions includes all structural and mechanical provisions to remove/replace selected vehicle components. Weight growth includes 5% of existing hardware weight and 15% on all other weights.

Center of Gravity. Figure 2.2.1-21 shows the cg movement for the 20k delivery missions and 7.5k manned roundtrip mission. The 20k mission establishes the engine gimbal angle requirement of 21 degrees. This angle provides 4 degrees of control authority if an engine were to fail shortly after the payload was delivered. The manned mission establishes the ballute diameter via the aerodynamic stability margin requirement. The relationship between the aerodynamic center and the cg for this mission is shown.

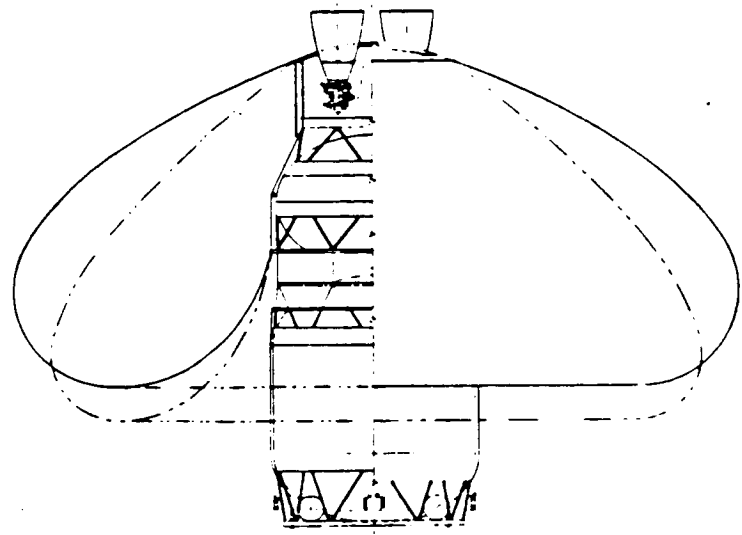
Weight Trending. For the above chronological history of configurations, figure 2.2.1-22 shows how the weights changed as the configurations changed. Table 2.2.1-2 presents a breakdown of the weight changes.

2.2.1.6 Configuration for Drag Modulation Trade

A system level trade was performed between configurations using ballute turndown for drag control as discussed above versus engine exhaust modulation. The complete trade is discussed in Volume III and thermal protection inputs are addressed in Section 5.0 of this document. Figure 2.2.1-23 shows the engine drag modulation vehicle configuration used in the trade. Besides drag modulation, the engine exhaust is also used to cool the boundary layer of the ballute resulting in a lower FSI weight.

The weight changes from the space based OTV with a 600 degree backwall temperature ballute using turndown are shown in table 2.2.1-3. Although the engine modulated vehicle has a structural weight savings, this savings is offset by the addition of main propellant and ballute pressurant required for the aeromaneuver. Additional pressurant is required to maintain the ballute at its nominal profile throughout the

- MAN-RATED SUBSYSTEMS
- 1500° B/W, 1.5 T/D BALLUTE SIZED FOR 7.5K PAYLOAD RETURN (50 FT. DIA.)



	<u>LBS</u>
STRUCTURES	4237
PROPULSION SYSTEMS	1019
THERMAL CONTROL AND PROTECTION	1168
GUIDANCE, NAVIGATION AND CONTROL	135
COMMUNICATIONS/DATA HANDLING	469
ELECTRICAL POWER	710
SPACE MAINTENANCE	323
WEIGHT GROWTH	1128
(DRY WEIGHT)	(9189)
RESIDUALS	669
(INERT WEIGHT)	(9858)
REACTANTS—EPS (INC. RESERVES)	34
PROPELLANTS—RCS (INC. RESERVES)	972
MAIN PROPELLANTS (INC. RESERVES)	61582
FLUID LOSSES	1694
(IGNITION WEIGHT)	(74140)
MASS FRACTION	.831

Figure 2.2.1-20 Weight Summary Space-Based, Ballute-Braked OTV—No. 8

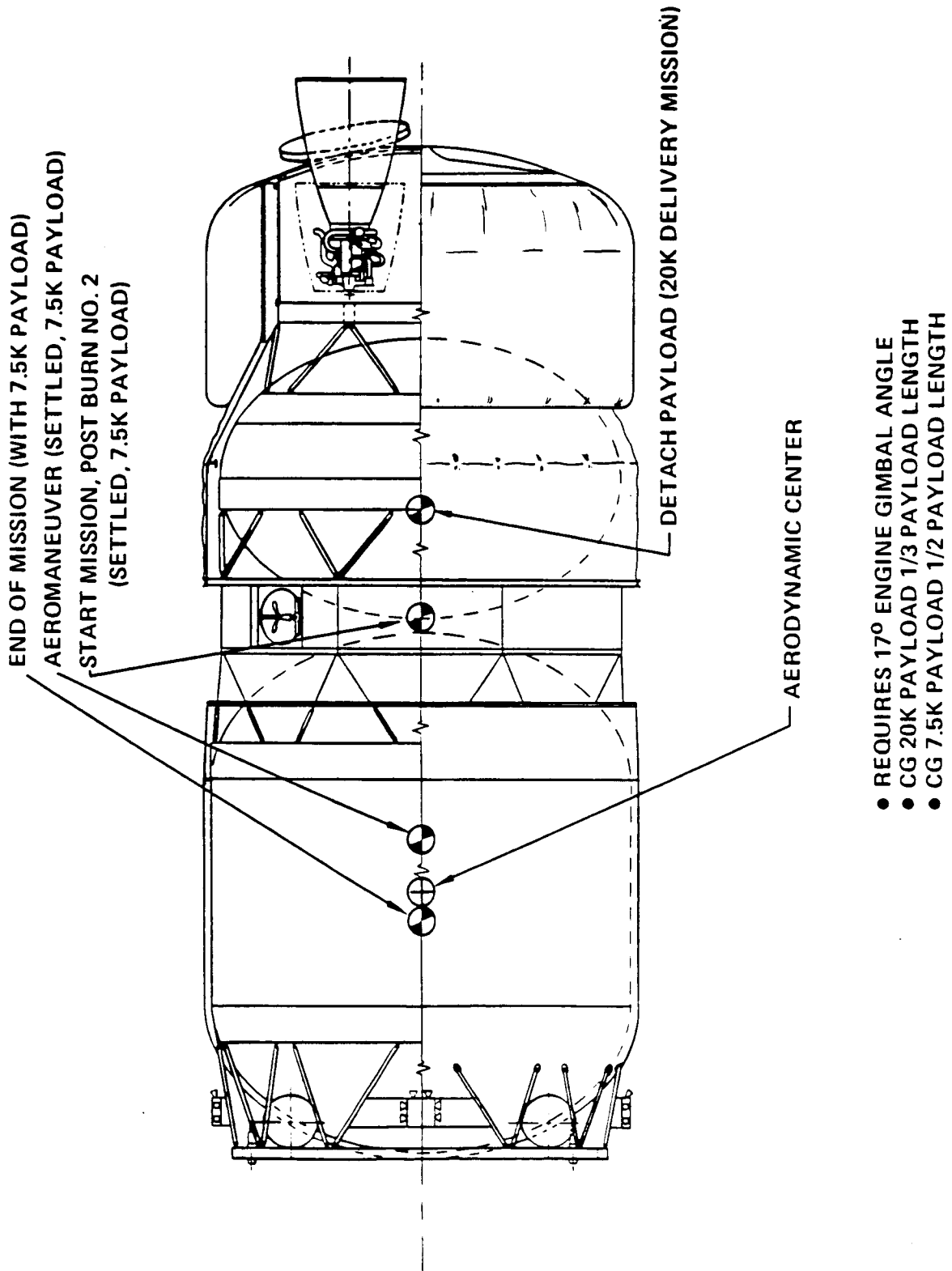


Figure 2.2.1-21 C. G. Locations Space-Based Ballute-Braked OTV

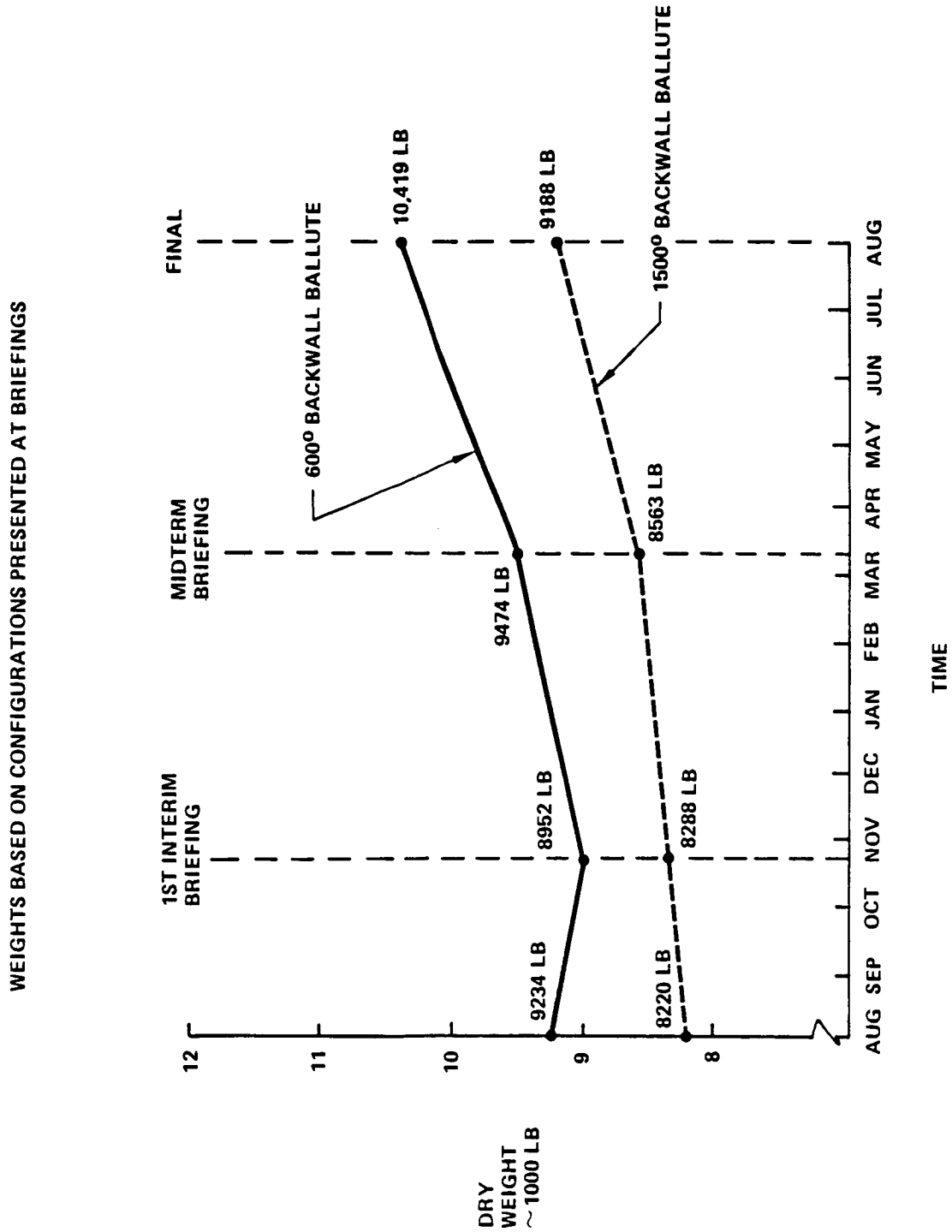


Figure 2.2.1-22 Dry Weight History Space-Based Ballute Braked OTV

Table 2.2.1-2. OTV Dry Weight History 15000 BW SB Ballute-Braked OTV

1ST CUT→1ST INTERIM BRIEF		1ST INTERIM BRIEF→MIDTERM		MIDTERM→3RD QUARTER	
CHANGE	WT Δ	CHANGE	WT Δ	CHANGE	WT Δ
MAIN TANK SIZE INCREASE	+41	UPDATE ELLIPT. TANK WEIGHTS	+80	INCREASE TANK SIZE	+72
IMPROVE STRUCT. DEF.	-325	UPDATE STRUCT. DEF.	+88	IMPROVE STRUCT. DEF.	-61
MOVE BALLUTE SYSTEM TO ENGINE END	+271	UPDATE BALLUTE SUPPORT STRUCT. DEF.	+171	INCLUDE JETTISONABLE BALLUTE SUPPORT STRUCT.	+193
UPDATE TPS	0	UPDATE TPS REQ'S	+32	UPDATE VEHICLE TPS REQ'T AND BALLUTE TPS ASS'Y	+97
IMPROVED GNC & TTC, + DMS DEFINITION	-41	SAME AVIONICS	0	UPDATE MAN-RATING, IMPROVE DMU WEIGHTS	-5
UPDATE FUEL CELL WEIGHTS, INCLUDE THERMAL CONTROL	+108	DECREASED EPS REACTANT REQ'T	-57	UPDATE EPS REACTANT REQ'T, + THERMAL CONTROL, MAN-RATE	+186
INCREASE RCS MANIFOLD LENGTH	+12	DECREASE RCS MANIFOLD LENGTH	-8	INCREASE RCS PROPR REQ'T, ADD EXT. PRESS., + MAN-RATE	+91
IMPROVE ENGINE WEIGHT,	-13	IMPROVE ENGINE WEIGHT,	-65	MISC. MPS PLUMBING CHANGE	+43
MISC.	+6	MISC.	-2	MISC.	-1
WEIGHT GROWTH ADJ.	+9	WEIGHT GROWTH ADJ.	+36	WEIGHT GROWTH ADJ.	+11
TOTAL (LBM)	+68	TOTAL (LBM)	+275	TOTAL (LBM)	+626

- CHANGES FROM BALLUTE DRAG MODULATED VEHICLE
- HEAT SHIELD STRUCTURE SHORTENED 17 INCHES TO EXPOSE END OF REGENERATIVELY COOLED SECTION OF NOZZLE
- DOORS OVER ENGINES REMOVED AND REPLACED BY THERMAL BLANKET WHICH PROTECTS ENGINE BODY AND INTERNAL CAVITY FROM PLUME RECIRCULATION
- BALLUTE REDUCED FROM 50 FT. TO 43 FT. DUE TO WEIGHT REDUCTION FROM ABOVE CHANGES
- BALLUTE MAINTAINED AT NOMINAL PROFILE AFTER INFLATION

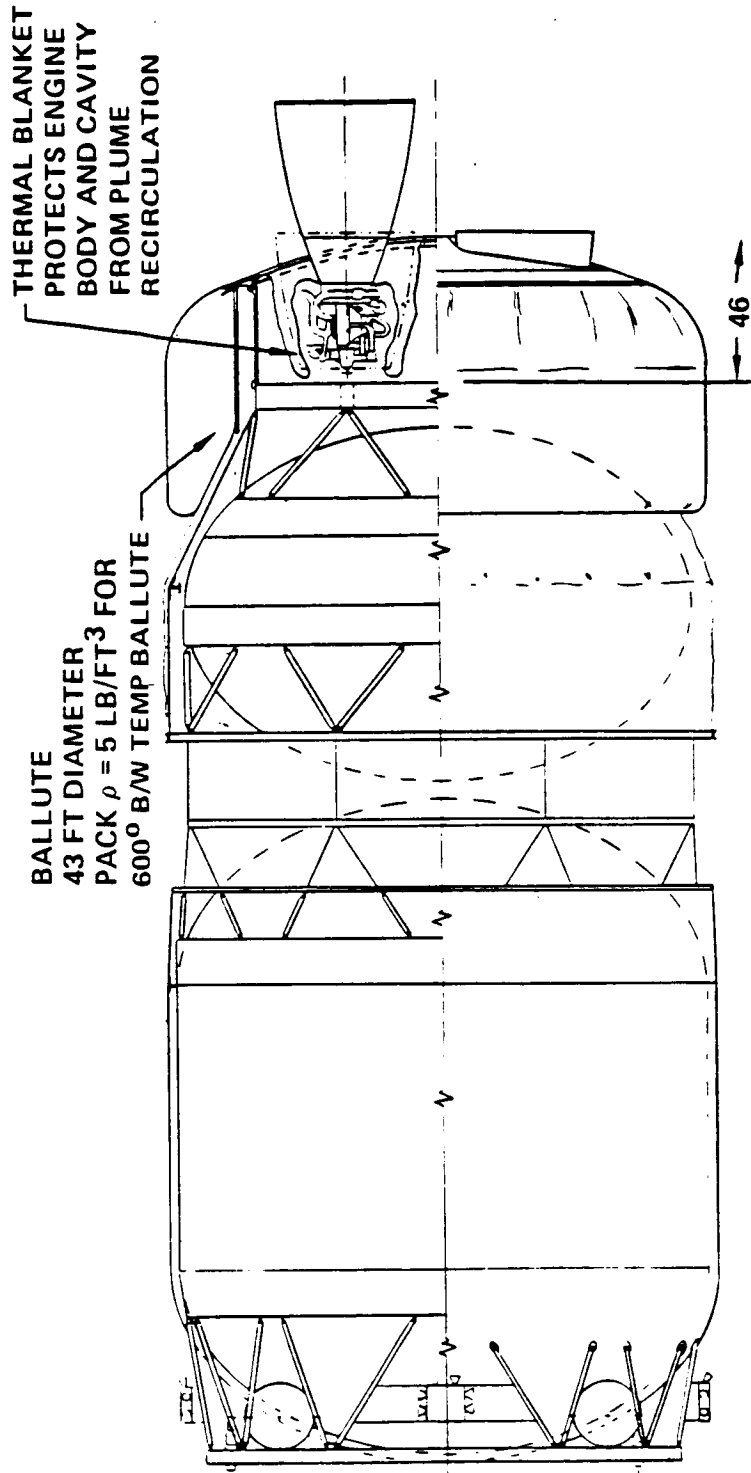


Figure 2.2.1-23 Space Based Ballute—Braked Engine Drag Modulated OTV—Single Stage

Table 2.2.1-3. Engine Drag-Modulation System Trade Weight Delta

- REFERENCE SYSTEM IS TDR = 1.5, 600° B/W TEMP BALLUTE
BALLUTE DIAMETER = 50 FT.
- ENGINE DRAG-MODULATED BALLUTE DIAMETER = 43 FT.

	REFERENCE SYSTEM	Δ LB. FOR EDM
AEROASSIST STRUCTURE	(1131)	(-200)
BALLUTE STRUCTURE--JETTISONABLE	392	- 95
SUPPORT STRUCTURE--JETTISONABLE	210	- 67
SUPPORT STRUCTURE--NON-JETTISONABLE	456	-111
INFLATION PROVISION--NON-JETTISONABLE	73	+ 73
THERMAL PROTECTION	(2054)	(-503)
BALLUTE--JETTISONABLE	1947	-444
RIGID--JETTISONABLE	16	- 16
FLEXIBLE--NON-JETTISONABLE	0	+ 48
RIGID--NON-JETTISONABLE	91	- 91
MAIN PROPELLANT FOR AEROMANEUVER	(0)	(+123)
BALLUTE PRESSURANT (N ₂)	(61)	(+104)
WEIGHT GROWTH (STRUCTURE, TPS ONLY)	(478)	(-105)
TOTAL	3724	-581

maneuver. Shortening the heat shield length changes the cg of the vehicle permitting a smaller ballute. The net weight savings results from this smaller ballute sizing.

2.2.2 Space Based Symmetrical Lifting Brake OTV

2.2.2.1 Initial Reference Configuration - Articulated Brake

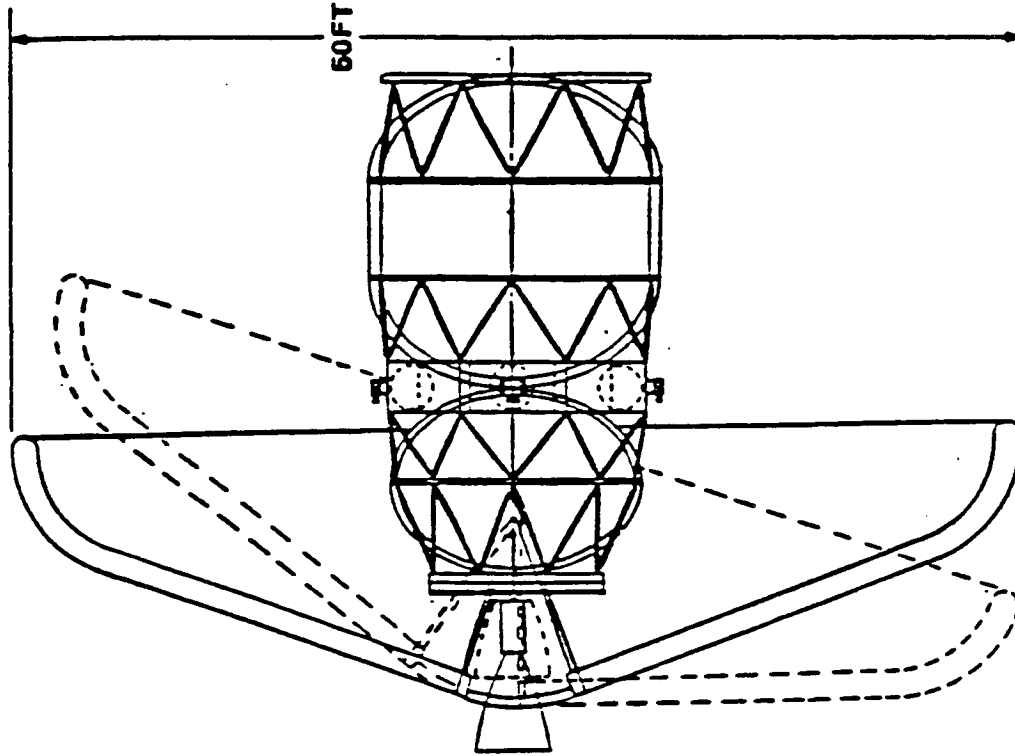
The lifting brake OTVs discussed in this section are transported to orbit in the Shuttle payload bay. Figure 2.2.2-1 shows our initial reference configuration. The lifting brake is articulated so the angle of attack and lift vector direction can be modified during the aeromaneuver to compensate for cg changes from flight to flight and to control the flight direction. Articulating the brake to one side shifts the vehicle cg off the brake centerline causing the vehicle to stabilize at an angle of attack. Flying the brake at an angle of attack produces lift. Controlling the lift vector direction allows the vehicle to be flown into or out of the atmosphere, that is, into denser air or less dense air. Flying through differing air densities controls the amount of velocity dissipated via the aeromaneuver.

The vehicle core consisting of the tankage, engines, and systems module was derived from the space based ballute braked vehicle. The core is an efficient design for carrying the predominately axial loads of the brake while minimizing the number of tanks and providing a symmetric interface for the articulated brake. Due to the fact that both together exceed the payload bay volumetric capability, the core and the brake are transported to orbit on different Shuttle flights and are integrated on orbit.

Figure 2.2.2-1 also shows a top level weight summary of the initial configuration.

2.2.2.2 Revised Reference Configuration

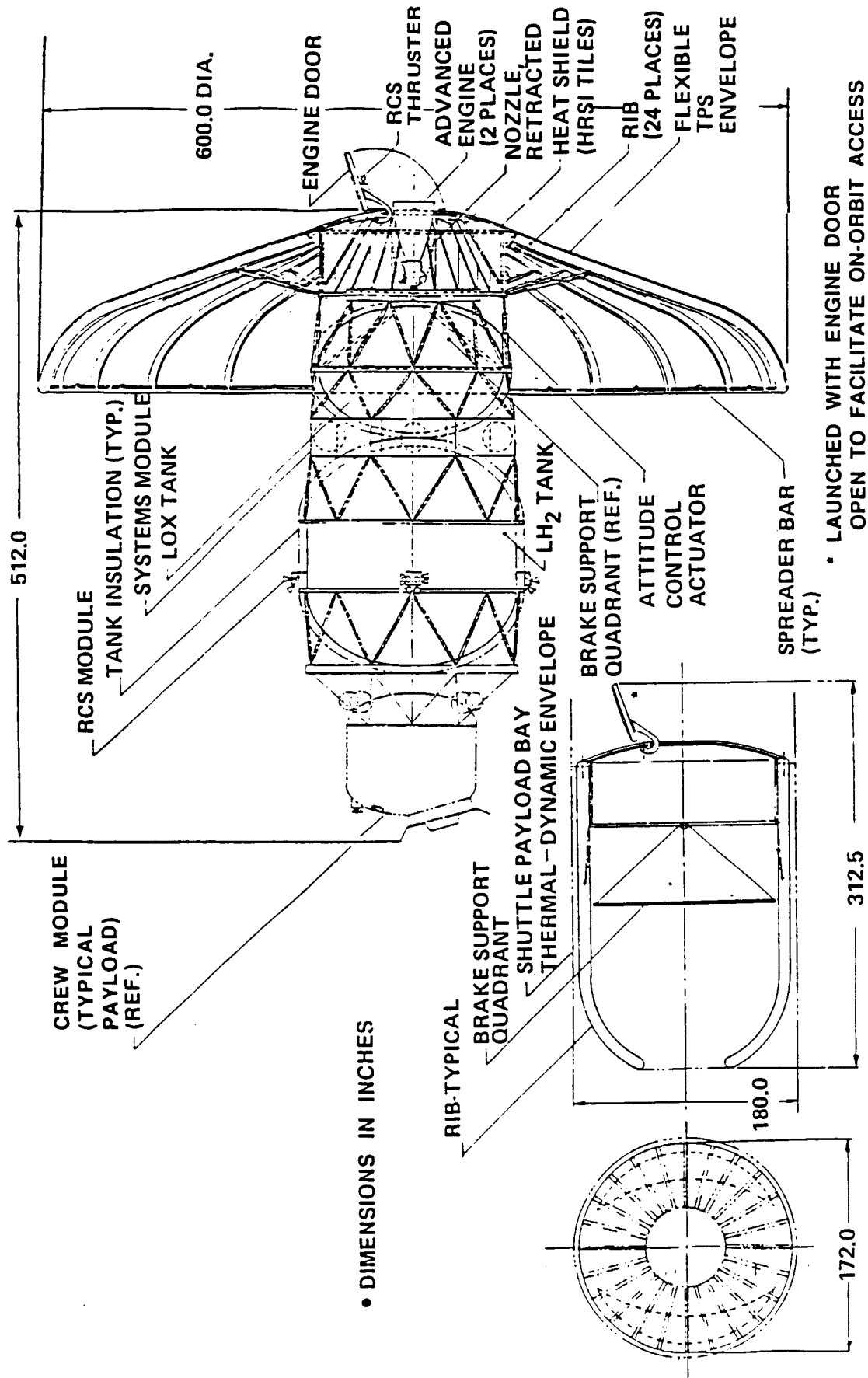
Further definition and a structural analysis (see section 3.0) of the articulated brake were performed resulting in the configuration shown in figure 2.2.2-2. The RCS thrusters were relocated forward to reduce impingement on the brake and associated loss of thrust. The brake is launched in a collapsed condition as shown. When expanded and mated with the core it is attached by bearings at the apex of the support quadrants and two actuators at 90 degrees to the supports. A deep cylindrical section with a heavy ring at the base collects the drag loads from the ribs and rib support struts and delivers it to the support quadrants and actuators. The relatively shallow angle and small rib attachment radius of the rib support struts results in a heavy brake framework as shown in table 2.2.2-1. When the TPS, support structures, and support mechanisms are added



STRUCTURE	2680
LIFTING BRAKE SYSTEM	3226
AVIONICS	609
ELECTRICAL POWER	659
MAIN PROPULSION	868
ATTITUDE CONTROL	185
SPACE MAINTENANCE	320
WEIGHT GROWTH	1284
(DRY WEIGHT)	(9841)
MPS RESIDUAL	565
ACS RESIDUAL	31
EPS RESIDUAL	23
(BURNOUT WEIGHT)	(10460)
MPS PROPELLANT	55,000
ACS PROPELLANT	545
EPS REACTANT	62
(GROSS WEIGHT)	(86279 LB)

Figure 2.2.2-1 SCB Lifting Brake OTV —
Initial Reference Configuration

OTV-1858



• DIMENSIONS IN INCHES

Figure 2.2.2-2 OTV Articulated Symmetric Lifting Brake Concept – Revised Reference Configuration

Table 2.2.2-1 Articulated Lifting Brake -- Weight Data

● BRAKE FRAMEWORK

RIBS (24)	850
RIB NON-OPTIMUM (5%)	42
RIB HARDWARE	72
CYLINDER STRUCTURE	627
CYLINDER NON-OPTIMUM (5%)	31
SUPPORT STRUT TUBES	115
SUPPORT STRUT TUBES NON-OPTIMUM (5%)	6
SUPPORT STRUT HARDWARE	72
TOTAL	1815 LBS
MIN. STRUCTURE FRACTION	0.88

to the framework the aeroassist device accounts for 25 percent of the total vehicle dry weight.

2.2.2.3 Trades and Analyses

Fixed Brake. Recognizing the dominant role of the brake weight in the vehicle sizing, we investigated an alternative fixed brake design. Figure 2.2.2-3 shows the fixed brake configuration. The vehicle core is angled relative to the brake to offset the cg causing the brake to fly at an angle of attack during the aeromaneuver. Pointing of the lift vector of the brake is accomplished by rolling the vehicle about its longitudinal axis. Since the brake does not gimbal, the rib struts can be attached directly to the vehicle core. Attaching the struts to the aft edge of the systems module and moving the rib interface outboard increases the efficiency of the strut system and reduces the bending loads in the ribs. Table 2.2.2-2 shows the reduced weight of this brake system.

Wake Heating. Thermal analysis of both of these configurations indicates severe wake heating problems as discussed in section 5.0. The entire return payload and a portion of the hydrogen tanks are subject to wake impingement. The severity of the wake heating resulted in the adoption of a design ground rule of no return payload wake heating. This ground rule combined with a nominal 22 degree wake heating boundary eliminated the two tank in-line configurations from further consideration and caused us to investigate multi-tank concepts.

Four Tank Concept. This concept was derived from our ACC configurations and is shown in figure 2.2.2-4. The LO2 tanks, LH2 tanks, brake and avionics ring/core structure are transported individually in the Shuttle bay and are assembled together on orbit. This configuration incurs weight, risk and cost penalties due to the amount of required on orbit assembly. Weight penalties include interface points to ASE for transport, EVA or RMS handling fixtures, and EVA mate/demate structural and electrical joints. The complexity of EVA, Quality Assurance, and the limited resources available if an error occurs increases the cost risk of a vehicle which is extensively assembled on orbit. Cost increases include astronaut training, EVA directly incurred costs, and increased checkout and leak detection required since major components of the MPS have to be assembled. A four tank configuration incurs a weight penalty relative to a three or two tank arrangement due to increased surface area which needs to be insulated and protected from meteoroids and debris. This configuration also incurs

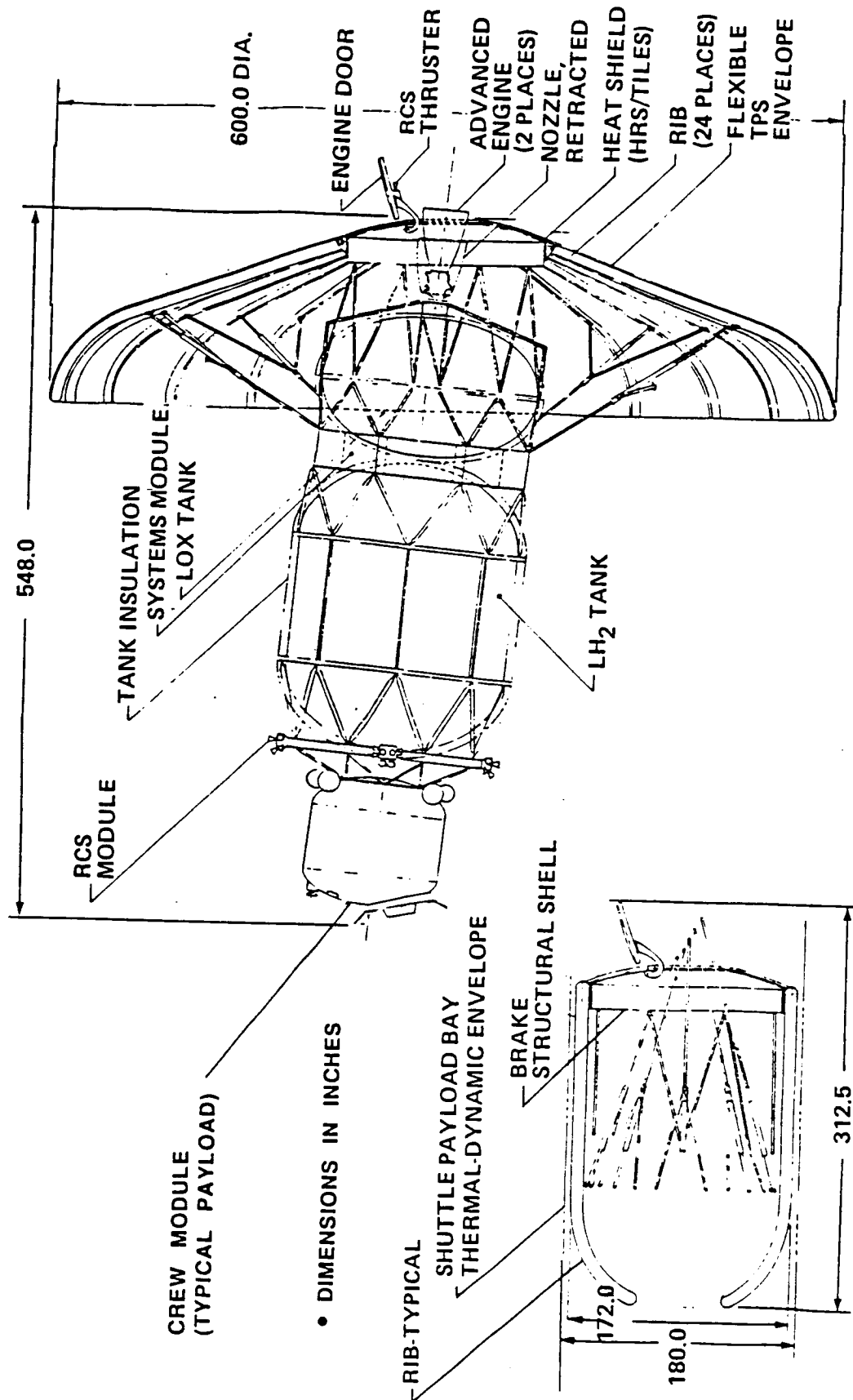
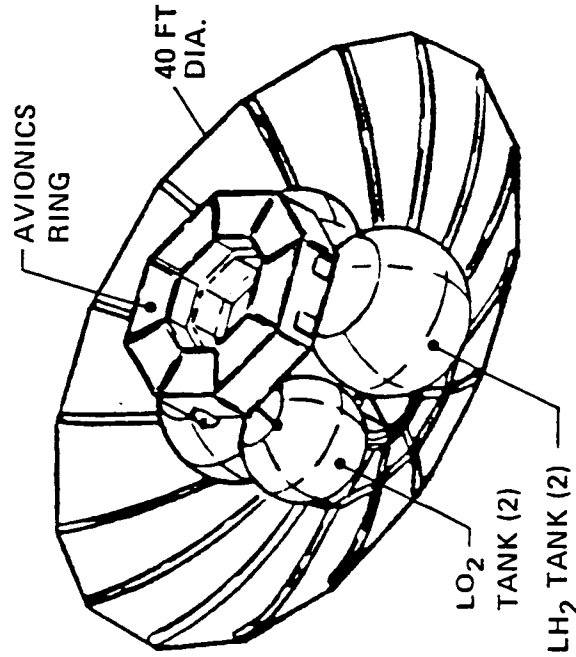


Figure 2.2.2-3 OTV Fixed Symmetric Lifting Brake Concept — Alternate Reference Configuration

Table 2.2.2-2. Fixed Lifting Brake Weight Data

● BRAKE FRAMEWORK	
RIBS (24)	576
RIB NON-OPTIMUM (5%)	29
RIB HARDWARE	72
CYLINDER STRUCTURE	399
CYLINDER NON-OPTIMUM (5%)	20
SUPPORT STRUT TUBES	134
SUPPORT STRUT TUBES	7
SUPPORT STRUT HARDWARE	96
TOTAL	<u>1333 LBS</u>



- MAJOR ORBITAL ASSEMBLIES 6-7
(O₂ TANKS; ENGINES; BRAKE;
TPS; AVIONICS)
- W/C_DA 11.0
- NUMBER FLUID/ELECTRICAL CONNECTIONS 4
- STRUCTURE CENTRAL BODY TRUSS
STRUCTURE WITH SPHERICAL
PROP. TANKS
- BRAKE STRUCTURE WEIGHT 1976 LBM
- USABLE PROP. LOAD 60,000 LBM
- STAGE DRY WEIGHT 9285 LBM

Figure 2.2.2-4 SB OTV Lifting Brake Concept, 4 Tank Configuration

the burden of having to be extensively disassembled for return to earth if a problem occurs which is not space repairable.

Three Tank Concept. Figure 2.2.2-5 shows tank configuration options which were explored for the lifting brake OTV. The tanks have been located transverse to the roll axis of the brake so the return payloads will not be subjected to wake impingement heating. Likewise, the brake is sized in diameter to prevent wake impingement heating on the tanks or the engines.

Besides wake heating, the aeromaneuver's L/D requirement drives the location and arrangement of the tanks. L/D results from flying the brake at an angle of attack which, in turn, is obtained by cg offset. As discussed in section 6.0, an aeroguidance trade study was performed for 10, 20, and 30 degree angles of attack to determine which resulted in the least weight system. The trade favored 10 degrees. A low angle of attack is also favorable from a configuration standpoint because of the conflicting requirements of cg offset verses no wake impingement heating. As the tanks are moved forward to increase the cg offset and, thereby, increase angle of attack, the angle between the brake and the wake impingement boundary line increases (22 degrees + angle of attack) forcing the tanks back. As a result, a 10 degree angle of attack was selected as a design requirement.

Five major elements whose cg position control the angle of attack are the; 1) lifting brake, 2) tankset, 3) engines, 4) propellant, and 5) return payload. The lifting brake, tankset, engines, and residual propellant cg positions combine to form an inert weight cg position which varies very little from flight to flight. For any OTV configuration to trim at a desired angle of attack, the tankset and engine positions must be juggled relative to the brake to locate the inert weight cg along the angle of attack trim line. On the other hand, the reserve propellant and return payload are masses that have large variations from flight to flight and have a large influence on the system cg. As a result, the reserve propellant and payload cg positions must individually be located on the angle of attack trim line so the system cg position will track the trim line despite their variations. Unfortunately, it is impossible to eliminate all sources of cg error or variation; however, their influence on the vehicle's angle of attack reduces as the cg moves closer to the nose of the brake. For example, 8 feet behind the brake the angle of attack changes 0.95 degrees per inch of cg error, whereas at 20 feet, 1.85 degrees/inch will occur. Therefore, a configuration which positions the vehicle and payload cgs close to the brake is desirable.

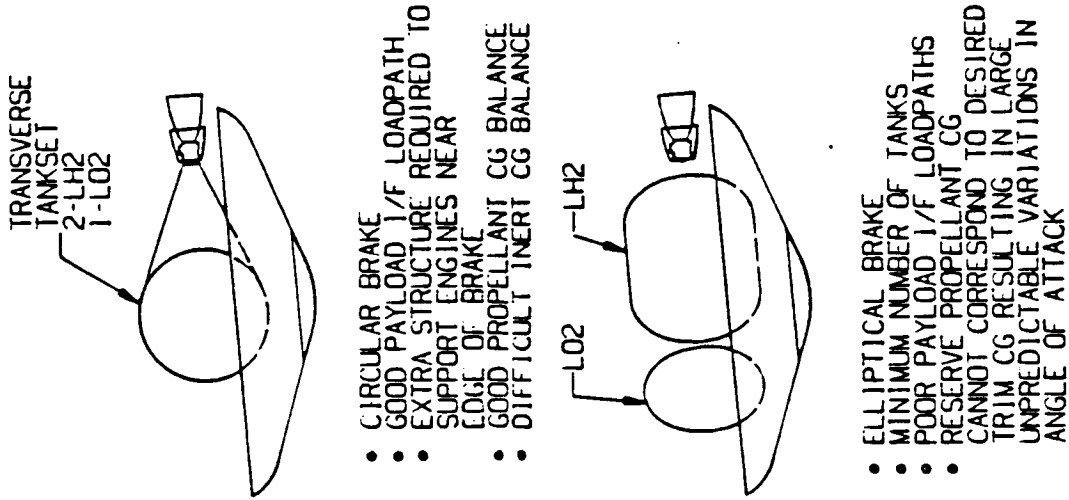
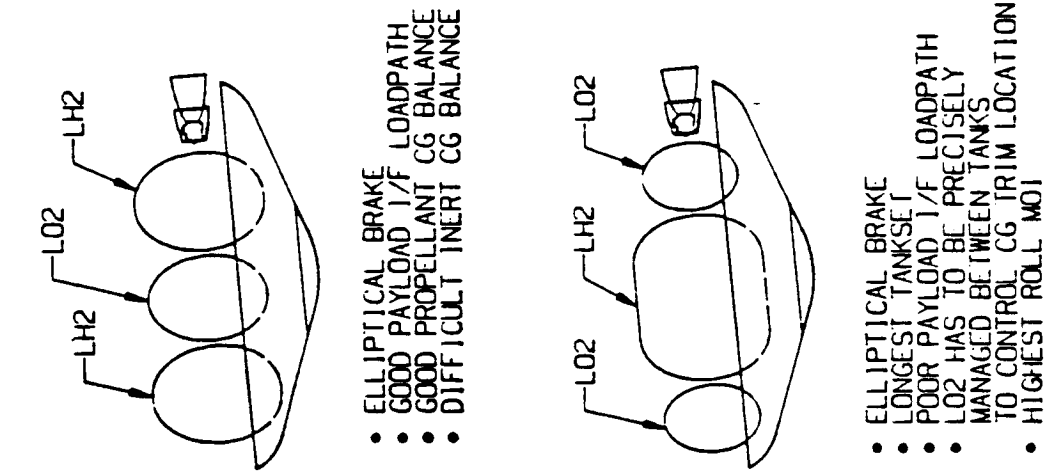
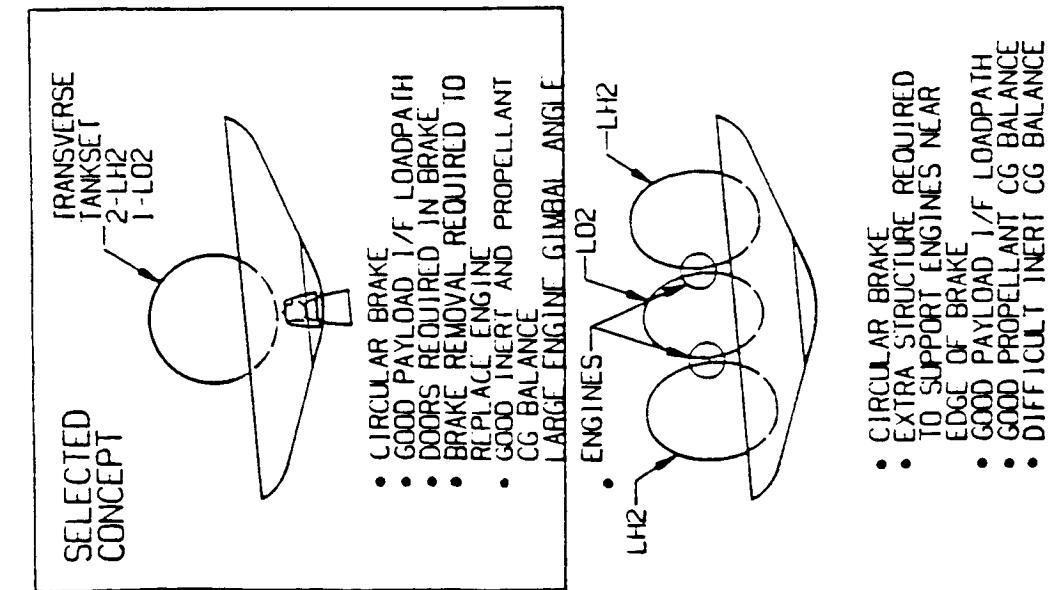


Figure 2.2.2-5 Tankage and Engine Arrangement Options Lifting Brake OTV

Based upon the aforementioned configuration guidelines, the multi-tank configurations shown in figure 2.2.2-5 can be evaluated and a reference configuration selected.

2.2.2.4 Selected Baseline Configuration

Figures 2.2.2-6 and 2.2.2-7 show our baseline space based lifting brake OTV employing 3 tanks. Relative to the four tank configuration, on orbit assembly costs and risks have been mitigated by making the tanks, propellant manifolds, avionics, EPS, RCS, engine interfaces, and payload interface one integral unit which is brought to orbit in the Orbiter PLB. Table 2.2.2-3 shows the key configuration features of the OTV concept.

Major Elements. Figure 2.2.2-8 shows the major elements which are individually transported in the Shuttle bay and are assembled on orbit. The TPS for the brake is transported separate from the collapsed brake structure to avoid damaging the fabric and allow for the installation of ASE on the brake structure.

When a main engine or the brake TPS has to be replaced on orbit the brake must be removed to provide the EVA astronaut access to the engine or TPS interface. A simple four point interface is maintained between the tankset and the brake to facilitate brake removal/reinstallation.

Brake Structural Configuration. The brake's basic form is a blunted 70 degree half angle cone as shown in figure 2.2.2-7 (see figure 2.2.2-11 for views and sections). An 87 inch radius hardshell dome covered with RSI forms the center of the brake. Doors are located in the dome for engine nozzle deployment. Ribs attach to a ring on the dome and support the fabric TPS covering. The ribs fold up for transport in the Orbiter bay. A triangular strut system transfers the brake loads to the tankset. One set of struts connects the dome to the tankset and another connects the ribs to the tankset. The rib struts minimize the bending loads in the ribs therefore allowing the ribs to be relatively light sections.

Besides the strut system which transfers the brake loads to the tankset, a strut system exists which transfers loads between the ribs as shown in figure 2.2.2-9. These struts laterally stabilize the ribs, prevent "racking" of the ribs during roll maneuvers, and transfer the rib strut kick loads between ribs.

Brake TPS. Figure 2.2.2-10 shows the flexible TPS assembly for the lifting brake. The TPS is designed to be installed with the brake structure assembled. The inner edge

- 43 FT. DIA. BRAKE
- MAN-RATED SUBSYSTEMS

LBS

4175

1161

1703

135

469

760

323

1221

(9947)

717

(10664)

34

1072

66490

1694

(79954)

.832

STRUCTURES

PROPULSION SYSTEMS

THERMAL CONTROL

GUIDANCE, NAVIGATION & CONTROL

COMMUNICATIONS/DATA HANDLING

ELECTRICAL POWER

SPACE MAINTENANCE

WEIGHT GROWTH

(DRY WEIGHT)

RESIDUALS

(INERT WEIGHT)

REACTANTS-EPS (INC. RESERVES)

PROPELLANTS-RCS (INC. RESERVES)

MAIN PROPELLANTS (INC. RESERVES)

FLUID LOSSES

(IGNITION WEIGHT)

MASS FRACTION

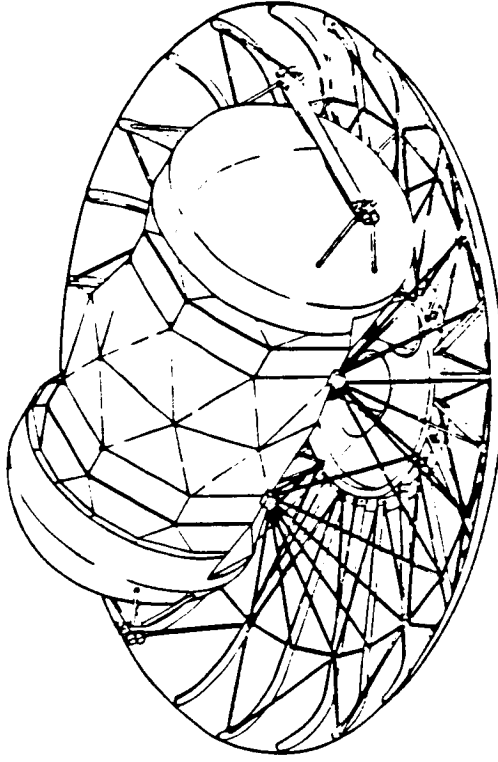


Figure 2.2.2-6 Weight Summary (lb) Space-Based Symmetric Lifting Brake OTV-No. 11

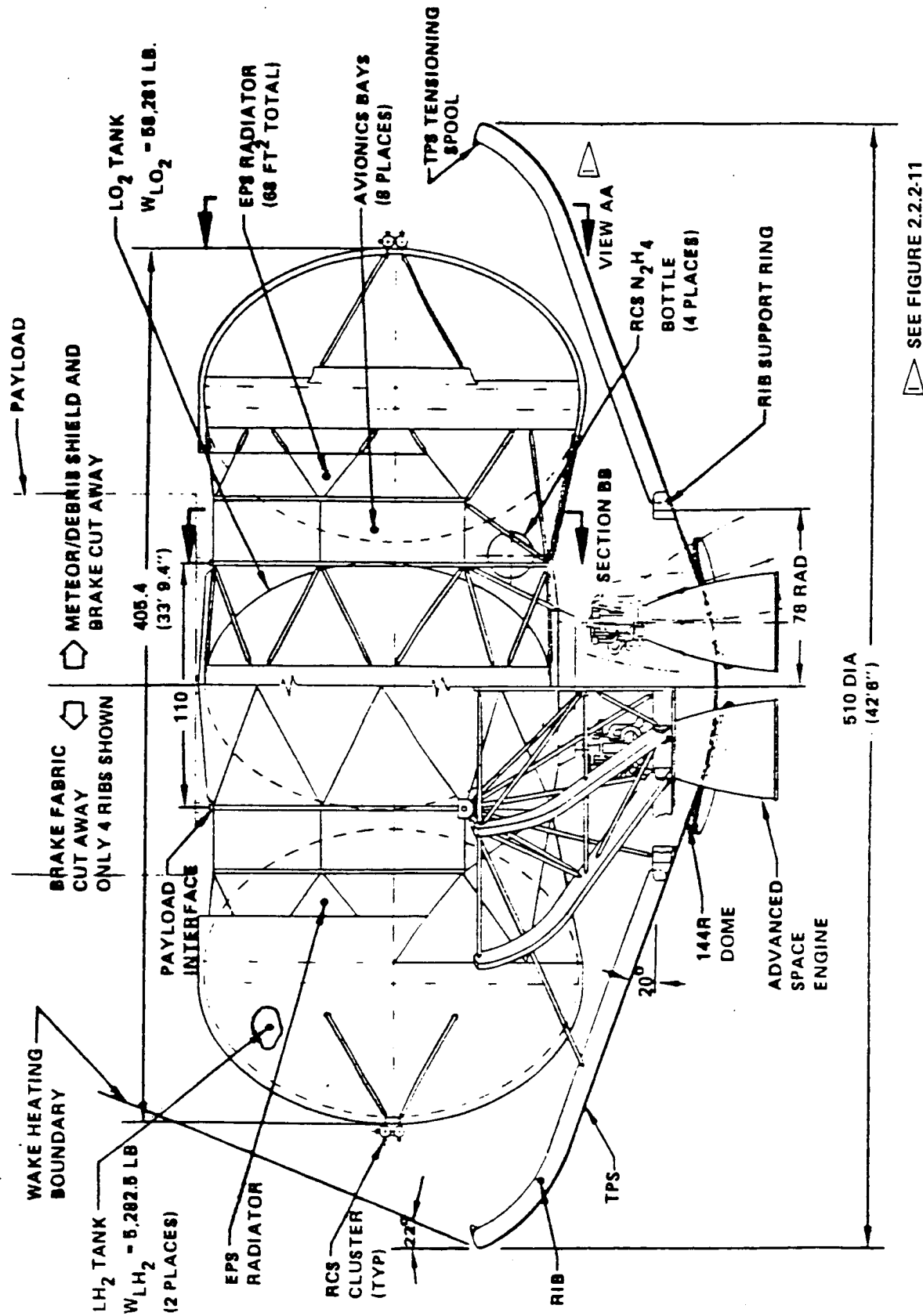


Figure 2.2.2-7. Final Configuration Space Based Lifting Brake OTV

Table 2.2.2-3 Configuration Features Space-Based Lifting Brake OTV

<u>FEATURE</u>	<u>RATIONALE</u>
<ul style="list-style-type: none"> ● PROPELLANT TANKS, LINES, ENGINE INTERFACES, AVIONICS, EPS, RCS AND PAYLOAD INTERFACE ARE INTEGRAL UNIT 	<ul style="list-style-type: none"> ● ELIMINATE COST AND RISK OF ON-ORBIT ASSEMBLY ● INTEGRAL UNIT LESS WEIGHT THAN IF ORBIT ASSEMBLED
<ul style="list-style-type: none"> ● 1 LO₂ TANK AND 2 LH₂ TANKS 	<ul style="list-style-type: none"> ● LOWEST NUMBER OF TANKS THAT PROVIDES BALANCED C.G. TRIM ● LOWER MOI AND SHORTER THAN 2 LO₂ AND LH₂ TANKS ● CANTILEVERING LIGHT LH₂ TANKS DOES NOT IMPOSE WEIGHT PENALTY
<ul style="list-style-type: none"> ● ENGINES AND PAYLOAD IN-LINE 	<ul style="list-style-type: none"> ● PAYLOAD LENGTH UNRESTRICTED BY ENGINE GIMBAL ANGLE
<ul style="list-style-type: none"> ● ENGINES AND BRAKE SHARE SAME PRIMARY STRUCTURE 	<ul style="list-style-type: none"> ● NO DUPLICATION OF STRUCTURE—CLEAN DESIGN
<ul style="list-style-type: none"> ● AVIONICS, MAIN ENGINES, FRSI, AND RCS THRUSTERS ARE ORUs 	<ul style="list-style-type: none"> ● EVA REPLACEMENT POSSIBLE AND COSTS LESS THAN EARTH RETURN
<ul style="list-style-type: none"> ● FRSI REMOVED/REPLACED WITHOUT FOLDING UP BRAKE RIB STRUCTURE 	<ul style="list-style-type: none"> ● SAVES COST AND REDUCES RISK OF REPLACEMENT ● FRSI REPLACED AFTER 5 FLIGHTS
<ul style="list-style-type: none"> ● 4 POINT BRAKE INTERFACE TO TANKSET 	<ul style="list-style-type: none"> ● ALLOWS EASY REMOVAL OF BRAKE FOR ENGINE ACCESS
<ul style="list-style-type: none"> ● RADIATORS SIZED ASSUMING OTV PERFORMS THERMAL ROLL 	<ul style="list-style-type: none"> ● RESULTS IN SMALLER RADIATOR AREA AND LESS WEIGHT ● PAYLOADS USUALLY REQUIRE ROLL FOR THERMAL CONTROL
<ul style="list-style-type: none"> ● EPS RADIATOR AND AVIONICS BAYS INTEGRATED WITH METEOROID/DEBRIS SHIELD 	<ul style="list-style-type: none"> ● ELIMINATED STRUCTURAL BOX AROUND AVIONICS ● LESS SHIELD AREA THAN CONFORMAL DOME DESIGN ● SHIELD SUPPORTED BY TANK SUPPORT STRUTS
<ul style="list-style-type: none"> ● NON-DEPLOYABLE METEOROID/DEBRIS SHIELD WITH 3" STANDOFF DISTANCE 	<ul style="list-style-type: none"> ● YIELDS MINIMUM GAGE SHIELD—LARGER SPACING DOES NOT REDUCE WEIGHT

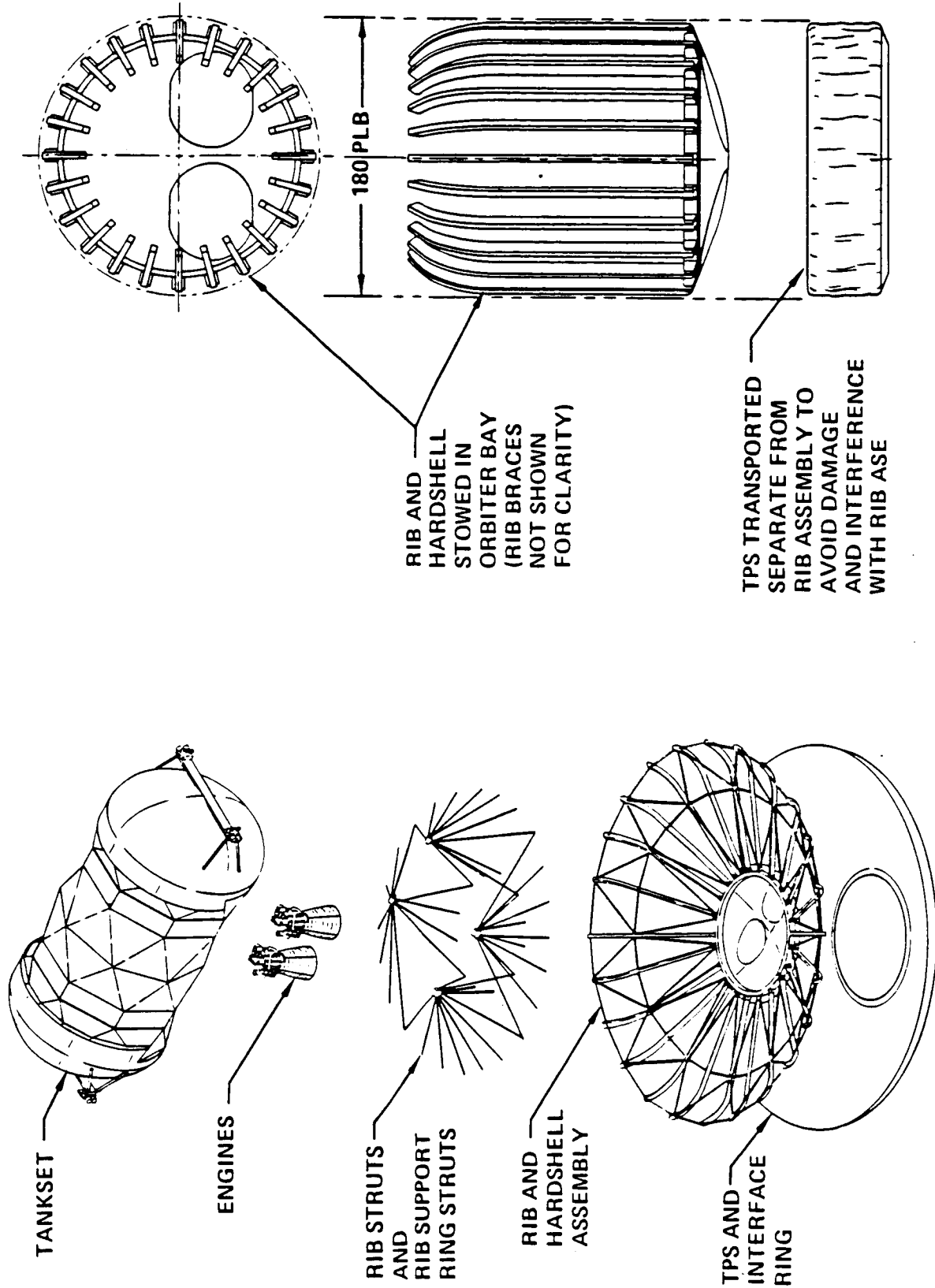


Figure 2.2.2.8 Lifting Brake Elements and Transport

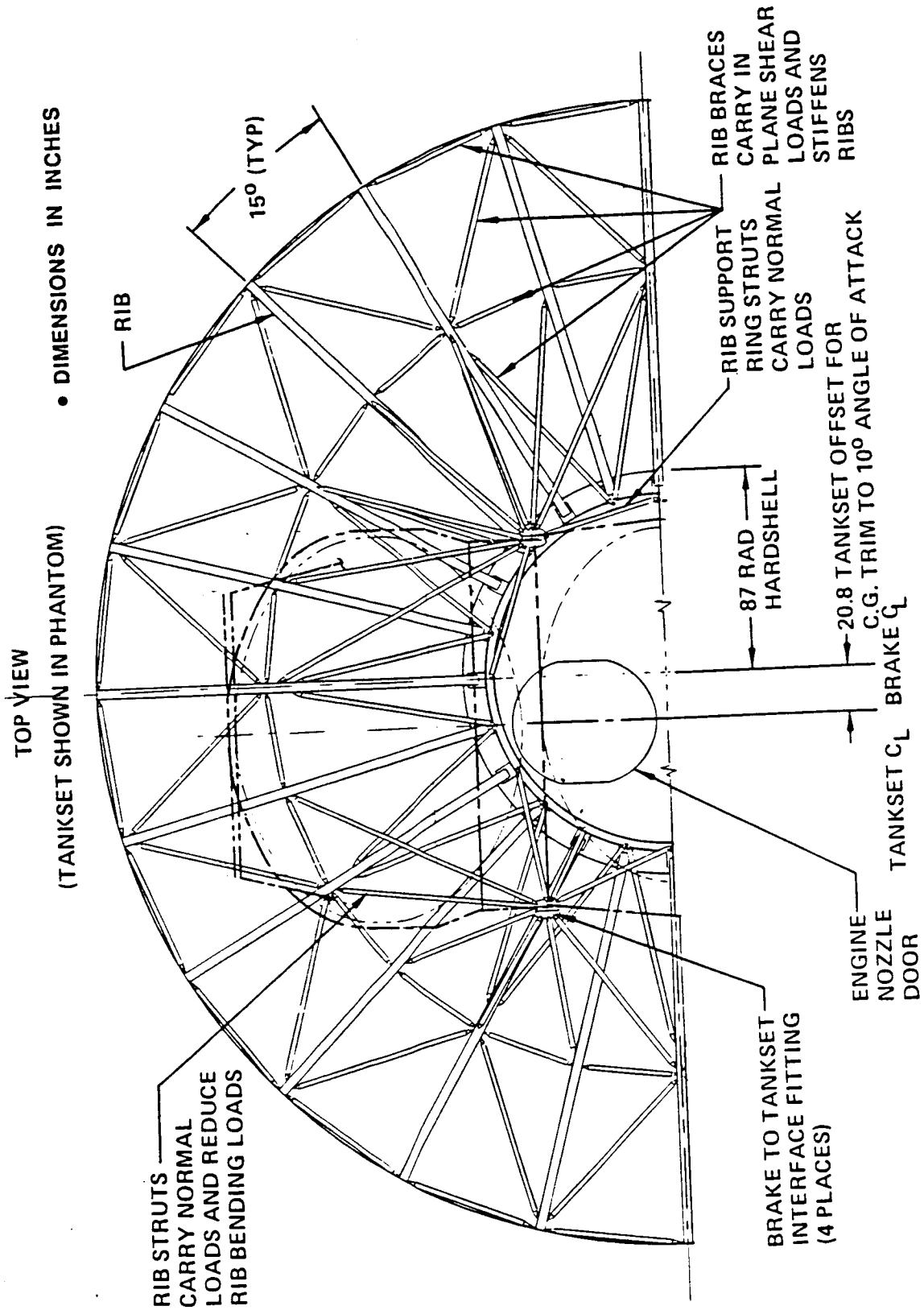


Figure 2.2.2-9 Lifting Brake

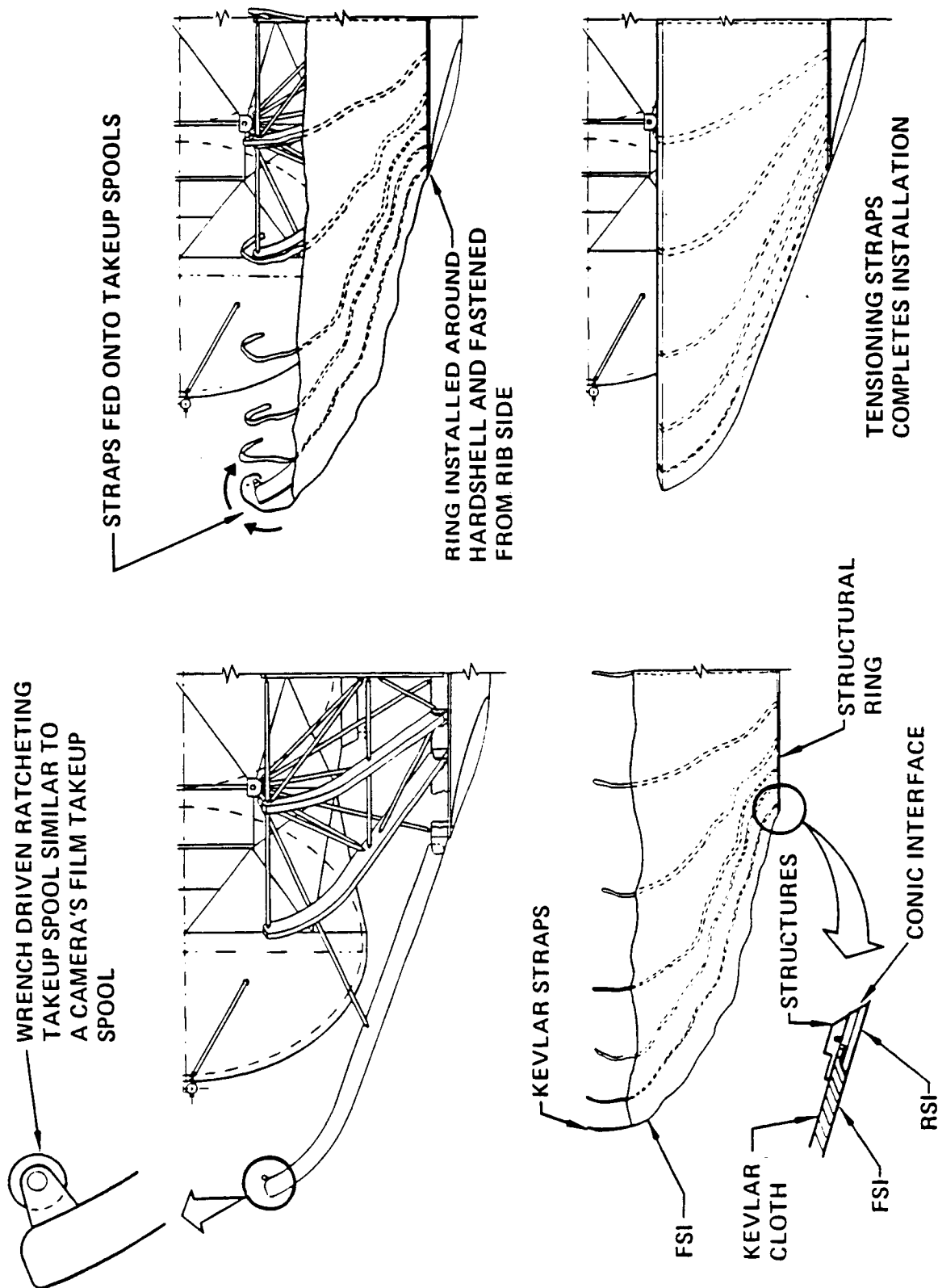


Figure 2.2.2-10 Lifting Brake TPS Installation

of the fabric is secured by a structural ring which is part of the TPS assembly. This ring fits concentrically to the dome of the brake and dome fasteners are used to secure it. This avoids having fasteners penetrate the RSI on the ring. Radial straps are sewn to the Kevlar base cloth corresponding to the rib locations. They are wound onto spools to tension the blanket.

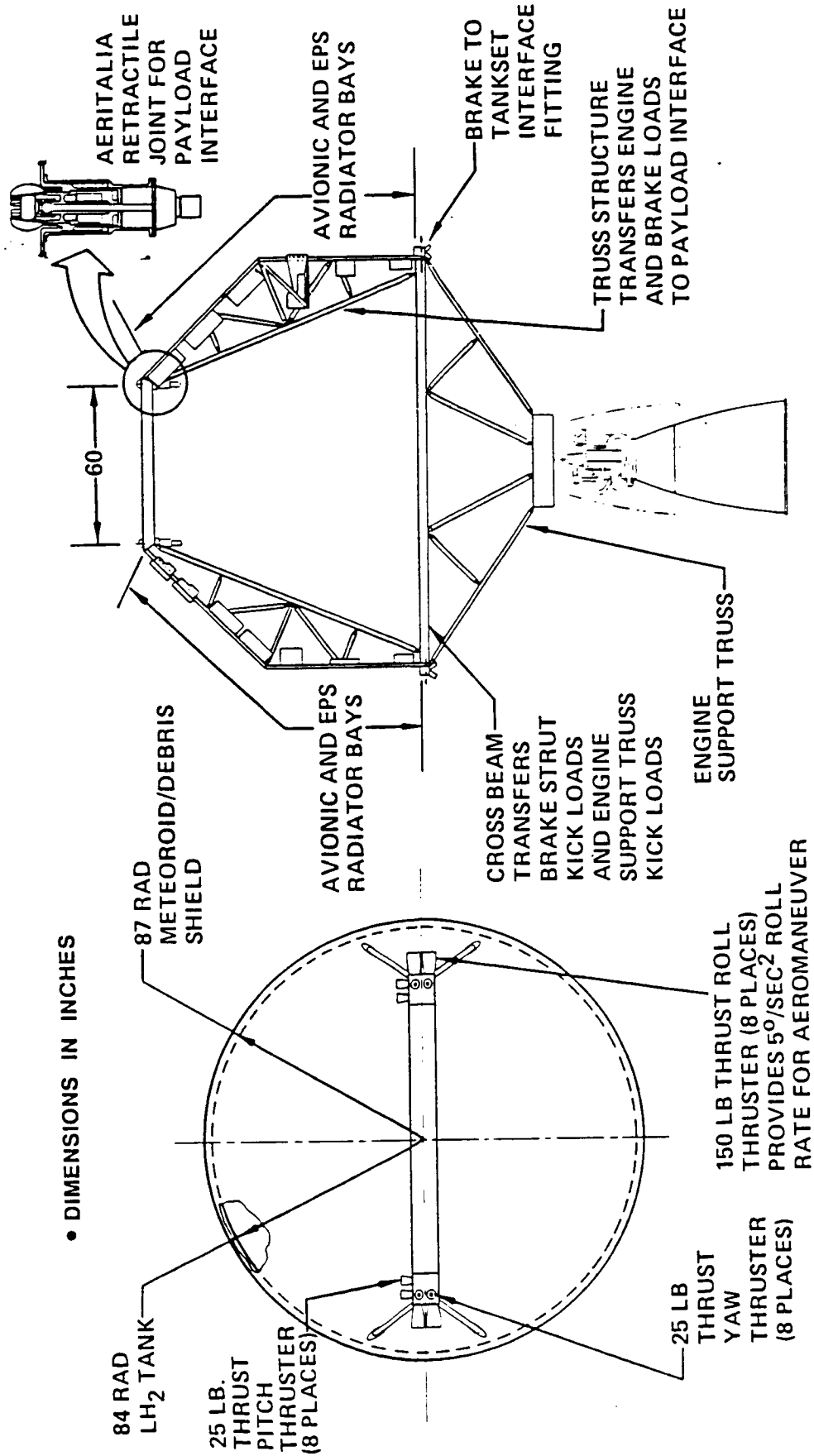
Tankset. The tankset consists of the tanks, propellant manifolds, avionics, EPS, RCS, and engine, brake and payload interfaces. As shown in figure 2.2.2-9, the tankset is offset from the center of the brake so the vehicle will trim to a 10 degree angle of attack during the aeromaneuver.

A bi-pod strut system interconnects the LO2 tank with the two LH2 tanks. There are eight avionic bays located between the LO2 and LH2 tanks similar to the space based ballute configuration discussed earlier. The bays and EPS radiator are identical in configuration as the ballute vehicle's design (reference figure 2.2.1-19); however, they have been located to minimize their view factor to the payload while maintaining a high view factor to space. Meteoroid/debris protection again parallels the ballute design with a 3 inch stand off shield conformal to the body lines integrated with the EPS radiators and equipment bays.

A four point interface connects the tankset to the lifting brake. Section BB of figure 2.2.2-11 shows the primary structure which transfers the engine and brake loads to the payload interface, the tank support strut connection points, and the avionic bays. This integrated engine and brake primary structure design provides a very efficient structural design despite the cantilevered design of the LH2 tanks. Placing the tanks perpendicular to the engine and brake load directions does not impose a weight penalty on the vehicle because of the high moment of inertia due to the large diameter of the vehicle and the light structural loads.

View AA in figure 2.2.2-11 taken from the side view of the lifting brake shows the RCS thruster clusters on the ends of the tankset. 150 lb roll thrusters are required to achieve a roll rate of 5 degrees per second squared. This roll rate is required to change the lift direction during the aeromaneuver so the guidance system can fly out atmospheric dispersion errors. The roll thrusters can also provide pitch authority except when the cg lies in their thrust plane. Forward pointing pitch thruster were added for this contingency although they present a potential payload contamination and heating problem; however, a payload has to be very large in diameter for this to occur. The forward pointing pitch thrusters are generally more efficient for pitch and yaw control

• DIMENSIONS IN INCHES



SECTIONS RELATE TO FIGURE 2.2.2-7

Figure 2.2.2-11 Lifting Brake View and Section

than the roll and yaw thrusters and could be used extensively on missions whose payloads are insensitive to their effects.

Brake Sizing. Figure 2.2.2-12 shows how the brake diameter is constrained. The heating line is developed from TPS temperature limits discussed in section 5. The other two lines show trending lines for a horizontal tankset with a circular brake. Ellipsoidal domes are used on the tanks to minimize the brake diameter. As the reentry weight increases due to increased propellant loads the tankset length increases requiring a larger brake to protect the tanks. Our configuration is sized by the manned sortie mission reentry weight and the heating limit curve.

Weights. A weight summary for the final lifting brake OTV configured for a manned sortie mission was shown in figure 2.2.2-6. All subsystems are man-rated. The summary contains the same elements as the ballute braked OTV discussed previously. In this case the lifting brake primary and secondary support structure as well as the flexible membrane are included in structures weights. Insulation on the face of the brake is included in thermal control and protection.

Center of Gravity. Figure 2.2.2-13 shows the cg movement for the 20k delivery missions and 7.5k roundtrip manned missions. The cg position for the final circularization burn after the aeromaneuver sets the engine gimbal angle requirement of 34 degrees. This angle provides 4 degrees of control authority if an engine were to fail. The high gimbal angle results from the low cg position designed to reduce the vehicle's angle of attack sensitivity to cg position errors. Accommodating this large gimbal angle is not possible with the current brake dome design due to diameter limitations.

Weight Trending. For the above chronological history of lifting brake configurations, figure 2.2.2-14 shows how the weights changed as the configurations changed. Table 2.2.2-4 presents a breakdown of the weight changes.

2.2.2.5 Revised Baseline Configuration

Further assessment of the symmetric lifting brake OTV was done in conjunction with refinement activity for the GB ACC OTV lifting brake. This analysis focused an update of the brake rib structure, and the brake thermal protection system. The weight improvement in these subsystems led to a performance improvement for the vehicle overall.

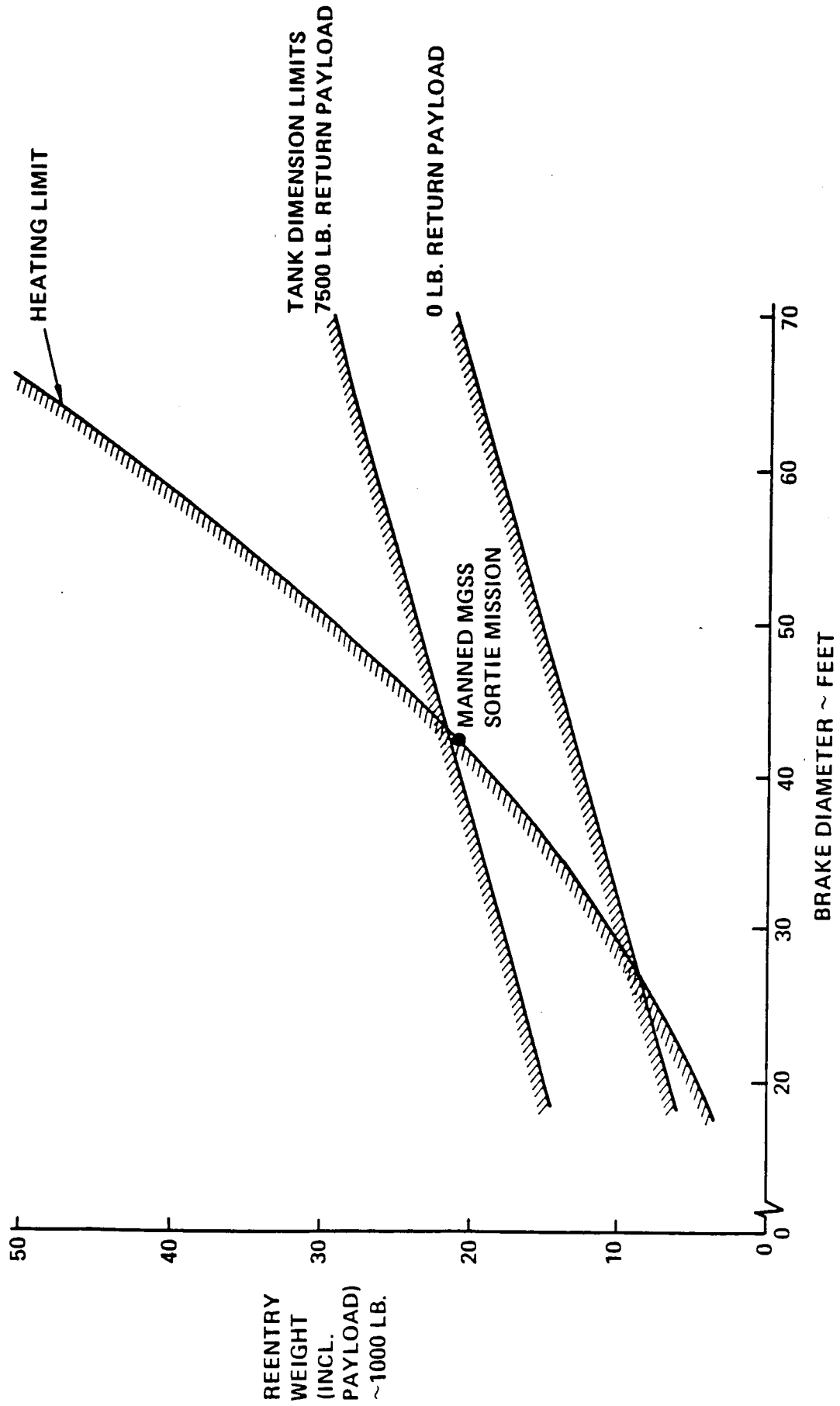


Figure 2.2.2-12 Brake Diameter Sizing Space-Based Symmetric Lifting Brake OTV

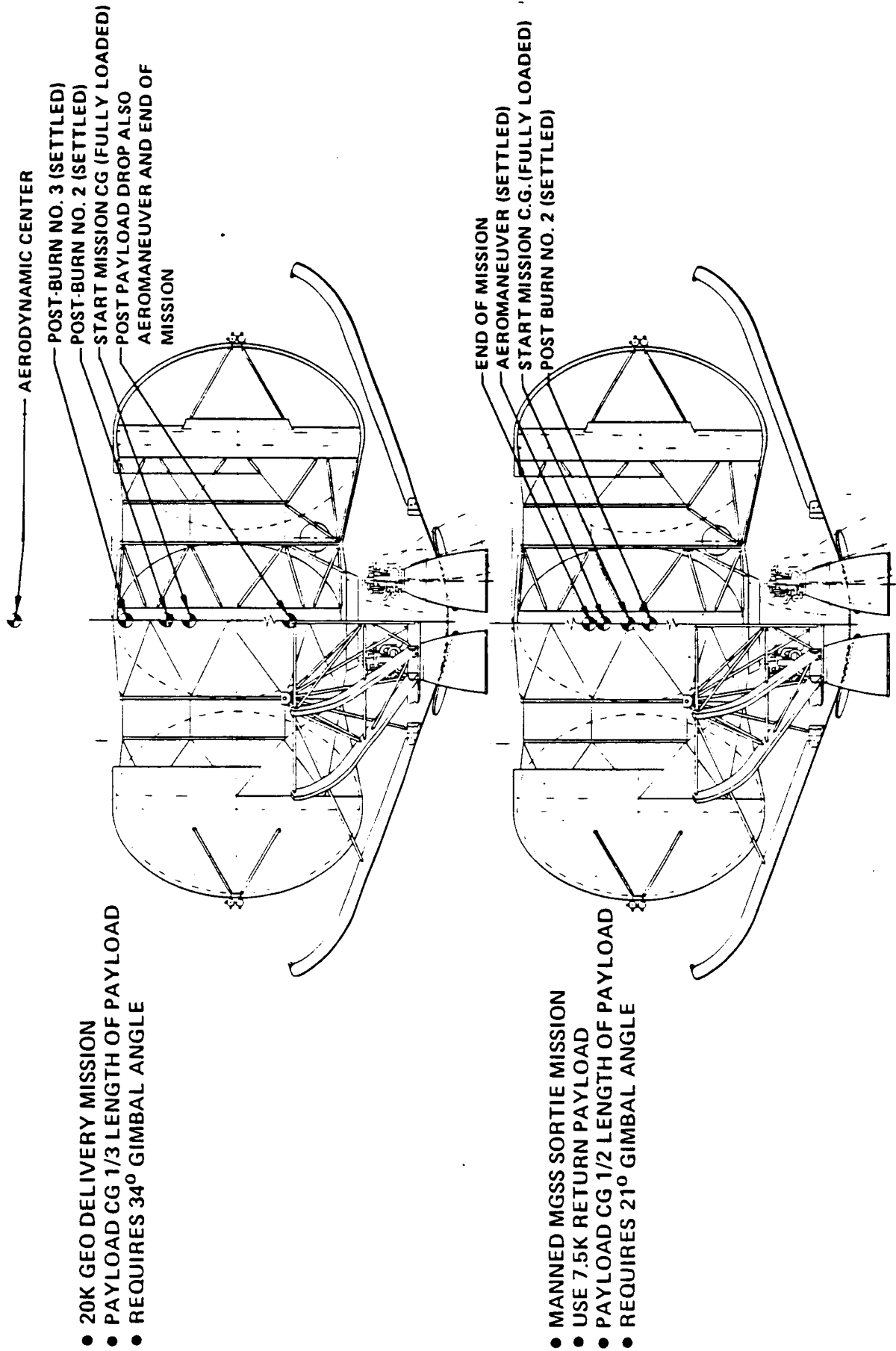


Figure 2.2.2-13 CG Locations Lifting Brake OTV

• WEIGHTS BASED ON CONFIGURATIONS PRESENTED AT BRIEFINGS

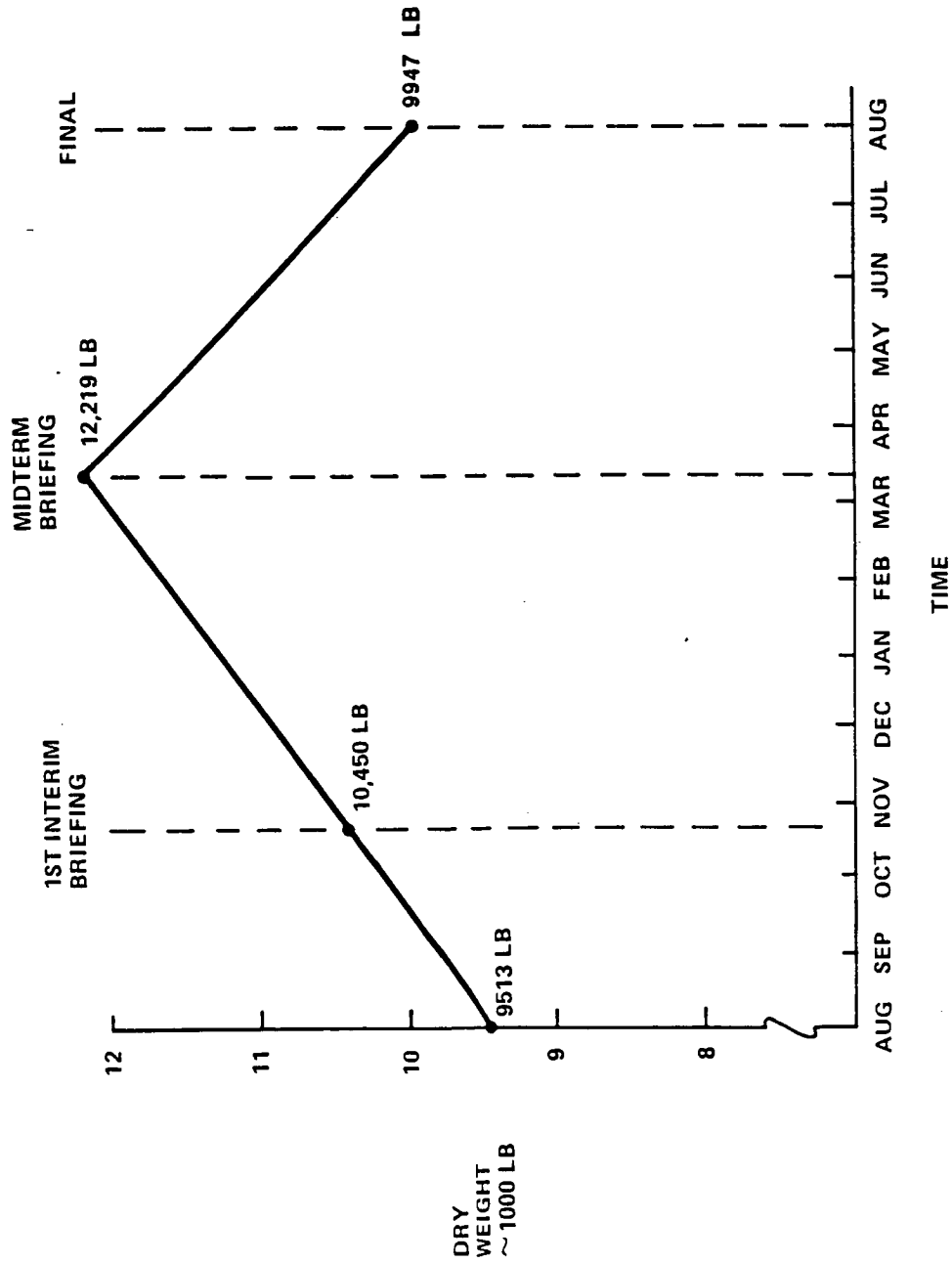


Figure 2.2.2-14 Dry Weight History Space-Based Symmetric Lifting Brake OTV

Table 2.2.2.4. OTV Dry Weight History SB Symmetric Lifting Brake OTV

1ST CUT → 1ST INTERIM BRIEF		1ST INTERIM BRIEF → MIDTERM		MIDTERM → 3RD QUARTER	
CHANGE	WT Δ	CHANGE	WT Δ	CHANGE	WT Δ
INCREASE MAIN TANK SIZE	+41	INCREASE MAIN TANK SIZE	+294	USE TWO LH ₂ TANKS	+34
UPDATE STRUCT., THERMAL CONTROL DEF.	+101	INCREASE VEHICLE SIZE + STRUCT.	+225	IMPROVE STRUCT. DEF.	-397
UPDATE BRAKE STRUCT. DEF. FOR ARTICULATION	+1114	UPDATE BRAKE STRUCT. DEF.	+915	FIX BRAKE W/CG OFFSET,	-1531
IMPROVED TPS DEF.	-457	UPDATE TPS REQ'T	+135	INCREASE TPS THICKNESS, BUT DECREASE AREA	-415
IMPROVED GNC, TTC, + DMS DEF.	-41		0	UPDATE AVIONICS MAN-RATING, IMPROVE DMU	-5
UPDATE FUEL CELL, INCLUDE THERMAL CONTROL	+108	DECREASED EPS REACTANT REQ'T	-30	UPDATE EPS REACT. REQ'T +UPDATE MAN-RATING	+209
INCREASED RCS MANIFOLD LENGTH	+12	INCREASED RCS MANIFOLD LENGTH	+15	UPDATE THRUSTERS, + PROP. REQ'T	+115
IMPROVE ENGINE WT;	-69	IMPROVE ENGINE WEIGHT, MISC. PLUMBING CHANGE	-50	UPDATE PLUMBING FOR MULTI-TANK	+128
MISC	+6	MISC	+34	MISC	-37
WEIGHT GROWTH ADJ	+122	WEIGHT GROWTH ADJ	+231	WEIGHT GROWTH ADJ	-373
TOTAL (LBM)	+937	TOTAL (LBM)	+1769	TOTAL (LBM)	-2272

The twenty-four deployable ribs in the symmetric brake can be tailored to the moment distribution along the rib in order to minimize weight. With this type of tailoring, as shown in figure 2.2.2-15, a weight savings of about 160 lb can be achieved. Also, the inter-rib support can be tension-only straps instead of tension/compression struts, as was designed originally. Use of straps instead of struts saves 260 lb.

In the area of TPS, the fabric assembly weight was updated, using an integrally woven assembly that includes both support fabric of NEXTEL and surface fabric of NICALON, rather than the original concept of an all-NICALON assembly supported by a KEVLAR cloth. This change resulted in a weight savings of 90 lb. Updated TPS insulation thickness resulted in a weight savings of 240 lb.

Overall, these updates resulted in weight savings of 860 lb., including weight growth of 110 lb. In terms of performance, this reduced the propellant requirement for performing the 20K lb delivery mission to GEO from 69,681 lb to 65,180 lb of LO2/LH2. The results of this analysis are shown in figure 2.2.2-16.

2.2.3 Space Based Shaped Brake OTV

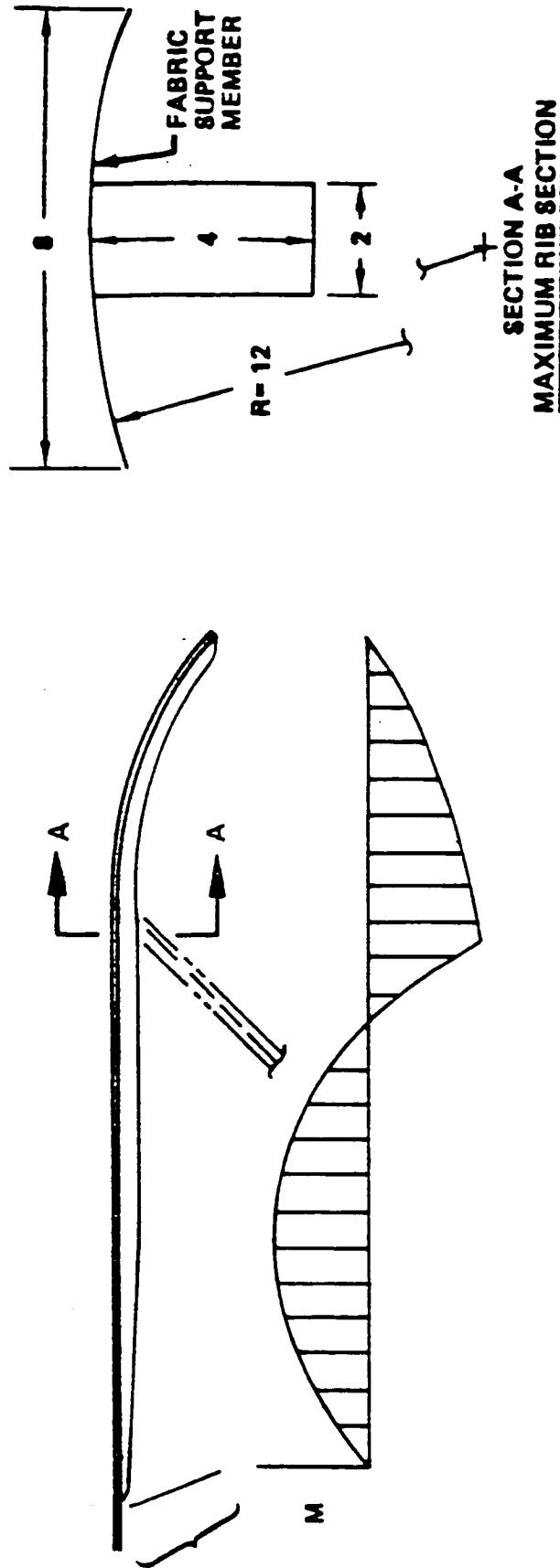
2.2.3.1 Initial Reference Configuration

The shaped brake OTVs discussed in this section are transported to orbit in the Shuttle payload bay. Figure 2.2.3-1 shows our initial reference configuration. The brake's shape, tankage and engine arrangement were based upon the Johnson Space Center configuration in NASA TM 58264.

The shaped brake is a blunted raked elliptical cone hardshell thermally protected by RSI. The brake diameter is affected by the same controlling factors as the symmetric lifting brake OTV, that is, protecting the tanks, engines and return payload from wake impingement heating and the TPS material heating limit. For the shaped brake, wake impingement tends to be the controlling constraint. The base of the cone (in the rake plane) is circular to allow packaging of the tanks and engines.

Once on orbit three LH2 tanks, one LO2 tank, the engines, and the avionics systems module are integrated to the brake via a structural truss system. The avionics systems module is identical to that used in the initial space based ballute braked OTV. Use of four tanks permits efficient packaging into a circular brake and good inert weight cg trim for the aeromaneuver. Each integrated element provides its own thermal protection system and meteoroid/debris shielding.

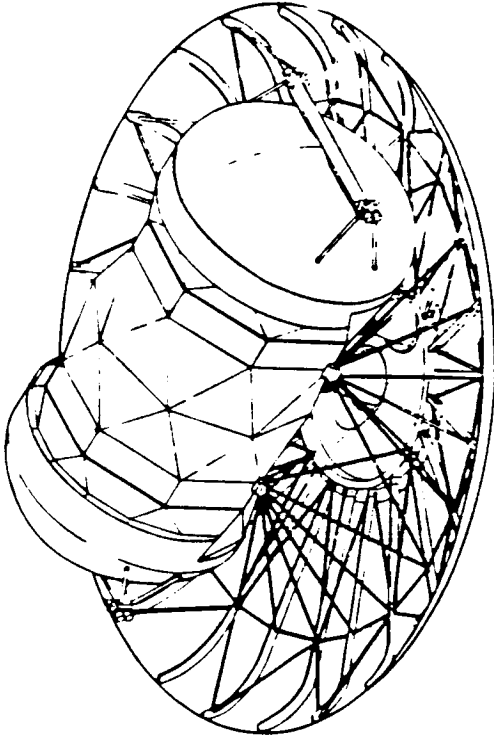
The structural design concept for this configuration is described in section 3.0. Basically, the inertia loads of the tanks and equipment are transferred via the strut



- CURVED CAP REDUCES CROSS-FLOW HEATING & PREVENTS INSULATION BURN-THROUGH
- RIBS TAILORED TO MOMENT DISTRIBUTION TO SAVE WEIGHT
- SUPPORT STRUT LOCATED TO MINIMIZE BENDING & RIB END DEFLECTIONS
- LIGHT WEIGHT GRAPHITE POLYIMIDE CONSTRUCTION
 - FILLED WITH 3.0 PCF H.C. CORE FOR STABILITY
 - $F_c = 55,000$ PSI

38

Figure 2.2.2-15 Symmetric Lifting Brake Structure



- CORE VEHICLE
- AEROASSIST DEVICE
 - STRUCTURE
 - TPS
 - WEIGHT GROWTH (DRY WEIGHT)
- TOTAL MAIN PROPELLANTS
- OTHER FLUIDS
- PAYLOAD
- START-BURN WEIGHT

WEIGHT SUMMARY (LBM)

<u>REF. CONFIG.</u>	<u>UPDATE</u>
6,671	6,587
3,276	2,495
● 1452	● 958
● 1397	● 1212
● 427	● 325
<u>(9947)</u>	<u>(9082)</u>
69,681	65,180
1,161	1,108
20,000	20,000
<u>(100,789)</u>	<u>(95,370)</u>

Figure 2.2.2-16 SB Symmetric Lifting Brake Weight and Performance Update

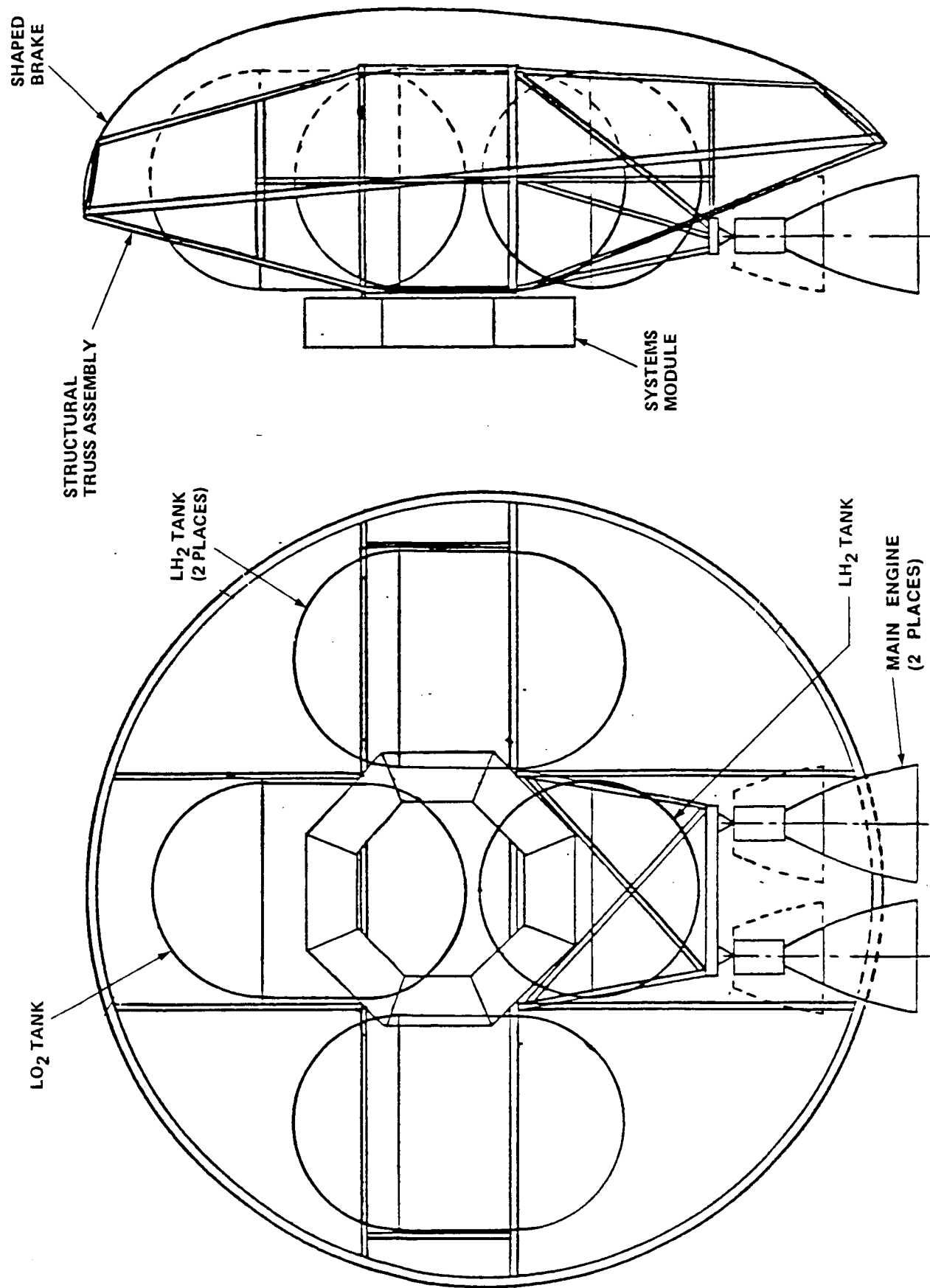


Figure 2.2.3-1 Space-Based Shaped Brake OTV—
Initial Reference Configuration

system to the brake periphery during the aeromaneuver. This causes the brake's hardshell to go into compression similar to squeezing an egg shell. Utilizing the doubly curved surface of the brake for overall stability allows the brake to be designed as a monocoque structure.

Control of the shaped brake during the aeromaneuver is the same as the fixed lifting brake OTV discussed above. Rolling the vehicle changes the lift vector direction allowing flight into or out of the atmosphere. The brake is flown at a 17 degree angle of attack relative to the base of the brake yielding an L/D of 0.275.

2.2.3.2 Revised Reference Configuration

Two successive design and analysis iterations were performed to establish a new reference configuration shown in figure 2.2.3-2. The primary changes for the first iteration include changing the structural design and updating the brake's RSI weights based on a thermal analysis.

Local brake hardshell stability, deflection and load distribution concerns resulted in the abandonment of the 'egg shell' structural design concept for a cruciform keel beam/bulkhead system. The cruciform concept uses keel beams and bulkheads to stabilize the shell structure and distribute loads to the tanks and equipment. The keel beams and bulkheads are deep webbed structures sized for deflection rather than strength. Deflections are limited by strain compatibility between the shell and the RSI tiles.

The primary changes for the second iteration include decreasing the tank sizing, improving the structural definition, and changing to advanced engines. Using advanced engines reduces the weight of the engines as well as the tank size due to improved performance. Section 4.0 presents the engine trades in depth. Further structural analysis resulted in an improved structural definition with a reduction in weight. This weight decrease also caused the tank size to decrease.

Figure 2.2.3-3 shows the major elements of the updated reference configuration and figure 2.2.3-4 shows a top level weight summary.

2.2.3.3 Trades and Analyses

The following trades and analyses were performed against the revised reference configuration.

Angle of Attack. As discussed in section 6.0, an aeroguidance trade study was performed for 10, 20, and 30 degree angles of attack to determine which resulted in the

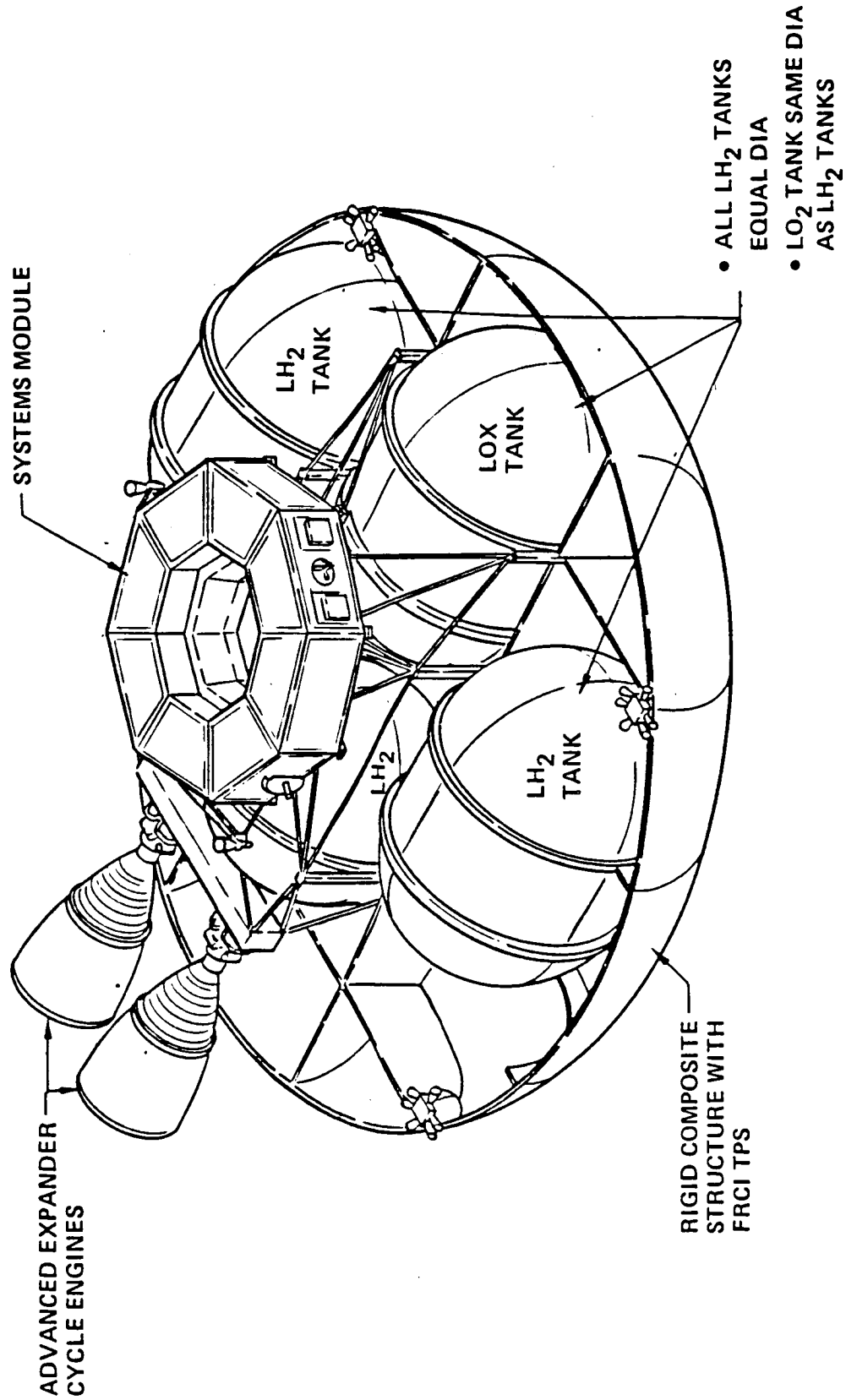


Figure 2.2.3.2 OTV Shaped Brake Concept —
Revised Reference Configuration

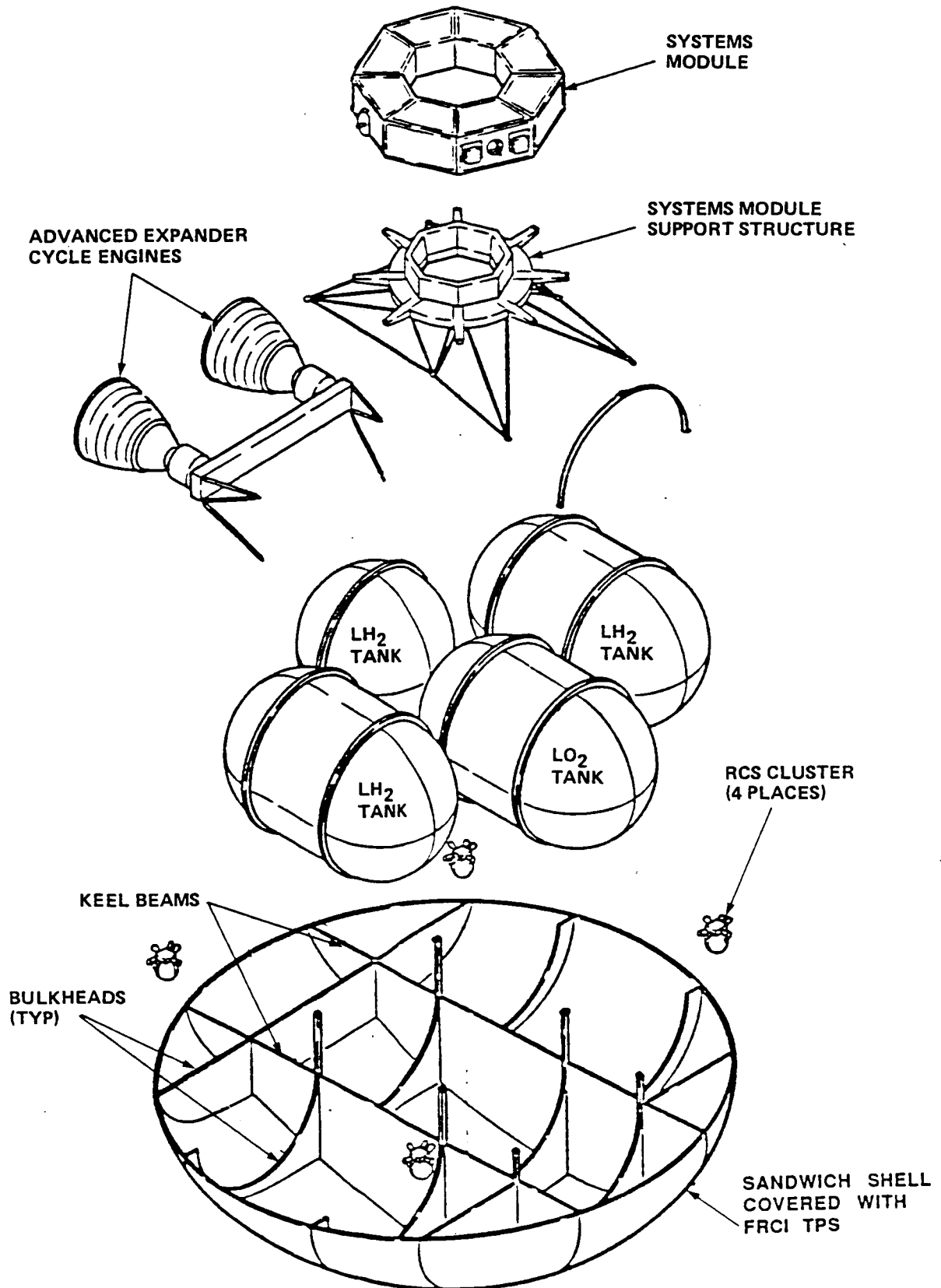
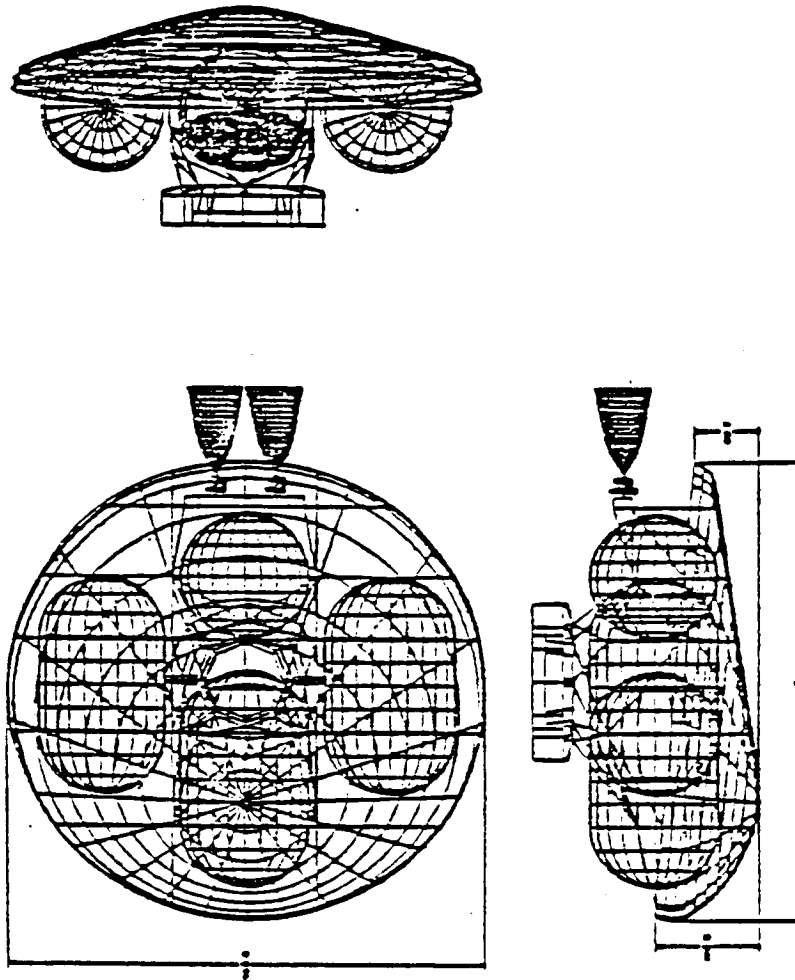


Figure 2.2.3-3 Shaped Brake OTV Major Elements



STRUCTURE	7,406*
THERMAL CONTROL	1,621
AVIONICS	609
ELECTRICAL POWER	665
MAIN PROPULSION	1,206
ATTITUDE CONTROL	205
SPACE MAINTENANCE	320
WEIGHT GROWTH	1,805
(DRY WEIGHT)	13,837
MPS RESIDUAL	824
ACS RESIDUAL	100
EPS RESIDUAL	94
(BURNOUT WEIGHT)	14,855
INFLIGHT LOSSES	415
MPS PROPELLANT	87,000
ACS PROPELLANT	720
EPS REACTANT	135
(GROSS WEIGHT)	103,125

*2010 LB SHELL WEIGHT TO LIMIT EDGE ROTATION TO ONE DEGREE (SPACE ASSEMBLY CRITERION)

Figure 2.2.3-4 Spaped Brake Point Design

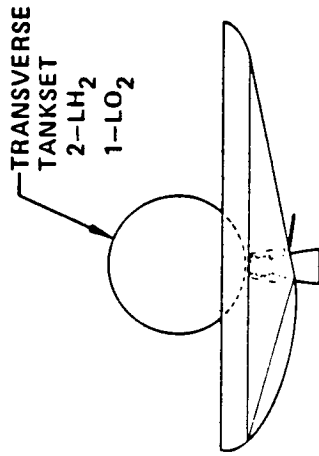
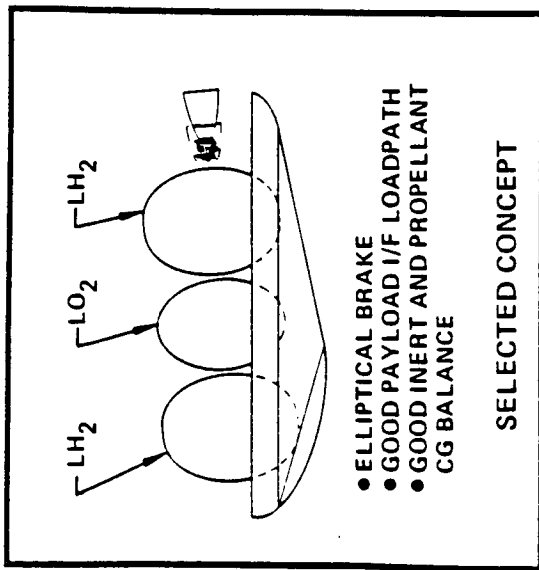
least weight system. The trade favored 10 degrees. The configuration implications of angle of attack for the shaped brake is the same as for the lifting brake and is discussed in section 2.2.2.4. A 10 degree angle of attack was selected as a design requirement based on this trade.

Tank Configurations. The reference configuration incurs weight, risk and cost penalties due to the amount of required on-orbit assembly. Weight penalties include interface points to ASE for transport, EVA or RMS handling fixtures, and EVA mate/demate structural and electrical joints. The complexity of EVA Quality Assurance and the limited resources available if an error occurs increases the cost risk of a vehicle which is extensively assembled on orbit. Cost increases include astronaut training, EVA directly incurred costs, and increased checkout and leak detection required since major components of the MPS have to be assembled. A four tank configuration incurs a weight penalty relative to a three or two tank arrangement due to increased surface area which needs to be insulated and protected from meteoroids and debris. This configuration also incurs the burden of having to be extensively disassembled for return to earth if a problem occurs which is not space repairable.

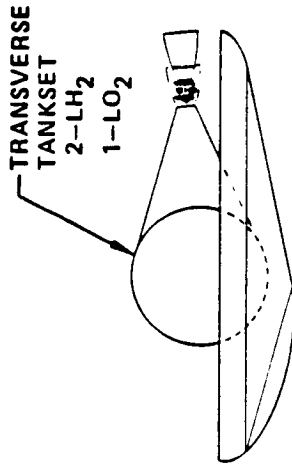
As a means of mitigating these on orbit assembly associated penalties, configuration concepts that have the tanks, propellant manifolds, avionics, EPS, RCS, engine interfaces, and payload interface as one integral unit were investigated. Figure 2.2.3-5 shows the tank configuration options that were explored. These configurations are the same as those investigated for the lifting brake OTV except for the brake itself; however, the selected concept changes because of this difference as discussed below.

The evaluation principals presented in section 2.2.2.4 for the lifting brake are also applicable to the shaped brake options. To reiterate, the inert weight cg, reserve propellant cg and payload cg positions need to fall along the angle of attack cg trim line for a configuration to be viable. The desirability for the reserve propellant cg position to fall along the trim line provides another reason for exploring alternative to the reference configuration described above since it fails to have this characteristic. The cg position is forward of the trim line due to the forward placement of the LO2 tank and center LH2 tank and their forward inclination due to the angle of attack.

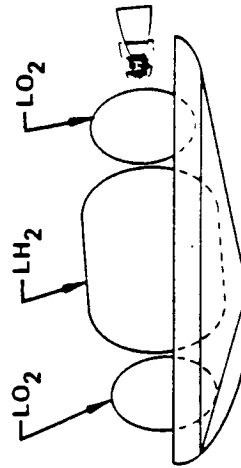
As previously mentioned, the shaped brake has a significant impact on the preferred configuration. This is because the shaped brake's inert cg position is well forward of the trim line. This forward cg can be balanced by locating the engines aft. There are three advantages to this concept; (1) no brake removal is required for engine access, (2) no nozzle doors are required in the hardshell, and (3) the engines can be



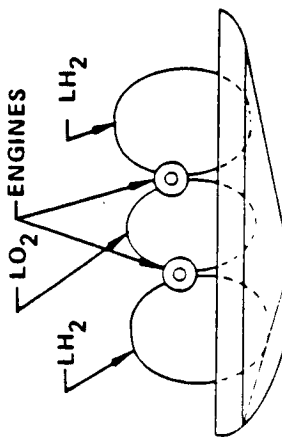
- CIRCULAR BRAKE
- GOOD PAYLOAD I/F LOADPATH
- DOORS REQUIRED IN BRAKE
- BRAKE REMOVAL REQUIRED TO REPLACE ENGINE
- GOOD INERT AND PROPELLANT CG BALANCE
- LARGE ENGINE GYMBAL ANGLE



- CIRCULAR BRAKE
- GOOD PAYLOAD I/F LOADPATH
- EXTRA STRUCTURE REQUIRED TO SUPPORT ENGINES NEAR EDGE OF BRAKE
- GOOD PROPELLANT CG BALANCE
- DIFFICULT INERT CG BALANCE



- ELLIPTICAL BRAKE
- LONGEST TANKSET
- POOR PAYLOAD I/F LOADPATH
- LO₂ HAS TO BE PRECISELY MANAGED BETWEEN TANKS TO CONTROL CG TRIM LOCATION
- HIGHEST ROLL MOI



- CIRCULAR BRAKE
- EXTRA STRUCTURE REQUIRED TO SUPPORT ENGINES NEAR EDGE OF BRAKE
- GOOD PAYLOAD I/F LOADPATH
- GOOD PROPELLANT CG BALANCE
- DIFFICULT INERT CG BALANCE

- ELLIPTICAL BRAKE
- MINIMUM NUMBER OF TANKS
- POOR PAYLOAD I/F LOADPATH
- RESERVE PROPELLANT CG CANNOT CORRESPOND TO DESIRED TRIM CG RESULTING IN LARGE UNPREDICTABLE VARIATIONS IN ANGLE OF ATTACK

Figure 2.2.3-5 Tankage and Engine Arrangement Options Shaped Brake OTV

brought to orbit integral with the tankset. As for the lifting brake concept, its brake cg is along the center of the brake and cannot balance a set of engines located near the edge of the brake. Therefore, the engines must be located under the tankset to achieve an inert weight cg balance.

2.2.3.4 Final Baseline Configuration

Figure 2.2.3-6 shows our final space based shaped brake OTV. The vehicle is based upon the results of the trades discussed above. Table 2.2.3-1 shows the key configuration features of this vehicle.

Major Elements. The major components which are transported in the Orbiter bay and are assembled on orbit are shown in figure 2.2.3-7. The brake is transported in three sections. The center section is transported on one Shuttle flight while the two side sections are transported overlapped on another shuttle flight. Removable jigs are used to rotate the sides into position on the center section. This precludes premature contact of the RSI. Shear cones are used to align the sections as they are rotated into place. Structural fastener installation completes the assembly and the jigs are removed.

Brake Structural Configuration. The brake's basic form is derived from the initial reference configuration described earlier. The brake has been scaled up in length and down in width to form an elliptical base. The brake has been made elliptical to accommodate the length of the tankset without increasing the area of the brake beyond that required by a four tank updated reference configuration.

Figure 2.2.3-8 shows the brake's structural design. The brake is divided into three 12 foot sections as shown in section AA of the figure. The tankset is attached to the brake keel beams located at the juncture of the sections via struts. Since the tankset is the stiffest element of the assembly due to its high moment of inertia, it is used to stiffen the brake. This eliminates the need for deep webbed keel beams and reduces the brake weight. A composite sandwich shell is stiffened by a series of cross ribs. The cross ribs are, in turn, stiffened by struts from the tankset. These struts allow the ribs to be relatively light while still maintaining a brake stiffness compatible with the RSI tile requirements. The net result of this design is a much lighter brake weight. Section 4.0 discusses this structural concept and the member sizing in depth.

Tankset. The tankset consists of the tanks, propellant manifolds, avionics, EPS, RCS, engines, and brake and payload interfaces. A side view of our configuration is

- MAN-RATED SUBSYSTEMS
- 44 FT x 36 FT. BRAKE

	LBS
STRUCTURES	4517
PROPULSION SYSTEMS	1162
THERMAL CONTROL AND PROTECTION	1679
GUIDANCE, NAVIGATION, AND CONTROL	135
COMMUNICATIONS/DATA HANDLING	469
ELECTRICAL POWER	760
SPACE MAINTENANCE	323
WEIGHT GROWTH	1269
(DRY WEIGHT)	(10314)
RESIDUALS	725
(INERT WEIGHT)	(11042)
REACTANTS—EPS (INC. RESERVES)	34
PROPELLANTS—RCS (INC. RESERVES)	1072
MAIN PROPELLANTS (INC. RESERVES)	67920
FLUID LOSSES	1694
(IGNITION WEIGHT)	(81762)
MASS FRACTION	.830

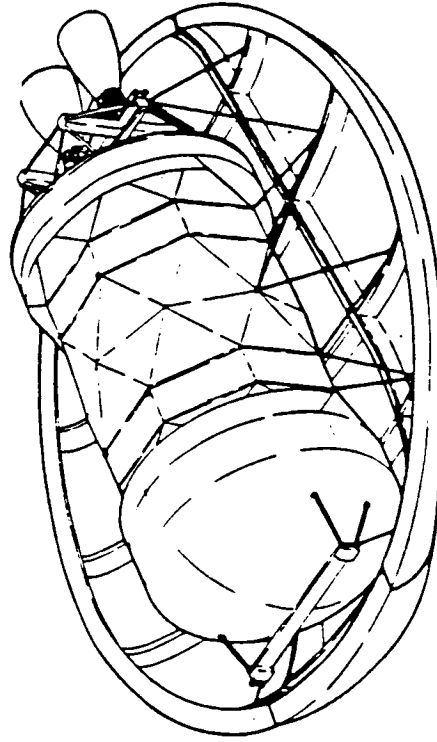


Figure 2.2.3-6 Weight Summary Space-Based Brake OTV—No. 16 —
Final Configuration

Table 2.2.3-1 Configuration Features Space-Based Shaped Brake OTV

<u>FEATURE</u>	<u>RATIONALE</u>
<ul style="list-style-type: none"> • PROPELLANT TANKS, LINES, ENGINES, AVIONICS, EPS, RCS AND PAYLOAD INTERFACE ARE INTEGRAL UNIT 	<ul style="list-style-type: none"> • ELIMINATE COST AND RISK OF ON-ORBIT ASSEMBLY • INTEGRAL UNIT LESS WEIGHT THAN IF ORBIT ASSEMBLED
<ul style="list-style-type: none"> • 1 LO₂ TANK AND 2 LH₂ TANKS 	<ul style="list-style-type: none"> • LOWEST NUMBER OF TANKS THAT PROVIDES BALANCED C.G. TRIM • LOWER MOI AND SHORTER THAN 2 LO₂ AND 1 LH₂ TANKS • CANTILEVERING LIGHT LH₂ TANKS DOES NOT IMPOSE WEIGHT PENALTY
<ul style="list-style-type: none"> • ELLIPTICAL BRAKE 	<ul style="list-style-type: none"> • ALLOWS ENGINES TO BE LOCATED ON END OF TANKSET ELIMINATING DOORS IN BRAKE AND NEED TO REMOVE BRAKE FOR ENGINE ACCESS • SPLITS INTO THREE STS PLB COMPATIBLE PIECES FOR TRANSPORT
<ul style="list-style-type: none"> • ENGINES NOT IN LINE WITH PAYLOAD 	<ul style="list-style-type: none"> • AEROMANEUVER TRIM AND WAKE HEATING RESTRICTS CREW MODULE PLACEMENT • ENGINE GIMBAL ANGLE LIMITS RESTRICT PAYLOAD C.G. LOCATION
<ul style="list-style-type: none"> • LO₂ AND LH₂ TANKS CARRY PRIMARY LOADS 	<ul style="list-style-type: none"> • ENGINE LOADS ARE RELATIVELY LOW • TANK PRESSURIZATION KEEPS TANKWALLS IN TENSION
<ul style="list-style-type: none"> • AVIONICS, MAIN ENGINES, RCS THRUSTERS ARE ORUs 	<ul style="list-style-type: none"> • EVA REPLACEMENT POSSIBLE AND COSTS LESS THAN EARTH RETURN
<ul style="list-style-type: none"> • RADIATORS SIZED ASSUMING OTV PERFORMS THERMAL ROLL 	<ul style="list-style-type: none"> • RESULTS IN SMALLER RADIATOR AREA AND LESS WEIGHT • PAYLOADS USUALLY REQUIRE ROLL FOR THERMAL CONTROL
<ul style="list-style-type: none"> • EPS RADIATOR AND AVIONICS BAYS INTEGRATED WITH METEOROID/DEBRIS SHIELD 	<ul style="list-style-type: none"> • ELIMINATED STRUCTURAL BOX AROUND AVIONICS • LESS SHIELD AREA THAN CONFORMAL DOME DESIGN • SHIELD SUPPORTED BY TANK SUPPORT STRUTS
<ul style="list-style-type: none"> • NON-DEPLOYABLE SHIELD WITH 3" STANDOFF DISTANCE 	<ul style="list-style-type: none"> • YIELDS MINIMUM GAGE SHIELD—LARGER SPACING DOES NOT REDUCE WEIGHT

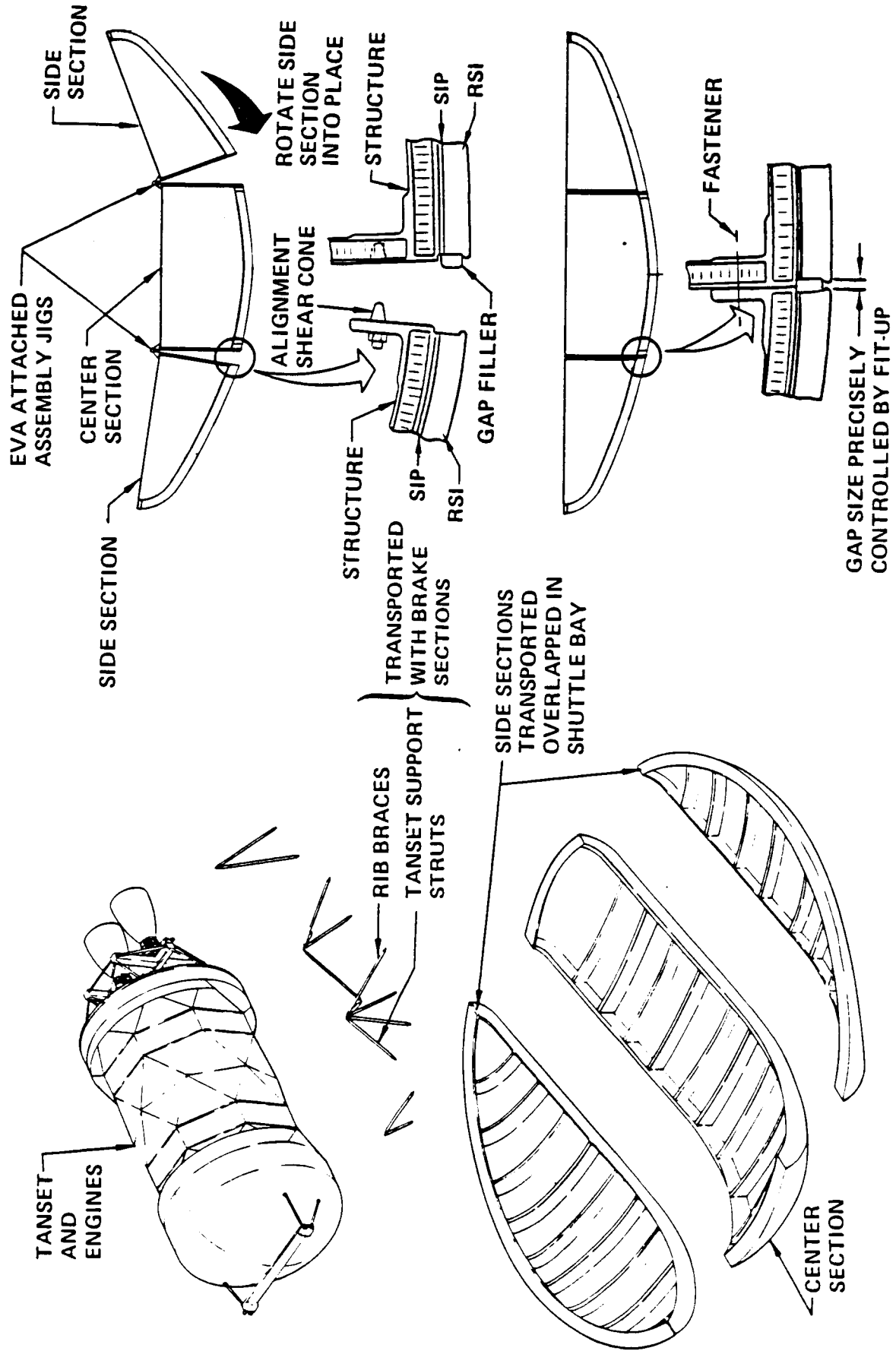


Figure 2.2.3.7 Shaped Brake Element Transport and Assembly



**Figure 2.2.3-8 Shaped-Brake OTV –
Final Configuration**

shown in figure 2.2.3-9. The brake is maintained at a 10 degree nominal angle of attack during the aeromaneuver by offsetting the cg of the vehicle. The location of the LO2 tank and the LH2 tank near the engines is critical to achieving a constant cg offset. These are the two tanks which still have propellant in them during the aeromaneuver. Since over 1200 lb of this propellant is reserves which may or may not be used on a given flight, the cg of the propellant (always 1/7 the distance between the LO2 and the LH2) must be located on the cg trim line. This is accomplished by designing the cylindrical sections of the two LH2 tanks to properly place the LO2 tank between them.

From an inert cg standpoint, the forward cg of the brake helps offset the aft cg of the engines. The avionics location would be used to fine tune the cg position. The crew module must be designed such that its cg is located on the trim line when it is on the vehicle.

A bi-pod strut system interconnects the LO2 tank, the two LH2 tanks and the cruciform engine support structure. The avionics, EPS radiators, RCS, payload interfaces, and meteoroid/debris protection are configured the same as for the lifting brake OTV's final configuration. The primary structure which transfers the brake loads to the return payload is shown in figure 2.2.3-8 section AA. Again, this structure is the same configuration as that used in our lifting brake OTV concept since the loading conditions and load paths are similar.

Brake Sizing. Figure 2.2.3-10 shows how the brake size is constrained. The heating lines are developed from TPS temperature limits. The other two lines show how the brake length must increase to prevent wake heating of the tankset as the tankset length increases due to increased propellant loading. Our configuration is sized by the tank length required to do the manned sortie mission.

Weights. A weight summary for the shaped brake OTV configured for a manned sortie mission is shown in figure 2.2.3-6. All subsystems are man-rated. Elements for each subsystem are the same as defined for the ballute braked OTV. In this case, the shaped brake primary and secondary structure including support structure is included in structures weights. Rigid tile insulation on the face of the brake is included in thermal control and protection.

Center of Gravity. Figure 2.2.3-11 shows the cg movement for the 20k delivery missions and 7.5k manned roundtrip mission. The "post burn number 2" cg position and the "end of mission" cg position set the gimbal angle requirement of 34 degrees. This

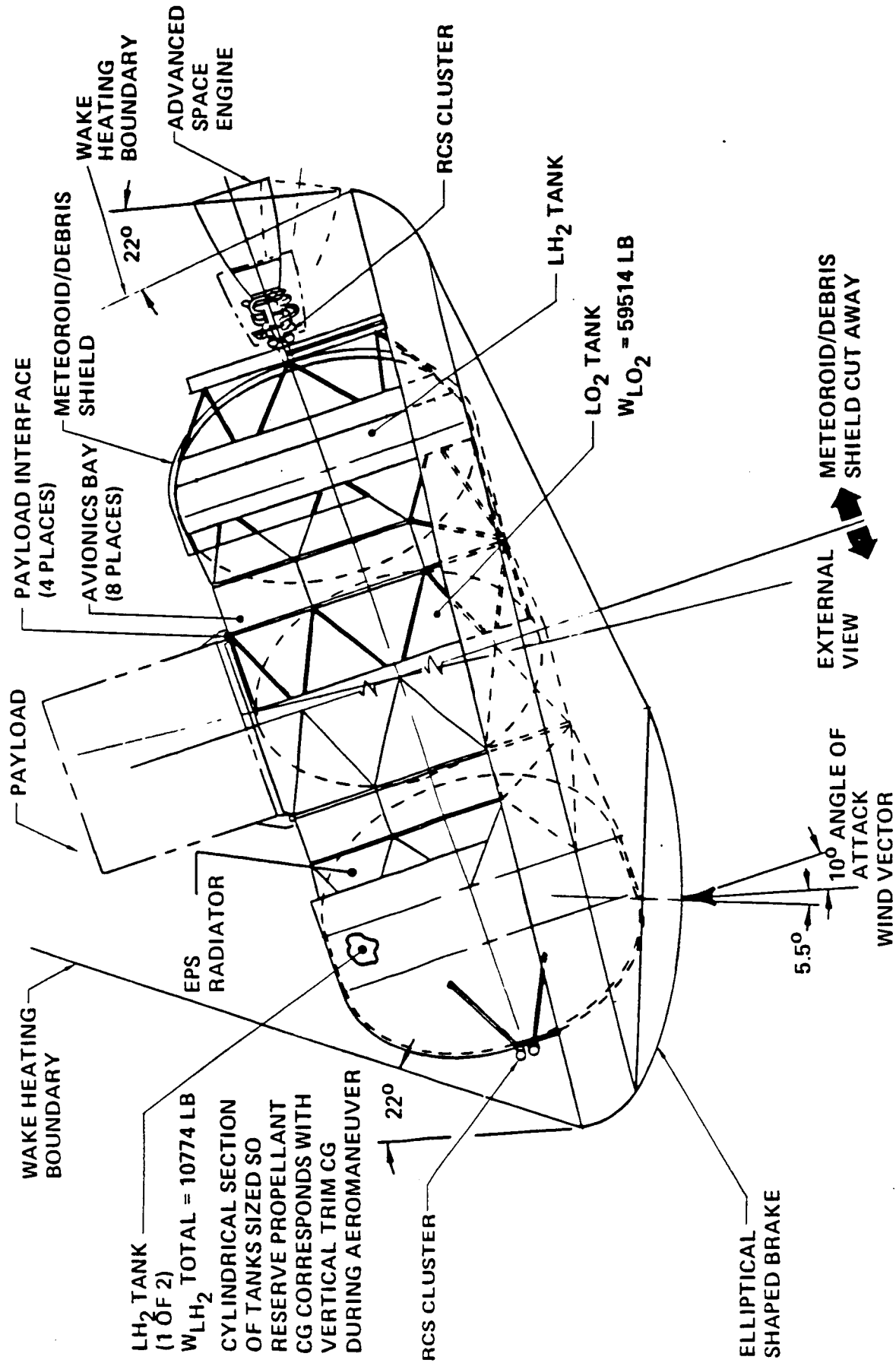


Figure 2.2.3-9 Configuration Space-Based Shaped Brake OTV

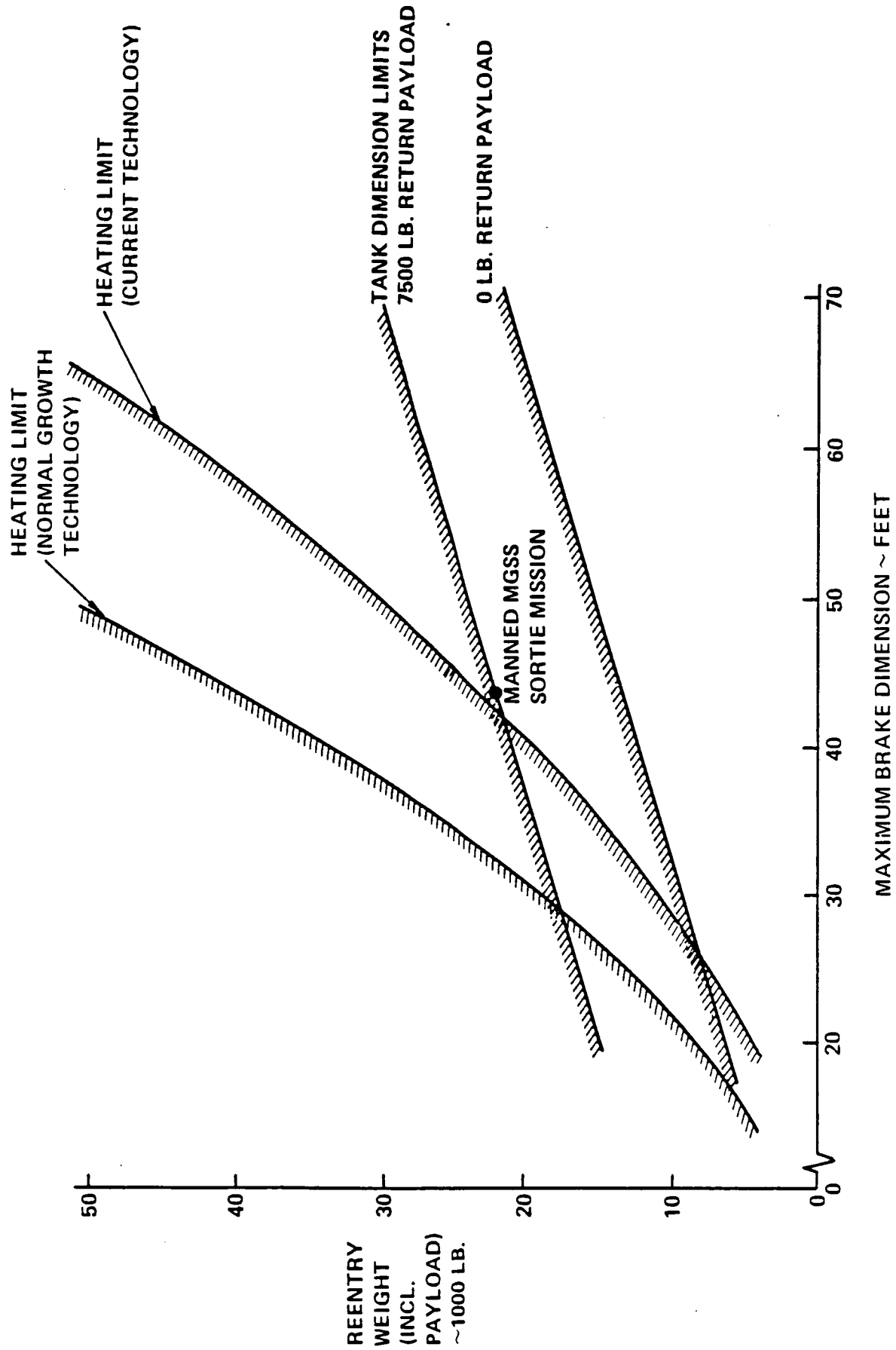


Figure 2.2.3-10 Brake Diameter Sizing Space-Based Shaped Brake OTV

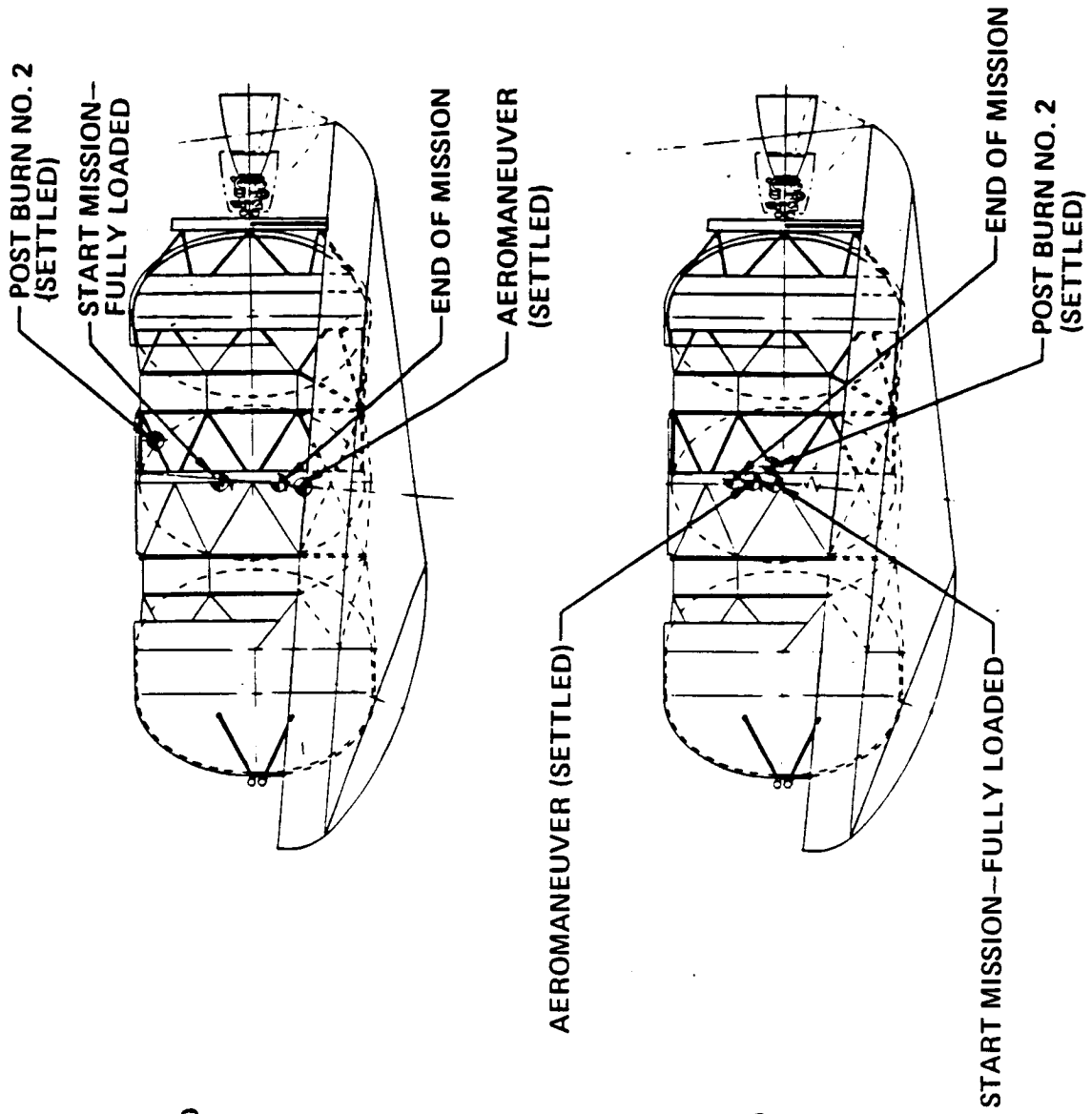


Figure 2.2.3-11 CG Location Shaped Brake OTV

angle provides 4 degrees of control authority if an engine were to fail. If the payload cg position was offset more than the assumed amount ($1/3$ length of the payload), the gimbal angle would increase further. The location of the engines for this configuration imposes limits on the tolerable gimbal angle resulting in payload cg limitations which a configuration like the lifting brake (engines below tankset) does not have.

Weight Trending. For the above chronological history of shaped brake configurations, figure 2.2.3-12 shows how the weights changed as the configurations changed. Table 2.2.3-2 presents a breakdown of the weight changes.

2.3 PROPELLANT LOGISTICS SYSTEMS

This section describes the configuration effort to develop propellant logistics systems necessary to support any of the SB OTV concepts. Propellant storage tanks are located at the Space Station and tankers deliver propellant from the Earth launch complex to the Station.

2.3.1 Propellant Storage Tanks

Figure 2.3.1-1 and figure 2.3.1-2 shows the LH₂ and LO₂ storage tanks, respectively. The trades and analyses performed to establish the design and sizing of the tanks are presented in section 3.0.

Both tanks share a common design and consist of a thin walled pressure vessel, surrounded by two vapor cooled shields, surrounded by a structural shell which provides meteoroid/debris protection. The shields and pressure vessel are supported by the shell via straps to minimize heat conduction paths and; therefore, reduce boiloff. MLI blankets are located between the shields to reduce radiant heat transfer and, again, to reduce boiloff. Boiloff is a critical concern because of the long propellant storage time.

The pressure vessel is pressure stabilized with helium during transport to orbit. Two ASE frames attach to the structural shell to transfer the tank loads to the Orbiter and are used to support the tanks at the Space Station. The tanks are designed to be launched independent of one another to allow multiple manifesting with heavier payloads and to allow flexibility in their placement at the Station.

2.3.2 Propellant Delivery Tanker

To transport propellant to the Space Station in the Orbiter a tanker has been configured and is shown in figure 2.3.2-1. Again, the trades and analyses which defined the type of tanker desired are presented in section 3.0 and in volume II, book 4.

WEIGHTS BASED ON CONFIGURATIONS PRESENTED AT BRIEFINGS

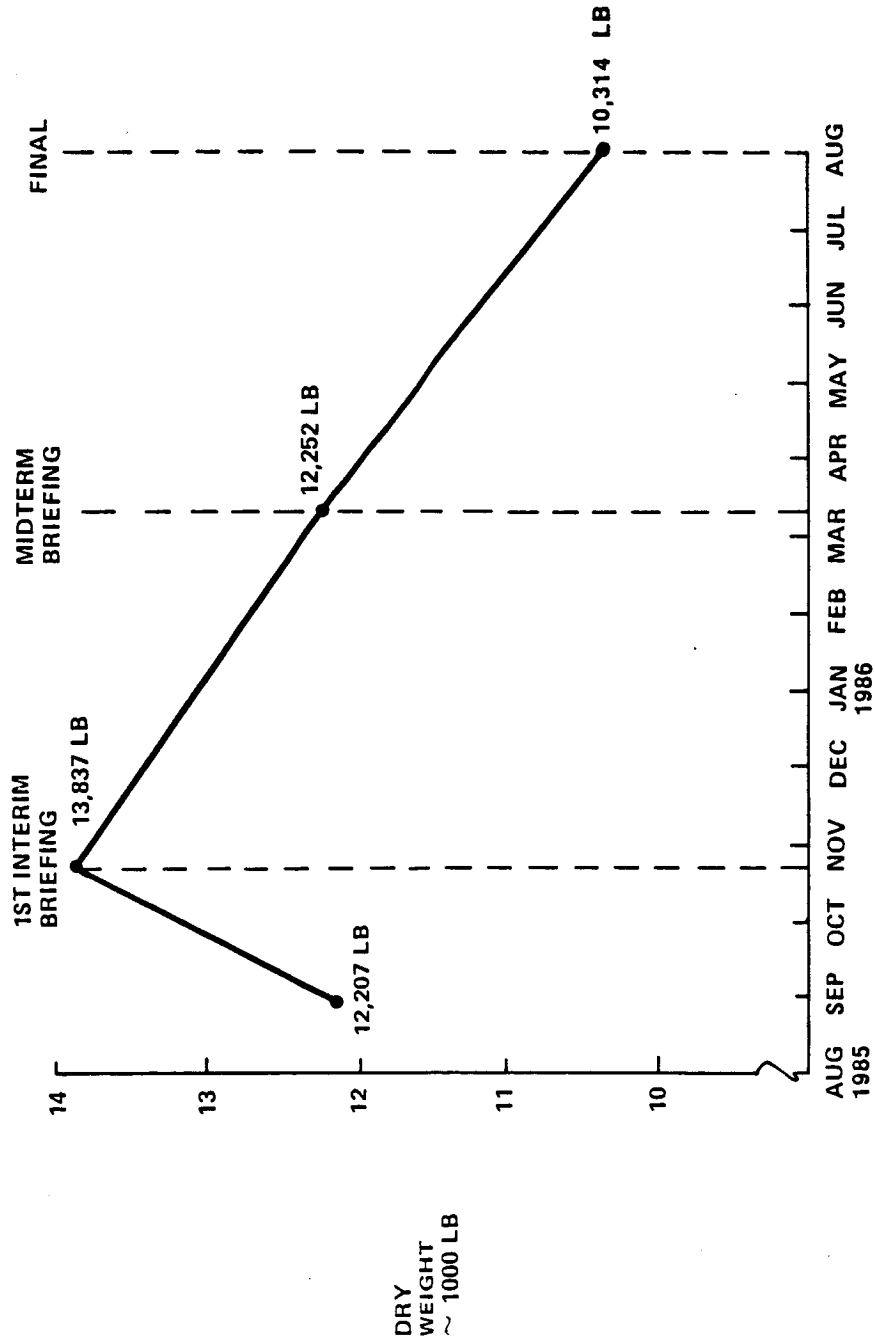
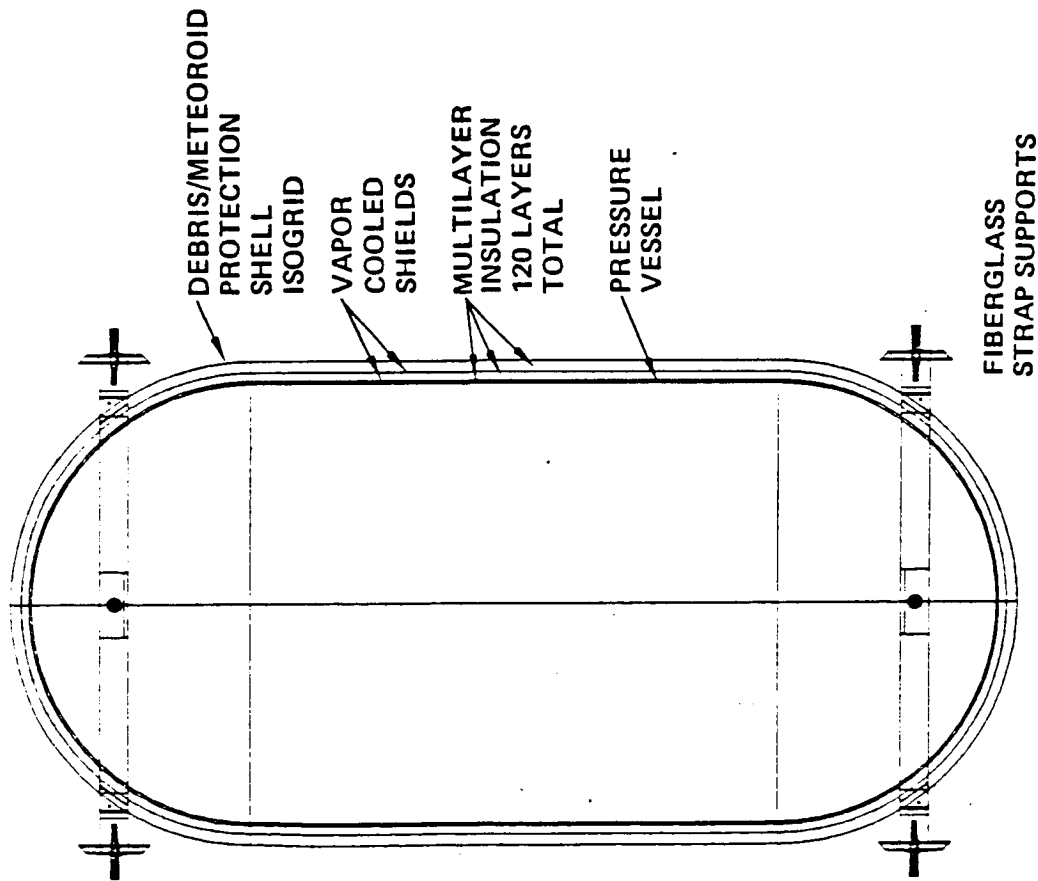


Figure 2.2.3-12 Dry Weight History Space-Based Shaped Brake OTV

Table 2.2.3.2. OTV Dry Weight History SB Shaped Brake OTV

1ST → 1ST INTERIM BRIEF		1ST INTERIM BRIEF → MIDTERM		MIDTERM → 3RD QUARTER	
CHANGE	WT Δ	CHANGE	WT Δ	CHANGE	WT Δ
NO CHANGE IN TANKAGE WT	Ø	DECREASED TANK SIZE	-495	USE ELLIPTICAL HEAD TANKS	+21
UPDATE STRUCT. DEF.	+1008	IMPROVED STRUCT' DEF.	-551	IMPROVED CONFIGURATION	-1427
UPDATE BRAKE STRUCT. DEF.	+1396	INCLUDED BRAKE ASSEMBLY ALLOWANCES	+126	IMPROVED BRAKE STRUCT. DEF.	-618
HEATING RATE UPDATE ON TPS	-1071	NO CHANGE IN TPS	Ø	MINOR TPS UPDATE	-1
IMPROVED GNC, TTC + DMS DEF	-41	NO AVIONICS CHANGE	Ø	IMPROVED DMU, UPDATE AVIONICS MAN-RATING	-5
UPDATE FUEL CELL' INCLUDE THERMAL CONTROL	+105	DECREASED EPS REACTANT REQ'T	-32	UPDATE EPS REACT REQ'T, +UPDATE MAN-RATING	+214
INCREASED RCS MANIFOLD LENGTH	+20	INCREASED RCS MANIFOLD LENGTH	+7	UPDATE THRUSTER REQ'T + RCS PROP	+115
NO CHANGE IN MPS	Ø	USE ADVANCED ENGINES,	-473	MISC PLUMBING INCREASE	+129
MISC	Ø	MISC	+40	MISC	-37
WEIGHT GROWTH ADJ	+213	WEIGHT GROWTH ADJ	-207	WEIGHT GROWTH ADJ	-329
TOTAL (LBM)	+1630	TOTAL (LBM)	-1585	TOTAL (LBM)	-1938



DESIGN PARAMETERS

- PRESSURE VESSEL
 - DIAMETER, 13 FT
 - LENGTH, 28.93 FT
 - WEIGHT, 1397 LBM
- DEBRIS/METEOROID SHELL
 - DIAMETER 14.33 FT
 - LENGTH 30.26 FT
 - WEIGHT, 1652 LBM
- CAPACITY AT 17.5 PSIA
 - 13286 LBM WITH 7% ULLAGE
- INSULATION SYSTEM
 - 120 LAYERS MLI
 - 2 VAPOR COOLED SHIELDS WITHIN MLI
 - BOILOFF ~ 7 LBM/DAY
 - WEIGHT, 1114 LBM
- LIQUID ACQUISITION SYSTEM
 - 8 CHANNELS ON MERIDIANS
 - CHANNELS 8 IN. BY 2 IN.
 - 2 SCREENS 325 x 2300
 - ONE SIDE OF CHANNEL
 - WEIGHT, 781 LBM
- TOTAL TANK WEIGHT, 5686
- ASE WEIGHT 598 LBM
- DEVELOPMENT COST, \$106.3 x 10⁶
- PRODUCTION COST, \$9.9 x 10⁶ FIRST UNIT

Figure 2.3.1-1 Space Station Hydrogen Storage Tank Baseline Concept

- DESIGN PARAMETERS**
- **PRESSURE VESSEL**
 - DIAMETER, 13 FT
 - LENGTH, 13.47 FT
 - WEIGHT, 438 LBM
 - **DEBRIS/METEOROID SHELL**
 - DIAMETER, 14.33 FT
 - LENGTH, 14.8 FT
 - WEIGHT, 829
 - **CAPACITY AT 17.5 PSIA**
 - 79714 LBM WITH 7% ULAG
 - **INSULATION SYSTEM**
 - 120 LAYERS MLI
 - 2 VAPOR COOLED SHIELDS WITHIN MLI
 - BOILOFF, 13 LBM/DAY
 - **LIQUID ACQUISITION SYSTEM**
 - 8 CHANNELS ON MERIDIANS
 - CHANNELS 4 IN. BY 1 IN.
 - 2 SCREENS 325 x 2300 ON ONE SIDE OF CHANNEL
 - WEIGHT, 260 LBM
 - **TOTAL TANK WEIGHT, 2063 LB**
 - **ASE WEIGHT, 598 LBM**
 - **DEVELOPMENT COSTS, \$48.8 x 10⁶**
 - **PRODUCTION COST, \$4.7 x 10⁶**

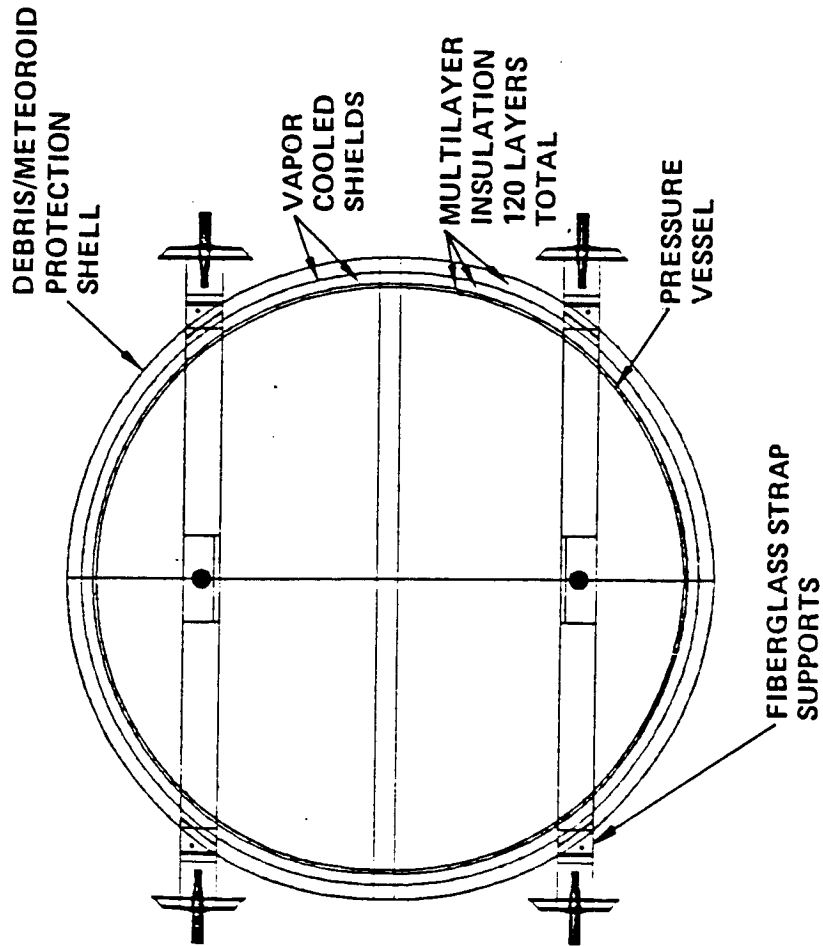
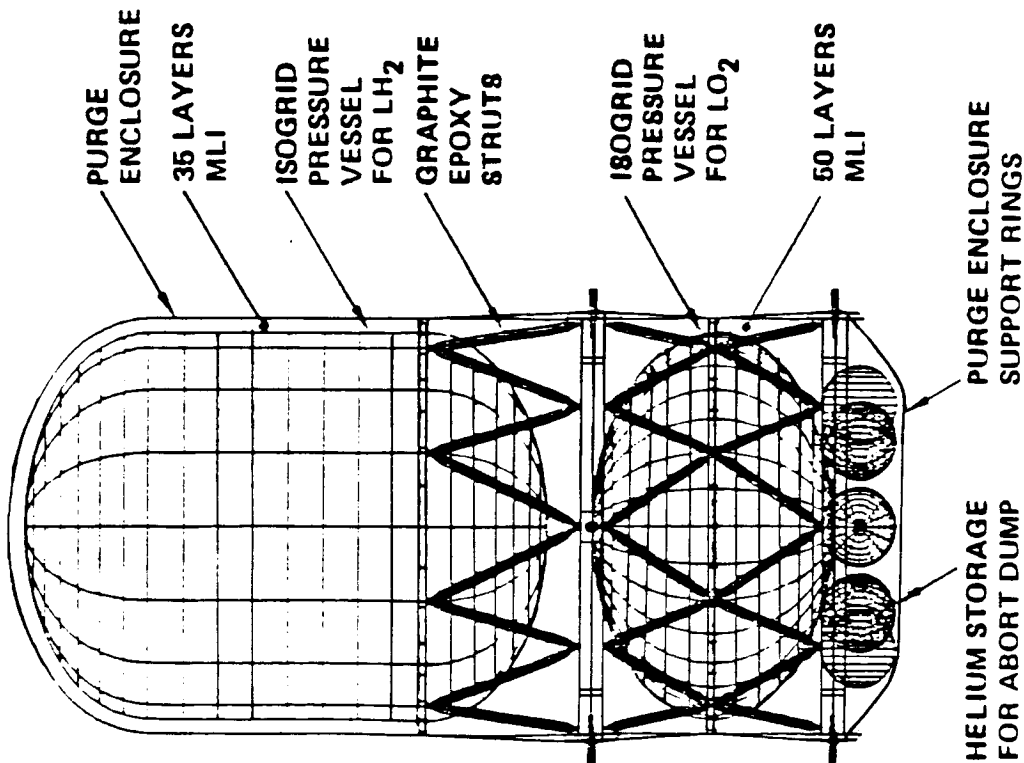


Figure 2.3.1-2 Space Station Oxygen Storage Tank Baseline Concept



• TANKER DESIGN PARAMETERS

- HYDROGEN TANK
 - PRESSURE VESSEL
 - DIAMETER, 13.33
 - LENGTH, 19.23
 - WEIGHT, 1002
 - VOLUME, 2176 FT³
 - CAPACITY AT 17.5 PSIA
 - 8858 LBM WITH 7% ULLAGE
 - INSULATION
 - HELIUM PURGED 35 LAYERS MLI
 - ACQUISITION SYSTEM WEIGHT 585 LBM
- OXYGEN TANK
 - PRESSURE VESSEL
 - DIAMETER, 13.33
 - LENGTH, 9.43
 - WEIGHT, 729
 - VOLUME, 808 FT³
 - CAPACITY AT 17.5 PSIA
 - 53146 LBM WITH 7% ULLAGE
 - INSULATION
 - HELIUM PURGED 50 LAYERS MLI
 - ACQUISITION SYSTEM WEIGHT, 217 LBM
- HELIUM STORAGE
 - CAPACITY 124 LBM
 - 4000 PSIA
- TOTAL TANKER SYSTEM WEIGHT INCLUDING PLUMBING IS 6479 LBM
 - DEVELOPMENT COST, \$185.5 X 10⁶
 - PRODUCTION COST, \$19.3 X 10⁸ FIRST UNIT

Figure 2.3.2-1 Tanker Tanks Configuration Baseline Concept

The tanker consists of LH2 and LO2 isogrid tanks supported by two structural rings via graphite/epoxy struts. Isogrid tanks are used to distribute the local strut loads into the tank. Struts are used to minimize heat conduction and; therefore, propellant boiloff. Surrounding each tank are MLI blankets and a purge enclosure. The purge enclosure permits a helium purge of the system on the ground to avoid liquid nitrogen from forming on the LH2 tank.

Helium bottles are located on the aft support ring and provide helium pressurant for dumping the propellant during a launch abort condition.

Forward and aft structural support rings are located on either side of the LO2 tank with the LH2 tank cantilevered from the forward ring. Since the forward ring also supports the keel pin, this design locates the keel pin approximately at the cg of the loaded tanker. This minimizes yaw coupling loads in the system and so reduces the structural loads. Cantilevering the LH2 tank imposes little weight penalty because the launch loads are predominately axial and landing always occurs with the tanks empty.

2.4 GROUND BASED OTV'S

This section discusses the configuration effort associated with OTV's launched within the shuttle cargo bay (SCB) or aft cargo carrier (ACC). Unless noted, the vehicles and their payloads or auxiliary propellant tanks are launched using an STS with 72k lbm capability (study groundrule). As in the case of SB OTV's the discussion is chronological in terms of configuration development.

2.4.1 Ground Based SCB Ballute Braked OTV

The GB SCB OTV concept consists of a main stage used on missions involving $\leq 12k$ lbm GEO delivery or equivalent and an auxiliary propellant tankset for more demanding missions.

2.4.1.1 Operational Description for Main Stage OTV

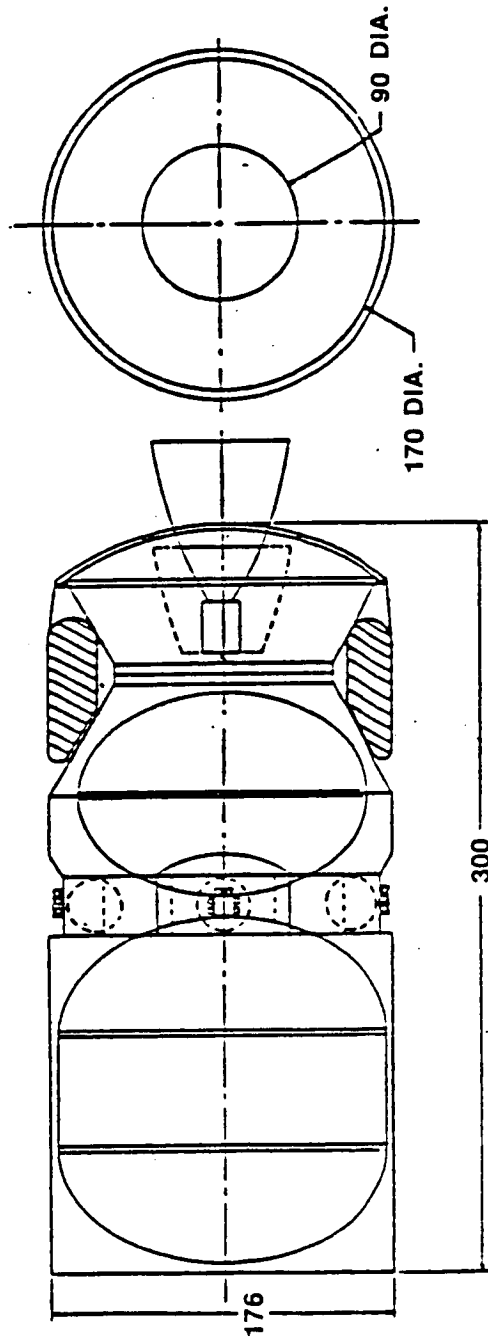
The ground based main stage OTV is transported to orbit in the Shuttle SCB fully fueled with a payload attached. On orbit, the OTV and payload are deployed and the OTV performs its mission. Upon return to LEO, the ballute is jettisoned and the OTV is restowed in the PLB for return to the ground. On the ground, the OTV is refurbished with a new ballute and is manifested for another mission.

2.4.1.2 Initial Reference Configuration

Figure 2.4.1-1 shows our initial reference configuration and a top level weight statement for the ground based ballute braked OTV. The configuration was based upon the OTV Concept Definition Study NAS8-33532 (Ref. 1). The OTV structure consists of an LH2 and LO2 tank, an external shell, avionics/RCS ring, engine support beams, and an aft shell for ballute support. Main propulsion is provided by a single RL10-IIB engine. Attitude control is provided by a blow-down hydrazine system with four thruster modules mounted on the avionics ring.

Design of the structural system for this vehicle is dominated by the attached payload cantelevered loads during ascent and abort conditions and the LO2 oxidizer loads during ascent. Propellant loads are not a structural driver for Orbiter abort landing conditions because the propellant is dumped overboard for safety and to meet Orbiter landing load restrictions. An exterior graphite/epoxy sandwich shell is used to gather the payload and LO2 tank loads and distribute them to the Orbiter interface trunnions and keel pins. The shell also provides meteoroid/debris protection for the vehicle.

• DIMENSIONS IN INCHES



STRUCTURE	3642	
AEROBRAKE SYSTEM	2438	
AVIONICS	609	
ELECTRICAL POWER	859	
MAIN PROPULSION	868	
ATTITUDE CONTROL	194	
WEIGHT GROWTH	1247	
(DRY WEIGHT)	(9557 LBM)	

MPS RESIDUAL	565	
ACS RESIDUAL	31	
EPS RESIDUAL	23	
(BURNOUT WEIGHT) (10,176)		
INFLIGHT LOSSES	212	
MPS PROPELLANT	55,000	
ACS PROPELLANT	545	
EPS REACTANT	62	
(GROSS WEIGHT)	(65,995 LBM)	

Figure 2.4.1-1 Ground-Based Ballute-Braked OTV Concept —
Initial Reference Configuration

Both the LH2 and LO2 tanks are made of 2219-T87 aluminum and have elliptical domes. Elliptical domes are used to reduce the vehicle length in the Orbiter bay so a reasonable payload length is available. The tanks are attached to the shell via graphite/epoxy struts. Struts are used to minimize heat conduction to the tanks and, thus, minimizes propellant boiloff losses.

The aerobrake is a 50 foot diameter, 60 degree half angle, 600 degree F backwall temperature ballute. The ballute is jettisoned after each flight so the OTV can be restowed in the Orbiter. To facilitate ballute installation on the ground, the aft dome and conical structure attached to the engine support structure can be removed.

The avionics ring is a 30 inch deep octagonal aluminum structure which supports the avionics, EPS, and RCS. An octagon was selected because its flat surfaces simplify the design of the doors and avionic support structure. No space maintenance provisions have been provided for the avionics. The avionics ring is located between the LO2 and LH2 tanks rather than on the forward end to reduce vehicle length so payload length is maximized.

2.4.1.3 Major Trades and Analyses

The same five top level trades and analyses that were presented for the space based ballute braked OTV in section 2.2.1.2 are applicable to the ground based OTV. These trades and analyses are; 1) ballute sizing analysis, 2) systems module (avionics ring) location trade, 3) tankage shape trade, 4) engine type and sizing trade, and 5) reliability analysis.

2.4.1.4 Revised Reference Configuration

Figure 2.4.1-2 shows the main stage OTV configuration with the above trade results incorporated. A separation plane has been added to the vehicle to accommodate ASE attachment and a 5 degree clearance angle for deployment has been provided.

2.4.1.5 Revised Reference Configuration Refinement

From this reference configuration further trades and analyses were conducted on the ballute, RCS, avionics and EPS, and TPS. Again, these trades and analyses are the same as those presented for the space based ballute braked OTV in section 2.2.1.4.

The avionics ring and the EPS radiator were changed to cylindrical shapes rather than octagonal or faceted. Both of these items carry large primary loads during launch on the ground based vehicle making it undesirable to disturb the load path from the circular shells to a faceted shape.

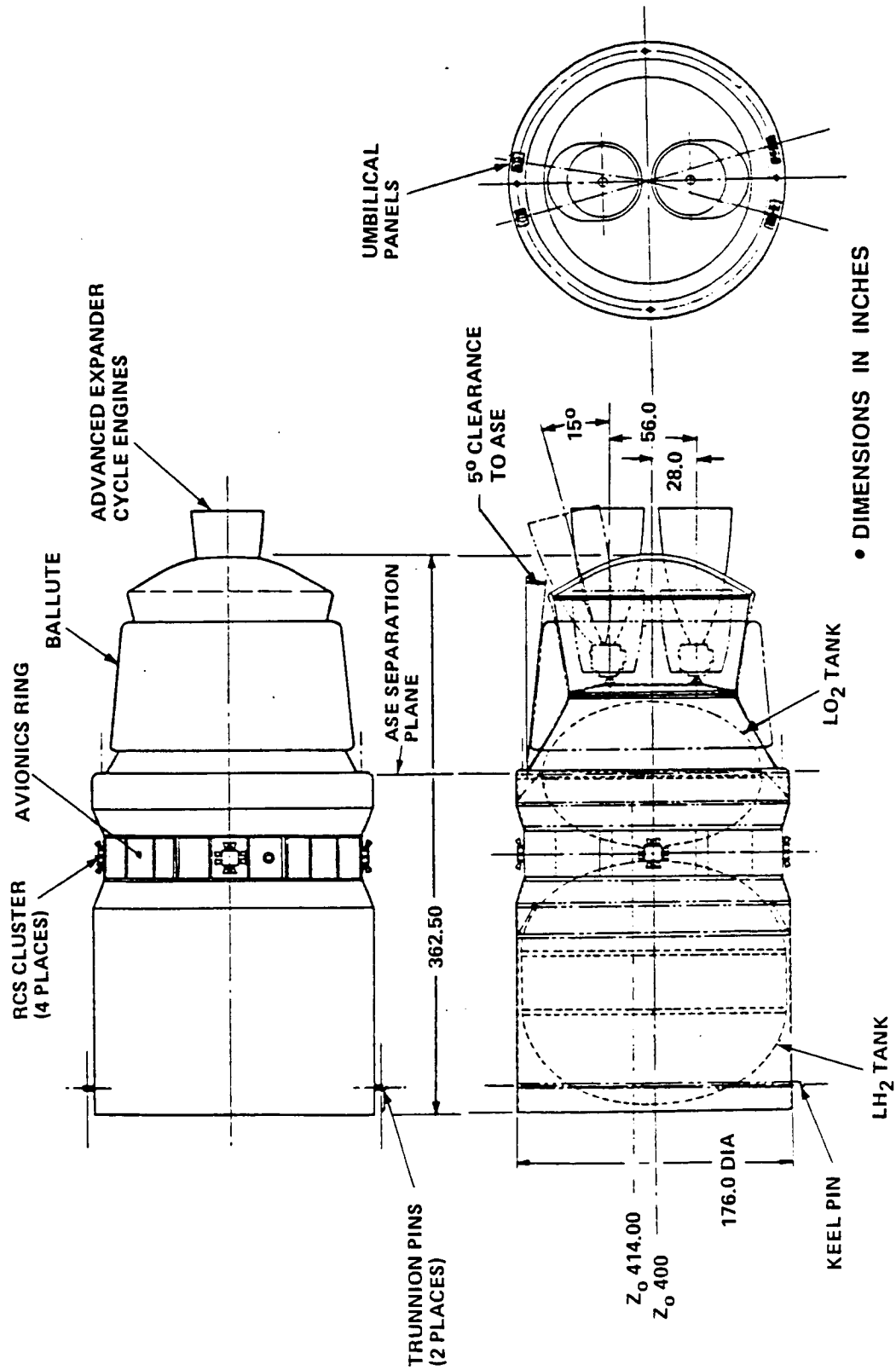


Figure 2.4.1-2 Ground-Based Ballute-Braked OTV—
Revised Reference Configuration

2.4.1.6 Baseline Main Stage OTV Configuration

Figure 2.4.1-3 shows our final baseline configuration for the ground based ballute braked OTV. Key configuration features are shown in table 2.4.1-1. The OTV is sized for payloads of 12000 pounds or less. The larger payloads in the mission model utilize an auxiliary tankset to increase the performance capability of the vehicle. The configuration of the auxiliary tankset and their vehicle implications are discussed in section 2.2.7.

Ballute. The vehicle utilizes a 33 foot diameter, 70 degree half angle cone ballute with a 1500 degree backwall temperature for the aeromaneuver. When an auxiliary tankset is utilized, the tankset changes the cg of the vehicle significantly and requires a larger ballute size. The forward and aft attachment points are spaced apart over half the radius of the 33 foot diameter ballute. The ASE interface to the vehicle precludes a larger spacing which would be desirable for the larger ballutes used with the auxiliary tankset.

Ballute inflation, control and jettison are accomplished using the same provisions and procedures as the space based ballute braked vehicle. Ballute installation, of course, is done on the ground.

Ballute Sizing. The ballute diameter sizing constraints are shown in figure 2.4.1-4. The manned sortie mission and low g GEO delivery mission are sized by the 5% static stability margin as discussed for the space based ballute braked vehicle. The unmanned multiple manifest mission corresponds to a 12k lb or less payload mission and is sized by the 1.5 turn-down limit. This limit is the smallest 70 degree ballute with a 63 inch forward attachment radius that will have a turn down ratio of 1.5.

ASE. An ASE has been designed to collect the axial loads and transfer them to the Orbiter, tilt the OTV out of the payload bay, and support the avionics, manifold, and helium bottles needed to interface the OTV with the Orbiter. The helium bottles provide pressurant for dumping the OTV propellents in 300 seconds for launch abort. The ASE attaches to the OTV via a series of mechanical latches. A five degree clearance angle has been provided between the ASE and the vehicle to accommodate deployment.

Figure 2.4.1-5 shows how the OTV is installed in and deployed from the Orbiter bay. The forward trunnion on the ASE transfers the 113K lb x axial loads to the orbiter. The placement of the vehicle is, therefore, constrained by the locations of 120 kip x

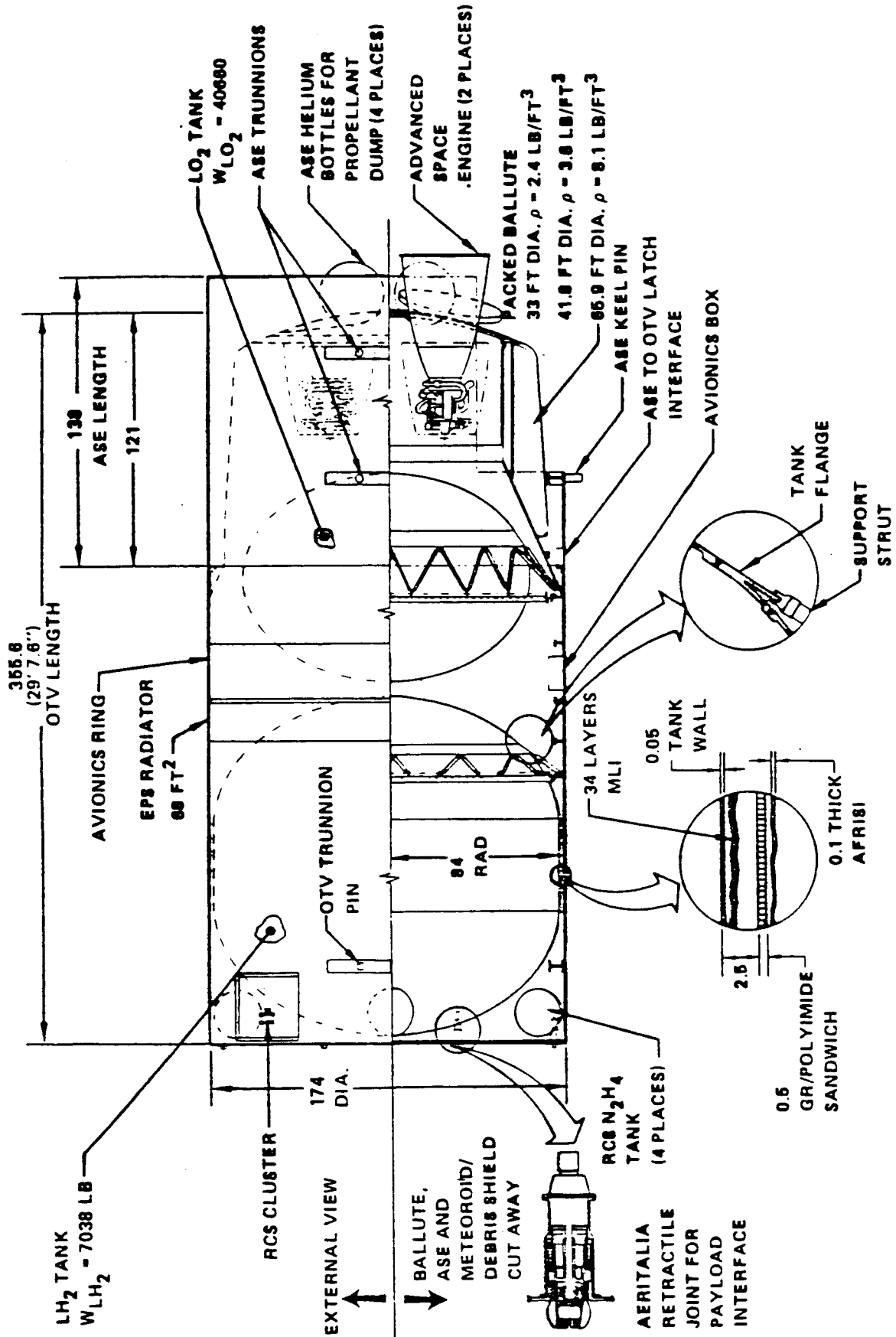


Figure 2.4.1-3 Ground-Based Ballute-Braked OTV-Single Stage—
Final Configuration

Table 2.4.1-1 Configuration Features Ground-Based Ballute Braked OTV

<u>FEATURE</u>	<u>RATIONALE</u>
• MID BODY AVIONICS RING	<ul style="list-style-type: none"> • AFT C.G. REDUCES BALLUTE DIAMETER SIZED FOR • AERO-STABILITY
• EPS RADIATOR LOCATED ADJACENT TO AVIONICS RING	<ul style="list-style-type: none"> • CO-LOCATES ALL RADIATORS ON VEHICLE • EPS RADIATOR ADJACENT TO EPS
• RADIATORS SIZED ASSUMING OTV PERFORMS THERMAL ROLL	<ul style="list-style-type: none"> • RESULTS IN SMALLER RADIATOR AREA AND LESS WEIGHT • PAYLOADS USUALLY REQUIRE ROLL FOR THERMAL CONTROL
• RCS LOCATED FORWARD	<ul style="list-style-type: none"> • ELIMINATE CONTAMINATION AND HEATING OF RADIATORS • REDUCE PLUME IMPINGEMENT ON BALLUTE
• MAXIMUM DIAMETER 174"	<ul style="list-style-type: none"> • 3" STATIC AND DYNAMIC CLEARANCE IN STS PLB
• PRIMARY LOADS CARRIED BY CYLINDRICAL STRUCTURE WHICH ALSO ACTS AS METEOROID/DEBRIS SHIELD	<ul style="list-style-type: none"> • HIGH LOADS INCURRED DURING LAUNCH AND ABORT LANDING WITH CANTILEVERED PAYLOAD
• AUXILIARY TANKSET USED TO INCREASE PERFORMANCE ALONG WITH MULTIPLE BALLUTE SIZES	<ul style="list-style-type: none"> • MOST COST EFFECTIVE APPROACH TO CAPTURING FULL MISSION MODEL
• 25 FT. MAX. LENGTH PAYLOAD MANIFESTED WITH OTV; 35 FT. MAX. WITH AUXILIARY TANKSET	<ul style="list-style-type: none"> • LENGTH CONSTRAINT OF PLB
• 70° JETTISONABLE BALLUTE WITH 1500°F BACKWALL TEMPERATURE	<ul style="list-style-type: none"> • LEAST WEIGHT BALLUTE SYSTEM • INSULATION REQUIRED AROUND TANKAGE
• BALLUTE FORWARD ATTACHMENT POINT HALF BALLUTE RADIUS FROM AFT ATTACHMENT POINT (33 FT DIA BALLUTE)	<ul style="list-style-type: none"> • PERMITS 1.5 TURN DOWN RATIO

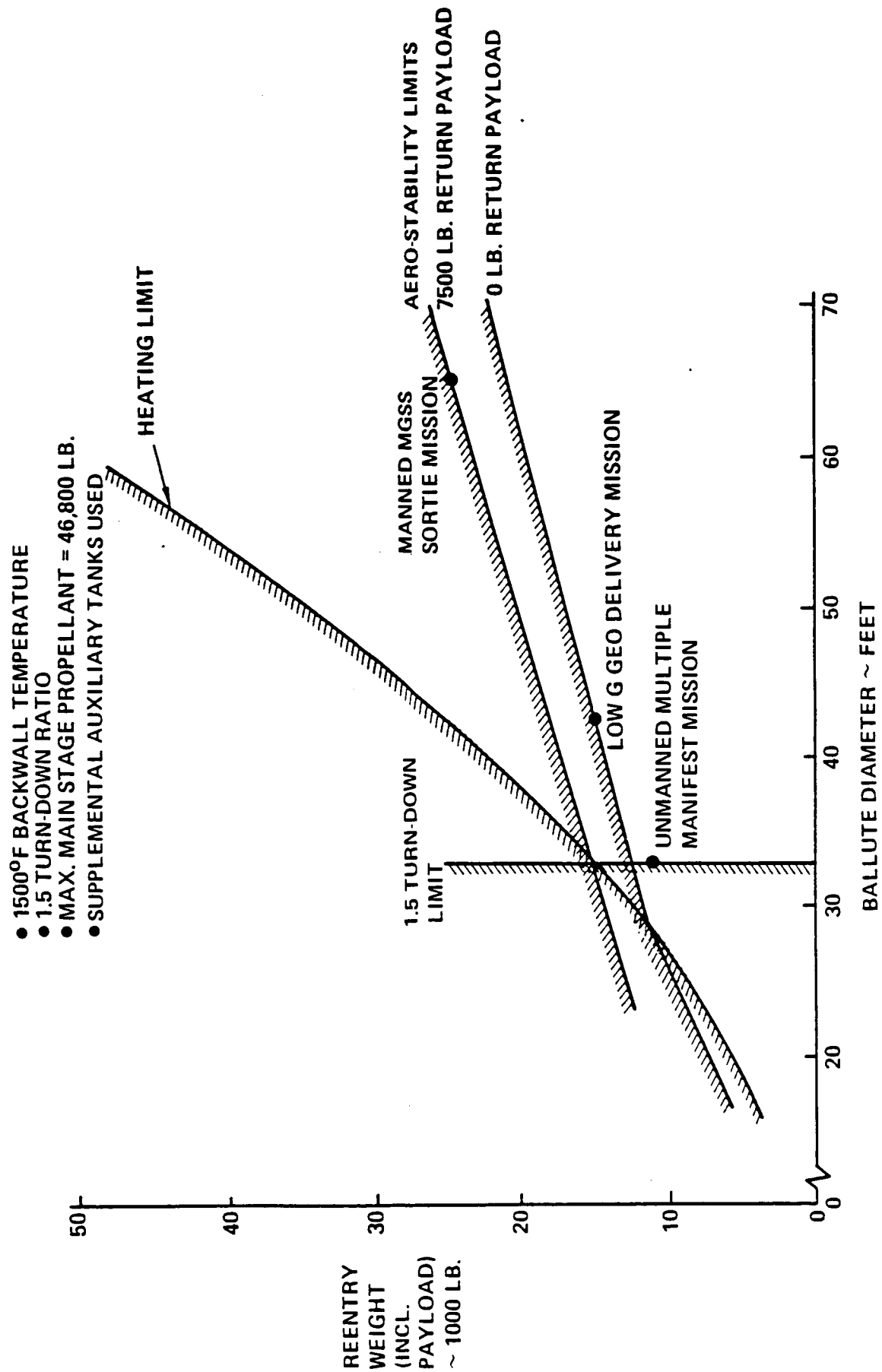


Figure 2.4.1-4 Brake Diameter Sizing Ground-Based Ballute—Braked OTV

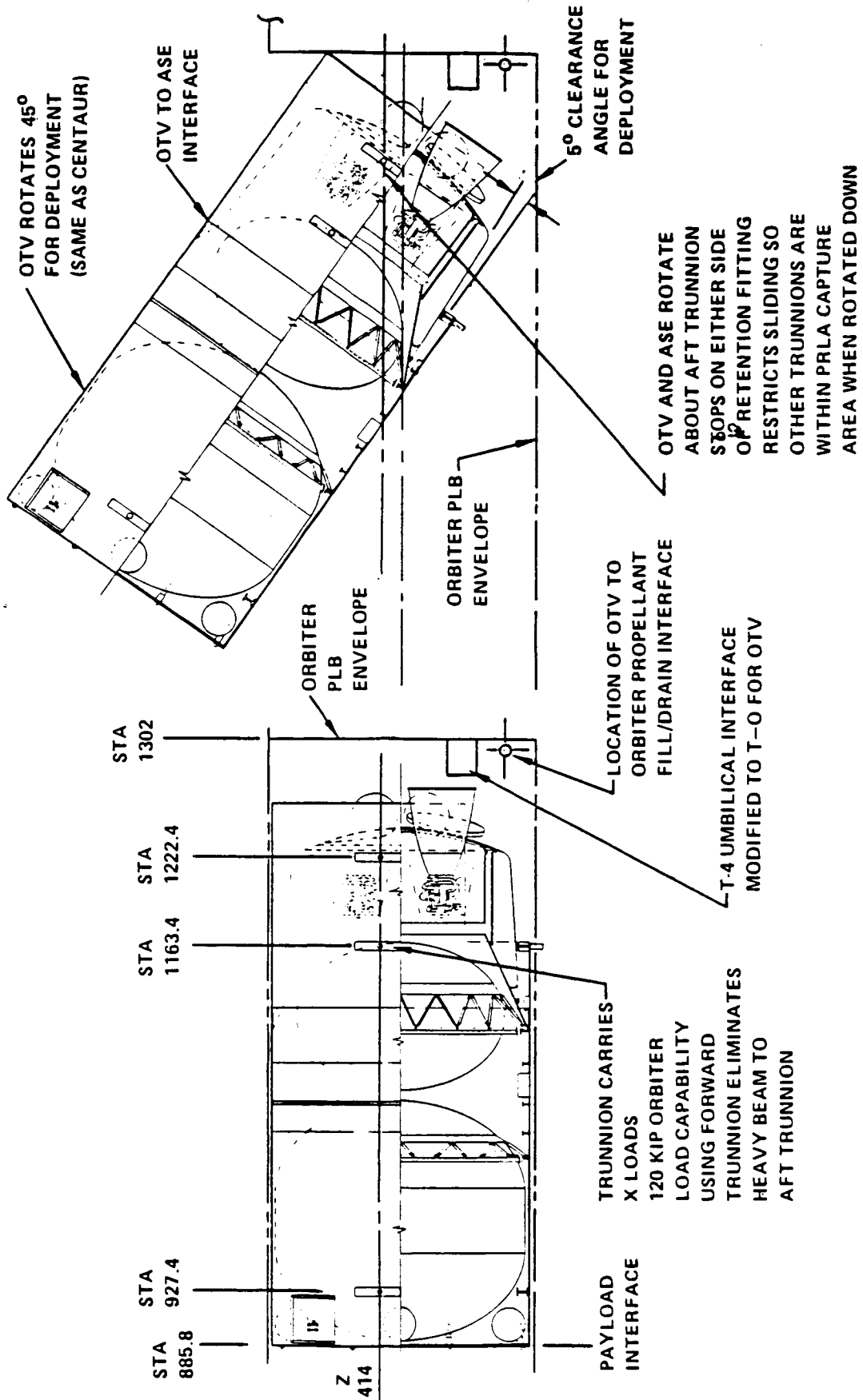


Figure 2.4.1-5 Shuttle Installation/Deployment Ground Based Ballute Braked OTV

load capability PRLAs (payload retention latch assembly) and the rotation clearance required by the ASE. A payload length of 25 feet can be accommodated. The vehicle is rotated 45 degrees for deployment via an aft tilt mechanism and is spring deployed after checkout.

An important part of the ASE necessary to launch a payload is the government-furnished portion, or that which is supplied by the launch vehicle that is charged to the payload weight. Generally, this includes fluid kits, electrical kits, wiring, and support fittings that are not normally manifested on the shuttle, but are necessary for integration of the payload in the shuttle.

In the case of the ground-based OTV, this support equipment must be provided for both the launch and return of the stage and payload. The weights for both the government and contractor furnished ASE are shown in table 2.4.1-2. The common government-furnished equipment is equipment that is common to most payloads loaded in the shuttle, and includes a Standard Mix Cabling Harness (SMCH), mid payload bay wiring harnesses, closed circuit TV, utility kits, and a 675 lb allowance for bridge and keel fittings that is part of the normal shuttle manifest. Payload-specific equipment includes longeron and keel bridge fittings, latches, and guides, as well as pressurization and vent kits, additional payload handling aids (extra RMS, MMU), and contractor-furnished structures. Weights for the standard longeron and keel bridge fittings, latches, and guides, as well as cabling and propellant handling kits, are per the February 25, 1985 Shuttle Systems Weight and Performance book, JSC-09095-79.

Weights. A weight summary is presented in figure 2.4.1-6 for a 10 klb multiple manifest mission with a 1 klb payload rack. Included in structure weights are body shell and stiffening ring structures, thrust structure, equipment support structures, tankage, as well as ballute primary and secondary structures. Included also are all ballute and heat shield support structures. Propulsion systems include both main propulsion and reaction control system weights. Thermal control and protection includes tank insulation, active thermal control, as well as ballute and body insulation for thermal protection during thermomaneuver. Other systems are as shown. Space maintenance provisions are not applicable on a ground based vehicle. Weight growth includes 5% of all existing hardware and 15% on all other hardware.

Center of Gravity. One important step in validating a ground based shuttle launched configuration is checking the compatibility of the proposed payload/vehicle combination with the shuttle payload bay cg envelope. The possible payload/vehicle

Table 2.4.1-2 Airborne Support Equipment (ASE) for Ground-Based SCB OTV System

WEIGHT AT LAUNCH (LBM)

	PAYLOAD ONLY	PAYLOAD & AUX. TANK	PAYLOAD & STAGE	STAGE ONLY
SCB EQUIPMENT				
COMMON GFE	323	323	323	323
FITTING ALLOWANCE	-675	-675	-675	-675
MISC.	998	998	998	998
PAYLOAD SUPPORT EQUIPMENT	936	100	100	-
ATTACH FTGS.	836			-
P/L KITS	100	100	100	-
CONTRACTOR - FURN. STRUCTURE	- *	- *	- *	-
AUX. TANK EQUIPMENT	-	4161	-	-
ATTACH FTGS.	-	1086	-	-
FLUID SYSTEMS, ETC.	-	285	-	-
CONTRACTOR - FURN. STRUCTURE	-	2790	-	-
OTV RETURN EQUIPMENT	-	-	6068	6068
ATTACH FTGS.	-	-	1705	1705
PRESS. SYSTEMS, TOOLS	-	-	370	370
CONTRACTOR - FURN. STRUCTURE	-	-	3993	3993
TOTAL	1259	4584	6491	6391

* INCL. IN PAYLOAD WEIGHT

- MANNED SCAR SUBSYSTEMS
- 1500° B/W, 1.5 T/D BALLUTE (33 FT. DIA.)
- SIZED FOR MULTI-MANIFEST MISSION

STRUCTURES	LBS
PROPULSION SYSTEMS	3605
THERMAL CONTROL AND PROTECTION	1251
GUIDANCE, NAVIGATION, AND CONTROL	994
COMMUNICATIONS/DATA HANDLING	115
ELECTRICAL POWER	409
SPACE MAINTENANCE	611
WEIGHT GROWTH	N/A
	976
(DRY WEIGHT)	(7961)
RESIDUALS	526
(INERT WEIGHT)	(8487)
REACTANTS-EPs (INC. RESERVES)	79
PROPELLANTS-RCS (INC. RESERVES)	624
MAIN PROPELLANTS (INC. RESERVES)	45981
FLUID LOSSES	338
(IGNITION WEIGHT)	(55509)
PAYLOAD	11000
CONTRACTOR-FURNISHED ASE	3993
GOVERNMENT-FURNISHED ASE	2398
(LAUNCH WEIGHT)	(72900)
MASS FRACTION	0.828

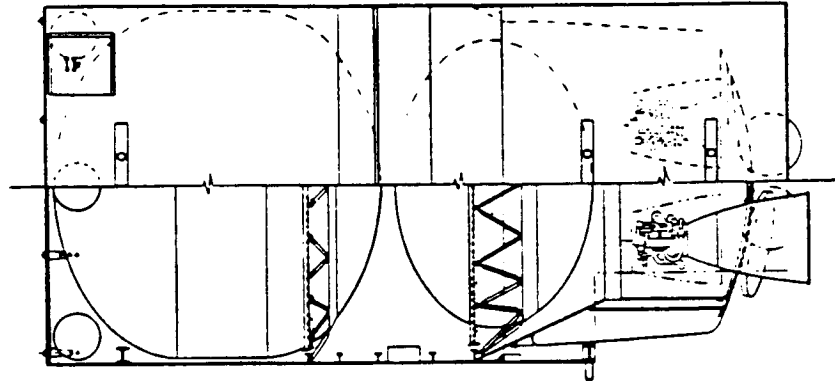


Figure 2.4.1-6 Weight Summary Ground-Based, Ballute-Braked OTV -No. 34

launch options are; 1) OTV with multi-manifest rack and payloads (33 foot ballute) or, 2) OTV only but configured for use with an auxiliary tankset (42 or 66 foot ballutes). Figure 2.4.1-7 shows the launch, abort, and landing cg locations for these options assuming all propellants are dumped prior to abort landing.

Weight Trending. For the above chronological history of ground based ballute braked configurations, figure 2.4.1-8 shows how the weights changed as the configurations changed. Table 2.4.1-3 presents a breakdown of the weight changes.

2.4.1.7 Auxiliary Tankset Configuration and Impact

Auxiliary propellant tanks (tankset) are used on those missions requiring propellant requirements exceeding the lift-off capability of the Space Shuttle.

2.4.1.7.1 Operation Description

When an auxiliary tankset is used with the OTV, the auxiliary tankset and payload are transported to the Space Station on one flight and the OTV is delivered on another flight. At the Station the tankset/payload is integrated to the OTV and the system is launched on its mission. After completion of its mission the OTV/tankset returns to the Station and are restowed in the Shuttle for return to the ground.

2.4.1.7.2 Baseline Configuration for Ground Based OTV Application

Figure 2.4.1-9 shows the auxiliary tankset configured for use with our final configuration ground based OTV described in section 2.4.1.6. The tankset extends the nominal performance capability of the OTV from 12 k-lb to 20 k-lb payload and also provides the capability to perform the manned sortie mission.

Tankset. The design of the tankset is similar to the OTV itself. A graphite/epoxy sandwich shell is used to transmit the payload and tank loads to the ASE. The tanks themselves are supported by graphite/epoxy tubes to minimize boiloff losses. External insulation protects the tankset from wake impingement and ballute radiation heating. The payload and ASE structural interfaces are the same as the OTV; however, the tankset also has the interface needed to mate it with the OTV. Electrical and fluid umbilical interfaces for both the ASE and OTV are also provided.

ASE. Rather than using the OTV's ASE, the auxiliary tankset has been designed with its own ASE so it can be located further aft in the Orbiter bay. A payload length

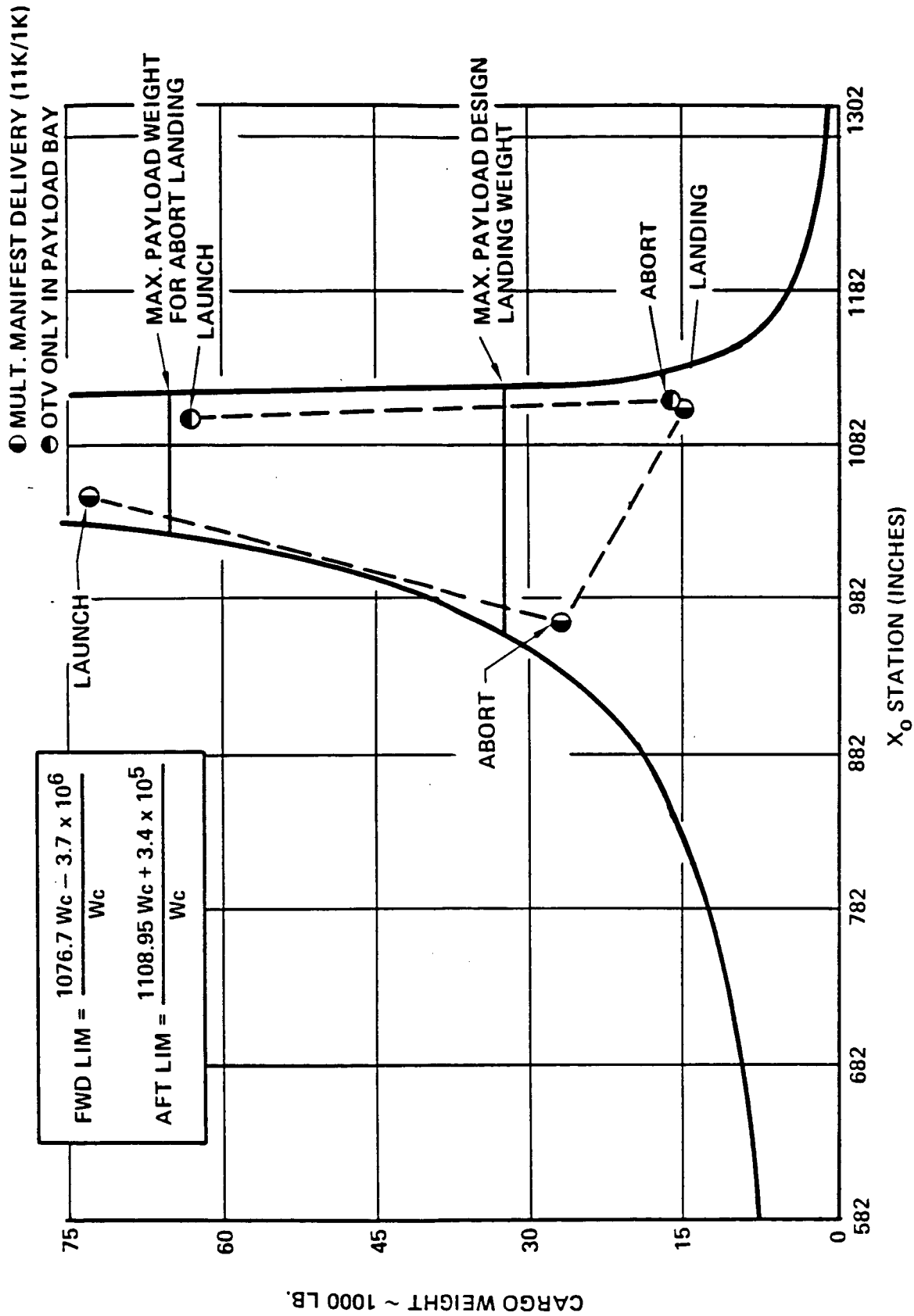


Figure 2.4.1-7 GB Ballute-Braked OTV Launch Orbiter Cargo C.G. Limits Ref.—JSC 07700 Vol XIV

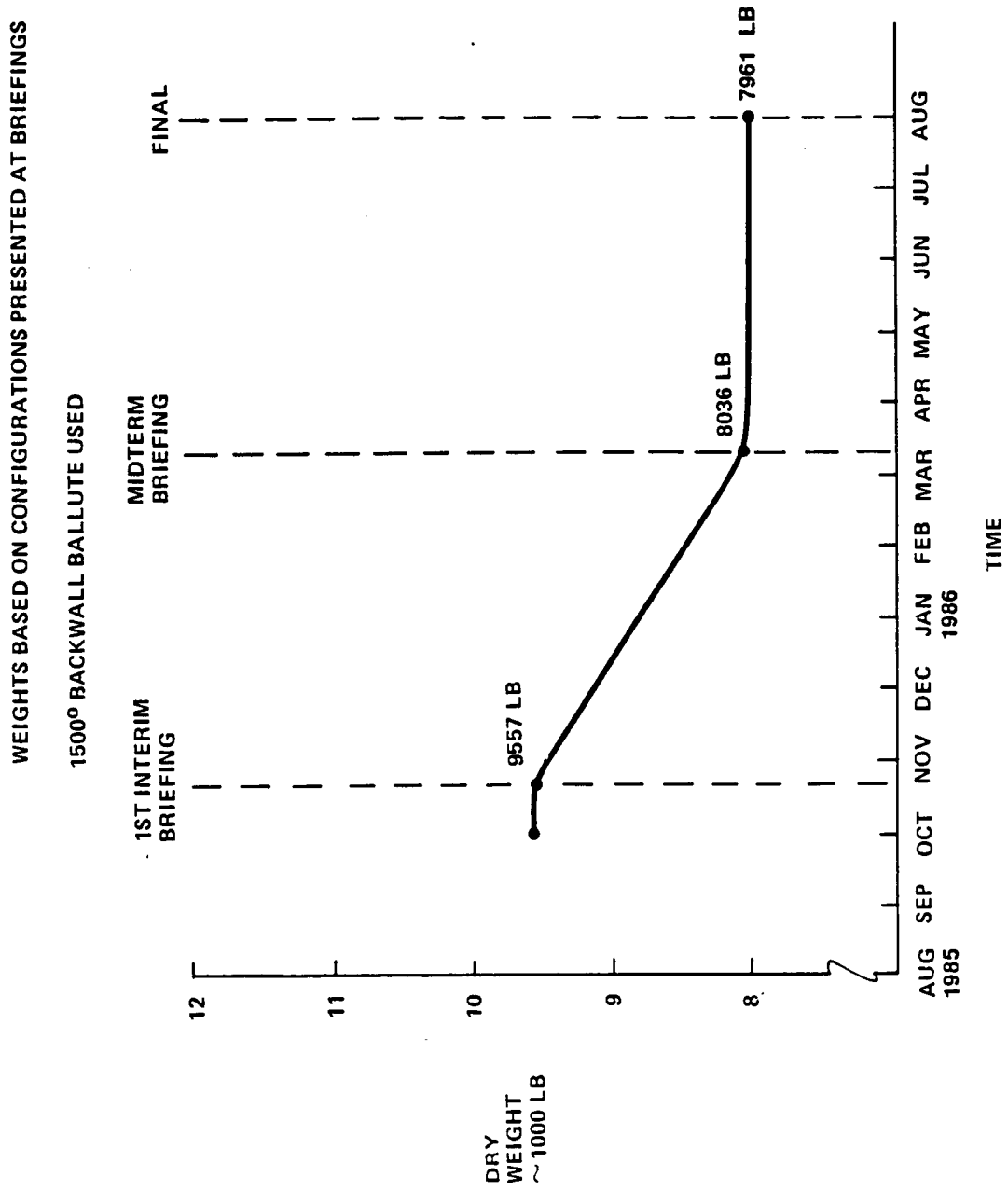


Figure 2.4.1-8 Dry Weight History Ground-Based Ballute-Braked OTV

Table 2.4.1-3 OTV Dry Weight History GB Ballute-Braked OTV –
1500° B/W Temperature Ballute

1ST INTERIM BRIEF→MIDTERM		MIDTERM→3RD QUARTER	
CHANGE	WT Δ	CHANGE	WT Δ
IMPROVE STRUCT. DEFINITION, DECREASE TANK SIZE	-412	IMPROVE STRUCT. DEFINITION, INCREASE TANK SIZE	-247
BEGIN USING 1500° BALLUTE	+341	DECREASE BALLUTE DIAMETER	-123
DECREASE BALLUTE INSULATION	-893	DECREASE TPS AREA AVIONICS –	-128
USE SINGLE THREAD AVIONICS	-154	USE COST OPTIMUM WITH MANNED SCAR	+69
USE COST-OPT ELECT POWER	-20	USE MANNED SCAR ELECT. POWER	+59
DECREASE NO. OF RCS THRUSTERS	-17	ADD RCS TANKAGE + PLUMBING	+81
IMPROVE ENGINE WEIGHT	-32	NO CHANGE IN ENGINES	Ø
MISC PLUMBING CHANGE-COST-OPS	-135	UPDATE PLUMBING TO MAN-RATED	+314
WEIGHT GROWTH ADJ	-199	WEIGHT GROWTH ADJ	-67
TOTAL (LBM)	-1521	TOTAL (LBM)	-42

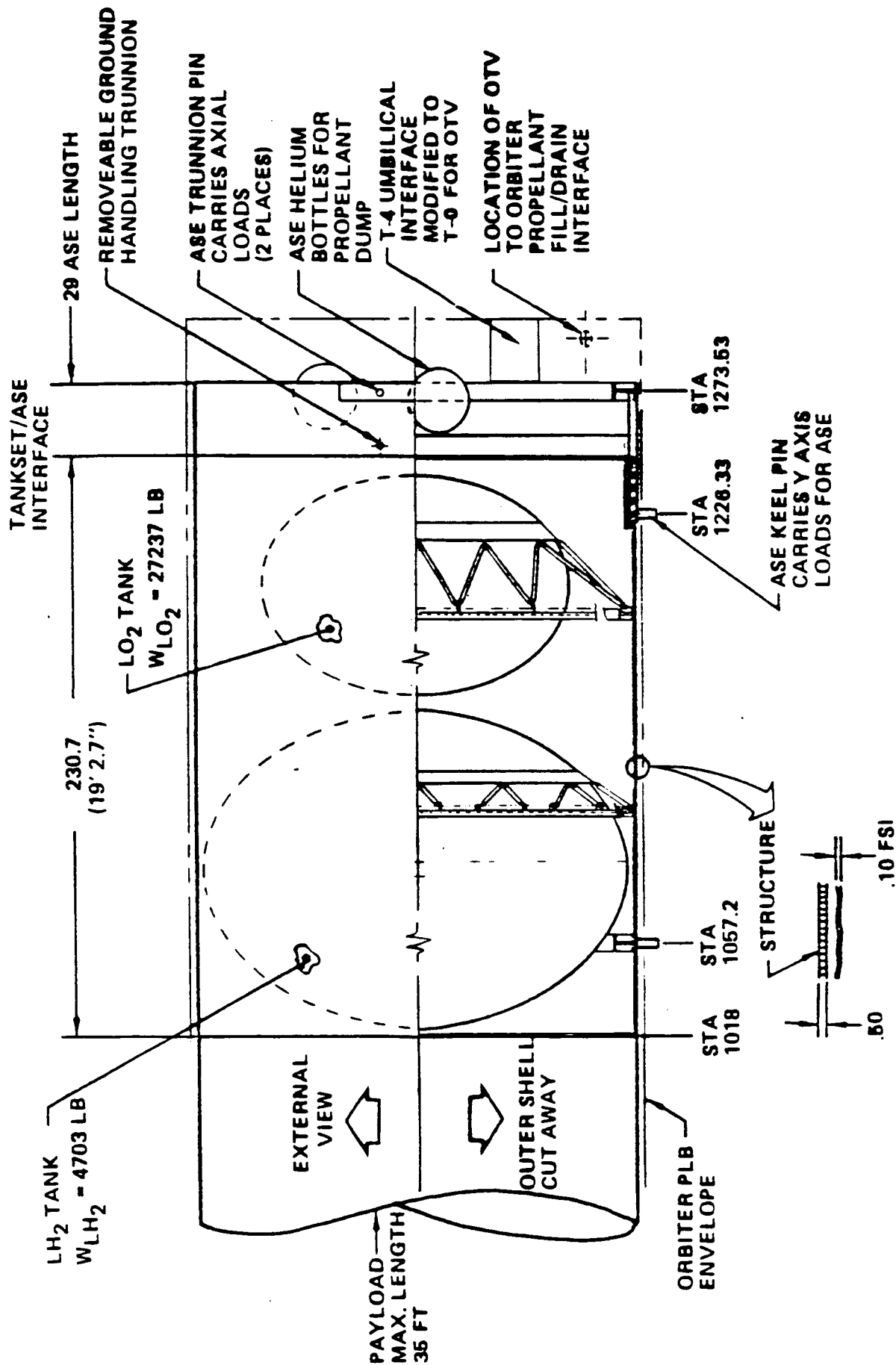


Figure 2.4.1-9 Auxiliary Tankset Ground Based Ballute Braked OTV

of 35 feet can be accommodated with this design. Deployment of the tankset is via the RMS rather than rotating the ASE. This was selected to maximize payload length. The ASE performs the same propellant fill/drain/dump and health monitoring functions as the OTV ASE.

The ASE has two trunnions which transfer X and Z loads to the Orbiter. We have assumed that the payload has a set of trunnions to carry Z loads so it does not have to be cantilevered from the tankset. There is a keel pin both on the ASE and on the tankset. The keel pin on the ASE provides a statically stable system when the ASE is returned to the ground after delivery of the tankset. This keel pin reaches forward from the ASE body to the Orbiter's most aft keel pin position. The pin support beam is relatively flexible compared to the tankset shell, and so, does not transmit primary yaw loads. Primary yaw loads are transmitted to the Orbiter via the keel pin on the tankset. The keel pin is located to avoid exceeding the Orbiter's X load carrying capability for the ASE's trunnions due to axial loads and yaw coupling loads. A payload cg position one half the payload length was used to determine this location.

Impact on Ballute Sizing. Three different aeromaneuver configurations are possible when using auxiliary tanksets; (1) the OTV alone goes through the aeromaneuver after a 12 klb delivery mission, (2) the OTV plus tankset after a 12-20 klb delivery mission, or (3) the OTV, tankset and crew module goes through the aeromaneuver. Each of these configurations have different weights and cg positions and; therefore, require different ballute sizes. Figure 2.4.1-10 shows the three configuration options and their corresponding ballutes. The 66 foot ballute ensures no wake impingement heating of the return payload; however, the wake heating boundary for the 42 foot diameter ballute intersects the auxiliary tankset. The tankset is insulated externally with AFRSI to preclude overheating the structure.

Figure 2.4.1-5 showed the ballute sizing criteria for each of these configurations.

Weights. Figure 2.4.1-11 presents a weight summary for a 7.5 klb return payload manned sortie mission involving the main stage and auxiliary tank. Included in the weights are increases in avionics, electrical power and propulsion systems to man-rate the vehicle, as well as increased ballute and TPS weights reflecting a 66 foot ballute. All other OTV elements are the same as the ground based OTV multi-manifest stage elements. The auxiliary tankset structures includes body shell, support rings, tankage and tankage support. Thermal control includes tank insulation. Propulsion system includes all manifolds and manifold interfaces. Data handling and electrical power

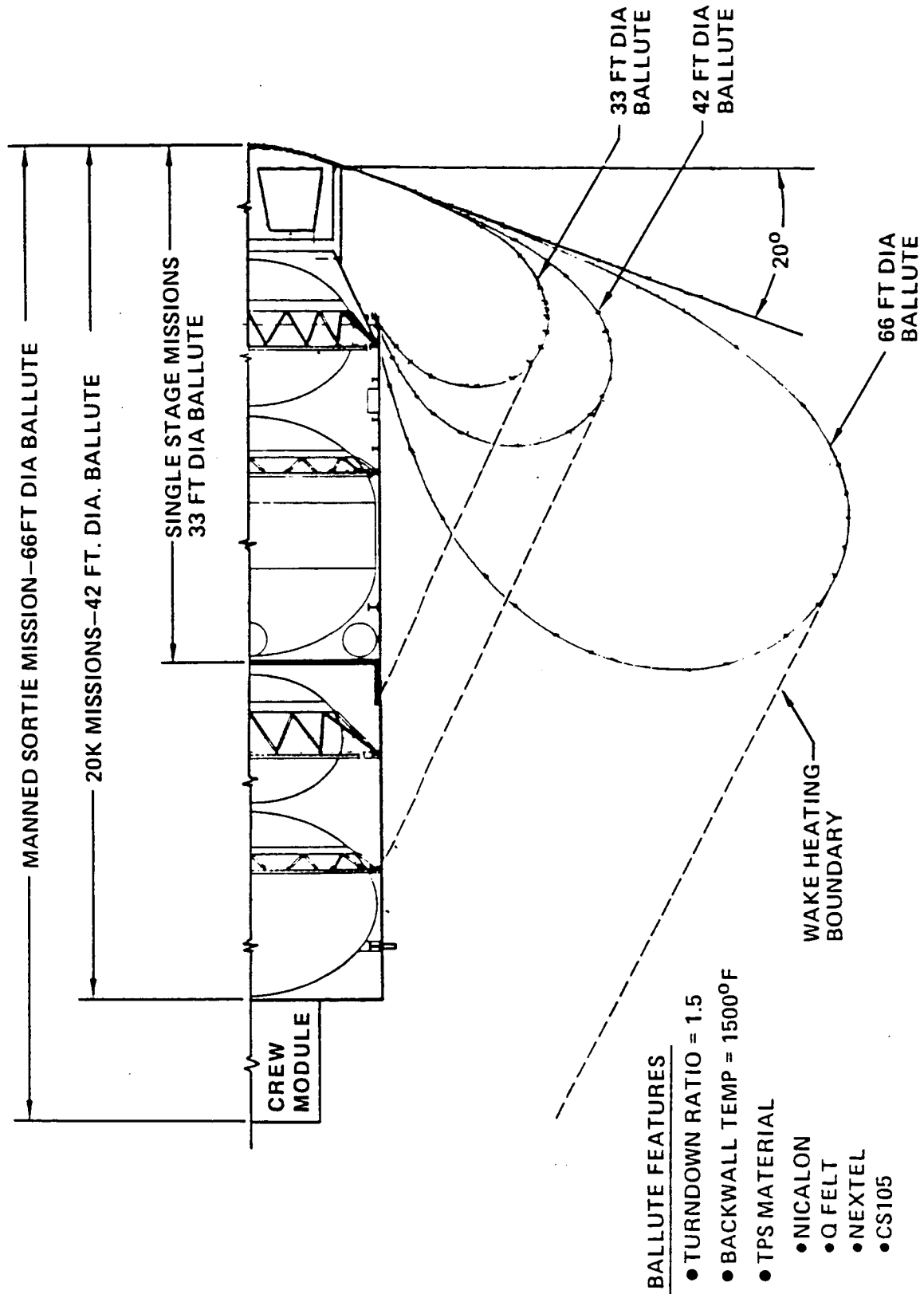


Figure 2.4.1-10 Ballute Aeroassist Provisions Ground Based OTV

- WEIGHT IN POUNDS
- MAN-RATED SUBSYSTEMS, ADDITIONAL RCS TANKAGE
- 1500° B/W, 1.5 T/D BALLUTE SIZED FOR 7.5K PAYLOAD RETURN (66 FT. DIA.)

	MAIN STAGE	AUX. TANKS
STRUCTURES	4494	1830
PROPULSION SYSTEMS	1348	410
THERMAL CONTROL	1521	175
GUIDANCE AND NAVIGATION	135	--
COMMUNICATIONS/DATA HANDLING	469	75
ELECTRICAL POWER	736	110
SPACE MAINTENANCE	N/A	N/A
WEIGHT GROWTH	1217	390
(DRY WEIGHT)	(9920)	(2990)
RESIDUALS	526	230
(INERT WEIGHT)	(10446)	(3220)
REACTANTS--EPS (INC. RESERVES)	37	--
PROPELLANTS--RCS (INC. RESERVES)	1563	--
MAIN PROPELLANTS (INC. RESERVES)	44489	30828
FLUID LOSSES	1832	180
(IGNITION WEIGHT)	(58367)	(34228)
PAYLOAD	--	7500
CONTRACTOR-FURNISHED ASE	3993	2792
GOVERNMENT-FURNISHED ASE	2398	1809
(LAUNCH WEIGHT)	(64758)	(46329)
TOTAL MASS FRACTION	0.813	

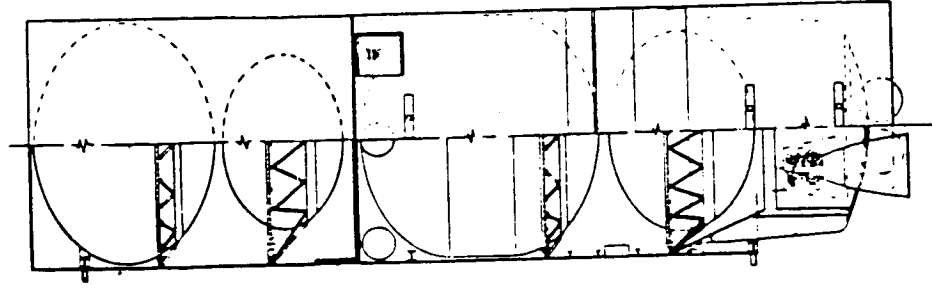


Figure 2.4.1-11 Weight Summary Ground Based, 1½ Stage, Ballute-Braked OTV—No. 36

subsystems include wiring, data bus, and interfaces between the OTV and payload, as well as propellant usage monitoring instrumentation.

Center of Gravity. Figure 2.4.1-12 shows the launch, abort, and landing cg locations in the Orbiter bay for the tankset with a 20 klb payload and the tankset alone. Although the auxiliary tankset only condition exceeds the aft cg envelope, multiple manifesting with additional payloads to fully utilize the payload bay would correct this problem. Abort conditions reflect complete dumping of propellants prior to abort.

2.4.1.7.3 Alternate Configurations

Several alternate auxiliary tankset designs were configured for the system level trades discussed in Volume III. The major options are shown in figure 2.4.1-13. The integral tankset concept with 4 tanks provides a lower cg location for small propellant loads because it is a shorter stage than a two tank system. However, as the propellant load increases the weight penalty for using cylindrical tanks increases. For ballute braked vehicles and for the propellant loads considered the weight penalty more than offsets the length benefit so the two tankset configuration provides a lower OTV/tankset cg location.

The jettisonable concept shown provides better performance than an integral concept but imposes the complexities of staging and disposal of the tanks.

The integral 4 tank arrangement was initially selected to conduct system level trades. The final auxiliary tankset made use of 2 tanks because of better performance characteristics.

2.4.1.8 Configuration for 65k STS

During the first part of the follow-on work to the Phase A OTV study, the sensitivity of the OTV systems to the launch capability of the shuttle was studied. For this analysis, a down-sized version of the ground-based OTV was studied, for launch in a shuttle with 65,000 lb payload capability. This configuration is shown in figure 2.4.1-14. All of the major subsystems on this vehicle are similar to those on the larger GB OTV, as well as design groundrules and features. The ballute sizing groundrules are also the same. The smallest ballute, 33 ft diameter, is sized by turn-down ratio criterion, and is used on the single stage delivery missions. The next size is 36 ft diameter, sized by a wake impingement criterion, and is used when the small auxiliary tankset is returned. When a large auxiliary tankset is used, a 43 ft diameter ballute is required for minimum wake impingement on the tankset. When a crew module is returned with the large

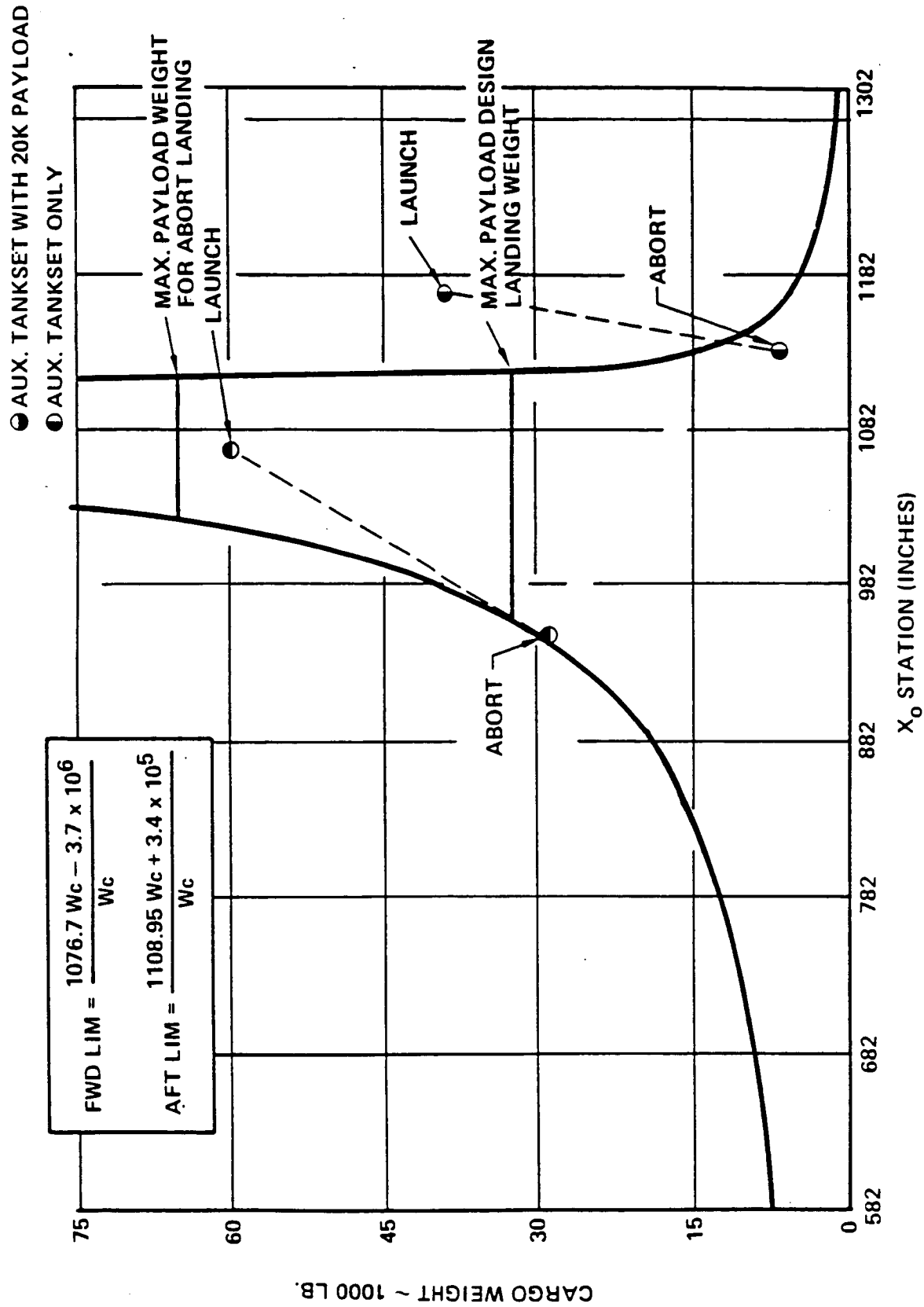


Figure 2.4.1-12 GB Auxiliary Tank Launch Orbiter Cargo C.G. Limits Ref.—JSC 07700 Vol XIV

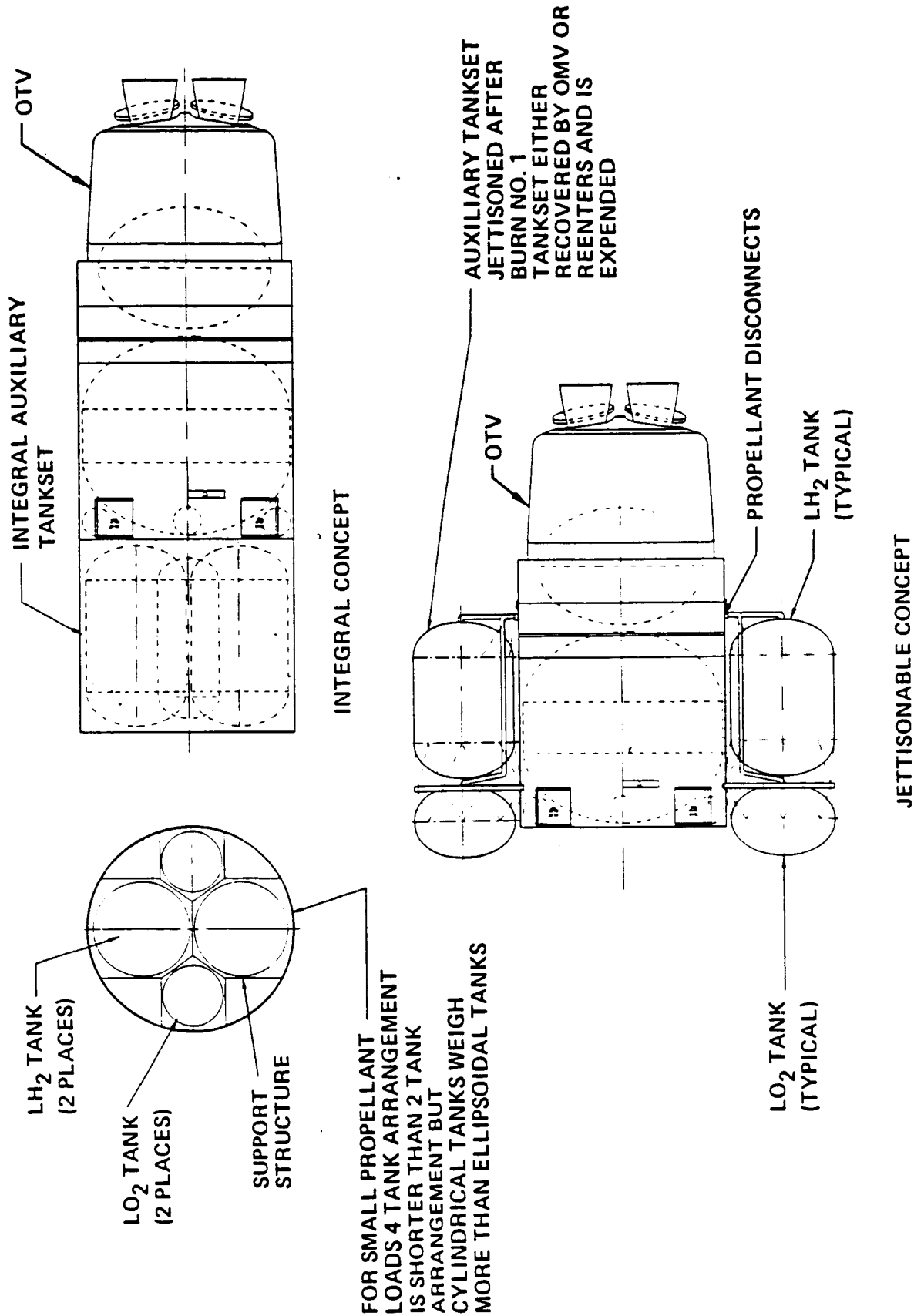
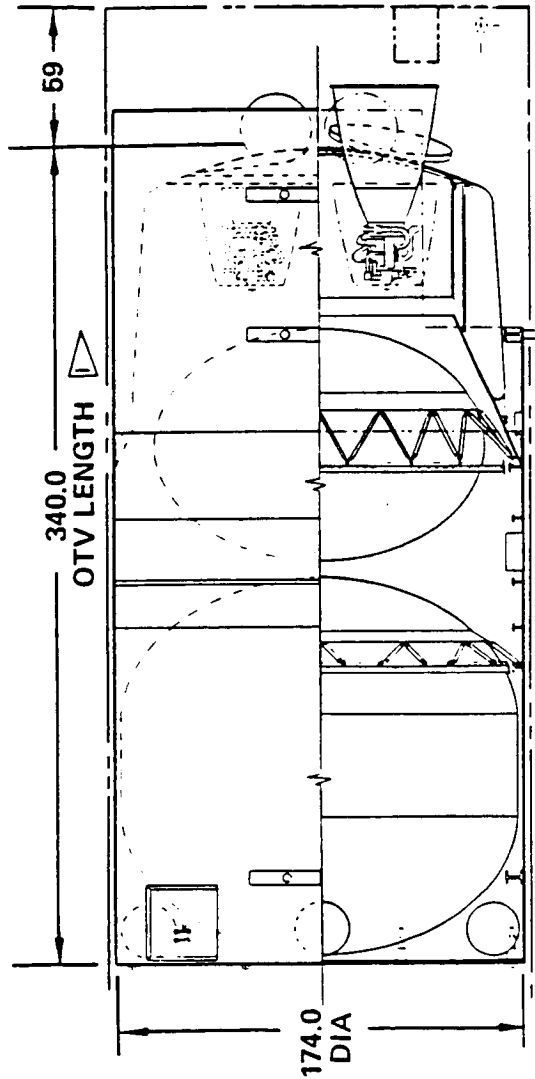


Figure 2.4.1-13 Alternate Auxiliary Tanksets Ground Based OTV



NOT TO SCALE

● DIMENSIONS IN INCHES

FEATURES

● LAUNCHED AND RETURNED IN ORBITER CARGO BAY

● BALLUTE AREOASSIST-EXPENDABLE

-33 FT. DIA. FOR MAIN STAGE RETURN

-36 FT. DIA. FOR RETURN W/SMALL AUX. TANKS

-43 FT. DIA. FOR RETURN W/LG. AUX. TANKS

-67 FT. DIA. FOR RETURN OF AUX. TANKS AND CREW MODULE

● ADVANCED CRYO ENGINES T = 5000 LBF EACH

● 2 TANKS

WEIGHT SUMMARY (LBM)

MAN-SCAR (33 FT. BALLUTE)	MAN-RATED (67 FT. BALLUTE)
7,784	9,684
40,850	40,850
1,173	1,242
49,807	51,776

● DRY

● MAIN PROP
(TOTAL)

● OTHER FLUIDS

● START BURN

Figure 2.4.1-14 GB SCB OTV Configuration Update-65K Orbiter Launch

auxiliary tankset, a 67 ft diameter ballute is required for aerostability. Summary weights of this smaller vehicle as applied to various missions, are shown in table 2.4.1-4.

2.4.2 Ground-Based ACC Lifting Brake OTV

This section describes the operation and configuration of the ground-based aft cargo carrier (ACC) OTV. This concept involves use of a main stage and auxiliary propellant tank.

2.4.2.1 Operational Description

The ground-based ACC OTV main stage is launched in the aft cargo carrier. For missions involving ≤ 8.4 k lbm, the payload is launched in the Shuttle Orbiter cargo bay. On orbit, the OTV and payload are mated, and the mission is performed similar to other ground-based OTV concepts. Upon return to LEO, the OTV jettisons the lifting brake, then is disassembled and stowed in the orbiter for the return to ground. On the ground, the OTV is refurbished and reassembled, then integrated into the ET ACC for re-launch. For payloads ≤ 8.4 k lbm, an auxiliary propellant tank is required and is launched along with payload in the Orbiter cargo bay. Again, on-orbit assembly of the main stage and auxiliary tank/payload are required.



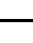

2.4.2.2 Initial Reference Configuration


The initial reference ground-based ACC OTV main stage configuration is shown in figure 2.4.2-1. The OTV structure consists of two fuel tanks and two oxidizer tanks, a central body truss structure, a forward support structure for avionics and electrical power systems, and an aft structure for engine mounting and aerobrake support. The portions of the forward and aft structures that support the LH2 tanks are collapsible to permit stowage in the orbiter payload bay. Avionics and electrical power components are supported by a rectangular composite structure with aluminum mounting doors, located at the forward end of the vehicle. Other body structures include disassembly provisions, payload interface latching provisions, and forward-mounted service connector panels for fluids, gases, and electrical power.

The tanks containing the liquid oxygen and hydrogen are all-welded 2219-T87 aluminum pressure vessels. Each tank has spherical heads, and is supported at the ends by conic ring structures. Each tank also has an internal support rod for transferring axial loads. Because of the disassembly requirement, the LH2 tanks and supports are equipped with latch fittings for easier tank removal. The fittings on the tanks serve also as the attach fittings for stowage of the tanks in the ASE for return to the ground.

Table 2.4.1-4 GB SCB OTV Weight Summary (lbm)

MAIN STAGE SIZED FOR 65K STS

	9K GEO DELIV. 	12K GEO DELIV.	20K GEO DELIV.	7.5K MANNED RETURN
STAGE DRY WEIGHT	7,784	7,886	8,151	9,684
AUX. TANK DRY WEIGHT	--	2,449	3,286	3,286
TOTAL MPS PROPELLANT	40,850	55,620	73,840	82,590
OTHER FLUIDS	975	1,345	1,542	1,804
PAYLOAD	9,000	12,000	20,000	7,500
START-BURN WEIGHT	58,609	79,300	106,819	104,864
ASE	6,391	 10,975	 10,975	 10,975
ACC	--	--	--	--
TOTAL LAUNCH WEIGHT	65,000	90,275	117,794	115,839

 65K STS LIMIT SIZING REFLECTS ASE FOR TWO STS LAUNCHES (1ST-P/L + AUX. TANK; 2ND-STAGE)

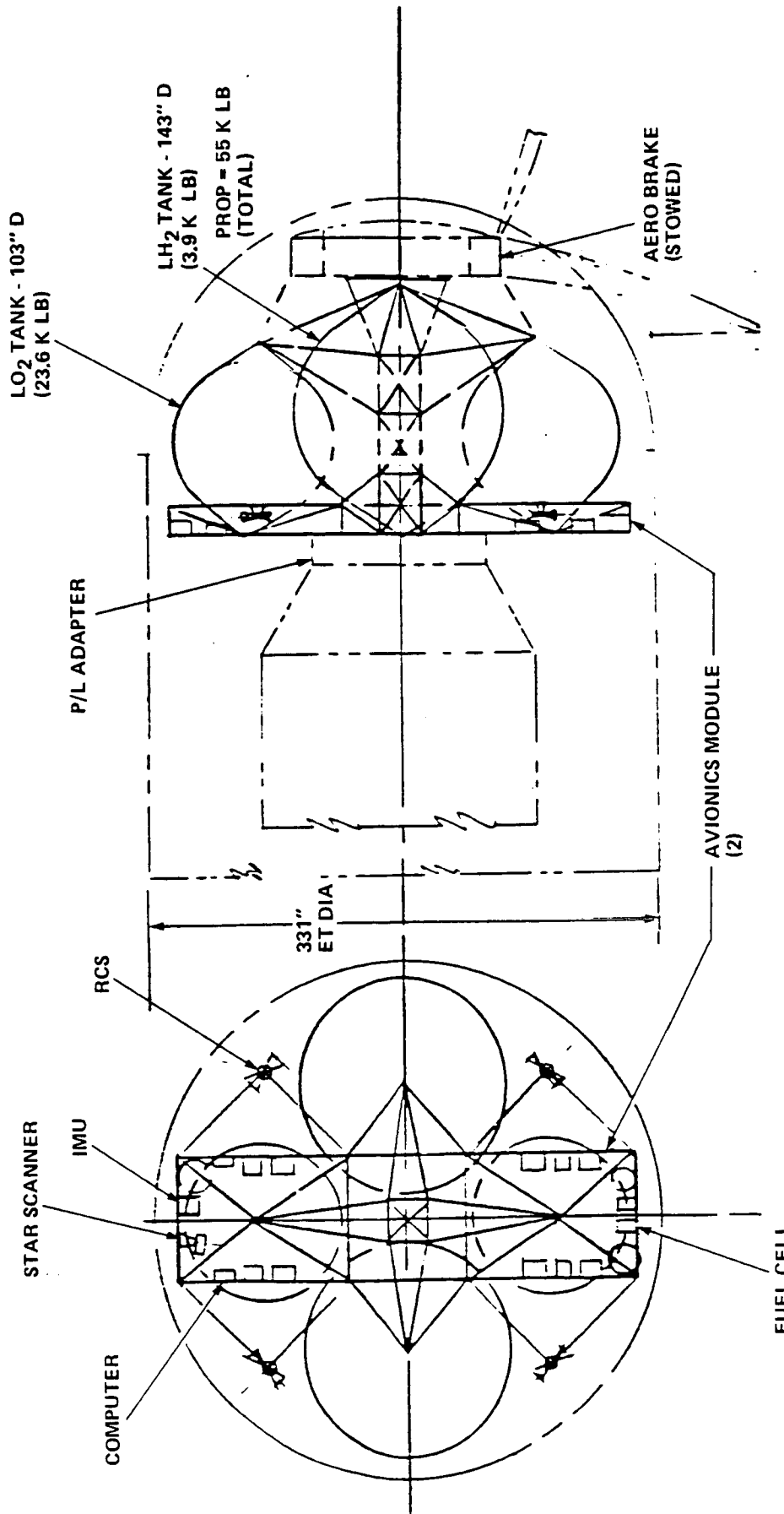


Figure 2.4.2-1 ACC/OTV Concept –
Initial Reference Configuration

Quick disconnect interfaces are also provided for this operation for the fuel and pressurization lines.

Meteoroid/debris shielding is provided by a double wall shielding around each propellant tank. A 0.006 in outer wall is located 6.0 inches from a 0.01 in backwall around each tank. This arrangement poses a significant problem in handling the main tanks, however, especially in disassembly and stowage on-orbit.

Main propulsion is provided by a single RL10-IIB LO2/LH2 engine, and attitude control is provided by a blow-down hydrazine system, with four thruster modules mounted on deployable support arms. All propellant feed systems are similar to those of the SCB ground-based OTV, except for extra disconnects required for removal of the LH2 tanks for stowage in the orbiter. Pressurization of the tanks is accomplished using an autogenous pressurization system similar to that of the SCB ground-based OTV system. Thrust vector control is also similar. The RCS thruster support arms must be collapsible in order to stow the OTV back in the orbiter cargo bay. RCS tankage, thrusters, and other hardware is similar to that on other OTVs.

The aerobrake is a 40 foot diameter symmetric lifting brake, with a 12 foot diameter central rigid heat shield, and a deployable fabric-membrane/composite-rib structure as the rest of the brake. The fabric membrane is of KEVLAR cloth, since the fabric temperature is limited to 600 degrees F (due to radiative heating from the backwall to the vehicle). The sixteen brake ribs are of graphite/polyimide composite structure, and are tailored to minimize deflections under aeromaneuver loading conditions. The brake design is similar to that of the space-based lifting brake, including the design of the central heat shield over the main engine. In this case, however, the shield has only one engine door.

Thermal protection of the lifting brake is similar to that of the space-based lifting brake OTV. It consists of an integrally woven NICALON cloth/Q-felt quilt attached to the brake fabric membrane, and rigid tile thermal protection bonded to the central heat shield.

Avionics and electrical power systems on the GB ACC OTV are similar to those on the SCB vehicle.

A summary weight statement for this configuration is given in table 2.4.2-1.

Airborne support equipment includes those structures and interfaces necessary to support the ACC OTV in the ACC for launch, as well as that equipment necessary to support the vehicle disassembled in the orbiter bay for return to earth. For launch, the ASE consists of a double cruciform beam structure at the aft end of the ET. Interfaces include electrical, data, and fluids, and equipment is provided on the ASE for backup

Table 2.4.2-1 Point Design ACC Lifting Brake OTV Ground Based

STRUCTURE	2078	MPS RESIDUAL	585
LIFTING BRAKE SYSTEM	3918	ACS RESIDUAL	31
AVIONICS	809	EPS RESIDUAL	23
ELECTRICAL POWER	659	(BURNOUT WEIGHT)	(10,146)
MAIN PROPULSION	837	INFLIGHT LOSSES	212
ATTITUDE CONTROL	185	MPS PROPELLANT	55,000
WEIGHT GROWTH	1243	ACS PROPELLANT	545
(DRY WEIGHT)	(9527 LBM)	EPS REACTANT	62
		(GROSS WEIGHT)	(65,965 LBM)

electrical power and control, and subsystem status monitoring. For return in the shuttle cargo bay, the equipment support structure serves as the primary support structure, with ASE cradles to be attached at both ends to secure the vehicle main segment and to support the hydrogen tanks. This arrangement is shown in figure 2.4.2-2. Pressurization tanks are also provided for pressurization of the tanks prior to return to the ground. These return ASE structures must be launched in the shuttle and therefore degrade the overall performance of this concept.

2.4.2.3 Baseline Main Stage Configuration

Two factors influenced the need to update the ACC vehicle configuration. These included the use of two advanced engines in the configuration, and the use of a stretched dedicated version of the ACC shroud. Two engines were incorporated due to cost optimum redundancy results as well as man-rating needs. The cylindrical section of the shroud was allowed to be 42 inches longer than that shown on the original configuration, allowing more length for the OTV based on studies performed by Martin Marietta. Because of this, the thrust structure was moved aft, resulting in a decreased engine gimbal angle for engine-out capability. This also allowed the thrust structure and engines to be included with the aerobrake central heat shield and support in a removable module that can be returned in the shuttle following the OTV mission.

The resulting baseline configuration for the ACC OTV is shown in figure 2.4.2-3. The stage is designed for a maximum propellant capacity of 43,000 lb LO₂/LH₂, and is able to deliver 8400 lb to GEO. In order to perform the larger mission requirements, an auxiliary tankset is added to the vehicle.

Lifting Brake. The lifting brake for the final ACC OTV configuration is a 42 ft diameter deployable flexible brake. The brake is sized to satisfy the criteria of no wake impingement on the vehicle, and also is the largest that can be easily stowed in the available space in the ACC. A 14.5 ft diameter rigid shell forms the center of the brake and is reusable. Doors are located in the dome for engine nozzle deployment. Twenty-four, rather than sixteen, ribs attach to a ring on the dome and support the fabric TPS portion of the brake. The ribs are supported by twenty-four spring-loaded lock-struts which transfer aero loads into a major ring at the vehicle mid-body. These ribs, along with the support rings, struts, and flexible TPS, are expended after each flight, and cannot be returned in the shuttle cargo bay. Other features of this lifting brake are similar to those of the updated SB symmetric lifting brake configuration.

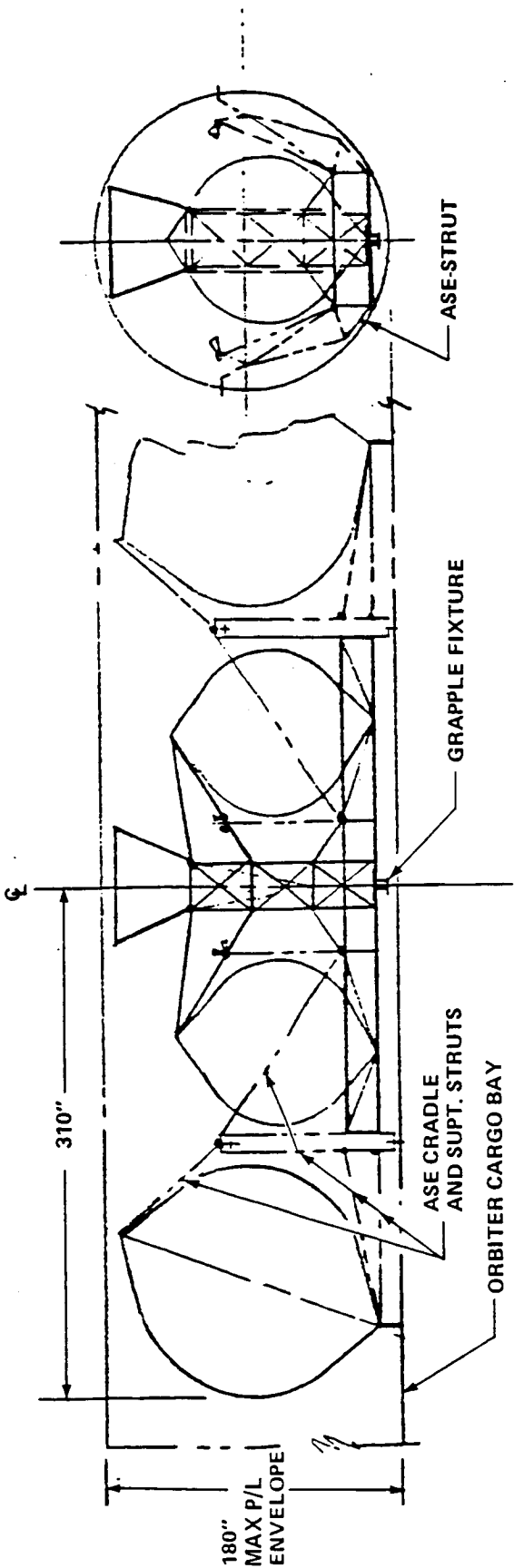
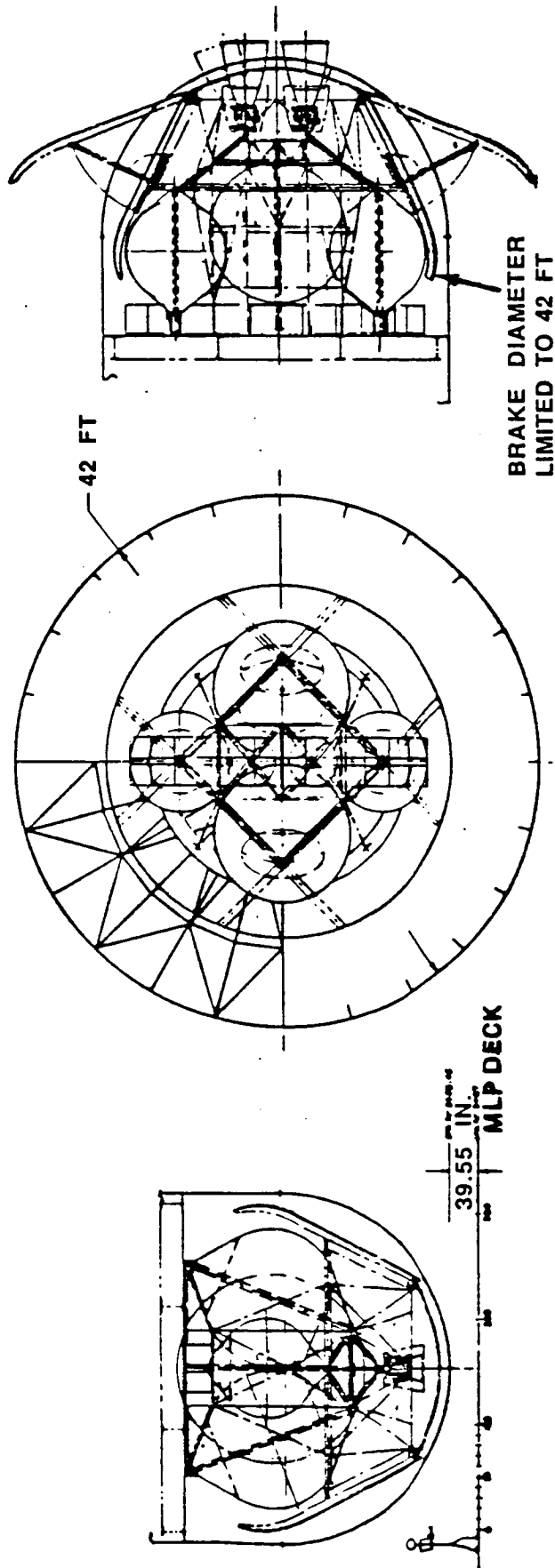


Figure 2.4.2.2 ACC/OTV Recovery Concept

**FEATURES:**

- LAUNCHED IN ET-OCB
- RETURNED IN STS-OCB
- LIFTING BRAKE AEROASSIST, -EXPENDABLE
- ADVANCED CRYO ENGINE T-5000 LBF
- 4 TANKS
- PROPULSION/HEATSHIELD MODULE

WEIGHT SUMMARY (LBM)

	MAN RATED	MAN SCAR ONLY
• DRY	8,430	8,179
• MAIN PROP. (TOTAL)	42,630	42,630
• OTHER FLUIDS	1,169	1,169
• START BURN	52,229	51,978

Figure 2.4.2-3 GB ACC OTV Concept 107 —
Final Configuration

Airborne Support Equipment. The support equipment necessary to support the OTV in the ACC for launch is similar to that in the initial reference configuration. For return to earth, however, the OTV is now disassembled into four parts: the core module, with the central truss structure and LO2 tanks; the two LH2 tanks; and the engine/heat shield module. The core module and the LH2 tanks have support structure built in, and can be attached directly to the shuttle longeron fittings. The engine module must have an ASE cradle for support. That same cradle, however, can be used to transport purge and pressurization Helium, as well as instrumentation for vehicle monitoring for the return trip. The arrangement of the disassembled OTV in the shuttle bay is shown in figure 2.4.2-4. Weights for the launch and return ASE, including government and contractor furnished ASE, are shown in table 2.4.2-2. The weight of the ACC shroud is actually an equivalent weight to orbit, since it is jettisoned before ET burnout.

Weights. A detail weight summary for this vehicle is given in table 2.4.2-3, and summary weights for various mission types are given in table 2.4.2-4.

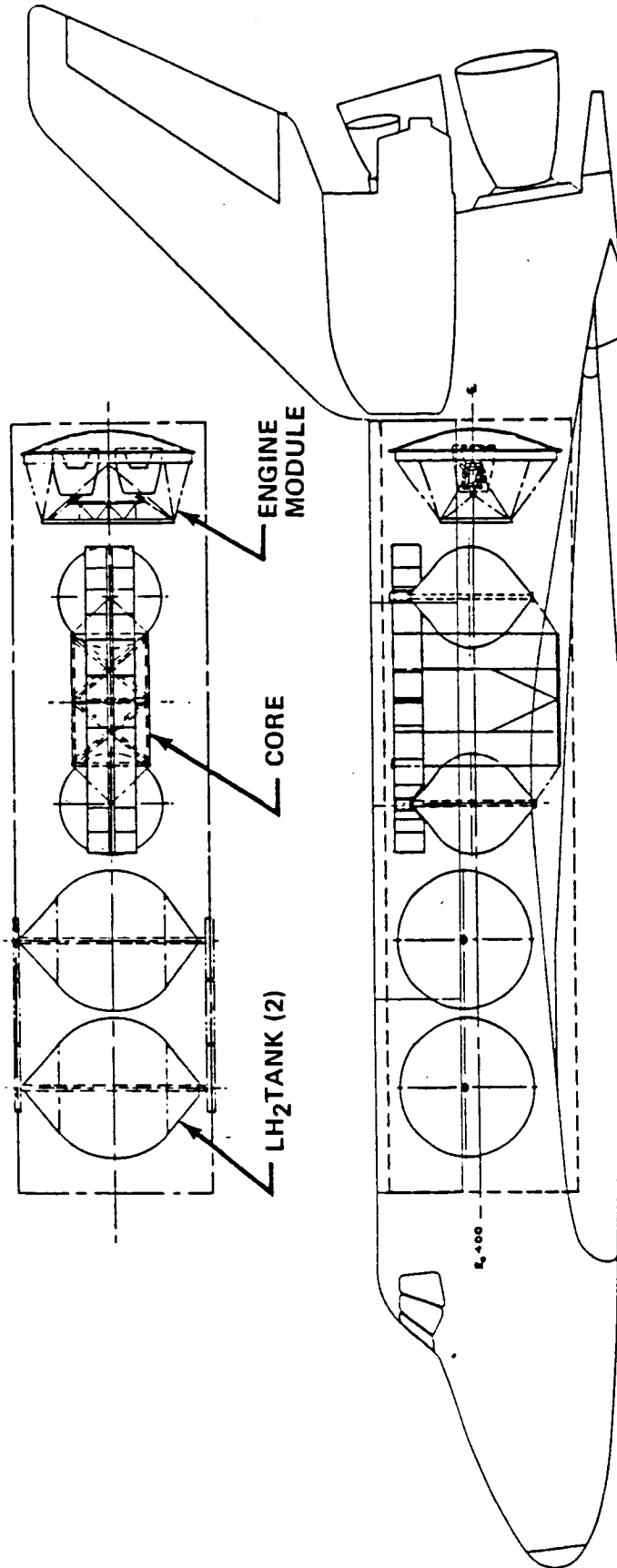
2.4.2.4 Alternate Configuration

Disassembly of the ACC OTV and stowage in the cargo bay for earth return is a major concern. An alternate approach to the updated configuration simplifies these operations through use of a different tank arrangement. This design incorporates a single large spherical LH2 tank and four small spherical LO2 tanks, as shown in figure 2.4.2-7. This configuration is sized for the same propellant loading as the updated configuration, and is only about 300 lb heavier. Whereas the reference configuration, when disassembled, takes up the entire shuttle payload bay, this configuration only fills half of the shuttle bay, as shown in figure 2.4.2-8. This is accomplished by rotating the LO2 tanks forward so that the vehicle can be returned in one piece, rather than four. A weight summary is shown for this vehicle for various missions in table 2.4.2-5.

The LCC comparison of configuration No. 104 indicated it to be about \$1.2 B less than concept 107, however, still more than the SCB GB OTV.

2.4.2.5 Baseline Auxiliary Tankset Configuration

Figure 2.4.2-5 and 2.4.2-6 show small and large auxiliary tanksets to be used with the baseline ACC mainstage to perform missions exceeding the capability of only the main stage. These tanksets are similar to those described for the SCB OTV in that they are launched in the shuttle cargo bay with the payload attached, then integrated with the main stage on-orbit.



FEATURES

- TWO LH₂ TANKS MOUNTED FORWARD
- VEHICLE BUSS WITH AVIONICS AND TWO LO₂ TANKS
- MODULE CONTAINING TWO ENGINES AND HEATSHIELD
- ALL TRUNNION MOUNTED AT BRIDGERAIL FITTINGS TO LONGERONS
- ASE WEIGHT FOR STAGE AND PAYLOAD---6760 LBS

Figure 2.4.2.4 GB ACC OTV No. 107 Return Configuration

Table 2.4.2-2 Airborne Support Equipment (ASE) for Ground-Based ACC OTV System (#107)

	WEIGHT AT LAUNCH (LBM)			
	PAYLOAD ONLY	PAYLOAD & AUX. TANK	PAYLOAD & STAGE	STAGE ONLY
ACC SHROUD, STRUCTURE (EQUIV.)	NA	NA	5000	5000
SCB EQUIPMENT	323	323	323	323
COMMON GFE	-675	-675	-675	-675
FITTING ALLOWANCE	998	998	998	998
MISC.				
PAYLOAD SUPPORT EQUIPMENT	936	100	936	-
ATTACH FTGS.	836	-	836	-
P/L KITS	100	100	100	-
CONTRACTOR - FURN. STRUCTURE	-*	-*	-*	-
AUX. TANK EQUIPMENT	-	4161	-	-
ATTACH FTGS.	-	1086	-	-
FLUID SYSTEMS, ETC.	-	285	-	-
CONTRACTOR - FURN. STRUCTURE	-	1790	-	-
OTV RETURN EQUIPMENT	-	-	5502	5502
ATTACH FTGS.	-	-	2242	2242
PRESS. SYSTEMS, TOOLS	-	-	1710	1710
CONTRACTOR - FURN. STRUCTURE	-	-	1550	1550
TOTAL	1259	4584	11,761	10,825

* INCLUDED IN PAYLOAD WEIGHT

Table 2.4.2-3 OTV Weight Summary (Pounds)

REUSABLE OR ACC OTV - CONCEPT 7

* SPHERICAL HEAD L02/LH2 TANKS

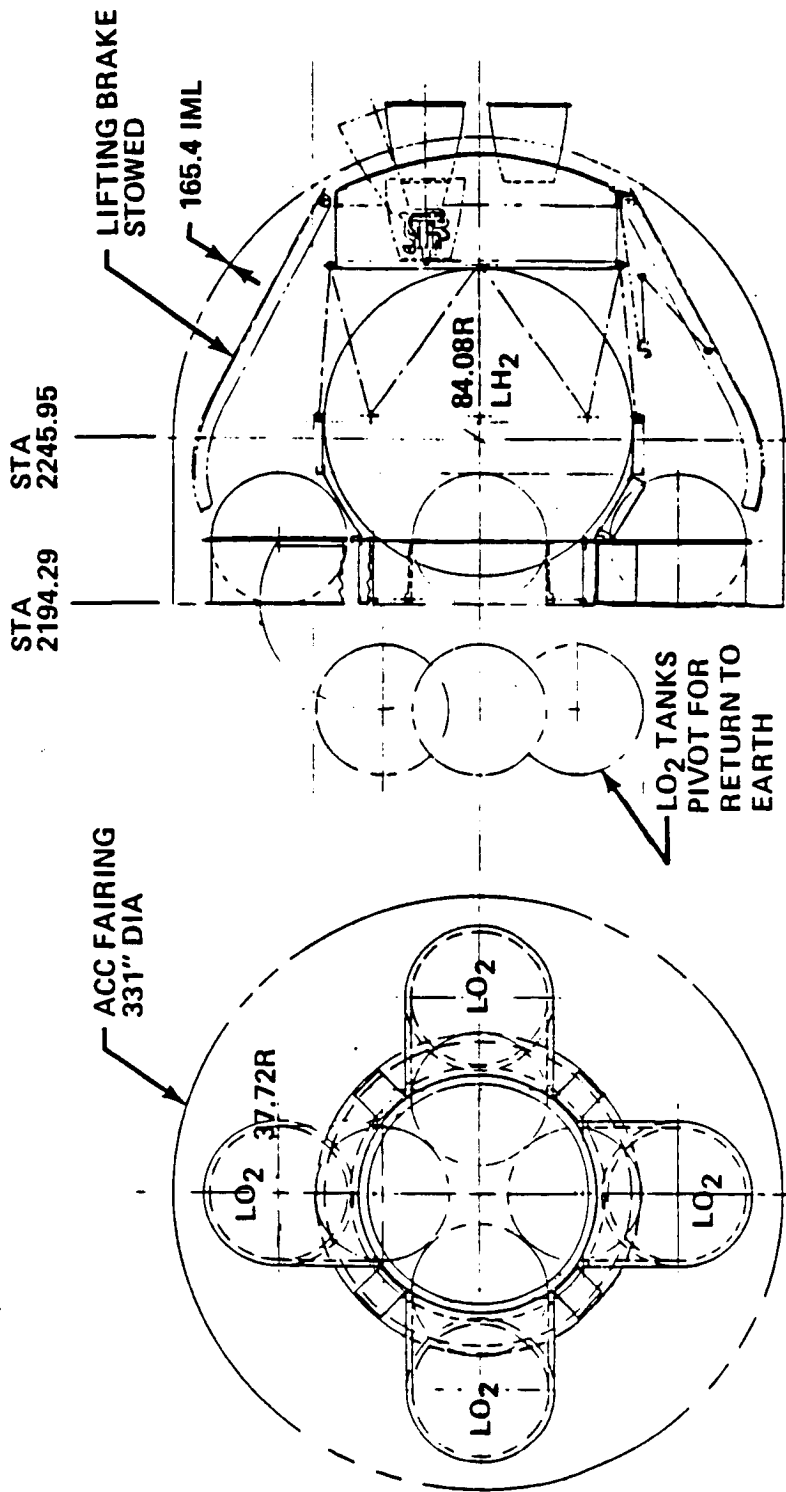
* MAN-SCAR

STRUCTURES AND MECHANISMS	2,052	
RECOVERY SYSTEM (41.5 FT DIA BRAKE)	2,327	
STRUCTURE	1,147	
THERMAL PROTECTION	1,180	
THERMAL PROTECTION AND CONTROL	305	
MAIN PROPULSION, LESS ENGINE	697	
MAIN ENGINES (2 5000 Lbf ASE)	396	
AUXILIARY PROPULSION	251	
GUIDANCE AND NAVIGATION	115	
COMMUNICATION AND DATA HANDLING	409	
ELECTRICAL POWER	601	
WEIGHT GROWTH	1,026	
(DRY WEIGHT)	(8,179)	
RESIDUALS	482	
JETT. ITEMS, INCL GROWTH	2,014	
(INERT EOM WEIGHT)	(6,647)	
JETT. ITEMS, INCL GROWTH	2,014	
EPS REACTANTS	80	
PRESSURANTS	37	
(INERT WEIGHT)	(8,778)	
RCS USABLE PROPELLANTS	1,000	
MPS USABLE PROPELLANTS	42,200	
(GROSS WEIGHT)	(51,978)	

Table 2.4.2.4 GB ACC Concept #107 Weight Summary (Pounds)

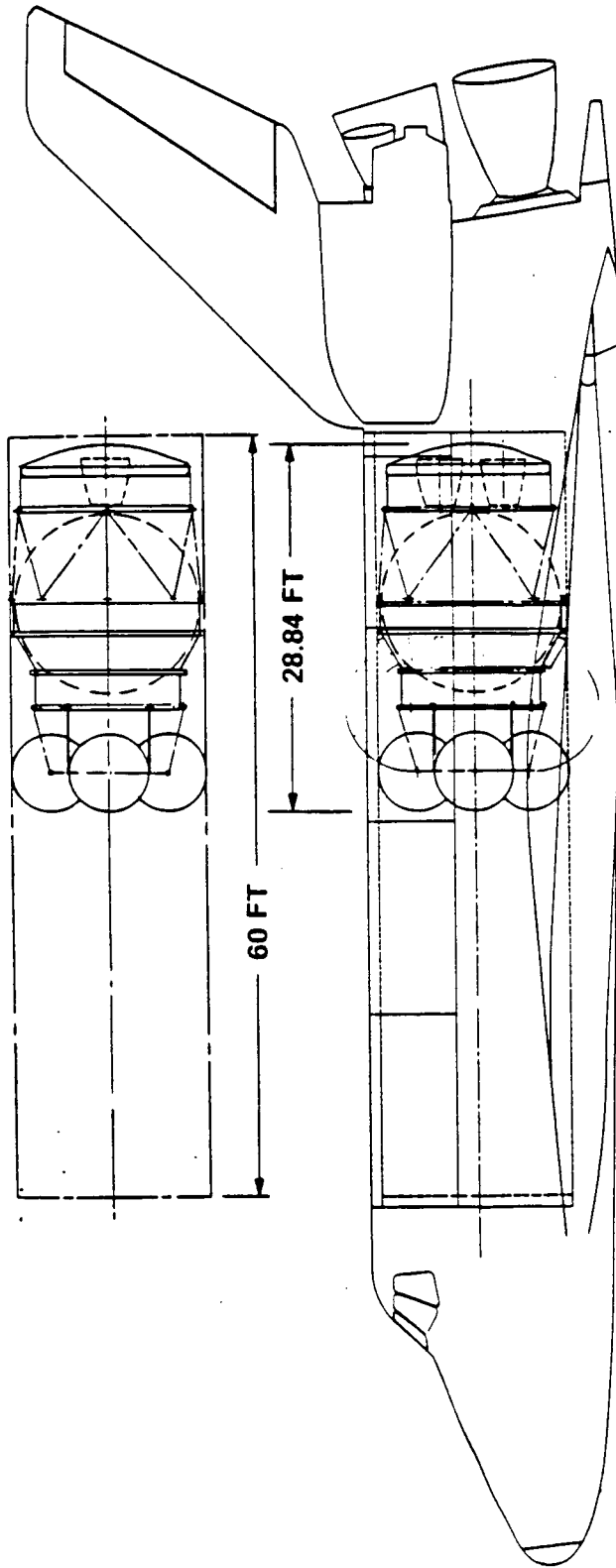
	5.3K GEO DELIV. ¹	8.4 K GEO DELIV.	12K GEO DELIV.	20K GEO DELIV.	7.5K MANNED RETURN
STAGE DRY WEIGHT ³	8,179	8,179	8,179	⁴ 8,179	⁵ 8,430
AUX. TANK DRY WEIGHT	--	--	2,395	2,990	2,990
TOTAL MPS PROPELLANT	38,810	43,040	57,010	73,855	75,455
OTHER FLUIDS	950	781	1,000	1,330	1,209
PAYLOAD ³	5,300	8,420	12,000	⁴ 20,000	⁵ 7,500
START-BURN WEIGHT	53,239	60,420	80,584	106,354	95,584
ASE	6,761	6,761	² 10,409	² 10,409	² 10,409
ACC	5,000	5,000	5,000	5,000	5,000
TOTAL LAUNCH WEIGHT	65,000	72,181	95,993	121,763	110,993

¹ 65K STS LIMIT SIZING² REFLECTS ASE FOR TWO STS LAUNCHES (1ST-P/L + AUX. TANK; 2ND-STAGE)³ REFLECTS MAX. BRAKE SIZE IN ACC⁴ IF BAC BRAKE REQ'T SATISFIED: BRAKE Δ WT + 870 LBS; PAYLOAD Δ WT-870 LBS⁵ IF BAC BRAKE REQ'T SATISFIED: BRAKE Δ WT + 1500 LBS; PAYLOAD Δ WT-1500 LBS



WEIGHT SUMMARY (LBM)			
FEATURES		MAN RATED	MAN SCAR ONLY
• ONE CENTRAL LH ₂ TANK	• DRY	8,751	8,499
• 4 LO ₂ TANKS	• MAIN PROPELLANT (USABLE + RESIDUALS)	42,630	42,630
• MINIMAL DISASSEMBLY FOR PAYLOAD BAY RETURN	• OTHER FLUIDS	1,169	1,169
• EXPENDABLE LIFTING BRAKE AEROASSIST	• START BURN	52,550	52,298

Figure 2.4.2-7 GB ACC OTV Concept 104 (5 Tank Set)









FEATURES

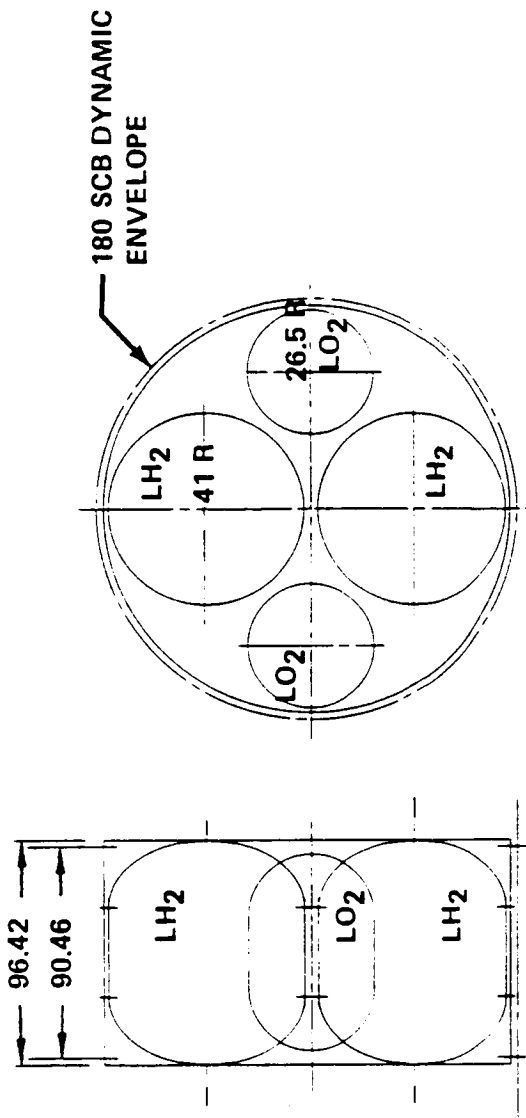
- 4 LO₂ TANKS THAT PIVOT FORWARD AND ARE SECURED
- OTV IS MOUNTED USING STANDARD FITTINGS, 4 TRUNNIONS AND ONE KEEL PIN
- USES 29 FEET OF ORBITER CARGO BAY LENGTH

Figure 2.4.2-8 GB ACC OTV Concept 104 SCB Return Configuration

Table 2.4.2-5 GB ACC Concept #104 Weight Summary (Pounds)

	5.46K GEO DELIV. 	12K GEO DELIV.	20K GEO DELIV	7.5K MANNED RETURN
STAGE DRY WEIGHT	8,499	8,499	8,499	8,751
AUX. TANK DRY WEIGHT	--	2,492	3,090	3,090
TOTAL MPS PROPELLANT	40,030	58,240	75,220	76,930
OTHER FLUIDS	930	1,050	1,347	1,267
PAYLOAD	5,460	12,000	20,000	7,500
START-BURN WEIGHT	54,919	82,281	108,156	97,538
ASE	5,081	 8,729	 8,729	 8,729
ACC	5,000	5,000	5,000	5,000
TOTAL LAUNCH WEIGHT	65,000	96,010	121,885	111,267

 65K STS LIMIT SIZING REFLECTS ASE FOR TWO STS LAUNCHES (1ST-P/L + AUX. TANK; 2ND-STAGE)



• DIMENSIONS IN INCHES

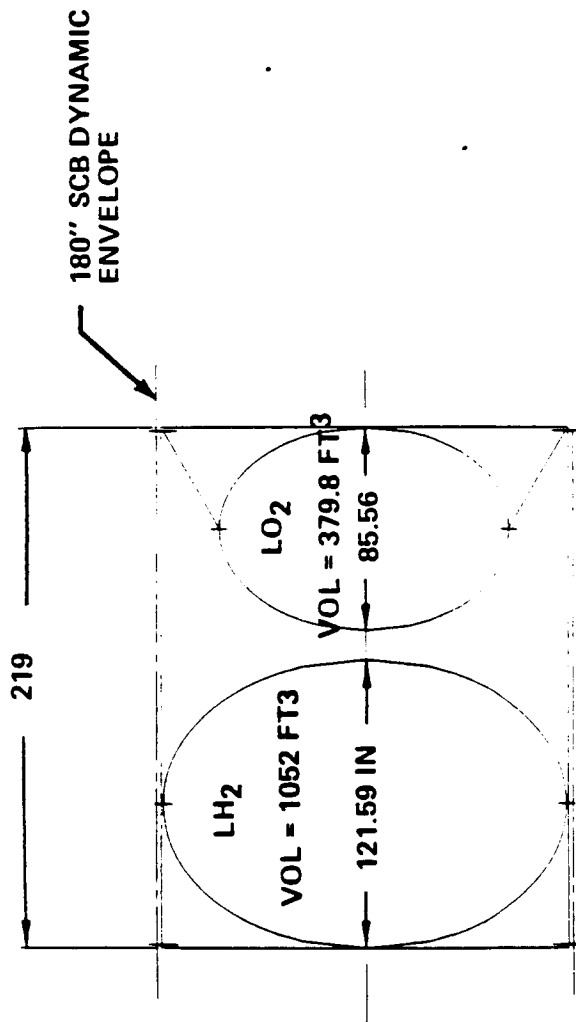
FEATURES

- TWO LH₂ TANKS 0.707 ELLIPTICAL HEADS
- TWO LO₂ TANKS SPHERICAL HEADS
- SCB-CARRIED THRU 4 TRUNNION AND ONE KEEL PIN

WEIGHT SUMMARY (LBM)

• USABLE PROPELLANT	13,800
• INERT	2,543
• TOTAL	16,343

Figure 2.4.2-5 13.8K Auxiliary Tank GB ACC OTV



FEATURES

- ONE LH₂ TANK 0.707 ELLIPTICAL HEADS
- ONE LO₂ TANK 0.707 ELLIPTICAL HEADS
- OCB—CARRIED THRU 4 TRUNNIONS AND ONE KEEL PIN

WEIGHT SUMMARY (LBM)

● USABLE PROPELLANT,	30,000
● INERT	3,220
● TOTAL	34,020

Figure 2.4.2-6 30.8K Auxiliary Tank – GB SCB OTV

OTV-1152

The small tankset is designed to extend the performance capability of the ACC OTV from 8.4 klbm. GEO delivery to 12-klbm GEO delivery. This tankset has four cylindrical tanks with 13.8 klbm total propellant capacity, supported in a GR/EP cylindrical shell. Propellant interfaces to the main stage are located at the perimeter of the 170 inch diameter interface ring, with L0₂ and LH₂ lines on opposite sides of the ring.

The large tankset extends the performance capability to 20 klb GEO delivery or 7.5 klb GEO roundtrip. This tankset has two 0.707 elliptical dome tanks with 30.8k lb propellant capacity. These tanks are also strut-supported within a GR/EP cylindrical shell. Propellant interfaces are similar to those of the small tankset.

2.2.2.6 Configuration Impact for 65K STS

The sensitivity of the ACC OTV system to a 65,000 lb shuttle launch capability was studied in the follow-on portion of the OTV study. The configuration used for this analysis was the same as used for the 72,000 lb lift capability shuttle, which was sized to the maximum envelope of the ACC. This vehicle was shown offloaded to 38,810 lb propellant, with 65,000 lb shuttle lift capability. With this condition, the optimized payload that could be delivered to GEO was reduced to 5300 lb. The summary weights for this configuration are shown in the first column of table 2.4.2-4. No further changes to the stage configuration were made for this sensitivity.

This Page
Intentionally
Left
Blank

3.0 STRUCTURES

The focus of the structures effort has included selection of the most efficient structural concepts, use of proper materials, propellant tankage design and meteoroid/space debris protection for those tanks.

3.1 STRUCTURAL REQUIREMENTS

3.1.1 Key Design Requirements

Structural design requirements for the OTV studies have been taken from applicable sections from References 8 through 13.

References 8, 9 and 10 were used as a composite structural design criteria for all OTV structural systems. Reference 8 was used for all space operations remote from the orbiter. Reference 9 was used to define interfaces and load factors while in the orbiter and 10 was used for the remaining structural requirements applicable to operation in the orbiter. References 11, 12 and 13 were used to define meteoroid and space debris environments at the space station and at GEO.

3.1.2 Main Tankage Design Requirements

OTV propellant tankage structural requirements are summarized in Table 3.1.2-1. In addition to these requirements, an additional requirement for "no explosive rupture in a meteoroid/debris environment" has been applied to any propellant tankage exposed in proximity to manned operations. This is a more severe criteria than the "leak before rupture" criteria and is applied because of the possible catastrophic effect of explosive rupture of a pressure vessel in proximity to manned operations. Explosive rupture is an area of particular concern and will need to be better understood as space transportation technology matures. It is discussed in more detail in Section 3.2.2.

Main propellant tankage associated with the OTV can be classed in three distinct functions, including vehicle main propulsion tankage, propellant transfer tankage, and on-orbit propellant tankage. Design operating conditions for the three tankage functions are given in Table 3.1.2-2.

3.1.3 Body Structure Loading Conditions

The development of body structure preliminary loads considers the following mission scenarios: a reusable delivery mission to GEO with a 11,000 lb multiple

Table 3.1.2-1 OTV Propellant Tankage Structure Design Requirements

- **VOLUME EFFICIENCY AND PROPELLANT ACQUISITION**
- **ENVIRONMENTAL COMPATIBILITY**
 - **LOX COMPATIBLE**
 - **CRYOGENIC TEMPERATURES**
 - **LOADS AND PRESSURES**
 - **METEOROID/DEBRIS**
- **LEAK BEFORE RUPTURE**
- **LOW SYSTEM WEIGHT**
- **DAMAGE TOLERANCE AND REPAIRABILITY**

D180-29108-2-3

Table 3.1.2-2 OTV Propellant Tankage Operating Conditions

	Space-Based Vehicle		Ground-Based Vehicle		Propellant Tanker		On-Orbit Storage Tanks	
	LO ₂	LH ₂	LO ₂	LH ₂	LO ₂	LH ₂	LO ₂	LH ₂
Operating temperature (°F)	-300	-423	-300	-423	-300	-423	-300	-423
Ullage vent pressure (PSIA)	20-22	18-22	20-22	18-22	20-22	18-22	16-20	16-20
Vapor pressure (PSIA)	N/A	N/A	18	18	18	18	N/A	N/A
Repressurization pressure (for return-PSIA)	N/A	N/A	18	18	18	18	N/A	N/A
Design service life (Missions/years)	45/-	45/-	45/-	45/-	100/-	100/-	-/5	-/5
Launch condition	Empty	Empty	Full	Full	Full	Full	Empty	Empty
Manned environment	Yes	Yes	Yes	Yes	Yes	Yes	Yes	Yes
Tank vent to refill	Yes <input type="checkbox"/>	Yes	Yes <input type="checkbox"/>	Yes	Yes <input type="checkbox"/>	Yes	No	No
Min. factor of safety to yield (Oper. temp)	1.5	1.5	1.5	1.5	1.5	1.5	1.5	1.5

☐ Not completely vented☐ Vented on ground

manifest payload including a 1,000 lb payload rack, a reusable delivery mission to GEO with a 20,000 lb payload, and a reusable manned sortie mission to GEO with a 7,500 lb up/7,500 lb return payload. Load factors considered for orbiter liftoff, landing, and boost are per JSC 007700, Vol. XIV. Other loading conditions considered include OTV main engine initial burn, and aeromaneuver, with combined limit load factors of 0.25 and 3.0, respectively. For ground-based vehicle body structures, the governing condition is orbiter liftoff. For space-based vehicle body structure the governing condition is aeromaneuver with a 7,500 lb return payload. For all aerobrake structures, the governing condition is aeromaneuver.

For all body primary structure, an ultimate factor of safety of 1.5 was assumed.

3.1.4 Meteoroid/Debris Design Requirements

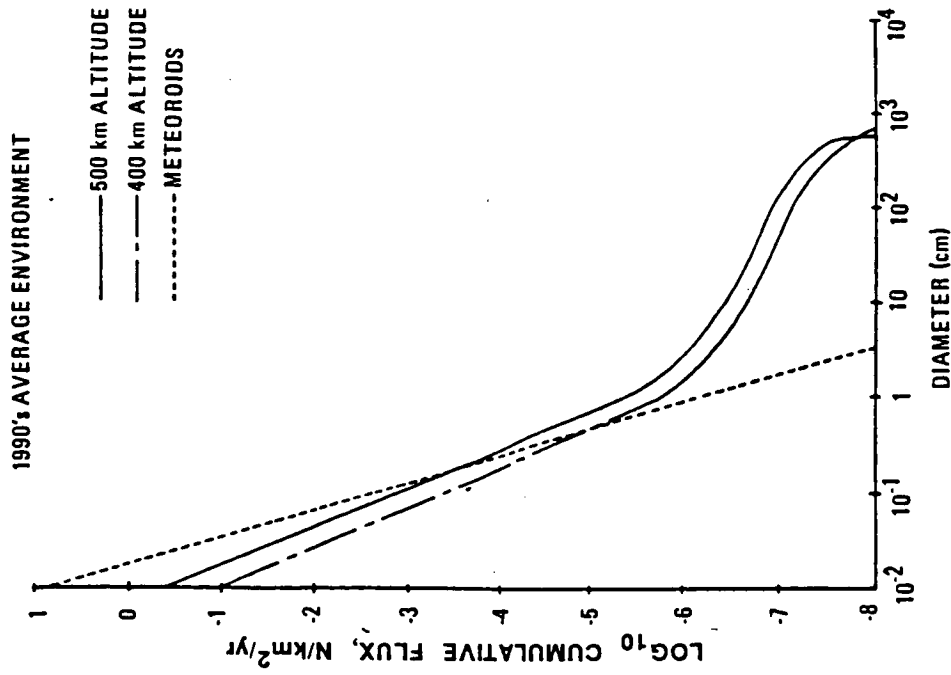
A major consideration in design of reusable space vehicles, and in particular, reusable cyclic pressure vessels, is to ensure protection against meteoroids and man-made debris particles in the space environment.

The meteoroid/space debris environments used in our analyses are shown in figure 3.1.4-1.

The meteoroids environments/flux reflected in our design and analysis correspond to those shown in figure 2-13 from NASA TM 82478 as cited in NASA TM 82585 per phase I Groundrules References No. 9. The debris flux was taken from JSC-20001 for 500 km altitude.

Minimum meteoroid/debris survival probability goals and design exposure times employed in this study are shown in Table 3.1.4-1. The minimum survival probabilities listed for the three distinctly different tankage classifications were selected to be compatible with the associated systems requirements. The goal of 0.999 per mission is essential for vehicle tankage to permit the vehicle to realize an overall probability of 0.995 for mission completion. The overall probability of 0.995 for vehicle reliability per mission was the result of cost optimization analysis. The design goals for the tanker and storage tanks were somewhat arbitrarily selected as being less critical than that required by the vehicle tankage.

The design exposure times shown are indicative of a manned sortie mission for the vehicle tankage, assuming storage in a hangar between missions at LEO, a propellant delivery to LEO for the transfer tankage, and a long-term stay at LEO for the storage tankage.



DEBRIS

JSC-20001, "ORBITAL DEBRIS ENVIRONMENT
FOR SPACE STATION", D. J. KESSLER, 1984.

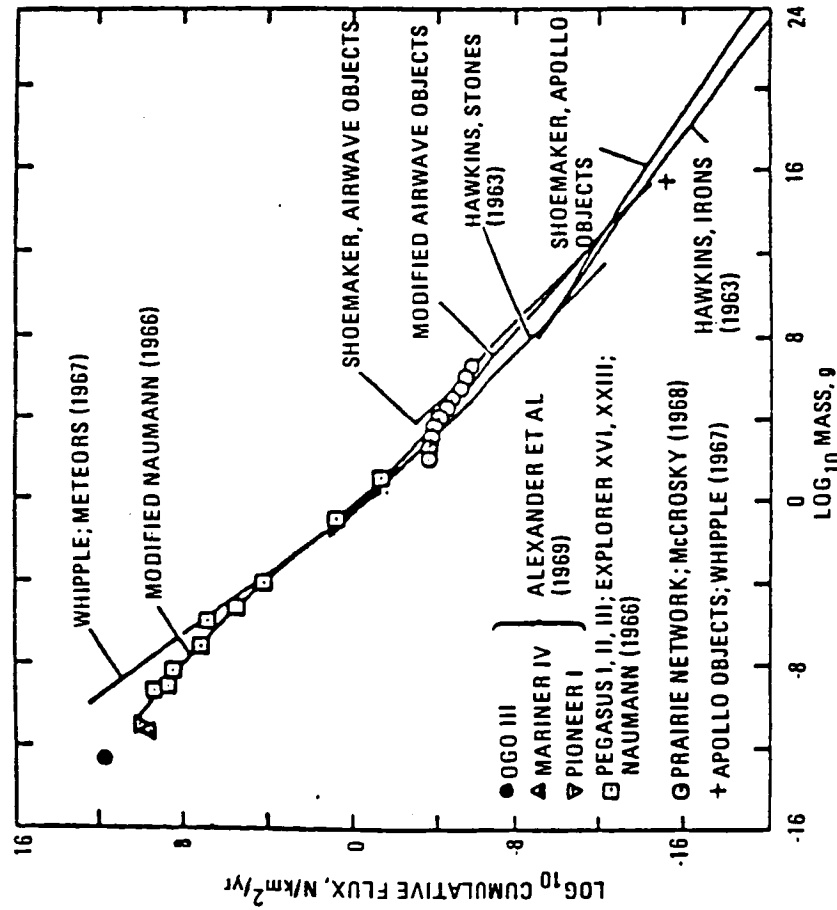


FIGURE 2-13. TERRESTRIAL MASS-INFLUX RATES OF METEORIODS.
N IS THE FLUX OF PARTICLES WITH MASS GREATER
THAN m (2-29).

METEORIODS

NASA TM 82478, "SPACE AND PLANETARY ENVIRONMENT
CRITERIA GUIDELINES FOR USE IN SPACE VEHICLE
DEVELOPMENT" REV 1982 VOLUME I

Figure 3.1.4-1 Meteoroid/Space Debris Environments

Table 3.1.4-1 Meteoroid/Debris Protection Design Requirements

	Min. Survival Probability	LEO Exposure Time (Days)	GEO Exposure Time (Days)
Vehicle Tankage	.999	0.5	18.0
Prop. Delivery Tanker	.997	1.0	0
Orbital Prop. Storage Tankage	.995	1825.0	0

Contribution to Overall Vehicle Survival Probability

Predominant Debris Environment

Predominant Meteoroid Environment

3.2 STRUCTURES DESIGN APPROACH

3.2.1 Main Tankage Design Approach

The tanks containing liquid hydrogen and liquid oxygen are all-welded 2219-T87 aluminum pressure vessels. They are designed by room temperature pneumostatic proof test conditions corresponding to critical flight conditions and to desired critical crack length capability at operating stress. This is to assure the mission service life requirement with low probability of leakage subsequent to a successful proof test and leakage check. For ground-based systems, the tanks are designed using "best fit" fracture mechanics design data, whereas for space-based systems, more conservative "lower boundary" data is used.

Figure 3.2.1-1 shows critical crack length versus operating stress for 2219-T87 aluminum tankage. This curve was developed from data for the indicated alloy at liquid nitrogen temperature from NASA CR-135369, "Analysis and Tests of Deep Flaws in Thin Sheets of Aluminum and Titanium", R. W. Finger, April 1978. Indicated on this plot are three companion sets of operating stresses with associated proof test approaches for cryogenic propellant tanks. The higher set of operating stresses correspond to the lightest weight tanks which could be obtained from 2219 by demonstrating the required residual fatigue life by conducting the required proof tests at the usage temperatures for the individual tanks. The corresponding critical flaw size is approximately 2.5 inches. Tanks designed to these stress levels would be expected to fatigue to leak or rupture if damaged even slightly following proof test. Also they could not be repaired if damaged in manufacturing or in service.

Furthermore, the associated damage tolerance is not adequate for large pressurized tanks spending their life in close proximity to the space station. The mid range indicated stress levels would permit conducting the required proof tests at room temperature with associated increases in damage tolerance and fatigue life. The lower indicated stress level is half the room temperature yield stress which would permit conducting a room temperature proof test of 2 x MEOP and would result in a critical crack length of approximately 8 inches. Fracture mechanics analysis shows that tanks designed to this stress level would require approximately 5,000 full pressure cycles to grow a 1/2 inch thru crack to rupture. Since a 1/2 inch thru crack would cause leaking and loss of pressure, it might appear that this statistic is meaningless. However, what it does mean is that a simple on-orbit mechanical repair could be made to the tanks following a reasonable sized penetration and that it would still have the residual fatigue

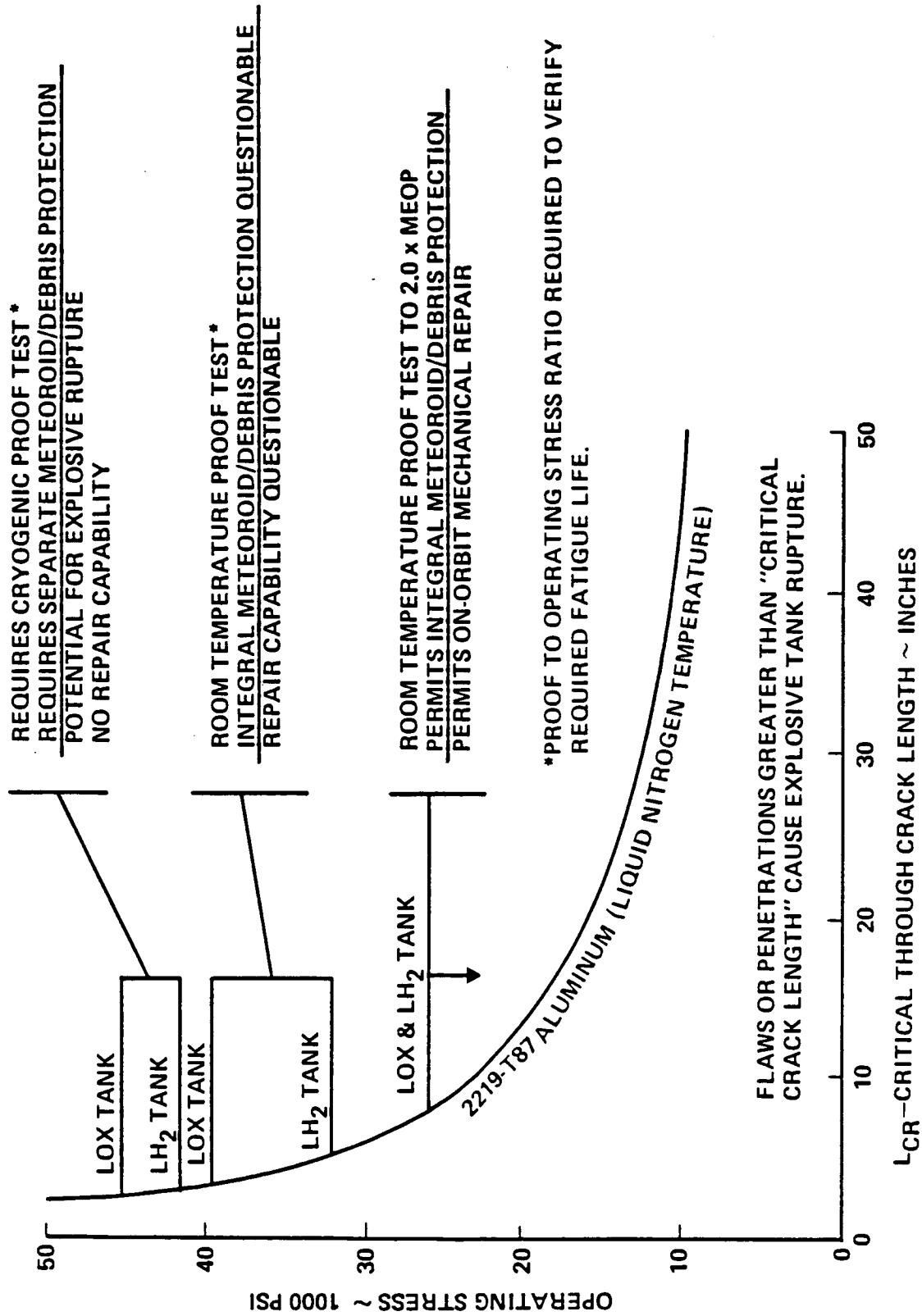


Figure 3.2.1-1 Tankage Critical Crack Length and Design Stresses

life to complete its required service life. The resultant damage tolerance and safety requirements for tankage in proximity to the space station would require further individual assessment.

Due to the nature of 2219-T87 aluminum, room temperature proof-testing is recommended, giving the tanks an inherent factor of safety due to improved strength characteristics at operating temperature. This will be discussed further for specific vehicle configurations.

3.2.2 Body Structures Design Approach

Body structure design efforts included material selection for reusable OTV systems, as well as loads and structural sizing analysis. Consistent with a lightweight design approach, maximum use was made of advanced composites, including Graphite/Epoxy and Graphite/Polyimide for body and aerobrake structures.

Loads and structural sizing analysis was based on determination of the following:

- a. Launch loads
 - 1. Fully fueled or empty.
 - 2. Payload or no payload.
 - 3. Orbiter or aft cargo carrier.
 - 4. Forward and aft ASE loads.
- b. Main engine burn
 - 1. Propellant loading.
 - 2. Payload.
- c. Aerobrake
 - 1. Return payload.
 - 2. Angle of attack.
 - 3. Thermal environment.

In general, static load analysis was the basis of structural sizing, with consideration for obvious dynamic load contributions. Specific structural sizings and descriptions for each vehicle are given under vehicle structures analysis Section # 3.3.

3.2.3 Meteoroids/Debris Shield Design Approach

A study of past analysis on the subject of meteoroid and debris protection, as well as recent developments in protection design philosophy, indicates the following major issues:

- a. Implications of a combined meteoroid/debris environment.

- b. Implications of meteoroid/debris shield failure.
- c. Implications of allowing the pressure vessel wall to contribute to meteoroid/debris shielding - including the effect on service life.
- d. Optimum meteoroid/debris protection design, including shield standoff, and use of alternate materials, such as MLI and GR/EP honeycomb sandwich.

Major trades and analyses were conducted to address these issues. A description of the protection analysis tool and summaries of the analyses performed are detailed in the following paragraphs. Table 3.2.3-1 summarizes unresolved issues and identifies work that needs to be accomplished to support these resolutions.

Analytical Method. We have conducted our meteoroid/debris protection analysis using a computer code "BUMPER" which was updated specifically to support our Space Station Common Module proposal effort. This code indicates shielding requirements which are less than those reported in the Future Orbital Transfer Vehicle Technology Study (NASA Contractor Report 3536). However, it does appear to be in reasonable agreement with other published analysis methods. Key features of the code are identified in Table 3.2.3-2. Input required by this code includes wetted surface area, time, standoff distance, shield thickness and backwall thickness, on an equivalent mass basis. Output from the code is the probability of no penetration through the given shield and backwall combination. The organization which maintains this code recently obtained a contract from JSC to conduct additional impact tests and analysis. Results from their efforts will be incorporated in the code as they become available.

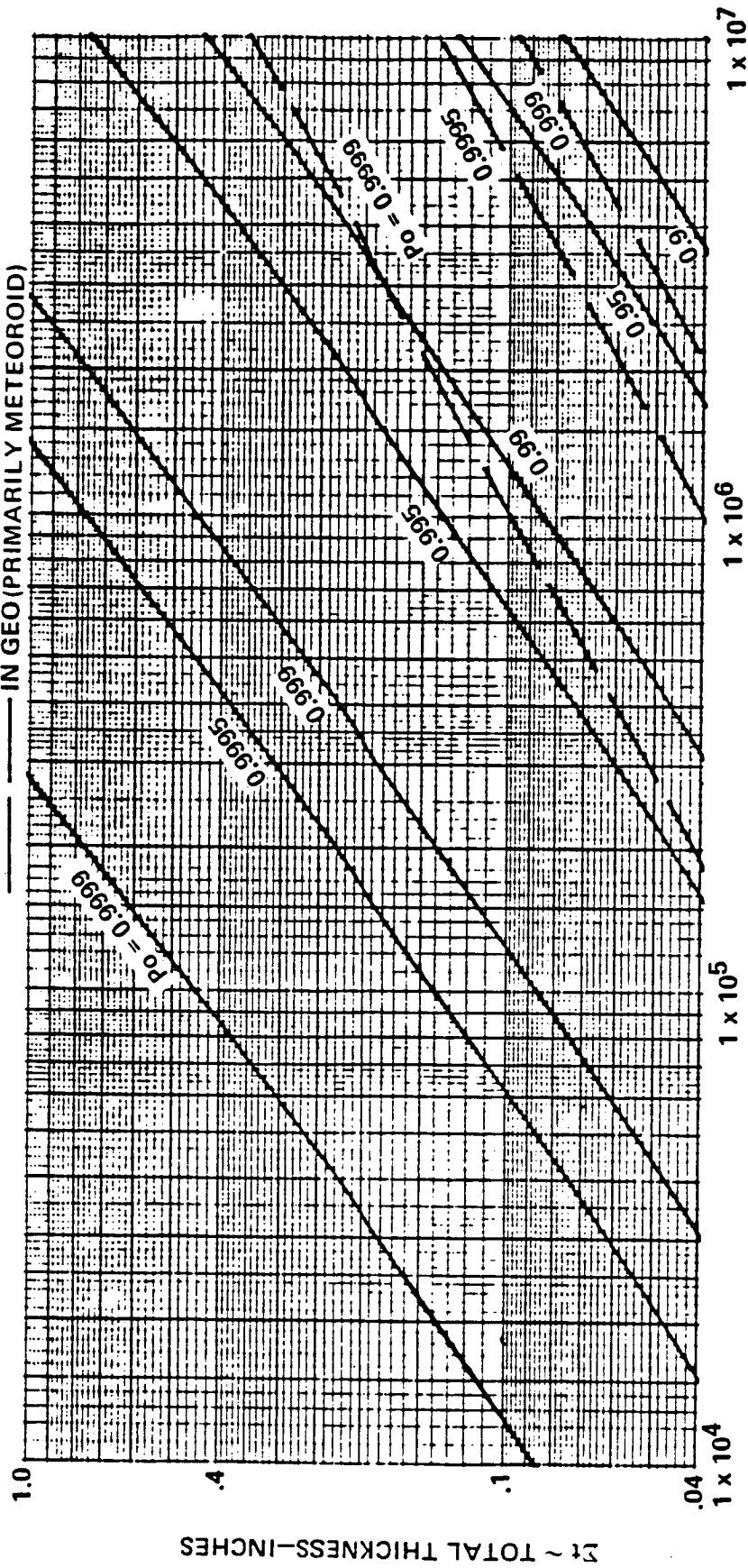
Combined Meteoroid/Debris Environment. The difference in protection requirements at GEO versus those at LEO is illustrated in figure 3.2.3-1. This plot was prepared using the "BUMPER" code for a range of surface area-time values.

Note that the combined thickness range begins at 0.040 inches. Much smaller combined thicknesses will provide predictable protection. However, realistic minimum shield and backwall thicknesses can not be represented by extending this particular plot. Once either thickness reaches minimum gage the thickness ratio can no longer be maintained. Therefore an extension of this plot to lower combined thicknesses would give unconservative or meaningless results. A different type of plot or analysis is needed when working in the minimum gage range, with varying shield to backwall thickness ratios or with varying standoff distances.

- **WHAT ARE THE DAMAGE TOLERANCE REQUIREMENTS?**
 - **VEHICLE IMPLICATIONS**
 - **SPACE STATION IMPLICATIONS**
- **IMPROVED 2219 FRACTURE MECHANICS DATA AT LH₂ TEMPERATURES.**
- **DAMAGE MECHANICS OF PRESSURIZED TANKS AND PROTECTION SYSTEMS.**
- **GROUND RULES FOR SEPARATE VERSUS INTEGRAL PROTECTION DECISIONS.**
- **EXPLOSIVE RUPTURE MECHANICS ANALYSIS AND PREVENTION REQUIREMENTS.**

- COMPUTER CODE "BUMPER", FOR ANALYSIS OF INPUT DESIGNS, AND USED TO SUPPORT SPACE STATION COMMON MODULE EFFORTS.
- BUMPER USES A VELOCITY SPECTRUM FOR BOTH METEORIODS AND DEBRIS.
- METEOROID PENETRATION ANALYSIS:
 - "A PENETRATION CRITERION FOR DOUBLE-WALLED STRUCTURES SUBJECT TO METEOROID IMPACT", J.P.D. WILKINSON, AIAA JOURNAL, VOL 7, NO. 10, OCT. 1969
- METEOROID FLUX:
 - $\text{LOG}_{10} (\text{FLUX}) = -14.37 - 1.213 \text{ LOG}_{10} (\text{MASS})$
 - FLUX IS IN IMPACTS/(METER²-SEC) MASS IS IN GRAMS
- DEBRIS PENETRATION ANALYSIS:
 - "METEOROID PROTECTION FOR SPACECRAFT STRUCTURES", J. F. LUNDBERG, P. H. STERN, R. J. BRISTOM, NASA CR-54201, OCTOBER 1965.
- DEBRIS FLUX:
 - $\text{LOG}_{10} (\text{FLUX}) = -5.46 - 2.52 \text{ LOG}_{10} (\text{DIAMETER})$
 - FLUX IS IN IMPACTS/(METER²-YEAR) DIAMETER IS IN CM
 - MASS = $2.80 \pi D^{3/6}$

- 2219 ALUMINUM PROTECTION SYSTEM
 - SHIELD THICKNESS = BACKWALL THICKNESS/3
 - STANDOFF DISTANCE = 3.0 INCHES
 - P_0 ~ PROBABILITY OF NO PENETRATION:
- IN LEO (PRIMARY DEBRIS)
 ——— IN GEO (PRIMARY METEOROID)



$A \times T$ - SURFACE AREA \times TIME - $\text{FT}^2 \times \text{DAYS}$

Figure 3.2.3-1 Meteoroid/Space Debris Protection

Thus, for the purpose of comparison, using the plot in figure 3.2.3-1, and given a surface area of 20,000 ft², a probability of no penetration of .9999, and stays at LEO and GEO for 0.5 days and 18 days, respectively, the design shielding thickness for the LEO stay would be about 0.09 in, as compared to about 0.056 in for the GEO stay. Thus, the short time in the debris environment at LEO is more critical.

Meteoroid/Debris Shield Failure. Table 3.2.3-3 presents a qualitative analysis of varying degrees of meteoroid/debris shield failure. Prior investigators have spent a considerable amount of effort in assessing meteoroid/space debris environments and developing shielding penetration analysis tools. However, relatively little effort has been spent assessing the phenomenon of explosive rupture of pressurized tanks. Understanding probable damage mechanics, cause and consequences of potential explosive rupture and establishing a realistic criteria for "no explosive rupture" needs to be addressed in greater depth and may prove to be one of the most important activities related to space based tankage structural design.

Figure 3.2.3-2 addresses the issues which lead to a selection of criteria dealing with meteoroid/debris induced explosive rupture of large pressurized tanks. If the pressure shell is penetrated by the debris from an impact on the outer shield, and the diameter of that penetration area is greater than the critical crack length of the tank, explosive rupture of the tank could occur. This is most critical for transfer tankage and storage tankage, which are exposed to impact in close proximity to manned structures over extended periods of time.

Pressure Vessel Impact/Penetration. A review of prior work on meteoroid/debris shielding indicates as a major issue the allowance for pressure vessel impact or penetration. In allowing pressure vessel impact, the pressure vessel effectively becomes part of the meteoroid/debris shielding. A previous NASA criteria for non-cycled tanks (NASA SP-8042, May 1970) allowed penetration up to 25% of the wall thickness. The FOTV study (NAS1-16088, May 1982) stated the position of allowing no damage to the pressure vessel for cyclic tanks as a conservative criteria, due to insufficient data on remaining service life of debris-damaged tanks.

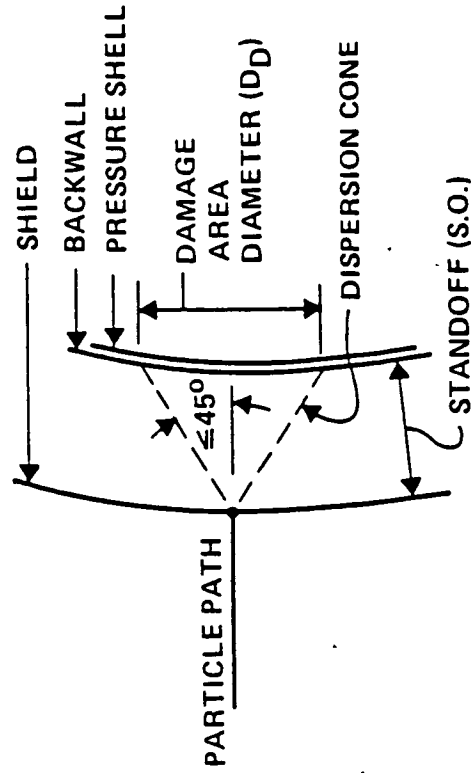
Analysis of this issue requires consideration of the following factors:

- a. Pressure vessel operating stress.
- b. Critical crack length or flaw size.
- c. Probability of no tank impact.
- d. Probability of no tank penetration.

Table 3.2.3-3 Meteoroid/Debris Shield Failure

Failure Type*	Verification	Effect	Repair/Solution
Penetration of shielding	Difficult	No Effect on Tank Life	None Required
Damage to tank surface (< CCL)	Difficult	Some Reduction of Tank Life	Inspection; Repair or Reproof
Damage to tank surface (\geq CCL)	Difficult	Severely Reduces Tank Life - Risk of Explosive Rupture	Non-repairable; Could Reproof
Penetration of tank (< CCL)	Pressure Loss From Tank	Some Reduction of Tank Life, Tank Leakage	Inspection; Repair and Reproof
Penetration of tank (\geq CCL)	Explosive Rupture	Loss of Vehicle, Surrounding Hardware	None Possible

* CCL: Critical Crack Length



- IF PRESSURE SHELL IS PENETRATED AND $D_D > L_{cr}$ AN EXPLOSIVE RUPTURE WILL OCCUR.
- MINIMUM CRITERIA FOR BALANCED DESIGN AND NO EXPLOSIVE RUPTURE MUST BE:

$L_{CR} \geq 2 \times \text{S.O.}$ UNLESS THE SHIELD IS TOO LIGHT TO BREAK UP THE LIGHTEST PARTICLE THAT COULD PENETRATE THE BACKWALL AND PRESSURE SHELL.

Figure 3.2.3-2 Meteoroid/Debris Protection and Damage Characteristics

- e. Probability of no explosive rupture.
- f. Residual service life.
- g. Combined weight.

A qualitative analysis of this issue is presented in Table 3.2.3-4. Quantitative analyses for each type of tankage considered are given in the vehicle-related sections. Conclusions based on the analysis are presented in Table 3.2.3-5.

Meteoroid/Debris Protection Design. Meteoroid/debris protection design is based on two factors: shielding requirement and structural requirement. Each vehicle or tankage set has specific design requirements for primary structure and thermal control. In some cases, this primary structure or thermal control structure can contribute to meteoroid/ debris protection.

Because of the lack of conclusive studies into the effect of alternate materials for meteoroid/debris protection, materials such as MLI and graphite/epoxy honeycomb sandwich were included on an equivalent mass basis as input to the "BUMPER" code. The use of these materials is discussed further for each vehicle type.

Meteoroid/debris shield outer wall thickness and stand-off distance are generally determined as a function of expected impact particle diameter and velocity. For separate shielding, shield-to-backwall thickness ratio is approximately 1:3. This is not true when either wall reaches minimum gage. The selection of 0.016 inch minimum thickness is based upon manufacturing and handling experience and extrapolation of those experiences to space. Greater attention to this problem might result in some reduction in the barrier gage but the reduction would be much less than 100% efficient in terms of weight reduction.

Table 3.2.3-4 Qualitative Analysis of Separate vs. Integral

	Separate Protection (Do Not Allow Tank Impact)	Integral Protection (Allow Tank Impact)
Pressure Vessel Operating Stress	<u>High</u> : Tank Wall Sized for R.T. Proof Test, Based on Service Life Req't.	<u>Low</u> : Tank Wall Sized for R.T. Proof Test, Based on "No Explosive Rupture" Criterion.
Critical Crack Length	Less Than 2.0 Times Shield Stand-off Distance	Equals 2.0 Times Stand-off Distance
Probability of No Tank Impact	High, Due to Separate Shielding (Some Particles May Hit Tank Wall in Both Cases)	Lower, Due to Allowing Tank Impact
Probability of No Tank Penetration	High, Due to Separate Shielding (Some Particles May Penetrate Tank in Both Cases)	Lower Than Separate, But Still High
Probability of No Explosive Rupture	Lower: High Percentage of Particles <u>That Penetrate</u> Could Cause Explosive Rupture	High: Tank Wall Sized for "No Explosive Rupture" Criterion
Residual Service Life	Good, Unless Tank is Impacted - Then Unknown	Very Good - Lower Stress Allows Longer Life, Even if Penetrated.
Combined Weight (Shield & Tank Wall)	High - Requires Additional Support Structure	Lower Than Separate Protection

Table 3.2.3-5 Separate vs. Integral Meteoroid/Debris Shielding Conclusions

- o Vehicle Tankage - Use Separate Protection System with Tankage Designed for Service-Life Determined Room Temperature Proof Test.
 - o Relatively Short LEO Exposure Time - Short Exposure Near Manned Systems.
 - o Minimum Gage Protection Required - Higher than Design Probabilities of No Tank Penetration
- o Transfer Tankage - Use Integral Protection System with Tankage Designed for "No Explosive Rupture" Room Temperature Proof Test.
 - o Relatively Short LEO Exposure, But All Exposure Time Near Manned Systems.
 - o Minimum Gage Protection Required - Probably Sized By Launch Support
- o Storage Tankage - Use Integral Protection System with Tankage Designed for "No Explosive Rupture" Room Temperature Proof Test.
 - o Long LEO Exposure Time Near Manned Systems
 - o Thermal Control Shields Contribute to Combined Shielding

3.3 VEHICLE STRUCTURAL ANALYSES

The major structural elements in the orbital transfer vehicles are as follows:

- a. Aerobrake,
- b. Thrust Structure,
- c. Equipment Support Section,
- d. Propellant Tanks,
- e. Support Struts/Body Structure,
- f. Rings Integral with Tanks,
- g. Payload Interface,
- h. Thermal/Handling/Meteoroid/Debris Protection,
- i. ASE.

Trades and analyses completed for each of the OTV concepts are detailed in the following paragraphs.

3.3.1 SB Ballute-Braked OTV

The space-based ballute braked vehicle concept is shown in figure 3.3.1-1.

Aerobrake. For this concept, a 50 ft diameter, high temperature fabric, lobed ballute is the aerobrake device. Because of high-temperature strength capability, Nextel was chosen as the ballute structural fabric material.

In support of the Aeroassist Flight Experiment (AFE) effort, Goodyear has performed fabric assembly detail design on a 25 ft diameter ballute operating at a maximum of 20 PSF. For OTV, a direct scale-up to 50 ft diameter was initially considered. However, because of the combination of small loads in the fabric membrane and meridians, and large fabric surface area (both byproducts of the "highly lobed" structural concept), a change to a modified scale-up having a variable stress structural concept was undertaken. The result is a "moderately lobed" ballute with 10% less fabric surface area. Key features of the three designs are shown in figure 3.3.1-2.

Weight trade studies indicate that the minimum weight of a throwaway ballute is attained by tailoring the TPS such that the Nextel structural fabric assembly reaches a maximum temperature of 1800°F during the aeromaneuver. The high ratio of fabric strength to load would appear to suggest considering a design with fewer meridians, a larger lobe radius and a lower lobe angle in the interest of reducing membrane area and fabrication costs.

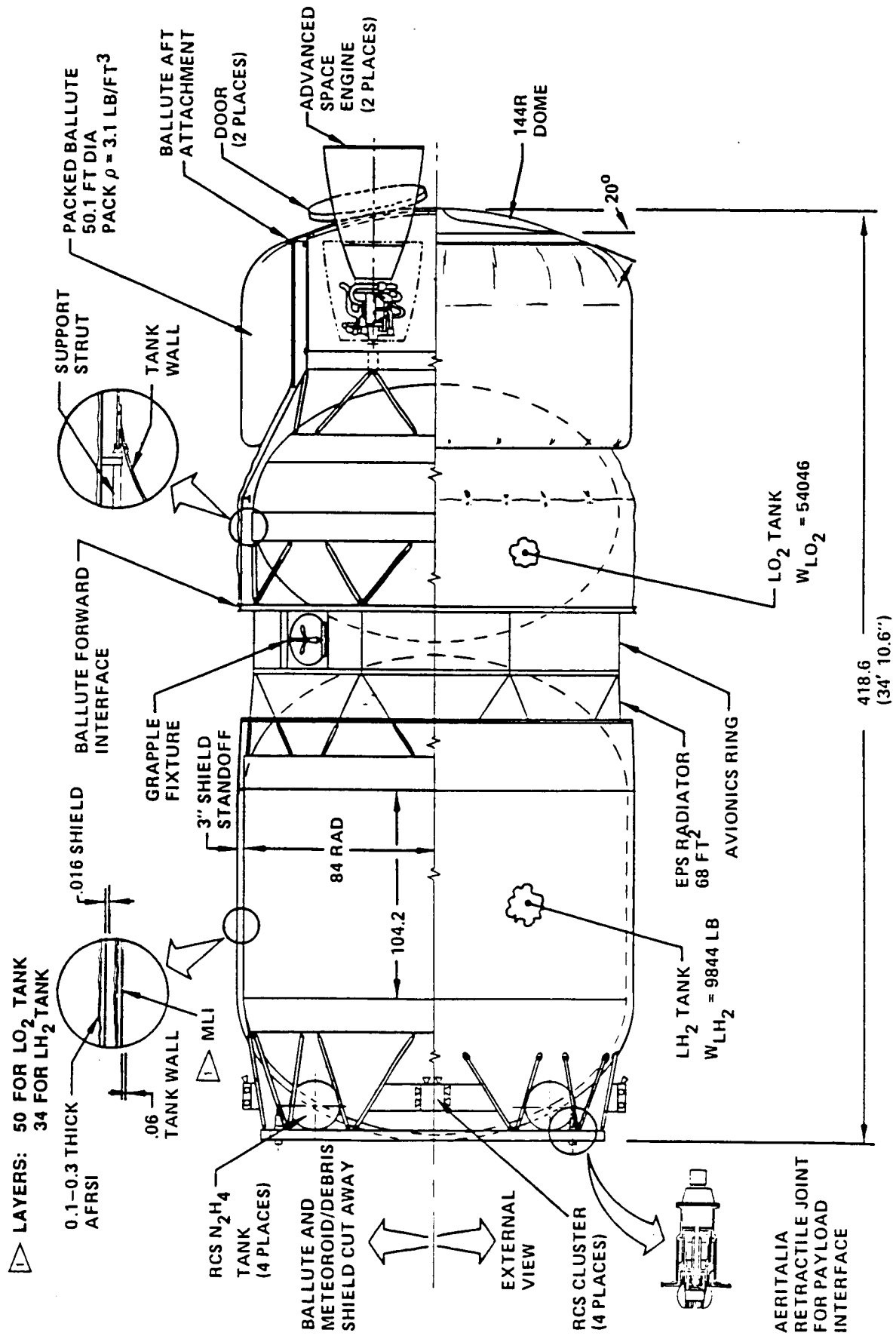
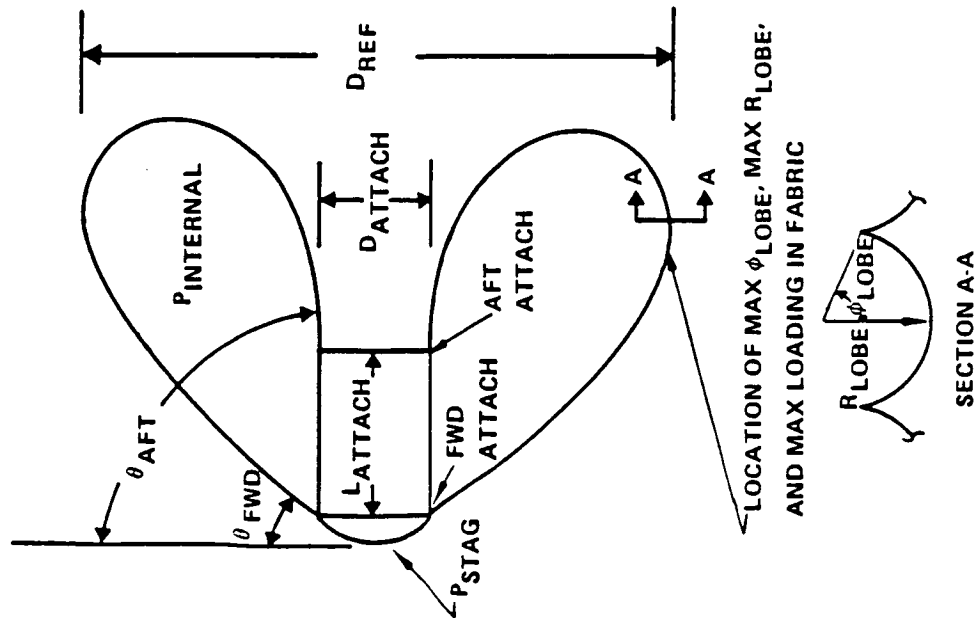


Figure 3.3.1-1 Configuration Space-Based Ballute-Braked OTV—Single Stage

BALLUTE DESIGN

GOODYEAR BASE DATA	DIRECT SCALE-UP	MODIFIED SCALE-UP
DREF (FT)	25.0	50.0
DATTACH/DREF	0.28	0.28
LATTACH/DREF	0.16	0.16
θ FWD ATTACH (DEG)	30	20
θ AFT ATTACH (DEG)	90	90
PSTAG (PSI)	0.267*	0.267
PINTERNAL/PSTAG	0.78	0.78
NUMBER OF MERIDIANS	240	240
MAX ϕ LOBE (DEG)	88	60
MAX R _{LOBE} (IN)	2.0	4.0
MAX LOADING IN FABRIC (LB/IN)	0.46	0.92
LOAD IN MERIDIAN (LB)	28	112
FABRIC SURFACE AREA (YD ²)	200	800
MERIDIAN LENGTH (YD)	9.5	19



*CORRESPONDS TO MAX $q = 20$ PSF

Figure 3.3.1-2 Ballute Structural Fabric Assembly Geometry and Loads

The central heat shield of the ballute vehicle is a GR/PI honeycomb sandwich structure situated over the main engine compartment, with structural doors to cover the retracted engine nozzles during aeromaneuver. Designed for stiffness and stability at aeromaneuver loading, the sandwich construction has 6-ply face sheets with a 1.0 in thick honeycomb core with 4 pcf density. The doors are of similar construction. For thermal protection, both heat shield and doors are covered with FRCI-12 rigid thermal tiles.

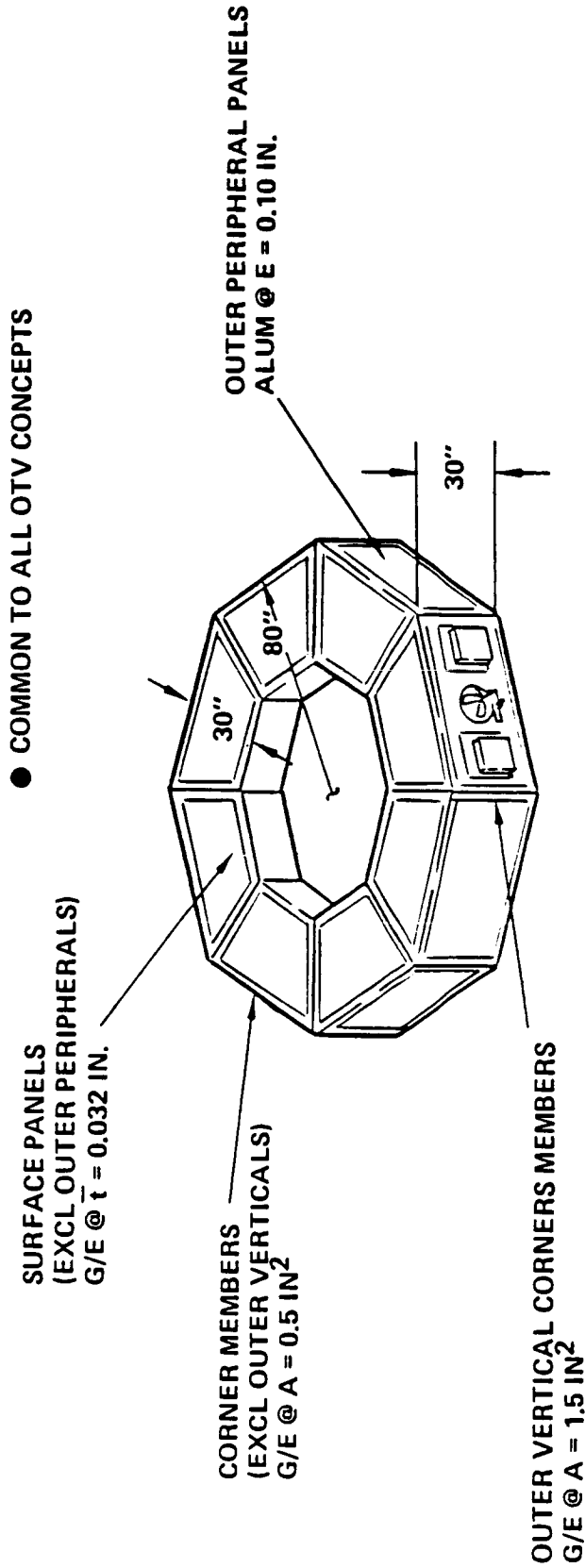
Thrust Structure. For this concept the thrust structure is a double cruciform, rectangular beam structure designed to distribute thrust loads evenly to a thrust ring and on to the aft support struts. The thrust beam structure is of graphite/epoxy design, with mounting provisions for two engines, including thrust vector controllers. Designed to minimize deflections at the center, assuming stiffness tailoring, the beams were found to have an average cross-sectional area of 4.3 in². Additional structure is necessary for assembly and attachment.

Equipment Support Section. The equipment support section is an octagonal GR/EP structure with aluminum doors for monitoring of avionics and electrical power components. Because it is located in the mid-body of the vehicle, this section must also be stiffness and strength designed to transfer forward and aft loads through the GR/EP structure only. Pertinent member sizings are shown in figure 3.3.1-3.

Propellant Tanks. The propellant tank pressure shells are sized to permit room temperature proof testing to 1.63 times the MEOP of 22.1 psi for the liquid hydrogen tank and 1.32 times the MEOP of 23.7 psi for the liquid oxygen tank.

With respect to the hydrogen tank, the MEOP of 22.1 psi occurs subsequent to the initial OTV main engine ignition and is based on an ullage maximum vent pressure of 22.0 psia plus a maximum head pressure of 0.1 psig. During operation, the ullage pressure may perturbate several times between 22.0 and 18.0 psia. After return, the tank is purged of its gaseous hydrogen before refueling. The hydrogen tank average dome thickness is 0.036 in and cylinder thickness in 0.06 in.

With respect to the oxygen tank, the MEOP of 23.1 psi occurs also subsequent to the OTV main engine initial burn and is based on a maximum ullage vent pressure of 22.0 psia plus a maximum head pressure of 1.1 psig. During operation, the ullage pressure may oscillate several times between 22.0 and 20.0 psia. After return, the oxygen tank is



SURFACE PANELS (EXCL OUTER PERIPHERALS)	75
OUTER PERIPHERAL PANELS	151
CORNER MEMBERS (EXCL OUTER VERTICALS)	78
OUTER VERTICAL CORNER MEMBERS	22
ASSEMBLY PROVISIONS	50
EQUIPMENT INSTALLATION PROVISIONS	100
TOTAL STRUCTURES WEIGHT	476 LB.

Figure 3.3.1-3 Equipment Module Structure

partially purged before refilling on-orbit. The oxygen tank average dome thickness is 0.029 in.

Due to the cryogenic operating conditions, and based on room-temperature proof-testing, the inherent ultimate factor of safety on strength is 2.84 for the hydrogen tank and 1.92 for the oxygen tank.

Support Struts/Body Structure. The support struts are fabricated from graphite/epoxy for economy, weight savings and to provide thermal isolation to the cryogenic tanks. They are designed as pin ended columns to sustain the loads developed during aeromaneuver. The struts were selected for tank support and to provide the vehicle primary load paths as being much lighter than a corresponding shell structure.

Strut cross-sectional areas vary from 0.7 to 0.8 in², depending on location on the vehicle.

Rings Integral With Tanks. The rings provided to permit the support struts to support the propellant tanks are fabricated integral with and internal to the tanks for structural weight and volume efficiency and to simplify thermal protection.

Typical ring cross-sectional areas vary from 1.2 to 1.75 in², for LH₂ and LO₂ tanks, respectively.

Payload Interface. The payload interface is a GR/EP ring fabricated with payload attachment pads and mechanism support, placed at the forward end of the vehicle to support the payload under OTV main engine burn conditions.

Thermal/Handling/Meteoroid/Debris Protection. The plot in figure 3.3.1-4 was developed specifically to assess meteoroid/debris protection for the tanks for the Space Based OTV with ballute brake. It reflects a total tankage surface area of 1200 square feet, a standoff distance of three inches, shields and backwalls as indicated, and 18 days exposure at GEO plus the indicated time at LEO.

The minimum thermal protection of 30 layers of MLI plus a protective shield of 0.016 inches of aluminum provides the minimum required protection of 0.999 for the 18 days at GEO plus 0.6 days at LEO.

If the tank wall is allowed to contribute to the meteoroid/debris shielding, the probability of no tank wall penetration exceeds 0.99995, making the possibility of explosive rupture very low. Thus, for this vehicle, a separate shielding system with tank

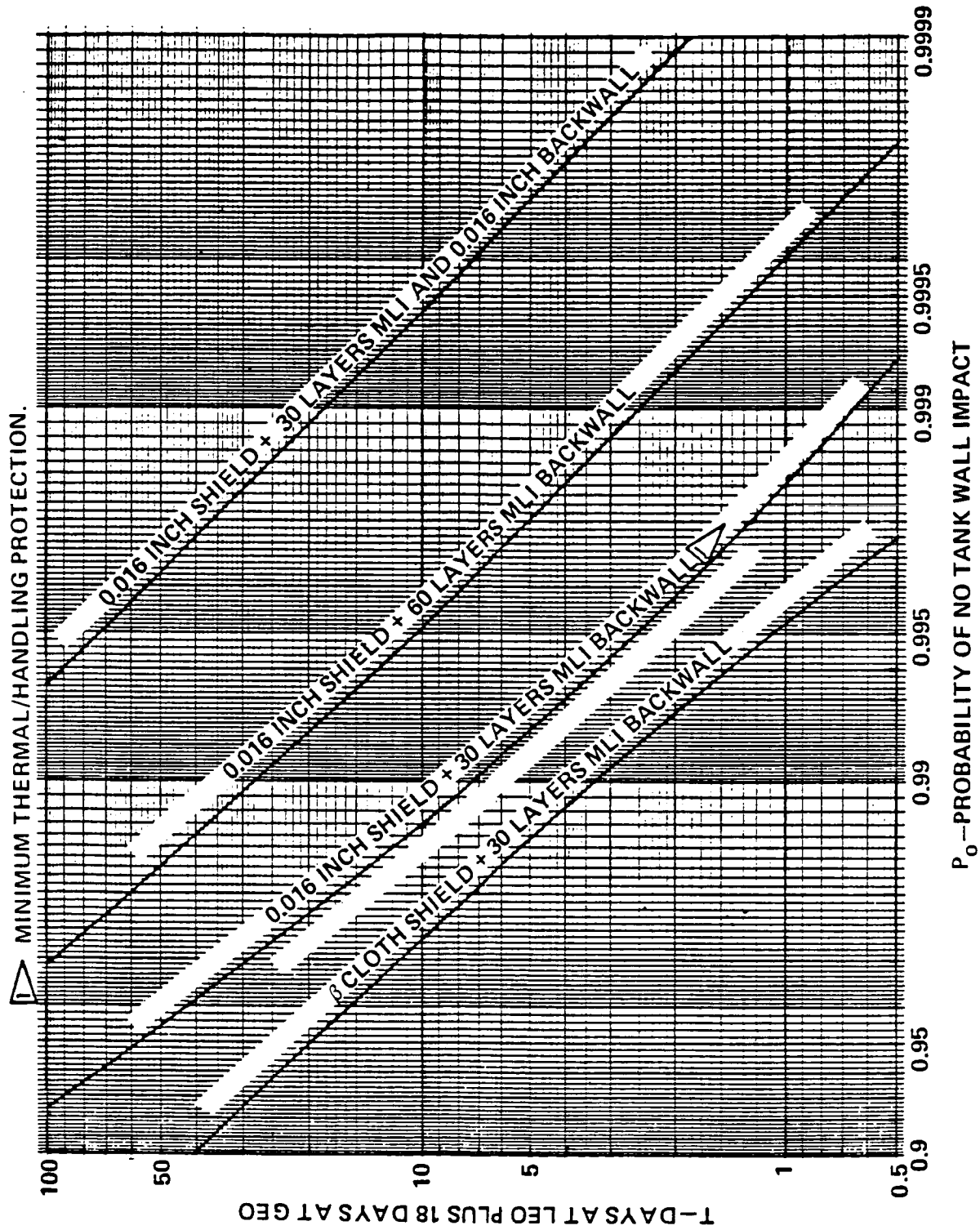


Figure 3.3.1-4 Space-Based OTV Meteoroid/Debris Protection

walls sized for service life requirement room temperature proof test is the preferred concept.

ASE. For transport to orbit the OTV is supported in the orbiter bay, unfueled, by a forward ASE ring which attaches to the P/L interface ring and at the thrust strut interface ring by an open, U-shaped, ASE segment. These ASE segments will be similar in concept but much lighter and simpler than the IUS ASE. Maturing the ASE design for this or other vehicle concepts is not considered a necessary part of this study. The particular OTV to ASE attachment locations were selected to facilitate installation and removal of the OTV from the orbiter and to minimize OTV scar weight.

3.3.2 Space-Based Lifting Brake OTV

The space-based lifting brake OTV is shown in figure 3.3.2-1.

Aerobrake. The brake structure for the SB lifting brake obviously is quite different than that for the SB ballute brake. Table 3.3.2-1 identifies the focus of lifting brake design activity. A qualitative analysis of two lifting brake structural concepts was performed to determine the most efficient concept. One type of brake is supported at the outer edge by an inflated fabric toroid, and the other is supported by rigid struts. This trade is shown in figure 3.3.2-2. The preferred concept is the strut-supported concept, as this provides the most stable structural concept, and minimizes possible brake deformations.

The SB lifting brake OTV reacts brake rib support loads into the equipment structure (ESS) through rib support struts. The ESS is sufficiently deep in local cross section that it is well suited to reacting these loads without major weight penalty. The rib support struts were designed to reduce bending moment in the rib and deflections at the end of the rib, resulting in increased overall stiffness while reducing total rib weight. The support struts are GR/PI struts with an average cross-sectional area of 0.6 in².

The rib cross section and the stresses in the rib at the location of maximum loading are provided in figure 3.3.2-3. The lifting brake ribs are designed to minimize deflections at all points along the rib, and can be tailored to match the bending moments along the rib. This is shown in figure 3.3.2-4.

The lifting brake ribs will be fabricated from graphite polyimide for structural efficiency, economy and to survive the thermal environment with tolerance for local hot spots, should they occur. The section is filled with honeycomb core to stabilize the 0.05

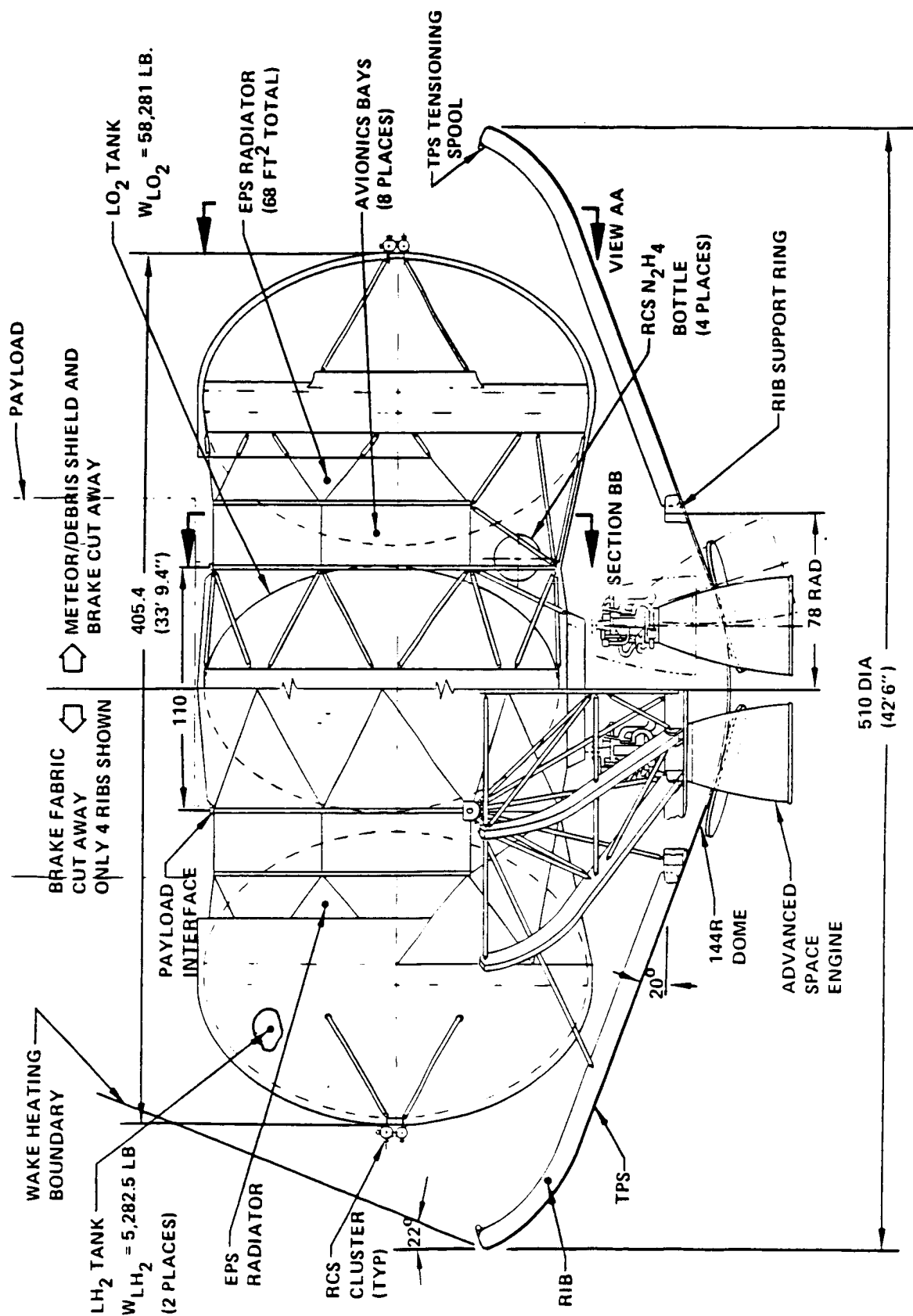
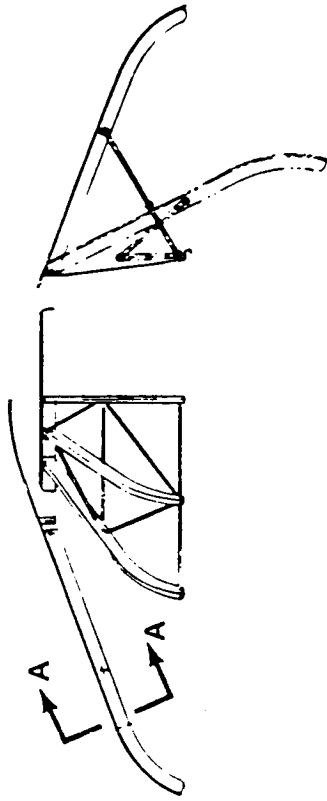


Figure 3.3.2-1 Configuration Space Based Lifting Brake OTV

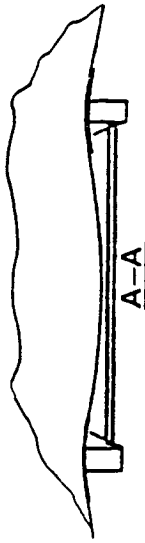
Table 3.3.2-1 Symmetric Lifting Brake Structure

- **RIB AND SUPPORT STRUT REDESIGNED TO REDUCE:**
 - **RIB BENDING**
 - **RIB WEIGHT**
- **ATTENTION FOCUSED ON FABRIC/INSULATION TO REDUCE**
 - **HEATING**
 - **FABRIC LOADS**
 - **AXIAL LOADS IN RIBS**



PREFERRED CONCEPT - RIGID STRUT AND BRACE SUPPORTED RIBS

- SUPPORT STRUTS ARE RIGID MEMBERS WHICH MAINTAIN BRAKE CONFIGURATION DURING AERO MANEUVERS
- SUPPORT STRUT IS PLACED TO MINIMIZE RIB BENDING & DEFLECTIONS
- DIAGONAL BRACES USED TO MAINTAIN RIB SEPARATION ARE POSITIONED BELOW THE FABRIC TO PREVENT CONTACT & LOCAL BURN-THROUGH



ALTERNATE CONCEPT - PRESSURIZED FABRIC TOROID SUPPORTING OUTER EDGE

- INCREASES RIB DEFLECTIONS & STRESS BY PLACING SUPPORT AT OUTER DIAMETER
- STABILITY OF STRUCTURE IN ASYMMETRIC 3-D FLOW FIELD IS DIFFICULT TO VERIFY
- COSTLY NONLINEAR ITERATIVE LARGE DEFLECTION MODELS OF FULL BRAKE & LOCAL SUBSTRUCTURE WITH ASYMMETRIC LOADS REQUIRED TO VERIFY INTEGRITY OF CONCEPT
- LOCAL TORUS CROSS-SECTIONAL DEFORMATIONS MAY CAUSE HIGH LOCAL HEATING & FABRIC BURN-THROUGH LEADING TO CATASTROPHIC SINGLE-POINT FAILURE OF THE BRAKE

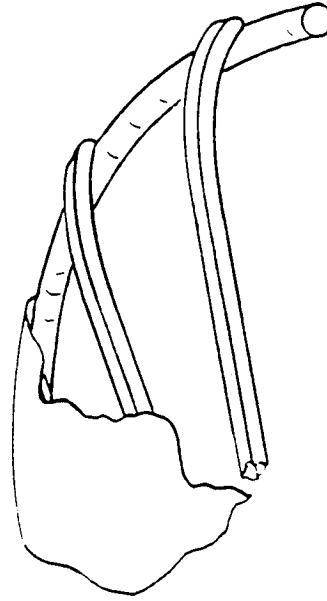
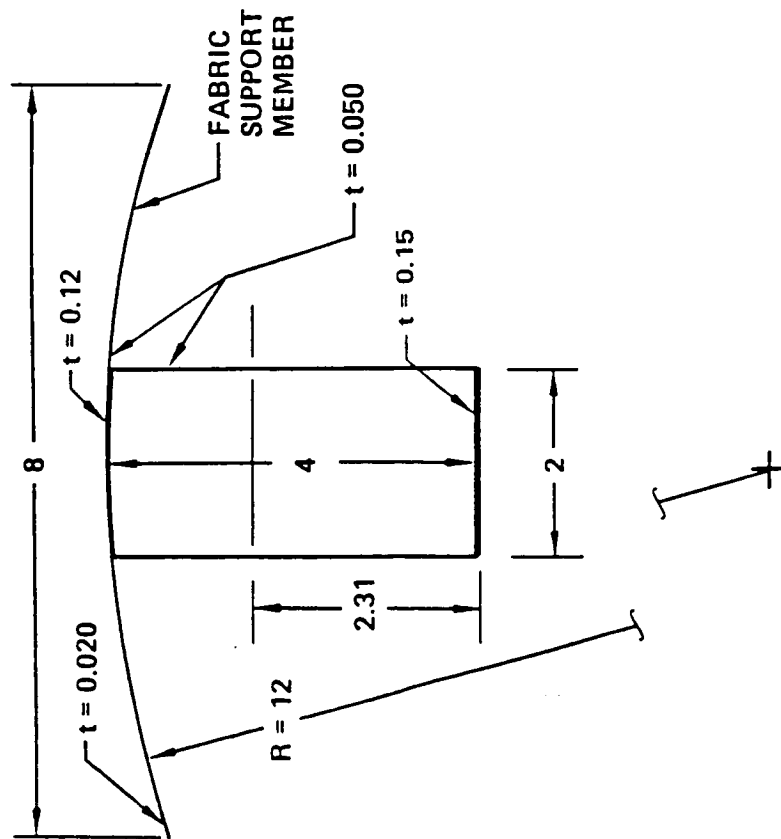


Figure 3.3.2-2 OTV Brake Structural Concepts



MAXIMUM RIB SECTION
(DIMENSIONS IN INCHES)

GRAPHITE POLYIMIDE CONSTRUCTION

FILLED WITH 3.0 PCF H.C. CORE FOR STABILITY.
 $F_c = 55,000$ PSI

ULTIMATE SECTION LOADS:

$M = 70,400$ LB. IN. $P = 4,000$ LB. $S = 2,400$ LB.

SECTION PROPERTIES:

$A = 1.15$ IN.² $I = 3.32$ IN.⁴ $C = 2.31$ IN.

MAXIMUM STRESSES:

$$f_c = \frac{MC}{I} + \frac{P}{A} = 52,400 \text{ PSI}$$

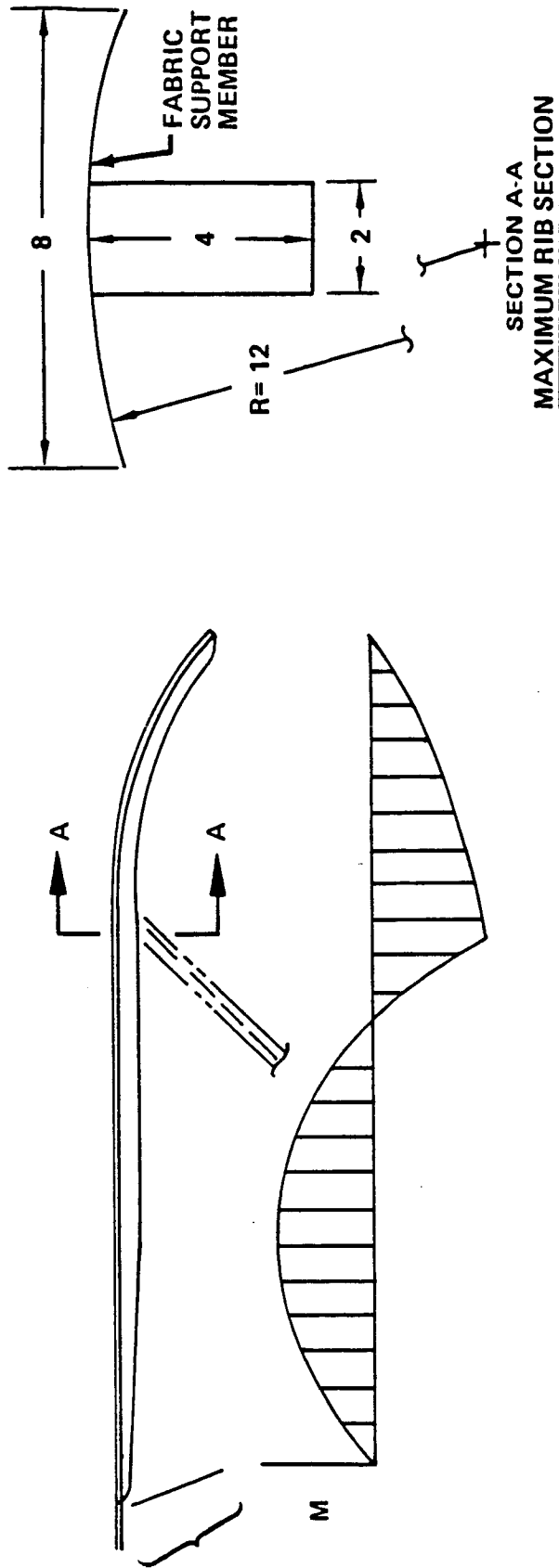
$$f_s = S/2th = 6,000 \text{ PSI}$$

FABRIC SUPPORT MEMBER:

$M = 18$ LB. IN./IN.

$$f = 6 M/t^2 = 6 \times 18/.05^2 = 43,000 \text{ PSI}$$

Figure 3.3.2.3 Symmetric Lifting Brake Rib Section Analysis



- CURVED CAP REDUCES CROSS-FLOW HEATING & PREVENTS INSULATION BURN-THROUGH
- RIBS TAILORED TO MOMENT DISTRIBUTION TO SAVE WEIGHT
- SUPPORT STRUT LOCATED TO MINIMIZE BENDING & RIB END DEFLECTIONS
- LIGHT WEIGHT GRAPHITE POLYIMIDE CONSTRUCTION
 - FILLED WITH 3.0 PCF H.C. CORE FOR STABILITY
 - $F_c = 55,000$ PSI

Figure 3.3.2.4 Symmetric Lifting Brake Structure

inch side walls against buckling due to the combined axial compression and shear loads. The central heat shield for this brake is similar in design to the ballute-braked OTV central heat shield, with structural doors over the nozzle opening. The heat shield is of GR/PI honeycomb sandwich construction.

Additional attention was also given to details of the various design sensitivities of the covering fabric. The objective was to avoid sharp crease lines at the rib which would cause excess local heating, limit fabric maximum tension loads and resultant axial compression loads in the ribs. Those sensitivities are addressed in figure 3.3.2-5. Excess local heating at the rib lines due to cross flow and local contour discontinuity is a major concern with the fabric covered symmetric lifting brake. The problem is eliminated by use of a wide radiused chord on the forward face of the rib section. Aerodynamic heating analysis indicates that a rib chord of 12 inches is adequate to avoid excess heating. Membrane analysis of the fabric spanning between adjacent ribs shows that a chord width (a) of 6 to 8 inches will eliminate local creases and permit acceptable installation tolerances without excessive deflections. With fabric strength in excess of 200 lb/inch the fabric loading is no problem.

The equations used to develop the plots in figure 3.3.2-5 are as follows:

$$\begin{aligned} a &= 24 \sin \phi \\ R_F &= (b/2 \sin \phi) - R_C \\ S &= (R_C + R_F) (1 - \cos \phi) \\ N_T &= P_{\max} \times R_F \\ P_{\max} &= 0.708 \text{ psi ult} \\ \Delta S &= (\phi \times \phi \times (R_C + R_F)/90) - b \end{aligned}$$

A major structural trade was made in regard to the lifting brake support method. The pre-midterm concept of the lifting brake OTV included a brake that was articulated to provide lift control. This type of design restricted the amount of vehicle-to-rib-support, causing large bending moments, excessive deflection, and excessive weight. In going to a design philosophy in which the brake is fixed so that the vehicle C. G. is permanently offset, the vehicle-to-rib-support can be improved, resulting in decreased bending and deflections, and weight. This redesign resulted in a weight savings of 725 lb of brake and support structure weight.

Thrust Structure. This lifting brake OTV thrust structure is similar to the SB ballute-braked OTV thrust structure, except instead of through a ring, the thrust loads

CONCERN: EXCESS HEATING DUE TO CROSS FLOW AND CONTOUR DISCONTINUITY AT RIB LINES.

SOLUTION: CONTOUR RIB FRONT CHORD TO ELIMINATE FABRIC CREASE LINE. TAPER RIB CHORD WIDTH (a) FROM 6 INCHES AT THE ROOT TO 8 INCHES AT MAXIMUM LOADING TO PERMIT INSTALLATION WITHOUT CRITICAL TOLERANCES, EXCESS FABRIC LOAD OR DEFLECTIONS.

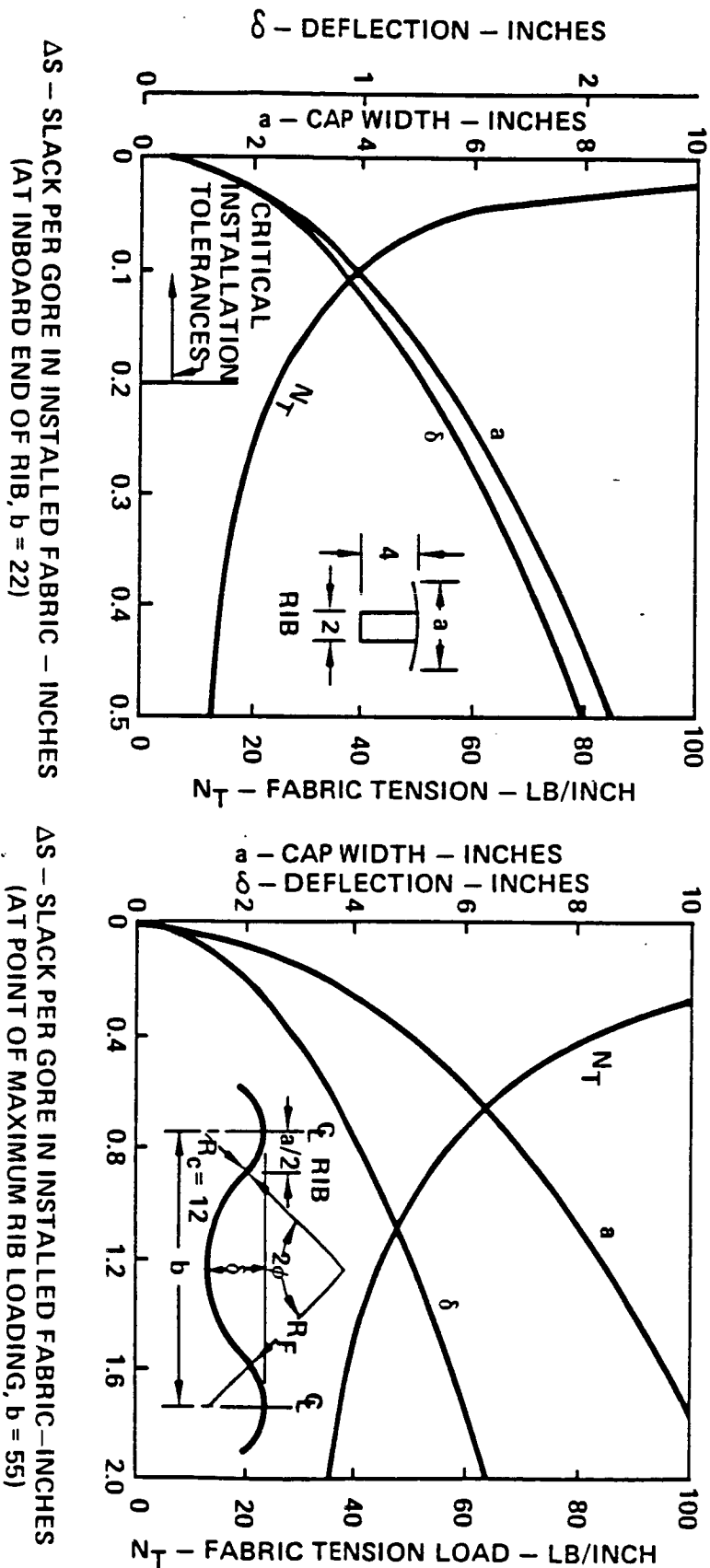


Figure 3.3.2-5 Symmetric Lifting Brake Fabric Installation

are directed into the engine support structure (ESS) through twelve struts. These struts are of GR/EP design and have an average cross-sectional area of 0.5 in².

Equipment Support Section. For this vehicle, the equipment support section is in two segments, each having similar construction to the single structure of the ballute-braked vehicle. Additional stiffening is needed at the payload interface and at the brake support/thrust structure interface.

Propellant Tanks. The propellant tank pressure shells are similar in design to the ballute-braked vehicle tanks. The tanks are loaded differently, however, at main engine initial burn, resulting in maximum pressures of 22.1 psia and 23.6 psia for the liquid hydrogen tanks and liquid oxygen tanks, respectively. Purge and refill operations, as well as flight perturbation conditions, are the same as the ballute-braked OTV. Inherent ultimate factors of safety are also the same.

Average tank dome thickness for the hydrogen tanks is 0.036 in, and cylinder thickness is 0.06 in. Average dome thickness for the oxygen tank is 0.029 in.

Support Struts/Body Structure. The support struts are similar to those for the ballute-braked OTV. For this vehicle, however, the tanks are cantilevered from the ESS, and so somewhat different conditions exist. The struts are stability-designed, and cross-sectional areas range from 0.35 to 0.5 in².

Rings Integral with Tanks. The tank rings are the same design as on the ballute-braked vehicle, but in this case have a cross sectional areas of 1.0 and 1.75 in² for hydrogen and oxygen tanks, respectively.

Payload Interface. For this vehicle, the payload interface structure is built into the equipment support sections and consists of support pads and mechanism support.

Thermal/Handling/Meteoroid/Debris Protection. This vehicle has a larger tank than the ballute-braked vehicle, but has partial shielding provided by the lifting brake. Therefore, the debris shielding has the same definition as that on the ballute-braked vehicle, providing in excess of .999 protection for the same mission.

Implications of meteoroid/debris impact to the aero brake surface are summarized in table 3.3.2-2. Although protection while in use is not feasible those periods of

Table 3.3.2-2 Meteoroid/Debris Implications of Aero Brake Surfaces

- PROTECTION WHILE IN USE IS NOT FEASIBLE.
- INSPECTION FOR DAMAGE WILL BE DIFFICULT.
- SIZE OF PENETRATION THAT BECOMES CRITICAL IS NOT KNOWN.
- REPAIR TECHNIQUES MAY BE REQUIRED.

D180-29108-2-3

exposure are sufficiently small that the probability of impact by a particle of significant size is also small.

The size of penetration which can be tolerated without resultant excess heating, rapid erosion and damage to the vehicle equipment is not known. Certainly that will vary with the type and design of the brake surface and location of the damage.

Inspection for critical damage to the brake surface will be difficult. A lightweight standoff witness plate aft of the brake may need to be considered to facilitate location of critical penetrations. On-orbit repair techniques applicable to the specific surfaces will probably be required.

ASE. This vehicle is transported to orbit in three pieces, including tank/equipment module, propulsion module, and lifting brake. The tank/equipment module is supported unfueled in the orbiter as an open, U-shaped pallet at the ESS location. The main engines are supported on a second pallet, and the aerobrake is launched separately, folded and attached to a fixture at the heat shield area.

3.3.3 Space-Based Shaped Brake OTV

Structures for the shaped brake OTV are similar in many respects to those used on the SB lifting brake OTV and are shown in figure 3.3.3-1. Body structures, tankage, ESS, and payload interface are all similar. The thrust structure, however, is similar to that used on the SB ballute-braked OTV. The major structural difference is the aerobrake structure that, along with debris/meteoroid protection considerations, and airborne support equipment, are discussed in the following.

Aerobrake. The shaped brake shell consists of three major segments sized for delivery to LEO in the orbiter. The elements of these segments are detailed to provide a compromise between weight and complexity of on-orbit assembly.

Table 3.3.3-1 identifies the major issues addressed in the structural design/analysis of the SB shaped brake OTV structure and figure 3.3.3-2 identifies the members providing the major load paths and illustrates types of construction and structural sizings.

Assembly consists of mating the three major segments to the tankage and propulsion module. When assembled the tankage and propulsion module provides the primary girder for the shaped brake. Since it is quite deep and is designed to withstand launch loads in the orbiter, the brake maneuvering loads will not be critical for the tankage and propulsion module. It provides relatively rigid support to the three major

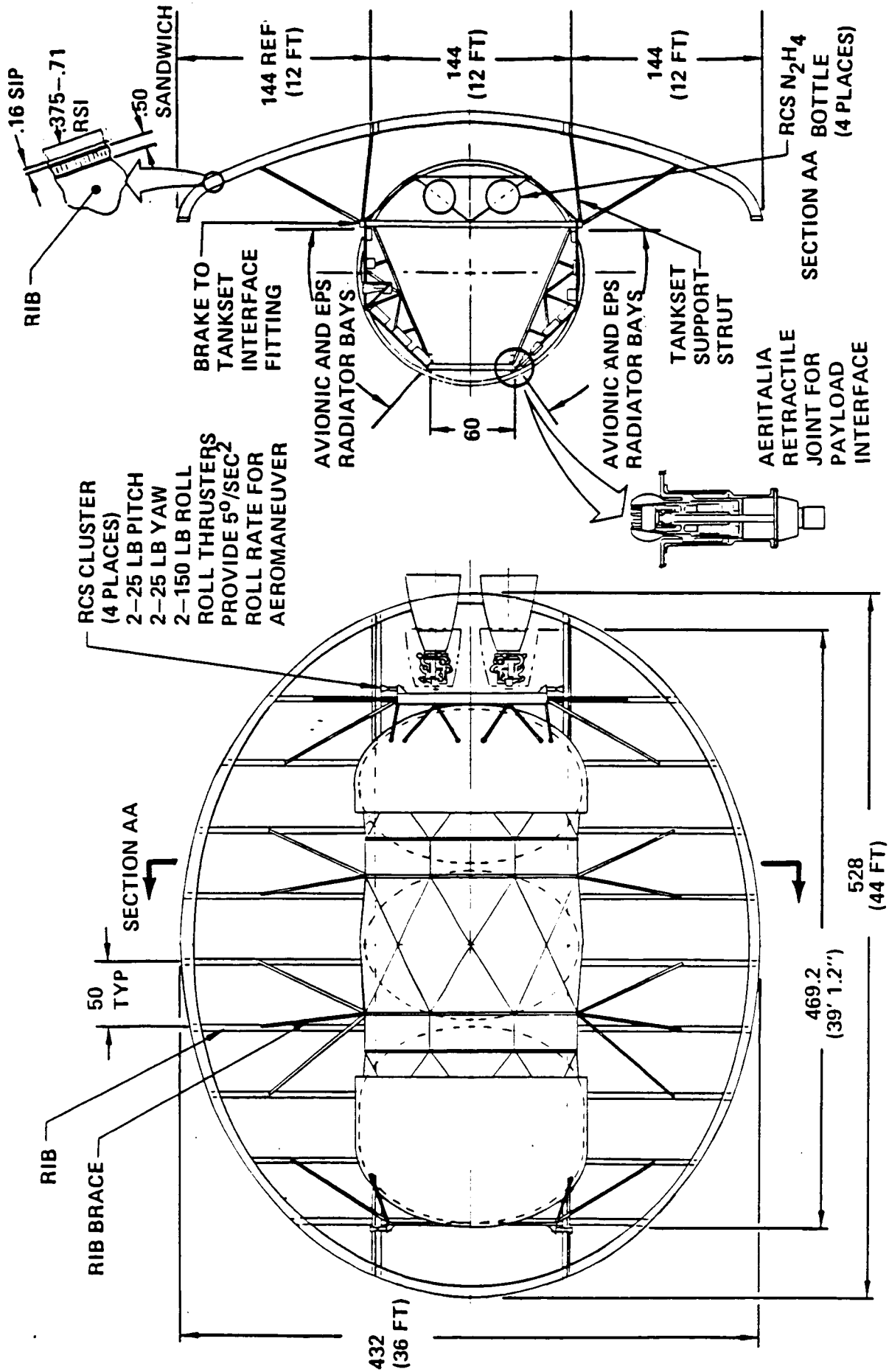


Figure 3.3.3-1 Shaped Brake OTV

Table 3.3.3-1 OTV Shaped Brake Structural System

- DEEP TANKAGE/PROPULSION MODULE PROVIDES PRIMARY GIRDER.
- TANKAGE/PROPULSION MODULE DEVELOPS CRITICAL LOADS DURING ORBITER LAUNCH.
- SHAPED BRAKE STRUCTURE SUPPORTS LOCAL LIFTING LOADS AND REACTS THEM INTO TANKAGE/PROPULSION MODULE.
- ULTIMATE PRESSURE = $q \times D.F. \times C_p \times F.S. \times \sin^2 a = P_{ult}$.
 $q = 28.7 \text{ psf}$, $D.F. = \text{DISPERSION FACTOR} = 1.25$, $C_p = \text{PRESSURE COEFFICIENT} = 1.95$, $F.S. = \text{FACTOR OF SAFETY} = 1.5$, $a = \text{ANGLE OF ATTACK}$, $P_{ult} = 105 \sin^2 a \text{ psf}$.
- FORWARD FACE IS CERAMIC TILE ATTACHED TO GRAPHITE/EPOXY SUPPORT PANEL BY STRAIN ISOLATION PAD (SIP).
- SHAPED BRAKE STRUCTURE IS DESIGNED FOR STRUCTURAL EFFICIENCY IN REACTING LIFTING LOADS AND TO RESTRICT SURFACE DEFLECTIONS SUFFICIENT TO AVOID PEELING TILES FROM SIP.

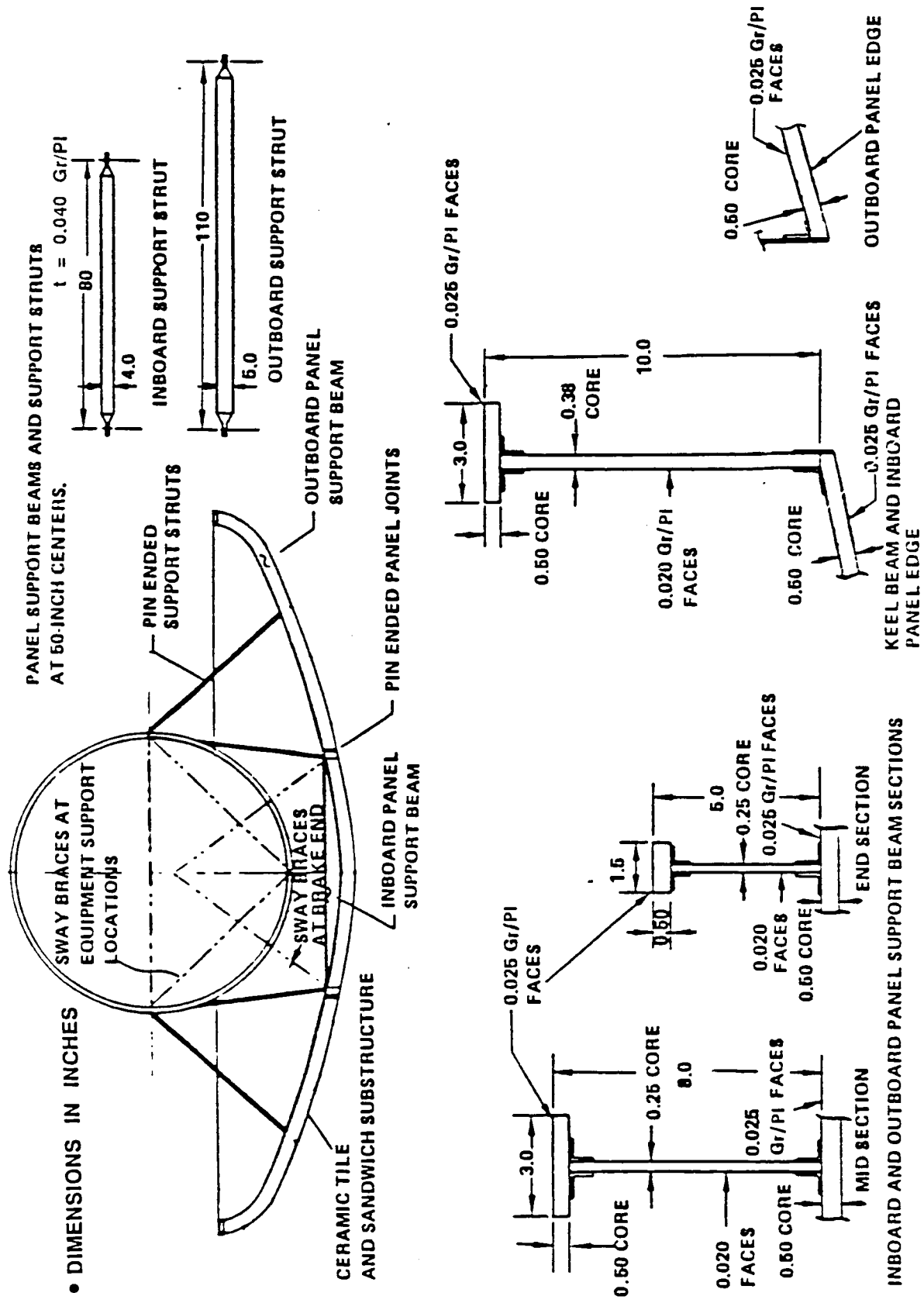


Figure 3.3.3-2 Shaped Brake Structural Sections

segments through a system of struts and transverse support beams located on 50 inch centers. Only the attachment points and internal transverse beams are delivered integral with that module. Sway braces at the module ends and at equipment support locations, shown by dashed lines, retain the section shape.

The ceramic tile/SIP support surface, the longitudinal keel beams and the transverse panel support beams, are all built up using graphite/polyimide (GR/PI) faces and lightweight honeycomb core. The panel face and honeycomb core thicknesses are selected to provide the strength to withstand the aero braking pressure induced loads and to restrict the maximum curvature at the supports to that which the SIP will tolerate. The core and face thicknesses in the keel and transverse beams are selected to stabilize the cross section and withstand the resultant beam bending and shear loads.

The side segment to center segment joints are primarily vertical shear load joints accomplished by a series of tension fasteners, in oversized holes, and tapered shear pins and/or keys to facilitate on-orbit assembly.

The brake shell and the tankage and propulsion module are joined by a series of pin ended graphite/epoxy tubular struts. All of these struts, except the end sway braces, are loaded in compression only. Thus, by match drilling for the pins on initial assembly, and selective slotting holes on disassembly the on-orbit assembly will be simplified. The joints will then be seated upon first loading.

Table 3.3.3-2 summarizes the tile support requirements. Providing a substructure to support the ceramic insulating tiles is the dominant driver in the design of the shaped brake shell structure. The primary issue is to avoid deflections of a magnitude that would exceed the limitations of the SIP and result in loss of the tile. However, we have not been able to obtain documentation of the SIP design characteristics. Therefore, we have made our design correspond to the worst case design condition reported by NASA/MSFC OTV personnel. Our analysis of that condition indicates a limit in the curvature of the support structure corresponding to a local EI/M or radius (R) or 160 inches. This corresponds to a maximum relative deflection of 0.02 inches under the 5 inch SIP. This limitation is reflected in the panel design for the brake panels.

Thermal/Handling/Meteoroid/Debris Protection. Tank areas for this vehicle are similar to the lifting brake OTV, so the same type of shielding can be used. As with the lifting brake, there are several unresolved issues with respect to the meteoroid/debris implications of the shaped brake surface. Although protection while in use is not feasible those periods of exposure are sufficiently small that the probability of impact by a particle of significant size is also small.

Table 3.3.3-2 OTV Shaped Brake Thermal Protection Tile Support

- **TILE/SIP (STRAIN ISOLATION PAD) DISPLACEMENT LIMITATIONS NOT WELL DEFINED.**
- **TILE/SIP/SUPPORT DEFLECTIONS ARE THE CRITICAL DESIGN CONCERN (NOT STRAINS).**
- **SHUTTLE TILES SHIFT AS MUCH AS 1/2 INCH OVER LONG DURATION FERRY FLIGHTS.**
- **ANALYSIS ASSUMPTIONS AND CONSIDERATIONS:**
 - **TYPICAL TILE SIZE 6 INCHES BY 8 INCHES**
 - **CORRESPONDING SIP UNDER LAYMENT 6 INCHES BY 6 INCHES**
 - **AVERAGE TILE GAP 1/10th INCH**
- **NASA/MSFC "WORST CASE" ALLOWABLE PEAK-TO-PEAK SINE WAVE DISPLACEMENT OF 2.2 INCHES IN SPAN OF 106 INCHES.**
- **BOEING CONFIGURATION INCORPORATES ADVANCED COMPOSITE GR/PI SANDWICH DESIGN TO LIMIT MAXIMUM LOCAL SUPPORT PANEL CURVATURE TO CORRESPOND TO A RADIUS OF NO LESS THAN 180 INCHES**

The size of penetration which can be tolerated without resultant excess heating, rapid erosion, and damage to the vehicle equipment is not known. Certainly that will vary with the type and design of the brake surface and location of the damage.

Inspection for critical damage to the brake surface will be difficult. A lightweight standoff witness plate aft of the brake may need to be considered to facilitate location of critical penetrations. On-orbit repair techniques applicable to the specific surfaces will probably be required.

ASE. Airborne support equipment for the tank module portion of this vehicle is similar to that for the tank module of the SB lifting brake OTV. Because of the engine placement, a separate ASE is not required to launch the main engines. The aerobrake, however, is launched in three separate pieces, and requires a support structure for launch.

3.3.4 On-Orbit Propellant Storage Tanks

The on-orbit storage tank body structures are inherently different from those of other vehicles as shown in Figure 3.3.4-1. The following paragraphs detail analysis performed in tank/body structure design, as well as meteoroid/debris protection.

Tank/Body Structure. The body and tank structure design of the two on-orbit propellant storage tanks is quite different from that of the candidate vehicle concepts. The differences are due to the fact that the usage scenarios and resultant design drivers are quite different. The LOX and LH₂ storage tanks are fabricated and launched as separate units rather than as a single unit sharing a common structural shell/meteoroid/debris protection system. The storage tanks are launched empty which results in minimal launch loads. The outer shell of waffle construction reacts the launch loads and supports the thin walled inner pressure shell by fiberglass straps which provide thermal isolation. This outer shell also interfaces with the ASE members in the spherical dome region of the tanks where clearance is available to permit a light weight ASE and is tailored to reflect the launch loads. The same ASE set is used for each of the tanks although it is designed for the heavier, LH₂, tank support loads. The pressure shells are submerged in water and hydrostatically proof tested before being integrated with the outer shells. The assembled tanks are loaded into a vacuum chamber which is evacuated with the annulus exposed to chamber pressure for thermal testing. Following thermal testing the annulus is filled with dry helium and sealed for removal and transportation to space, where it is again opened to the environment of space. Thus the storage tanks

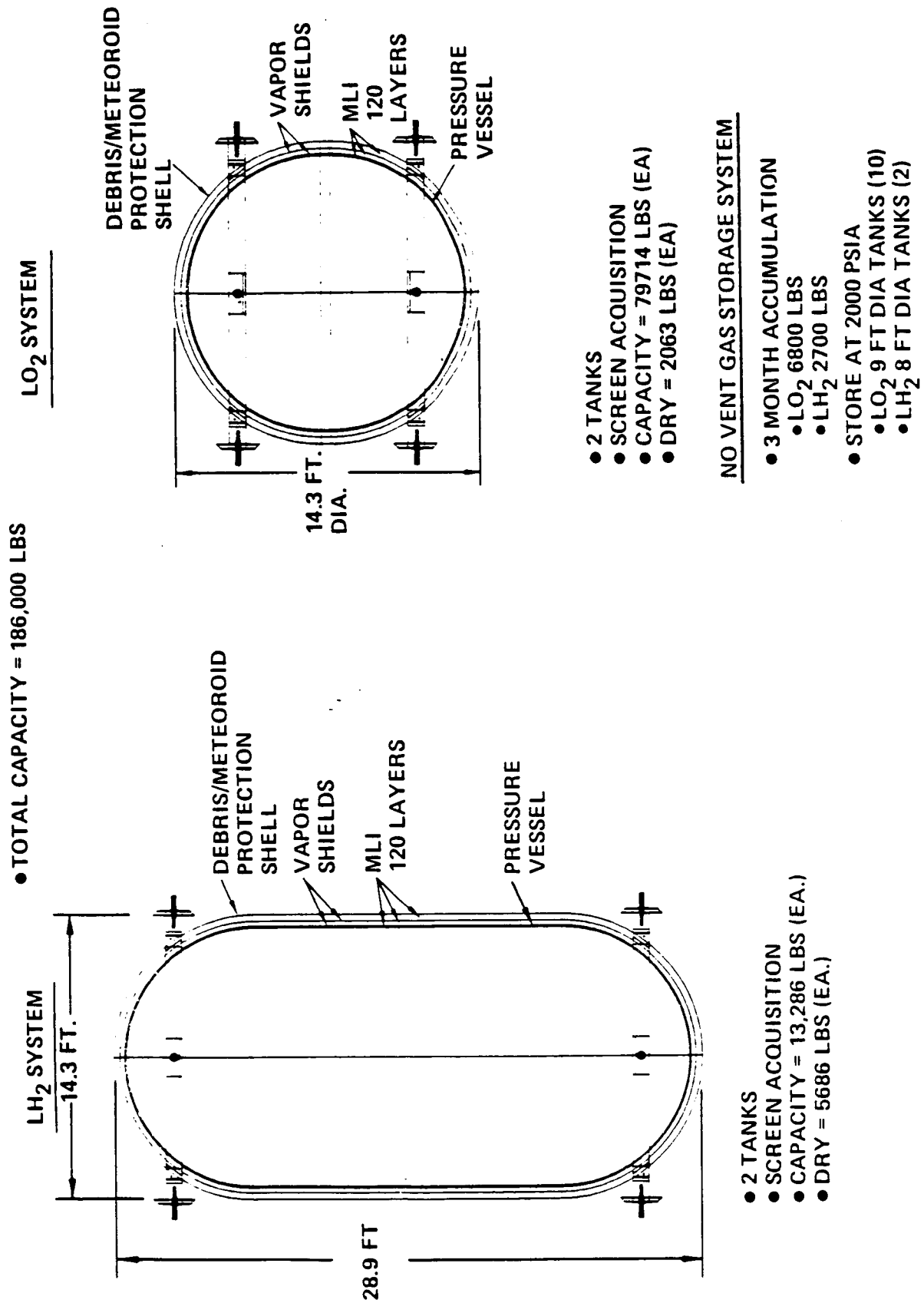


Figure 3.3.4-1 Propellant Orbital Storage System

function as dewars but never have to withstand the loads of being evacuated within the atmosphere.

A number of separate requirements or considerations have led to the selection of this design concept. The degree of thermal isolation required dictated limiting load paths and thermal paths between the two shells. That plus orbiter launch capability would dictate launching the LOX tank only partially filled. Launching the LH₂ tank filled is a possibility and was evaluated in terms of tank and ASE weight impact. Complications of maintaining helium pressure while being filled with LH₂ will probably dictate launching the LH₂ tank empty.

Several factors support the decision to fabricate the two tanks as separate units. The most important is the consequence of building them integral with a common meteoroid/debris protection shield and then sustaining punctures or otherwise developing leaks in each. Separate units simplified changeout. Also it would be poor orbiter utilization to manifest two large low density items simultaneously.

Thermal/Handling/Meteoroid/Debris Protection. Structural considerations dictate a minimum outer wall of aluminum isogrid ($t_{min} = 0.05$ in.) for this configuration. In addition, two major-cooled shields ($t = .01$ in. each) and 120 layers of MLI contribute to meteoroid/debris shielding, assuming the effectiveness of the vapor-cooled shields and MLI as meteoroid/debris protection to be 50 percent on an equivalent mass basis. Using a stand off distance of 6.0 in., an analysis was conducted to determine the optimum backwall and whether or not the tank wall would contribute to meteoroid/debris shielding. Using the critical crack length data explained in Section 3.2.1, as well as shield sizing data generated by the "BUMPER" code, a comparison was made of separate and integral shielding concepts. Fig. 3.3.4-2 shows a typical plot of probability and critical crack length versus combined wall thickness (outer wall, vapor, coded shields, backwall, and tank wall) for the on-orbit LO₂ tank. The plot of the same data for the LH₂ tank is similar but more complex, due to the significant cylindrical section in the LH₂ tank configuration. Pertinent data used in the trade are shown in Table 3.3.4-1.

With separate shielding, using a design condition of .995 probability of no impact on the tank wall, and using a tank wall sized for service-life proof test, probability of explosive rupture could be up to .003, and total system weight is 1240 lb, for the LO₂ tank. With integral shielding, using a tank designed for no explosive rupture, although the probability of impact on the tank is greater, and probability of tank penetration is also greater, the probability of explosive rupture of the tank is negligible because the critical crack length is not exceeded. In addition, the combined weight of the system is

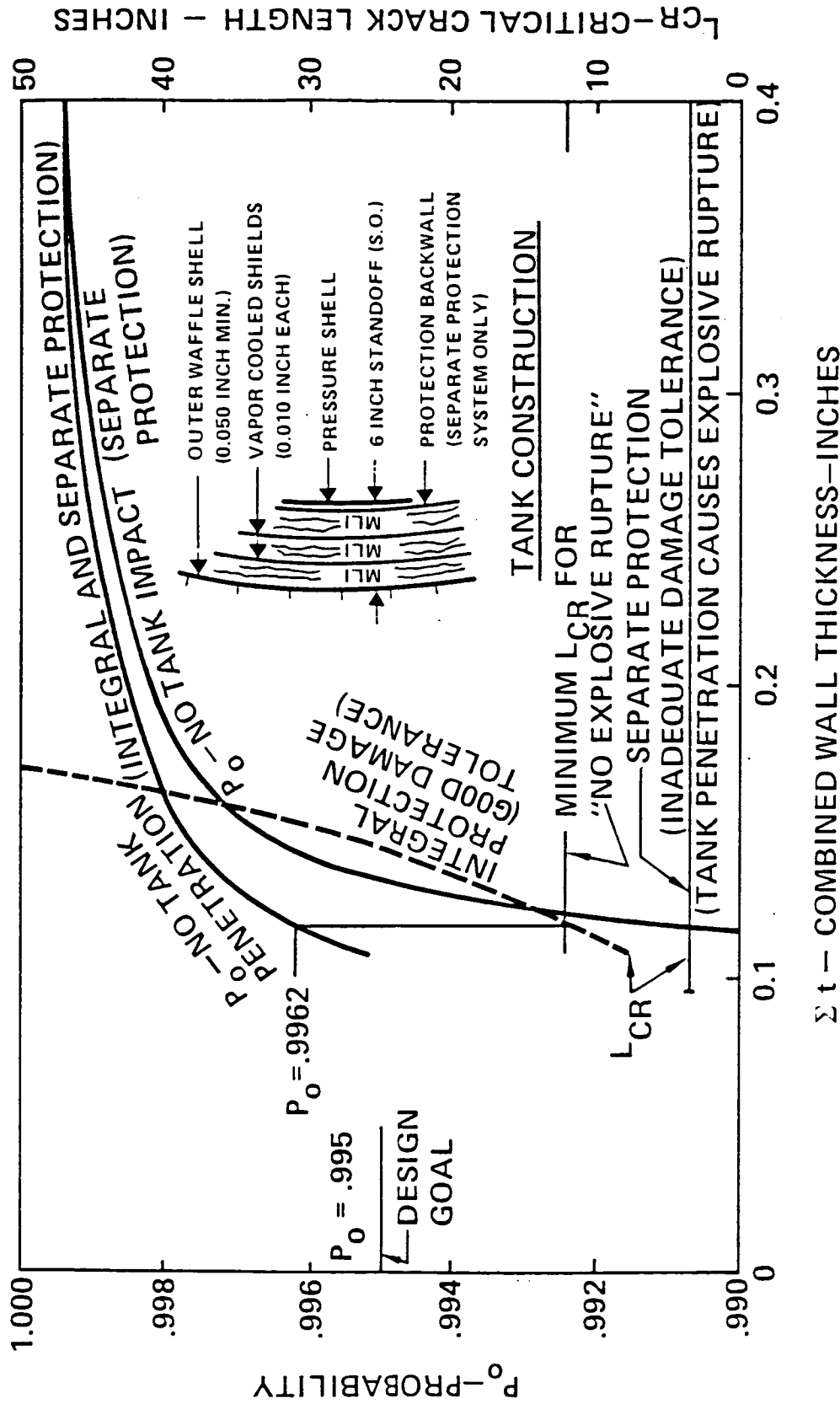


Figure 3.3.4-2 Separate Versus Integral Meteoroid/Debris Protection for Space-Based LOX Storage Tank

Table 3.3.4-1 *LO₂/LH₂ Storage Tank Integral Vs. Separate Meteoroid/Debris Protection*

	LO ₂ Tank		LH ₂ Tank			
	Separate Shielding	Integral Shielding	Separate Shielding		Integral Shielding	
			Heads	Cylinder	Heads	Cylinder
Operating Stress—ksi	39.4	21.1	31.1	31.1	21.1	21.1
Critical Crack Length—in.	3.4	12.0*	5.0	5.0	12.0*	12.0*
P _O —No impact	.995*	.991	.995*		.981	
P _O —No penetration	.997	.9962	.9967		.9958	
Probability of explosive rupture	≈ .003	Negl.	≈ .0033		Negligible	
Outer shield weight—lb. (t—in.)	686 (.07)	686 (.07)	686 (.07)	737 (.07)	686 (.07)	737 (.07)
Backwall weight—lb. (t—in.)	344 (.039)	0 (0)	705 (.08)	757 (.08)	0 (0)	0 (0)
Tank wall weight—lb. (t—in.)	210 (.026)	388 (.048)	267 (.033)	630 (.066)	388 (.048)	917 (.096)
Combined weight—lb. (t—in.)	1240 (.135)	1074 (.118)	1658 (.183)	2124 (.216)	1074 (.118)	1654 (.166)

*Design condition

only 1074 lbs for the LO₂ tank. Similar results are shown for the LH₂ tank. From this trade, it was determined that the on-orbit storage tanks should be allowed to contribute to the meteoroid/debris shielding and be designed for a "no explosive rupture" condition.

3.3.5 Propellant Resupply Tanker

Tank and Body Structure. The propellant resupply tanker shown in Fig. 3.3.5-1 was evolved and selected as a result of a trade study. The design selected employs isogrid tank pressure shells supported by fiberglass struts which also serve as primary structure for the module. The thermal protection system provides the outer wall for meteoroid/debris protection and consists of 50 layers of MLI and purge containment. The alternate concept employed struts to support the tanks and an outer structural shell to serve as primary structure for the module. Analysis showed that a minimum structural shell weight is considerably greater than the weight of the struts for the selected concept and that the selected concept is more than 800 pounds lighter than the alternate concept. Both concepts employ two trunnion support rings fabricated integral with the module with the keel fin supported by the trunnion support ring between the two tanks.

The inboard chord of a kick ring (not shown in sketch) is fabricated integral with the isogrid pattern at the location where adjacent struts meet to support the tanks.

Thermal/Handling/Meteoroid/Debris Protection. Structural considerations on this vehicle dictate using isogrid tanks to supply stiffness for launch. Because of operation in proximity to manned systems, the condition of "no explosive rupture" was applied to the tanks, and the tanks were allowed to contribute to meteoroid/debris shielding. Because of the short stay of LEO, however, the minimum 50-layer MLI/purge containment system was found to provide the .997 probability of no tank impact alone. Allowing the tank wall to contribute to the meteoroid/debris protection gives a very high probability of no tank penetration, and the chance of explosive rupture is negligible, due to the tank design.

3.3.6 GB Ballute - Braked OTV

The configuration of the ground-based ballute-braked vehicle is shown in Figure 3.3.6-1.

Aerobrake. For this concept, three sizes of ballutes were designed: 33 feet diameter for unmanned multiple manifest missions, 40 feet diameter for GEO delivery

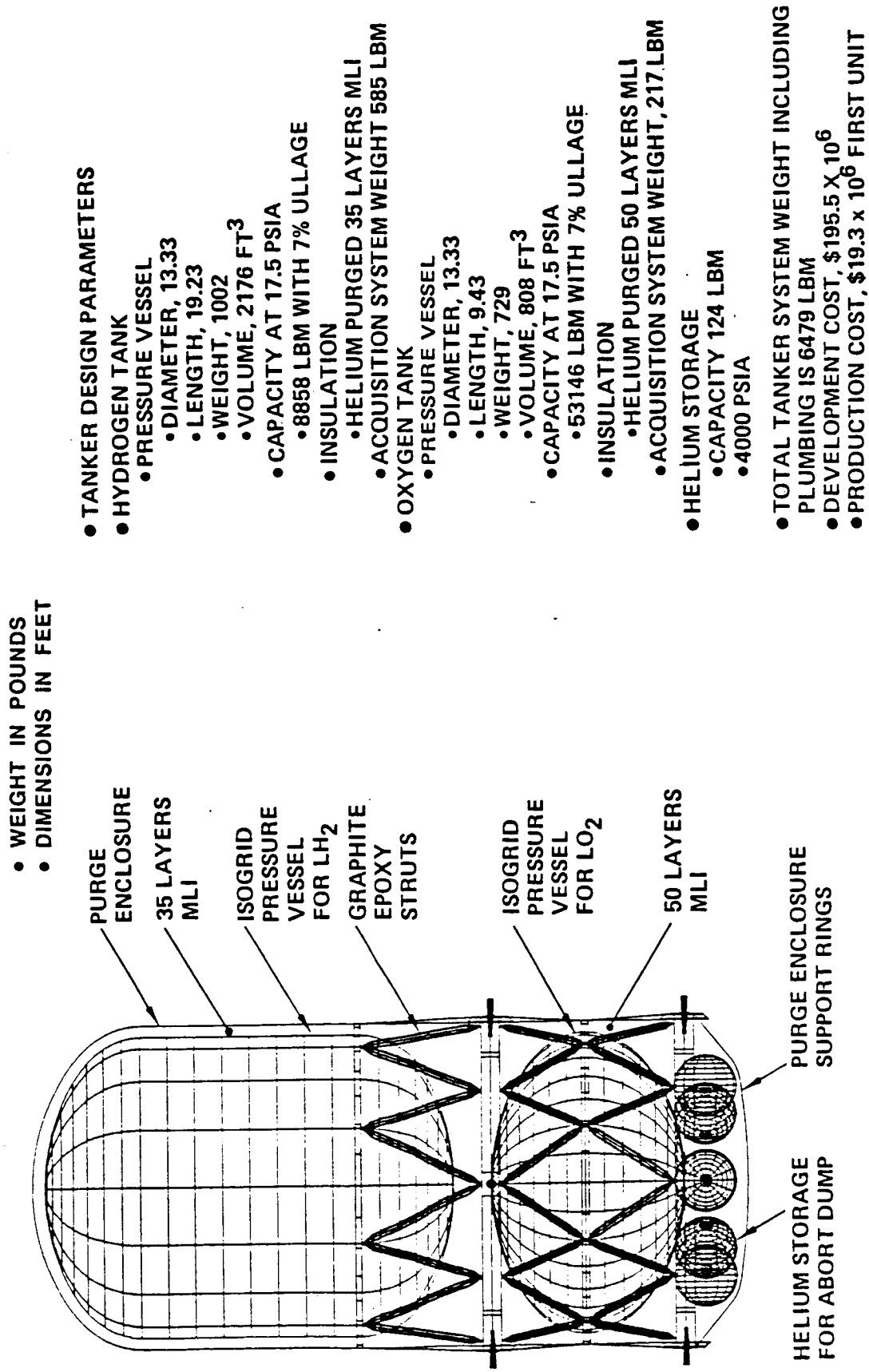
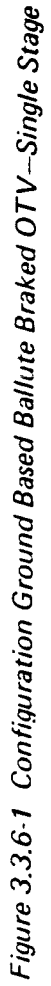


Figure 3.3.5-1 Tanker Tanks Configuration Baseline Concept



missions when auxiliary tanks are used, and 65 feet diameter for manned missions when auxiliary tanks are used and a manned capsule is returned. Ballute design is similar to that of the SB Ballute - braked OTV.

Thrust Structure. The thrust structure for this vehicle is similar to that of the SB Ballute - braked OTV.

Equipment Support Structure. The equipment support structure for this vehicle is similar to that of the SB Ballute - braked OTV, except that it is a circular structure to be compatible with the vehicle body shell. Also, the mounting doors are assumed to be load carrying so that the whole structure can be made lighter. This is possible because equipment maintenance can be performed on the ground.

Propellant Tanks. The propellant tank pressure shells are sized to permit room temperature proof testing to 1.37 (best-fit fracture mechanics data) times the MEOP of 22.1 psi for the liquid hydrogen tank and 1.32 times the MEOP of 33.3 psi for the liquid oxygen tank.

With respect to the hydrogen tank, the MEOP of 22.1 psi occurs subsequent to the initial OTV main engine ignition, and is based on an ullage maximum vent pressure of 22.0 psi plus a maximum head pressure of 0.1 psig. During operations, the ullage pressure may perturbate several times between 22.0 and 18.0 psia. After return, the tank is purged of its gaseous hydrogen and repressurized with helium before return to the ground. The hydrogen tank average dome thickness is 0.030 in. and cylinder thickness is 0.05 in.

With respect to the oxygen tank the MEOP of 33.3 psi occurs subsequent to shuttle ET burnout during launch, and is based on a propellant vapor pressure of 20.0 psia plus a maximum head pressure of 13.3 psig. During operating, the ullage pressure may perturbate several times between 22.0 and 20.0 psia. After return, the oxygen tank is partially purged and allowed to warm and pressurize before return to the ground. The oxygen tank average dome thickness is 0.031 in.

Due to cryogenic operating conditions, and based on room-temperature proof-testing, the inherent ultimate factor of safety of strength is 2.39 for the hydrogen tank and 1.92 for the oxygen tank.

Body Shell Structure. The body shell is fabricated from graphite epoxy with a NOMEX honeycomb core. This type of structure was chosen for the ground-based

vehicle as being the most effective for supporting a payload, as well as the fuel and oxidizer tanks, during launch. The design of this structural shell is based on analysis given in the Orbital Transfer Vehicle Concept Definition Study Vol. 4 (NA58-33532, 1980). Forward of the equipment support section, the shell is made up of 3-ply GR/EP face sheets with a 0.5 in., 4 pcf NOMEX honeycomb core. Aft of this, to the ASE interface, 6 ply face sheets are used with a 0.5 in., 4 pcf core.

Rings Integral with Tanks. Rings are similar to those in the space-based ballute-braked vehicle, but are sized for launch load conditions. Typical ring cross-sectional areas vary from 1.5 in² to 2.0 in² for the LH₂ and LO₂ tanks, respectively.

Payload Interface. Similar to SB Ballute - braked OTV

Thermal/Handling/Meteoroid/Debris Protection. Because of mission type and duration, this vehicle, like the SB vehicles, needs only minimum protection, and the tanks can be designed for service life requirements, instead of a "no explosive rupture" condition. The GR/EP honeycomb sandwich body shell and 34-50 layers of MLI more than adequately provide the necessary protection. Additional protection must be provided at the payload interface area only.

ASE. The aft ASE for this vehicle is a GR/EP cylindrical shell with longerons at the orbiter trunnion fitting locations for load distribution. The design is based on analysis from NAS8-33532 (Ref. 1). Forward ASE is included as a heavy ring and fittings integral to the vehicle body shell.

3.3.7 Auxiliary Propellant Tank

The design of the integral auxiliary propellant tank is conceptually quite similar to that of the GB OTV. A sketch is provided in Fig. 3.3.7-1. The two tank heads and supports for the LH₂ tanks are substantially identical to those for the OTV. The auxiliary LH₂ tank differs from the OTV LH₂ tank only in the elimination of cylindrical section whereas the auxiliary LOX tank is smaller than the OTV LOX tank. The structural shell for the module and its support in the orbiter are quite similar to that for the OTV. The major distinction is a different aft ASE with the keel pin support cantilevered forward of the ASE ring to reduce the yawing moments. The module structural shell is locally recessed to provide clearance for the keel in support. The clearance available for the aft ASE, and not available for the OTV aft ASE permits a

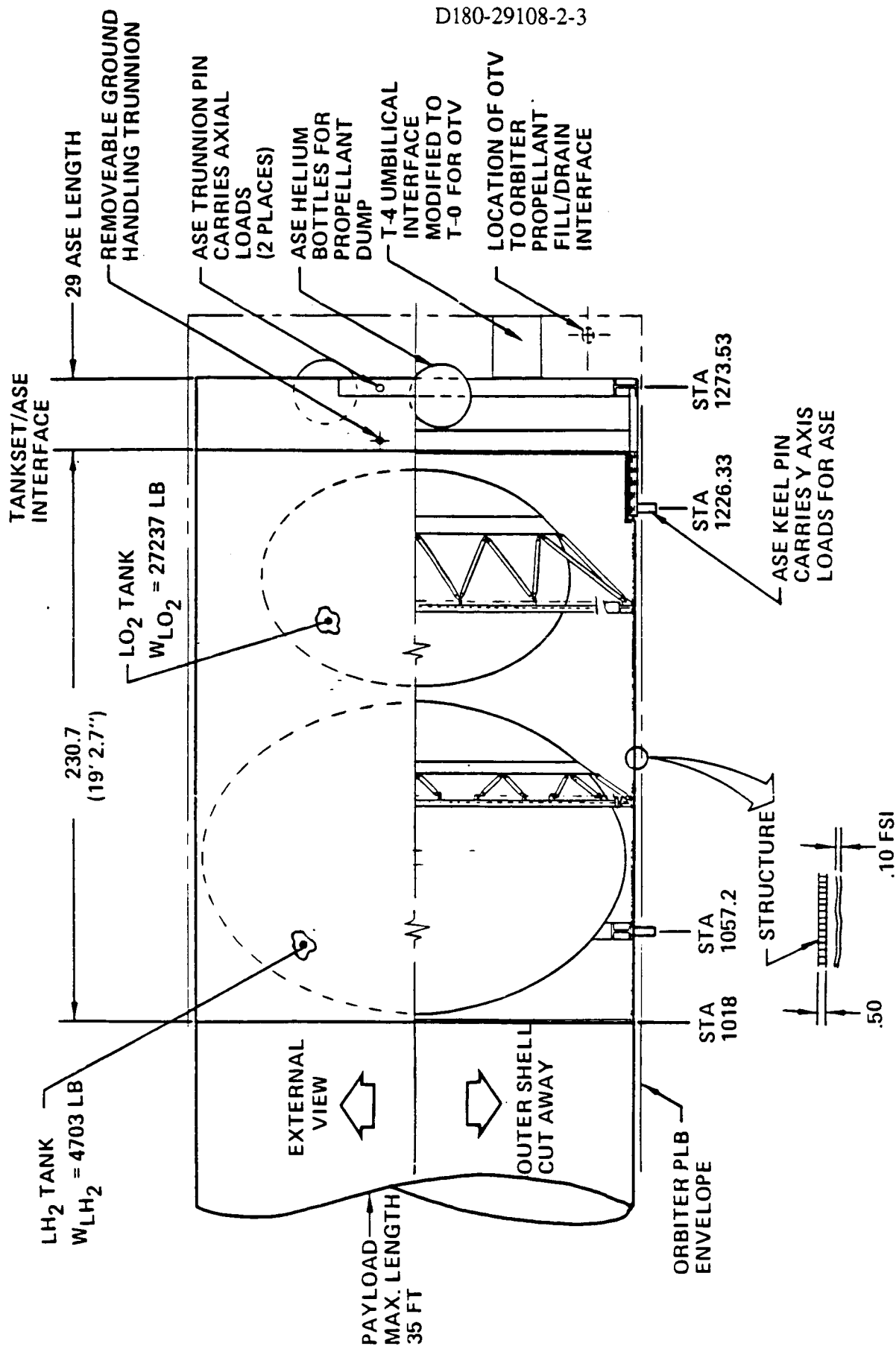


Figure 3.3.7.1 Auxiliary Tankset Ground Based Ballute Braked OTV

much deeper and lighter ASE structure. The forward trunnion support is substantially identical to that for the OTV.

3.3.8 GB ACC Lifting Brake OTV

The final configuration of the ground-based lifting brake OTV is provided in figure 3.3.8-1. This design is similar to the original reference configuration, except that it is longer, and has two advanced engines, rather than a single RL10. The thrust structure is larger and heavier, as well as the aerobrake support structure. The structural design loadings and features are given in table 3.3.8-1. These features are discussed in detail in the following paragraphs.

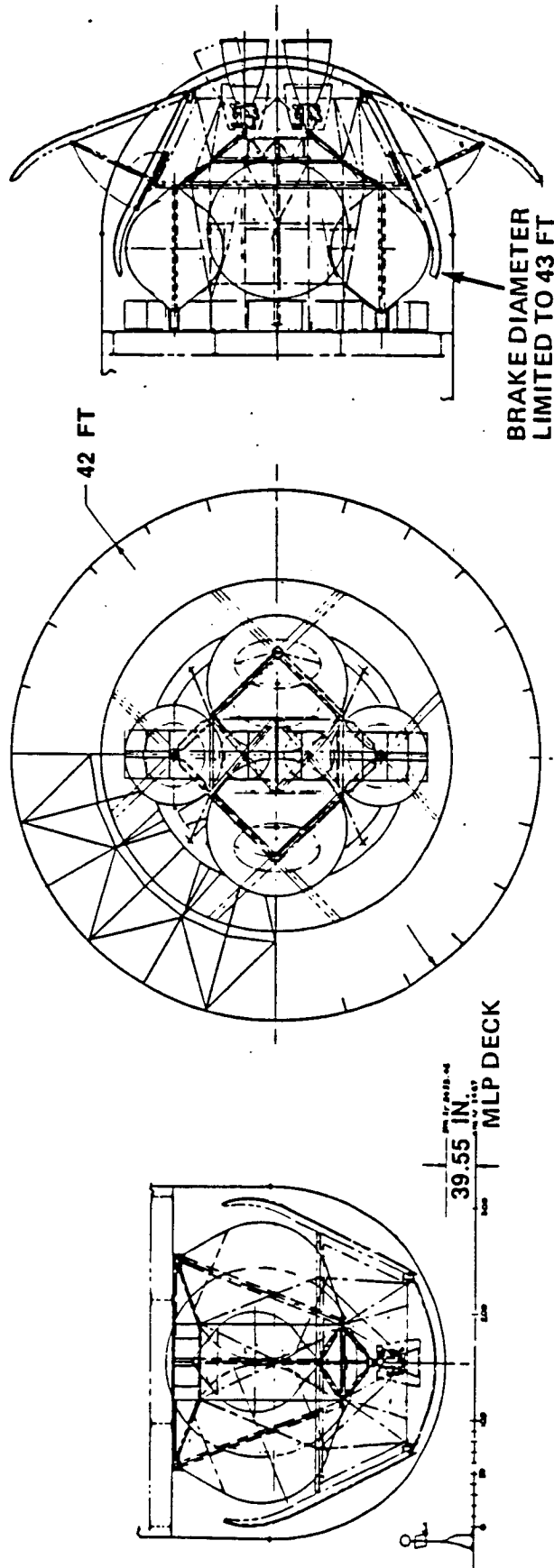
Aerobrake. Structural design of the GB ACC lifting brake is similar to that of the SB lifting brake, except the diameter of the brake is 42 feet, and the rib support struts are deployable, and are tied into a heavy support ring around the vehicle. Like the SB lifting brake, the brake ribs are tailored to the bending moment distribution in order to minimize deflections of the brake. Because of the need to recover and return the vehicle, the lifting brake is expended after each flight, so separation provisions are included. The flexible portion of the brake, including ribs and support struts are expended, while the heat shield remains intact.

The original reference design of the GB ACC lifting brake OTV had a 40 ft diameter deployable lifting brake that tied into the central truss structure of the vehicle.

Thrust Structure. The thrust structure for this vehicle is a strut-supported beam structure that transfers thrust loads to the central vehicle truss structure, as well as directly into the propellant tanks. The thrust beam is of GR/EP design, with mounting provisions for two advanced engines, and associated thrust vector controllers. Average cross-sectional area of the beam is 3.5 in². Additional structure is necessary for assembly and attachment.

The original reference configuration had a deep-beam thrust structure that distributed thrust loads from a single engine into the central box-truss structure and into the propellant tanks.

Equipment Support Section. The equipment support section is a rectangular box structure at the forward end of the vehicle at the payload interface. The ESS consists



FEATURES:

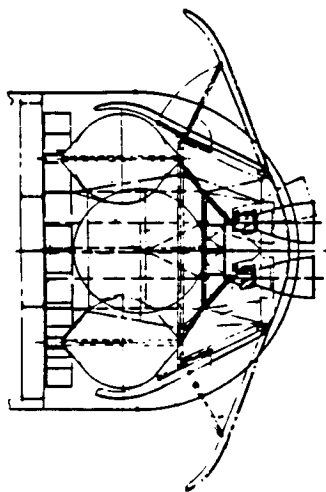
- LAUNCHED IN ET-OCB
- RETURNED IN STS-OCB
- LIFTING BRAKE AEROASSIST, -EXPENDABLE
- ADVANCED CRYO ENGINE T=5000 LBF
- 4 TANKS
- PROPULSION/HEATSHIELD MODULE

WEIGHT SUMMARY (LBM)

	MAN-RATED	MAN SCAR ONLY
• DRY	8,430	8,179
• MAIN PROP. (TOTAL)	42,630	42,630
• OTHER FLUIDS	1,169	1,169
• START BURN	52,229	51,978

Figure 3.3.8-1 GB ACC OTV Concept 107 Configuration

Table 3.3.8-1 GB ACC OTV No. 107 Structural Overview



● MAJOR STRUCTURE DESIGNED TO WITHSTAND LIFTOFF LOADS

- $N_x = -3.2 \text{ G (LIMIT)}$
 - $N_y = \pm 1.4 \text{ G (LIMIT)}$
 - $N_z = \pm 2.5 \text{ G (LIMIT)}$
- $N_{ult} = 1.5 \times N \text{ limit}$

● PROPELLANT TANKS ATTACHED DIRECTLY TO ACC SUPPORTS TO SAVE WEIGHT

- $N_x \text{ (ULT)} \times \text{WT (LOX)} = 91,000 \text{ LBF/TANK}$
- REINFORCED BOSSES AND INTERNAL RODS USED TO TRANSFER LOADS THROUGH TANKS

● REACTION OF TANK SIDE LOADS IS MAJOR STRUCTURAL CONCERN

- $N_y \text{ (UTL)} \times \text{LOX} = 71,000 \text{ LBF/TANK}$
- LIGHT WEIGHT TRUSS STRUCTURE USED TO REACT SIDE LOADS
- LIGHT WEIGHT GRAPHITE EPOXY AND GRAPHITE POLYIMIDE CONSTRUCTION

of GR/EP truss structures designed to support the equipment during aeromaneuver conditions, and aluminum load-carrying plates for attachment of avionics.

Propellant Tanks. The propellant tank pressure shells are sized to permit room temperature proof testing to 1.37 times the MEOP of 31.72 psia for the fuel tanks and 1.32 times the MEOP of 22.1 psia for the oxidizer tanks.

Design conditions for these tanks are the same as for the GB Ballute-braked OTV. The fuel tanks are designed for OTV main engine ignition, with a maximum head pressure of 0.1 psig. The oxidizer tanks are designed for ET burnout condition, with a head pressure of 13.7 psig. After return from orbit, the fuel tanks are purged and repressurized with helium, but the oxidizer tanks are only partially purged prior to return to ground.

Because of the nature of these tanks, the structural design is different from those of other OTV classes. A central support rod is included in each tank, and attachment is at either end of the tank, instead of at mid-tank rings. The hydrogen tank average dome thickness is 0.025 in. and the oxygen tank average dome thickness is also 0.025 in.

For the case of the ACC OTV configuration re-design, with a single LH₂ tank, and four LO₂ tanks, the tanks have the same design conditions, but do not have the central support rods. These tanks are supported at the outer ring structure. The hydrogen tank average skin thickness is 0.025 inches, and the oxygen tank average skin thickness is 0.025 inches.

Body Structure. The body structure for this vehicle consists of a central web-truss structure with lateral stiffening struts, and a deep-beam forward equipment support structure. For launch, all propellant loads are supported directly by the ACC support beam. The loads are distributed into the tank structure through the internal support rods. Thrust loads and aeromaneuver loads are reacted into the tanks and into the central body structure.

The central web structure is made up of GR/EP composites, and has an average unit weight of 1.9 lb/ft². The LH₂ tank support struts are of GR/EP design and have an average cross-sectional area of 0.5 square inches. The LO₂ tank lateral sway struts are of GR/EP, and have an average cross-sectional area of 1.2 square inches. The equipment support beam is a GR/EP box beam, with cross-sectional area of 4.0 square inches. Other structures include equipment support and installation provisions, latch assemblies for tank removal, umbilical interface plates and mechanisms, and orbiter-return support fittings.

In the original reference ACC OTV, the central body structure was a box truss structure with GR/EP struts. Other structures were similar to the current reference design.

With the vehicle design trade, alteration of the basic structural concept of the vehicle caused the primary structure to change from a central truss structure to an external cylindrical body shell. This cylindrical shell supports the single LH₂ tank, thrust structure, and aerobrake during launch, and provides the load path for thrust and aeromaneuver as well. The four LO₂ tanks are cantilevered from the cylindrical shell during thrust and aeromaneuver, but are directly supported by the ACC beam structure during launch. The cylindrical shell is of GR/EP sandwich, and has a unit weight of 0.71 lb/sq ft. Avionics equipment is supported from the conic section of the body shell. Other structure includes LO₂ tank support structure and disassembly mechanisms, aft thrust structure support struts, equipment installation provisions, umbilical interfaces, and shuttle-return fittings.

Rings Integral with Tanks. Rings are included in the tanks for this vehicle concept for stabilizing the tank walls during launch. Cross sectional areas average 0.3 in².

Payload Interface. The payload interface is integral with the forward body beam structure and equipment support structure. Pads for payload attachment and mechanism support are provided at 8 locations on the forward end of the vehicle.

Thermal/Handling/Meteoroid/Debris Protection. Like the other vehicles, the ACC vehicle has a limited LEO exposure to debris and has limited operation in proximity to manned systems, so the meteoroid/debris protection can be separate from the tanks, and the tanks sized for service life requirements. For this configuration, protection must be provided for 1280 ft² of wetted area, and the protection must be attached directly to the tanks themselves because of the vehicle configuration. The minimum gage shielding (0.016 in aluminum) and the minimum MLI for thermal control (30 layers) provides adequate protection for the vehicle tankage. Fiberglass supports are used to provide the 3.0 in outer shield standoff, and to minimize heat leak to the propellant tanks. This presents a potential problem and will need further analysis to determine the feasibility of such a method.

ASE. The ASE structure provided in the aft cargo carrier is a double cruciform deep-beam structure which interfaces with the OTV at the forward end. Attachment

provides direct support of the propellant tanks and of segments of the equipment support structure.

The ASE required to return the ACC OTV in the Shuttle includes a support cradle for the heat-shield/engine module, and support for the two LH₂ tanks and vehicle core module. The support cradle is a GR/EP truss cradle, with interfaces to the Shuttle at two longeron fittings and one keel fitting. This cradle also provides support for the repressurization tankage, as well as the vehicle-return instrumentation. The structure required for the LH₂ tanks and vehicle core module is built into the vehicle structure, and includes longeron and keel pins. All other structure required is government-furnished support structure in the Shuttle, such as longeron and keel bridge fittings and latches, and cabling support structure.

This Page
Intentionally
Left
Blank

4.0 PROPULSION

The OTV propulsion systems include the main propulsion system (MPS) and the reaction control system (RCS). The main propulsion system analyses are discussed in paragraph 4.1. The reaction control system analyses are discussed in paragraph 4.2. The analyses discussed in the following paragraphs was based on use of a ballute aeroassisted space based OTV although similar results would be anticipated for any of the vehicles described in Section 2.0.

4.1 Main Propulsion System

The main propulsion analyses focused on the selection of the propellant and engine.

4.1.1 Main Propulsion System Requirements

The primary requirement of the main propulsion is to provide thrust for the vehicle on demand in order to produce velocity changes for orbit transfers. Specific MPS burn requirements are:

- a. Perigee burns for insertion into LEO-GEO transfer orbit.
- b. Circularization at geosynchronous altitude if required for the mission.
- c. De-orbit from geosynchronous orbit to low earth orbit or aerobrake maneuver altitude as required for the mission.
- d. Velocity corrections if the required delta-velocity is greater than 20 feet/second.
- e. Provide velocity corrections prior to aeromaneuver for aeroassisted vehicles.
- f. Provide velocity corrections required after the aerobrake mission phase due to atmospheric dispersions.
- g. Circularize the orbit for recovery by the Shuttle or for recovery at the space station.

Other requirements of a more general nature are:

- a. Be reuseable for at least 10 missions to minimize recurring costs.
- b. Satisfy man-rating requirements.
- c. Be compatible with Shuttle launch capability.
- d. Be capable of operating in either a ground based or space based mode.

4.1.2 Main Propellant Selection

This trade was conducted as part of the midterm effort and used the BAC version of the Rev. 7 nominal mission model. This version had 252 OTV flights (vs 450 for the NASA model) and turned out to be essentially the same as the NASA Rev. 8 nominal model (257 flights). Although the Rev. 8 low model (145 flights) would have reduced the difference between the high and low performance concepts it was judged the conclusion would still be the same so the trade was not rerun. The other difference associated with the mid-term trade was that the weight of the vehicles was lower and, should the high final weights have been used, the higher performance concepts would again be more desirable. The remaining paragraphs of this section describe the trade as it was conducted.

Nine different propellant combinations were initially considered. Performance characteristics for the propellants are presented in figure 4.1-1. The development cost characteristics for engines which use these propellants is shown in figure 4.1-2. There are essentially two groupings relative to cost. Applying a screening criterion of selecting the highest performer (I_{sp}) from each group based on development cost, in addition to a non-cryo propellant and a propellant suitable for system evolution, resulted in selecting LF_2/LH_2 , LO_2/LH_2 , MMH and N_2O_4 , and a hybrid using N_2O_4/MMH and LO_2/LH_2 for further examination.

The configuration and performance characteristics for OTV's using the four candidate propellants are presented in figure 4.1-3. The use of single stages for the cryo options is the result of preliminary studies showing less than a 2-3% propellant penalty relative to two stages for an aerobraked OTV. A major contributor to this situation is the duplication of systems when two stages are used. The storable option however did benefit using two stages primarily because of the staging of inert weight offset the lower specific impulse. Specific impulse and bulk density contribute to the dry weight which in turn influences the propellant requirement. Based on these factors the LF_2/LH_2 systems require the least propellant followed by LO_2/LH_2 . The storable system even using two stages required nearly twice the propellant as the LO_2/LH_2 system. The hybrid system provided an improvement over the storable but still required considerably more propellant than the all cryo systems.

The undiscounted and discounted life cycle cost (LCC) comparison of OTV programs using the candidate propellants is shown in figure 4.1-4. All hardware and operations elements identified in Section 2.0 are included. The N_2O_4/MMH system has the least development cost but its high operations cost associated with propellant delivery (due to low I_{sp}) resulted in the highest LCC. A LO_2/LH_2 system gives the least

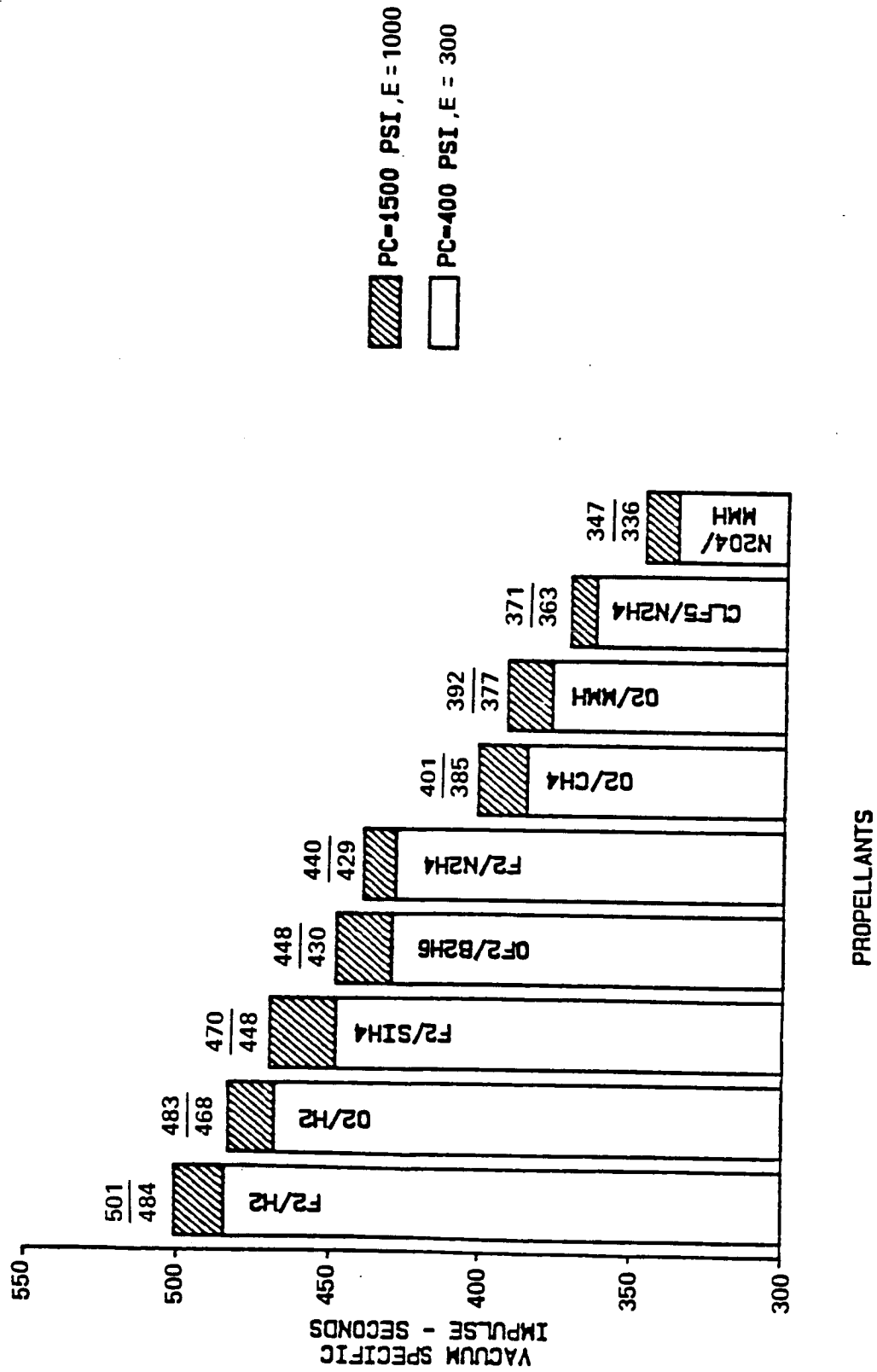
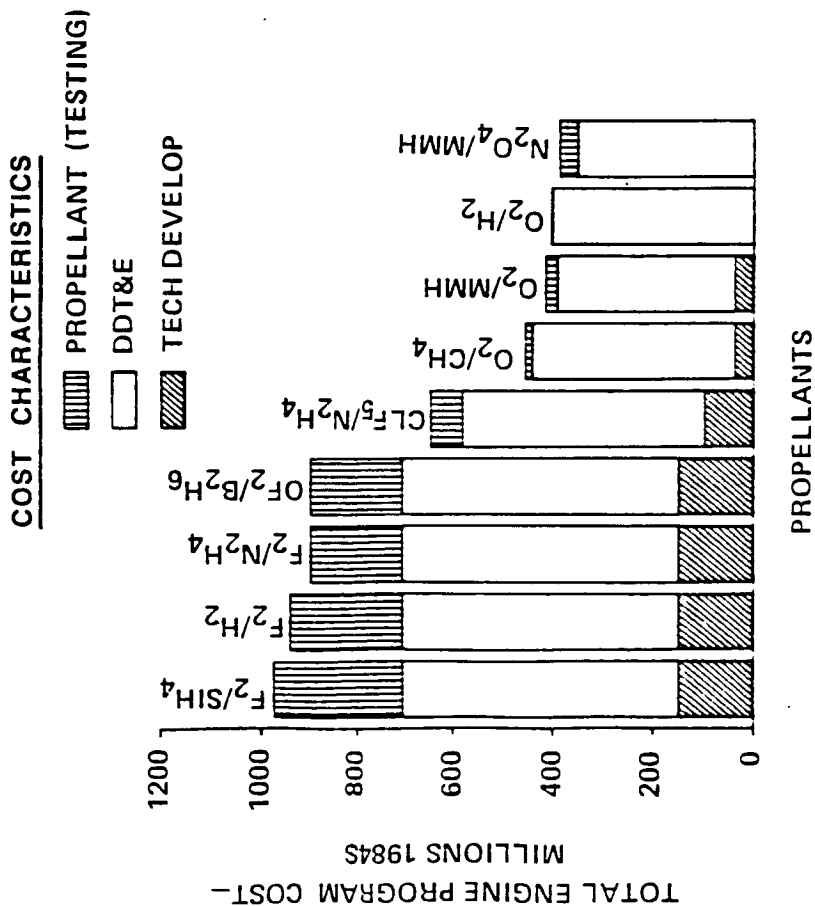


Figure 4.1-1 Propellant Performance Characteristics



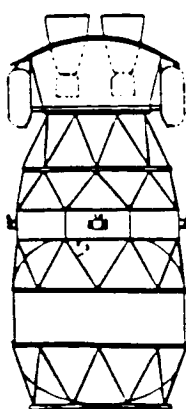
SELECTION

- CRITERIA—USE HIGHEST PERFORMER FOR EACH LEVEL OF DEV. COST
- HIGHEST DEV COST GROUP
USE LF₂/LH₂ (I_{SP} = 501)
NEXT CLOSEST (I_{SP} = 470)
- LOWEST DEV. COST GROUP
USE LO₂/LH₂ (I_{SP} = 483)
- OTHER CONSIDERATIONS
NON CRYO—N₂O₄/MMH
(I_{SP} = 346)
- PROP. EVOLUTION
BEGIN—N₂O₄/MMH STAGE
ADD—LO₂/LH₂ STAGE

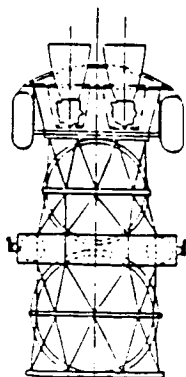
Figure A.1-2 OTV Propellant Candidates

● SECOND QUARTER TRADE

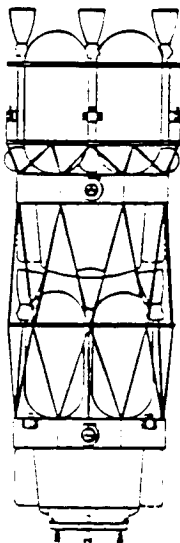
32 FT



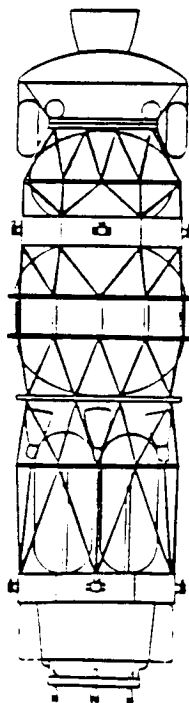
24 FT



45 FT



58 FT



PROPELLANT
SINGLE STAGE
LO₂/LH₂

I_{SP}
483

OTV DRY WEIGHT
8560

PROPELLANT WEIGHT
61,075

PROPELLANT
SINGLE STAGE
LF₂/LH₂

501

7700

54,400

PROPELLANT
TWO STAGE
N₂O₄/MMH

346

15000
(7780)
(7220)

114,400
(61,200)
(53,200)

PROPELLANT
TWO STAGE
LO₂/LH₂
N₂O₄/MMH

483
346

14990
(7910)
(7080)

90,980
(44,230)
(46,760)

[1] - ALL ENGINES P_C = 1500 PSIA, ε = 1000

[2] - SIZED FOR MAN SORTIE

D180-29108-2-3

Figure 4.1.3 Main Propellant Influence on OTV Configuration

BAC NOMINAL MISSION MODEL
1985 DOLLARS

UNDISCOUNTED

DISCOUNTED (10%)

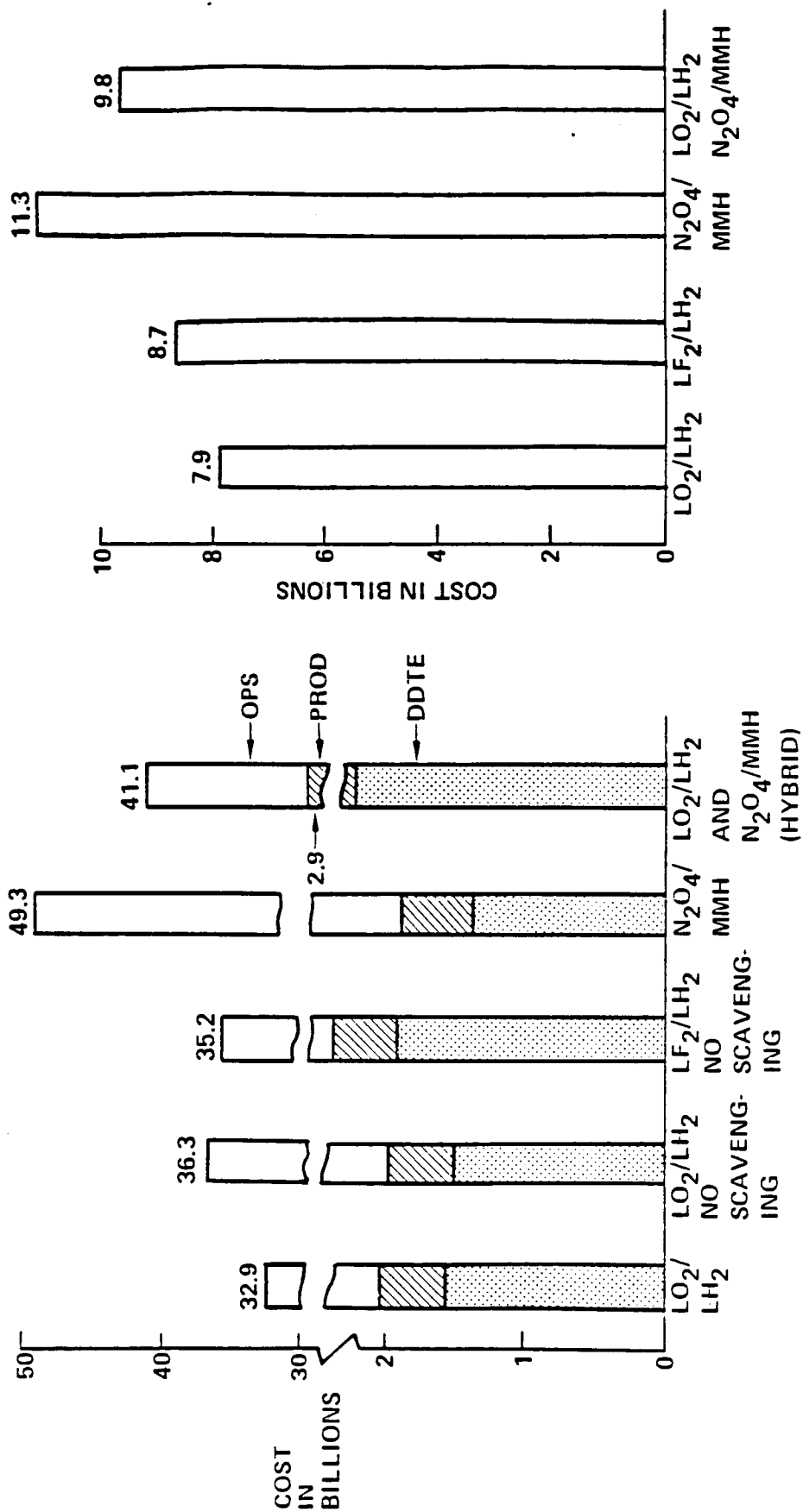


Figure A.1-3 OTV Program LCC Comparison Main Propellant Influence

LCC if propellant scavenging is used even though its performance is not as good as LF_2/LH_2 . This occurs because over 30% of the propellant is delivered via scavenging which reduces the net propellant delivery cost by 30% relative to a system that does not use scavenging. Although LH_2 could be scavenged for the LF_2/LH_2 option it represents only a small fraction of the total propellant requirement and was judged not worth the complexity. The hybrid system had even a higher development cost than the LF_2/LH_2 system primarily because two stages rather than one required development.

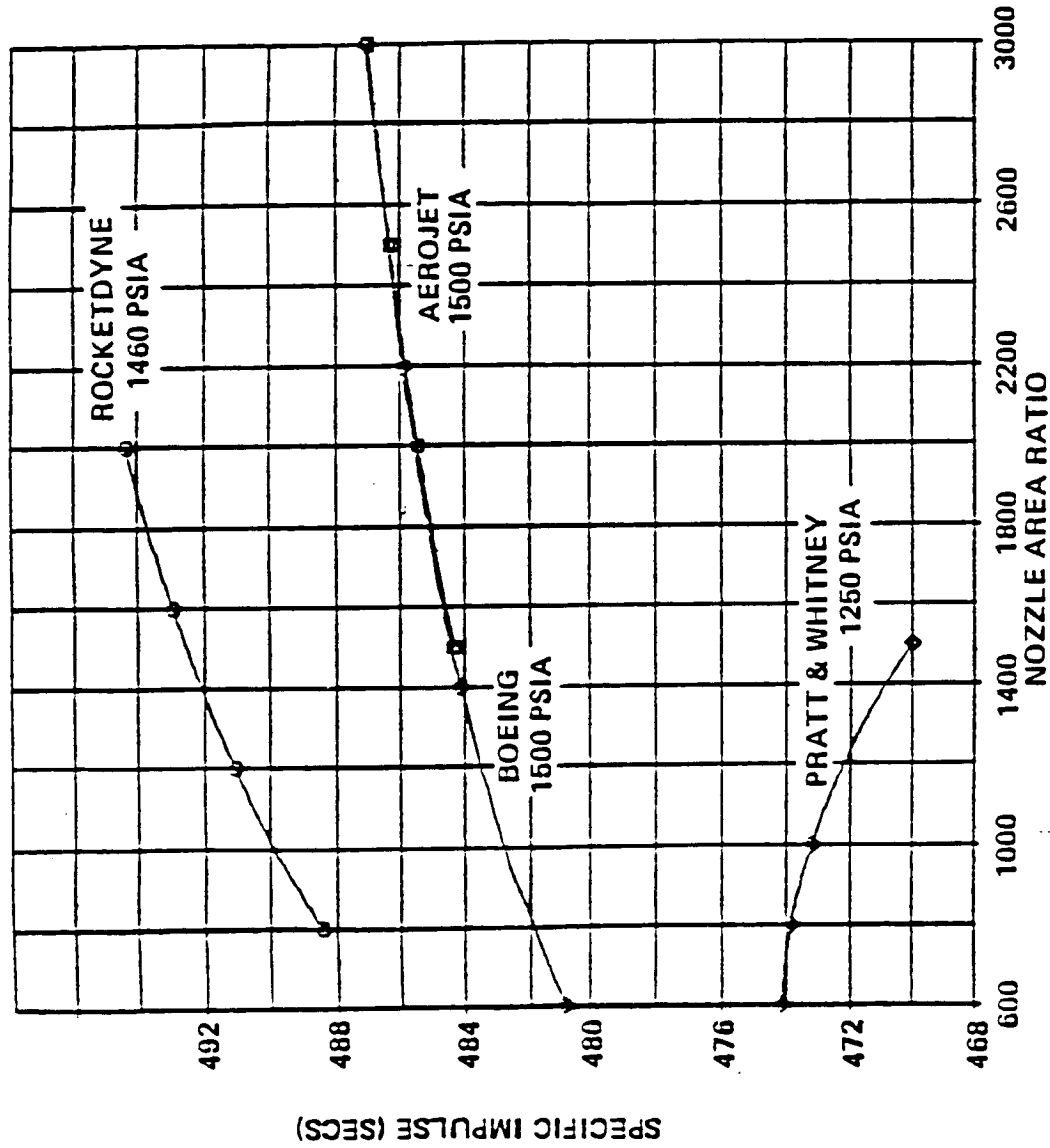
Our recommendation for main propellant is LO_2/LH_2 . This system provides a discounted life cycle cost advantage of 9% over the LF_2/LH_2 when propellant scavenging is used. In addition, the LO_2/LH_2 does not have the risks associated with handling and the extra equipment and operational procedures associated with LF_2 . The recommended LO_2/LH_2 system provides a 30% LCC advantage over the storable system due to the differences in operations cost resulting from its performance characteristics. For performance reasons the storable system required use of two stages and this would also be additional operational complexity relative to the one stage LO_2/LH_2 system.

4.1.3 Main Engine Selection

The analysis of main engine candidates was focused on those using LO_2/LH_2 since that was the selected propellant. The candidates consisted of derivatives of existing engines as well as a new advanced engine. The following paragraphs discuss the performance characteristics of the advanced engine and the program level comparison of the candidates.

4.1.3.1 Advanced Engine Characteristics

Specific Impulse and Weight. Engine performance data were available from Pratt and Whitney, Rocketdyne and Aerojet for advanced oxygen/hydrogen engines currently being studied under NASA contracts. Typical specific impulse data from these studies are shown by figure 4.1-5. The large variations in specific impulse between the manufacturers results from the lack of test data for nozzle expansion ratios greater than 400/1. The differences in performance are due to different methods of extrapolating nozzle performance from the lower area ratios and these discrepancies can only be finally resolved when higher area ratio test data are available. The manufacturers weights data shown by figure 4.1-6 also exhibit large differences. The weight differences are, in part, due to different type designs. The Aerojet weights shown do not include retractable nozzles and zero NPSH pumps as do the Rocketdyne and Pratt and Whitney data. Adding estimated weights for a retractable nozzle and



DIVERGENCE IN PERFORMANCE RESULTS IS A MAJOR CONCERN WITH RESPECT TO ENGINE TRADES

Figure 1.1-5 Specific Impulse Comparison

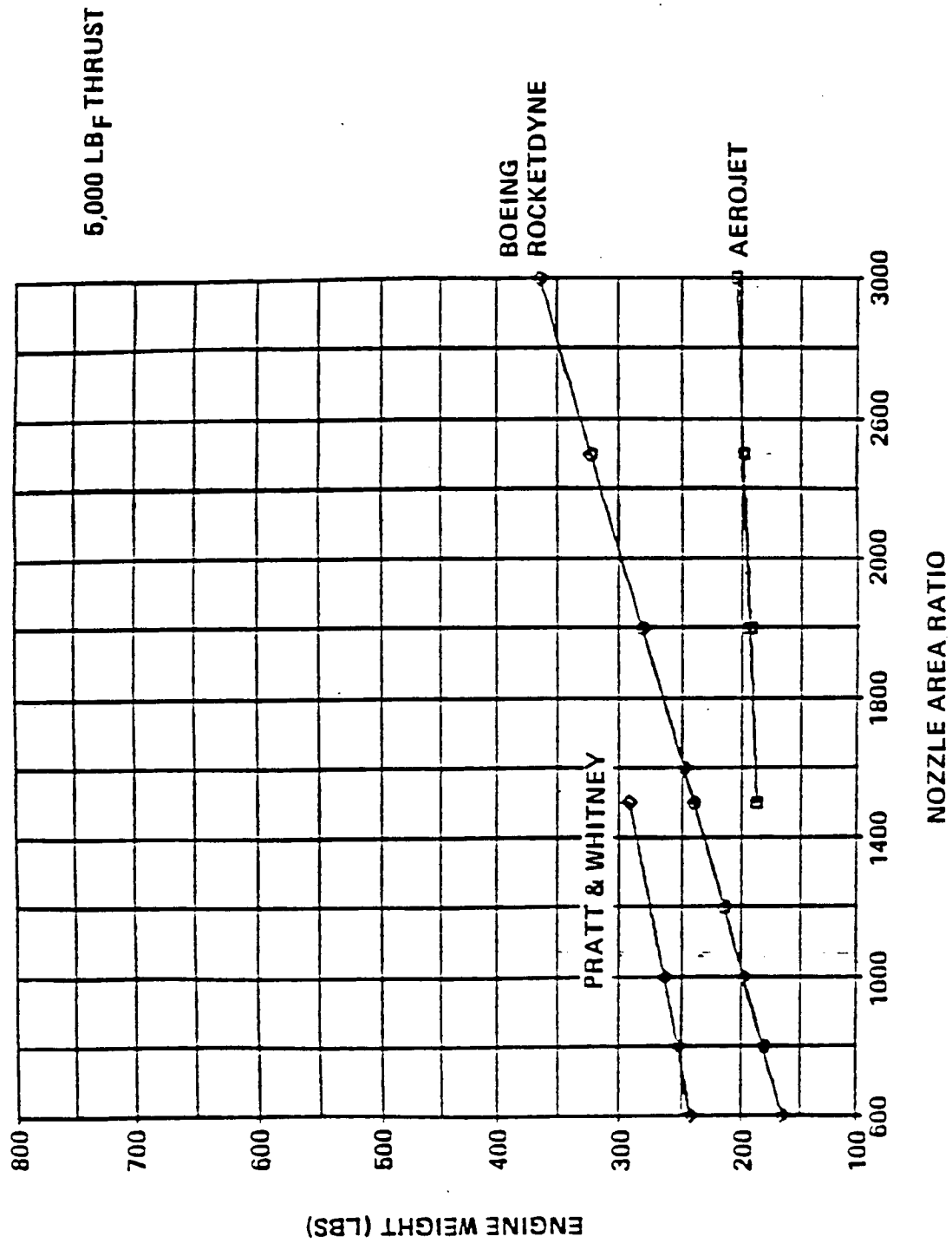


Figure 3.1-6 Engine Weights Comparison

zero NPSH pumps to the Aerojet data at 5000 lbf, 1000/1 area ratio results in approximately the same weight as shown by Rocketdyne but does not fully reconcile area ratio-weight trends. Trade studies investigating the effect of thrust were conducted using the Aerojet specific impulse data, which is reasonably conservative, and the Rocketdyne weight trends.

Thrust Level. Thrust level selection for the advanced engine took into account the number of engines required and the influence of propellant loading. Two engines have been incorporated as a result of the cost optimum reliability analysis performed for unmanned OTV application and described in Volume III. In addition, the criteria of no single point failures for manned OTV missions was best satisfied by two fully operational engines.

The influence of thrust level on propellant loading is shown in figure 4.1-7. Also included in this data is the influence of the number of perigee burns used on the up leg of a mission. The minimum loading is achieved using two perigee burns and a thrust level of 4000 lbf per engine. An engine thrust level of 5000 lbf was selected to provide for margin and growth potential.

4.1.3.2 Engine Comparison and Selection

The key characteristics of the investigated engines are shown in table 4.1-1. In the case of the advanced engine it should be noted that several of the parameters have a value specified for both space and ground versions of the engine. Most significant of the differences between engines are those involving weight (value shown is for one engine and two is the baseline), I_{sp} particularly for low g applications, life, and development time and cost. The key issue in this trade was whether the benefits of the advanced space engine (ASE) can offset its higher development cost.

Propellant requirement and payload capability for OTV's using the candidate engines is presented in figure 4.1-8. For the case of performing the manned GEO servicing sortie (MGSS) mission, the ASE provides an 8.6% and 14% advantage over the RL10-III and RL10-IIB, respectively. Using a fixed amount of usable propellant for a GEO payload delivery mission, the ASE provides a 16.2% and 29% advantage over the RL10-III and RL10-IIB, respectively. In both cases, the high I_{sp} and lower weight per engine are the major contributing factors.

The undiscounted and discounted life cycle cost (LCC) comparison of the main engines are presented in figure 4.1-9 in terms of their influence on total OTV program cost. An OTV with ASE's provides a 4.4% and 8.4% advantage over the RL10-III and

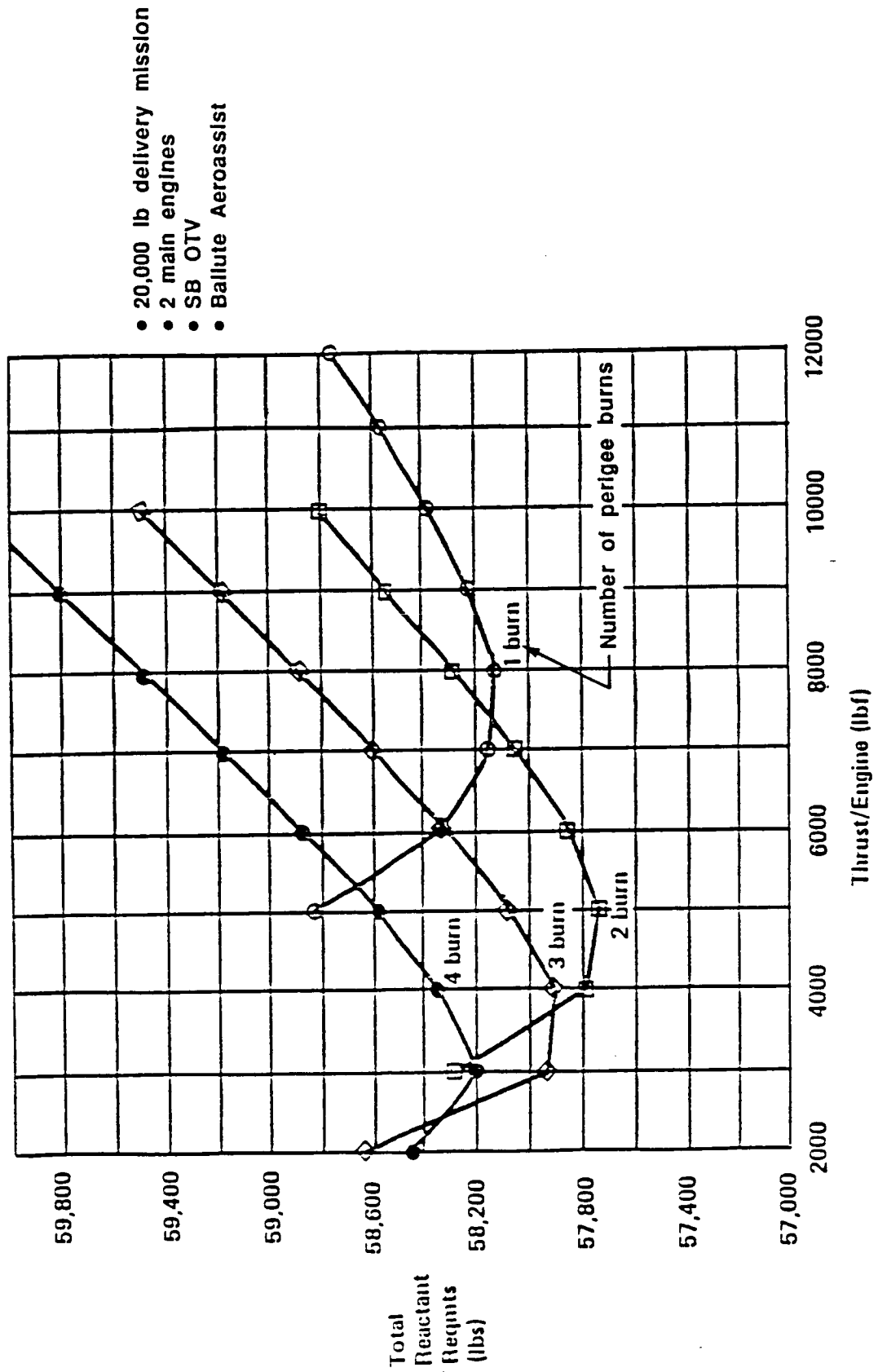






Figure 4.1-7 Two Engine Thrust Optimization

Table 4.1-1 LO₂/LH₂ Main Engine Candidates

PARAMETER	OPTIONS		
	RL 10-IIB	RL 10-III	ADVANCED 
• WEIGHT (LBS)	392	380	200
• THRUST (LB _F)	15,000	7,500	5000
• I _{SP} (SEC)	460	470	483
• LOW G TRANSFER I _{SP} (1 ENGINE OPERATING)	445	458	481
• LIFE (HOURS)	5	5	10
(FLIGHTS)	10	10	20
• DEVELOPMENT TIME (YRS)	3	3	6 (5)
• DDTE COST (\$M)	98	104	350 (300)
• UNIT COST (\$M)	1.9	2.0	3
• PROP LOAD 	75.8	71.3	65.2
 COMMON FOR SB AND GB OTV'S EXCEPT THOSE IN PARENTHESIS (UNIQUE TO GB)			
 FOR MANNED SORTIE MISSION			

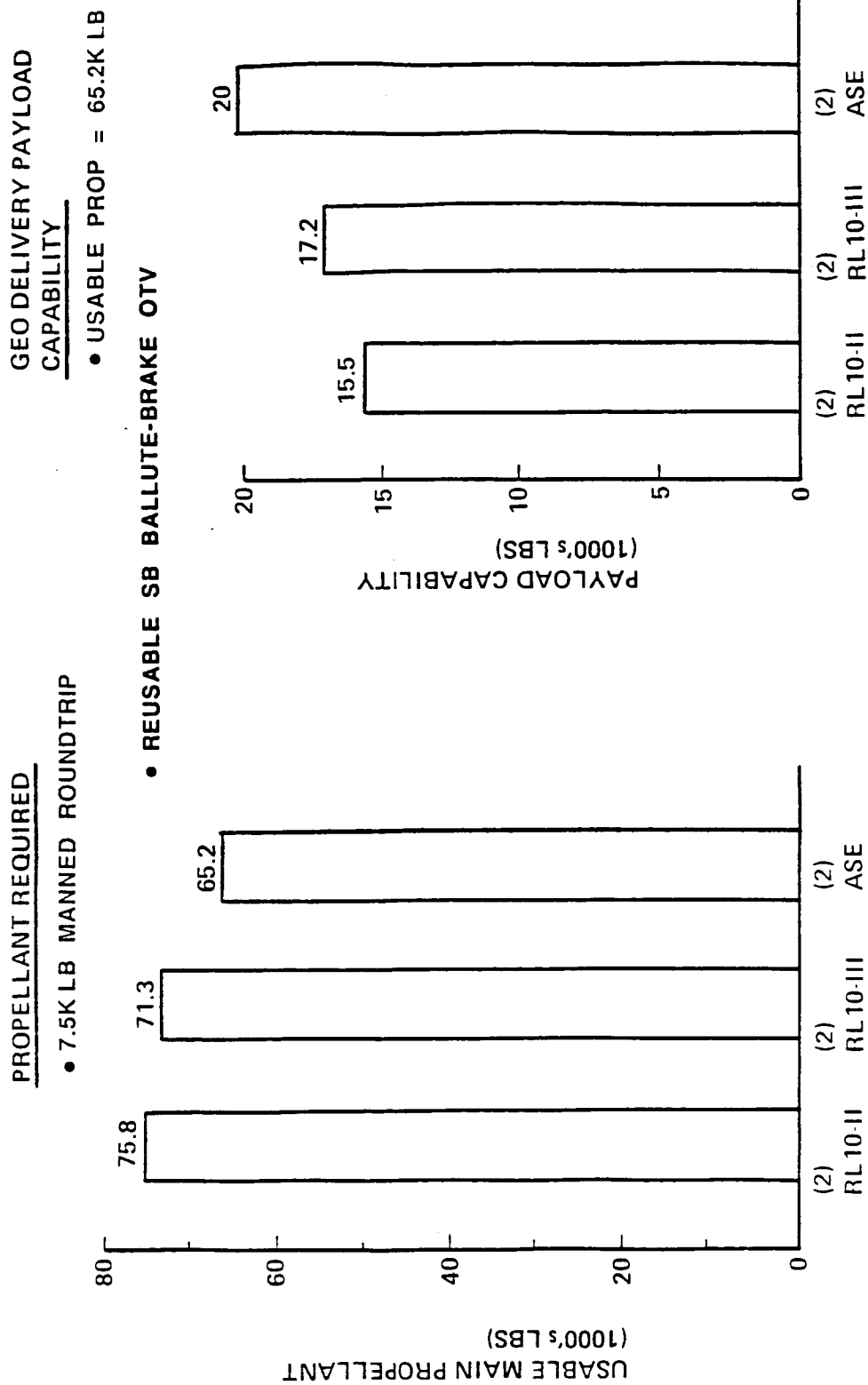


Figure 4.1-8 Performance Comparison LO₂/LH₂ Engine Candidates

- SB BALLUTE BRAKE OTV
- LOW MISSION MODEL 1997-2010

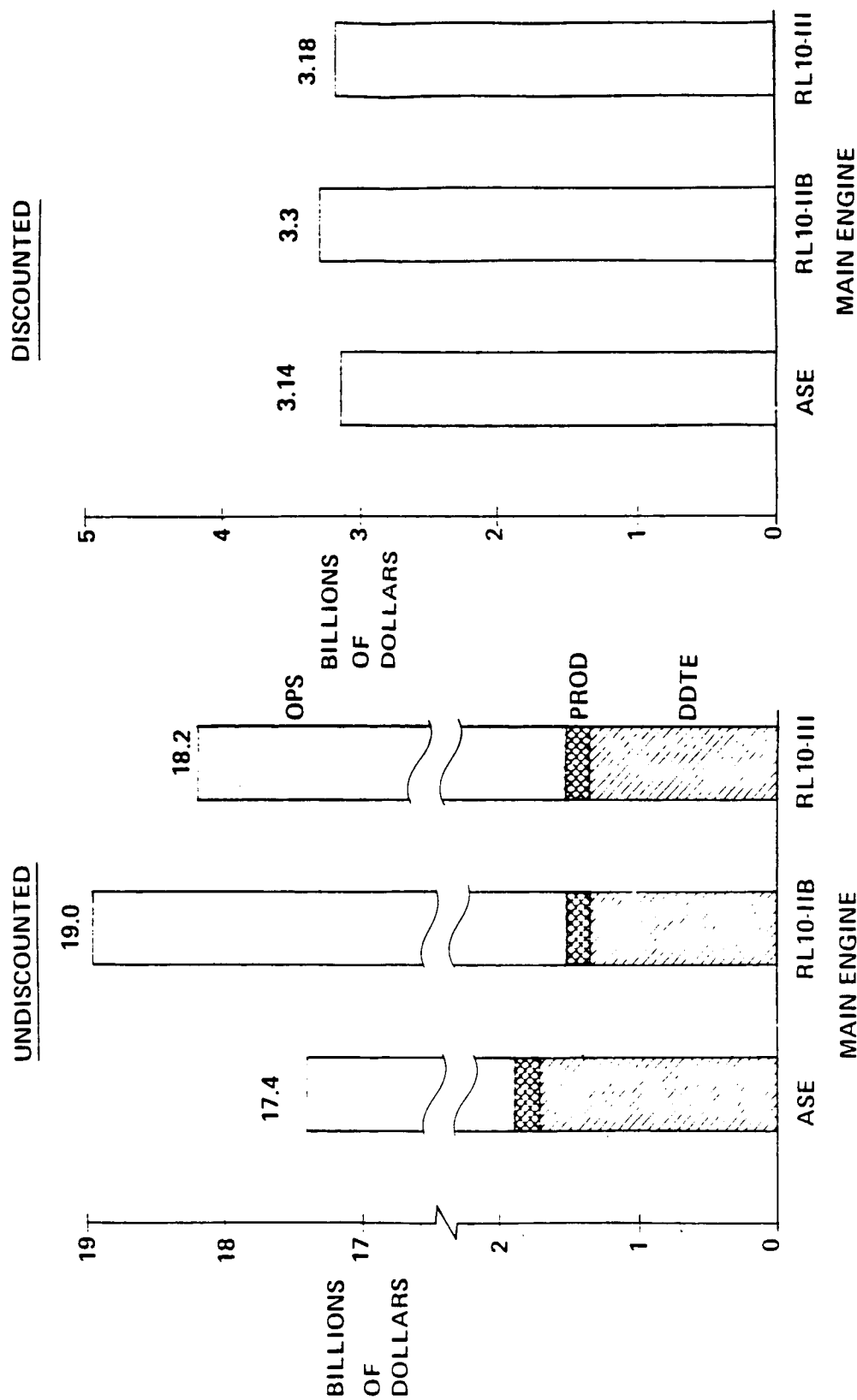


Figure 4.1-9 Main Engine Influence on OTV Program LCC

RL10-IIB, respectively. However, the ASE does have higher development cost and thus the discounted LCC comparison is closer which makes the time phased cost comparison an important parameter.

The plots shown in figure 4.1-10 present the cum LCC difference by year between a reference vehicle and any alternate vehicle in both discounted and undiscounted dollars. The influence of discounting in terms of how soon a given option begins to payback is clearly indicated. The reference vehicle has been chosen as one which uses ASE'S and as such is indicated by the zero dollar line. For the discounted case, which is most significant in terms of decisions when considering advanced hardware/programs, the data indicates the reference vehicle using ASE is increasingly more expensive than the alternative out to the point of beginning to fly the missions in 1994. In subsequent years however, the ASE is more efficient in terms of performance and requires less propellant thus lower recurring cost. By about 2001 the reference OTV with ASE's becomes cheaper than an RL10-11B OTV and cheaper than an OTV with RL10-111 in 2005.

Our recommendations for main engine for OTV application is the advanced LO₂/LH₂ system. Each engine has a thrust level of 5000 lbf, $P_c = 1500$ psia, expansion ratio of 1000, and Isp of 483 sec. Although the discounted payback relative to the closest competitor (RL10-111) takes a little longer than desired, other advantages such as additional performance capability to handle changes in mission requirements and better operations features in terms of dealing with design life and maintenance justify the selection of the ASE.

4.1.3.3 GB OTV Engine Selection

Only the advanced engine was considered for GB OTV application because the other engines did not have sufficient performance to allow a 12k lbm payload to be flown in a single 72k lbm STS flight (reusable mode). Discussion of the GB OTV performance is presented in Vol. III.

4.1.4 Baseline System Description

Key characteristics of the baseline main propulsion system resulting from the trades and analyses is shown in figure 4.1-11. This system which uses LO₂/LH₂ propellant and advanced engines provided the least program cost (discounted), good growth capability and a minimum of risk. Two engines and redundant valves throughout the system result in a cost optimum design for unmanned missions and satisfies manned mission criteria of no credible single point failures. The retractable nozzle feature

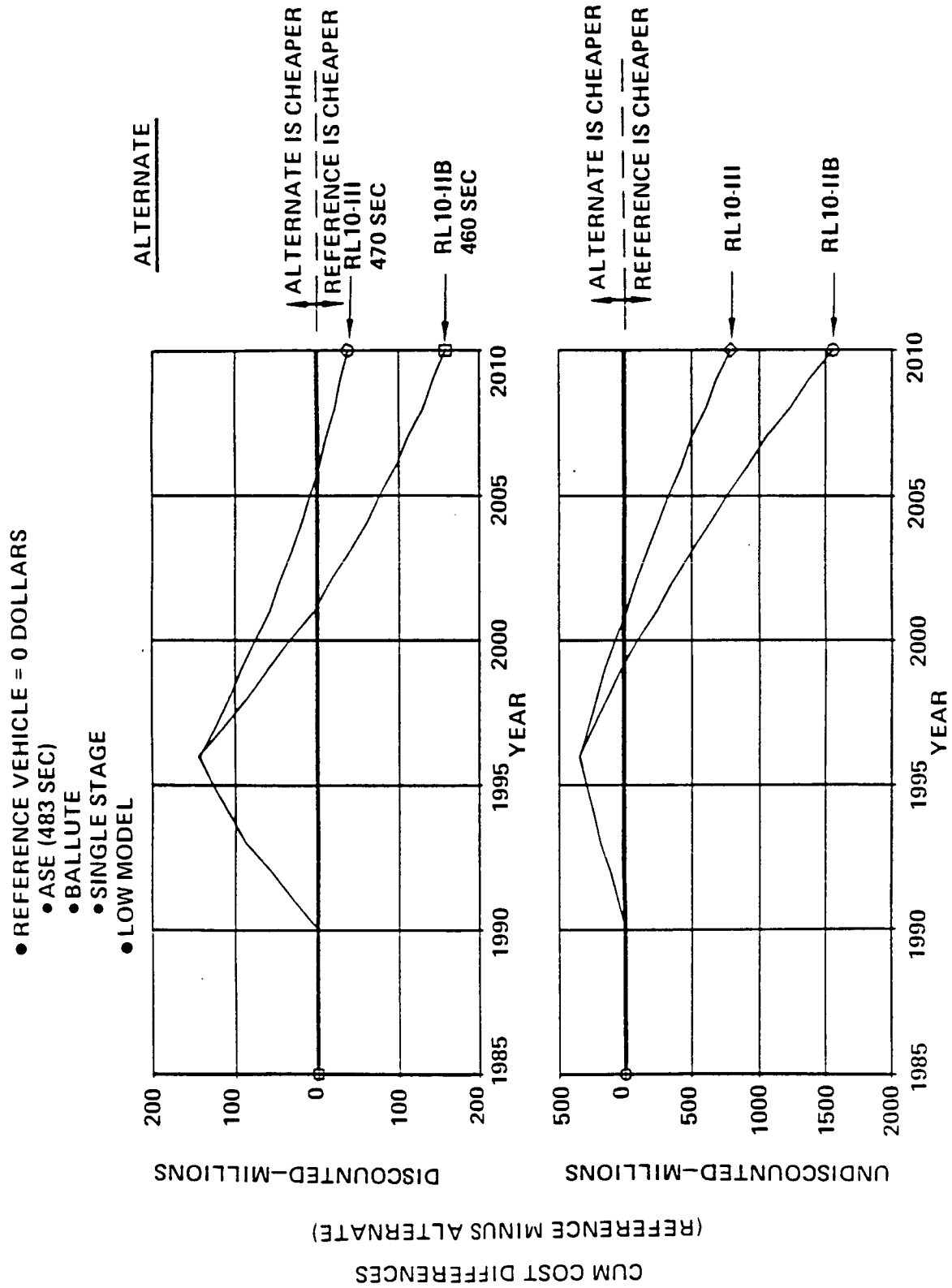


Figure 4.1-10 Time Phased LCC Comparison SBOTV Main Engine Trade

- DUAL FAILURE TOLERANT DUAL ENGINES
- HIGH RELIABILITY (0.99573)
- AT LEAST FAIL SAFE IN ALL COMPONENTS
- MAIN ENGINES:
 - $F = 5000 \text{ LB}_F \text{ EACH}$
 - $P_{CH} = 1500 \text{ PSIA}$
 - $\epsilon = 1000$
 - $I_{SP} = 483 \text{ SEC}$
 - $W_{ENG} = 200 \text{ LBS}$
- RETRACTABLE NOZZLE

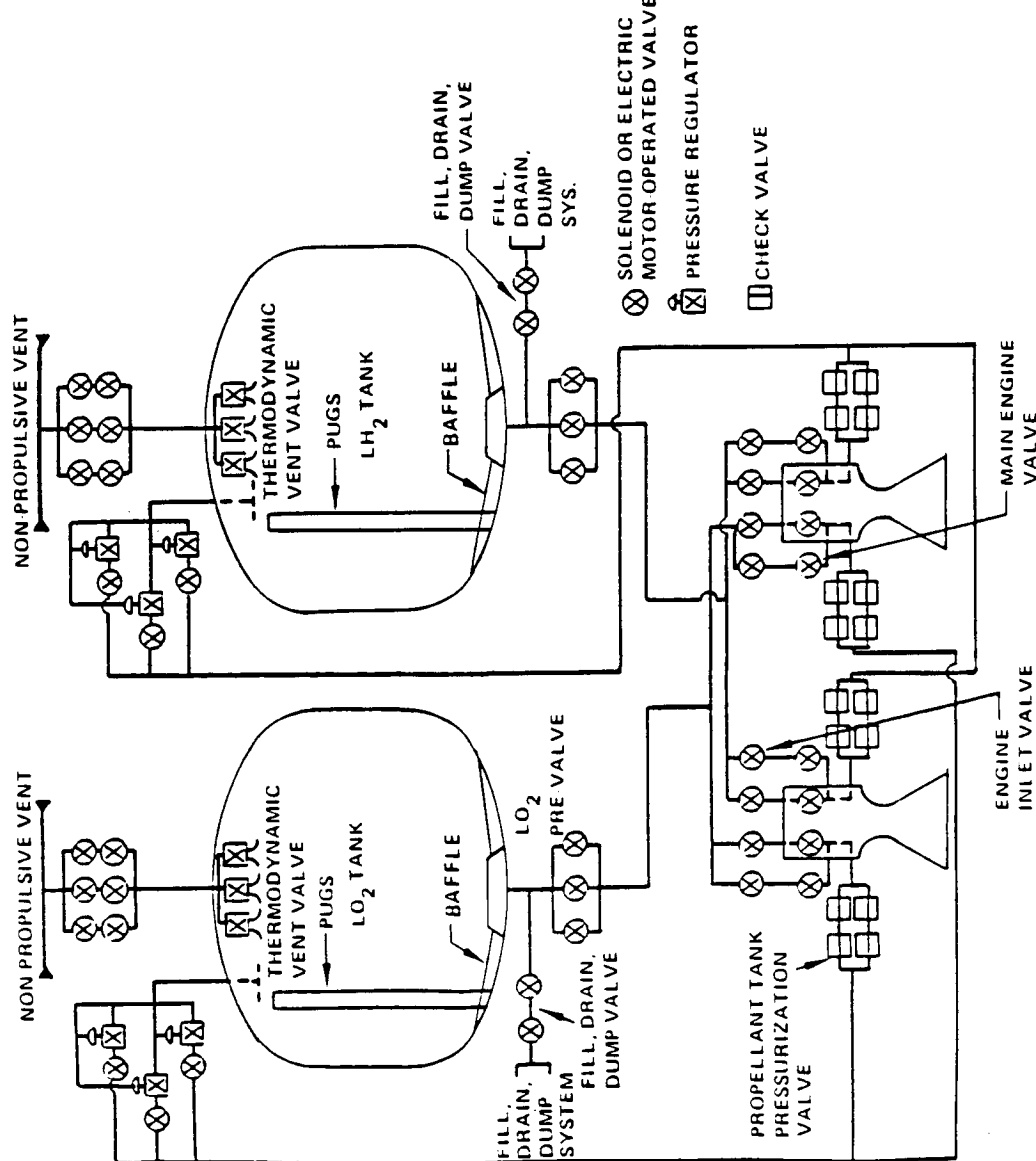


Figure 4.1-11 Baseline Main Propulsion Subsystem

allow the engines to be stowed behind the heat shield during the aeromaneuver. The engines also incorporate the features necessary to allow autogeneous pressurization.

The propellant loading sensitivity of the system to engine thrust level and Isp is shown in figure 4.1-12. For example, if specific impulse is two seconds lower than the baseline of 483 sec only a 600 lb propellant penalty will result. Should the optimum thrust level of 4000 lbf be used instead of 5000 lbf the propellant savings would only be 250 lbs.

4.2 Reaction Control System

The primary emphasis in the RCS area was to compare alternative propellants and their overall system impact.

4.2.1 RCS Requirements

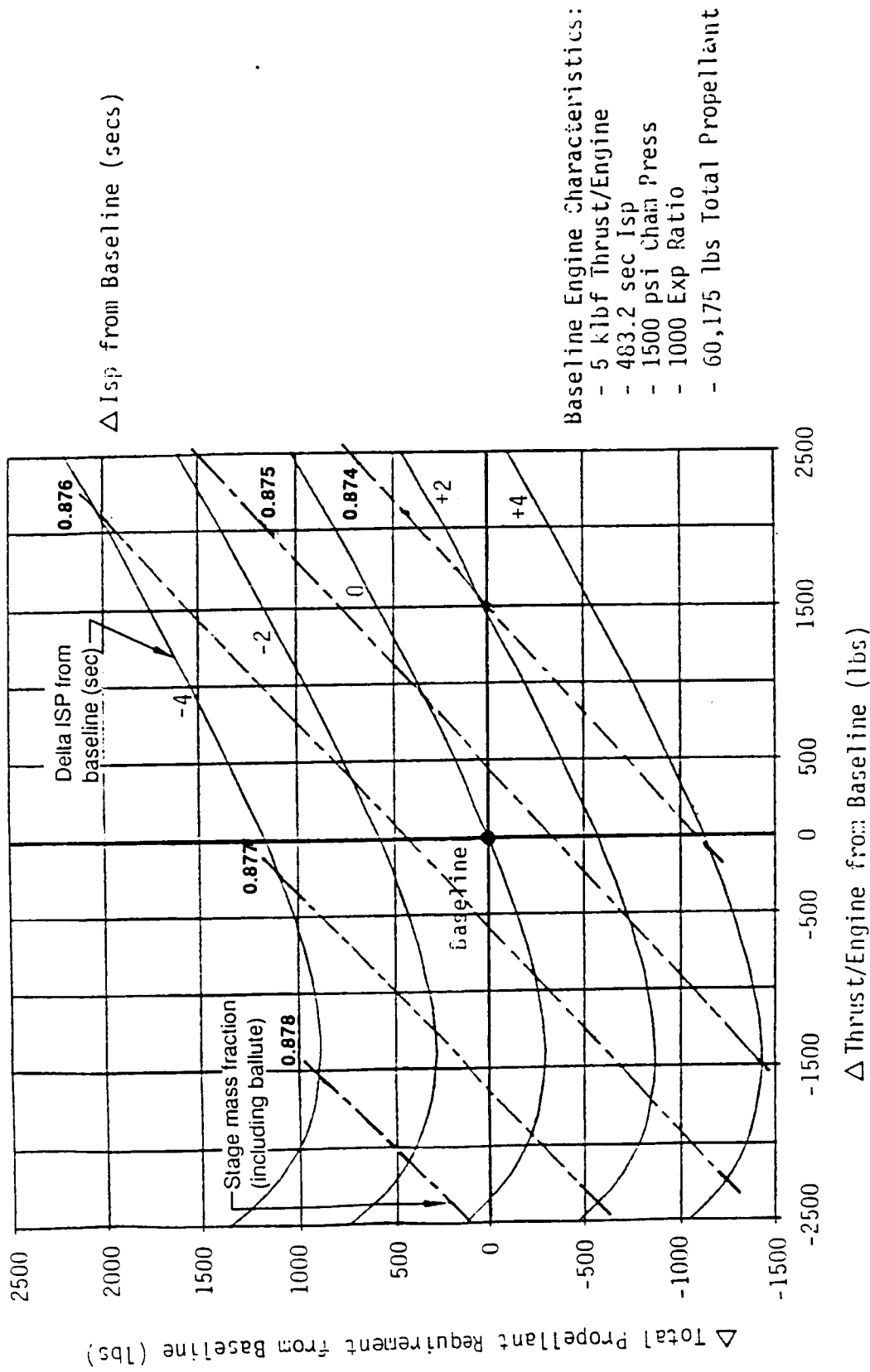
The purpose for the reaction control system (RCS) is to control the vehicle orientation during coasting periods and perform maneuvers which do not warrant use of the main propulsion system. Top level requirements to support the OTV missions and objectives are:

- a. Provide thrust for delta-velocity maneuvers of less than 20 fps.
- b. Be reuseable for at least 20 missions to minimize recurring costs.
- c. Satisfy man-rating requirements.
- d. Control orientation of the vehicle and provide initial pointing for main propulsion system start.
- e. Be capable of operating in either a ground based or space based mode.
- f. Be compatible with Shuttle launch.
- g. Provide six degree of freedom control for docking maneuvers.

The delta V budget for the RCS is shown in table 4.2-1. The modifications proposed and used by Boeing primarily reflect use of the MPS rather than RCS for any individual orbit correction burn greater than 20 fps.

4.2.2 RCS Propellant Trade

Comparison of the RCS propellant alternatives were done using a ballute braked space based OTV. The results of this trade however are applicable to all vehicle configurations described in section 2.0. The only differences in the RCS for the different vehicles would be the engine sizes needed to provide the control authority



Engine Operation Effects on Mission Propellant Requirement; 2 ASEs
 Nominal Engine Start/Stop and Boiloff Losses; Adv LOX/LI12 Values
 2 Perigee Burn GEO Servicing Mission with MGSS- 7500 lbs Roundtrip
 Jetisonable Ballute Configuration

Figure 4.1-12 Engine Design Perturbation Effects 7500 lb GEO Round Trip with MGSS

Table 4.2-1 Reaction Control System Requirements

- GENERAL REQUIREMENTS
 - FAIL OPERATIONAL/FAIL SAFE
 - FULLY REUSABLE, REFUEL AT SPACE STATION
 - 6 DEGREES OF FREEDOM
- PERFORMANCE REQUIREMENTS

MISSION PHASE	NASA ATTITUDE CONTROL EQUIVALENT ΔV , FT/SEC	BOEING ATTITUDE CONTROL & ORBIT TRIM EQUIVALENT ΔV , FT/SEC	
		RCS	MPS
SEPARATE FROM STATION	10	10	—
COAST TO FIRST PERIGEE BURN	0	10	—
INTERMEDIATE ORBIT TRANSFER	20	20	—
TRANSFER TO GEO COAST	10	10	—
GEO PAYLOAD POSITIONING	15	15	—
COAST AT GEO (24 HOURS)	50	50	—
DEORBIT TO LEO COAST	50	10	50
AEROBRAKE INTO PHASING ORBIT	50	—	~250 (TYPICAL)
PHASING ORBIT TRIM	15	20	—
LEO CIRCULARIZATION	10	40 ∇	—
TOTAL	230	185	300

∇ > INCLUDES RENDEVOUS AND DOCKING ALLOCATIONS

required for the different moments of inertia and a small variation in propellant quantity.

4.2.2.1 RCS Configuration Concepts

The reaction control systems analyzed for the OTV were a monopropellant hydrazine system and a hydrogen/oxygen system using common storage of the propellants with the fuel cell reactants.

The schematic of the hydrazine system shown in figure 4.2-1 indicates the functional arrangement of the thrusters, tanks and other components. Redundancy for manned missions required 24 thrusters to provide six degrees of control. Only 16 thrusters would be required for unmanned missions. Thrusters are arranged in four clusters with six thrusters each. Steady state thrust of each thruster is approximately 30 lbf at the maximum operating pressure of 380 psia. The minimum impulse bit is 0.30 lbf-sec. The thrusters are provided with thermostatically controlled electrical heaters to prevent propellant freezing. The propellant tanks contain bladders to separate the hydrazine from the nitrogen pressurizing gas and provide positive liquid expulsion. Each tank is connected to a manifold to distribute the propellant to the thruster clusters. Thermostatically controlled electrical heaters maintain the tanks, manifold and connecting lines above the freezing temperature of the hydrazine propellant. Six tanks are used because packing within the available envelope was found to be difficult with a fewer number of larger tanks.

The concept for the supercritical cryogenic oxygen/hydrogen system is shown in figure 4.2-2. The propellant has common storage with the fuel cell reactants. The electrical heaters in the cryogenic tanks are controlled by pressure switches to maintain approximately 300 psia pressure in the hydrogen tank and 900 psia in the oxygen tank. The advanced technology RCS thrusters provide approximately 410 seconds specific impulse. The system uses 24 thrusters the same as the monopropellant system to provide redundancy and satisfy man rating requirements.

4.2.2.2 Concept Comparison and Selection

Weight characteristics and trends were developed for monopropellant hydrazine and cryogenic oxygen/hydrogen reaction control systems as a function of total impulse requirements as shown in figure 4.2-3. The simpler monopropellant system has the lowest dry weight but the total weight including propellant is higher than the oxygen/hydrogen system for total impulse requirements higher than about 60,000 lbf-sec. A typical OTV delivery mission with 20,000 lbm payload requires an RCS total

- 6 DEGREE OF FREEDOM CONTROL
- COMPLETE DUAL REDUNDANCY
- NITROGEN PRESSURIZATION
- 24 THRUSTERS
- 25 LBF THRUST
- 1500 LBM HYDRAZINE PROPELLANT

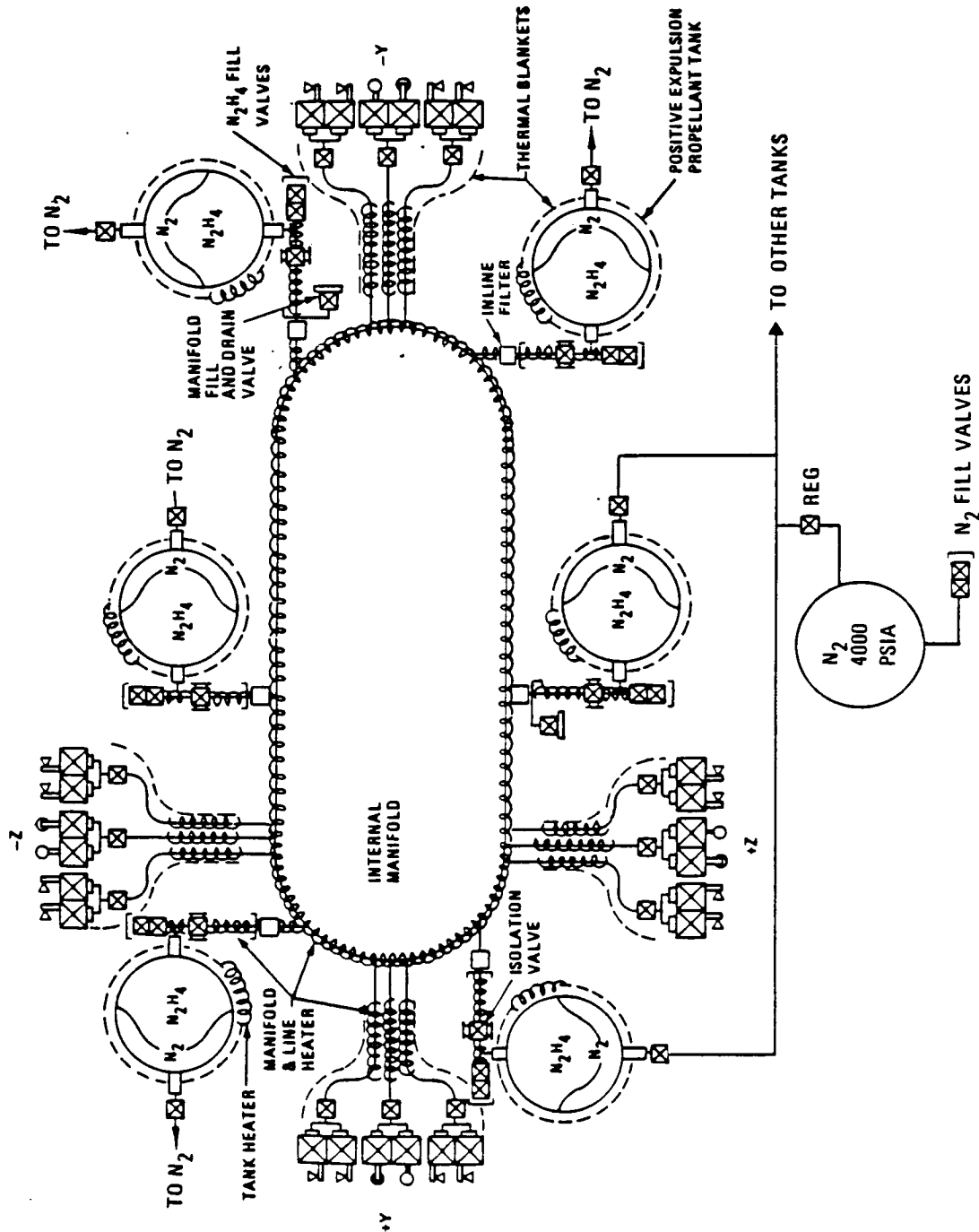


Figure 4.2-1 Baseline Reaction Control Subsystem

OTV-851

- **SYSTEM CHARACTERISTICS**
 - PROPELLANT STORAGE COMMON WITH FUELS CELLS
 - THRUST, 25 LBF
 - SPECIFIC IMPULSE 410 SEC. (CONSERVATIVE)
- **ADVANTAGES**
 - LOGISTICS-MINIMUM NO. OF FLUIDS REQUIRED
 - NON-CONTAMINATING EXHAUST
 - MINIMUM NO. COMPONENTS FOR RCS PLUS FUEL CELLS.
- **DISADVANTAGES**
 - ADVANCED TECHNOLOGY LIGHT WEIGHT TANKS REQUIRED
 - THRUSTER DEVELOPMENT REQUIRED. (BEING DONE FOR SPACE STATION.)
- **CONCERNS**
 - TRANSIENT PRESSURES WITH CRYOGENIC FLUIDS AND WARM LINES.

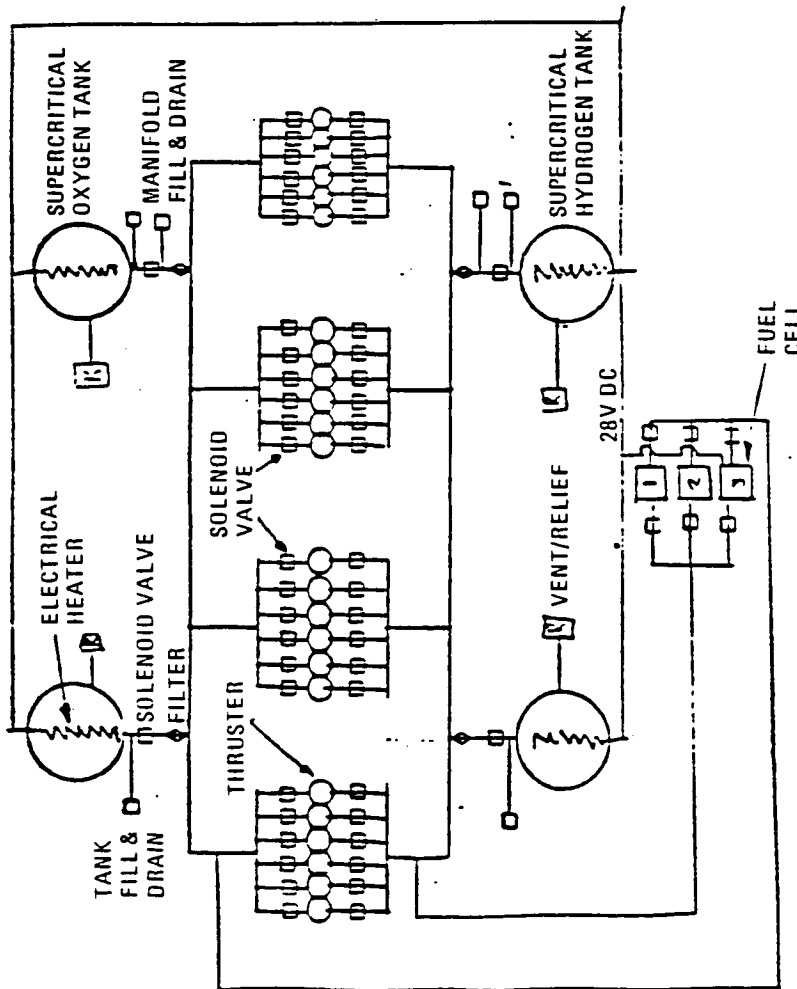


Figure 4.2-2 Reaction Control Subsystem—Supercritical Oxygen-Hydrogen

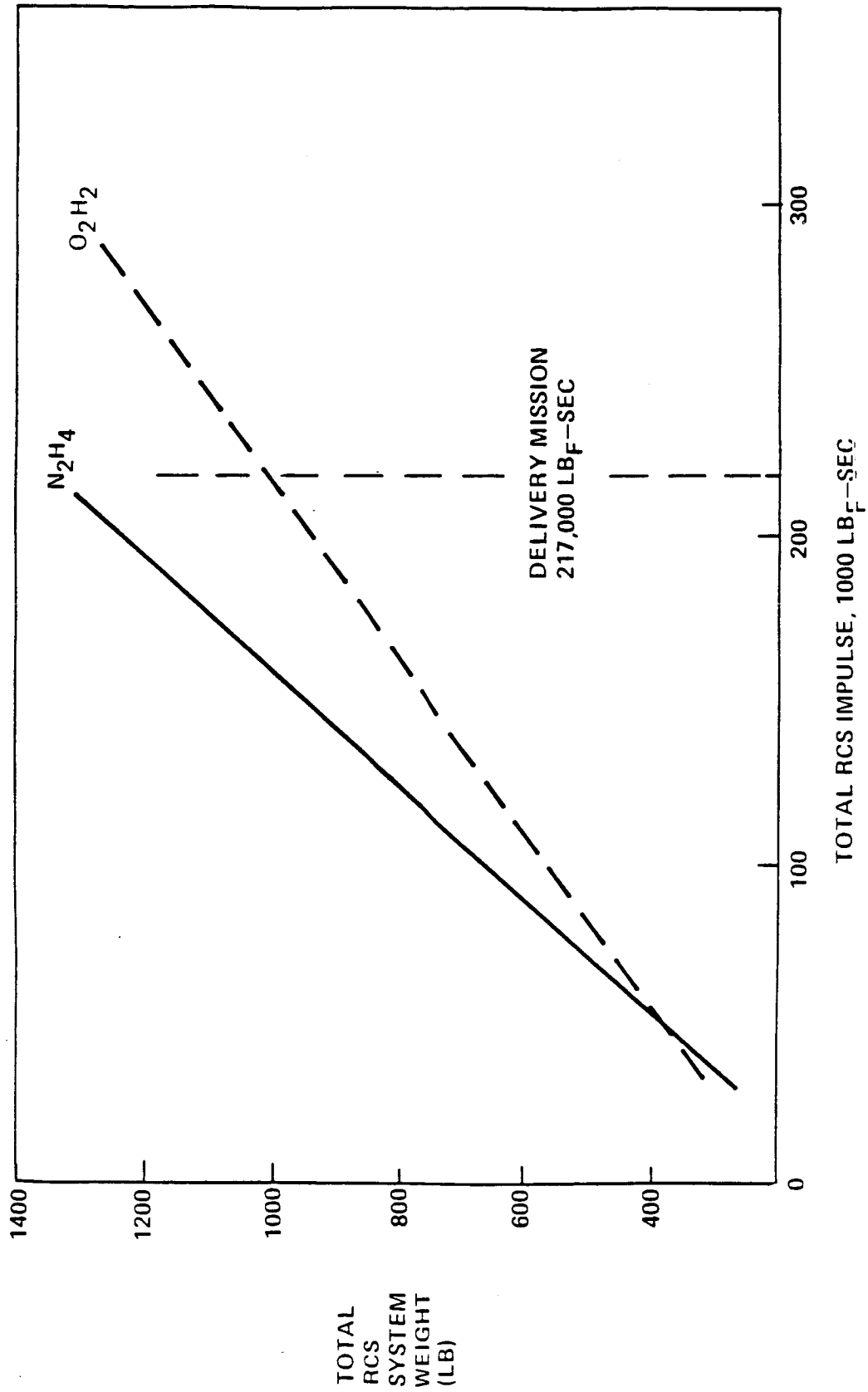


Figure 4.2.3 Reaction Control System Weight Comparison

impulse of approximately 21,7000 lbf-sec. The oxygen/hydrogen RCS weight including propellant for this total impulse is 385 lbm lower in weight than the monopropellant system for the same mission requirement.

Summary characteristics for the two concepts are presented in table 4.2-2. The dry weight of the cryogenic oxygen/hydrogen system is approximately 75 lbm heavier than the hydrazine system. The cryogenic RCS propellant quantity is less however because of having a higher I_{sp} . The total system weight for the oxygen/hydrogen concept is also lower resulting in less MPS propellant. The net benefit of the cryo system on a per flight resupply basis is 660 lbs.

Total program life cycle cost comparisons shown in figure 4.2-4 found the two systems extremely close but with a small advantage for the hydrazine system. The comparison of LCC on a time-phased basis, shown in figure 4.2-5, illustrates that the higher specific impulse of the oxygen system was not sufficient to offset the higher development and hardware costs of that system.

Our recommendation for RCS propellant is monopropellant hydrazine because its life cycle costs were lower and it is a less complex system. Should the RCS delta V budgets be substantially higher than those assumed and/or the development cost for the cryo system be shared with another program then further consideration should be given to O_2/H_2 RCS.

- SB B/B OTV
- LOW MODEL (1997-2010)

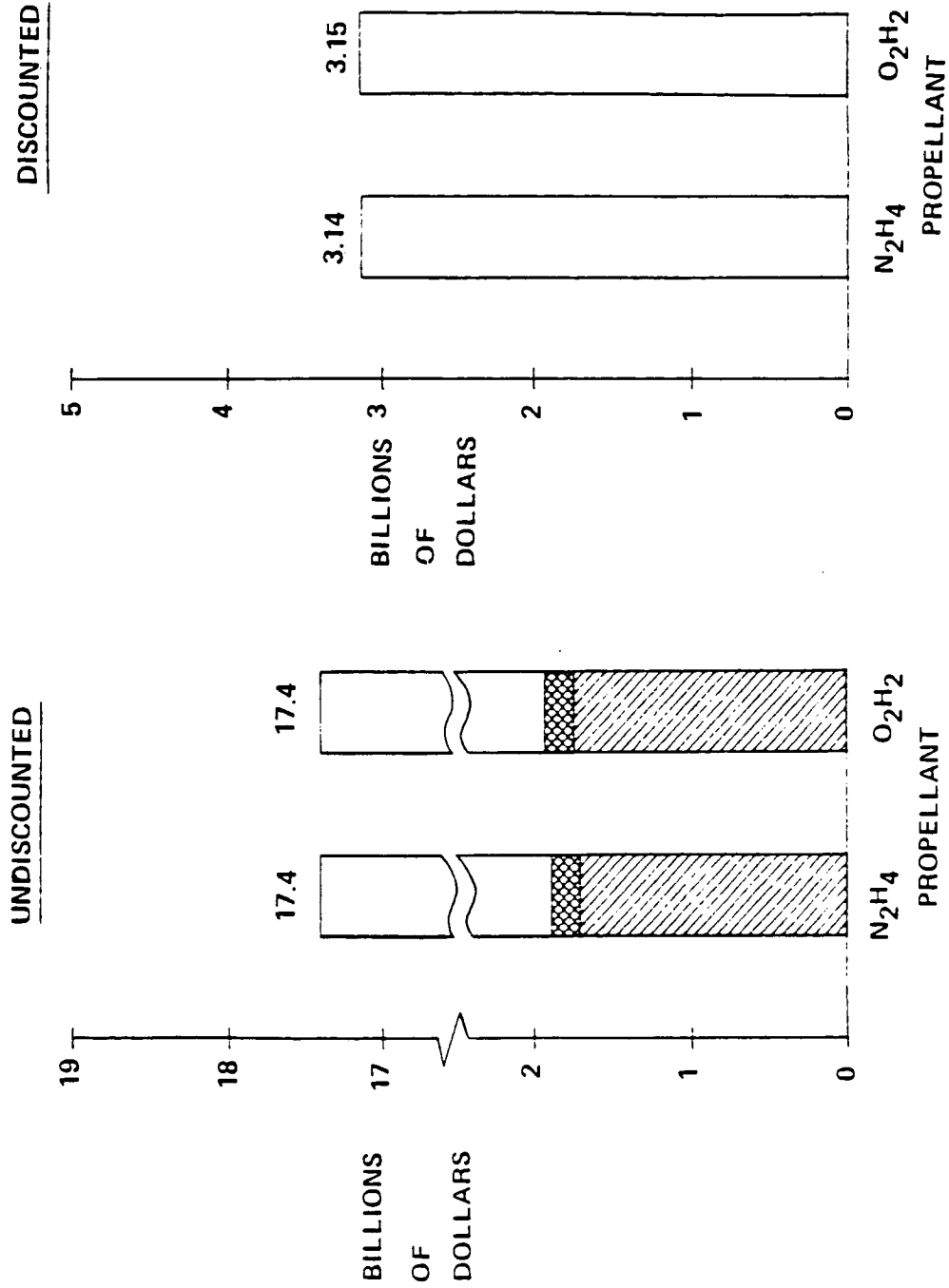


Figure 1.2-4 OTV Program LCC Comparison RCS Influence

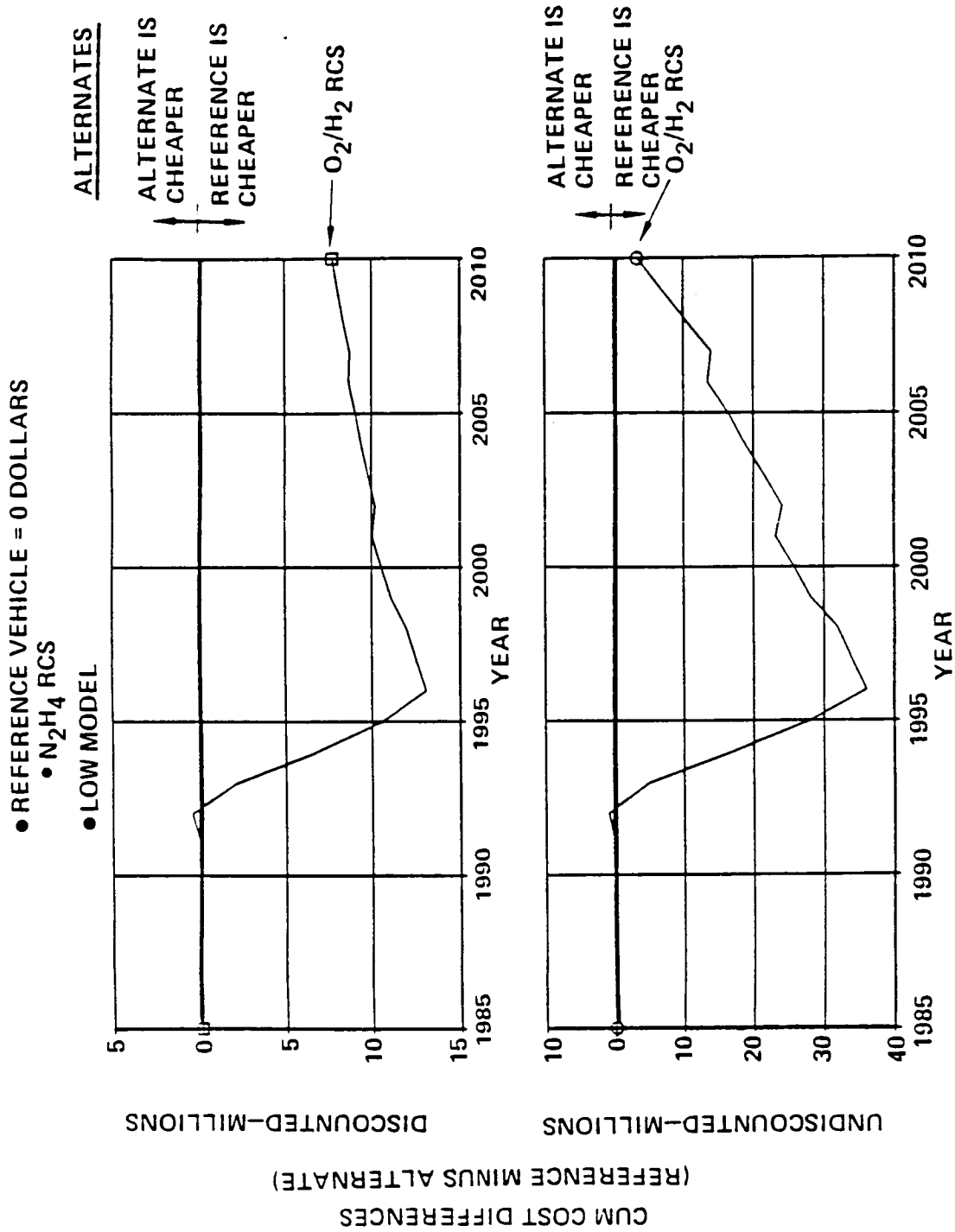


Figure 4.2-5 Time-Phased LCC Comparison SBOTV RCS Trade

5.0 THERMAL PROTECTION AND CONTROL

This section presents the Thermal Protection and Control (TP&C) analysis performed on each of the candidate OTV concepts. The material includes a summary of the requirements, a description of the generic types of TP&C concepts, the approach used to conduct analysis and a description of the TP&C system for each OTV concept. The majority of the analysis deals with thermal protection systems (section 5.2 through 5.9) associated with or affected by the aerobraking maneuver. This has occurred because of there being a greater degree of uncertainty and higher weight contribution of the TPS than that associated with thermal control. Section 5.10 however does summarize the thermal control approach.

5.1 TOP LEVEL REQUIREMENTS

Thermal protection systems (TPS) must:

- a. Provide an aerodynamic surface capable of operating while subjected to the aerothermal environments associated with the aeropass maneuver.
- b. Protect the primary structure from effects of the aerothermal environment.
- c. Maintain component temperatures within acceptable limits.
- d. Minimize propellant heating.

The TPS design environments are dependent on configuration shape and trajectories, but typical maximum heating rates on windward brake range from 20 to 40 BTU/ft²-sec. Other required features include:

- a. Light weight.
- b. Reusability or easy replacement.
- c. Capable of being assembled or deployed in orbit.

The thermal control system must provide a means of dissipating heat generated by the avionics unit, and also of protecting the avionics components from the aerothermal environment during the aeropass maneuver.

5.2 THERMAL PROTECTION SYSTEMS (TPS)

5.2.1 Thermal Protection Concepts

Candidate TPS concepts for the OTV vehicles consist of a flexible surface insulation (FSI) blankets and rigid surface insulation (RSI) tiles bonded to strain isolation pads (SIP) as shown in figure 5.2-1. The most promising FSI concept appears to be a Tailorable Advanced Blanket Insulation (TABI), which has been developed by NASA/ARC (reference 14). TABI features a 3-dimensional integrally woven structure with cells filled with quartz felt insulation, and provides smoother surfaces and better durability than the quilted design used on earlier systems. However, the TABI manufacturers (Woven Structures, Inc.), state that thicknesses less than about 3/8 inch are probably not practical due to fabrication problems. Consequently, quilted blankets similar to Advanced Flexible Reusable Surface Insulation (AFRSI, ref. 5.2-1) are proposed where required insulation thicknesses less than 3/8 inch are predicted.

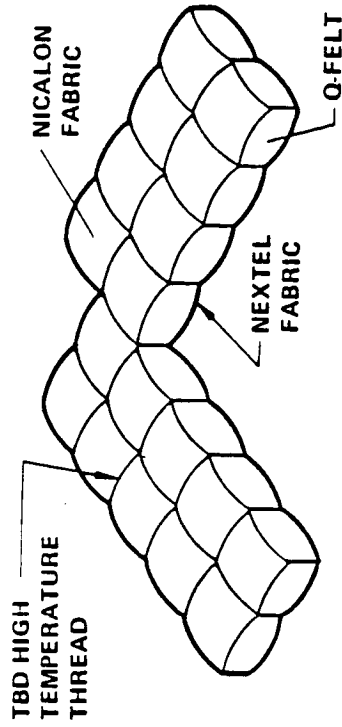
The RSI system is similar to that used on the Space Shuttle except that hexagonal shaped tiles are proposed where practical to minimize heating in the gaps between the tiles. The SIP is required on the Orbiter because of large differences in thermal expansion between the tiles and aluminum primary structure. For composite structures, where thermally induced strains are much smaller, the direct bonding of RSI tiles to primary structures has been proposed (ref. 15). However, we feel that a SIP is still required for OTV because of airload-induced deflections.

5.2.2 TPS Material Capabilities

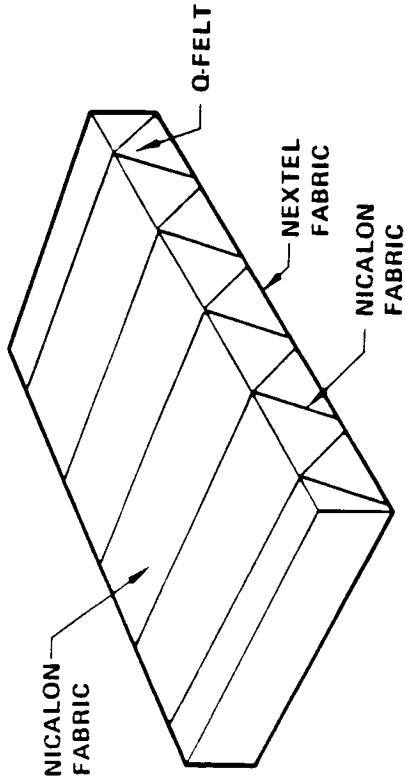
Our assessment of current and future TPS material capabilities are shown in table 5.2-1. All three types are, or are derived, from systems currently in use on the Space Shuttle Orbiter. Heat transfer rates are used as the measure of thermal capability instead of temperature to avoid the need for assuming surface optical properties.

The greatest gains in thermal capability are projected for FSI. The 1990 normal growth capability may be close at hand. Silicon carbide (Nicalon^R) fabrics have been successfully tested to about 34 BTU/ft²-sec with only minor degradation (ref. 16). TABI specimens have been fabricated with silicon carbide surface and cell wall fabrics, and will be thermally tested later this year.

The RSI material is assumed to be or to evolve from fibrous refractory composite insulation (FRCI). FRCI is basically sintered alumina and aluminoborosilicate fibers, and is a second generation tile for the Space Shuttle Orbiters. Development activities are in progress to enhance the capability of these types of materials.

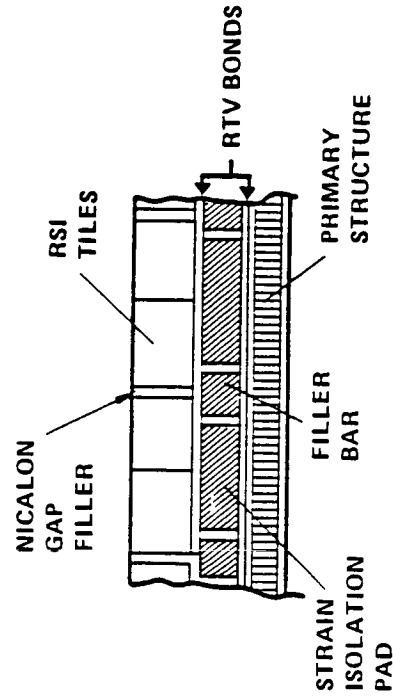
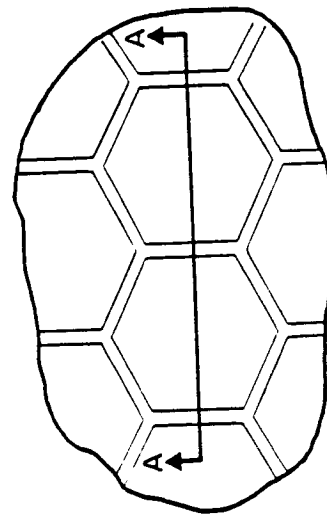


QUILTED FSI
(AFRSI DERIVATIVE)
PROPOSED ONLY WHEN THICKNESSES
LESS THAN 3/8 IN. ARE NEEDED



TAILORABLE ADVANCED BLANKET
INSULATION (TABI)

FLEXIBLE SURFACE INSULATION (FSI)



SECTION A-A

RIGID SURFACE INSULATION

Figure 5.2-1 TPS Concepts

Table 5.2-1 TPS Heating Limits

TPS TYPE	TPS LIFE (MISSIONS)	CURRENT TECHNOLOGY	HEATING RATE (BTU/FT ² - SEC)	
			1990 TECHNOLOGY NORMAL GROWTH	ACCELERATED GROWTH
FLEXIBLE SURFACE INSULATION (FSI)	5	4-6 (AFRSI)	30	50
	1	6-8	35	50
RIGID SURFACE INSULATION (RSI)	20	38 (FRCI)	50	90
HIGH DENSITY REFRACTORY (HIDR)	20	70 (ACC)	90	150

HDR materials are not proposed for OTV applications primarily because of weight, but are considered as alternates in case that future predictions of aerothermal environments exceed the capability of RSI.

5.2.3 Insulation Sizing Criteria

Criteria used in selecting FSI and RSI thicknesses are shown in figure 5.2-2. FSI thicknesses are selected to maintain backwall temperatures below designated limits, which are 600°F for Kevlar^R sealed with Viton^R, and 1500°F for Nextel^R sealed with CS105. RSI is sized to maintain temperatures below 550°F at the RSI/SIP bondline. If the temperature capability of suitable adhesives can be improved to the extent that a graphite/polyimide structure temperature limit of 600°F becomes the limiting condition, then RSI thicknesses can be reduced by roughly 25%.

The FSI and RSI thermal conductivities used to establish insulation thicknesses are shown in figure 5.2-3. FSI conductivities are based on AFRSI data presented in reference 18 for a pressure 0.01 atmospheres. Data presented in reference 17 also showed that FRCI 20-12 conductivity is about 20 percent greater than that of LI-900 (a first generation Shuttle tile) at 1.0 and 0.0001 atmospheres. Consequently, FSI conductivities are assumed to be 20 percent greater than LI-900 at 0.01 atmospheres. The 0.01 atmosphere pressure was selected as a mean value between the roughly 0.02 atmosphere stagnation pressure occurring at the stagnation point at the time of peak heating and the 0.001 to 0.005 atmospheres occurring when the backwall temperatures reaches its peak.

5.3 ANALYSIS APPROACH

Analyses were conducted to define the external aerothermal environments for each vehicle concept. Results were then used as a basis for shaping and dimensioning vehicle configurations, selecting candidate TPS materials, determining insulation thicknesses, and assessing aerothermal and TPS technology requirements. The aerothermal predictions represent design heating environments.

The general approach was to use conventional boundary layer methods to establish nominal heat transfer distributions, and then to apply appropriate factors to account for surface roughness, gas radiation, surface catalysis, rarefied flow effects, and atmospheric variations. Specific factors used are given in table 5.3-1. With the exception of the atmospheric density term, all of the factors shown are considered to be adjustments, and not uncertainties. Therefore, the terms are multiplied, and not root-sum-squared. The net result is that a factor 1.05 plus a vorticity correction of 8 to 20 percent is

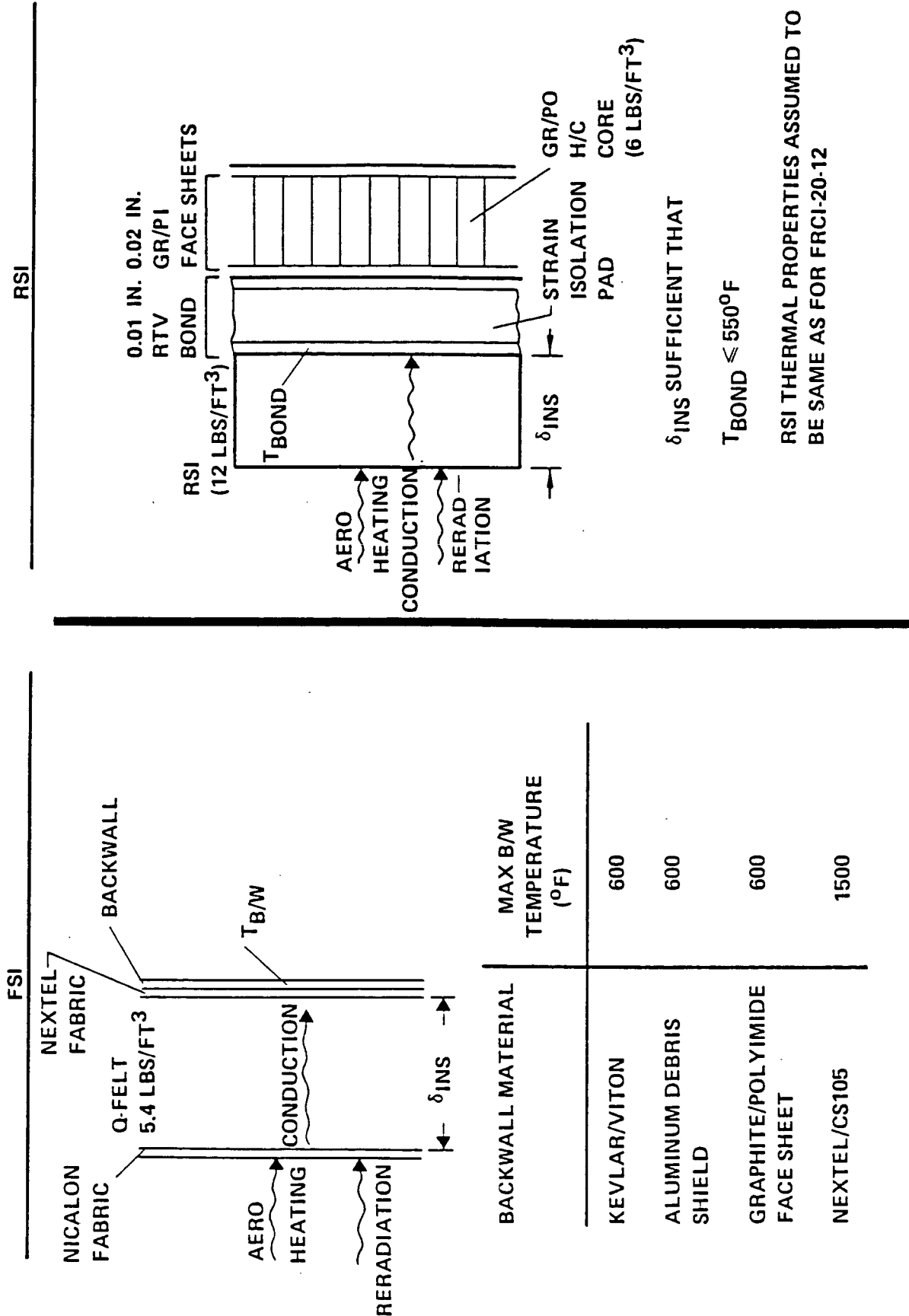


Figure 5.2-2 Insulation Sizing Criteria

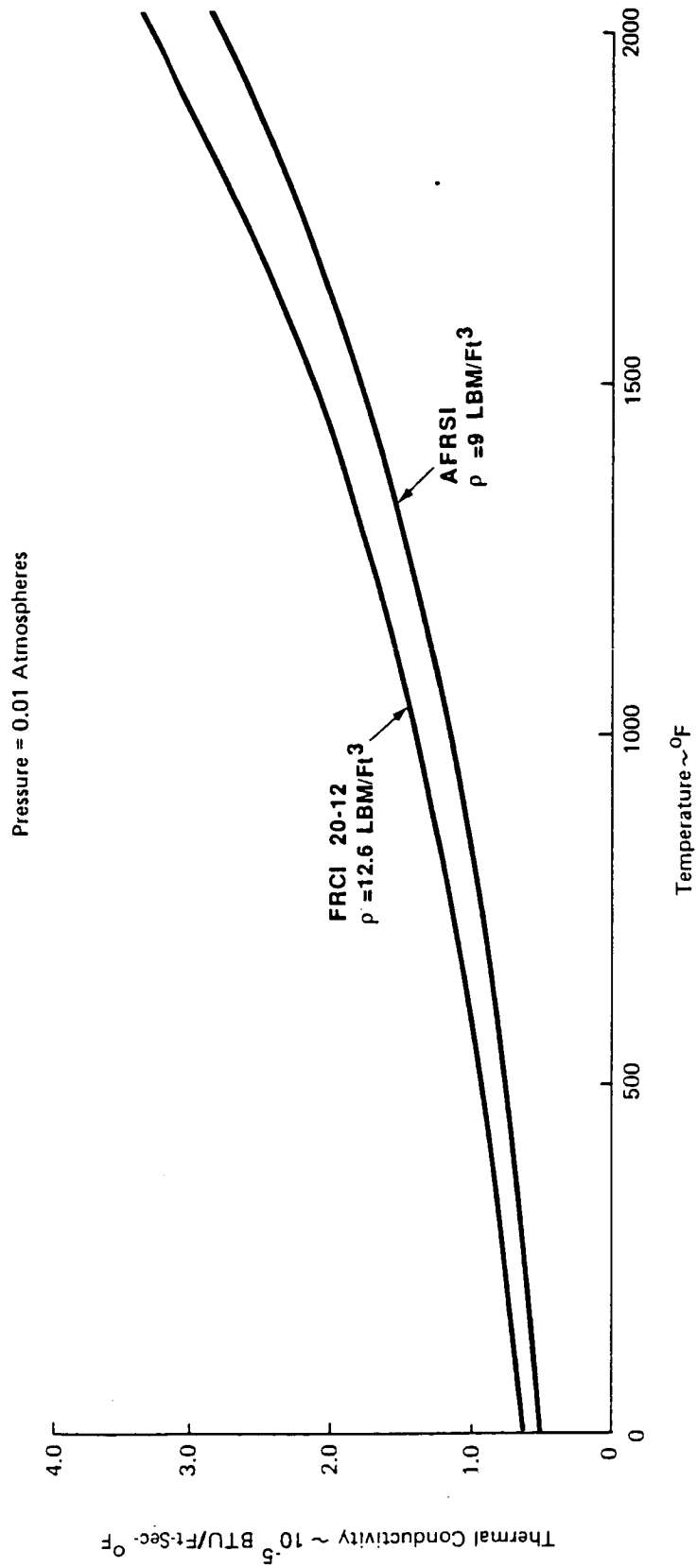


Figure 5.2.3 TPS Thermal Conductivities

Table 5.3-1 Heating Factors for Design Environments

ADJUSTMENT FOR	FACTOR q/q_{NOM}
SURFACE CATALYSIS	0.7
NON-EQUIL RADIATION	1.2
ATMOSPHERIC VARIATIONS	1.13
SURFACE ROUGHNESS	1.1
VORTICITY	f(ALTITUDE, NOSE RADIUS)

applied to all nominal heating rates. The justification and rationale for these factors is discussed below.

5.3.1 Nominal Heating Computations

Heating distributions on windward surfaces were computed using the rho-mu method described in reference 18, which is basically a boundary layer momentum integral method.

The general approach was to compute heating patterns consisting of \dot{q}/\dot{q}_0 ratios for each vehicle shape, where q_0 is the convective heating rate at the stagnation point of a one-foot radius hemisphere. These patterns are essentially independent of trajectory providing that the boundary layer remains laminar. The possibility of boundary layer transition occurring was assessed using the transition onset criteria used for the Space Shuttle Orbiter, but results indicated that the flow will remain laminar for all ballistic cases considered in this study.

Reference heating rates, q_0 , and reference heat loads, Q_0 , were computed for each trajectory, where

$$Q_0 = \int \dot{q}_0 dt$$

These data were then used to determine the maximum heating rates and heat load for each ballistic brake concept. Maximum heating rates are used in selecting and assessing TPS materials, and the heat load used to establish insulation requirements to avoid excessive structural temperatures.

Effects of atomic diffusion were estimated by assuming thermo/chemical equilibrium using the approach suggested by Fay and Riddell (ref. 19), given by:

$$\frac{H}{H_{(L_e=1)}} = 1 + (L_e^{0.52} - 1) \frac{i_D}{i_0}$$

Where H is the heat transfer coefficient, L_e the Lewis number, i_D the dissociation enthalpy, and i_0 the total enthalpy. Effects of ionization were approximated by including the energy absorbed in ionization in the dissociation enthalpy (i_D).

Surface pressure distributions on windward surfaces were estimated using modified Newtonian theory. With this approach, the stagnation heating rates are dependent only on the radius of curvature of the nose cap, and are independent of the ballute or brake

diameter. Results are valid for cases where the sonic line remains on the hemisphere, but tend to be conservative for most of the configurations studied, as is illustrated by the data-theory comparisons shown in figure 5.3-1. The predictions over most of the case are in good agreement with the data, but the stagnation heating is over predicted by nearly 30 percent. Agreement would be better on a 60° cone, which would be representative of the baseline ballute configuration, since the stagnation flow will be less influenced by the cone. Also, the tests were conducted in an ideal gas ($\gamma = 1.4$). In the OTV flight regime, the bow shock will lie much closer to the body, and the pressures will be closer to Newtonian. Consequently, predictions are felt to be realistic, but somewhat conservative near the stagnation point.

5.3.2 Surface Catalysis

The sensitivity of convective heating rates on a ballute configuration to the catalytic efficiency of the surface with regard to the recombination of atomic oxygen and nitrogen is shown in figure 5.3-2. These results indicate that assuming equilibrium gas chemistry may be overly conservative, and that large reductions in convective heating can be realized by selecting materials or surface coatings with low catalytic efficiency.

The figure 5.3-2 predictions were generated using the non-equilibrium chemistry Boundary Layer Integral Matrix Procedure (BLIMPK, ref. 20) assuming equilibrium chemistry exists at the edge of the boundary layer. Analyses of reentry heating data obtained during STS-2 reentry suggests that the catalytic efficiency (k_W) of the tile coatings was of the order of 100 cm/sec (ref. 21). Comparable performance should be achievable for OTV through the selection of appropriate materials and coatings, and the catalysis factor of 0.7 used in the present study for nominal estimates is felt to be appropriate.

5.3.3 Gas Radiation

Most previous analyses of radiation from high temperature air are based on the assumption that the gas is in chemical equilibrium. With this assumption, the predicted gas radiation contribution to the OTV TPS is small compared with convection term. However, analysis results presented in references 22 and 23 indicate that for conditions associated with critical OTV heating the stagnation region flow gas chemistry will deviate significantly from its equilibrium state, which could result in radiative heating rates of the same order to magnitude as the convective values. Other investigators (refs. 24 and 25) conclude that for these conditions, gas radiation intensities will be

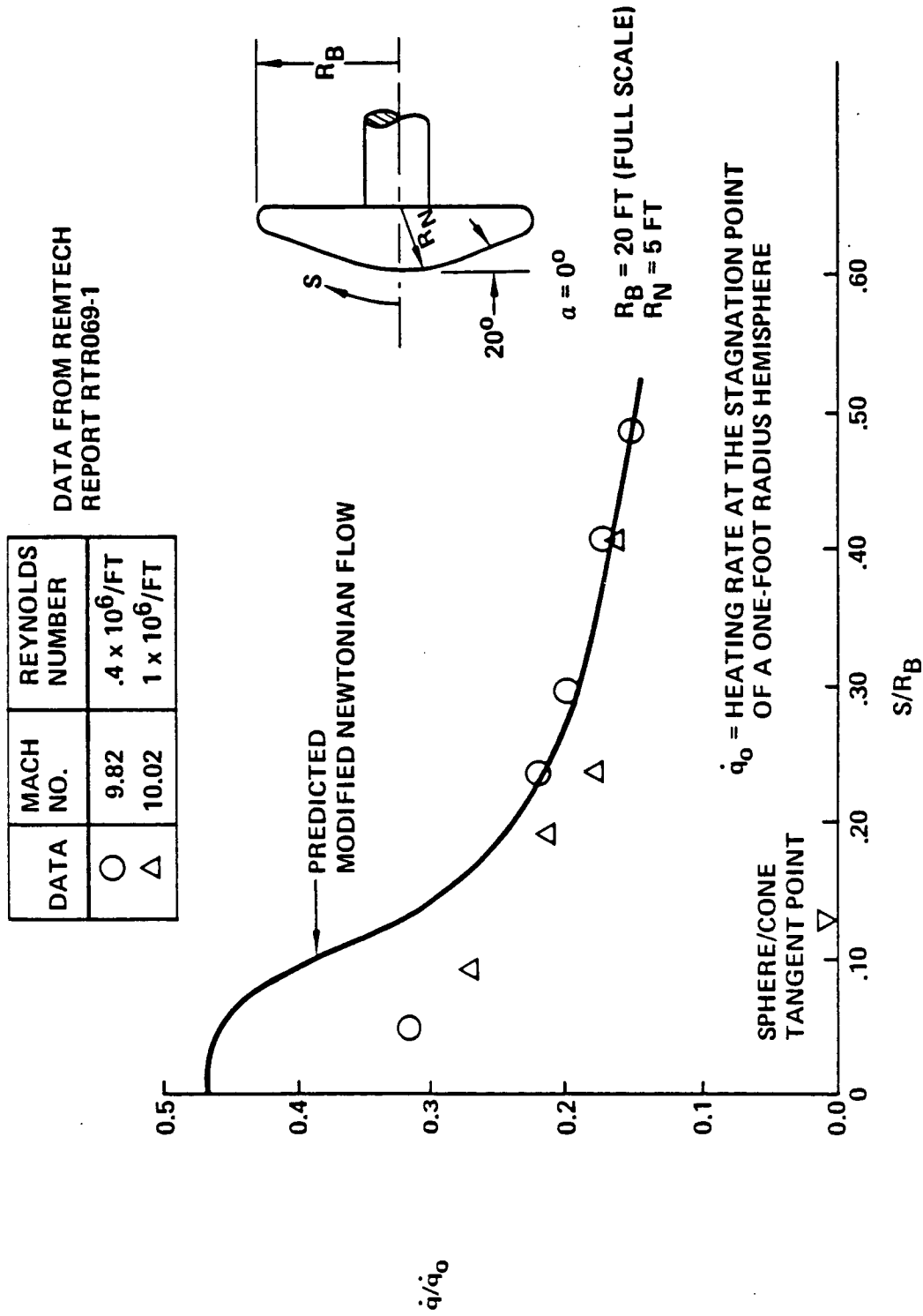


Figure 5.3-1 Blunt Cone Data—Theory Comparison

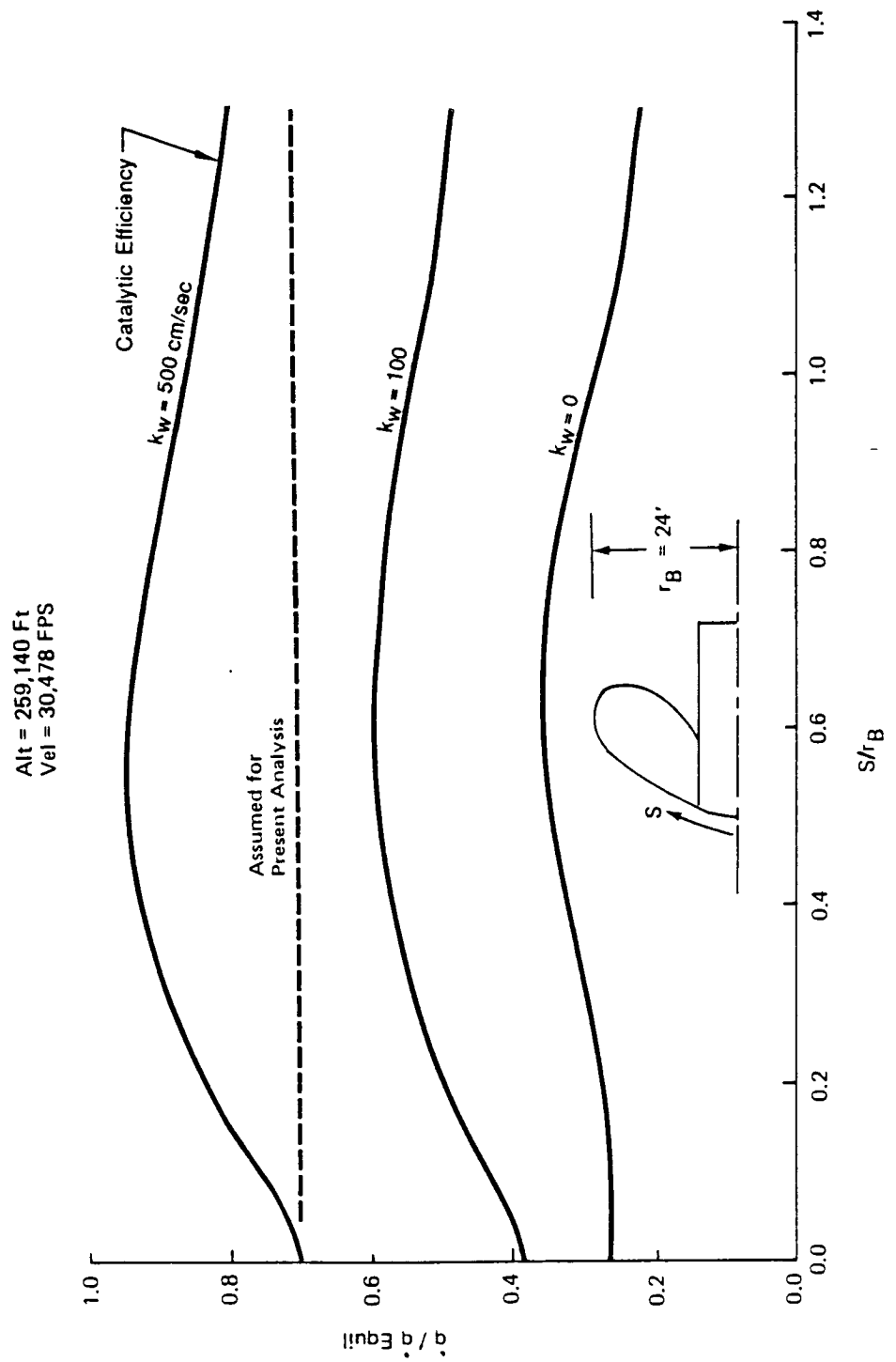


Figure 5.3-2 Surface Catalysis Effects

much less than the convection heating, even when non-equilibrium effects are considered. Current estimates of stagnation point radiation intensities for OTV vary from less than 1 BTU/ft²-sec to 26 BTU/ft²-sec. No reliable guidelines are available for accounting for velocity, altitude, body radius, or location on the body.

Equally important as radiation intensity is the absorptivity of the surface or surface coating to non-equilibrium radiation, which is primarily in the visible and UV spectral bands. Recent studies at NASA/ARC indicate that optical coatings using refraction and back-scattering to reject most of the radiant energy are practical, at least on rigid surfaces.

For this investigation, a factor of 1.2 was applied to convective heating predictions to account for non-equilibrium radiation for nominal estimates. Effects of velocity, altitude, and vehicle shape on radiative heating are different than on convection. However, use of a simple factor greatly simplifies analyses required to support the various trade studies, and is felt to be justified considering that the influence of these parameters on non-equilibrium radiation is not defined at this time. Stagnation heating rates on ballute brake configurations are typically about 35 BTU/ft²-sec, so a factor of 1.2 is roughly equivalent to a radiation intensity of 23 BTU/ft²-sec with an absorptivity of 0.3.

5.3.4 Surface Roughness

Fabric texture, seams, manufacturing tolerances, and joints all tend to enhance convective heating. A reliable assessment of roughness heating associated with the proposed TPS concepts is not possible at this time. Heating is sensitive to boundary layer thickness as well as surface condition, and decreases with increasing boundary layer thickness. Considering the relatively thick boundary layers that will cover the OTV, a factor of 1.1 is felt to be realistic.

5.3.5 Atmospheric Dispersions

Analyses of measurements obtained during reentry of STS-2, 4, and 6 indicate that relatively large variations in air density can occur at altitudes above about 230,000 ft (ref. 26), which is below the perigee altitude of all of the low L/D OTV concept studied. Trajectories were generated for the ballute aerobrake for each of these density profiles, and the impact on thermal environment assessed. The 1962 Standard Atmosphere was used as the basis for comparison. It was found that the impact of the density variations on trajectory were negligible, and the peak reference heating rates computed with the STS derived density profiles were in all cases lower than the corresponding values

obtained with the 1962 Standard Atmosphere, as shown in figure 5.3-3. This result is probably fortuitous in that the high density regions did not happen to occur at the peak heating altitudes. The nominal heating factor of 1.13 selected for the present study corresponds to a density approximately 28 percent greater than the reference value at the peak heating altitude. This variation roughly corresponds to the maximum value derived from the STS measurements, although the STS variations occurred significantly above the peak heating altitude.

5.3.6 Rarefied Flow Effects

During much of the aeropass maneuver the OTV will be operating in flight regimes commonly referred to as free-molecular and transitional, where the term transitional denotes that the flow is neither free-molecular nor continuum as shown in figure 5.3-4. However, the most severe heating environment will occur near perigee, where continuum flow methods are valid. Also, more than 95 percent of the total heat is generated in the continuum flight regime. Consequently, aerothermal predictions for this study are based on the usual continuum flow assumptions, although corrections are made to account for vorticity. Conventional boundary layer methods for predicting convective heating rates are predicated on the assumption that the viscous boundary layer is thin compared with the inviscid portion of the shock layer. For the OTV flight regime, Reynolds numbers are relatively low, and this condition is not satisfied. When the boundary layer thickness is of the same order-of-magnitude as the shock layer thickness, the boundary layer flow is influenced by vorticity induced by shock curvature. Stagnation point heat transfer rates were corrected for vorticity effects using data shown in figure 5.3-5, which was derived from correlations presented in reference 27. Away from the nose cap, vorticity corrections were assumed to be one-half of the stagnation value.

5.3.7 Base Heating

The thermal environment is much less severe in the base region than on windward surfaces, but is also much more difficult to predict. In this study, base heating estimates and wake closure envelopes are based on computations made using a Navier-Stokes solver, and wind tunnel and flight measurements, depending on location and vehicle concept. More detail is provided in the appropriate subsection for each vehicle concept.

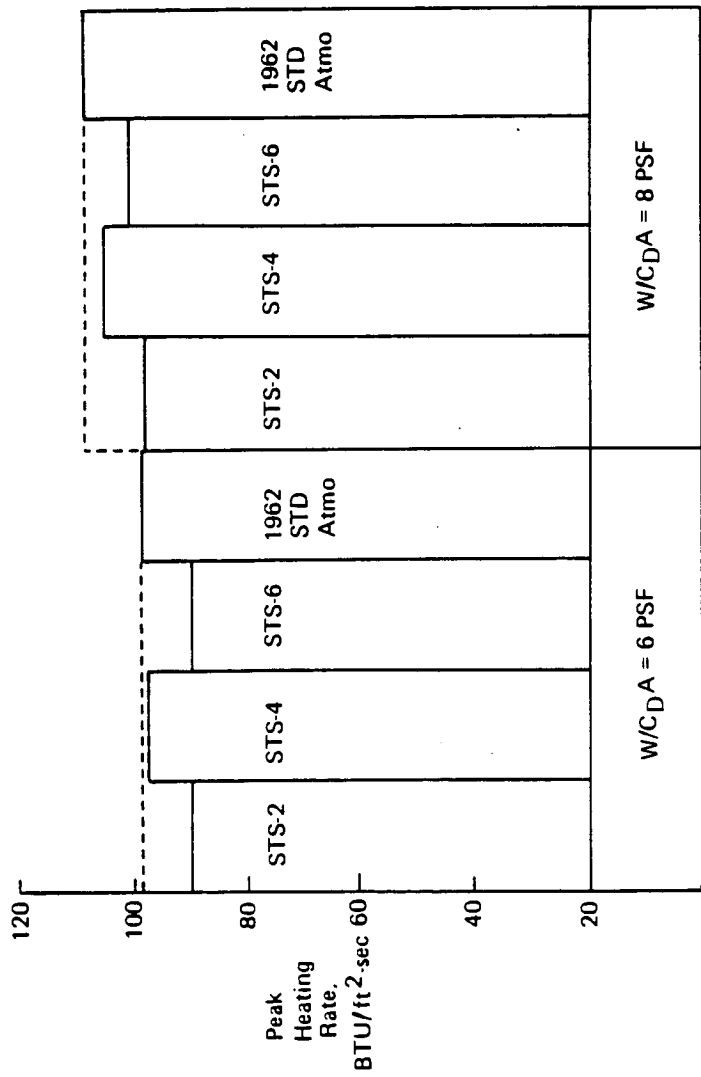


Figure 5.3-3 Impact of STS Derived Densities on Reference AOTV Heating

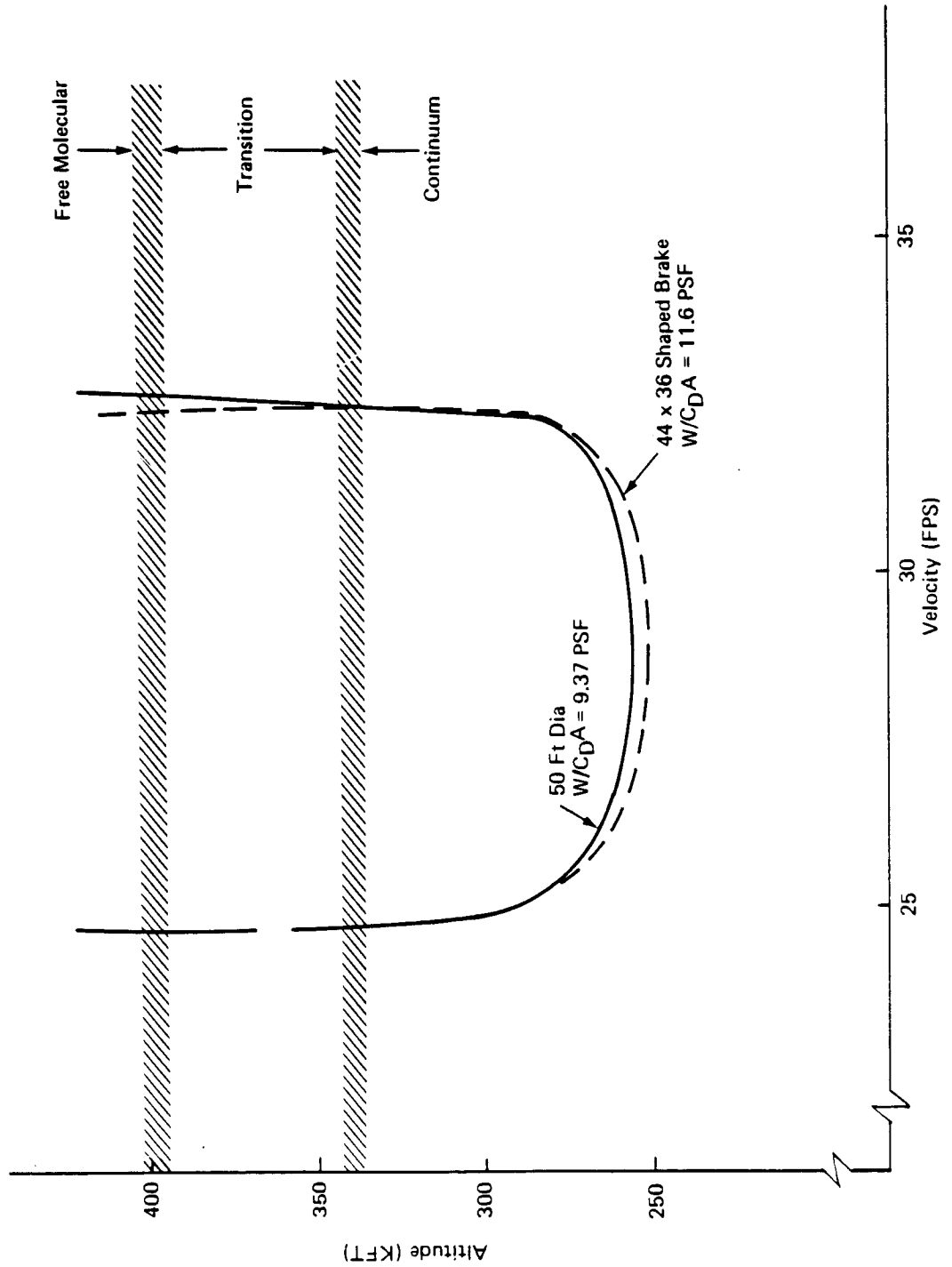


Figure 5.3-4 OTV Flight Regime

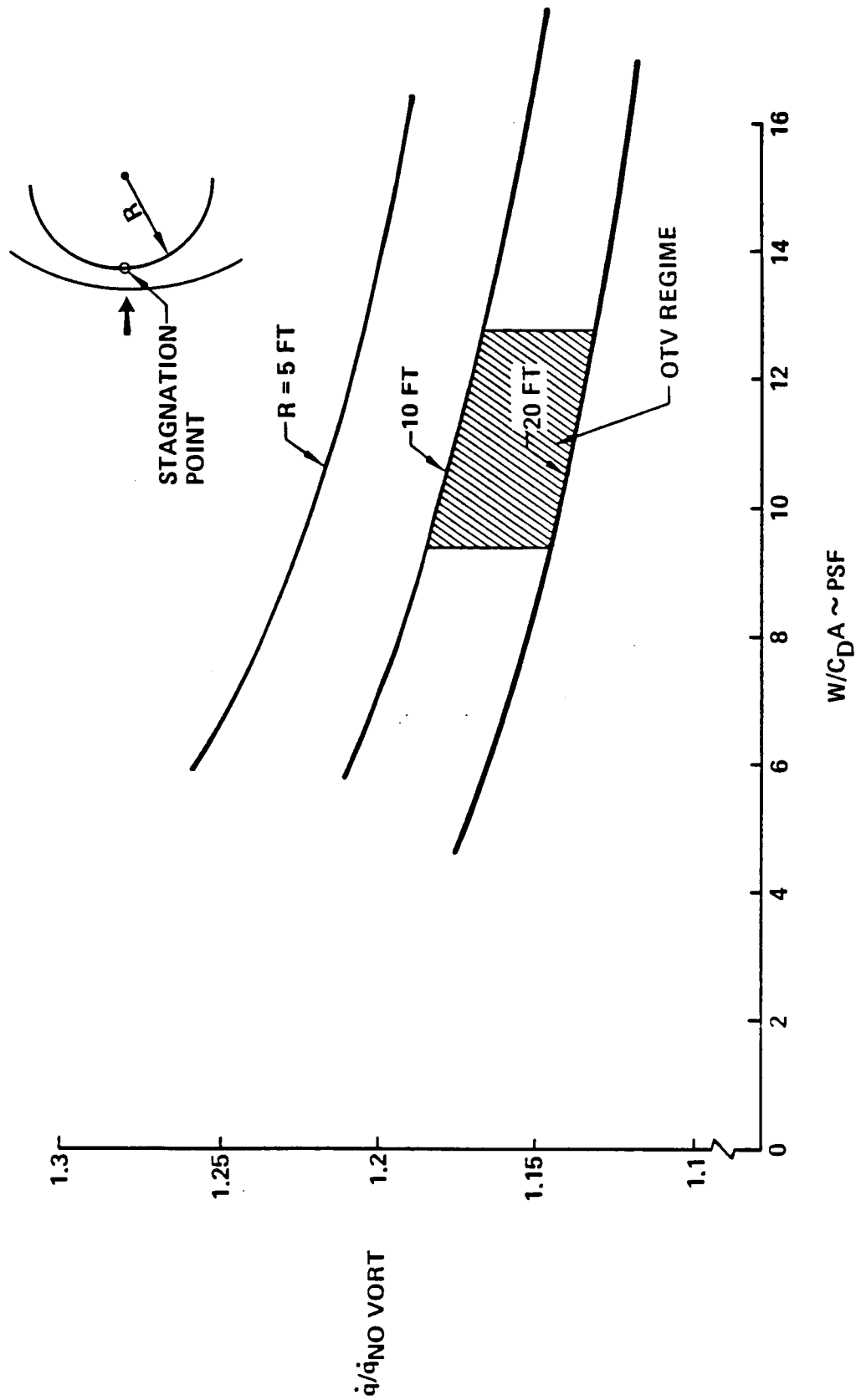


Figure 5.3-5 Vorticity Effects on Hemisphere Stagnation Heating

5.3.8 Wake Impingement Analysis

A major concern in aeroassist device design is the size required of the aerobrake because of weight, cost, and packaging concerns. Aerobrake size is a major contributor to ballistic coefficient ($W/C_D A$) and, as a result, to reentry heating and aeroguidance dynamics.

There exists another factor that, analysis reveals, often sets the brake diameter for a symmetric brake above that indicated by brake heating concerns. This factor is brake impingement heating on the payload and forces brake diameter to be driven by payload length for cases of lengthy payloads.

Remtech Report RTR 069-1 presents wake impingement heating data as a function of vehicle angle-of-attack. Most payloads returned via the aerobrake do not have high temperature TPS on their exterior because of weight constraints, windows, sensors, etc. A maximum allowable heating rate during the aerobrake maneuver was determined to be $0.5 \text{ BTU/ft}^2 \text{ sec}$ which results in a radiation equilibrium temperature of slightly over 600°F . 650°F is considered as a realistic limit for uninsulated structure. This value correlates to a non-dimensionalized heating rate, as presented in the Remtech data, of 0.005 (referenced to a one foot radius hemisphere stagnation point heating rate of $100 \text{ BTU/ft}^2 \text{ sec}$). Figure 5.3-6 presents the wake turning angle, θ , as a function of angle-of-attack, α , for a constant 0.005 heating rate ratio. It is seen that, at 10° angle-of-attack, the wake angle, relative to the freestream flow direction, is about 22° and, relative to the vehicle centerline, is about 32° . These angles increase slowly with angle-of-attack as shown in figure 5.3-6. For comparison, a NASA/LaRC calculation for the ballute wake angle is about 25° (ballutes will always operate at 0° angle-of-attack). As a result of examining the Remtech data, the wake impingement turning angle criterion adopted has been 32° relative to vehicle centerline (22° wake angle and 10° angle-of-attack). Table 5.3-2 shows a comparison of the impact on brake diameter and weight for the selection of 17.5° and 32° turning angle.

The data from the Remtech report, while valuable, are subject to interpretation. Also, it was necessary to extrapolate the normalized heating rate from about 0.02 to 0.005, which significantly reduces data reliability. In view of the significant impact on the vehicle, it is recommended that a more detailed study of wake impingement heating be conducted.

5.3.9 Heating Trajectories

For the reference mission which is a return from geosynchronous orbit, braking to a 270 nm apogee orbit, it was found that maximum reference heating rate (\dot{q}_0),

SYMMETRIC BRAKE PREDICTIONS ARE
DERIVED FROM DATA PRESENTED IN
REMTECH REPORT RTR 069-1

○ CURRENT BALLUTE CONSTRAINT
● CURRENT SYMMETRIC & SHAPED
BRAKE CONSTRAINTS

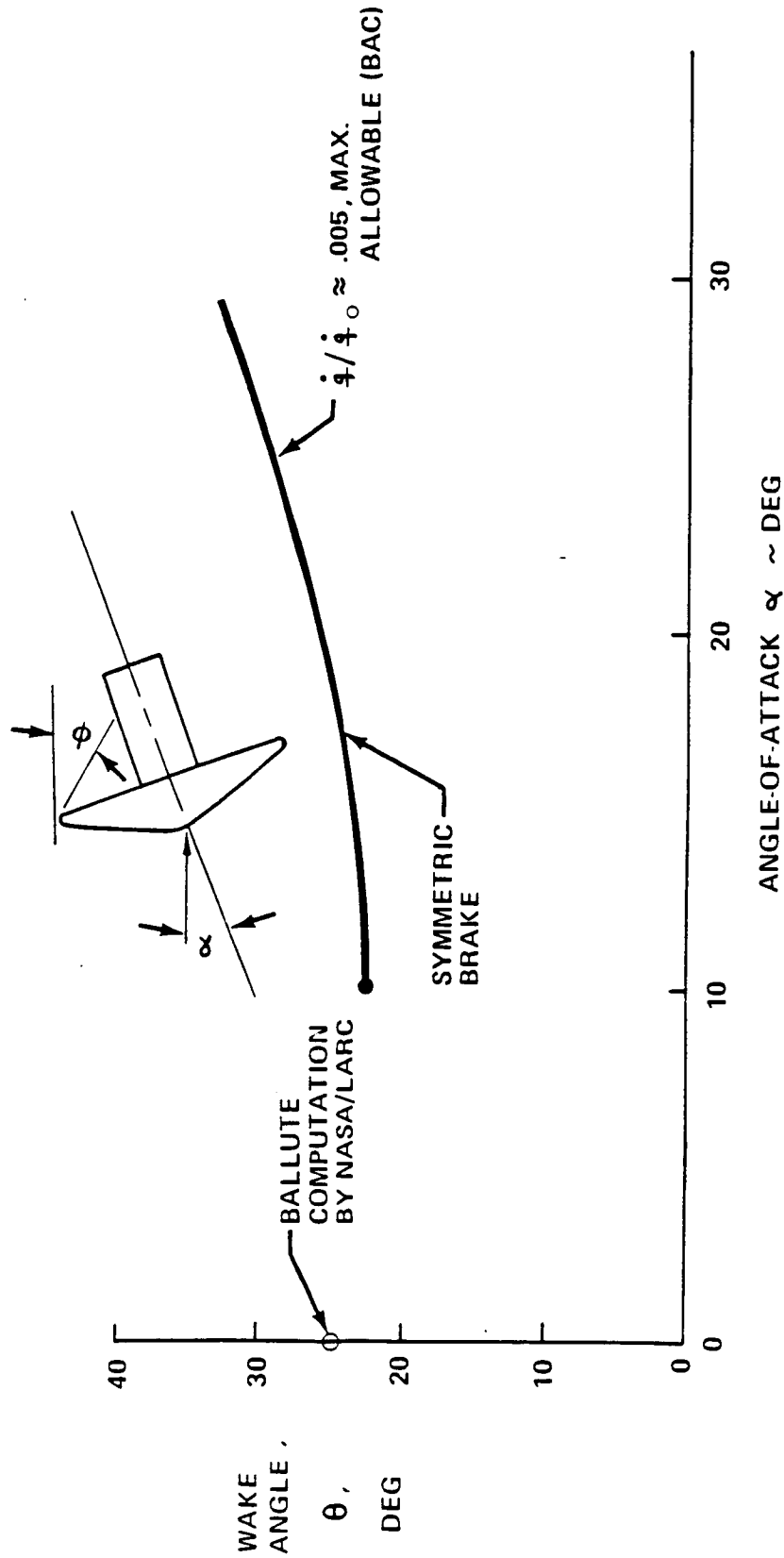


Figure 5.3-6 Wake Heating Constraints

OTV-1169

Table 5.3-2 ACC Lifting Brake—Wake Impingement Sizing

FLOW TURNING ANGLE	CONCEPT A		CONCEPT B	
	WAKE ANGLE, θ ANGLE OF ATTACK, α ATTITUDE DYNAMICS TOTAL ANGLE	BRAKE DIA (FT)	APPROX.* BRAKE WT (LB)	BRAKE DIA (FT)
	8.0° 7.5° 2.0° 17.5°		22.0° 10.0° — 32.0°	
VEHICLE				
OTV ONLY	35.0	1595	41.5	2014
OTV + APT (30.8K)	37.0	1718	53.0	2890
OTV + APT + MANNED CAB	38.5	1814	60.0	3508

* INCLUDES ONLY JETTISONABLE PORTION—RIBS, FABRIC, TPS—INCLUDING WT. GROWTH

reference heat load (Q_0) and maximum dynamic pressure can be defined as a function of ballistic coefficient ($W/C_D A$), as shown in figure 5.3-7. The ballistic coefficients used in establishing thermal environments were 22.5 percent greater than the minimum (fully inflated ballute) value to provide a margin for correcting for atmospheric and GN&C errors.

5.4 BALLUTE BRAKE OTV

This section discusses the specific types of TPS concepts investigated for space and ground based OTV's and the aerothermal predictions resulting from the analysis.

5.4.1 TPS Concepts

The four ballute concepts considered in this study are shown in figure 5.4-1. The most conservative, and heaviest, employs Kevlar ^R cloth sealed with Viton ^R as the load carrying gas bag, which requires flexible insulation to limit the Kevlar backwall to 600°F (upper left). Aerodynamic drag is modulated by varying the internal pressure to control the external shape of the ballute. The second configuration (upper right) also uses shape change to control drag, but the Kevlar/Viton gas bag is replaced by Nextel AB-312 ^R sealed with an elastomer, glass frits coating (CS-105), which can be used one time at temperatures in excess of 1500°F (ref. 28). The higher allowable bag temperatures significantly reduce the insulation weight on the outside of the ballute.

The third concept (lower left) requires that the engines be operated at either tankhead or low pumped idle during the aeropass. Because of the interaction between the jet counter flow provided by the engine exhaust plume and the ambient flow, the tankhead idle provides a drag level nearly an order of magnitude higher than that occurring at pumped idle, which provides the control authority required to correct for trajectory errors and atmospheric dispersions (ref. 29). In addition, the exhaust flow, which is much cooler than the ambient gas, provides cooling for the nozzles and over some or all of the windward surface. The fourth approach studied was to include both the high temperature gas bag and jet counterflow.

Two concepts for attaching FSI to the load carrying fabric are shown in figure 5.4-2. Most of the heat transferred to the FSI during the aeropass is reradiated to space. However, radiation to space is partially blocked in the crevices between the lobes (see subsection 5.4.2.3). Consequently, lobing of the external FSI should be minimized. With either of the concepts shown, it should be possible to essentially eliminate lobing of the FSI for a fully inflated ballute, which would also minimize crevices for a partially (turned down) ballute.

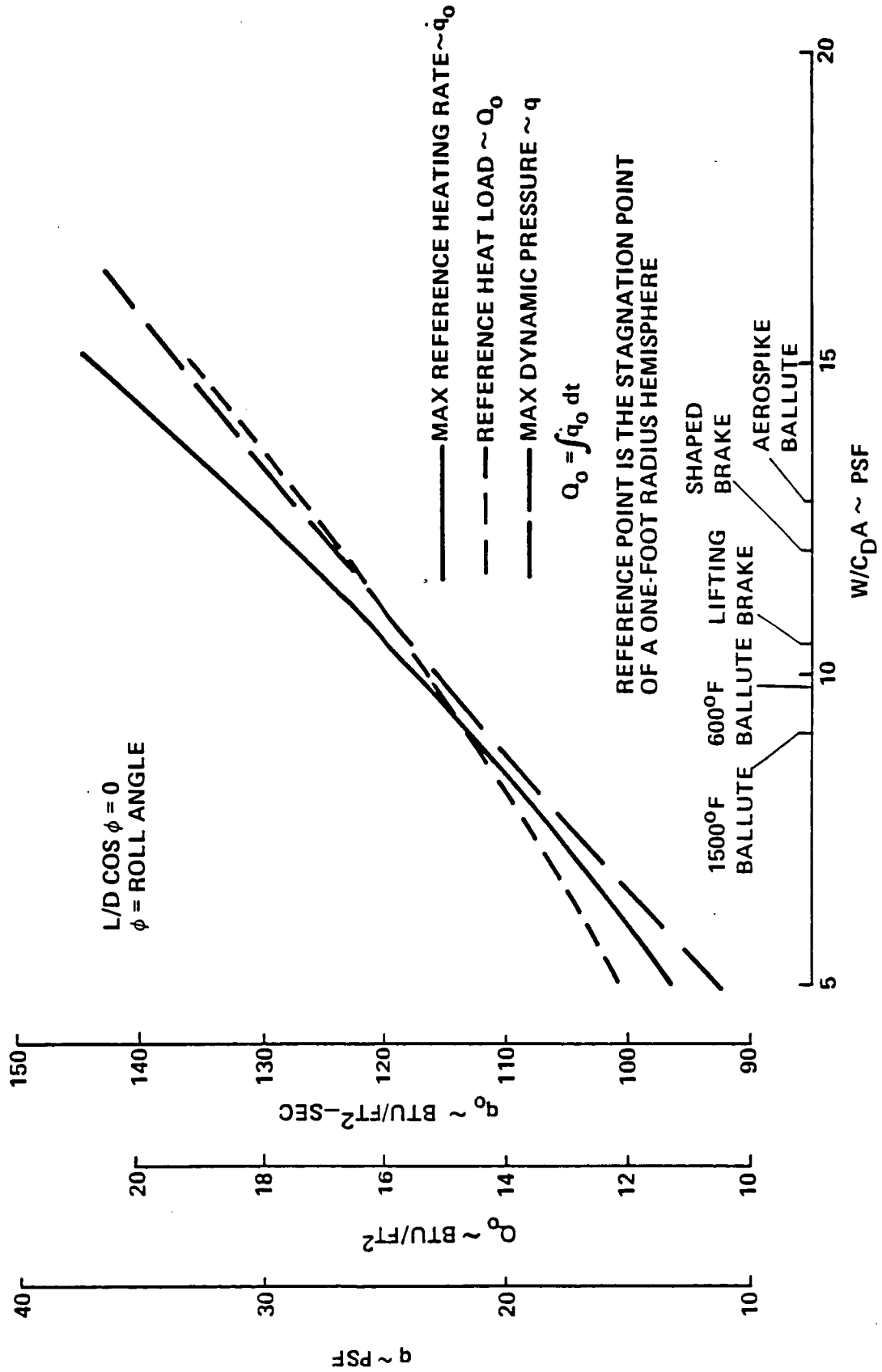


Figure 5.3-7 Effect of Ballistic Coefficient on Aerothermal Environment

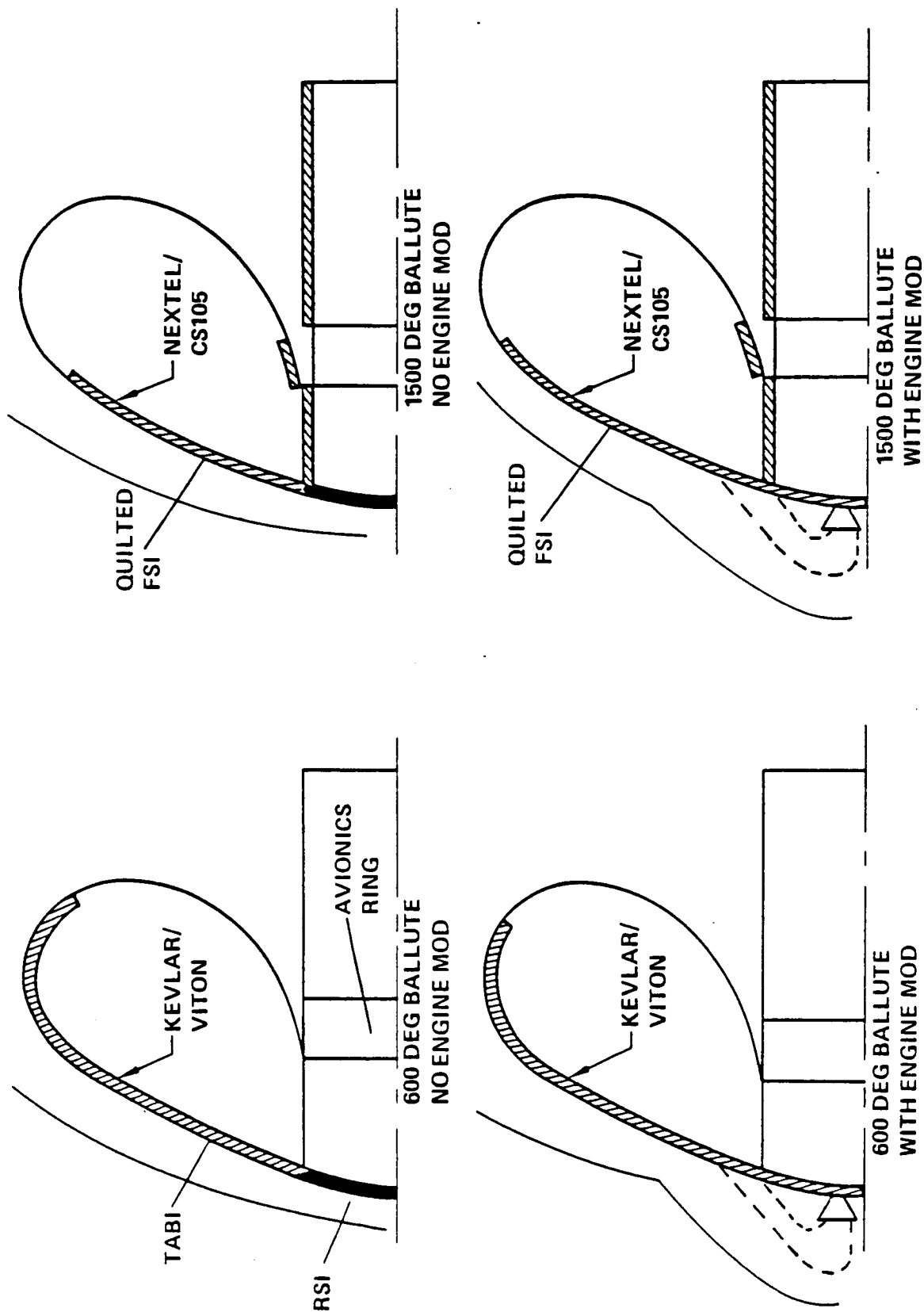


Figure 5.4-1 Ballute TPS Concepts

OTV 555

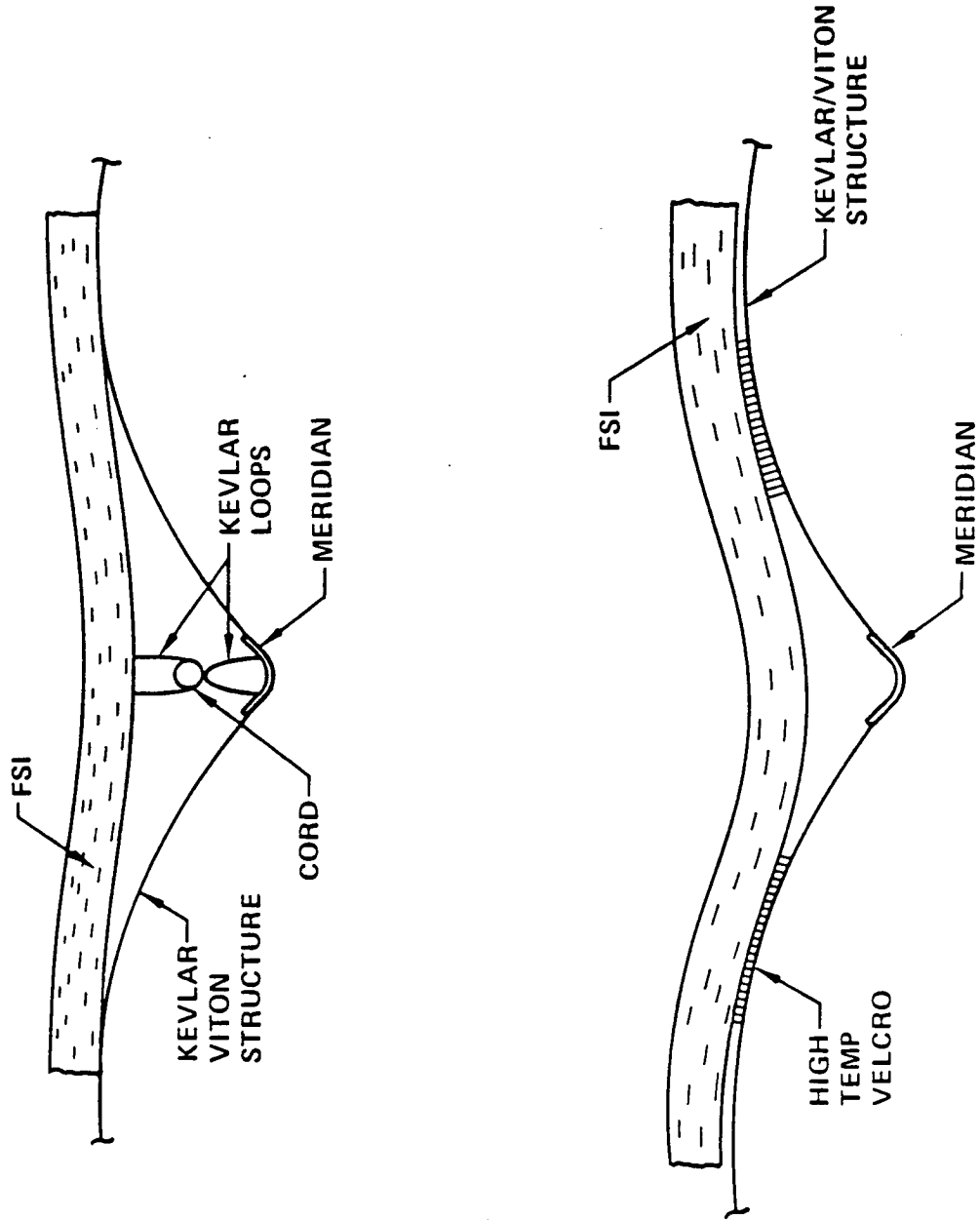


Figure 5.4-2 Ballute/FSI Attachment Concepts

OTV-854

5.4.2 Aerothermal Predictions

5.4.2.1 Ballute Angle Effects

The initial ballute design assumed for this study provided a surface angle of 60 degrees relative to the free-stream flow when the ballute was fully inflated. Subsequent studies indicated that increasing this angle to 70 degrees would provide several advantages, including improved stability and turndown capability. The impact on heat transfer distribution is shown in figure 5.4-3. The 70 degree ballute provides a significant reduction in heat transfer near the nose. These results are based on modified Newtonian pressures, which may not be valid at these large angles. Experimental verification of these trends is needed.

5.4.2.2 Turndown Effects

Decreasing the ratio of internal ballute pressure to that of the ambient flow reduces both the drag coefficient (C_D) and projected area (A) to provide a means for controlling flight path during the aeropass maneuver. Local surface angles are also reduced, resulting in lower heat transfer rates, as shown in figure 5.4-4. Except for figure 5.4-4, all heating rates and heat loads presented are based on a fully pressurized ballute, since it must be assumed that the maximum drag condition could be required at any time during the aeropass. Also, the lower heating levels associated with turndown are at least partially compensated by the increased lobing associated with decreased cross-sectional areas, resulting in deeper crevices where radiation to space is impeded.

5.4.2.3 Crevice Heating

A worst case analysis was conducted to assess the potential severity of the crevice radiation blockage problem. Assumptions include an isotenoid ballute shape with $\frac{1}{2}$ inches of FSI lying directly on the ballute surface and no reduction in convective heating rate in the crevice. If all of the convective heating is assumed to be re-radiated to space, the effective heating rate in the crevice is

$$\dot{q}_{\text{eff}} = \dot{q}_{\text{conv}}/VF$$

where, VF is the view factor to space.

Effective heating rates in the crevices are shown for both a fully inflated and a fully turned down ballute configuration in figure 5.4-5. Results show that the most

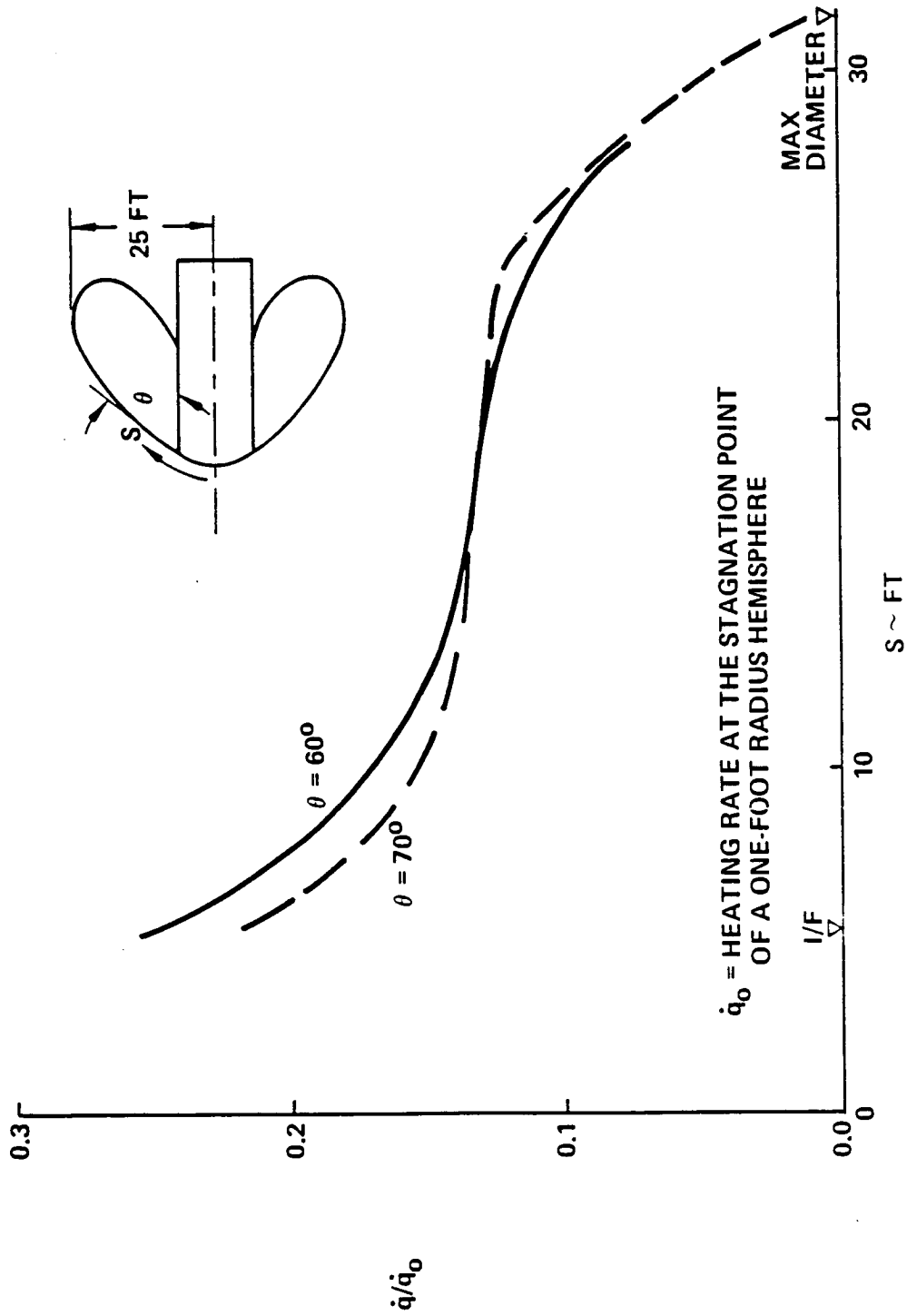


Figure 5.4-3 Effect of Interface Angle on Ballute Heating Distribution

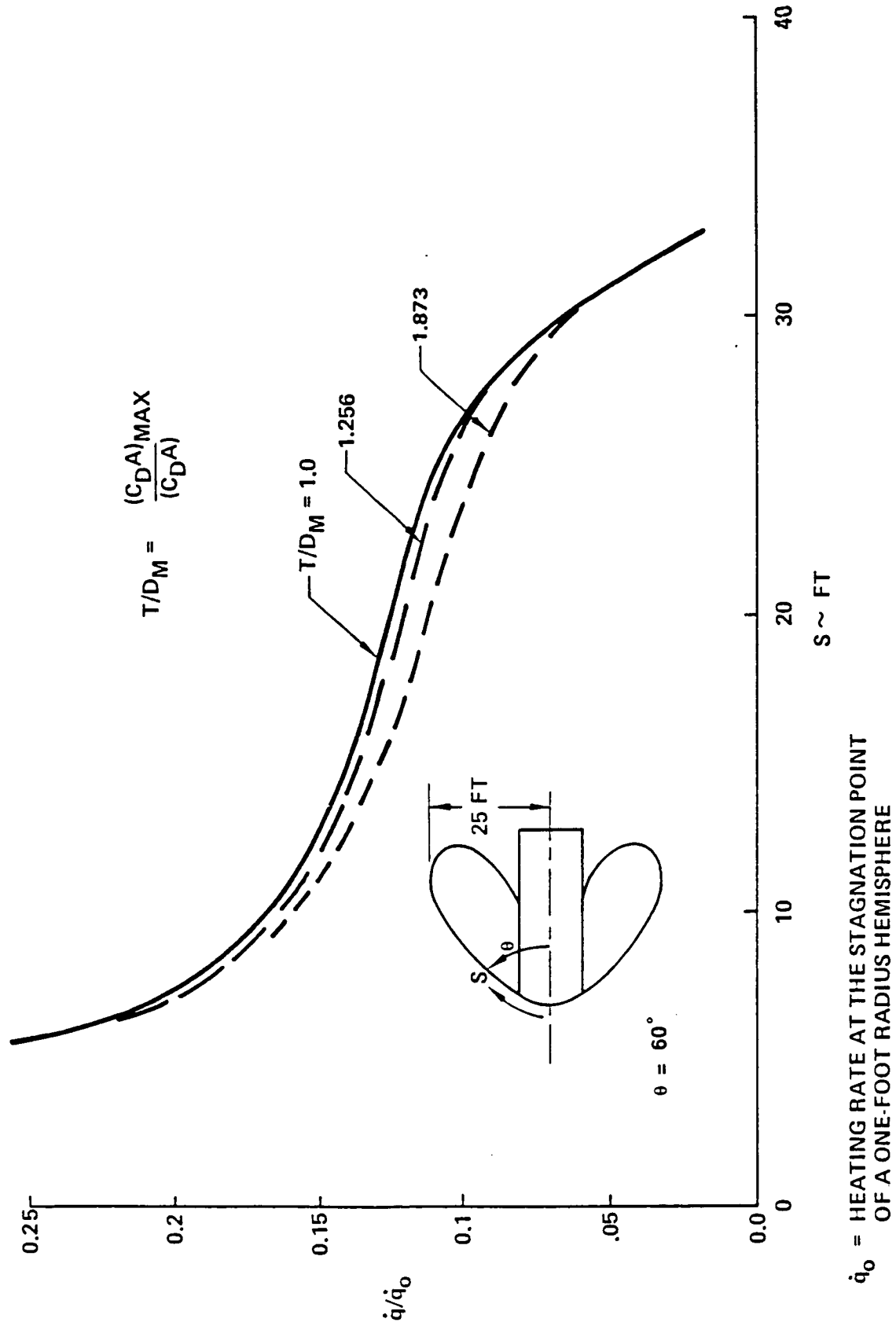


Figure 5.4-4 Effect of Turndown on Ballute Heating Distribution

WORST CASE

- NO REDUCTION IN CONVECTIVE HEATING
- ISOTENSOID DESIGN WITH 0.5" FSI

VF = VIEW FACTOR TO SPACE IN CREVICE

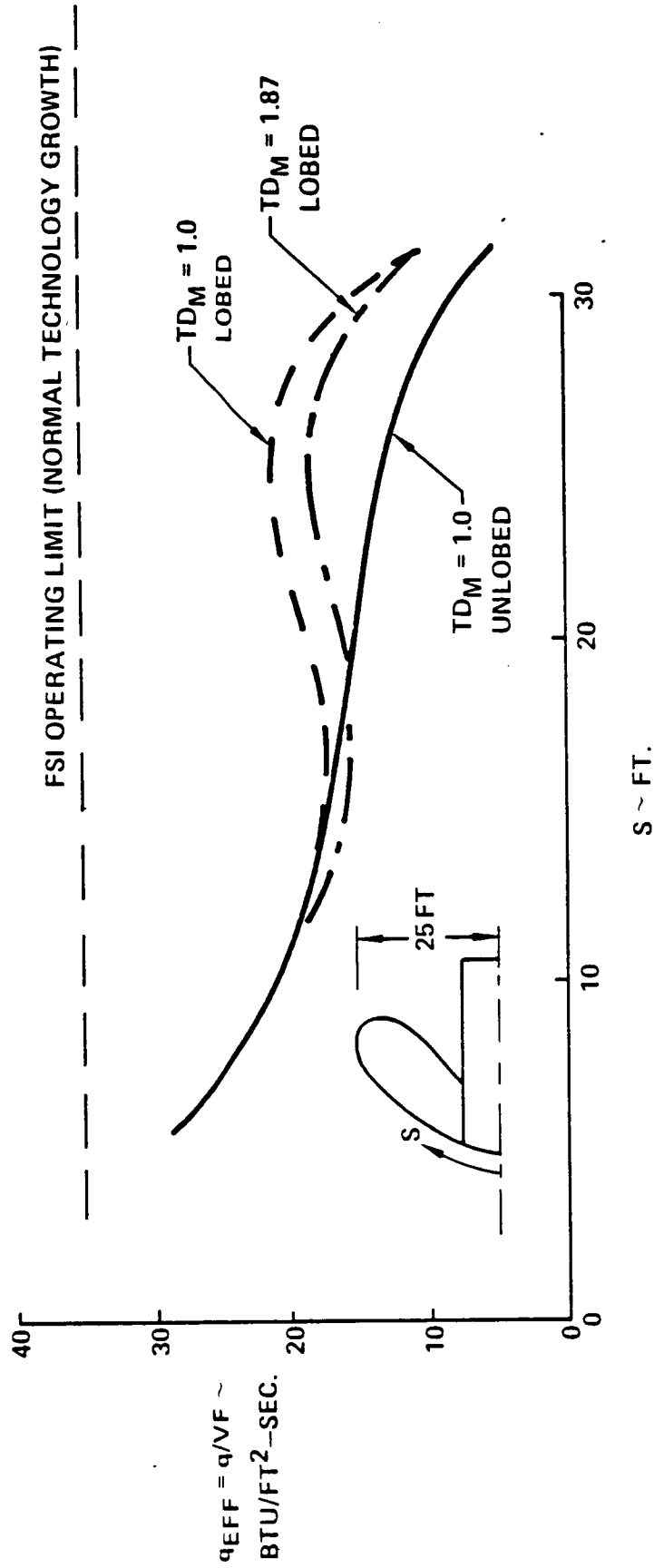


Figure 5.4-5 Radiation Blockage Effects on Lobe Crevice Heating

severe FSI heating condition is at the ballute (aeroshell interface), where lobing is insignificant, and that heating is well below the 35 BTU/ft²-sec limit for an expendable FSI system. Using FSI attachment techniques discussed in subsection 5.4.1, it should be possible to essentially eliminate crevices in the FSI with the ballute fully inflated, with relatively shallow crevices occurring at the minimum drag condition.

5.4.2.4 Engine Modulation Effects

Drag modulation using engine exhaust has been considered as an alternative to controlling drag by varying ballute shape. Drag modulation is accomplished by operating the engines at either tank head idle or low pumped idle with the engine exhaust directed into the free-stream flow. In addition to controlling drag, the exhaust flow should also provide some cooling of the windward surface, since the enthalpy of the exhaust gas is much lower than that of the free-stream.

Balance tests of ballute configurations with and without jet counterflow were conducted in the NASA Langley 22 inch Mach 20 helium tunnel (ref. 29). Results shown in figure 5.4-6 indicate that the ballute drag can be varied by nearly an order of magnitude by modulating the ratio of the momentum flux of the engine exhaust to that of the ambient flow. Note the drag coefficient shown in figure 5.4-6 represents only the drag on the ballute, and does not include the contributions of the center body. Using two 7500 lbf thrust RL 10-3 engines, it is estimated that tank head idle will provide about 25 lbf thrust from each engine, resulting in a total momentum ratio of approximately 0.000057. Pumped idle can achieve up to about 10 percent thrust, or 1500 lbf, which should provide a drag coefficient nearly an order of magnitude lower than the pumped idle value.

The thermal design of the engine modulated ballute must be based on the tankhead idle thrust levels, since that condition results in the more severe heating environment. Reliable methods and data needed to establish reliable thermal predictions in this area are lacking, so these predictions are subject to large uncertainties. The "no mixing" prediction shown in figure 5.4-7 is based on the assumption that the exhaust flow expands isentropically around the vehicle, and is not influenced by the ambient flow. A more realistic, but still optimistic approach is to assume that the heating levels are the same as for a transpiration cooled surface where the exhaust flow is injected into boundary layer flow uniformly over the upstream surface area. These results indicate that the exhaust flow will significantly reduce heating rates near the nose, but these effects will diminish about half-way around the windward face. The heating distribution assumed for the present studies is probably conservative except possibly at boundary

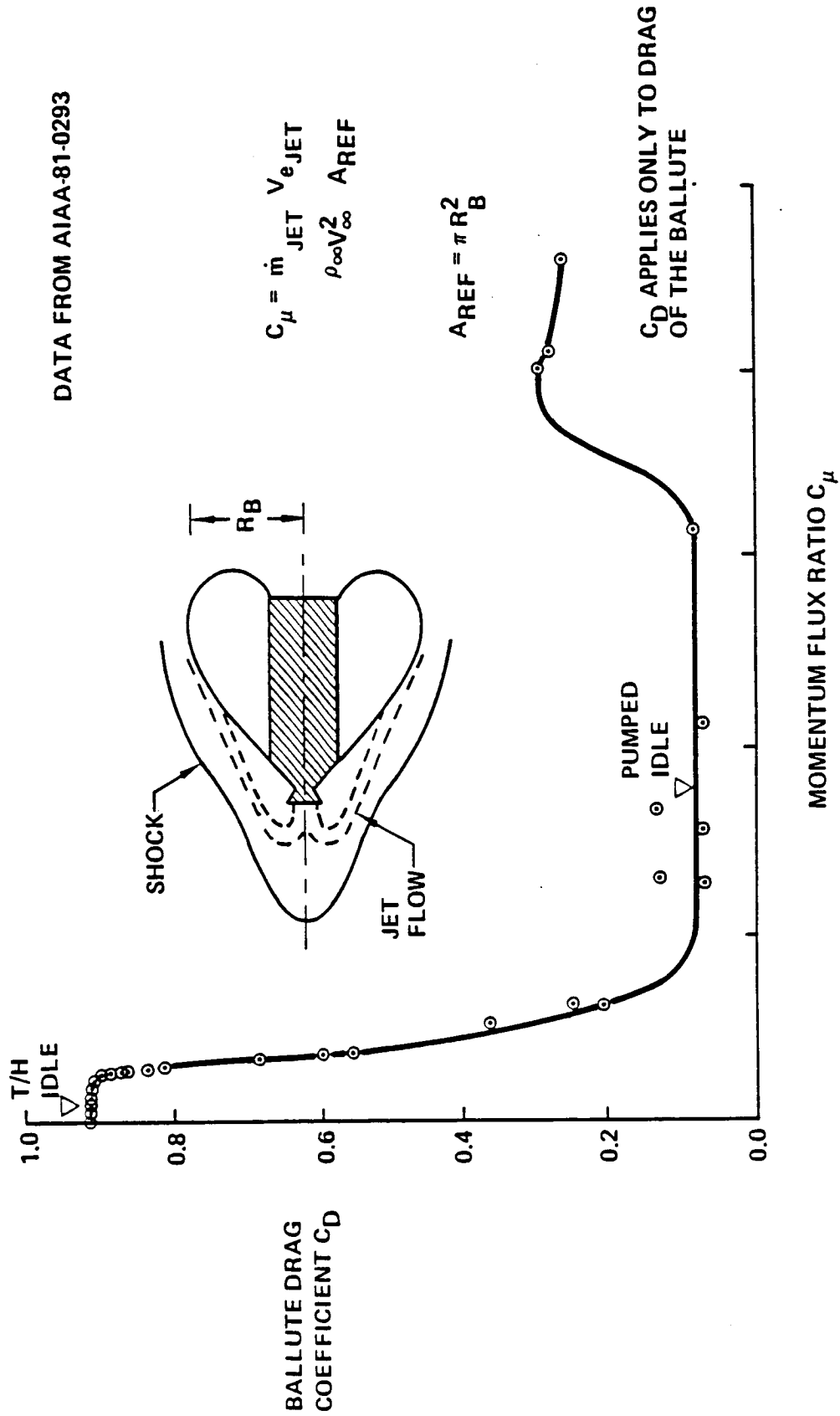


Figure 5.4-6 Effect of Engine Modulation on Ballute Drag

TANKHEAD IDLE
43-FT BALLUTE
ATTACHED FLOW

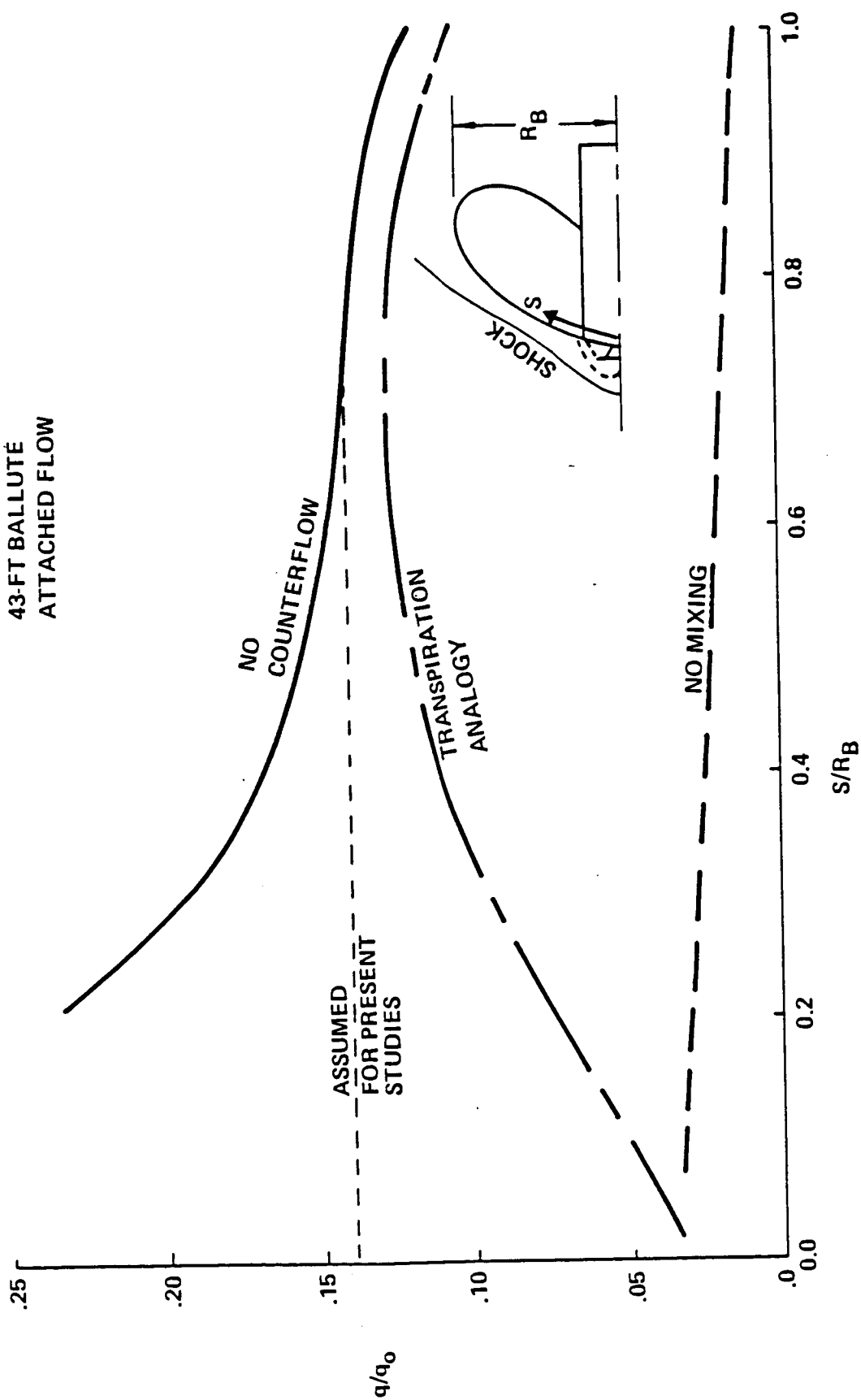


Figure 5.4-7 Effect of Engine Modulation on Ballute Heating Distribution

OTV-554

layer reattachment locations. Boundary layer reattachment is usually characterized by large but highly localized heating spikes. The boundary layer will be separated near the engine nozzles, but the reattachment location cannot be determined for the low thrust condition. For the pumped idle condition reattachment will probably occur at an S/RB of 0.6 or more, but the higher mass flow rates should result in heating rates less than the values shown, even at reattachment.

5.4.2.5 Base Heating

The heating distributions on the aft surface of the ballute are extrapolated from computations made by Dr. Peter Gnoffo of NASA/LaRC on a 25 foot diameter ballute using the Solution Adaptive Finite Volume Algorithm (SOFIA, ref. 30). Results are shown in figure 5.4-8. It was necessary to modify the base geometry as shown in order to obtain a solution. Consequently, results are probably not valid for expansion angles greater than about 90 degrees. Heating estimates at other base locations are shown in figure 5.4-9. Heating ratios on the side of the debris shield covering the cryogenic tanks and OTV structure was estimated using extrapolations of wind tunnel data obtained on a Venus Orbiting Imaging Radar (VIOR) configuration (reference 31). On the aft facing surface near the vehicle axis it was assumed that:

$$\dot{q} / \dot{q}_{\text{ref}} = 0.02$$

where q_{ref} is the predicted stagnation point heating rate for a hemisphere of the same radius as the brake. This approximation is consistent with Viking wind tunnel data presented in reference 32, and Apollo wind tunnel and flight data found in references 33 and 34. Thus, for a 25 foot radius ballute,

$$\dot{q} / \dot{q}_0 = 0.02 / \sqrt{25} = 0.004$$

Predictions based on correlations published by Bulmer (reference 35) were less than one-third of this value. Analyses were conducted using both methods to determine the sensitivity of TPS and thermal control requirements to methodology used in predicting environments. No methods or data are available for assessing effects of engine modulation on base heating, but these effects are expected to be small.

5.4.3 Insulation Requirements

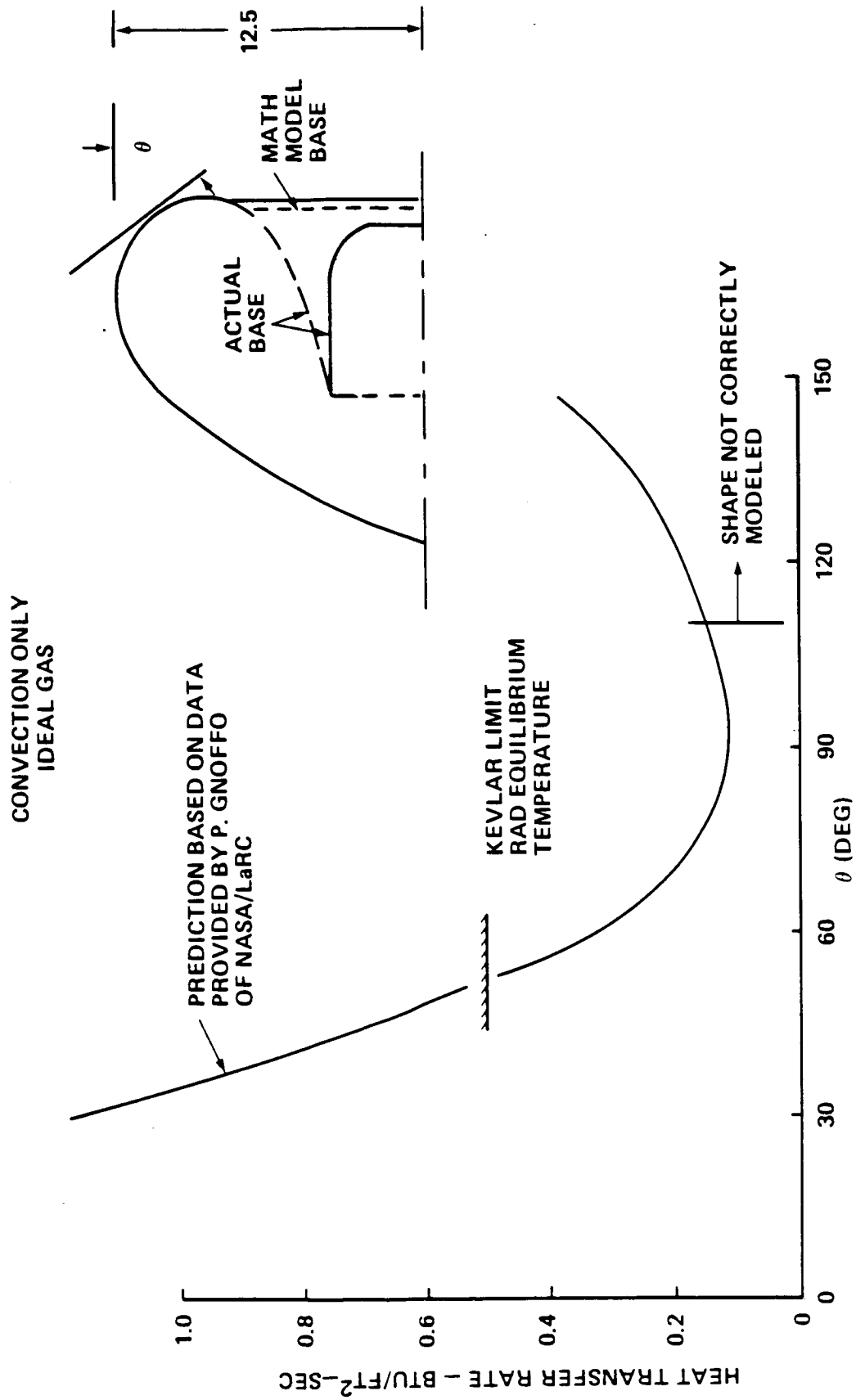


Figure 5.4-8. Base Heating Predictions

OTV-407

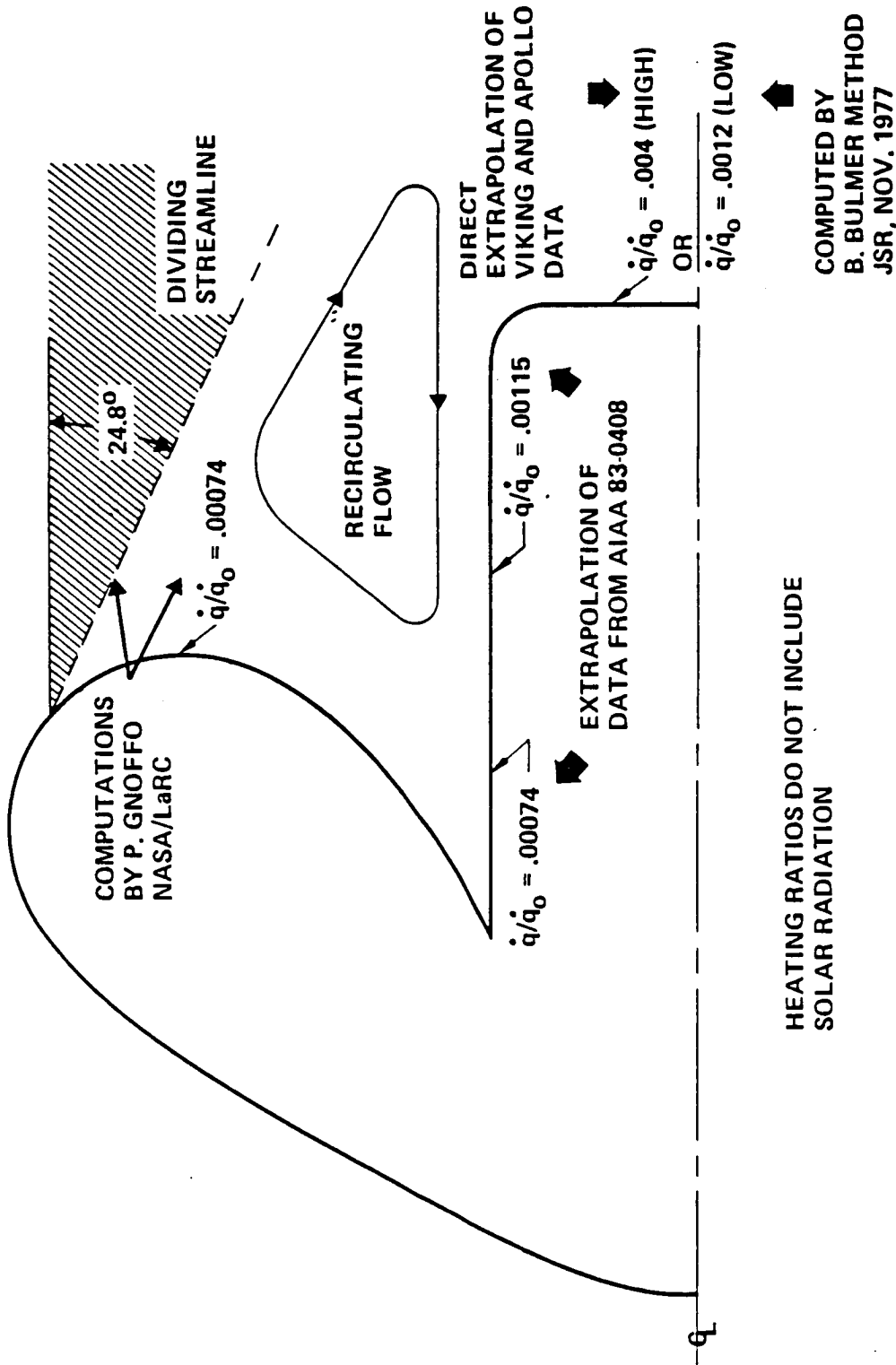


Figure 5.4-9 Ballute Base Heating Predictions

5.4.3.1 Thermal Models

Transient temperature analyses were conducted using the Boeing Engineering Thermal Analyses (BETA, ref. 36) based on axisymmetric thermal models such as the one shown in figure 5.4-10. Thermal transport modes considered include ballute internal radiation and radiation between ballute external surfaces and debris shield covering the OTV structure and cryogenic tankage. Results from these analyses were used to verify and supplement transient temperature predictions obtained with one-dimensional analyses made using the Convective Heating and Ablation Program (CHAP, ref. 37), which were used for most of the insulation sizing trades.

5.4.3.2 Space Based OTV Ballutes

600 Degree F Ballute - Maximum temperatures and required insulation thicknesses for the 600°F backwall ballute without engine modulation are shown in figure 5.4-11. Results indicate that no insulation is required on the base of the ballute or over the aluminum debris shield with the possible exception of the aft facing surface. With the aft facing surface no insulation is required with the lower heating rates based on reference 5.4-10 correlations, but some insulation could be required for the higher predictions obtained by direct extrapolation of Viking and Apollo data.

1500 Degree F Ballute - Increasing the backwall temperature of the ballute greatly increases the quantity of heat that is dissipated by radiation from the base of the ballute. For this reason insulation thicknesses on the windward face of the ballute can be reduced to about 0.1 inches for the high temperature condition, as shown in figure 5.4-12. Even less insulation is required over much of the ballute, but lower thicknesses are felt to be impractical from a fabrication standpoint.

A negative feature of this approach is that the ballute radiates much more heat to the OTV structure and debris shield, necessitating the addition of insulation to these components. Also, 3/8 inch of insulation is required on the base of the ballute to prevent overheating avionics components (see subsection 5.4.4).

Engine Modulated Ballute - Insulation requirements for the 1500°F backwall ballute with engine modulation are nearly the same as for the no-engine modulation concept except that no rigid TPS is required on the aeroshell. Insulation requirements for the 600°F backwall ballutes with and without engine modulation are shown in figure 5.4-13.

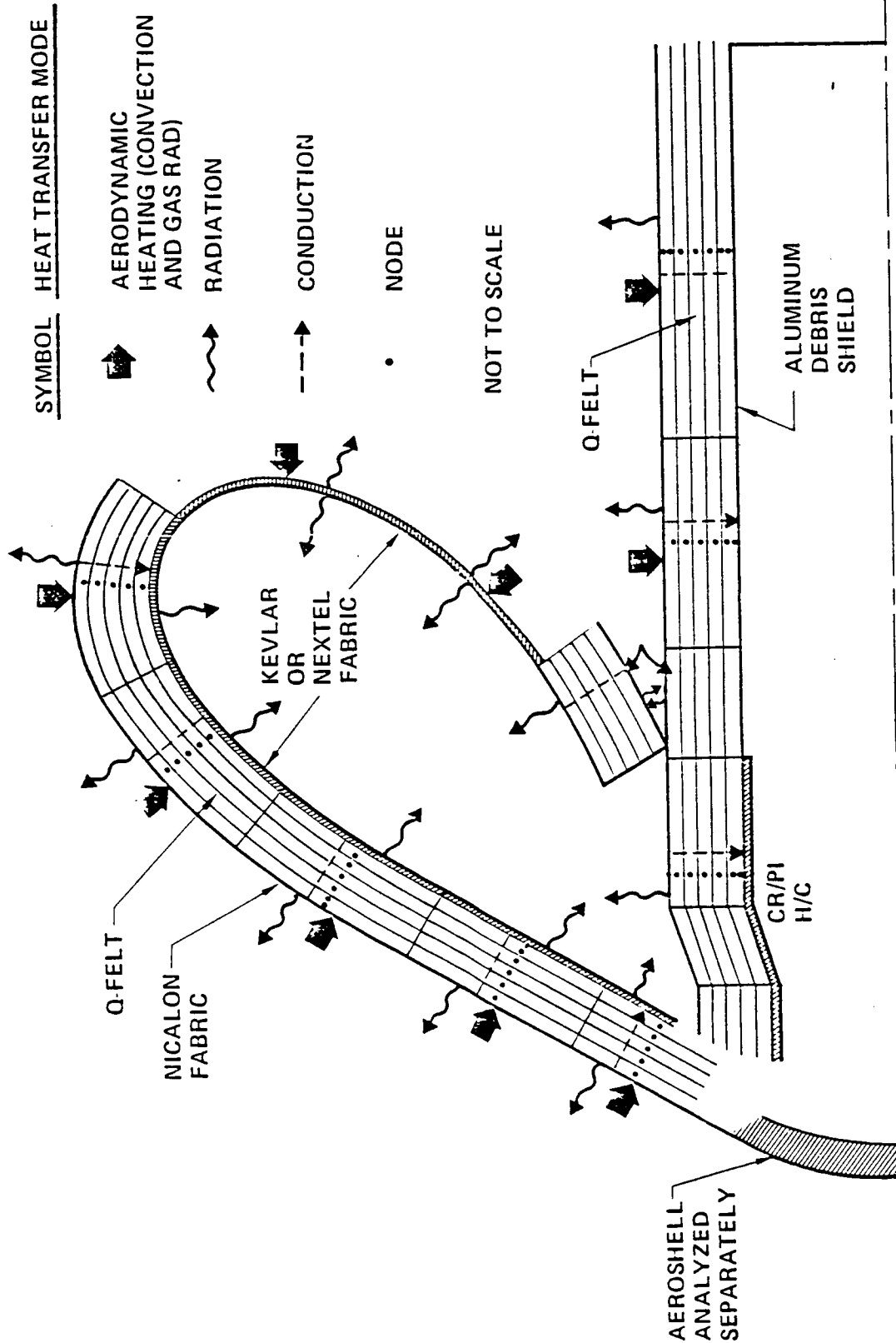


Figure 5.4-10 Ballute Thermal Model

OTV-505

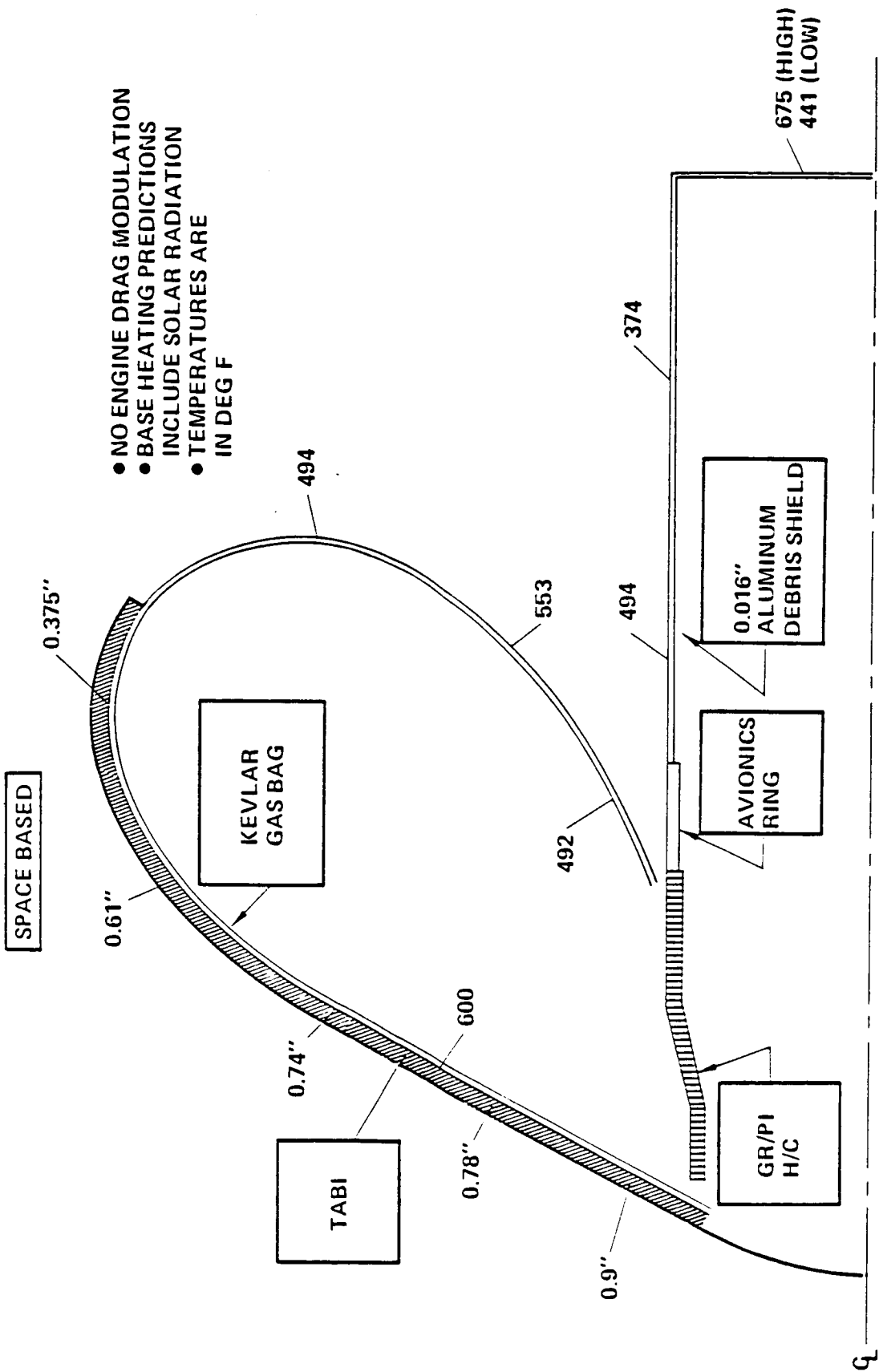


Figure 5.4-11 Maximum Temperatures on a 6000 F B/W Ballute

QTV 536

- NO ENGINE DRAG MODULATION
 - BASE HEATING PREDICTIONS INCLUDE SOLAR RADIATION
 - TEMPERATURES ARE IN DEG F
 - SPACE BASED
- DIAM= 50.1 FT
W/CDA = 9.37 PSE

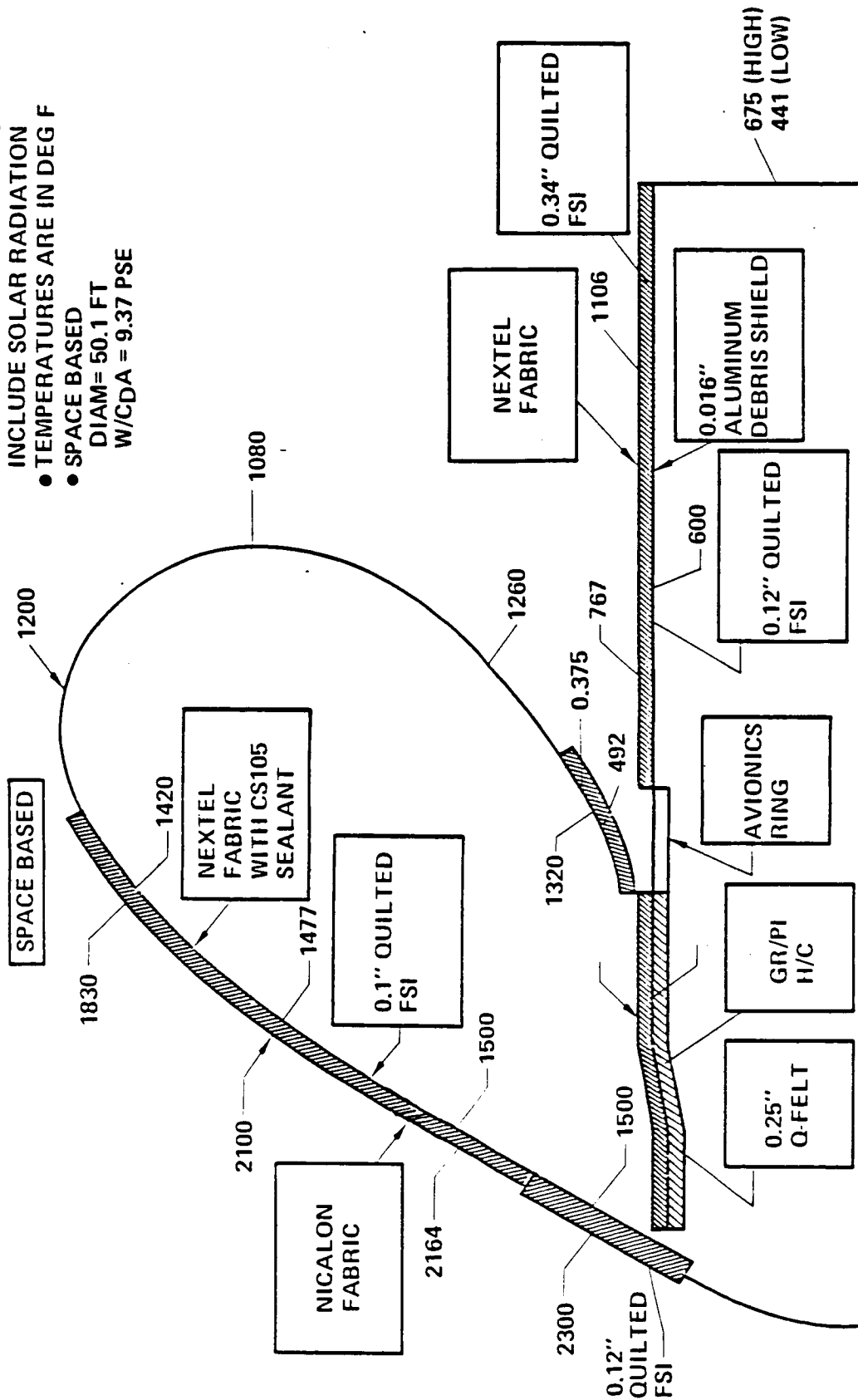


Figure 5.4-12 Maximum Temperatures on an 15000°F B/W Ballute

600°F B/W

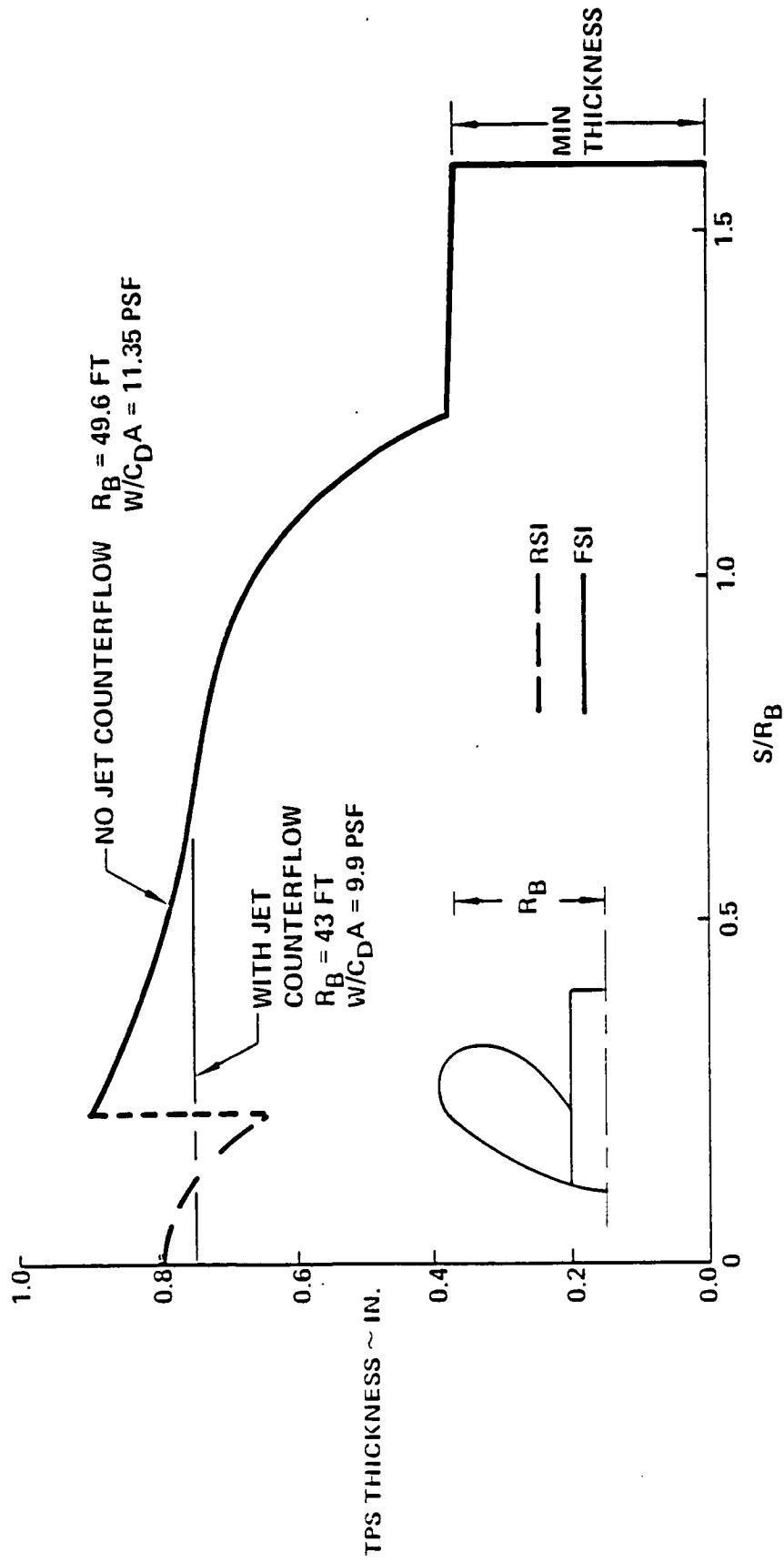


Figure 5.4-13 Ballute Insulation Thickness Requirements

5.4.3.5 Ground Based OTV Ballutes

Maximum temperatures and insulation thickness requirements for a 1500 degree 33 foot ballute used for a GB OTV are shown in figure 5.4-14. This configuration is proposed for delivery payloads up to 12,000 lbm and no return payload. Insulation thicknesses are nearly double those shown for the 50 foot ballute previously shown in figure 5.4-12 because of a higher ballistic coefficient and smaller ballute size. The aluminum debris shield over the aft structure and cryogenic tankage shown for the space based systems has been replaced with a graphite/polyimide structure. Results show that minimum thickness (0.1 inch) FSI over this structure will prevent the graphite/polyimide temperatures from exceeding the 600°F limit.

Results are inconclusive with regard to insulation requirements on the aluminum debris shield covering the base of the vehicle. Since it is a non-load carrying structure, a temperature limit of 600°F has been assumed. Some insulation is required based on the high estimate ($\dot{q}/\dot{q}_{ref} = 0.02$), but not for the low (Bulmer) prediction. The debris shield temperatures are for a surface in radiation equilibrium, and are probably conservative. The location of the separation streamline indicates that wake impingement heating may occur on the aft structure. However, since insulation is already required on these surfaces, the impact on TPS weight should be small.

Corresponding temperature and insulation data for a 66 foot diameter ballute are presented in figure 5.4-15. This ballute is sized for manned sortie missions, and includes a 7500 lbm return payload. Because of a lower ballistic coefficient and larger ballute size, the insulation thicknesses required on the front face of the ballute is one-half that required on the 33 foot ballute. Convective heating rates on the base structure are much lower than for the smaller ballutes, but benefits of the lower convective heating is offset by increased radiation from the base of the ballute due to a higher view factor. The location of the separation streamline indicates that wake impingement heating on the manned cab will not be a problem, but better methods for predicting recirculation heating are required before a meaningful determination of insulation requirements on the manned cab can be made.

5.4.4 Aeromaneuver Impact on Avionics

Due to the close proximity of the avionics ring with the ballute, the avionics thermal environment is dominated by radiation from the base of the ballute. Temperature profiles for the ballute base are shown in figure 5.4-16. The uninsulated base of the 1500°F ballute reaches a maximum temperature in excess of 1000°F, but

- NO ENGINE DRAG MODULATION
- BASE HEATING PREDICTIONS INCLUDE SOLAR RADIATION
- TEMPERATURES IN DEG F

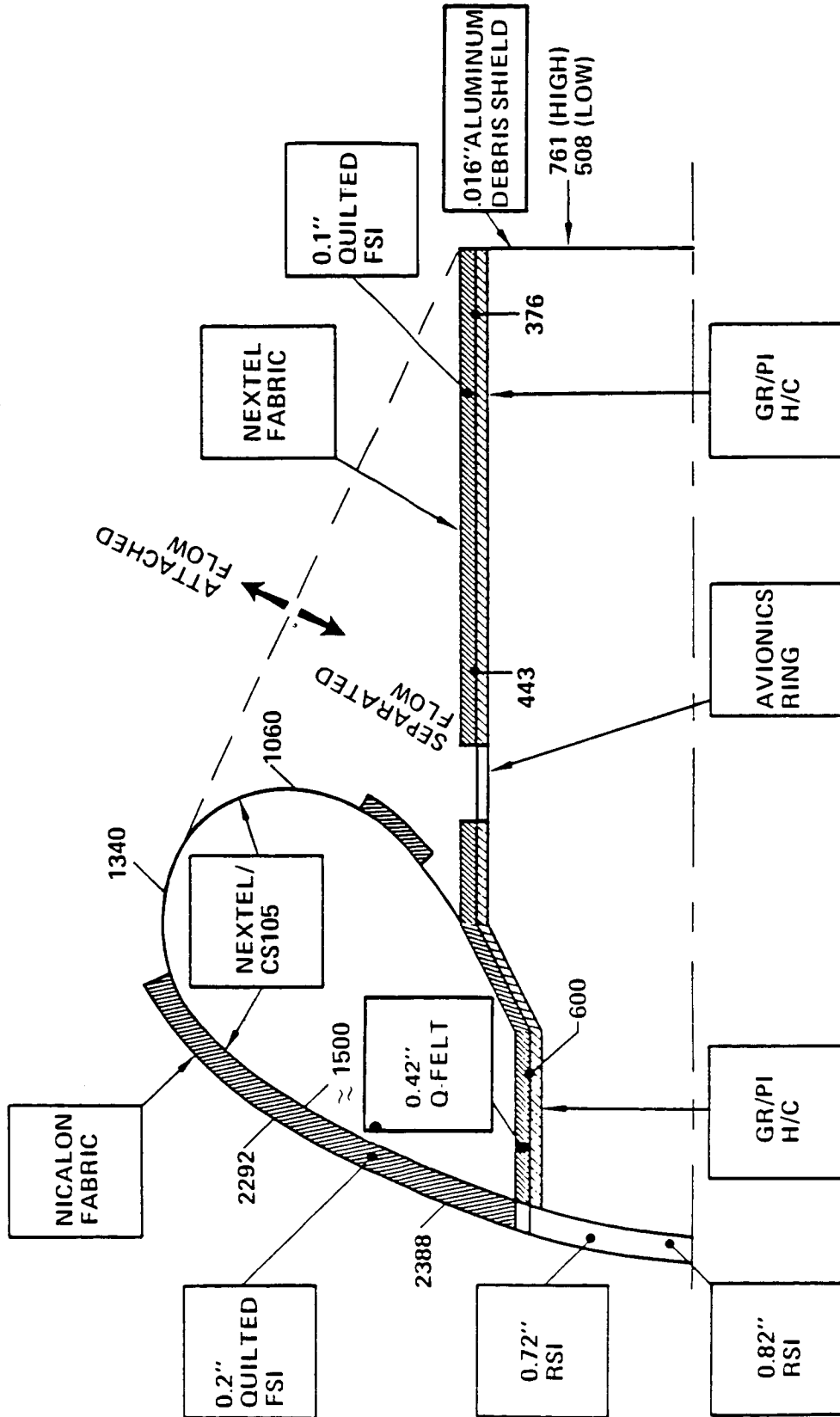


Figure 5.4-14 Maximum Temperatures on a 33 Ft. Ground Based Ballute

OTV 901

- NO ENGINE DRAG MODULATION
- BASE HEATING PREDICTIONS INCLUDE SOLAR RADIATION
- TEMPERATURES IN DEG F

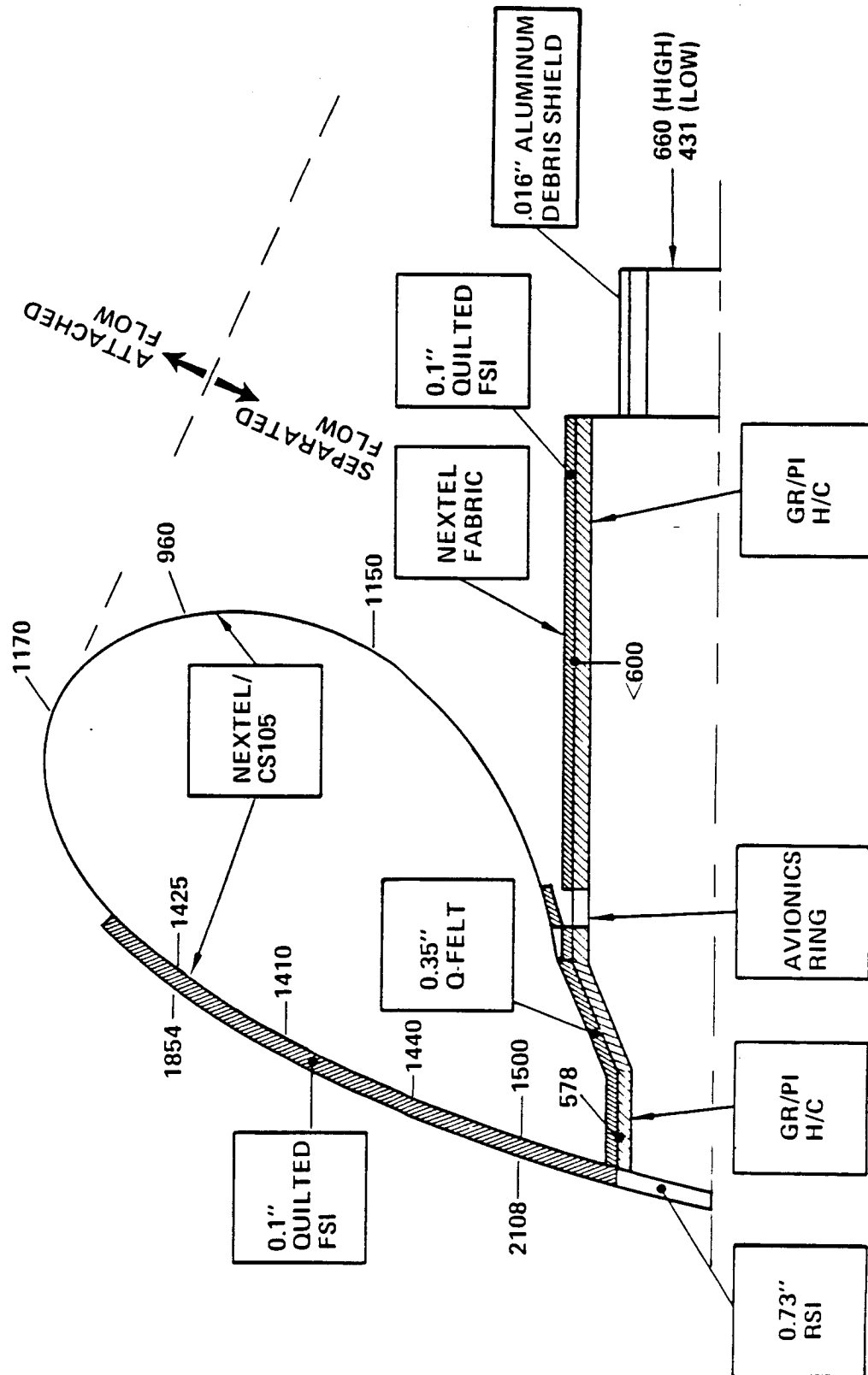


Figure 5.4-15 Maximum Temperatures on a 66 Ft. Ground Based Ballute

OTV 897

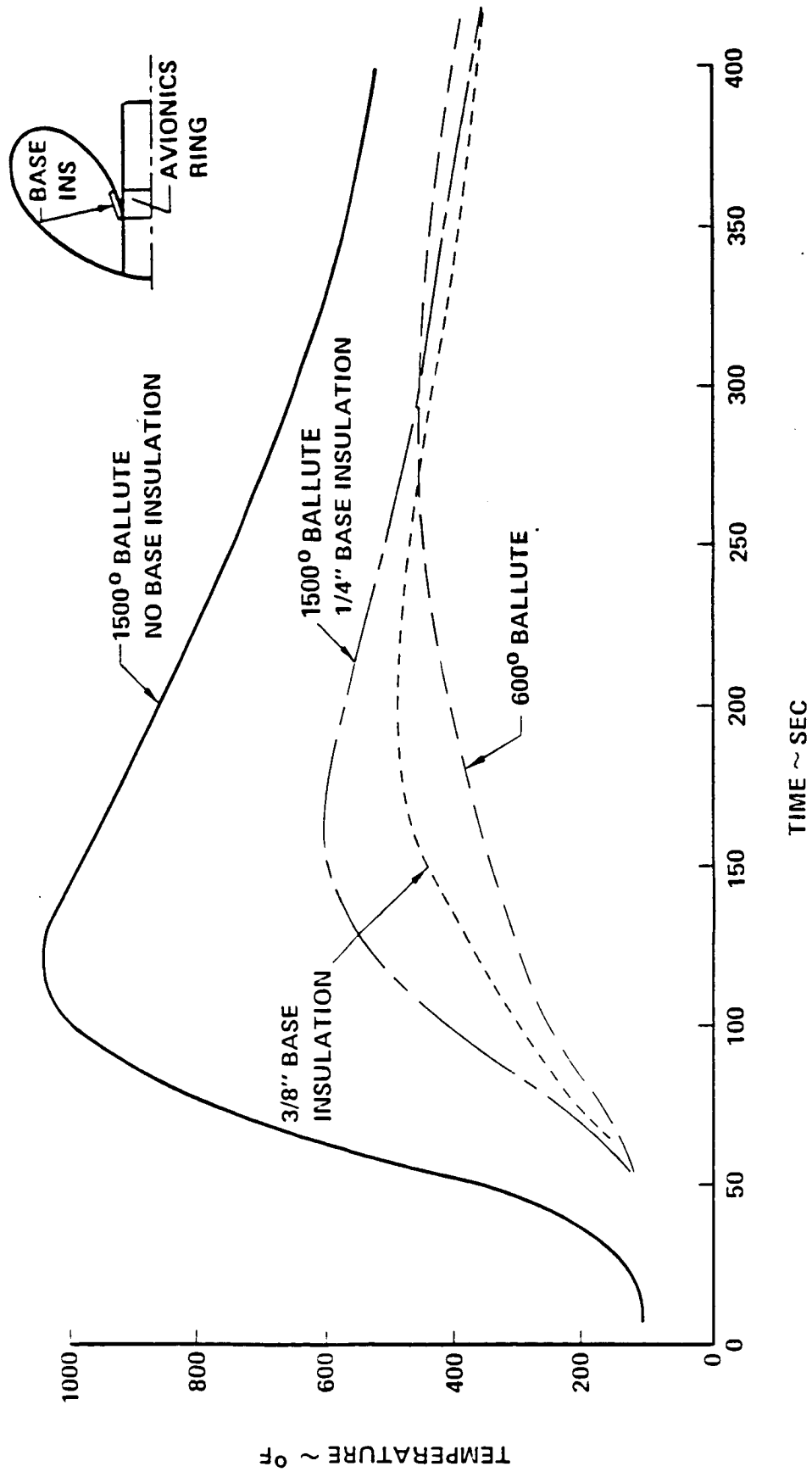


Figure 5.4-16 Ballute Temperatures Adjacent to Avionics Ring

3/8 inches of FSI reduces this temperature to less than 500°F, which is about the same level as with the 600°F backwall ballute.

The impact on selected avionics components is shown in table 5.4-1. Either active cooling or additional heat sink capacity is required in all cases to prevent the power amplifier from exceeding its qualification temperature. Probably the simplest and most reliable methods of passively cooling electronics for short periods is to use materials with a melt temperature slightly below the allowable component temperature, thus utilizing the latent heat of fusion to absorb excess heat. In this case myrietic acid, which has a melting temperature of 150°F, was selected as the phase change material (PCM). The weights shown are for the PCM only, and do not include the structure required to contain the PCM in its molten state.

5.5 LIFTING BRAKE OTV

5.5.1 TPS Concept



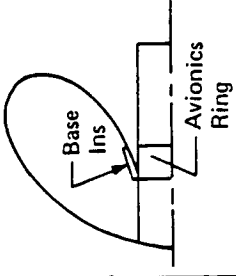
The lifting brake TPS concept is similar to that for the ballute in that it consists of RSI/SIP over a rigid aeroshell, and FSI over Kevlar sealed with Viton providing most of the brake surface, as shown in figure 5.5-1. The FSI/Kevlar flexible surface is supported by 24 ribs as shown. Methods for attaching the FSI/Kevlar to the aeroshell and ribs are shown in subsection 2.2.2.

5.5.2 Aerothermal Predictions

Heating patterns on the windward face are shown in figure 5.5-2 for 10°, 20°, and 30° angles-of-attack. These patterns are derived from experimental data obtained on a 4 inch diameter model in the NASA/Langley 31 Inch Mach 10 Tunnel (ref. 38). Heat transfer ratios near the nose cap and trailing edge were adjusted to account for differences in nose and trailing edge radii. No data were obtained at 20° angle-of-attack, so the patterns for 20° shown in figure 5.5-2 were interpolated from data obtained at 15° and 30°. Results indicate that peak heating rates do not vary much with angle-of-attack on either the FSI or RSI surfaces, although the peak heating location on the FSI moves from near the leading edge to the fabric/aeroshell interface as angle-of-attack is reduced from 30° to 10°.

Heating ratios in the base region are shown in figure 5.5-3 for 10° angle-of-attack. Methods used to estimate the heating near the axis are the same as were assumed for the ballute, with the high value based on extrapolation of Viking and Apollo data, and the low value computed using methods presented in reference 5.4-6. The envelope

Table 5.4-1 Ballute Avionics Thermal Assessment

Concept	Component	No Thermal		With PCM 		 Phase Change Material (Myrietic Acid)
		Max Qual Temp (°F)	Predicted Max Temp (°F)	PCM Needed (Lbm)	Predicted Max Temp (°F)	
600 Deg F Ballute	power amp IRU DMU No. 1	160	201 167 152	2.0	150	
1500 Deg F Ballute	Power Amp IRU DMU No. 1	160	480 218 193	15.6	150	
1500 Deg F Ballute with 3/8" Base Ins.	Power Amp IRU DMU No. 1	160	213 169 154	2.5	150	

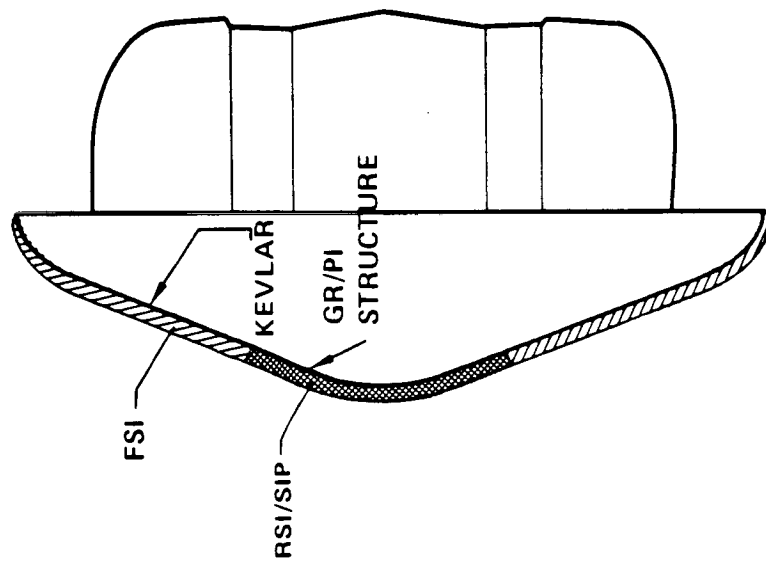
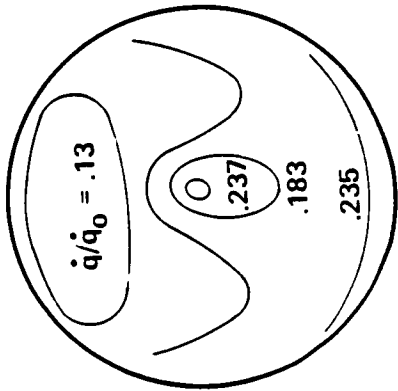
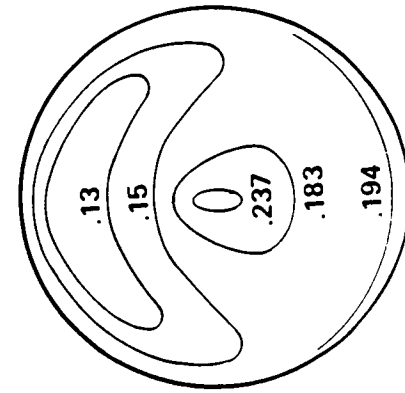


Figure 5.5-1 Lifting Brake TPS Concept

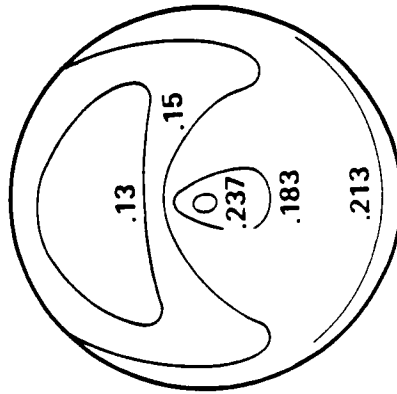
PREDICTIONS EXTRAPOLATED
FROM REMTECH REPORT
RTR 069-1 DATA



$\alpha = 30^\circ$



$\alpha = 10^\circ$



$\alpha = 20^\circ$

Figure 5.5-2 Lifting Brake Heating Patterns

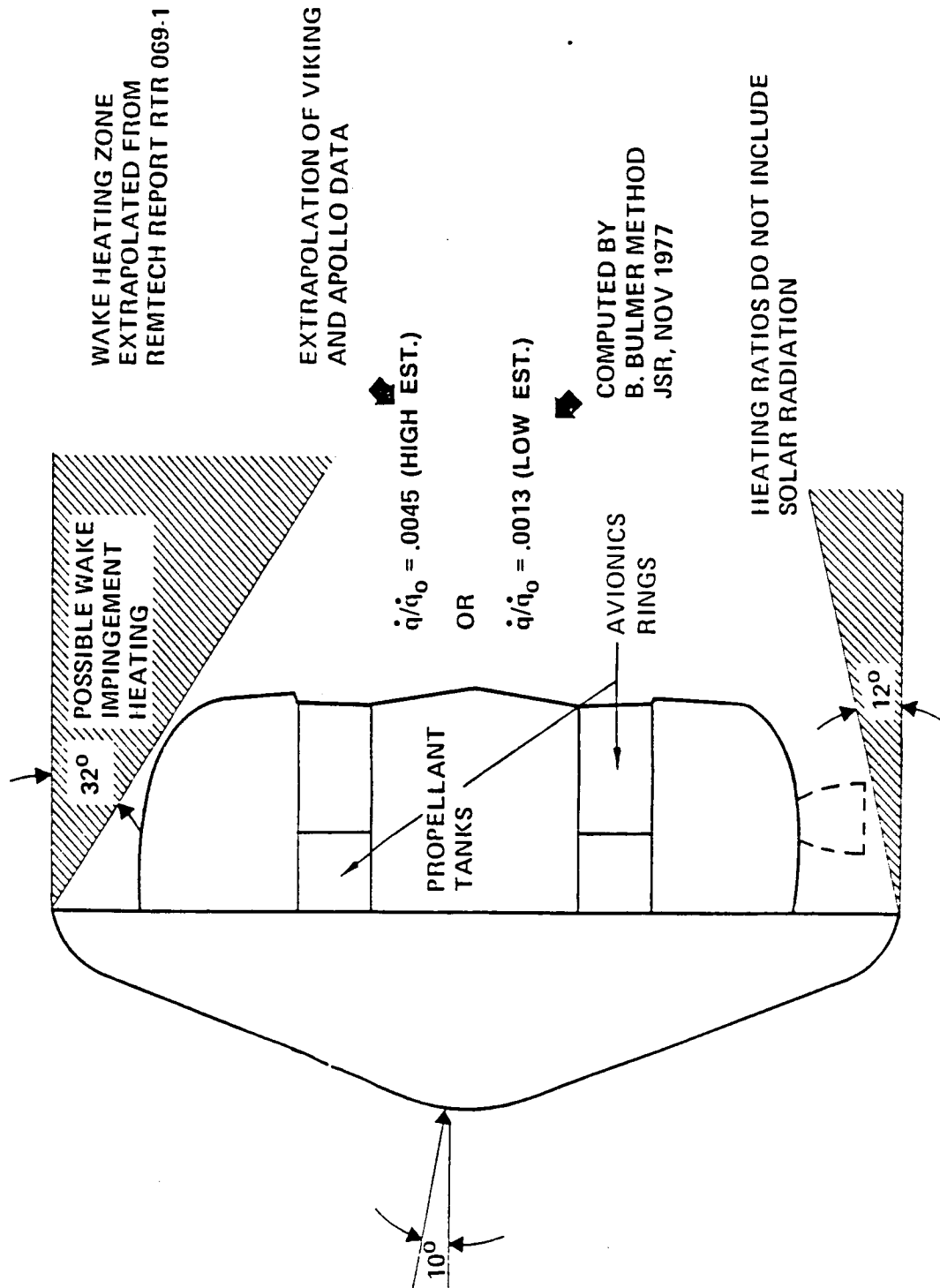


Figure 5.5-3 Lifting Brake Base Heating Predictions

required to avoid excessive wake impingement heating was derived from wind tunnel data presented in reference 5.5-1, and plotted in figure 5.5-4. The envelope boundary was selected to ensure that impingement heating ratios (\dot{q}/\dot{q}_0) do not exceed 0.005, which will limit maximum heating rates to roughly 0.5 BTU/ft²-sec. These predictions are subject to large uncertainties due to real gas effects and possible distortions in separation patterns resulting from the sting position.

5.5.3 Insulation Requirements

FSI and RSI thicknesses required to satisfy the insulation sizing criteria given in subsection 5.2.3 are shown in figure 5.5-5 for an angle-of-attack of 10°. The FSI thicknesses are based on view factors to space varying from 0.2 near the aeroshell to 0.625 on the trailing edge.

A brief analysis was also conducted to determine potential savings in insulation from increasing the allowable temperature of the load carrying fabric from 600°F to 1500°F. As with the ballute, the increase in temperature capability could be achieved by replacing the Kevlar/Viton fabric with Nextel AB312/CS105. Results are shown in figure 5.5-6. The increased backwall temperatures necessitate the addition of insulation over the structure behind the brake. Total insulation on the brake and debris shield is reduced by about 30 percent, excluding the insulation that must be added to the ribs and braces. The reason that the increase in backwall temperature did not result in the dramatic reduction in insulation that was obtained on the ballute is that the reduction in insulation is possible because of increased heat dissipation by radiation from the base, but with the lifting brake, much of this radiation is blocked by the debris shield covering the aft structure and cryo tanks. For a space based system the reduction in insulation weight is not considered to be sufficient to compensate for the loss in reusability, especially when the added rib and brace insulation is factored in.

5.5.4 Aeromaneuver Impact on Avionics

Predicted peak temperatures of selected avionics components is shown in table 5.5-1. Solar radiation effects were included. Results are inconclusive with regard to the need for additional cooling. Predictions based on the high estimate (Viking and Apollo data) show that 2.1 lbm of PCM are required to protect the power amplifier, but no PCM is required for the lower heating estimate (Bulmer).

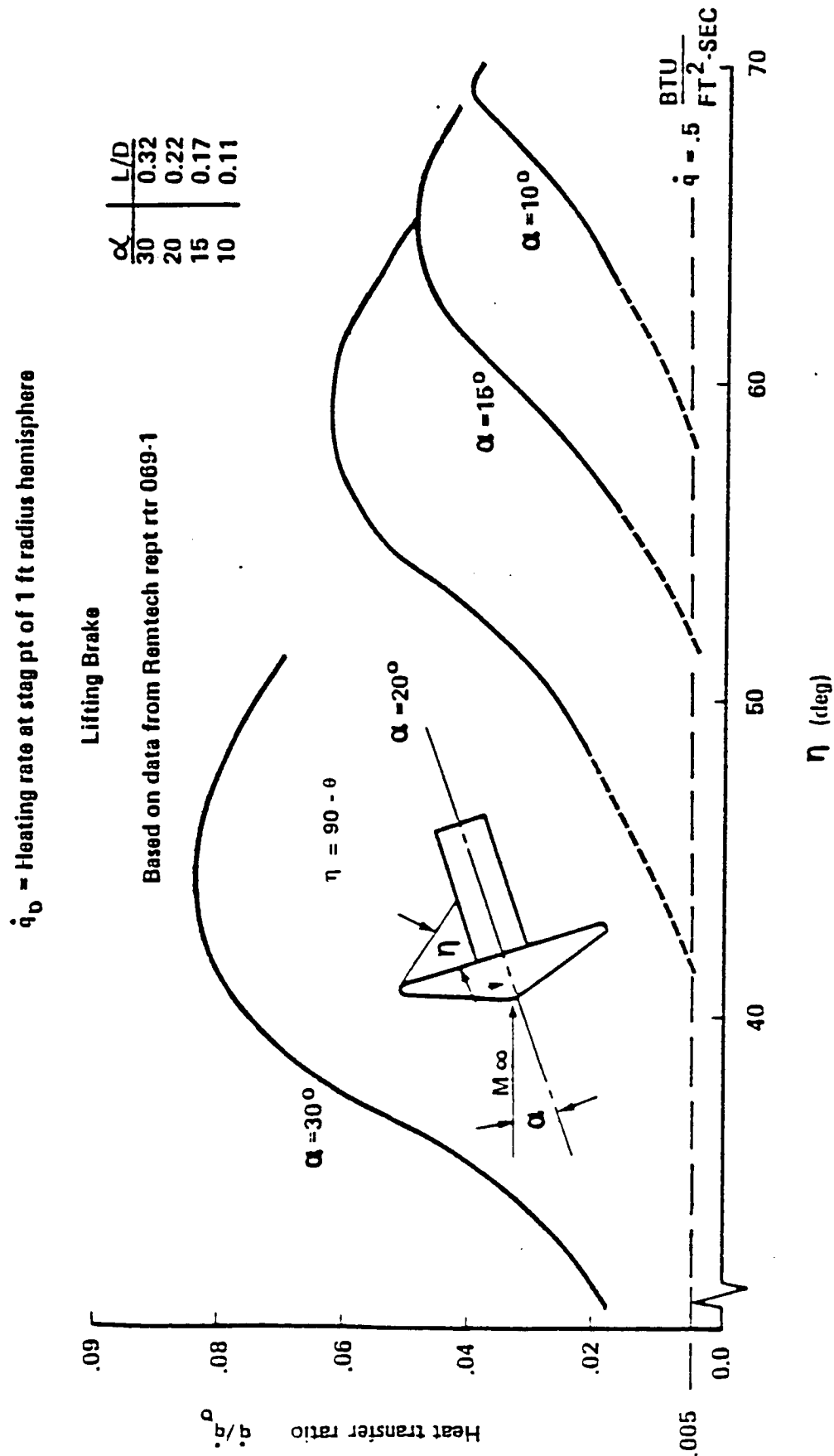


Figure 5.5-4 OTV Impingement Heating Distribution

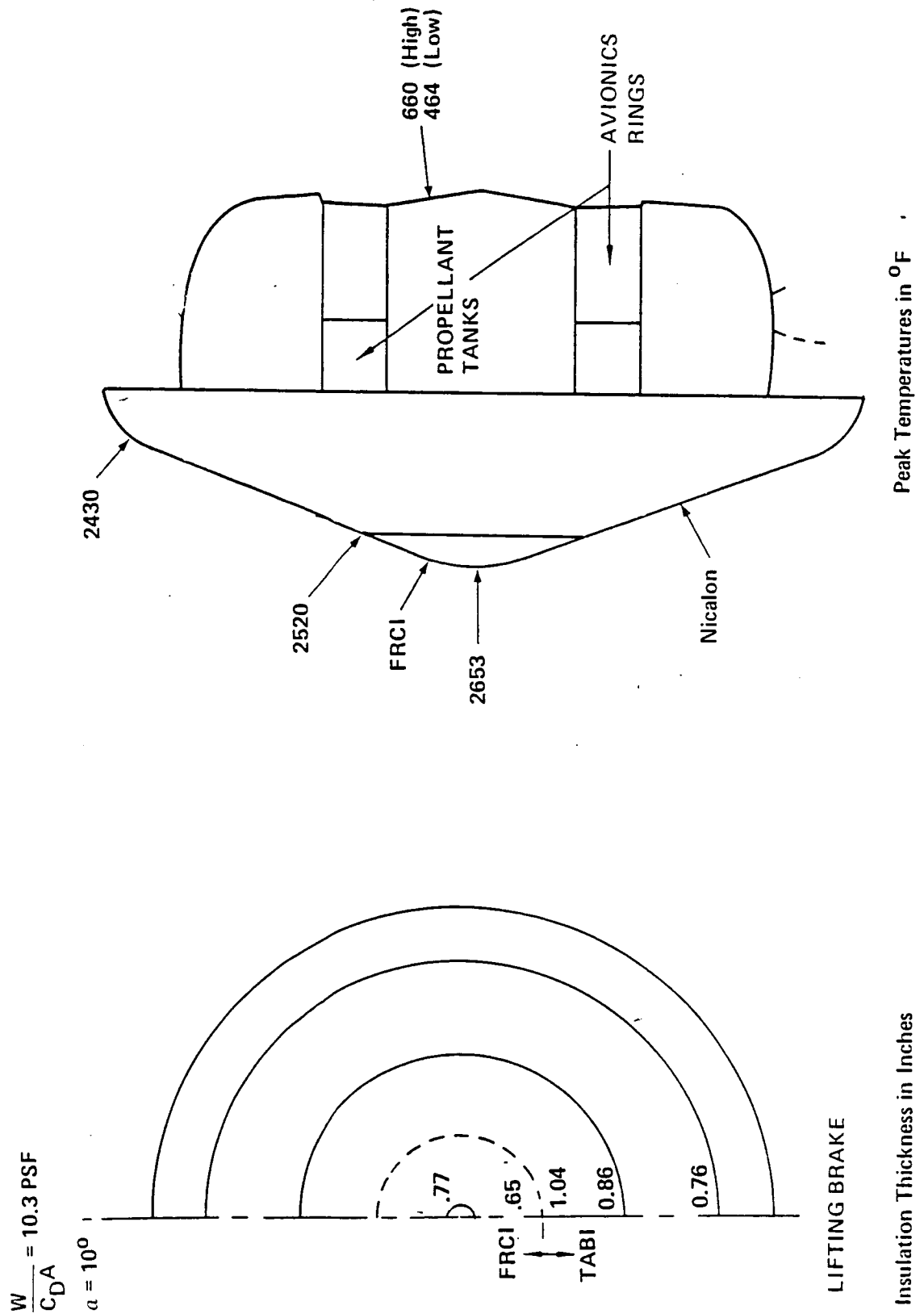


Figure 5.5-5 Lifting Brake Peak Temperatures and Insulation Requirements

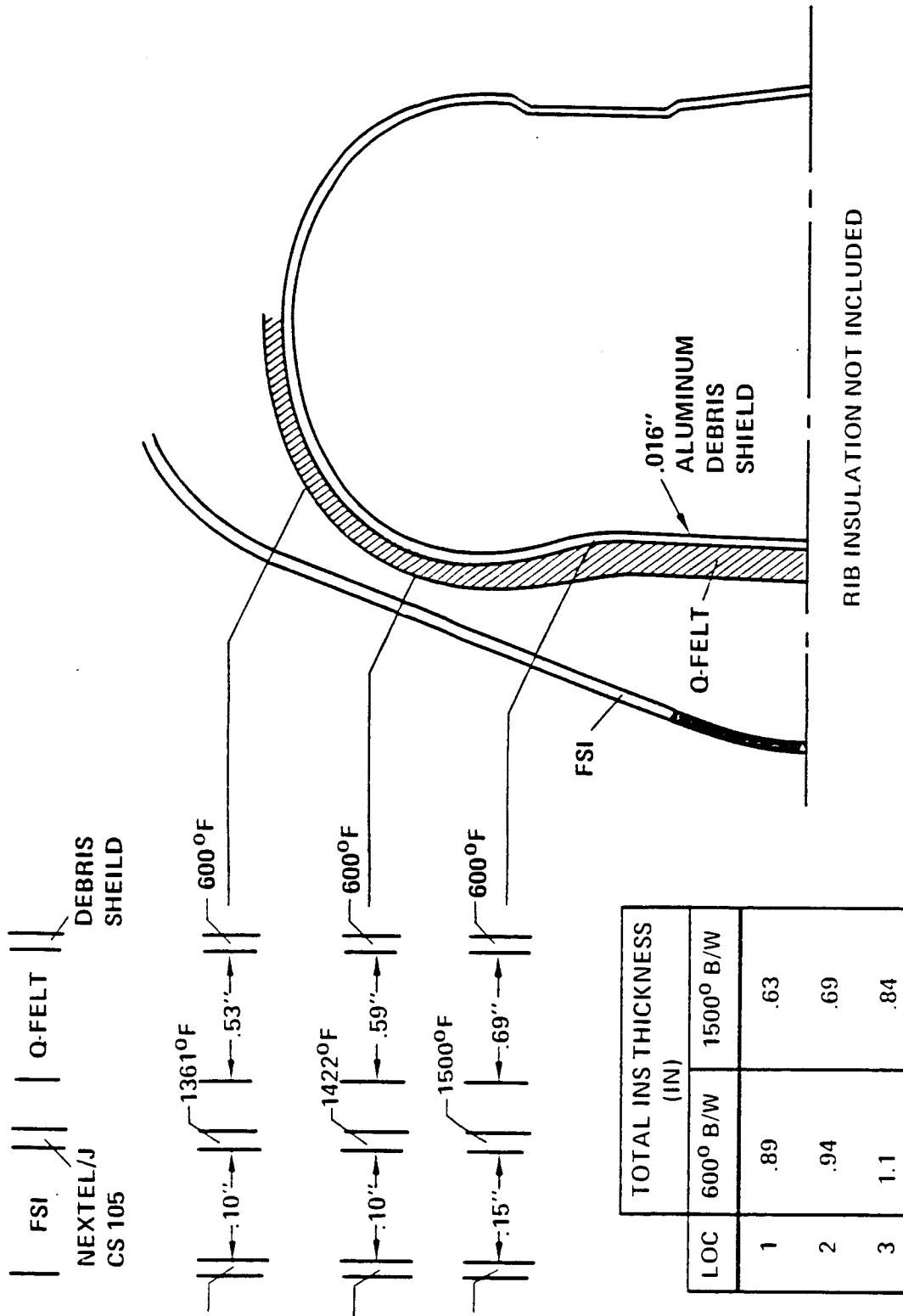


Figure 5.5-5 Maximum Temperatures on a 1500 Deg. Lifting Brake

Table 5.5-1 Predicted Peak Temperatures

CONCEPT	COMPONENT	NO THERMAL		WITH PCM 1		PHASE CHANGE MATERIAL (MYRIETIC ACID)
		MAX QUAL TEMP (°F)	PREDICTED MAX TEMP (°F)	PCM NEEDED (LBS)	PREDICTED MAX TEMP (°F)	
HIGH HEATING	POWER AMP IRU DMU NO. 1	160	201 173 157	2.1	150	
	POWER AMP IRU DMU NO.1	160	132 161 148	—	—	
LOW HEATING						

5.6 SHAPED BRAKE OTV

5.6.1 TPS Concept

The TPS concept on the windward brake surface is the same as for the rigid aeroshell surfaces on the ballute and lifting brakes as shown in figure 5.6-1. Hexagonal FRCI type tiles are bonded to a SIP, which is then bonded to the graphite/polyimide structure. If required, FSI will be used in the base region to protect the debris shield.

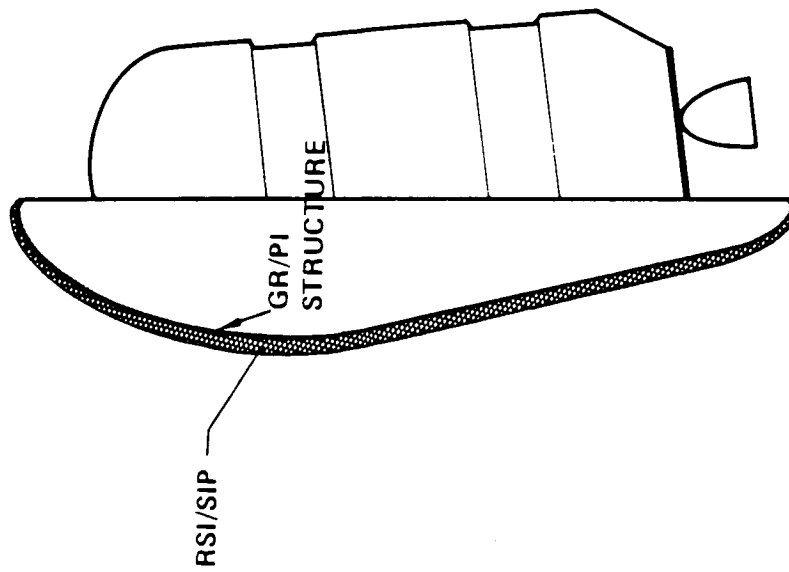
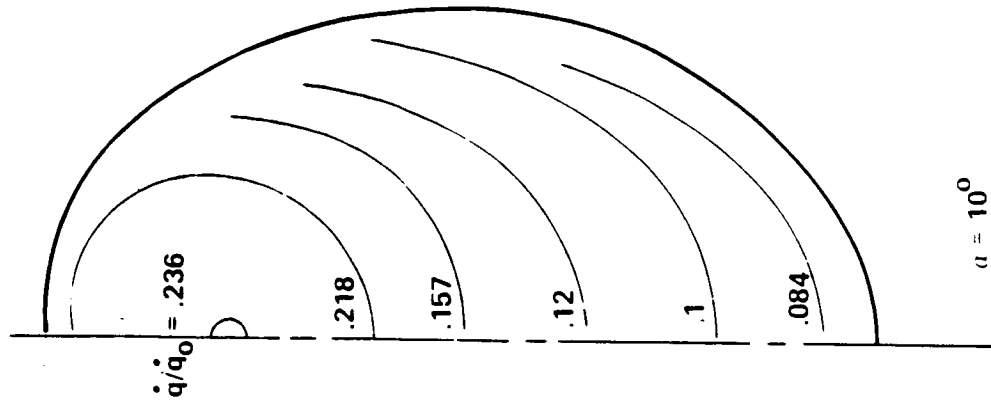
5.6.2 Aerothermal Predictions

Heating patterns on the windward face are shown in figure 5.6-2. The heating distribution along the line of symmetry projecting downward from the nose cap in figure 5.6-2 was computed using the rho-mu code assuming a modified Newtonian pressure distribution. The stagnation point heat transfer ratio is based on an effective hemispherical nose radius of 18 feet. Heating ratios on the rest of the nose cap were obtained by adjusting the stagnation point value for surface angle relative to the stagnation point. Similarly, distributions on the remaining windward surface areas were obtained by adjusting the heating rates along the line of symmetry to account for surface angle relative to the free-stream flow.

Heating predictions in the base region presented in figure 5.6-3 are essentially the same as for the lifting brake. The wake impingement envelope was established from data previously presented in figure 5.5-7, and is considered to be very approximate.

5.6.3 Thermal Analysis Verification

The BAC Boundary Layer Analysis Program (BLAP) has been used to determine heating rates for and thermal response of shaped aerobrake concepts. Testing conducted by NASA/LARC has provided data with which BLAP can be compared. Figures 5.6-4 and 5.6-5 show this comparison for points along the shaped brake centerline and for points perpendicular to the centerline, respectively. It will be noted that the computer program tends to overpredict heating rate at or near the stagnation point and tends to underpredict heating rate near the edge of the brake. This difference is primarily due to real gas effects which are included in the program while, due to the low tunnel air temperatures, the test closely approximates an ideal gas response. Actual heating rates are expected to match more closely with the BLAP results. The overall program/data correlation is considered excellent and verification established.



SHAPED BRAKE

Figure 5.6-2 Shaped Brake Heating Patterns

Figure 5.6-1 Shaped Brake TPS Concept

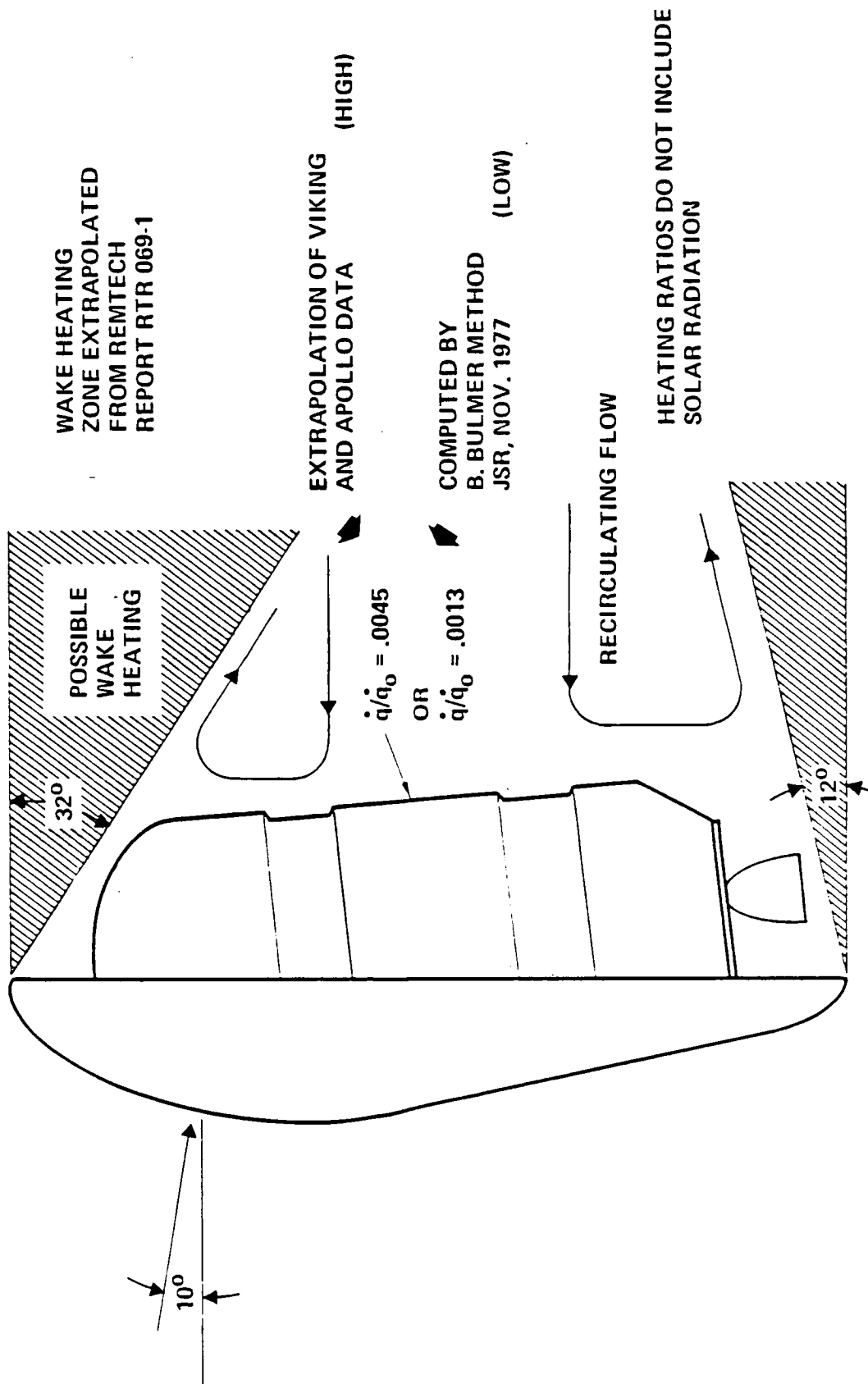


Figure 5.6-3 Shaped Brake Base Heating Predictions

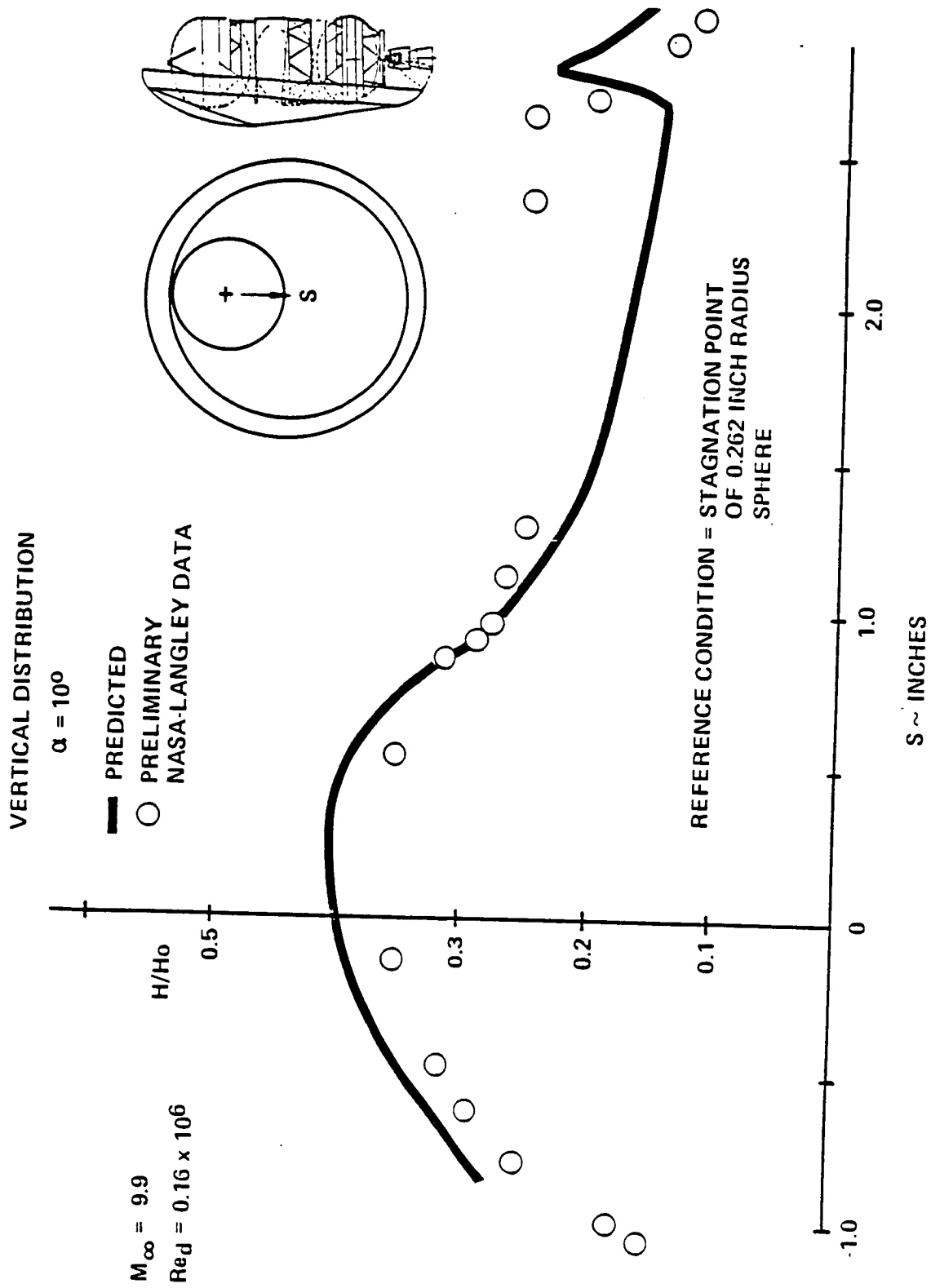


Figure 5.6-4 Shaped Brake—Data-Theory Comparison

QTV-1161

JSC 002 RAKED CONE

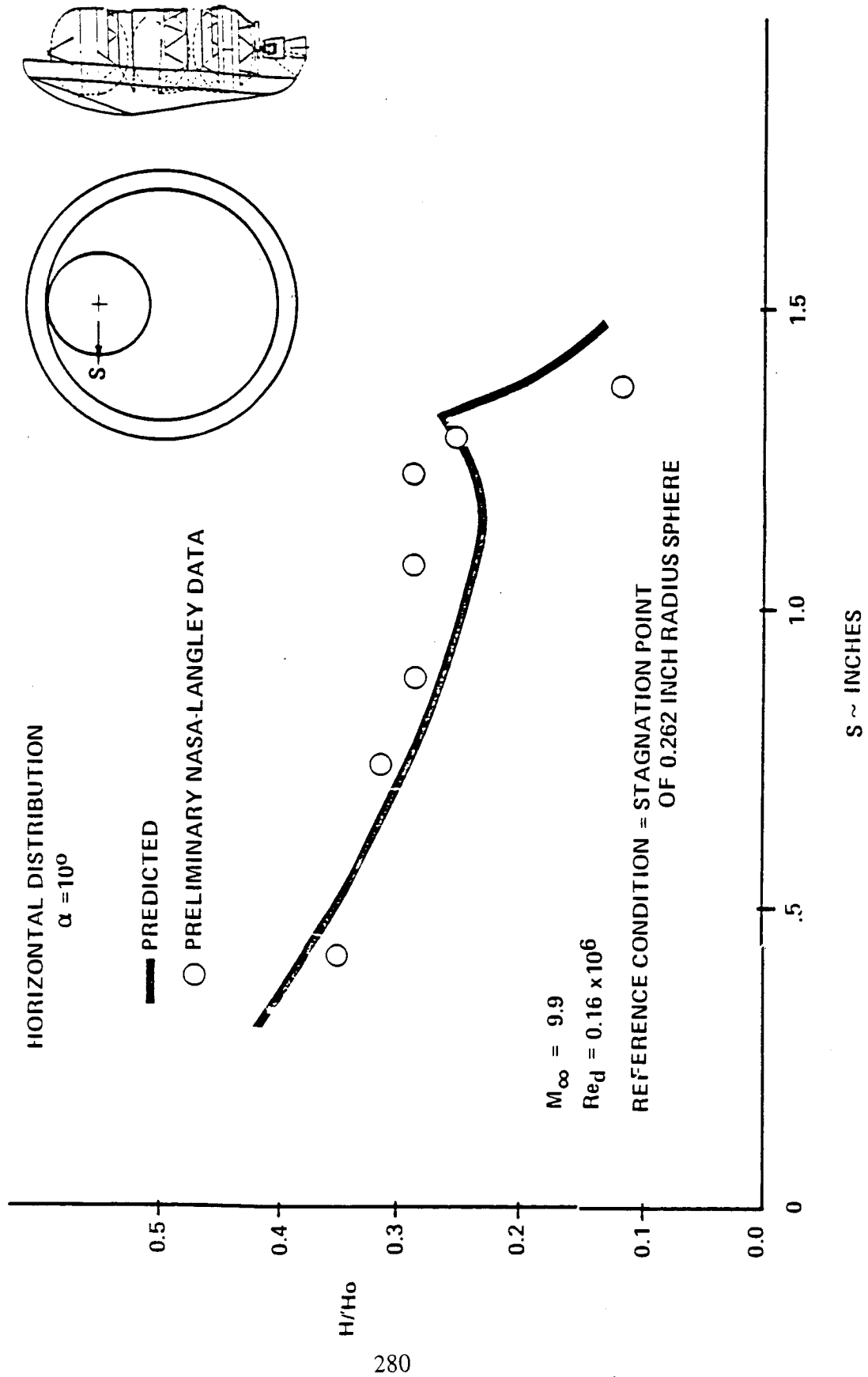


Figure 5.6-5 Shaped Brake—Data-Theory Comparison

5.6.4 Insulation Requirements

RSI thickness requirements for the shaped brake are presented in figure 5.6-6. These thicknesses are based on a maximum RSI/SIP temperature of 550°F with a tile density of 12 lbm/ft³ with a specific heat and thermal conductance properties equivalent to FRCI-20-12. As with the ballute and lifting brake configurations, more reliable base heating predictions are required before a meaningful assessment of insulation requirements in this area can be made.

5.6.5 Aeromaneuver Impact on Avionics

Thermal control requirements for the shaped brake are identical to those for the lifting brake (see subsection 5.6.3 and figure 5.5-6).

5.7 MISSION IMPACT AND AEROTHERMAL UNCERTAINTIES

The aerobraked return from lunar and planetary trajectories results in a thermal environment significantly more severe than a return from a geosynchronous orbit. Uncertainties in the thermal environment limit predictive capability and may result in excessive conservatism with attendant weight penalties. These subjects are discussed in detail in the following sections.

5.7.1 Mission Impact

Predicted heating rates for three aerobrake types and three mission types are shown in Table 5.7-1 for both flexible and rigid surface insulations (FSI and RSI). Also shown in this figure are materials limits projected for 1990 assuming normal growth (NG) of materials technology and advanced growth (AG). The circled values highlight predictions that exceed expected normal technology growth capability by 1990. It is seen that advanced technology growth is expected to satisfy the requirements for the worse-case mission.

An evaluation of the impact on total TPS weight for up to a 50% increase in heat load over that resulting from GEO return has been made for the shaped, symmetric, and ballute brakes. This evaluation is depicted in figure 5.7-1. For comparison, the percentage increase due to planetary and lunar return are shown. It is seen that the lunar return results in a TPS weight increase of between 60 and 110 lbm, depending on the brake concept used. Figure 5.7-2 illustrates, for the ballute concept, the change in TPS thicknesses dictated by a 50% increase in heat load over GEO return. It is seen that the changes are small.

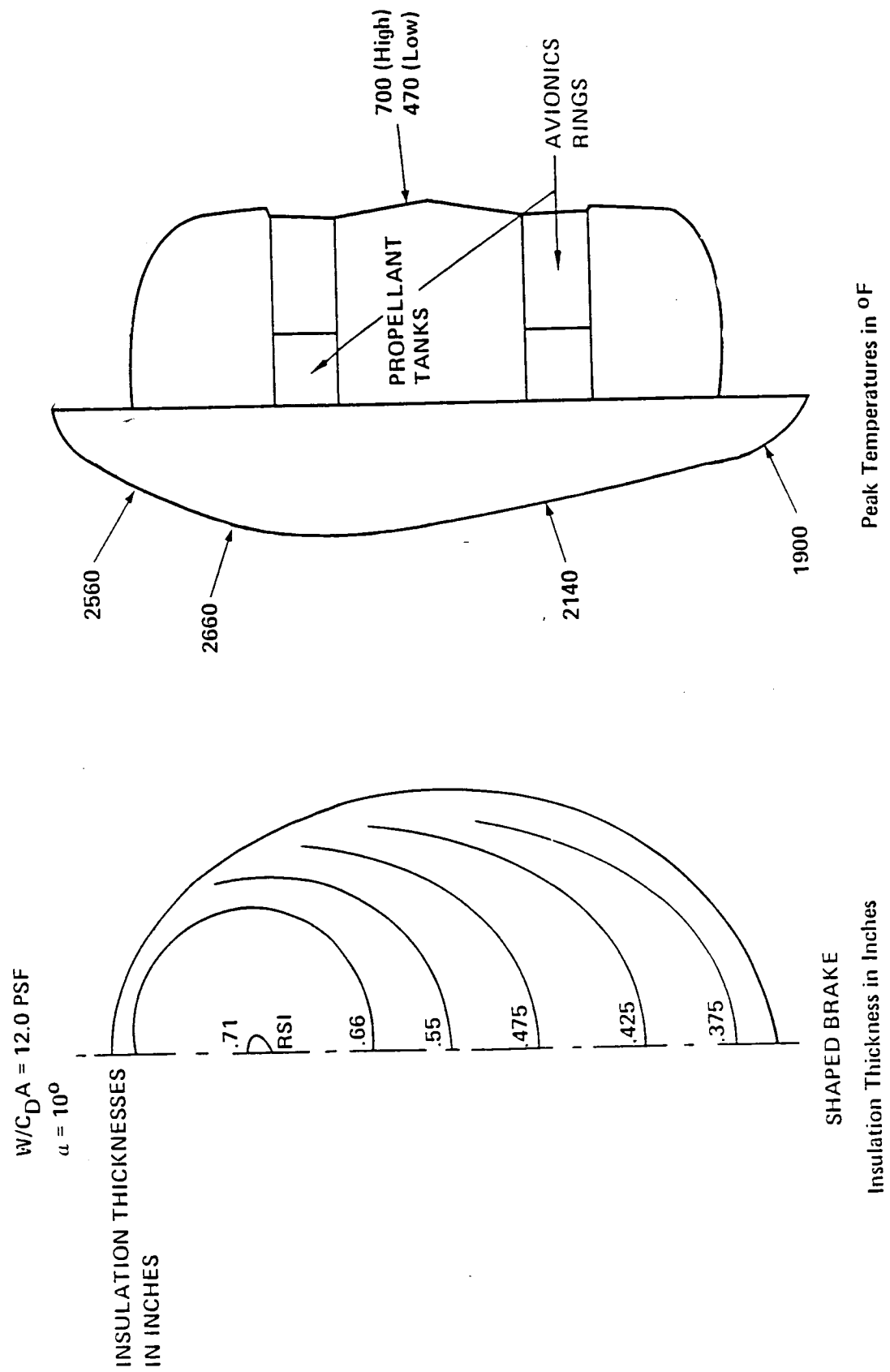


Figure 5.6-6 Shaped Brake Peak Temperatures and Insulation Requirements

Table 5.7-1 Mission Impact on Thermal Environment

HEATING RATES (BTU/FT ² - SEC)							
FSI				RSI			
CONCEPT	MISSION	PREDICTED	MATERIAL LIMITS		PREDICTED	MATERIAL LIMITS	
			NG	AG		NG	AG
BALLUTE BRAKE	GEO	28	34*	50	41	50	94
	LUNAR	(43)			(63)		
	PLANETARY	(40)			(58)		
LIFTING BRAKE	GEO	30	30		36		
	LUNAR	(46)			(55)		
	PLANETARY	(43)			(51)		
SHAPED BRAKE	GEO	N/A			36		
	LUNAR				(55)		
	PLANETARY				(51)		

* SINGLE USAGE

○ CIRCLED VALUES EXCEED NORMAL GROWTH MATERIAL LIMITS

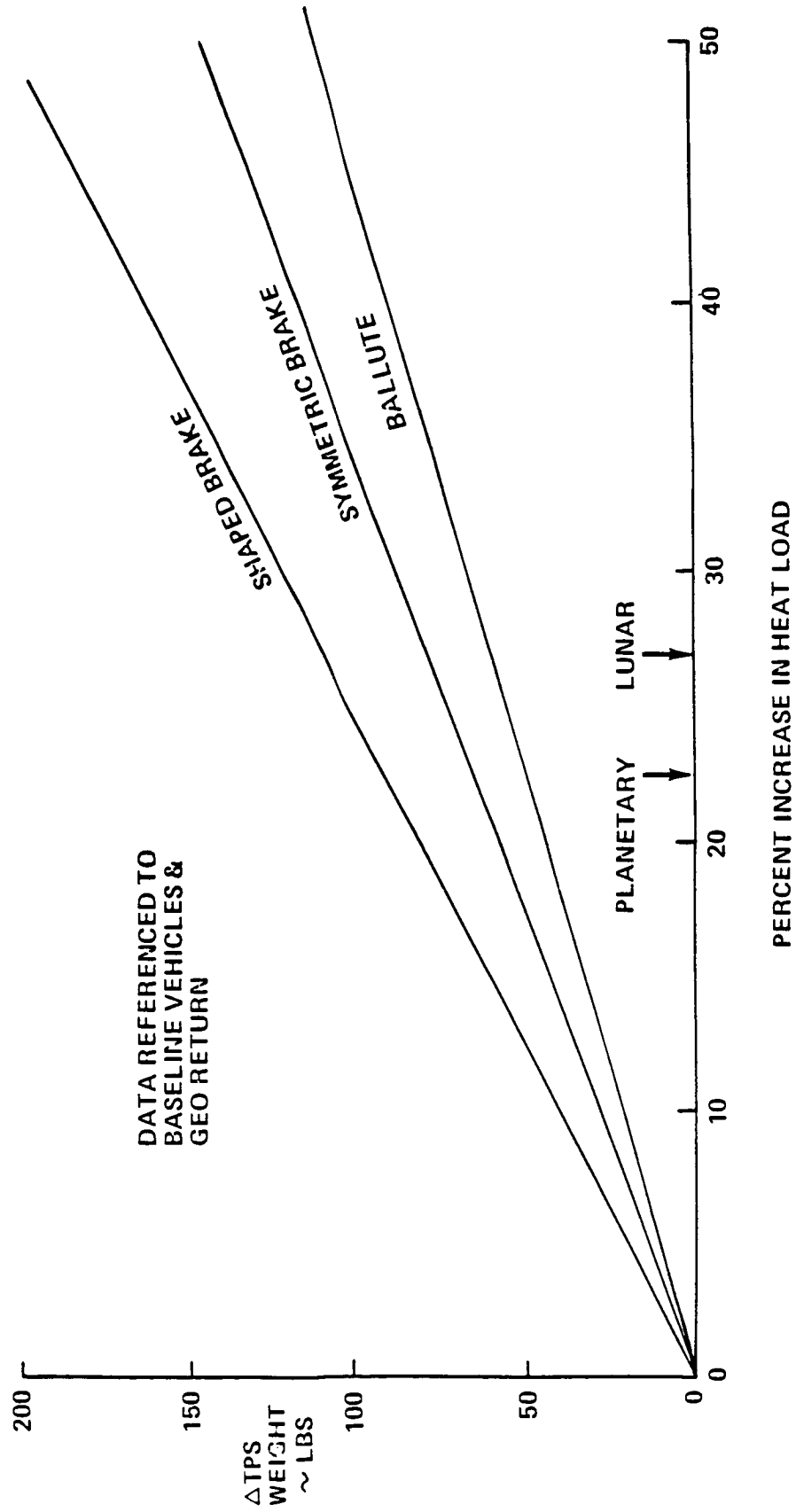
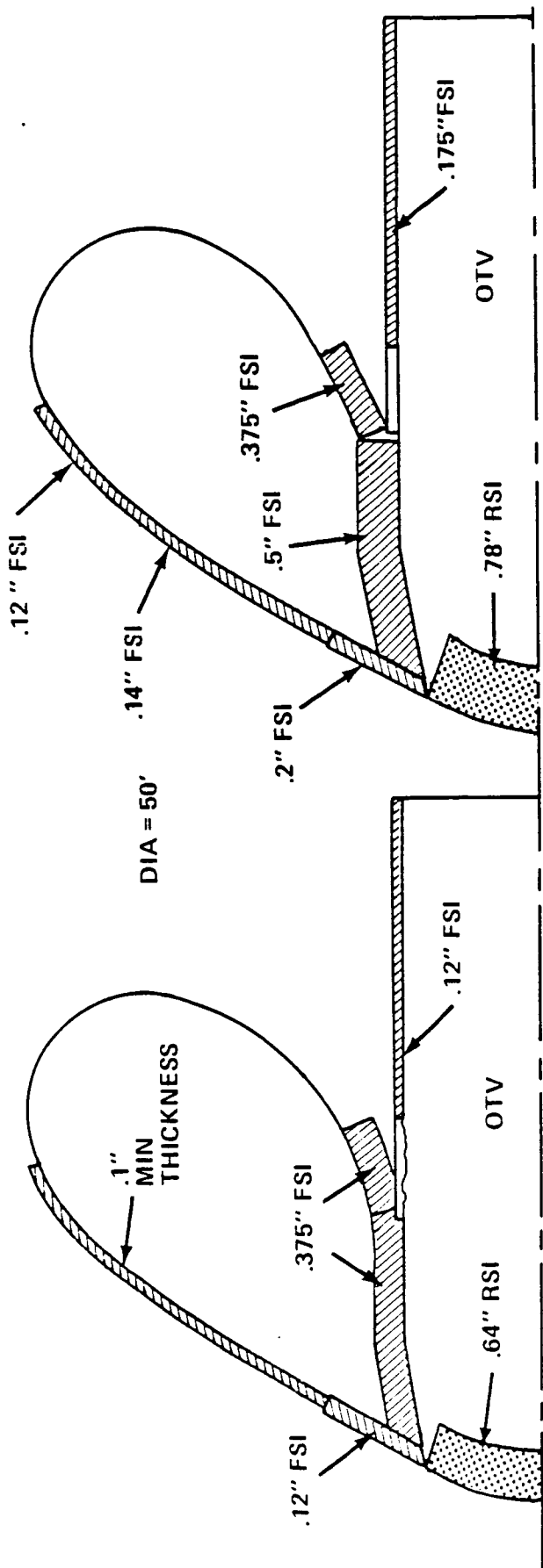


Figure 5.7-1 Sensitivity of TPS Weight to Heat Load

OTV-1170



● 1.5 TIMES BASELINE HTG

FSI WEIGHT (LBM)	961
RSI WEIGHT (LBM)	110
TOTAL INSULATION WT	1071 LBM

$\Delta = 105 \text{ LBM}$

● BASELINE SB BALLUTE HTG

FSI WEIGHT (LBM)	869
RSI WEIGHT (LBM)	97
TOTAL INSULATION WT	966 LBM

Figure 5.7-2 Impact of Aero Heating on Ballute Insulation Requirements

5.7.2 Aerothermal Uncertainties

The approach used to determine the aerothermal environment was to use conventional boundary layer methods to establish nominal heat transfer distributions, and then to apply appropriate factors to account for surface roughness, gas radiation, surface catalysis, rarified flow effects, and atmospheric variations. Specific factors used are given in Table 5.7-2. The net result is that a factor of 1.05 plus a vorticity correction of 8 to 20 percent is applied to all nominal heating rates. The justification and rationale for these factors is discussed in Section 5.3 where the nominal values used are derived. This subsection will discuss the uncertainties associated with catalysis, non-equilibrium radiation, and atmosphere dispersions. Surface roughness variations are considered to be primarily dependent on specific surface details and, hence, are not addressed.

Catalysis. Surface catalysis is affected, to a significant extent, by materials used. Therefore, uncertainties or dispersions from an average can be large. The nominal value used is 0.7 but can vary from 1.0 to as low as 0.4.

Non-Equilibrium Radiation. The uncertainty in establishing a value for non-equilibrium radiation stems from a sparsity of data for very high Mach number reentry and variances in surface absorptivity for various materials and also as a result of response to heating. The maximum non-equilibrium heating is considered to be 36% higher than the nominal and the minimum 22% lower.

Atmosphere Dispersions. The dispersions in atmospheric density will result in peak heating rate excursions of $\pm 10\%$.

Summary. Table 5.7-3 shows a compilation of the predicted heating rates with the high and low extremes for the three aerobrake concepts for both flexible and rigid surface insulations. Limits for these materials, assuming normal technology growth (NG) and accelerated technology growth (AG) to 1990, are shown. The circled values represent requirements that exceed normal 1990 technology growth projections. The shaped brake uses only rigid insulation so no FSI data are shown. Note that the lifting and shaped brake require the least technology growth for the RSI while the ballute is somewhat less demanding than the lifting brake for the FSI.

Table 5.7-2 Heating Factors for Design Environments

ADJUSTMENT FOR	FACTOR q/q_{NOM}
SURFACE CATALYSIS	0.7
NON-EQUIL RADIATION	1.2
ATMOSPHERIC VARIATIONS	1.13
SURFACE ROUGHNESS	1.1
VORTICITY	f(ALTITUDE, NOSE RADIUS)

Table 5.7-3 Impact of Thermal Issues on Environment

1. HEATING SENSITIVITY		HEATING RATES (BTU/FT ² -SEC)									
		FSI					RSI				
		PREDICTED			MATERIAL LIMITS		PREDICTED			MATERIAL LIMITS	
		HI	NOM	LO	NG	AG	HI	NOM	LO	NG	AG
BALLUTE BRAKE	N. E. RADIATION	(38)	28	23	34*	50	(55)	41	34	50	90
	SURFACE CATALYSIS	(40)		16			(59)		23		
	ATMOS. DENSITY	31		25			45		37		
LIFTING BRAKE	N.E. RADIATION	(40)	30	25	30		48	36	30		
	SURFACE CATALYSIS	(43)		17			(51)		21		
	ATMOS. DENSITY	(33)		27			39		32		
SHAPED BRAKE	N.E. RADIATION						48	36	30		
	SURFACE CATALYSIS			N/A			(51)		21		
	ATMOS. DENSITY						39		32		
		• POTENTIAL IMPACT • INCREASED TPS WEIGHT • REDUCED TPS LIFE • HIGHER RISK					• POSSIBLE FIXES • RECONFIGURE • REDUCE W/C _D A • ACCELERATED GROWTH TPS				

*SINGLE USAGE

○ CIRCLED VALUES EXCEED NORMAL GROWTH MATERIAL LIMITS

5.8 SUMMARY COMPARISONS

A summary of the thermal environments to which each OTV concept will be subjected are shown in tables 5.8-1 and 5.8-2 for space based and ground based vehicles, respectively. Reference heating rates range from 103 to 131 BTU/ft²-sec. In all cases the maximum heating rate predicted for the FSI surfaces exceed the capability of the AFRSI blankets, but TABI with silicon carbide external fabric, which is currently undergoing thermal tests, is expected to provide the needed capability. FRCI-20-12, which is employed on space shuttle orbiters starting with "Discovery" appears to be adequate as an RSI system for the lifting and shaped brake, but an increase in maximum heating rate capability of roughly 10 percent is needed for the ballute configurations. Development programs are underway that are expected to provide the required RSI capability prior to 1990.

Advantages and disadvantages of each ballute OTV concept, with regard to thermal protection, are tabulated in table 5.8-3. The ballute and associated TPS is considered expendable for all of the ballute concepts. The most conservative, and least risk, ballute design is the 600 degree backwall case without engine drag modulation. A major concern regarding this concept is the effectiveness of controlling the drag, which relies on varying the ratio of internal to ambient pressure to achieve shape changes. It should be noted, however, that the feasibility of this concept does not rest on turndown effectiveness, since trajectory errors not corrected aerodynamically can be corrected propulsively, but with a weight penalty (see section 6).

Increasing the ballute temperature to 1500 degrees F significantly reduces insulation requirements. Risks associated with this concept are considered to be slightly higher than for the 600 degree F Kevlar/Viton ballute, although Nextel AB-312 fabrics have been tested to temperatures over 2000 degrees F, and CS105 sealant has been tested to 1500 degrees F (reference 28).

The engine modulated ballute offers the potential for the minimum weight system, and also eliminates the need for turndown through ballute shape change and nozzle cover doors. However, this system is the least understood and, consequently, most risky of the ballute OTV concepts. The greatest concerns are in regard to interactions between the exhaust and ambient flows, with the potential for unsteady flow resulting in non-uniform cooling and ballute flutter. We feel that potential advantages of this system justify additional research.

A similar assessment of the lifting and shaped brake is given in table 5.8-4. The lifting brake exhibits many of the same concerns as the ballute concepts, except that the drag modulation problems are eliminated. The concern with debris damage is that a

Table 5.8-1 Aerothermal/TPS Summary

SPACE BASED

CONCEPT	DIAMETER (FT)	REENTRY WEIGHT (LBS)	W/C _D A (PSF)	\dot{q}_0 (BTU/ FT ² -SEC)	Q ₀ (BTU/FT ²)	\dot{q}_{MAX} (BTU/ FT ² -SEC)		TPS WEIGHT (LBS)	
						FSI	RSI	FSI	RSI
600°F BALLUTE	50.1	21,000	10.04	117	15,200	28.8	42.5	2238	123
600°F BALLUTE WITH ENGINE MOD	43.4	19,960	12.70	131	19,200	21.0	N/A	1784	0
1500°F BALLUTE	50.1	19,600	9.37	114	14,700	28.2	41.1	918	122
1500°F BALLUTE WITH ENGINE MOD	42.5	19,200	12.76	131	19,200	21.0	N/A	845	0
LIFTING BRAKE	42.5	20,980	10.3	119	15,500	30.0	35.7	1235	222
SHAPED BRAKE	44 x 36	21,400	11.6	126	16,700	N/A	36.0	0	1576

TPS TYPE	TPS LIFE (MISSIONS)	CURRENT TECHNOLOGY	1990 TECHNOLOGY	
			NORMAL GROWTH	ACCELERATED GROWTH
FLEXIBLE SURFACE INSULATION (FSI)	5	4-6 (AFRSI)	30	50
	1	6-8	35	50
RIGID SURFACE INSULATION (RSI)	20	38 (FRCI)	50	90
HEATING RATE (BTU/FT ² -SEC)				

Table 5.8-2 Aerothermal/TPS Summary

GROUND BASED 1500°F BALLUTE

MISSION	DIAMETER (FT)	REENTRY WEIGHT (LBS)	W/CDA (PSF)	(BTU/ FT ² SEC) \dot{q}_o	Q _o (BTU/FT ²)	\dot{q} MAX (BTU FT ² SEC)		TPS WEIGHT (LBS)	
						FSI	RSI	FSI	RSI
UNMANNED MULTI MANIFEST	33	10,926	12.05	128	16,700	31.5	45.8	626	125
UNMANNED 20K PAYLOAD	40	13,900	10.43	103	15,550	29.3	42.6	722	125
MANNED 75K RETURN	66	23,934	6.60	119	13,050	25.4	36.8	1244	125

TPS TYPE	TPS LIFE (MISSIONS)	HEATING RATE (BTU/FT ² - SEC)		
		CURRENT TECHNOLOGY	1990 TECHNOLOGY	
			NORMAL GROWTH	ACCELERATED GROWTH
FLEXIBLE SURFACE INSULATION (FSI)	15	4-6 (AFRSI)	30	50
	1	6-8	35	50
RIGID SURFACE INSULATION (RSI)	20	38 (FRCI)	50	90

OTV 1732

Table 5.8-3 Ballute Concept Assessment

CONCEPT	ADVANTAGES	DISADVANTAGES AND CONCERNS
<ul style="list-style-type: none"> • 600 DEG BALLUTE NO JET ENGINE MODULATED 	<ul style="list-style-type: none"> • LEAST RISK BALLUTE CONCEPT 	<ul style="list-style-type: none"> • REQUIRES TURNDOWN • BALLUTE/TPS MUST BE REPLACED AFTER EACH MISSION • NOZZLE DOOR ACTUATION AND SEALS
<ul style="list-style-type: none"> • 1500 DEG BALLUTE NO ENGINE MOD 	<ul style="list-style-type: none"> • LOW WEIGHT 	<ul style="list-style-type: none"> • SAME AS ABOVE
<ul style="list-style-type: none"> • ENGINE MODULATED BALLUTE (600 & 1500 DEG) 	<ul style="list-style-type: none"> • NO TURNDOWN REQUIRED • NO RSI REQUIRED • NO NOZZLE DOORS • SMALLER DIAMETER • MINIMAL LOBING 	<ul style="list-style-type: none"> • POTENTIAL FOR UNSTEADY FLOW • NON-UNIFORM COOLING • FLUTTER • COOLING MAY BE MARGINAL AT THI • LARGE UNCERTAINTIES IN HEATING PREDICTIONS • ENGINE OUT PERFORMANCE NOT KNOWN • AERO STABILITY • COOLING EFFECTIVENESS

OTV 558

Table 5.8-4 Lifting and Shaped Concept Assessment

CONCEPT	ADVANTAGES	DISADVANTAGES AND CONCERNS
600 DEG LIFTING BRAKE	<ul style="list-style-type: none"> • NO DRAG MODULATION REQUIRED • 5 REUSES FOR BRAKE/TPS 	<ul style="list-style-type: none"> • BRAKE/TPS REPLACEMENT ON SPACE BASED VEHICLE • WAKE HEATING • NOZZLE DOOR ACTUATION AND SEALS • DEBRIS DAMAGE TO FSI
1500 DEG LIFTING BRAKE	<ul style="list-style-type: none"> • SMALL REDUCTION IN INSULATION WEIGHT 	<ul style="list-style-type: none"> • SAME AS ABOVE PLUS • RIB INSULATION REQUIRED • NO REUSE OF BRAKE/TPS
SHAPED BRAKE	<ul style="list-style-type: none"> • NO DRAG MODULATION REQUIRED • 20 REUSES 	<ul style="list-style-type: none"> • TILE REPLACEMENT

hole in the FSI would be very difficult to detect, and flow of the hot boundary layer gas through a hole could be catastrophic. The disadvantage of the 1500 degree F. lifting brake is that the savings in insulation weight is less than for the ballute, and the brake and TPS will probably have to be replaced after each flight. The replacement of the brake fabric is deemed to be much more difficult than replacing a ballute (see subsection 2.2.2). The replacement requirement is the result of the CS105 sealant, which we feel is required to prevent the hot boundary layer gas from penetrating into the FSI.

Our analyses indicate that space shuttle TPS technology is adequate for the shaped brake. Consequently, from a thermal standpoint, the shaped brake is deemed the least risk approach of all of the concepts studied. A potential disadvantage of a space based system is that, if tile damage should occur, replacement in orbit could be difficult. The same concern applies to RSI surfaces on the ballute and lifting brakes, but the risk is less because of the smaller areas involved.

5.9 AEROTHERMAL ISSUES

Three key aerothermal issues are identified in table 5.9-1, the first two of which are common to all of OTV concepts studied. The discrepancies in predicted gas radiation heating rates are unacceptable, and resolving this issue is considered a top priority technology item.

Although heating levels in base regions are orders of magnitude less than on windward surfaces, a more accurate determination of the environment in these regions is required to optimize packaging arrangement, define insulation requirements, and establish avionics thermal control requirements.

The engine modulation (jet counterflow) method for modulating drag and actively cooling the ballute offered a small (1%) advantage in performance over an active turndown approach and may merit further investigation.

The effects of mission variations and aerothermal uncertainties also has been examined. Table 5.9-2 summarizes the effects of these factors on TPS weight for the three aerobrake types studied. The ballute is the least affected while the shaped brake is the most affected. These magnitudes and brake-to-brake differences are small but, at a factor of 8:1 for lift-off weight to propellant to GEO, an 80 lbm TPS difference is, in reality, a 640 lbm launch penalty. Aerothermal uncertainties are more significant than mission differences and, since the mission to be flown is an absolute, offers the most opportunity for resolution and potential weight reduction.

Table 5.9-1 Key Aerothermal Issues

ISSUE	APPLICABLE TO	CURRENT ASSESSMENT	PROPOSED SOLUTION
NON-EQUILIBRIUM GAS RADIATION	ALL	VERY LARGE UNCERTAINTIES OTV PREDICTIONS	<ul style="list-style-type: none"> • CONTINUE ANALYSES AND GROUND TEST PROGRAM • AFE
BASE HEATING	ALL	LARGE UNCERTAINTIES IN BOTH WAKE IMPINGEMENT AND RECIRCULATION HEATING TPS MAY OR MAY NOT BE NEEDED IN BASE REGION	<ul style="list-style-type: none"> • WIND TUNNEL TESTS • ANALYSES USING SOA COMPUTER CODES • AFE
POSSIBLE UNSTEADY FLOW DUE TO INTER-ACTION BETWEEN ENGINE EXHAUST AND AMBIENT FLOW	ENGINE MODULATED BALLUTE	PREVIOUS TESTS INDICATE THAT DISTURBANCE FREQUENCIES MAY BE HIGH ENOUGH TO AVOID STABILITY, FLUTTER, AND HEATING PROBLEMS	<ul style="list-style-type: none"> • ADDITIONAL WIND TUNNEL TESTING • 2 NOZZLES • SIMULATE AREA AND PRESSURE RATIOS

Table 5.9-2 TPS Weight Sensitivities

CONCEPT	SENSITIVITY TO MISSION		SENSITIVITY TO AEROTHERMAL ISSUES	
	MISSION	Δ TPS WGT (LBS)	UNCERTAINTY SOURCE	Δ TPS WGT (LBS)
BALLUTE BRAKE	GEO	0	N.E. RADIATION	75
	LUNAR	60	SURFACE CATALYSIS	97
	PLANETARY	50	ATMOS. DENSITY	18
SYMMETRIC BRAKE	GEO	0	N.E. RADIATION	102
	LUNAR	83	SURFACE CATALYSIS	125
	PLANETARY	74	ATMOS. DENSITY	28
SHAPED BRAKE	GEO	0	N.E. RADIATION	132
	LUNAR	118	SURFACE CATALYSIS	175
	PLANETARY	97	ATMOS. DENSITY	41

5.10 THERMAL CONTROL

Thermal control of an OTV's fuel cells, RCS, cryo propellant, and avionics is essentially the same for each of the concepts investigated. A description of the approach used in each area follows.

Thermal control of the fuel cells is provided by an active thermal conditioning system consisting of a Freon 11 fluid loop with a radiator, located on the body shell exterior, and the associated pumps, valves, and control elements. The passive thermal control techniques include insulation blankets, thermal control coatings, and selected radiative surfaces. The thickness of the aluminum used for the avionics ring assembly is controlled to provide for proper heat flow from internally mounted components and its exterior surface is covered with flexible optical solar reflector (FOSR) to provide the radiative surface. Electrical heaters are provided for RCS components and avionics equipment as required. The LH₂ and LO₂ tanks are insulated using MLI. The MLI consists of layers of doubly aluminized kapton with a dacron net spacer. Thirty-four layers of MLI are used on the LH₂ tank and fifty layers on the LO₂ tank. The selected MLI layers result from the data shown in figure 5.10-1 which shows the minimum combined weight for the MLI and propellant boil-off. A mission time of 96 hours was used in the selection process. The selected MLI approach results in an average propellant boil-off rate of 2.9 lbs/hr for GEO delivery missions. The MLI wrapped tanks are enclosed within purge barriers which are purged with dry gas (helium for the LH₂ tank and nitrogen for the LO₂ tank) prior to launch.

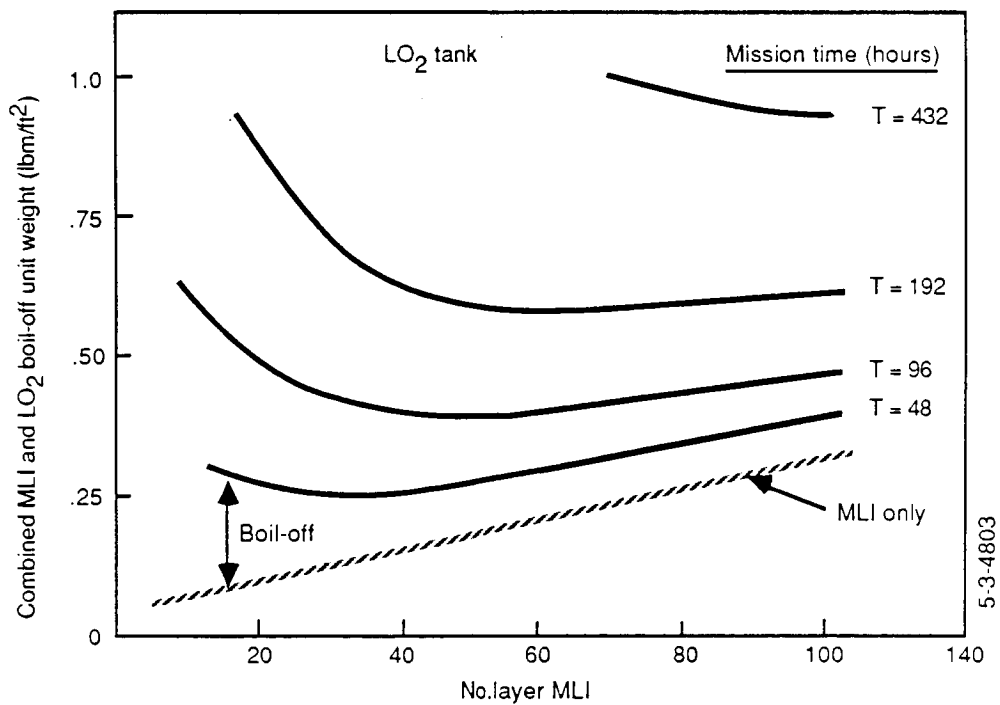
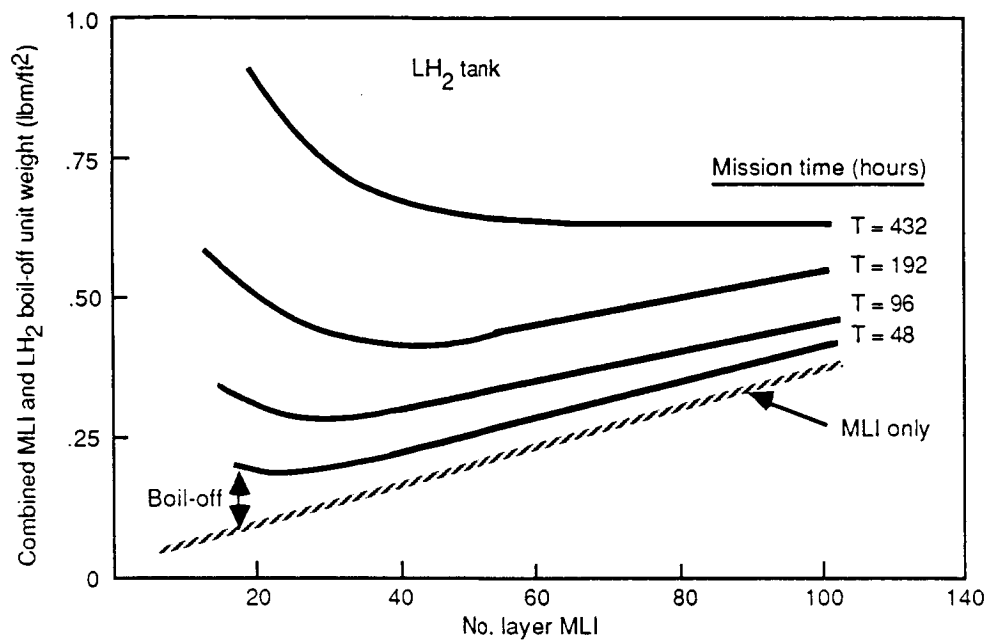


Figure 5.10-1 MLI for SB OTV Cryo Tanks

6.0 GUIDANCE AND NAVIGATION

The guidance and navigation (G&N) analysis was focused on those aspects dealing with an OTV using aeroassist for return back into low earth orbit. One goal was to develop a generic guidance algorithm which is applicable to all aeroassist concepts. This algorithm was then used to evaluate the impact of atmospheric dispersions on the guidance performance for the different vehicle designs. The output from the guidance analyses is an assessment of the propulsive Δ velocity allowances to be carried by each aeroassist vehicle concept to correct for guidance errors after the aeroassist maneuver.

6.1 AEROASSIST GUIDANCE AND NAVIGATION CONSIDERATIONS

This paragraph addresses the systems to be used to support the transfer from GEO to reentry and the resulting errors, the aeromaneuver error sources, and the guidance algorithm used during the aeromaneuver.

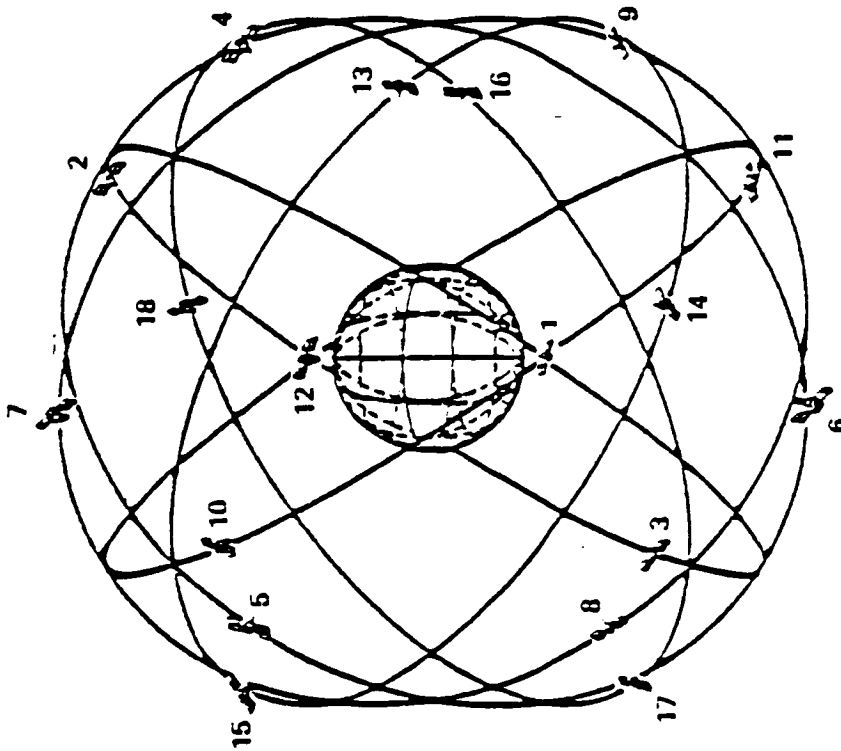
6.1.1 GEO to Atmosphere Entry Analysis

A precise navigation system is required to meet the accurate atmospheric reentry requirements of the OTV mission. Accurate position, velocity, body attitude, and acceleration measurements are necessary to effect the transfer. Navigation components needed may include a Navstar global position system (GPS) navigator (ref. 39), a star tracker, an accurate rotational inertial reference unit (IRU) and orbit propagator, and an accurate clock.

The Navstar GPS will provide the autonomous and accurate position and velocity measurements desired. Navstar GPS is a satellite-based navigation system that provides accurate three-dimensional position and velocity information to users on or near Earth. The system employs 18 satellites in 55-deg, inclined, circular, 12-hr orbits. Figure 6.1.1-1 shows the GPS configuration.

The near-Earth user measures pseudo-range and pseudo-range rate values using the navigation signal from each of four GPS satellites, where "pseudo" is the true value plus an offset due to the user's clock error. Each signal contains ephemeris data and system timing information for that GPS satellite, allowing the user to estimate its three-dimensional position and velocity. For the near-Earth OTV burn, the user can expect one standard deviation position error of 15 to 50 ft (ref. 40).

The geosynchronous user also measures pseudo-range and pseudo-range rate to one or two or, on rare occasions, three GPS satellites. Figure 6.1.1-2 shows the expected



- 18 SATELLITES IN 12 HOUR CIRCULAR ORBIT
- GPS SATELLITES ARE VISIBLE TO GEO USER WHEN ON OPPOSITE SIDE OF, BUT NOT BEHIND, THE EARTH
- GPS SUPPLIES RANGE AND RANGE RATE INFORMATION

Figure 6.1.1-1. NAVSTAR/GLOBAL Positioning System

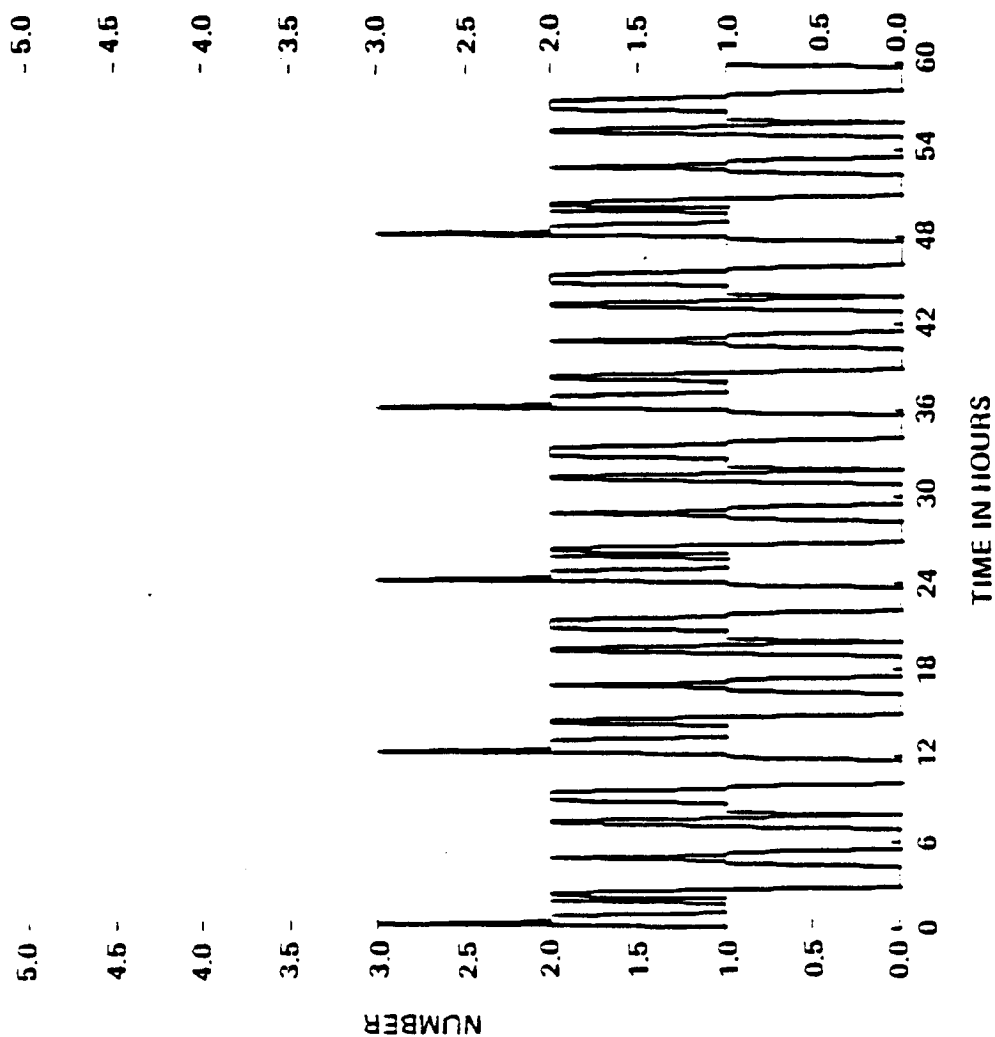


Figure 6.1.1-2. Number of GPS Satellites in View From GEO

number of GPS satellites in view. User measurements can be made sequentially with a simple 5-or 10-turn helical antenna as the GPS satellites become visible. Orbital dynamics, GPS signals, and the user's clock information must be combined to accurately navigate the geosynchronous satellite. Figure 6.1.1-3 shows the steady state estimated 3-sigma spacecraft position error using this system. Figure 6.1.1-4 shows the same data using a highly accurate user clock. The tables show that the OTV user can expect worst-case root mean square (RMS) position errors on the order of 300 ft prior to the geosynchronous deorbit burn.

After the deorbit burn, a period of time is required to acquire GPS satellite observations and improve the user's position and velocity estimate. In some cases this process may require waiting until the user is below the GPS constellation (10,000 nmi), about 1 hr prior to atmospheric reentry. When four GPS satellites can be acquired at one time, an accurate position and velocity fix can be computed in about 5 min. When the new GPS fix is computed, midcourse corrections can be made if necessary.

The accuracy of the geosynchronous deorbit burn is also related to the navigation estimate of the vehicle attitude and the accumulated ΔV during the burn. Prior to the deorbit burn, a star tracker update will reduce the navigation attitude errors and hence improve the burn direction control. Because the postburn GPS update will take some time to acquire, the IRU must accumulate acceleration for ΔV control and the orbit propagator must provide the position, velocity, and attitude estimate. Table 6.1.1-1 shows expected errors of presently available sensors. Table 6.1.1-2 shows the effect of those errors on the OTV burn control.

Experience with the IUS has shown that guidance and navigation errors are nearly independent. Independent error sources can be combined with root square sum (RSS) to obtain a total system accuracy estimate. Table 6.1.1-3 shows the guidance and navigation errors and the combination of those errors into altitude, velocity, flightpath angle, bank angle, and angle of attack to be quite small. The fuel used to remove the initial dispersion is also shown. The combined reentry errors of the described OTV avionics system are quite small.

6.1.2 Aeromaneuver Error Sources

The principal source of error during the aeromaneuver trajectory is due to the unpredictable density variations in the thermosphere. Data from STS flights indicate that there are atmospheric dispersions that have not been predicted by existing atmospheric models. More knowledge of the thermosphere will mean expanded mission

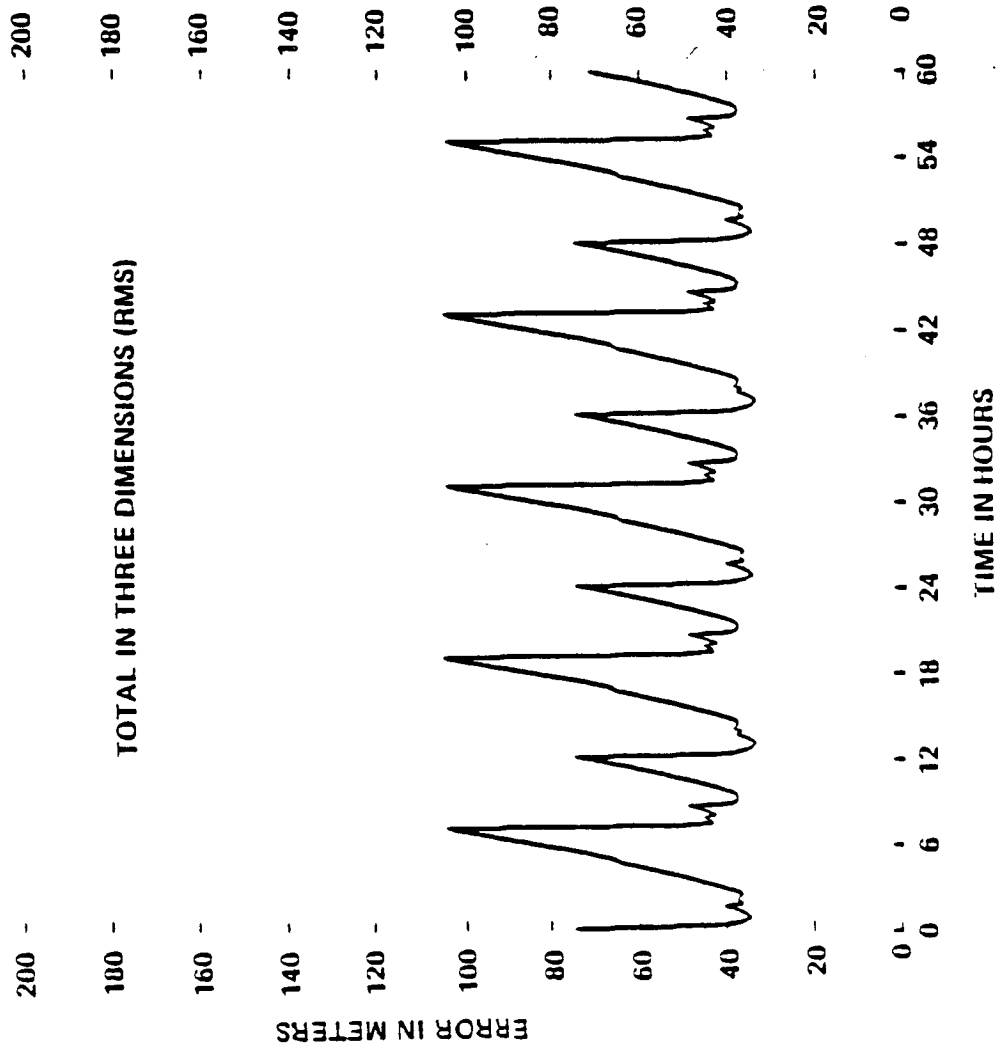


Figure 6.1.1-3. Spacecraft Position Error in GEO

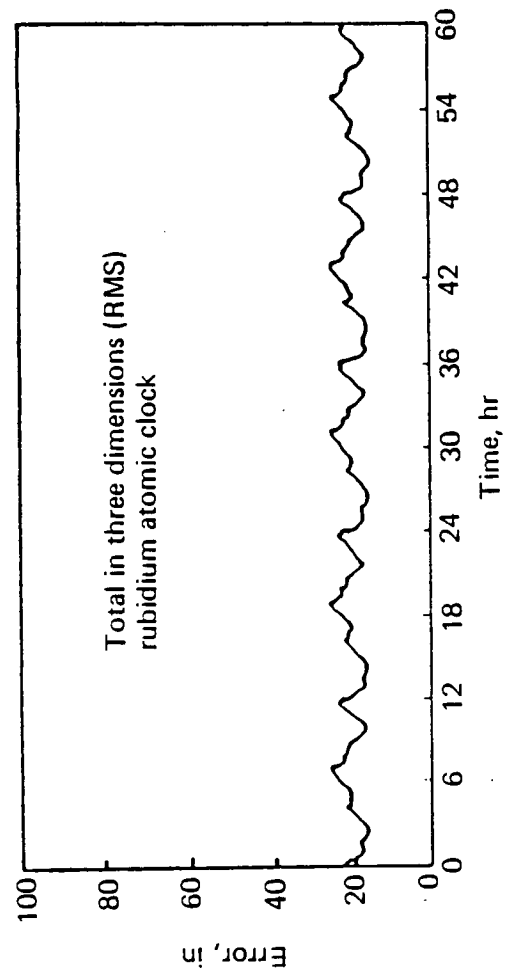


Figure 6.1.1-4. Spacecraft Position Error

Table 6.1.1-1. Inertial Sensor and RIMU Attitude Propagation AccuracyAccelerometer Accuracy

Bias	(1-sigma)	27.3 mg
	(3-sigma)	0.00264 ft/s ²
Scale Factor	(1-sigma)	17.2 ppm
	(3-sigma)	0.00088 ft/s ²
RSS (bias and scale factor)	(3-sigma)	0.00278 ft/s ²

Star Scanner Accuracy (3-Sigma)

2.0 arc min per axis capability
 4.8 arc min per axis IUS specification

The IUS specification is conservative, 2.0 arc min per axis is attainable; 2.0 arc min = 0.033 deg.

Attitude Propagation, GEO to LEO (3-sigma)

0.31-deg RM per axis

Table 6.1.1-2. Effect of Inertial Sensor and Navigation Errors on AOTV GEO and LEO Burn AccuracyGeosynchronous Deorbit Burn (330-Sec Nominal Duration)

Accelerometer Error	0.91 ft/s (3-sigma)
Vehicle Attitude Error	4.6 ft/s (3-sigma)

LEO Burn (10-Sec Nominal Duration)

Accelerometer Error	0.028 ft/s (3-sigma)
Vehicle Attitude Error	0.89 ft/s (3-sigma)

Table 6.1.1-3. Re-Entry Error Analysis

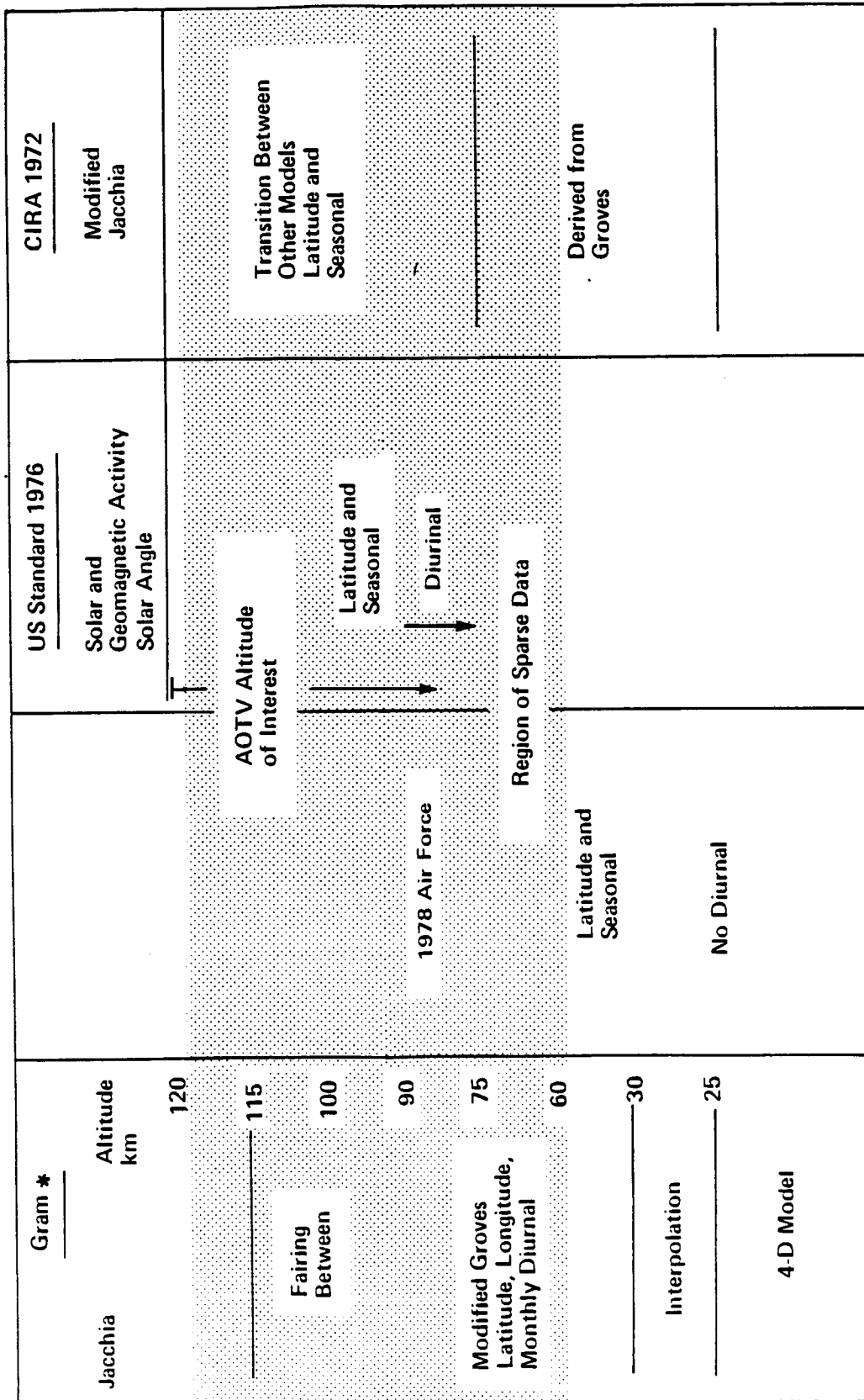
ERROR SOURCES	3 σ ERROR	3 σ DISPERSION DURING TRAJECTORY
ATMOSPHERIC UNCERTAINTY (ESTIMATED)	DENSITY = 20%	$\Delta = 20\%$
NAVIGATION ACCURACY (WITH GPS)	POSITION = 60 FT VELOCITY = 0.2 FPS ENTRY ANGLE = 0.0004 DEG	$\Delta H = 120 \text{ FT}$ $\Delta V = 0.6 \text{ FPS}$ $\Delta Y = 0.00184 \text{ DEG}$
GUIDANCE ACCURACY (GAMMA GUIDANCE)	POSITION = 104 FT VELOCITY = 0.57 FPS ENTRY ANGLE = 0.0018 DEG	
INERTIAL SENSORS (UPDATED AT GEO)	0.30 DEG IN PITCH, ROLL AND YAW	$\Delta \alpha = 0.31 \text{ DEG}$ $\Delta \beta = 0.31 \text{ DEG}$
AERODYNAMIC CHARACTERISTICS* (ESTIMATED FROM STS DATA)	$C_A = 5\%$ $C_N = 3\%$ $C_M = \text{N/A}$ 500 LB	$\Delta C_D = 3\%$ $\Delta L/D = 3\%$
PROPELLANT CONSUMPTION		$\Delta W = 3\%$

*VISCIOUS INTERACTION EFFECTS INCLUDED IN NOMINAL TRAJECTORY
(100% ERROR IN C_A POSSIBLE IF VISCIOUS EFFECTS IGNORED)

THE DOMINANT SOURCE OF ERROR DURING RE-ENTRY
APPEARS TO BE ATMOSPHERIC DENSITY DISPERSION

capability and fewer design restrictions. A survey of existing atmosphere models identified deficiencies and methods of improving the models.

The four atmosphere models surveyed were GRAM, Global Reference Model (ref. 41); Air Force Reference Atmosphere (ref. 42); U.S. Standard Atmosphere 1976; and CIRA 1972, COSPAR International Reference Atmosphere 1972 (ref. 43). Of the four models GRAM is the most appropriate for OTV application. Although CIRA was not considered, J.T. Findlay et.al., (ref. 44) share the conclusion that GRAM is the best atmosphere model available for OTV. The Air Force 1978 model was rejected because it is limited to 90 km which is below the effective atmospheric limit for OTV. Although the U.S. Standard 1976 atmosphere covers the entire altitude range of interest it was rejected because it is known to have deficiencies above 70 km. CIRA was rejected because it is similar to GRAM, but does not have as many variables modeled. Figure 6.1.2-1 summarizes the differences between the models.



*Models Winds and Random Parturbations

Figure 6.1.2-1 Candidate Atmosphere Models for OTV

OTV 1755

The advantages of using GRAM for the OTV reference atmosphere model are that it includes more of the predictable atmospheric variables than any of the other models and that it includes wind and perturbation models. GRAM includes solar and geomagnetic activity, diurnal, semi-annual, seasonal, latitudinal, and longitudinal variation. Of particular interest is the random atmosphere model which will produce a perturbed atmosphere with realistic time and spatial correlations. Some of the drawbacks to the GRAM model that are also shared with other models are that the OTV region of interest overlaps the region of sparse data, that the southern hemisphere is modeled as a six month displacement of the northern hemisphere, and that the overall data base is old. Another problem with GRAM is that between 90 and 115 km the data is generated by a fairing technique between the Jacchia and Groves models. This smoothing is achieved at the cost of accuracy. Discussions with C. G. Justus, one of the authors of GRAM, have provided ideas for improving GRAM for OTV. He suggested that the Groves model is more reliable in the region of overlap than the Jacchia, and that it would be a relatively straight forward task to update the mean data base as well as the statistical data base as more data becomes available.

Although the CIRA 1972 model does not have any advantages compared to GRAM, discussions with K.S.W. Champion at the Air Force Geophysics Laboratory revealed that the model is being updated to include more data and more variations. In particular the new version will have longitudinal variations and will use southern and northern hemisphere data. The first phase of the revision to cover the 18-80 km range will be available in late 1985. The second phase covering 80-120 km will be available late in 1986 or early 1987. It is possible that the revised CIRA data could be incorporated into GRAM. More work, however, would still have to be done to update the GRAM statistical base.

By reviewing the four atmosphere models and the STS measured density profiles it has been shown that a more accurate model of the mean atmosphere, as well as better temporal and spatial correlations of the dispersions are needed. As previously mentioned, the work associated with CIRA will provide some update to the mean data base. T. J. Findlay et.al., have been studying STS data to provide an OTV data base. The STS profiles do provide a detailed realistic picture of what a typical atmosphere would be, but the number of flights is limited which makes any statistical analysis difficult. On the other hand, there is a plentiful supply of Robin Sphere data available in the region of interest. In particular, Ascension Island (7°59' S 14°25' W) and Kwajalein (8°44' N 16°44' E). Nick Engler of the University of Dayton Research Institute indicated that there are at least five years and 500 flights worth of Robin Sphere data on tape

ready for processing. He also described the following Robin Sphere experiments that have been performed: every Wednesday at noon for five years; at Barking Sands and Point Magu simultaneously. The primary drawbacks to relying solely on Robin Sphere data are that no wave phenomena can be observed above 70 km and that it is not sufficient for temporal and spatial correlations.

Data from lidar experiments, unlike the Robin Sphere, can be used to show the existence, propagation, and dissipation of gravity waves. Density profiles from lidar soundings at the observatory of Haute Provence (44°N, 6°E, 30-100 km) (ref. 45) have shown systematic wavelike structures. Lidar data can be used to provide temporal and spatial correlations not readily available from other sources. An extensive experimental lidar data base is not available for an immediate update to the models but these experiments do indicate the potential of using lidar.

Another source of error is unpredictable variations in vehicle aerodynamic characteristics caused by errors in angles of attack, bank, or yaw; variations in aerodynamic coefficients; or navigation error sensing of vehicle attitude during the maneuver. As can be seen in Figure 6.1.2-2, the angle of attack is equal to the flight path angle plus the pitch angle, both of which are known very accurately at entry. Hence, the vehicle can always be trimmed to within one-third of a degree of the proper angle-of-attack, bank, or yaw using the inertial measurement accuracy available.

Unexpected variations in vehicle aerodynamic coefficients (C_A , C_M , C_N) are of two types. The first comes from improper extrapolation or analysis of test data and is generally caused by mach number, real gas, or Reynolds number effects. These variations are generally corrected during the flight test phase of vehicle development and cease to be a factor after the vehicle becomes operational. The second type of variation is caused by unexpected variations in atmospheric conditions or changes in vehicle shape (caused by wear, misrigging of controls, etc). This second type of error is of concern here and is estimated to be 3% to 5% of the aerodynamic coefficients based on current STS data. Note that variations in C_M will appear as errors in C_L and C_D because the vehicle will always be trimmed at a constant angle of attack.

6.1.3 Guidance Algorithms

One of the purposes of this study was to address the feasibility of guiding a low L/D OTV through the atmospheric portion of its flight. Guidance during this portion of the trajectory must respond to three primary sources of error. These are errors in knowledge of state of the vehicle at atmospheric entry, uncertainties in the aerodynamic characteristics of the vehicle, and uncertainties in the estimation of

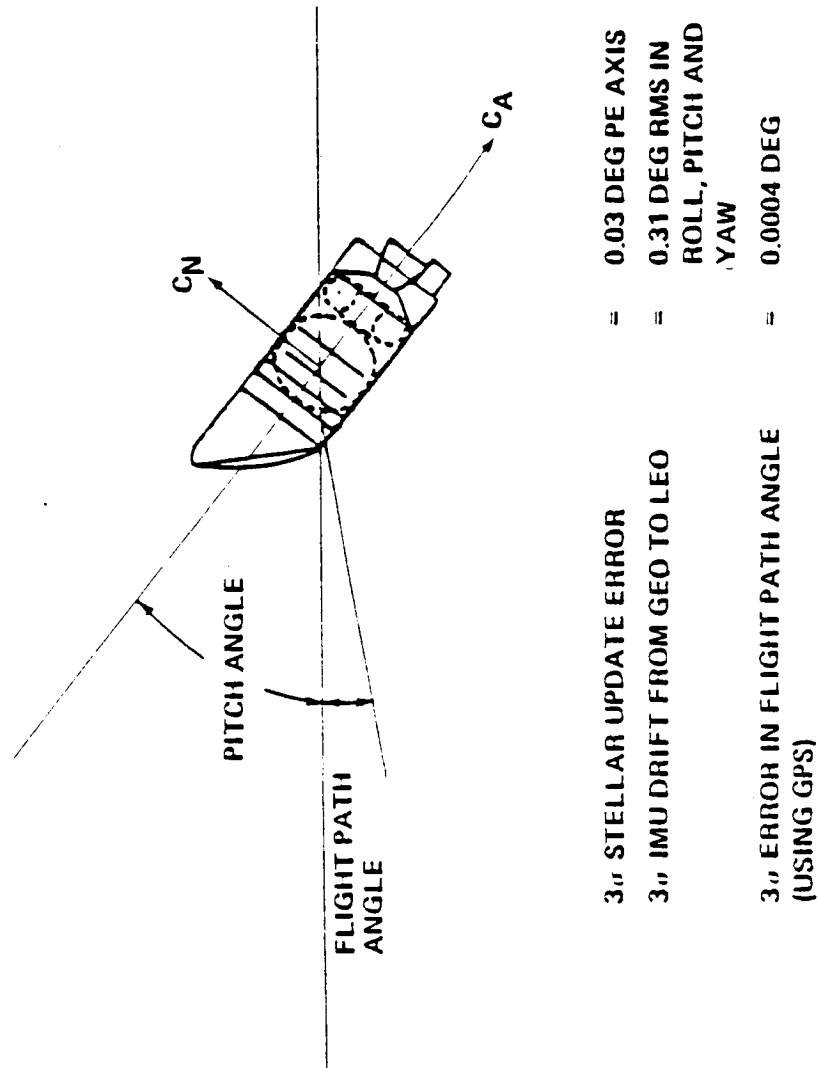


Figure 6.1.2-2. Angle of Attack Accurately Known

atmospheric density. Knowledge of entry-state errors are a result of navigation and guidance errors during the transfer from GEO to atmospheric entry. Uncertainties in the aerodynamic characteristics of the vehicle are the result of inaccurate analytical models and imprecise simulation of the entry environment. The atmospheric density varies spatially, seasonally and diurnally. Errors arise because standard atmospheric models do not address these variations.

The large uncertainties inherent in the environment of the thermosphere and the desire for mission flexibility dictate an adaptive guidance algorithm for the OTV. Guidance algorithms could be developed using the special characteristics of each vehicle concept. However, in consideration of the diversity of concepts and total mission requirements, a generic approach has been taken. The general guidance algorithm being developed is an expansion of Gamma Guidance (ref. 46) used on the Inertial Upper Stage. This approach will require minimal "tuning" and with its general modular structure is readily adaptable to a large variety of vehicle concepts and mission requirements.

For the application to OTV, the equations of motion for the vehicle are shown in figure 6.1.3-1.

The constraint equations, C_i , are targeted orbital parameters at atmospheric exit (e.g. altitude-at-apogee, inclination, etc.). $G(\lambda)$ is a scalar function which may be used for optimal guidance analysis. The general flow of the algorithm is illustrated in Figure 6.1.3-2.

This guidance approach links the development of ground software with that for flight software because the same or similar algorithms can be used for both. It also reduces the magnitude of preflight analysis because no preflight reference trajectory is required. The algorithm responds to large variations in flight conditions because it continually targets for the desired end conditions based on the current state of the vehicle.

The major drawback to this algorithm is that it places heavy demands on the flight computer, but with the advances being made in computer technology, this does not appear to be a serious concern.

6.2 TRADES AND ANALYSES

Four different OTV vehicles have been simulated. Two vehicles use ballutes to control entirely or assist in controlling the drag during the aeromaneuver. One ballute concept is controlled by varying the internal pressure to change the shape for controlling C_{DA} . The other ballute concept uses engine mass flux modulation to modify the flow field for C_D control. The other vehicles are rigid aerodynamic bodies

$$\ddot{\bar{X}} = \frac{d\dot{\bar{X}}}{dt} = -\frac{\mu \bar{X}}{|\bar{X}|^3} + \frac{\bar{L}}{m} + \frac{\bar{D}}{m} = \bar{F}(\bar{X}, \bar{\lambda}) \quad \text{Eq. 1}$$

where

$$\begin{aligned} \bar{X} &= \text{Earth centered inertial position} \\ &= [X, Y, Z]^T \end{aligned}$$

$$\bar{L} = \text{Lift vector}$$

$$\bar{D} = \text{Drag vector}$$

$$m = \text{Mass of vehicle}$$

and

$$\bar{\lambda} = \text{Control vector}$$

The lift and drag vectors are given by:

$$\bar{L} = \frac{1}{2} \rho V_R^2 C_L(\alpha) A \hat{\delta}_L \quad \text{Eq. 2}$$

and

$$\bar{D} = \frac{1}{2} \rho V_R^2 C_D(\alpha) A \hat{\delta}_D \quad \text{Eq. 3}$$

where

$$C_D = \text{Coefficient of drag}$$

$$C_L = \text{Coefficient of lift}$$

$$A = \text{Reference area}$$

$$\rho = \text{Atmospheric density}$$

$$\alpha = \text{Angle of attack}$$

\bar{V}_R is the Earth relative velocity vector given by

$$\bar{V}_R = \dot{\bar{X}} - (\bar{\omega} \times \bar{X}) \quad \text{Eq. 4}$$

where

$$\dot{\bar{X}} = \frac{d\bar{X}}{dt}$$

$$\bar{\omega} = \text{Earth rotation vector}$$

$$= \omega[0, 0, 1]^T$$

The unit vectors specifying the direction of the lift ($\hat{\delta}_L$) and drag ($\hat{\delta}_D$) are given by

$$\hat{\delta}_L = \frac{\bar{X} \times \bar{V}_R}{|\bar{X} \times \bar{V}_R|} \sin \beta - \frac{\bar{V}_R \times \bar{X} \times \bar{V}_R}{|\bar{V}_R \times \bar{X} \times \bar{V}_R|} \cos \beta \quad \text{Eq. 5}$$

$$\hat{\delta}_D = -\frac{\bar{V}_R}{|\bar{V}_R|} \quad \text{Eq. 6}$$

where β = vehicle bank angle.

The guidance algorithm determines a control vector, which is the solution to the following nonlinear, constrained optimization problem:

Find the minimum value of the scalar function $G(\lambda)$ subject to the m constraint equations,

$$C_i(\bar{X}_F, \dot{\bar{X}}_F, t_F, \bar{\lambda}) \leq 0, \quad i = 1, \dots, m \quad \text{Eq. 7}$$

where \bar{X}_F and $\dot{\bar{X}}_F$ are solutions to the differential equation

$$\ddot{\bar{X}} = \bar{F}(\bar{X}, \bar{\lambda}) \text{ at } t = t_F$$

For the OTV, the function $\bar{F}(\bar{X}, \bar{\lambda})$ is given by Eq. 1

Figure 6.1.3-1. Equations of Motion and Guidance Algorithm

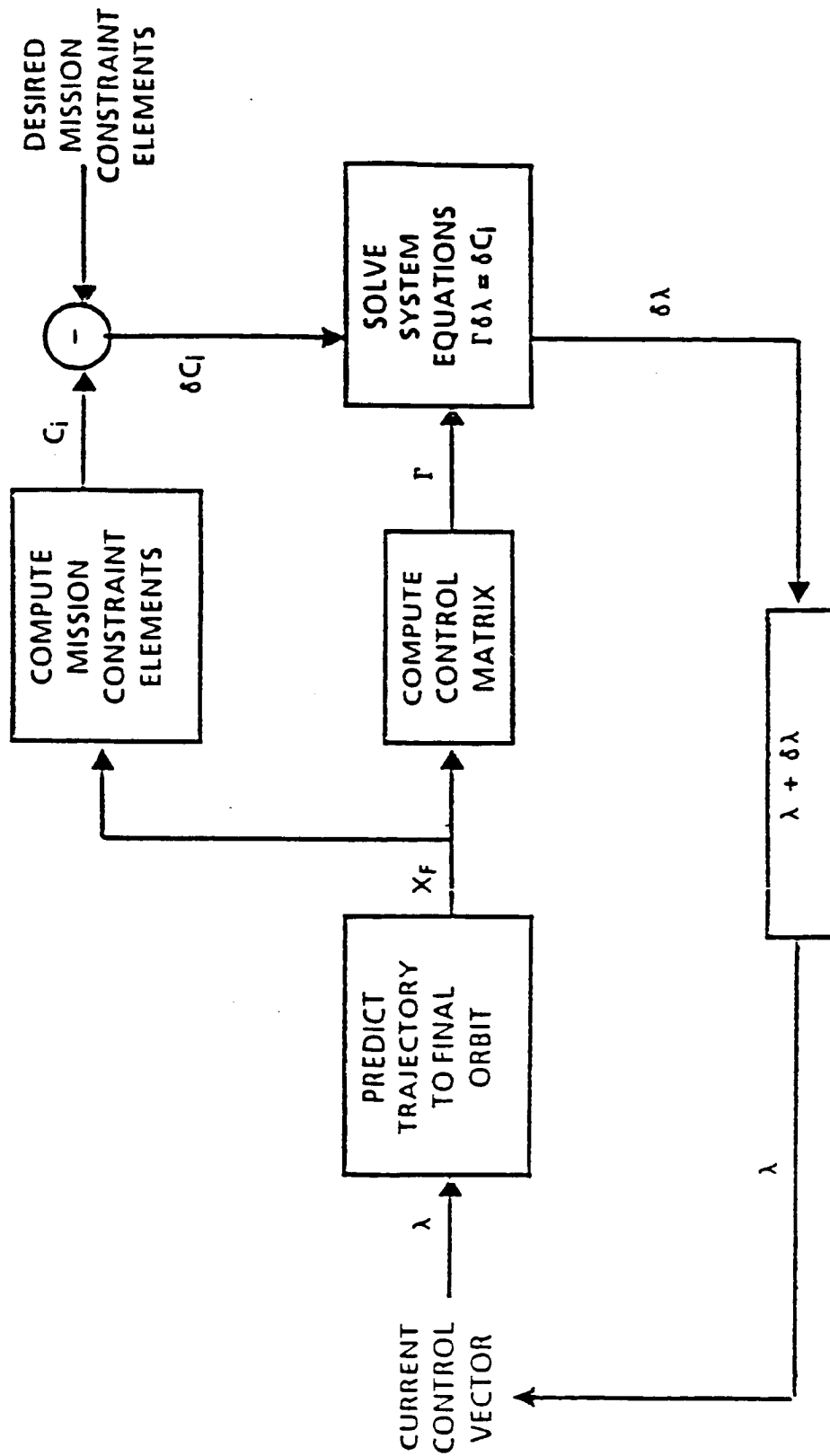


Figure 6.1.3-2 Adaptive Guidance Algorithm

configured to have a low L/D. For these studies the low L/D vehicles are flown at a constant angle of attack and are controlled by varying the bank angle.

The simulated flight for each of the vehicles is represented in Figure 6.2-1. The reentry conditions are based on a return flight from GEO altitude. The aeropass maneuver slows the vehicle to lower the apogee of the orbit. After exiting the atmosphere a propulsive maneuver at apogee will either circularize the orbit or place the OTV in a phasing orbit for rendezvous with an orbiter.

Three "real" density profiles were used for this study. They were the profiles derived from measurements on the STS-2, STS-4, and STS-6 shuttle flights, as shown in figure 6.2-2. The targeted end-condition for all flights was to exit the atmosphere in a transfer orbit with a radius of apogee of 260 nautical miles that would allow recovery at a Space Station. The measure of the aeroassisted vehicle performance was the error in the atmospheric exit velocity. This error was the magnitude of the delta-velocity which had to be added at atmospheric exit in order to reach the targeted radius of apogee within a tolerance of 1000 ft.

The guidance performance analysis was performed with a closed loop computer simulation called OPTIC. The inner loop of this simulation is the implementation of the guidance algorithm using simplified vehicle dynamics and a Standard-62 atmospheric density model. At each guidance update interval, a new set of guidance control variables is issued to the outer loop which consists of detailed vehicle dynamics and a representative, real atmospheric density profile. The simulated vehicle motion is propagated to the next guidance update time. At that time the current vehicle position and velocity are passed to the guidance algorithm in the inner loop for determination of a new guidance command based on the current vehicle state.

6.2.1 Ballute Brake OTV

This section discusses the analysis as it pertains to an OTV that uses only a ballute to perform the aeromaneuver.

6.2.1.1 Fixed Maximum Diameter Ballute

The initial guidance analysis for the ballute was designed to determine an acceptable turn-down ratio to be used in the design of a baseline ballute vehicle for the OTV analysis. The characteristics of the assumed vehicle and reentry state are shown in figure 6.2.1-1. The vehicle weighed 20,573 lbs and had a maximum diameter of 50 ft for all turndown ratios ($TDR = C_{DA_{max}}/C_{DA_{min}}$) in the range from 1.1 to 2.2. These vehicles have nominal ballistic coefficients in the range from 8.5 to 12.9 lbs/ft².

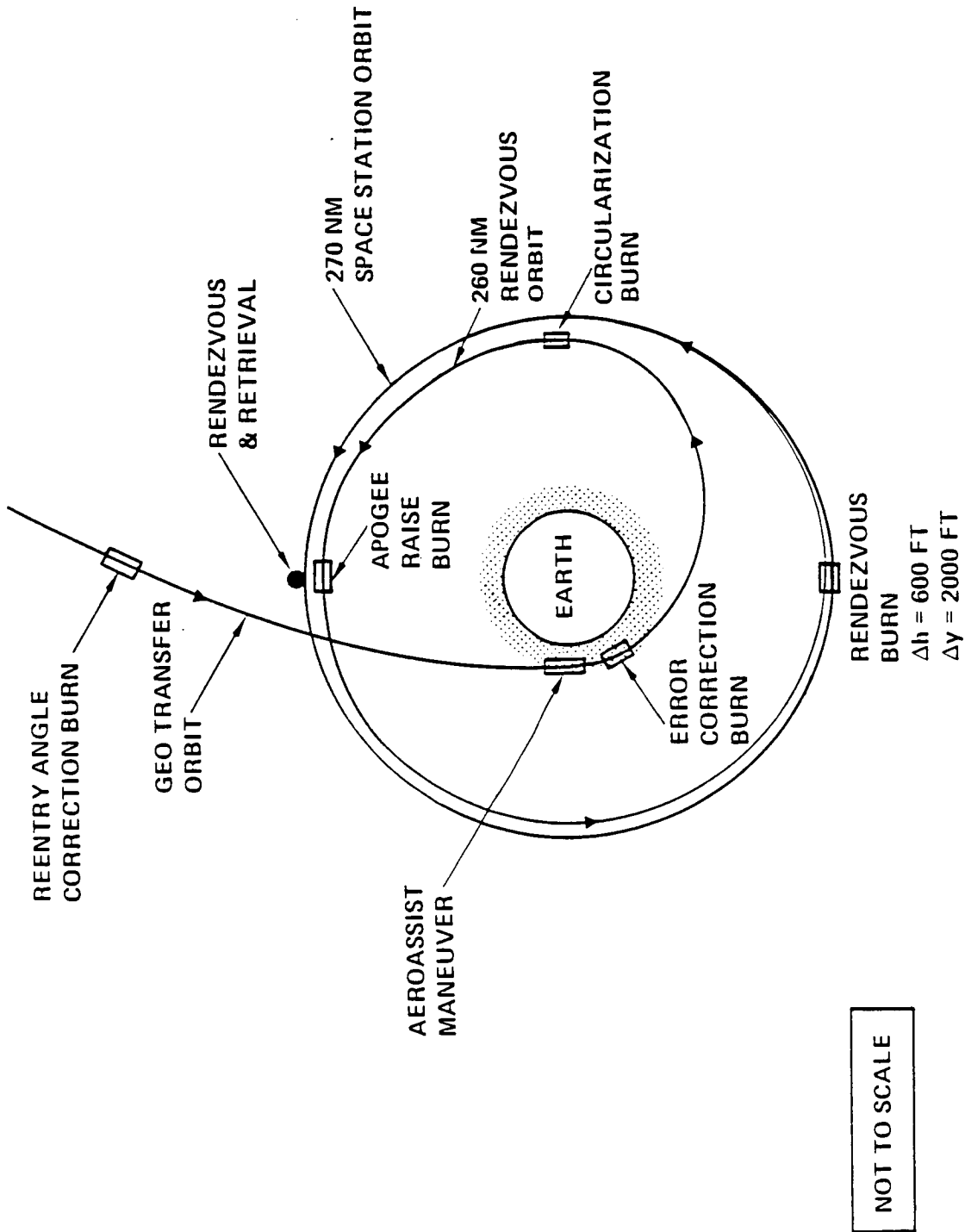


Figure 6.2-1 OTV Mission - Terminal Phase Key Guidance Events

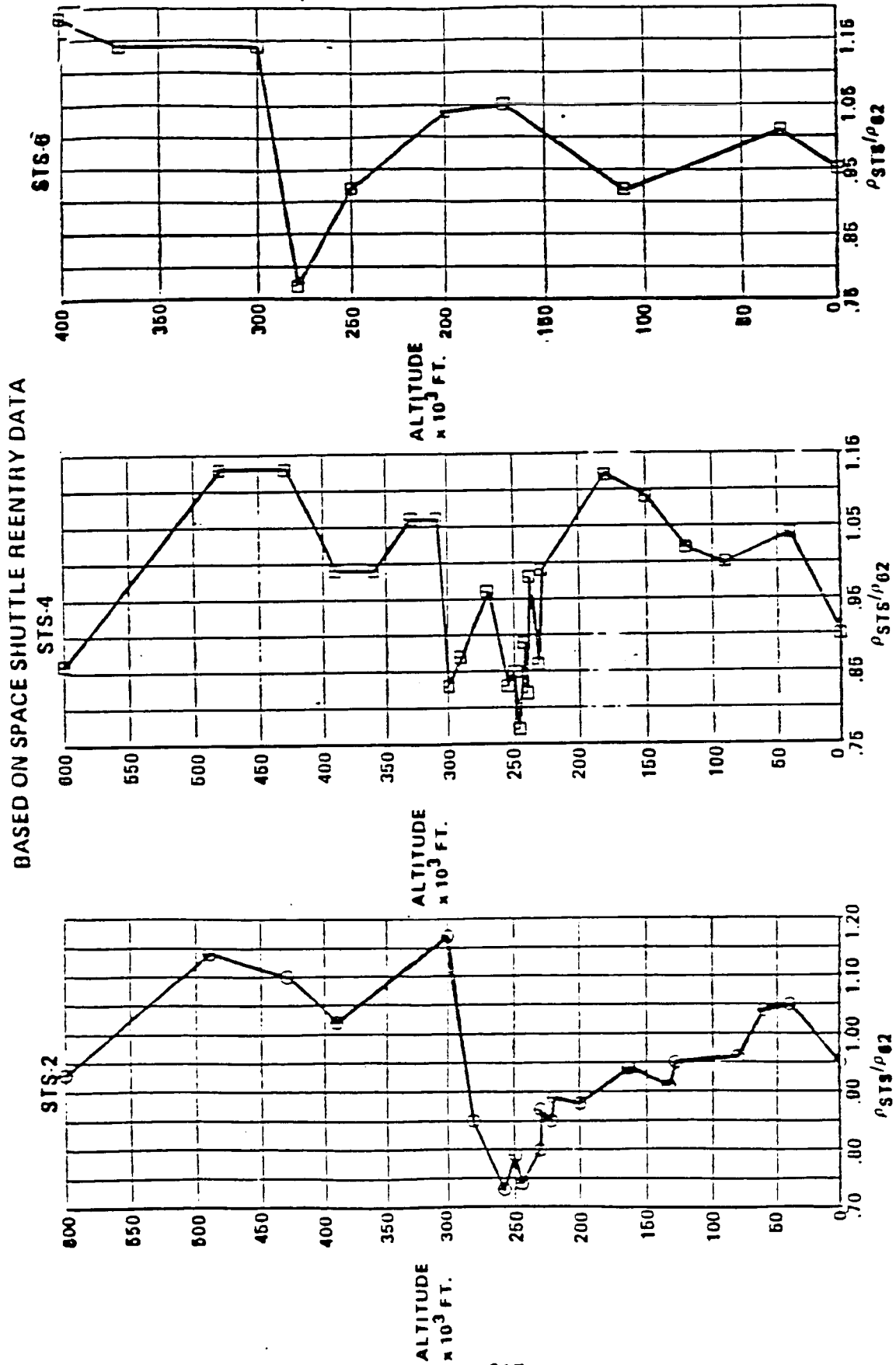


Figure 6.2-2 Simulated Atmospheric Dispersions



- REENTRY WEIGHT = 20,573 LBS
- MAXIMUM DIAMETER = 50 FT
- MAXIMUM $C_{D,A}$ = 2553 FT^2
- TURNDOWN RATIO RANGE = 1.1–2.2
- NOMINAL GEO-RETURN TRANSFER ORBIT
- PHASING ORBIT AT 260 NMI

REENTRY STATE

$R = 400,000 \text{ FT}$
 $V = 33,828.6 \text{ FT/SEC}$
 $\gamma = \text{DEPENDS ON TDR}$
 $\text{LAT} = 4.985^\circ \text{S}$
 $\text{LONG} = 9.244^\circ \text{W}$
 $\text{AZIMUTH} = 60.612^\circ$

TARGETED EXIT CONDITION

RADIUS-OF-APOGEE = 260 NMI

Figure 6.2.1-1. Ballute Used in Guidance Analysis

The guidance control variables for the ballute are C_{DA} (coefficient of drag times reference area) and velocity impulse at atmospheric exit. At each guidance update, the guidance algorithm solves the boundary value problem defined by current vehicle state vector and the desired exit condition which is an orbit with altitude-of-apogee (R_A) equal to 260 nm. The trajectory flown in the guidance algorithm is for a constant C_{DA} through a Standard-62 atmosphere with a velocity impulse added at atmospheric exit to ensure that the end constraint ($R_A = 260$ nm) is within the tolerance of 1000 ft. Because this solution always reaches the correct R_A , the measure of guidance error through the atmosphere is the magnitude of the velocity impulse required for convergence of the guidance algorithm.

The ballute model in the vehicle simulation used an equilibrium thermodynamics model to control the inflation dynamics. The guidance C_{DA} command was converted into an internal pressure command. Figure 6.2.1-2 shows the nonlinear ballute response curve which was used to model the relation between C_{DA} and the ratio of internal pressure to dynamic pressure. The computational flow through the model is shown in Figure 6.2.1-3. The ballute pressure lag model is detailed in Figure 6.2.1-4. It can be used to study the effects of tank size and temperature on the ballute response and to obtain information on the quantity of gas required to inflate and control the ballute through an aeromaneuver. It can also be used to investigate outflow valving strategy. For this study, a simple, two-position valve was used. At the first negative inflow command past perigee, the valve was opened fully and remained open for the remainder of the flight.

The time history of the inflation gas used for the 50 ft. ballute with a TDR = 1.5 is shown in Figure 6.2.1-5 for flights through the STS-2, -4, and -6 atmosphere. The sharp increase in the slope of the inflow gas occurs when the exit valve is opened.

Typical plots of the altitude and velocity along a ballute aeromaneuver trajectory are shown in Figure 6.2.1-6. This profile is for TDR = 1.5 through an STS-2 density profile.

The guidance command for the TDR = 1.5 and the actual vehicle response are shown in Figure 6.2.1-7. The shape of the vehicle C_{DA} response is the mirror image of the shape of the density perturbation as long as the response is within the turndown capability of the ballute. If the ballute response were linear, the actual drag and commanded drag would be the same and the C_{DA} command would be constant as long as the response remained within the vehicle capability. However, the assumed nonlinear response causes the actual drag to depart from the commanded drag. This effect results

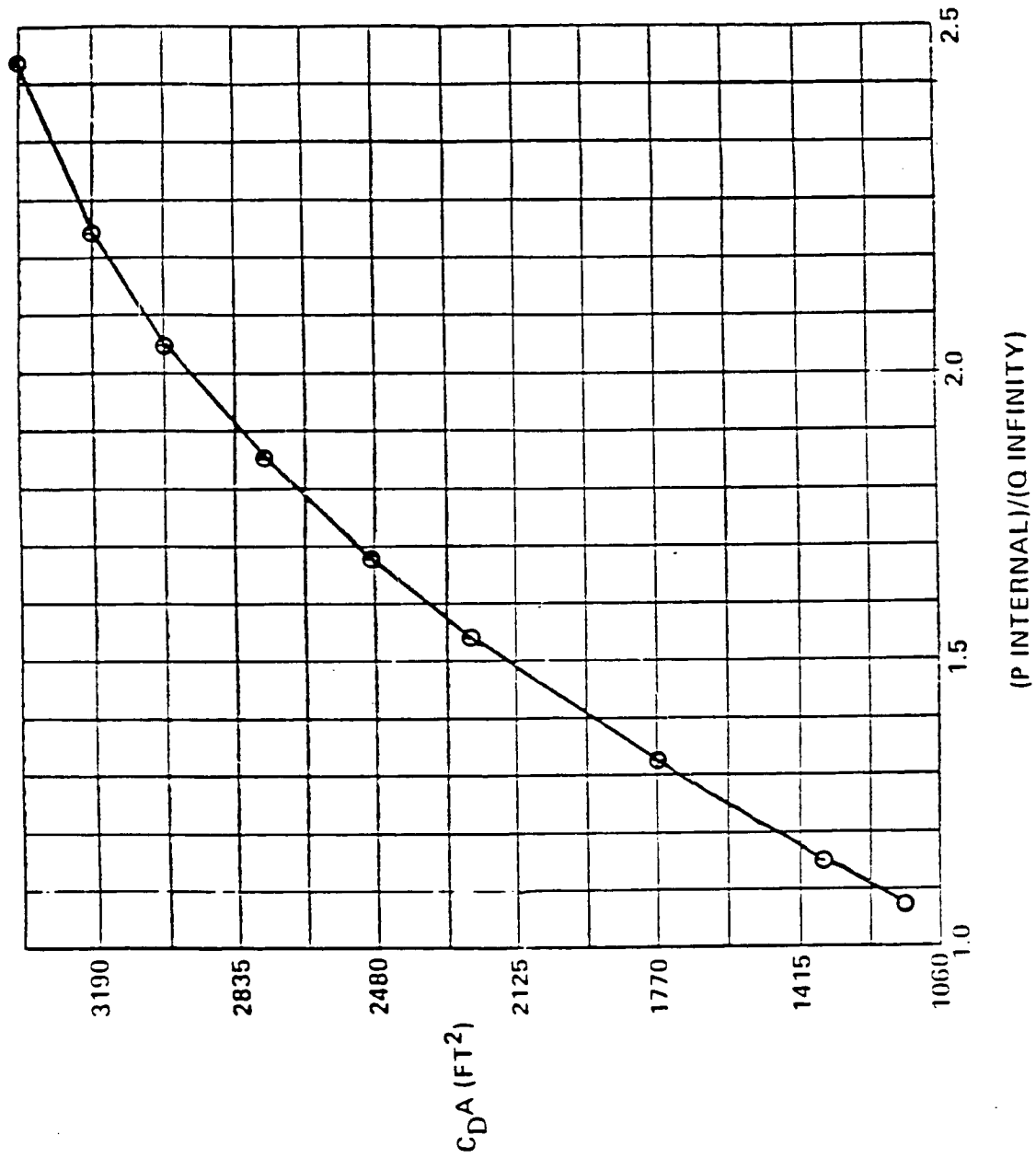


Figure 6.2.1-2 Ballute Response Characteristics

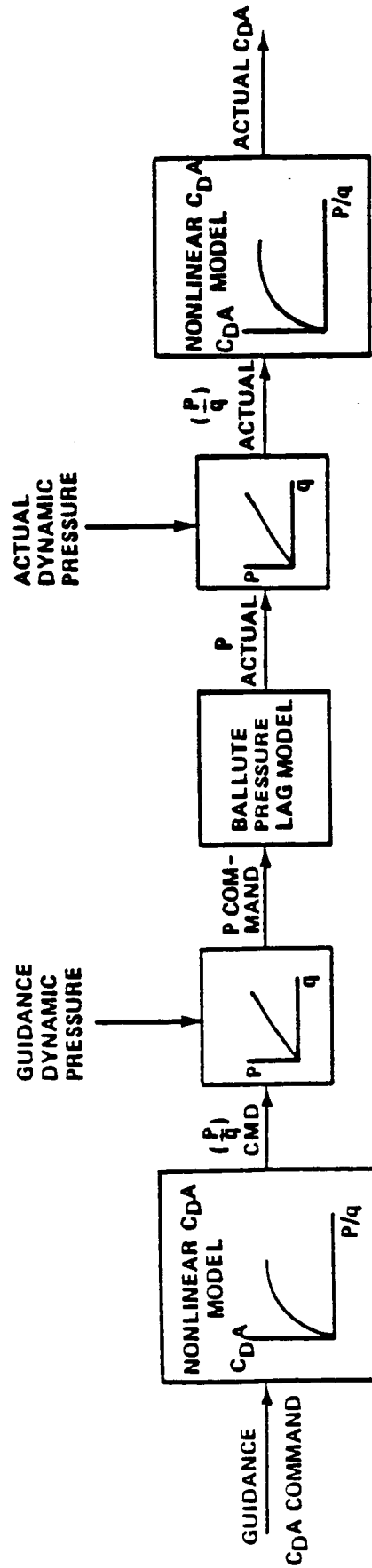


Figure 6.2.1-3. Ballute Pressure Lag Model Implementation

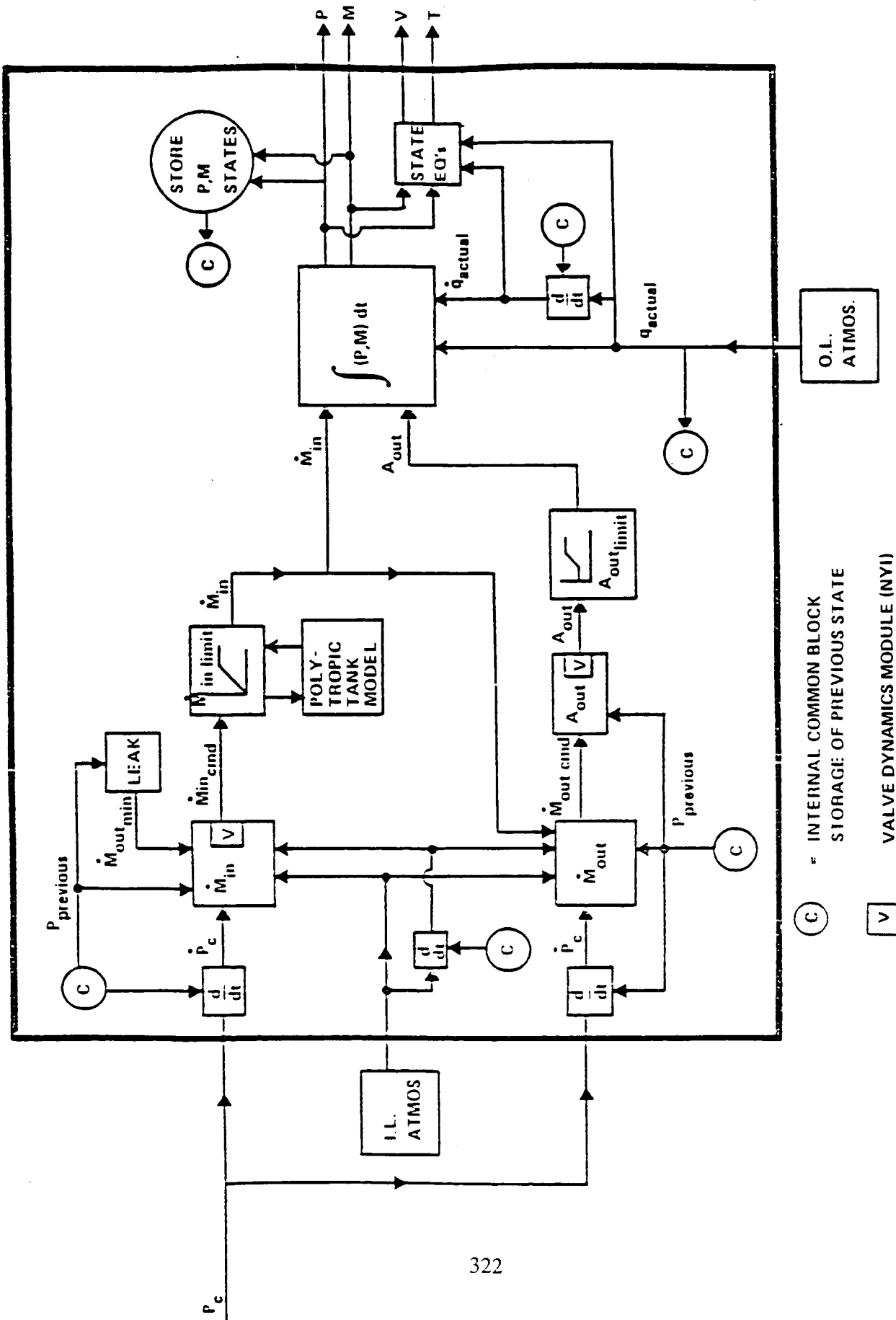
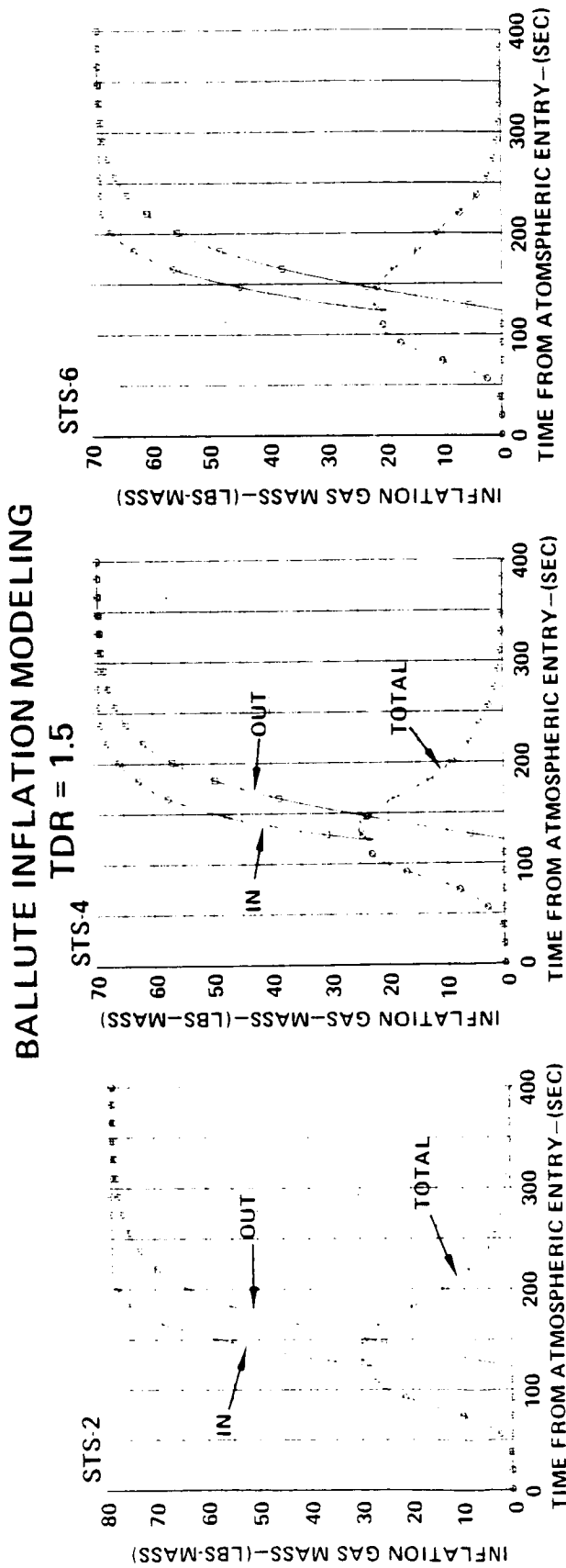


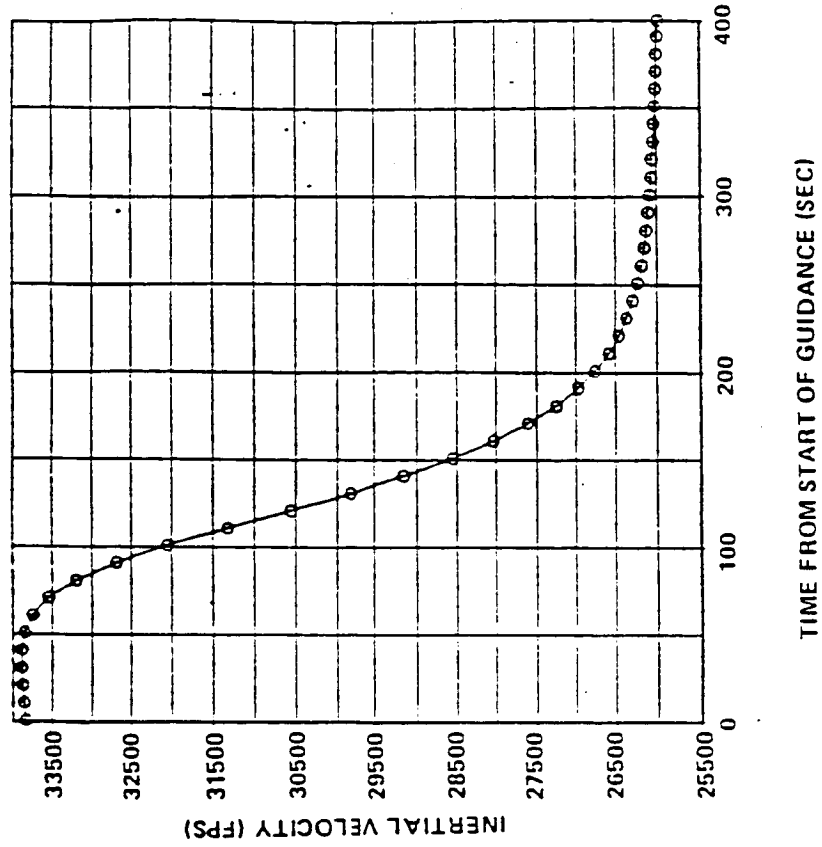
Figure 6.2.1-4 Ballute Pressure Lag Model



- EQUILIBRIUM THERMODYNAMIC MODEL ALLOWS STUDY OF:
 - INFLATION STRATEGY
 - GAS TANK SIZE
 - TANK PRESSURIZATION
 - MASS REQUIREMENTS
 - GAS GENERATOR
 - OUTFLOW STRATEGY
 - CONTROLLED EXIT VALVE
 - TWO POSITION VALVE
 - GAS LEAKAGE

Figure 6.2.1-5 Ballute Inflation Gas Time History

VELOCITY



ALTITUDE

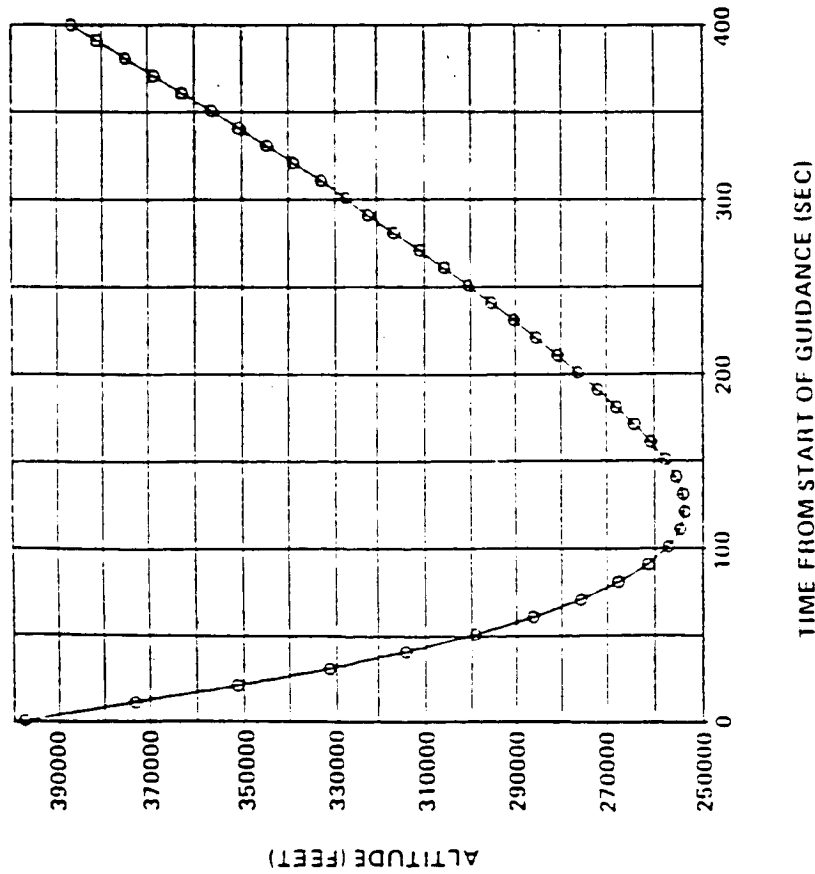


Figure 6.2.1-6 Ballute Aeropass Trajectory

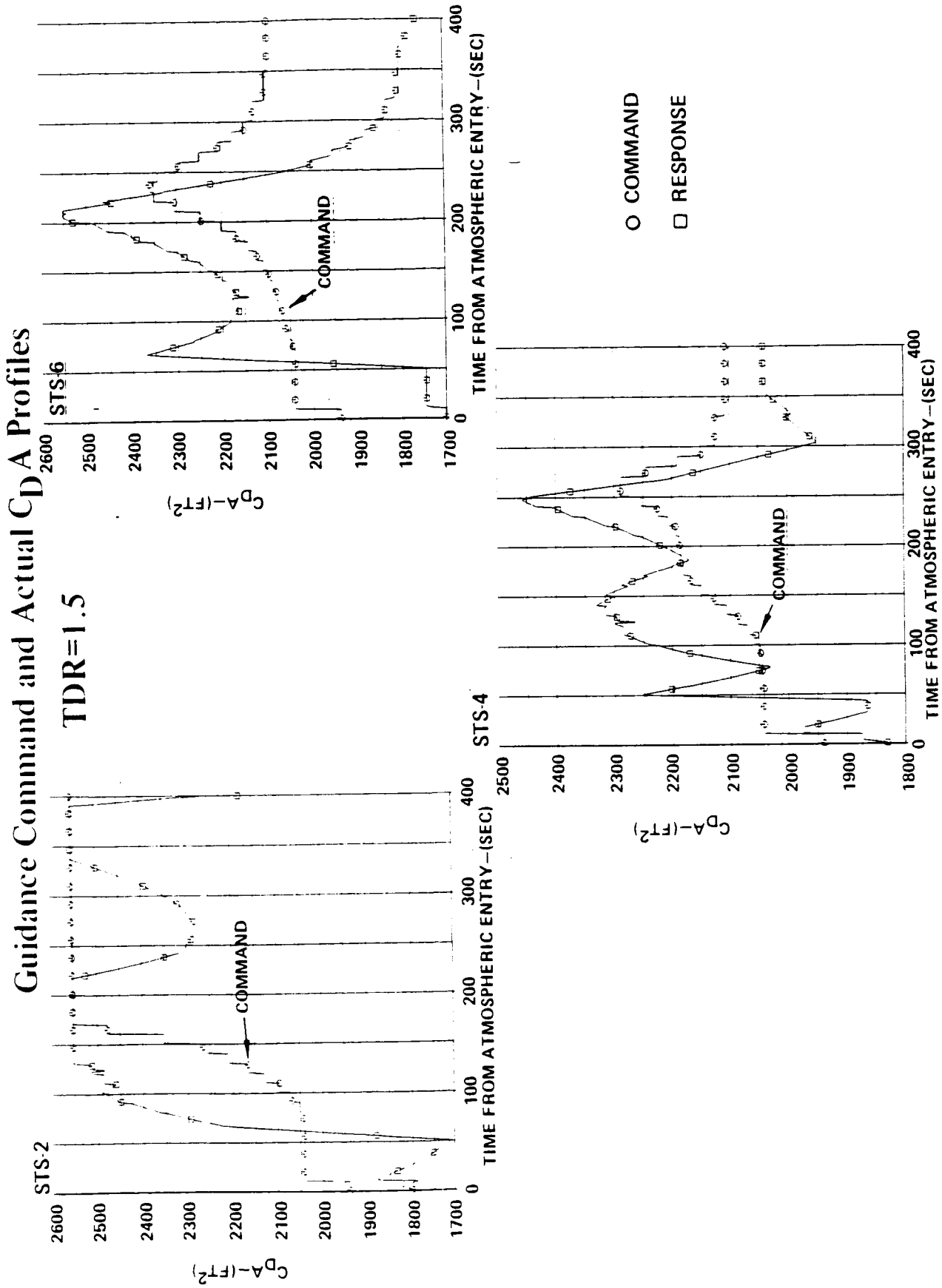


Figure 6.2.1-7 Ballute Guidance Command and C_{DA} Profiles

in a changing $C_D A$ command even if the response stays within the limits. This can be seen in the STS-4 and STS-6 command profiles.

The measure of the guidance error is the velocity excess or deficit at atmospheric exit. For a TDR = 1.5 the velocity errors are shown in Figure 6.2.1-8 for the three STS atmospheres.

A summary of the guidance analysis for the 50 ft ballute is shown in Figure 6.2.1-9. Using the STS-2 results as a conservative measure, it is shown that for a TDR = 1.5, the propulsive velocity correction to make up for atmospheric guidance errors is about 250 ft/sec.

6.2.1.2 Variable Maximum Diameter Ballute

The next phase of the ballute guidance analysis was to assess the effects of vehicle designs having different size ballutes and reentry weights. Three turndown ratios were picked and ballutes were sized for delivery of a 7500 lb. payload.

For a TDR = 1.25, the vehicle had a 45 ft maximum diameter ballute and a reentry weight of 13,287 lbs. The nominal ballistic coefficient of the vehicle was 7.2 lbs/ft². The altitude and velocity profiles of the trajectory for the TDR = 1.25 vehicle are shown in Figures 6.2.1-10 and 11. Figure 6.2.1-12 shows the commanded and actual $C_D A$ response for this vehicle. The command remained at the upper limit for most of the exit leg of the aeromaneuver. The present implementation of the command simulation does not drive the actual response to the ballute angle limit when this happens. Rather it commands an internal pressure which would inflate to the angle limit if the ballute were flying in a nominal atmosphere. On the exit leg of the trajectory, the density is greater than nominal which leads to an actual ballute response of less than the maximum $C_D A$. This contributes to the guidance velocity error during the aeromaneuver. For this trajectory this contribution is small, but for perturbations near perigee it could be significant. This part of the algorithm will be changed in the future. From Figure 6.2.1-13, which shows the accumulation of the guidance velocity error, it can be seen that the major contribution occurs during the time that the actual ballute response has reached the maximum ballute angle. This occurs in the time period from 120 sec to 200 sec along the flight path where the projected error grows to 420 ft/sec.

The ballute with a TDR = 1.5 had a maximum diameter of 50.1 ft and an entry weight of 13,077 lbs. This vehicle had a nominal ballistic coefficient of 6.38 lbs/ft². The aeromaneuver trajectory is shown in Figures 6.2.1-14 and 15. The command and actual $C_D A$ profile for the TDR = 1.5 vehicle are shown in Figure 6.2.1-16. The projected velocity error is shown in Figure 6.2.1-17. Comparing the two Figures, it can

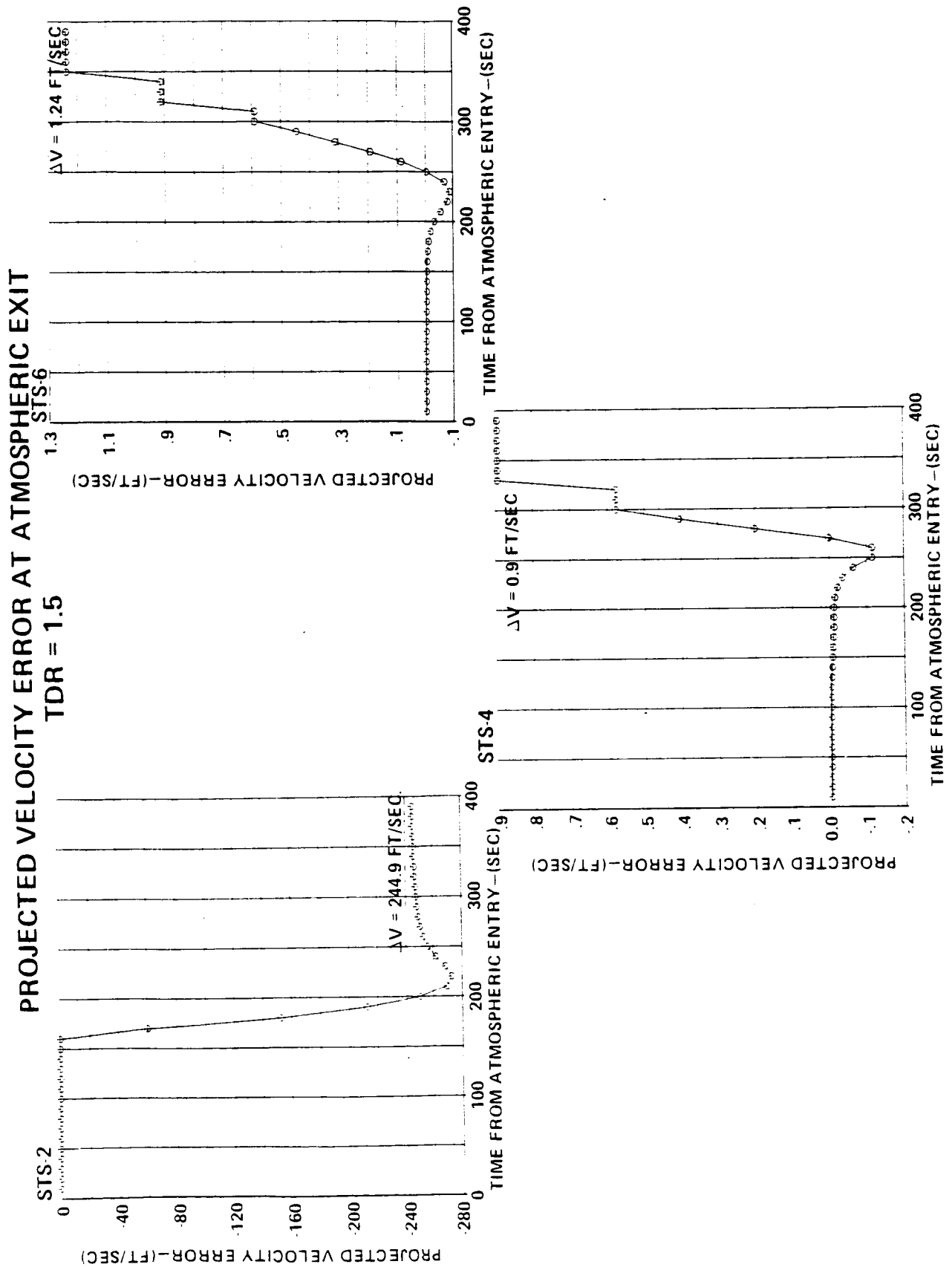


Figure 6.2.1-8 Ballute Guidance Velocity Errors

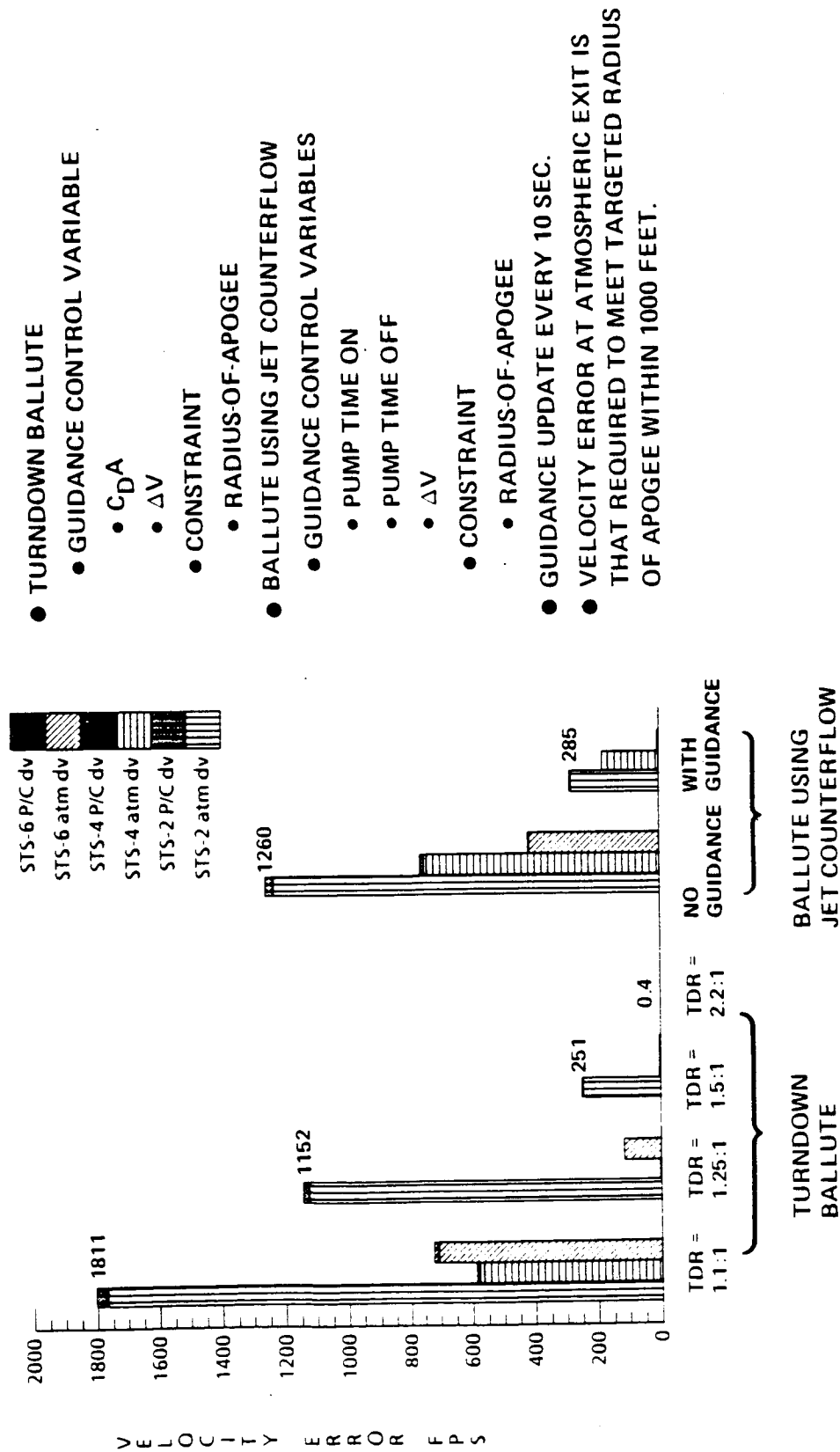
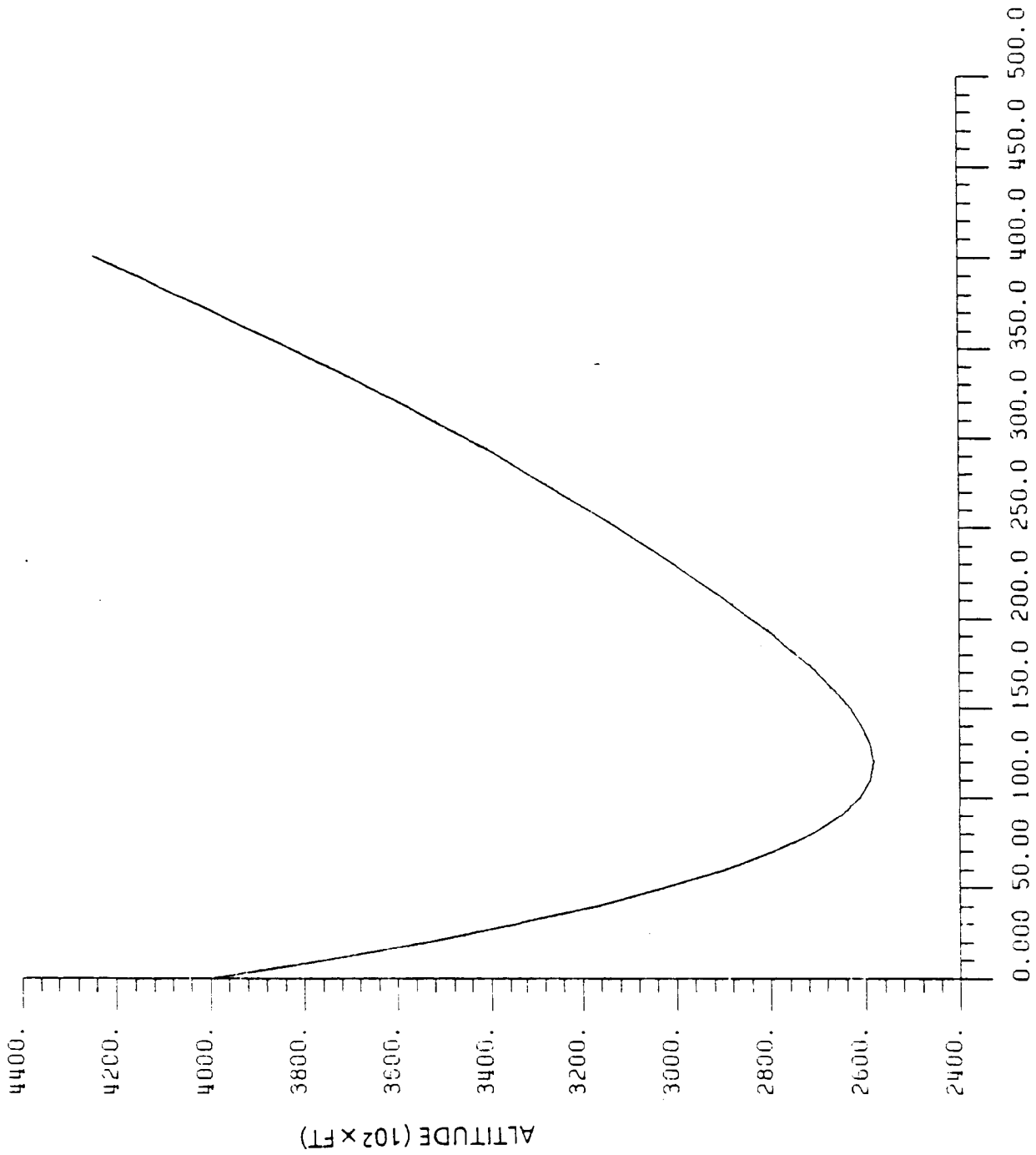
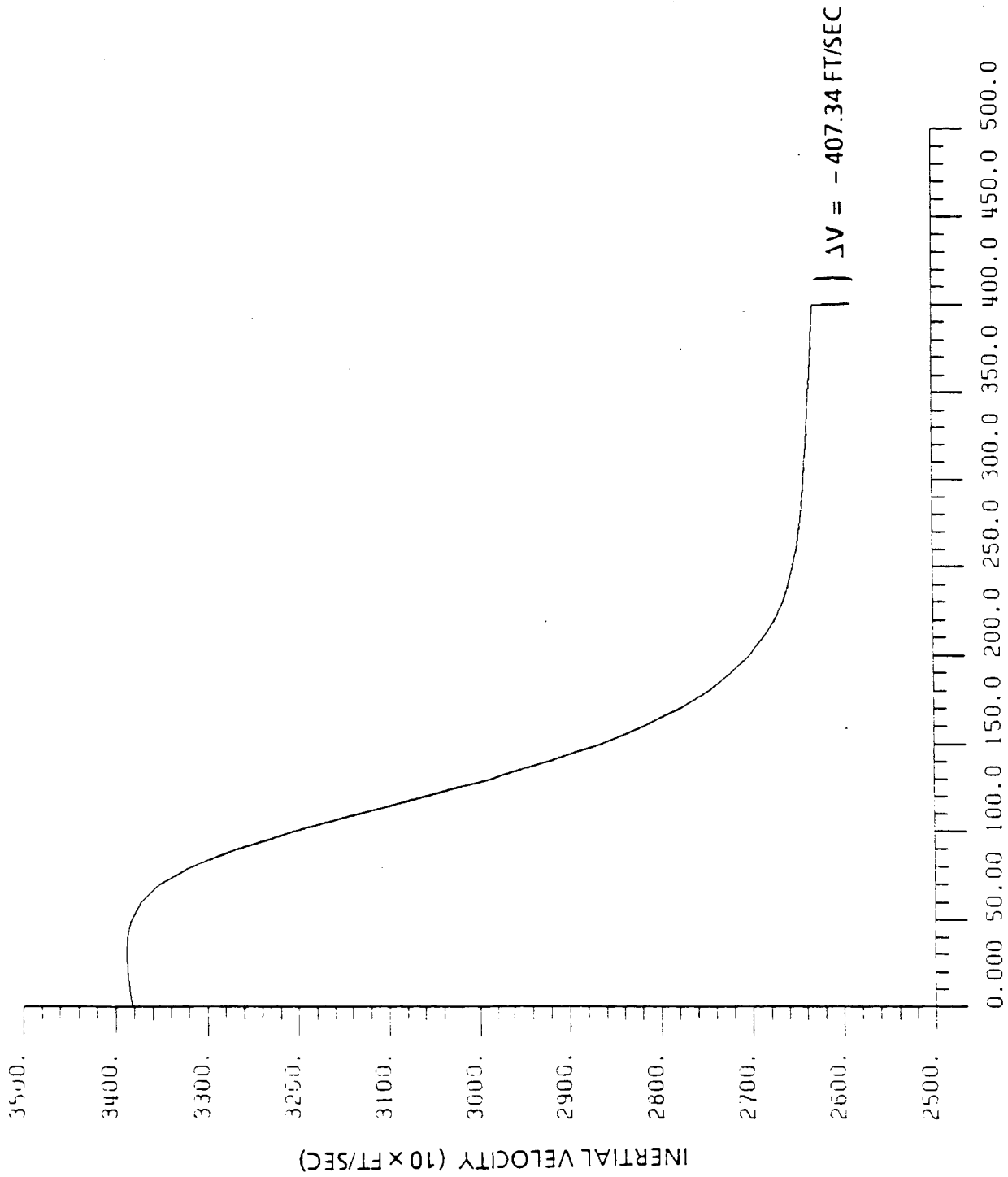


Figure 6.2.1-9. Ballute Response to Atmospheric Dispersions

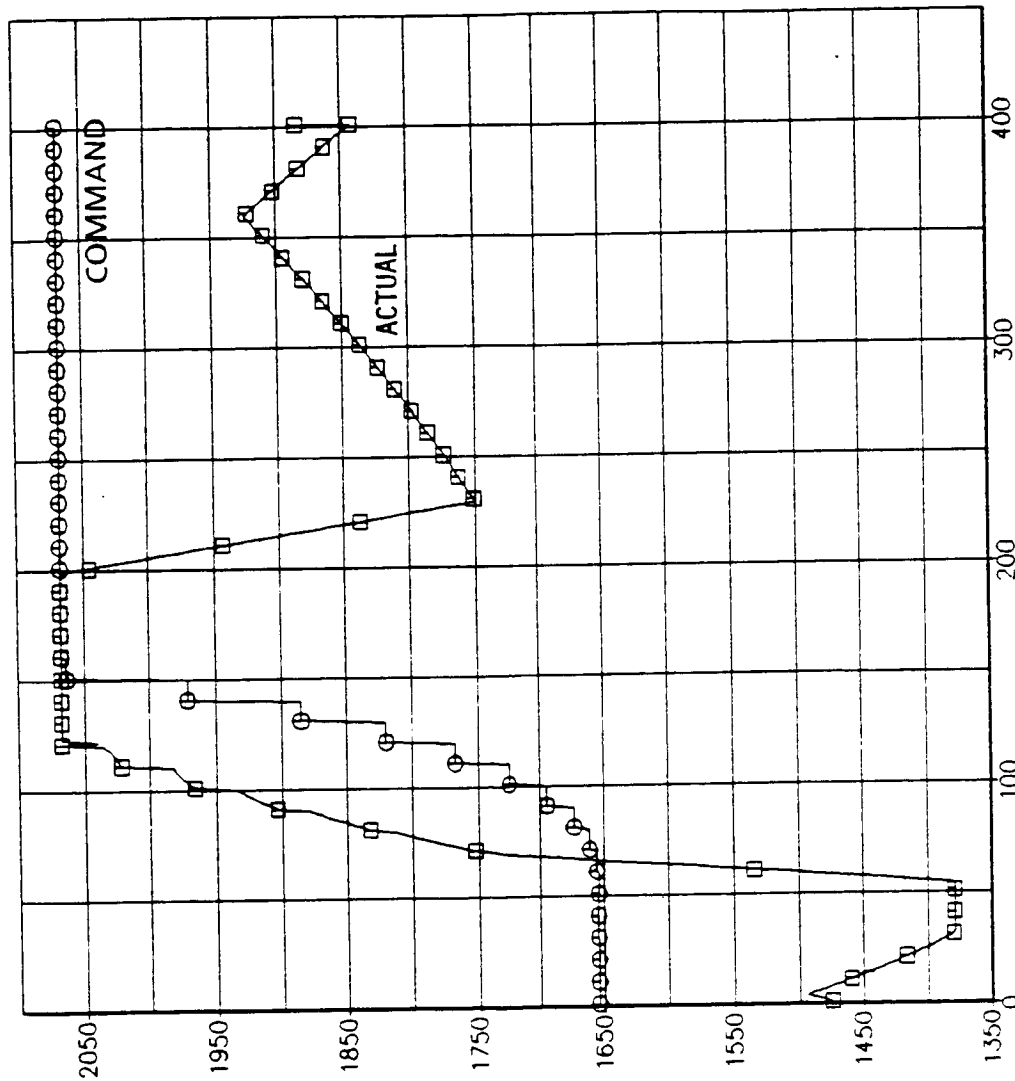


TIME FROM ATMOSPHERIC ENTRY (SEC)
 Figure 6.2.1-10. Altitude Profile for 45 ft, TDR = 1.25 Ballute



TIME FROM ATMOSPHERIC ENTRY (SEC)

Figure 6.2.1-11. Velocity Profile for 45 ft, TDR = 1.25 Ballute



TIME FROM ATMOSPHERIC ENTRY (SEC)

Figure 6.2.1-12. Command and C_{DA} Response for 45 ft, TDR = 1.25 Ballute

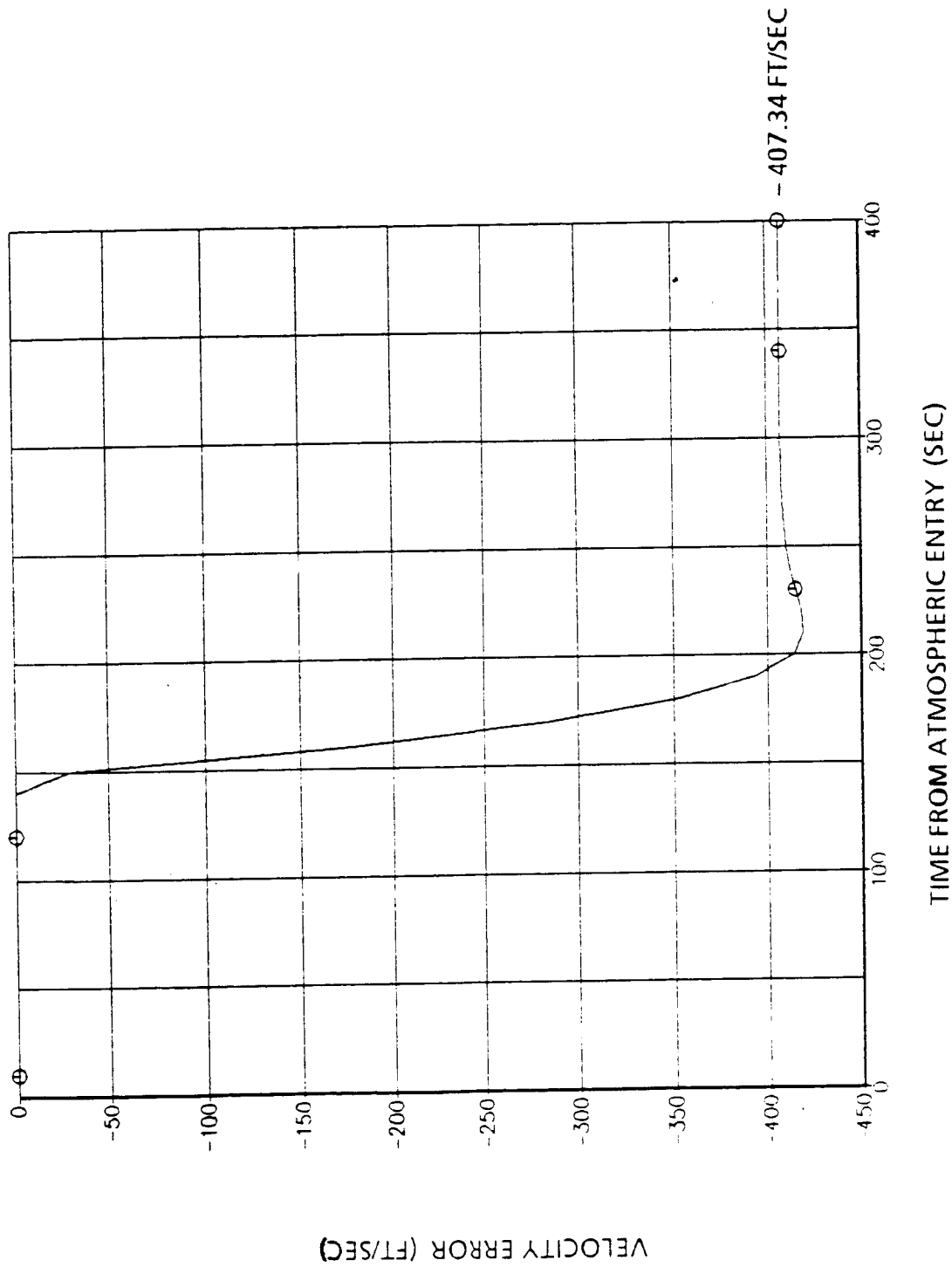
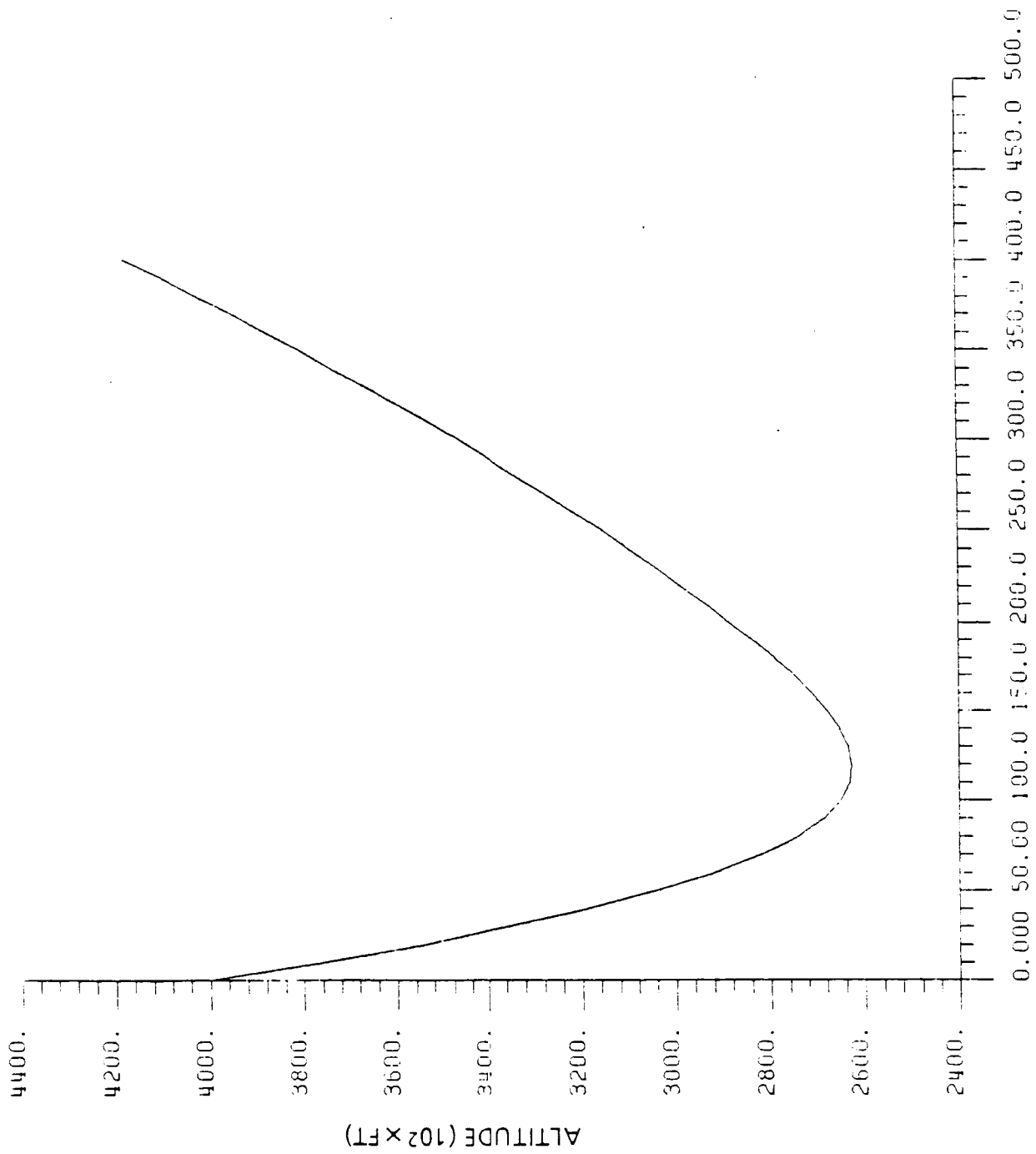
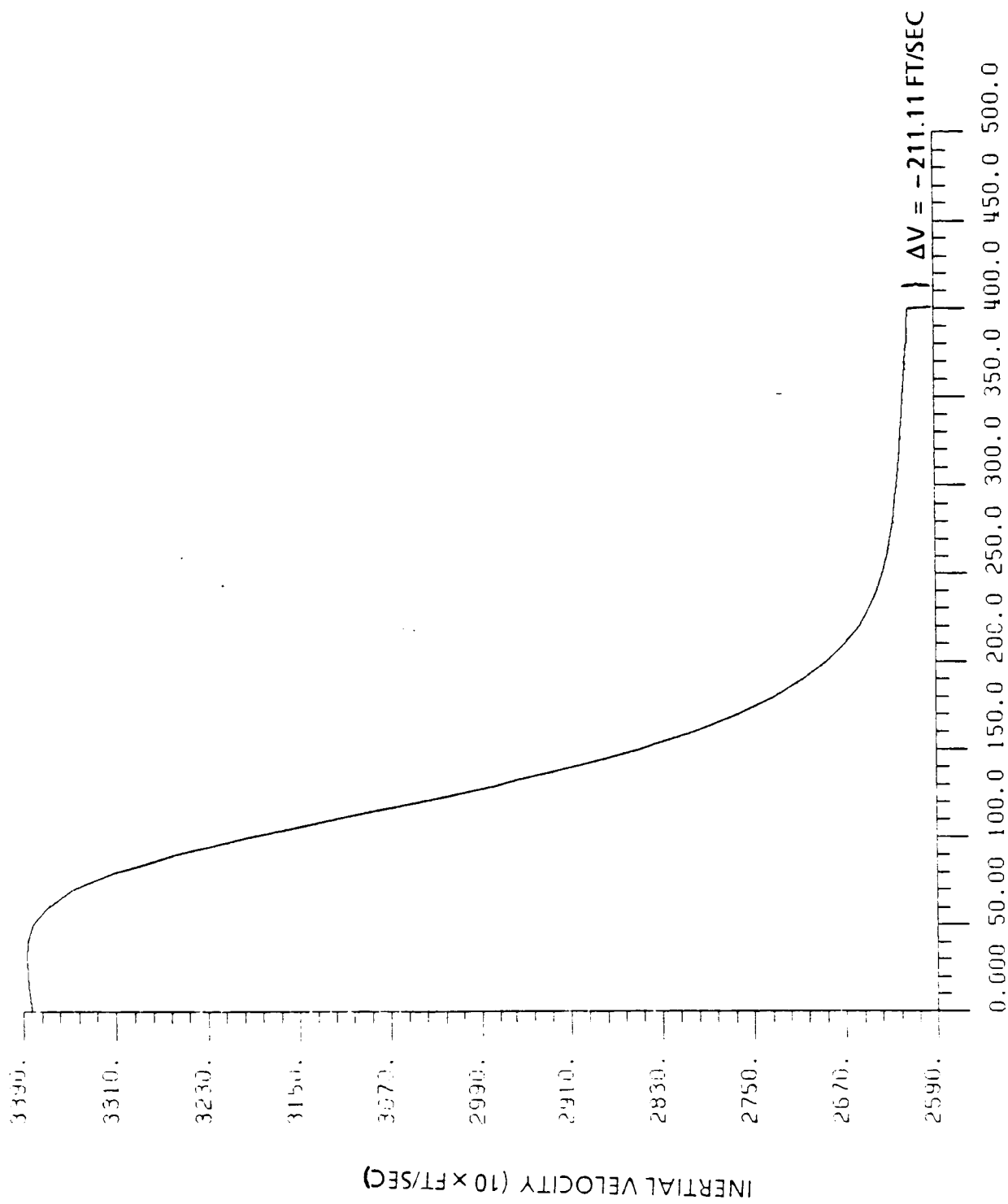


Figure 6.2.1-13. Projected Velocity Error for 45 ft, TDR = 1.25 Ballute



TIME FROM ATMOSPHERIC ENTRY (SEC)

Figure 6.2.1-14. Altitude Profile for 50.1 ft, TDR = 1.5 Ballute



TIME FROM ATMOSPHERIC ENTRY (SEC)

Figure 6.2.1-15. Velocity Profile for 50.1 ft, TDR = 1.5 Ballute

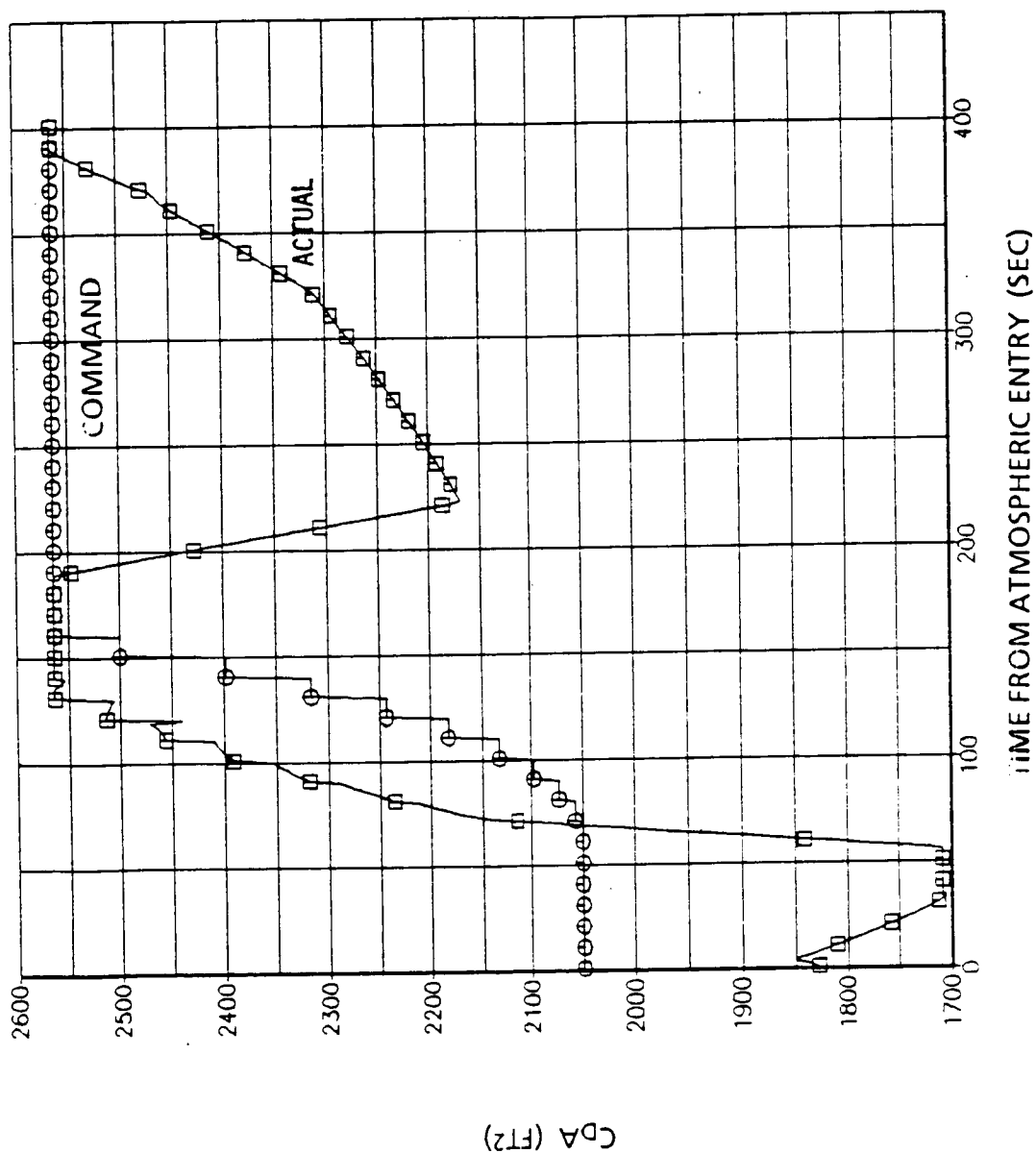


Figure 6.2.1-16. Command and C_{DA} Response for 50.1 ft, $TDR = 1.5$ Ballute

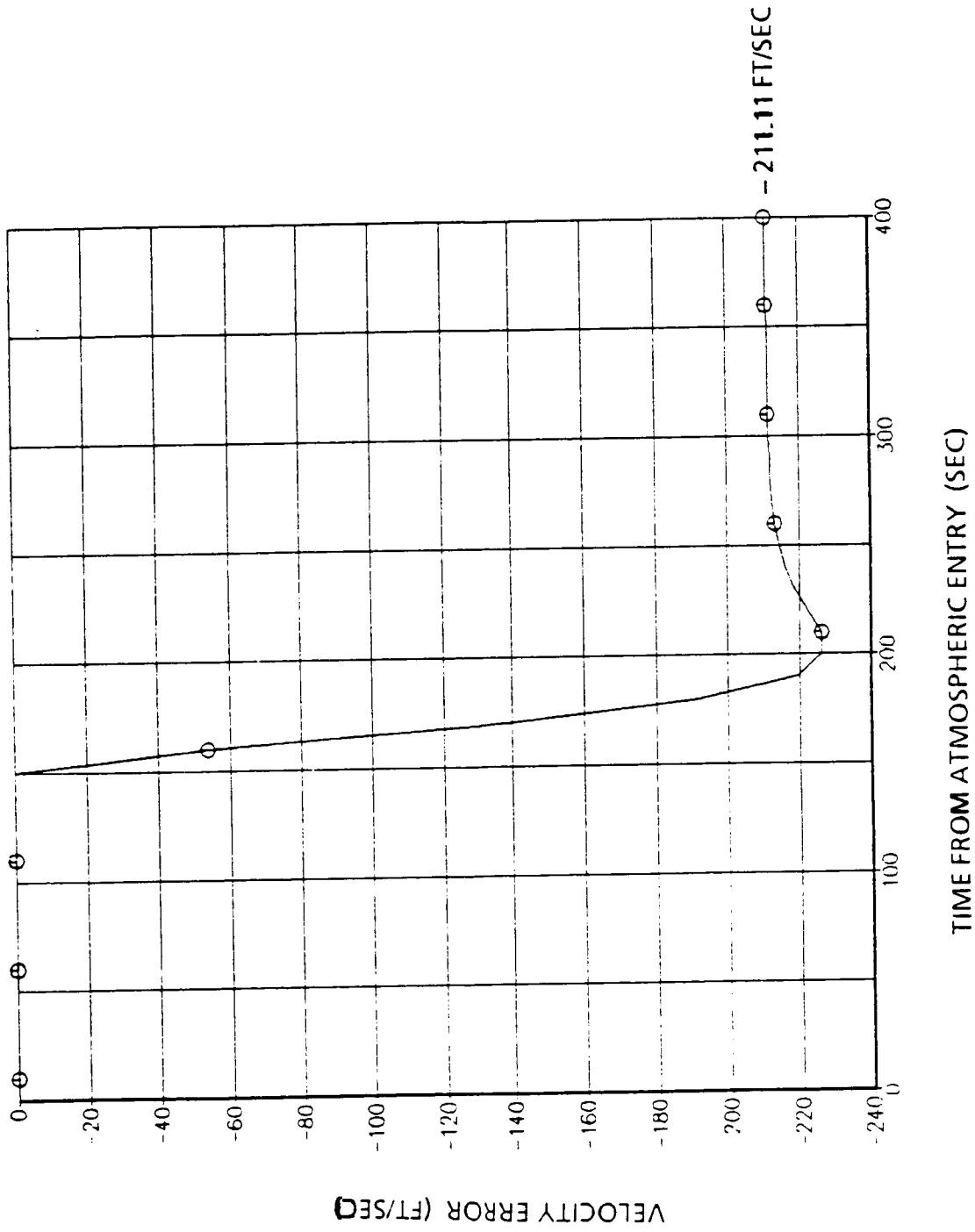


Figure 6.2.1-17. Projected Velocity Error for 50.1 ft, TDR = 1.5 Ballute

be seen that the projected error grows most rapidly during the time from 150 sec to 200 sec when the actual response is limited by the maximum ballute angle.

The TDR = 2.2 vehicle had a reentry weight of 15,176 lbs and a maximum diameter of 67.0 ft. The nominal ballistic coefficient for this vehicle was 5.30 lbs/ft². Figures 6.2.1-18 and 19 show the altitude and velocity of the STS-2 aeromaneuver trajectory for this vehicle. The C_DA command and response are shown in Figure 6.2.1-20. For this vehicle excess drag occurred during the down leg and pass through perigee leading to a commanded C_DA at the minimum ballute angle. However, there was an outflow lag which led to an increasing ballute size during a significant portion of the trajectory from 220 sec to the end. This resulted in an accumulated velocity deficit which would have to be made up propulsively. The projected velocity error is shown in Figure 6.2.1-21. This ballute was considerably larger than the others considered, but the same size exit valve was used. The outflow lag could have been eliminated by increasing the size of the exit valve.

6.2.1.3 Ballute Turndown Guidance Assessment

The results of the guidance analysis on the ballute vehicles have demonstrated the capability of the guidance algorithm and of the ballute concept to execute an aeroassist maneuver. A turndown ratio of 1.5 provides capability to correct for atmospheric dispersions as demonstrated by the STS-2, -4, and -6 profiles. A conservative propulsive allowance of 250 ft/sec is determined by the most demanding profile, STS-2.

6.2.2 Ballute OTV Using Jet Counterflow

Preliminary guidance analyses were performed for an OTV using a ballute and engine jet counterflow during the aeromaneuver. This vehicle concept was eliminated from consideration for other reasons, so the guidance analysis was not pursued in depth. The ballute studied was 42 ft in diameter and weighed 18,915 lbs at entry. The initial and targeted conditions are shown in Figure 6.2.2-1. The drag modulation of this vehicle is controlled by using engine exhaust momentum flux to control the point of bow shock separation. In this vehicle, the engines are directed forward during the aeromaneuver. At atmospheric entry, the engine is at tank head idle. Modulation is accomplished by turning the pump on or off and varying the thrust between tank head idle and pumped idle. The exhaust momentum flux at pumped idle results in an increased bow shock stand off distance and a reduction in the coefficient of drag (C_D) by an order of magnitude. Figure 6.2.2-2 shows the variation of C_D as a function of the momentum flux. For the preliminary guidance analysis a simple guidance law was used which

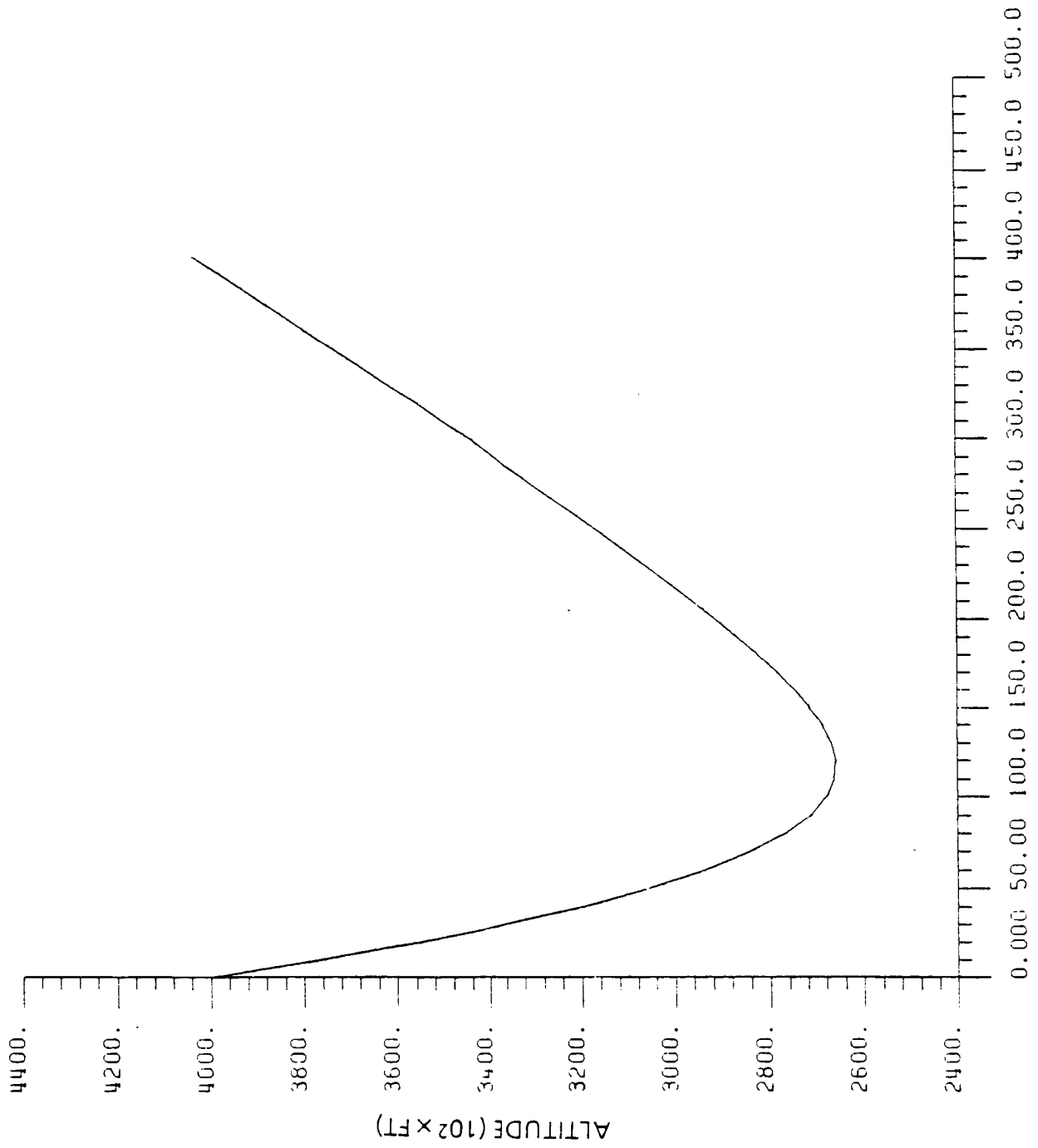


Figure 6.2.1-18. Altitude Profile for 67 ft, TDR = 2.2 Ballute

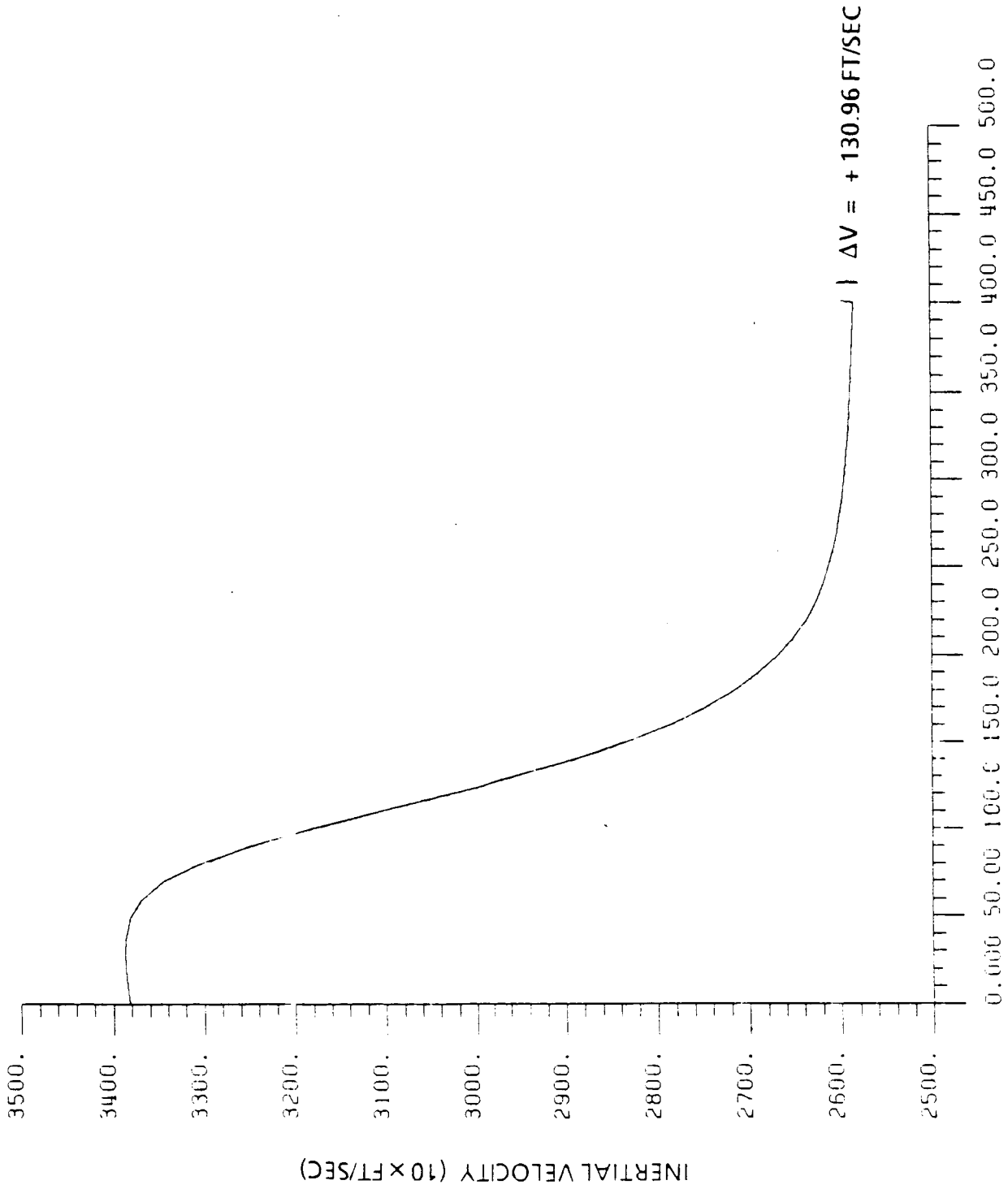


Figure 6.2.1-19. Velocity Profile for 67 ft, TDR = 2.2 Ballute

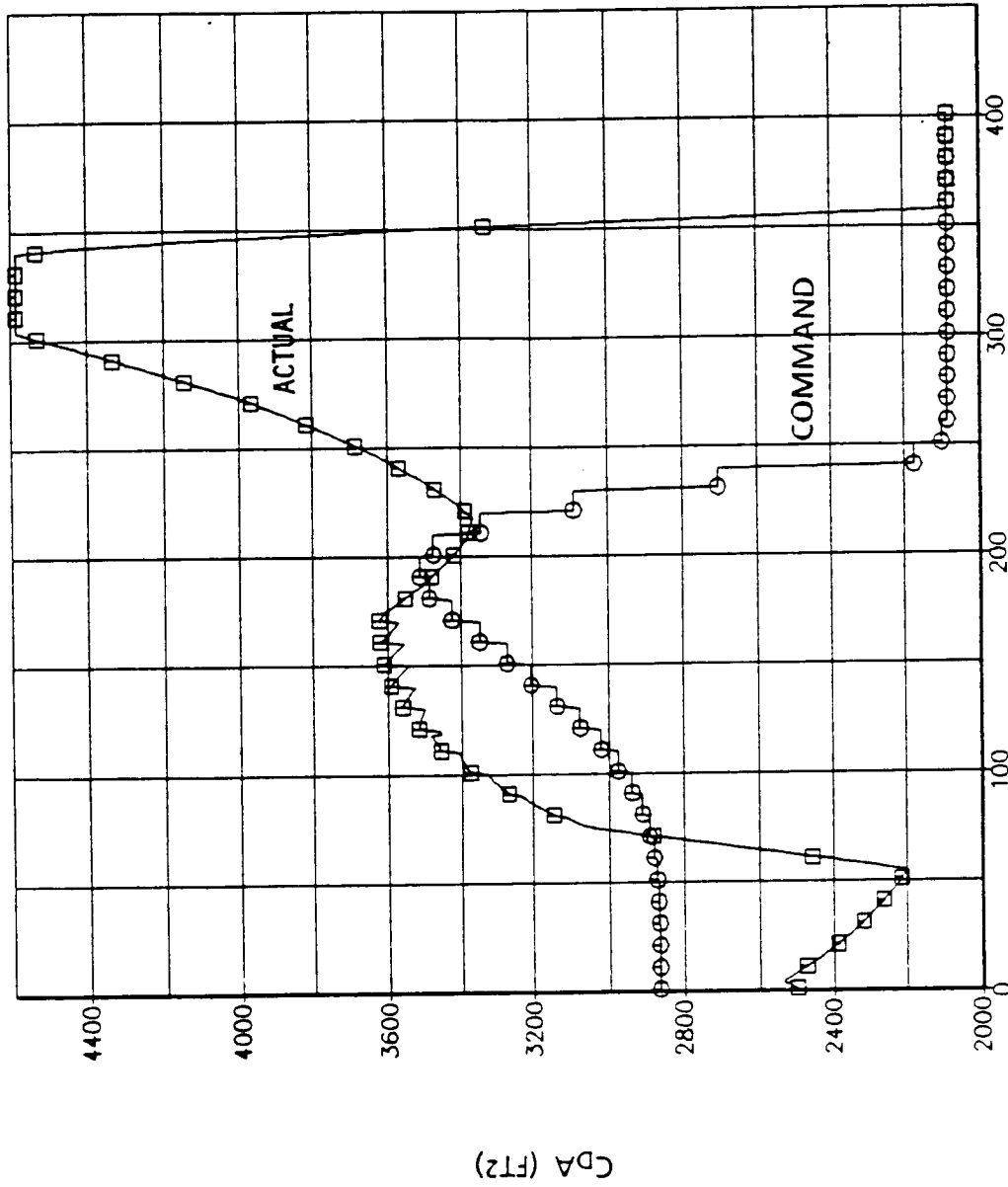


Figure 6.2.1-20. Command and C_{DA} Response for 67 ft, TDR = 2.2 Ballute

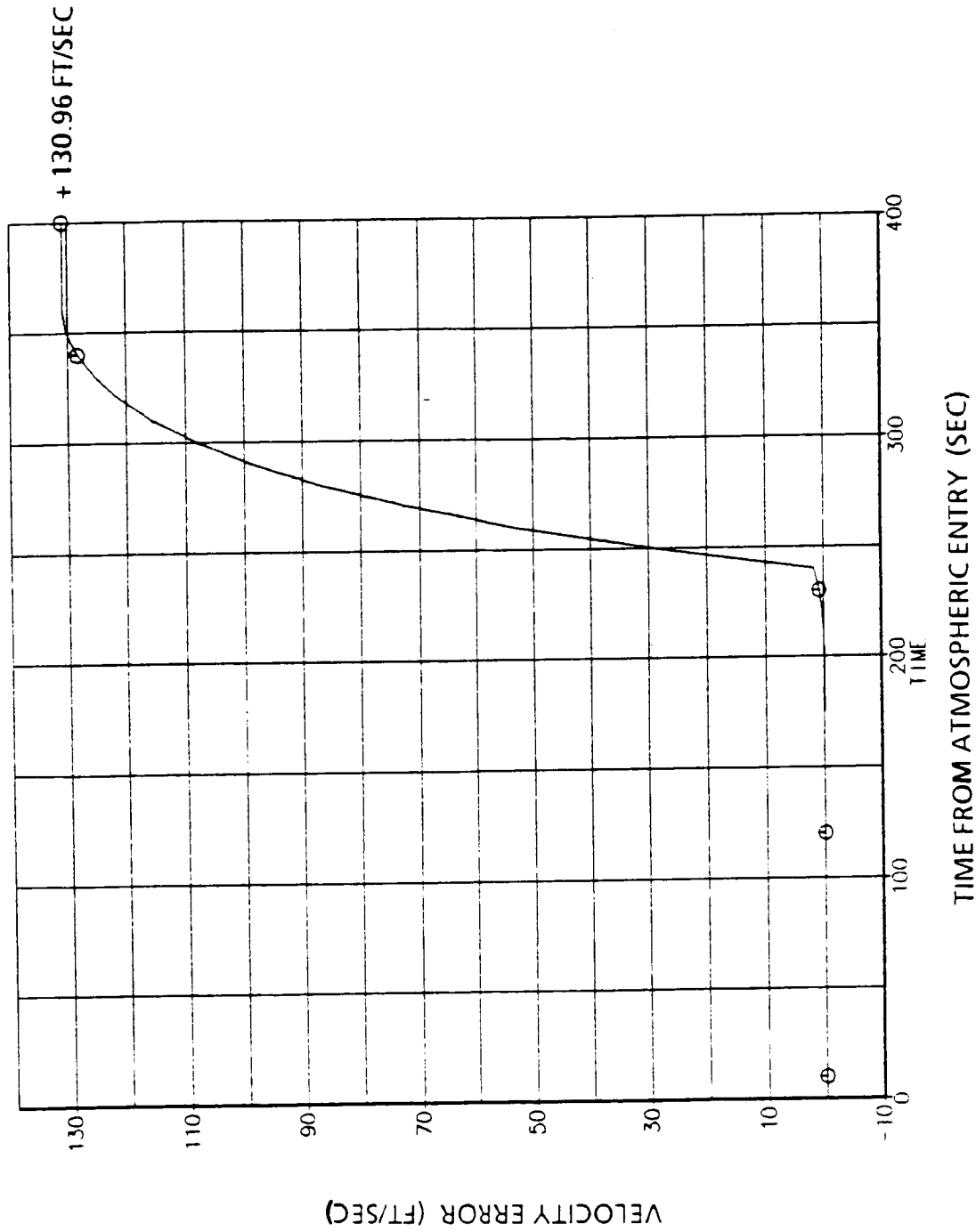


Figure 6.2.1-21. Project Velocity Error for 67 ft, TDR = 2.2 Ballute

- REENTRY WEIGHT = 18915 LBS
- DIAMETER = 42 FT
- $C_D A$ VALUES = 1886 FT², 188.6 FT²
- NOMINAL GEO-RETURN TRANSFER ORBIT
- PHASING ORBIT AT 260 NMI

REENTRY STATE

$R = 400,000$ FT
 $V = 33,828.6$ FT/SEC
 $\gamma = -4.973^\circ$
 $LAT = 4.985^\circ S$
 $LONG = 9.244^\circ W$
 $AZIMUTH = 60.612^\circ$

TARGETED EXIT CONDITIONS

RADIUS-AT-APOGEE = 260 NMI

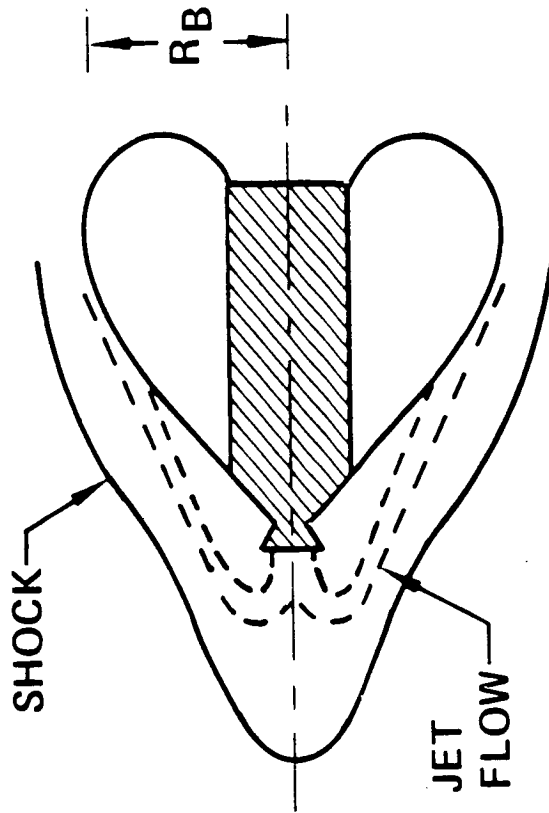


Figure 6.2.2-1. Ballute Using Jet Counterflow in Guidance Analysis

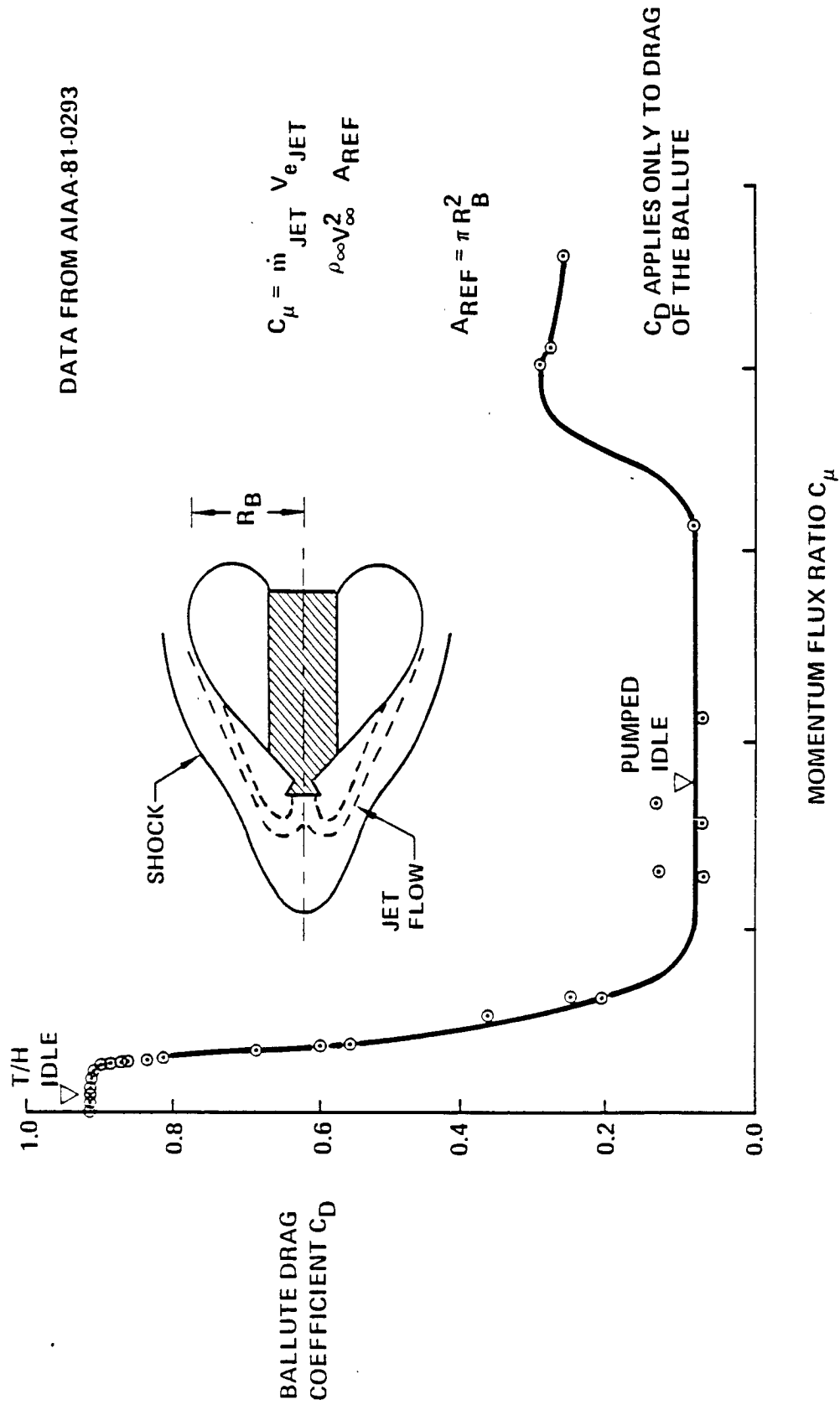


Figure 6.2.2-2 Effect of Engine Modulation on Ballute Drag

allowed only one cycle of the pump. The control variables for the guidance algorithm were the time after reentry to turn the pump on and the time to turn it off. The only drag modulation was accomplished by changing the engine momentum flux level. To maintain a constant ballute reference area required active inflation control. For this simulation, a variable diameter exit valve was used instead of the simple two position valve used for the ballute simulations discussed in section 6.2.1. The variable valve area is shown in Figure 6.2.2-3. This Figure also shows the gas inflow, outflow, and total volume. It can be seen that inflow is used to control the ballute volume until perigee. Then the volume control switches to outflow for control. There is a small variation in the ballute volume because of lags in the inflation system.

The altitude and velocity along the STS-2 aeromaneuver are shown in Figures 6.2.2-4 and 6.2.2-5. The velocity profile shows the effect of the order of magnitude change in C_D when the pump is turned on and off. The commanded and actual drag profiles are shown in Figure 6.2.2-6. The profiles for STS-4 and STS-6 show that the guidance algorithm did not command the pump to shut off before atmospheric exit. These profiles had accumulated more drag than desired. The projected velocity errors at atmospheric exit are shown in Figure 6.2.2-7.

A comparison of the 50 ft turndown ballute and the ballute using jet counterflow was previously shown in Figure 6.2.1-9. It is shown for the jet counterflow ballute that guidance can significantly reduce the propulsive correction required to reach a 260 nm apogee. It is also shown that jet counterflow gives comparable control to the turndown ballute. A combination of turndown and jet counterflow could give capability to respond to very large sources of error.

6.2.3 Low L/D OTV's

The application of the guidance algorithm to the lifting OTV concepts required a change in the control and constraint variables. The OTV's with lift have the capability to correct for out-of-plane error and to execute an out of plane maneuver. For the following guidance analysis, it was assumed that the total OTV plane change was accomplished propulsively at GEO. During the aeromaneuver, the OTV was constrained to exit the atmosphere in the same orbital plane as at entry. No plane change maneuver was planned.

The constraints applied at atmospheric exit were that the orbit should have an altitude of apogee of 260 nm and have an inclination and right ascension of the ascending node (RAAN) the same as at entry. For the following guidance trades the inclination was 28.5° and the RAAN was 0° .

BALLUTE INFLATION CONTROL*

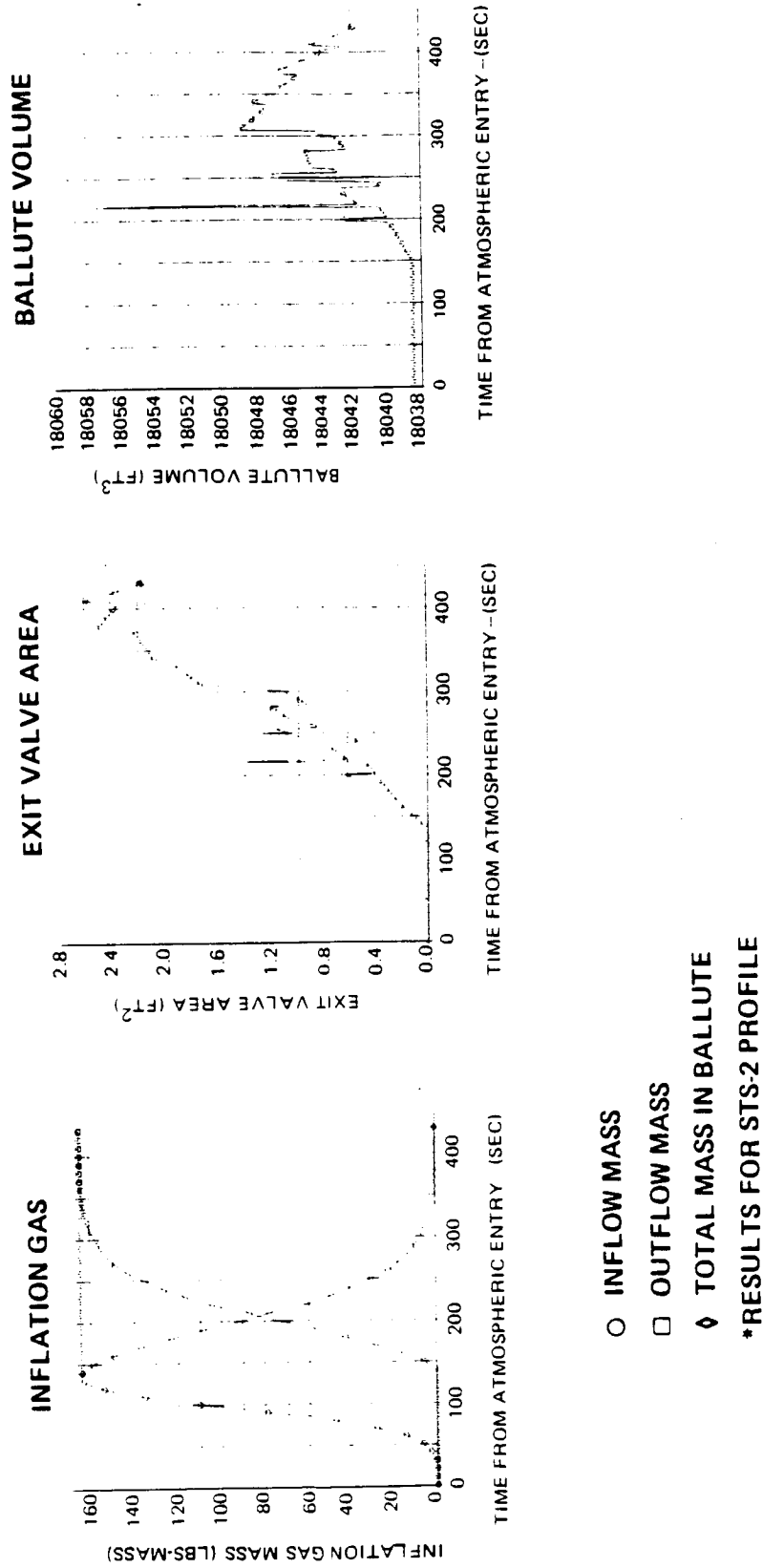


Figure 6.2.2-3 Ballute OTV Inflation Control Using Jet Counterflow

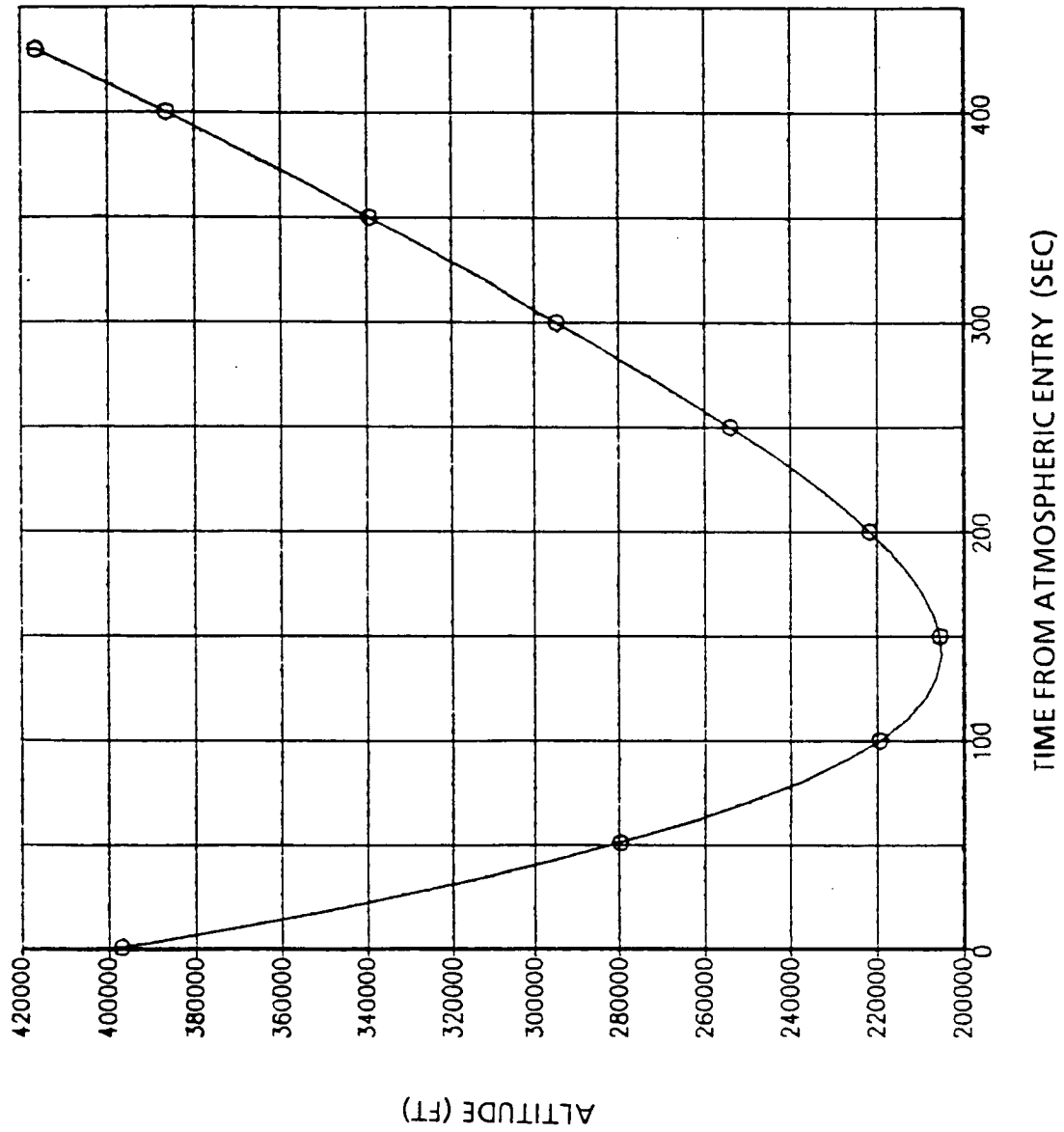


Figure 6.2.2.4. Altitude Profile for Ballute Using Jet Counterflow

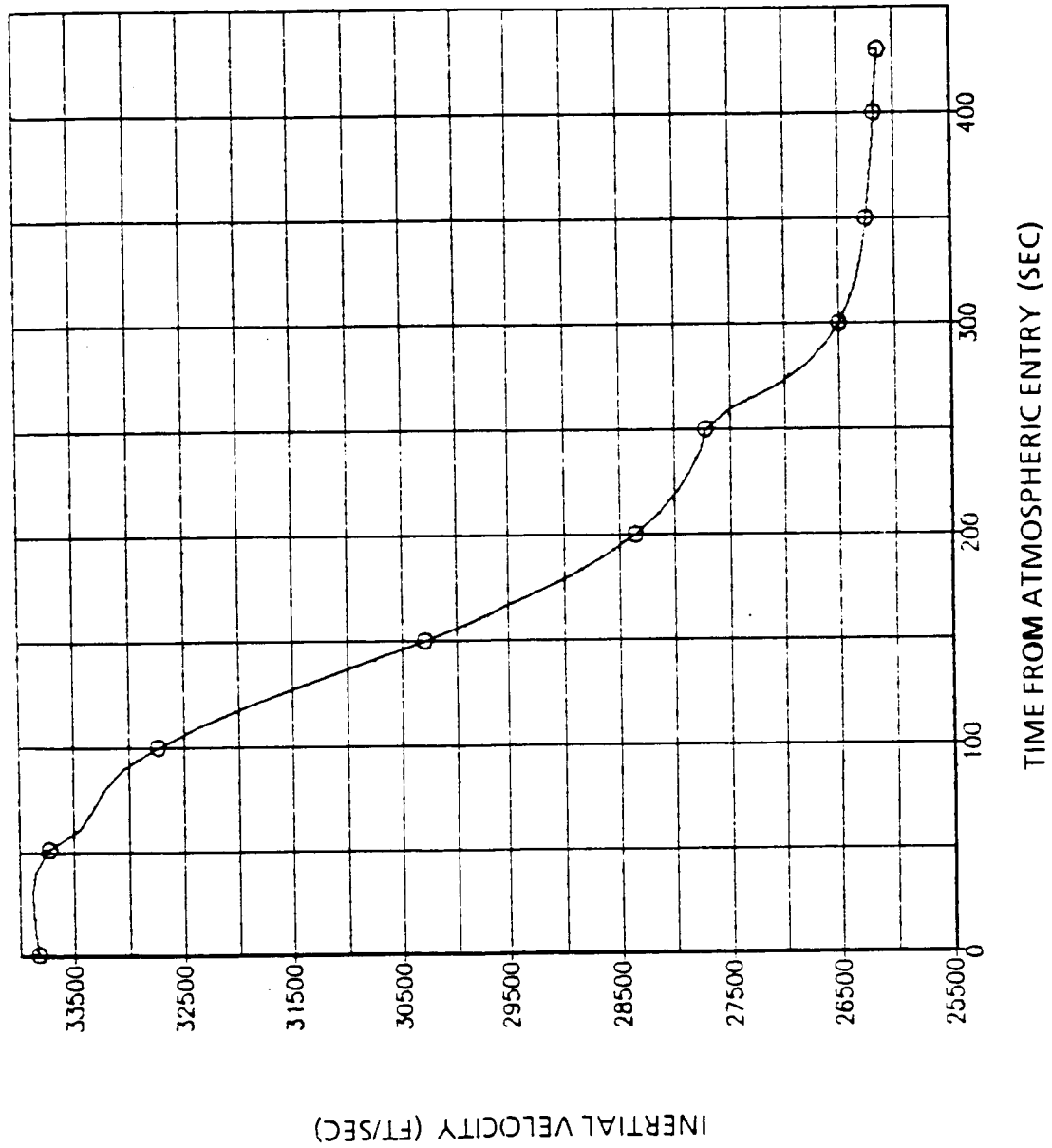


Figure 6.2.2-5. Velocity Profile for Ballute Using Jet Counterflow

COMMANDED AND ACTUAL DRAG PROFILES

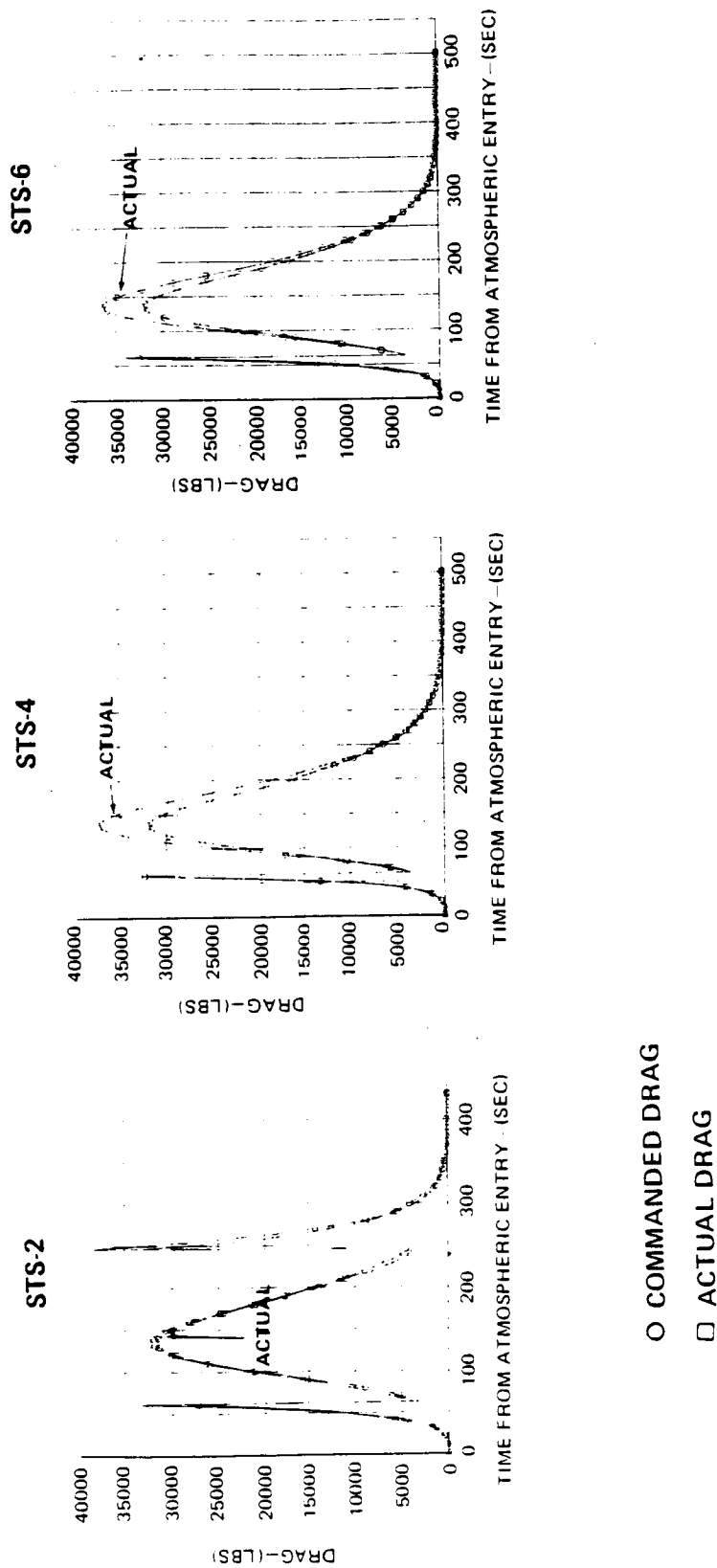
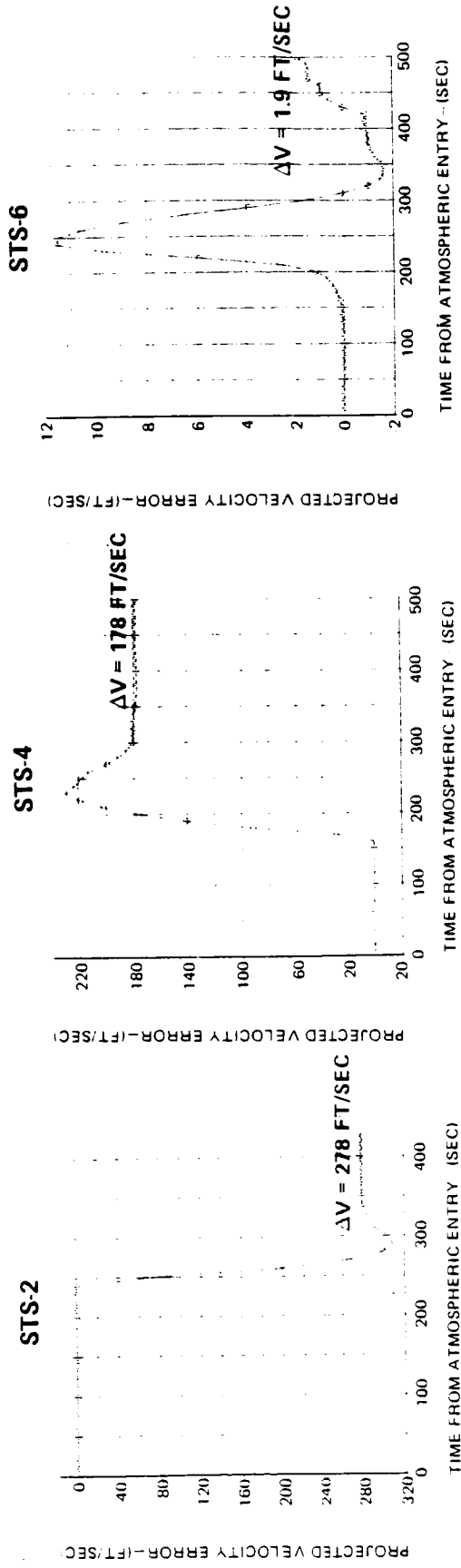


Figure 6.2.2-6 Ballute OTV Drag Profiles Using Jet Counterflow

PROJECTED VELOCITY ERROR AT ATMOSPHERIC EXIT



VELOCITY ERROR AT ATMOSPHERIC EXIT IS THE PROPULSIVE
 ΔV REQUIRED TO MEET THE RADIUS-OF-APOGEE CONSTRAINT
 WITHIN 1000 FT.

Figure 6.2.2-7 Ballute OTV Velocity Error Using Jet Counterflow

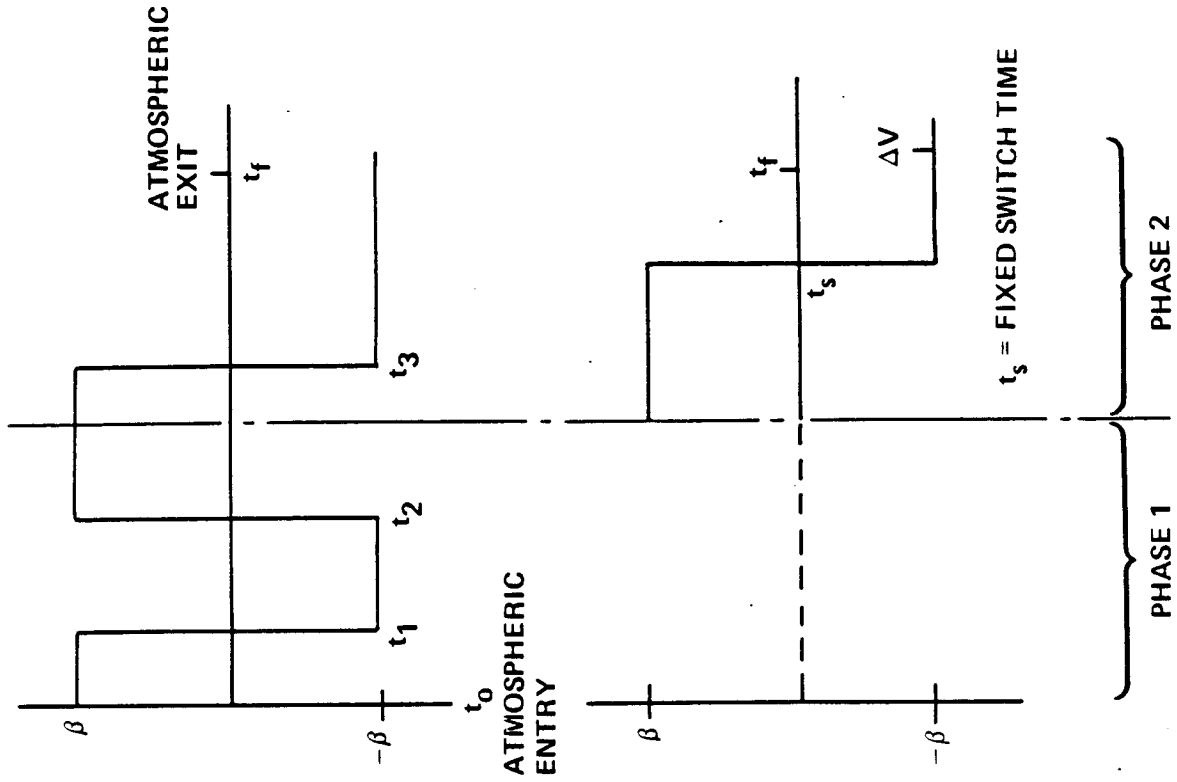
Using the experience gained with Gamma Guidance on the inertial Upper Stage and preliminary simulated low L/D aeromaneuver flights, a two phase application of the guidance algorithm was planned to increase the stability and robustness. In phase one, the control variables were the magnitude of the bank angle and three time variables for execution of bank angle reversals. This set of control variables is used with the three orbit constraints: altitude-of-apogee, inclination, and RAAN. At 160 sec after the start of guidance, phase two begins. At this time the bank angle reversal times are removed as active control variables and are set to the values determined in the last phase one guidance update. During phase two, the control variables are the magnitude of the bank angle and an impulsive ΔV applied in the direction of the velocity vector at atmospheric exit. The only constraint applied during phase two is the altitude-of-apogee constraint. After 160 sec there is little control capability available for changing the orbital plane. Therefore, during phase two, the guidance algorithm concentrates only on attaining the targeted altitude-of-apogee. The guidance command profile for the low L/D vehicle is shown in Figure 6.2.3-1. Guidance updates are performed at 80 sec, then every 10 sec until 160 sec. After 160 sec the updates are performed every 40 sec.

6.2.3.1 Symmetrical Lifting Brake OTV

The vehicle characteristics and entry conditions are shown in Figure 6.2.3.1-1. The assumed vehicle characteristics for the lifting brake were an entry weight of 20,209 lbs. and reference area of 1,256.6 ft². Three different L/D ratios were simulated. These were for the vehicle flying at an angle-of-attack of $\delta=10^\circ$, 20° , and 30° . The vehicle is trimmed at a constant angle-of-attack by a designed c.g. offset. The L/D ratios for each of these were 0.12, 0.23, and 0.32, respectively.

The lifting brake aeromaneuver was simulated through the STS-2, -4, and -6 density profiles at each of the three angles-of-attack. The STS-2 profile was again the most difficult to fly. The results which follow are all for flights through the STS-2 profile.

The altitude and velocity profiles for the flight at $\delta=10^\circ$ are shown in Figures 6.2.3.1-2 and -3. The solid lines are for the actual flight with guidance updates. The initial guidance command (dashed) with no guidance update and the actual flight profile (solid) are shown in Figure 6.2.3.1-4 for L/D=0.12 through the STS-2 atmosphere. The 451.9 ft/sec velocity impulse required to correct to a 260 nm apogee is indicated in Figure 6.2.3.1-3. The Keplerian inclination and RAAN of the atmospheric trajectory are shown in Figures 6.2.3.1-5 and -6. The dashed lines indicate the path which would have



PHASE 1:

CONTROL VARIABLES:

- BANK ANGLE MAGNITUDE, β
- 3 BANK REVERSAL TIMES, t_1, t_2, t_3

CONSTRAINTS

- RADIUS-OF-APOGEE
- INCLINATION
- RAAN

PHASE 2:

CONTROL VARIABLES:

- BANK ANGLE, β

- ΔV

CONSTRAINT

- RADIUS-OF-APOGEE

Figure 6.2.3-1. Guidance Problem Formulation for Low L/D

- REENTRY WEIGHT = 20,209 LBS
- REFERENCE AREA = 1,256.6 FT²
- L/D = 0.12, 0.23, 0.32
- NOMINAL GEO-RETURN TRANSFER ORBIT
- PHASING ORBIT AT 260 NMI

REENTRY STATE

R = 400,000 FT
 V = 33,828.6 FT/SEC
 γ = DEPENDS ON L/D
 LAT = 4.985°S
 LONG = 9.244°W
 AZIMUTH = 60.612°

TARGETED EXIT CONDITIONS

RADIUS-AT-APOGEE = 260 NMI
 INCLINATION = 28.5°
 RAAN = 0°

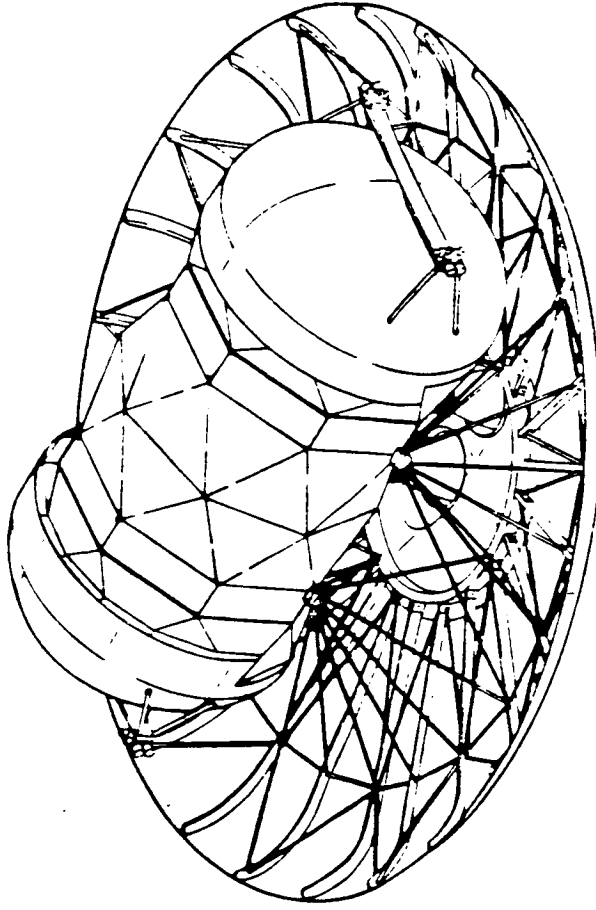


Figure 6.2.3.1-1. Lifting Brake Used in Guidance Analysis

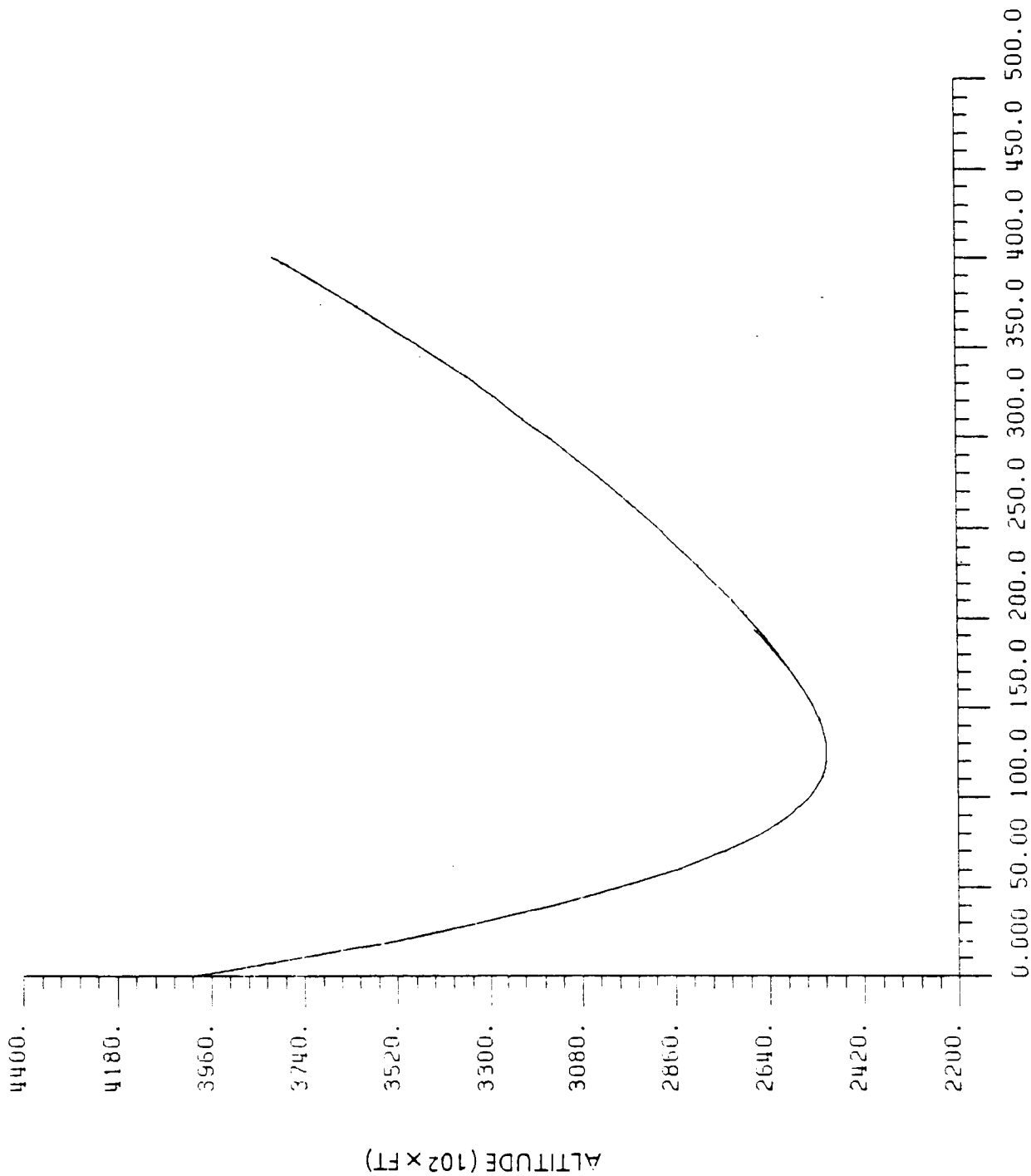


Figure 6.2.3.1-2. Altitude Profile for the Lifting Brake at $\alpha = 10^\circ$

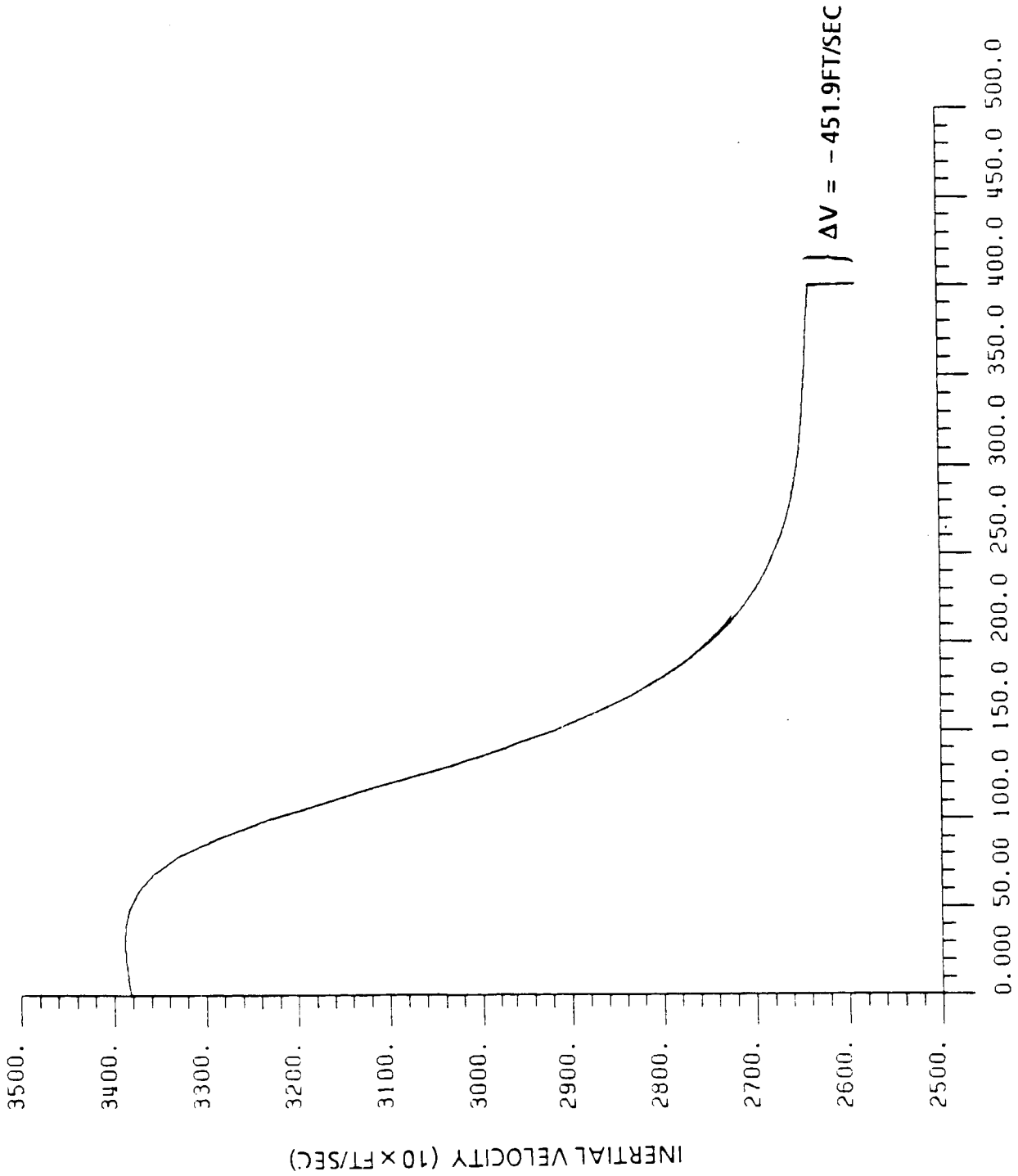


Figure 6.2.3.1-3. Velocity Profile for the Lifting Brake at $\alpha = 10^\circ$

OTV-1685

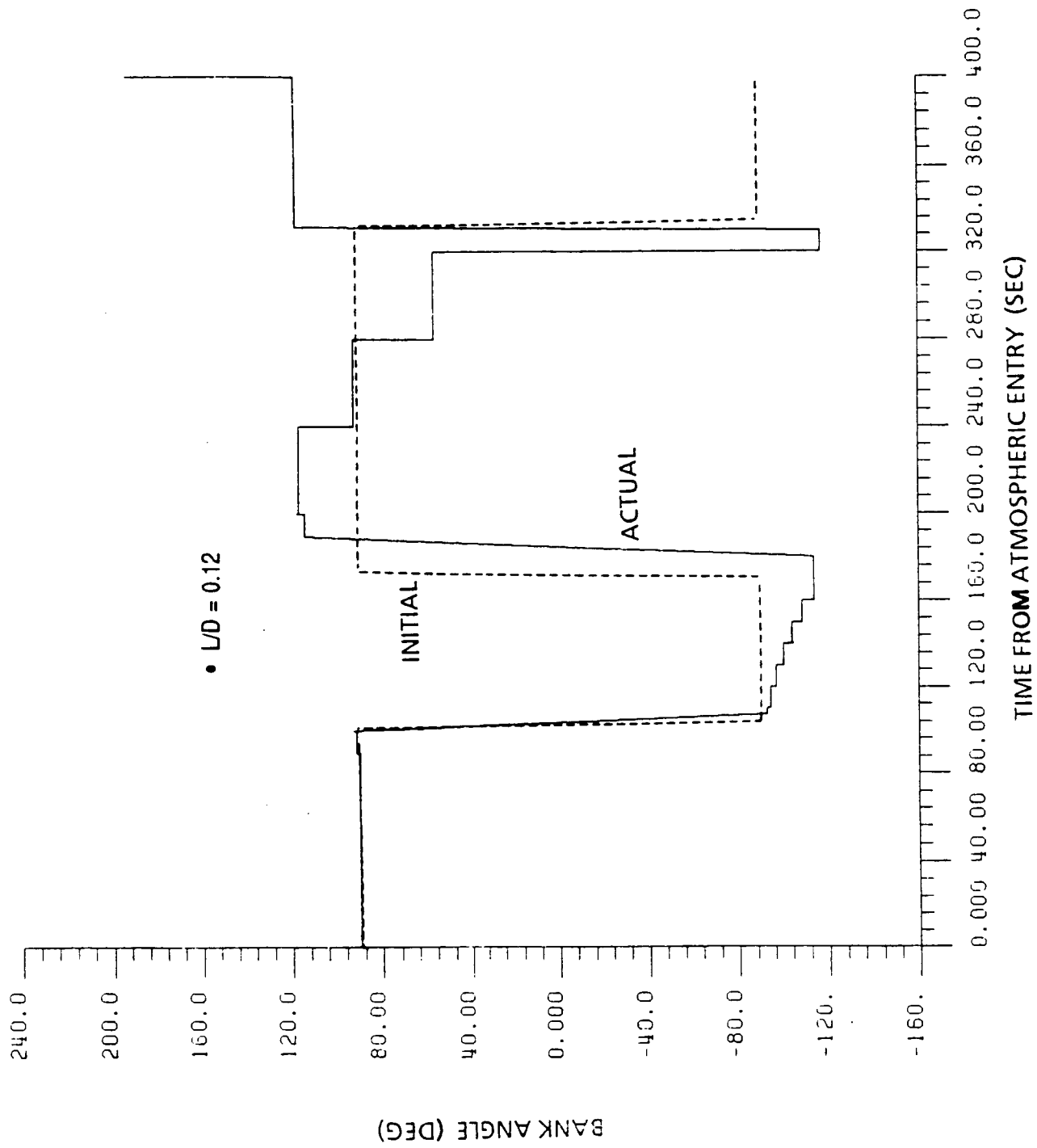


Figure 6.2.3.1-4. Initial Command and Actual Bank Angle Profile for the Lifting Brake at $\alpha = 10^\circ$

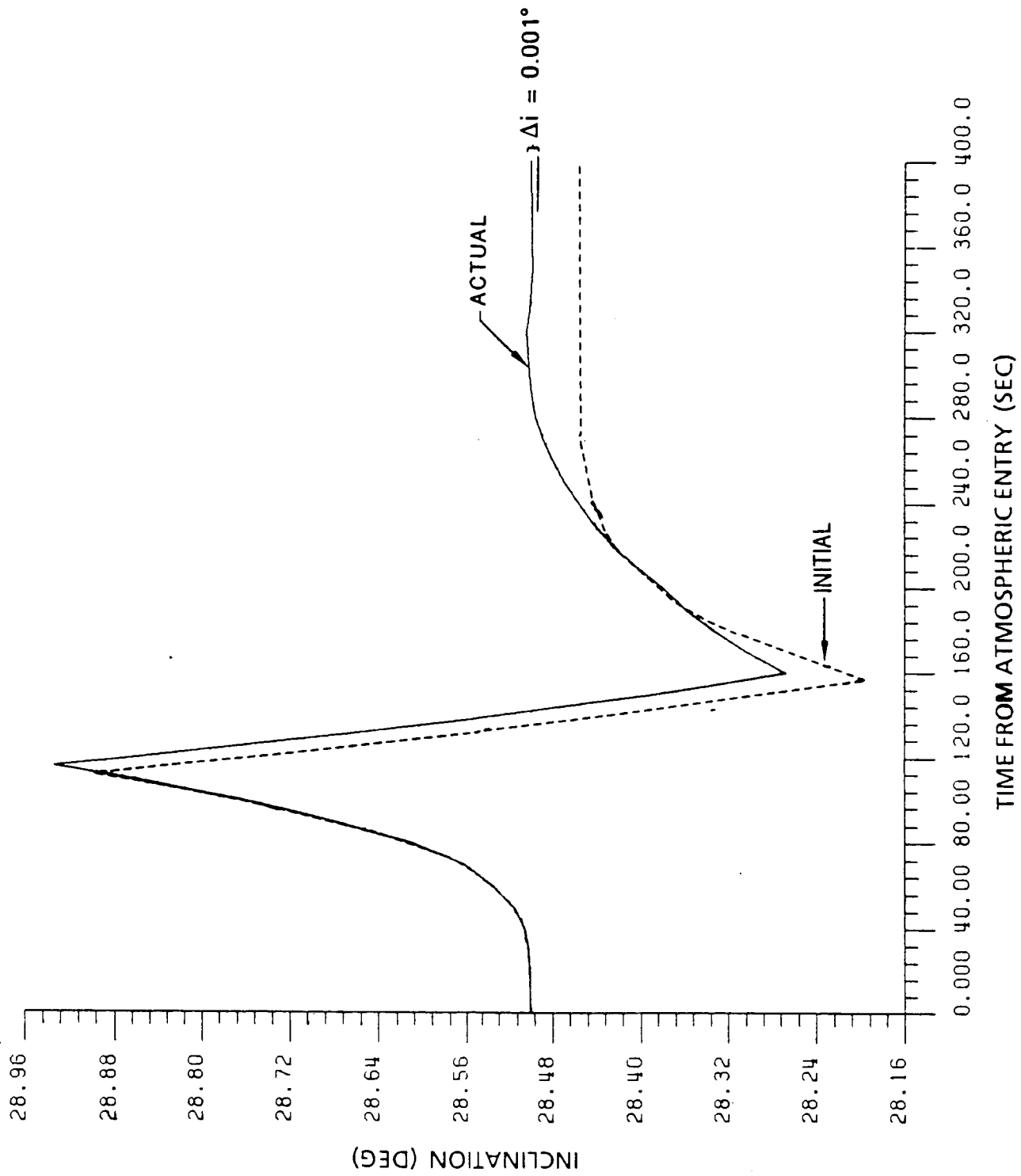


Figure 6.2.3.1-5. Inclination Profile for the Lifting Brake at $\alpha = 10^\circ$

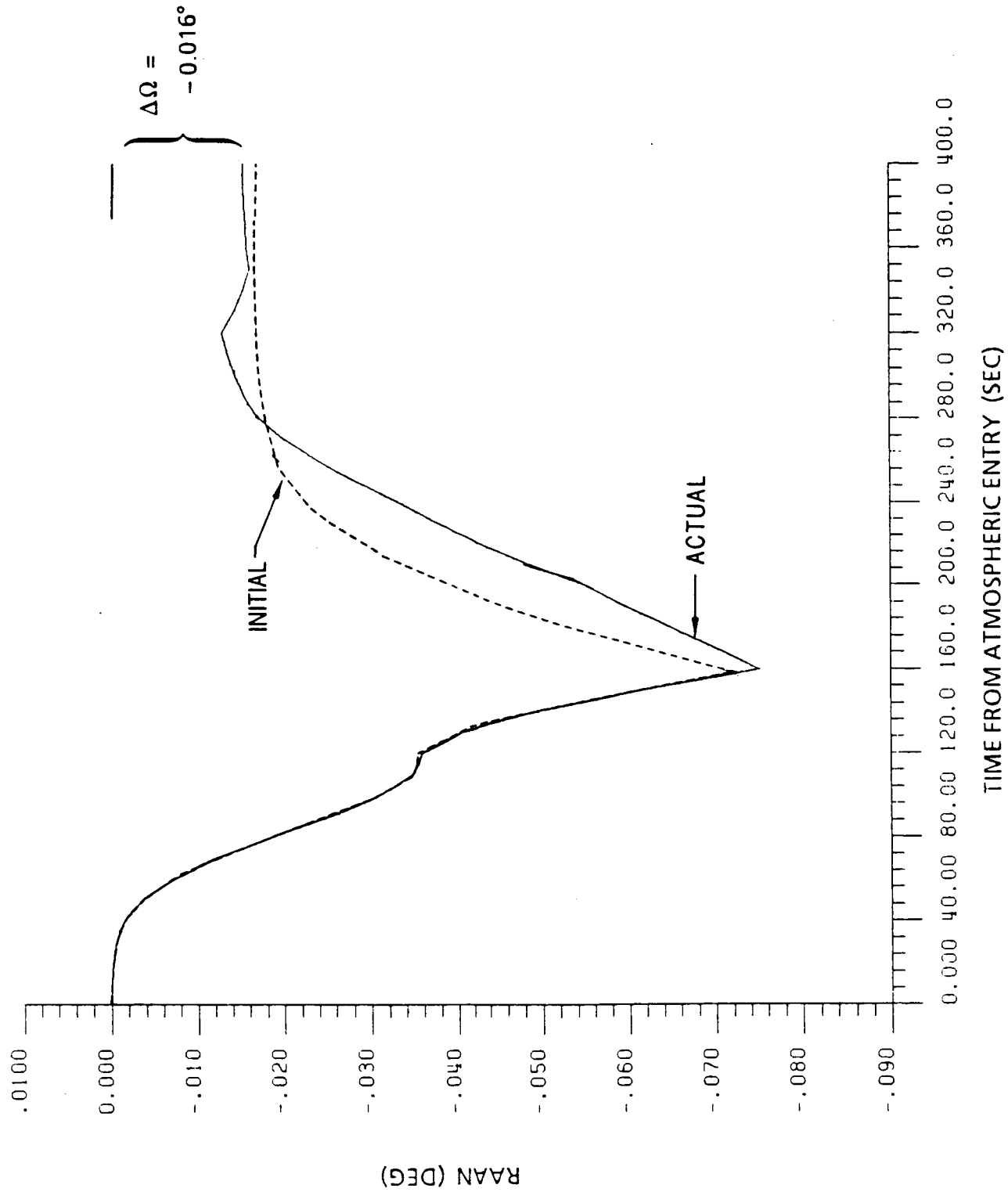


Figure 6.2.3.1-6. RAAN Profile for the Lifting Brake at $\alpha = 10^\circ$

been flown with no guidance update during the aeromaneuver. The solid lines indicate the actual path flown. The errors in inclinations and RAAN are indicated on the graphs.

Figure 6.2.3.1-7 and -8 show the altitude and velocity for the $\delta=20^\circ$ L/D=0.23 trajectory through the STS-2 atmosphere. The -532.9 ft/sec velocity impulse required to reach the 260 nm apogee is indicated on Figure 6.2.3.1-8. The initial guidance command (dashed) and actual flight profile for the L/D=0.23 lifting brake are shown in Figure 6.2.3.1-9. The inclination and RAAN of the trajectory are shown in Figures 6.2.3.1-10 and -11 with the plane errors at atmospheric exit indicated.

The final configuration of the lifting brake examined was for an angle-of-attack of 30° or L/D=0.32. The trajectory is shown in Figures 6.2.3.1-12 and -13 with the velocity error of -611.8 ft/sec indicated. The bank angle profile, inclination and RAAN profiles are shown in Figures 6.2.3.1-14, -15, and -16.

6.2.3.2 Shaped Brake OTV

The shaped brake OTV investigated had the characteristics shown in figure 6.2.3.2-1. This vehicle was flown with the same constraints and control variables as the lifting brake. The altitude and velocity of the aeromaneuver trajectory through the STS-2 atmosphere are shown in Figures 6.2.3.2-2 and -3. The velocity error at exit of -494.0 ft/sec is indicated on the velocity graph. The shaped brake bank angle commands are shown in Figure 6.2.3.2-4. The dashed line is the initial guidance command. The solid line is the actual bank angle profile flown through the STS-2 atmosphere. Figure 6.2.3.2- 5 and -6 show the inclination and RAAN for flight through the STS-2 atmosphere without guidance updates (dashed) and with guidance updates (solid). The plane errors at atmospheric exit are marked on the graphs. Further analysis of this concept for other L/D ratios was not completed because the shaped brake was eliminated from consideration based on other criteria.

6.2.3.3 Low L/D OTV Summary

The low L/D guidance algorithm did not use an atmospheric density predictor because only three perturbed density profiles were flown and because the vehicle sensed a profile which was symmetric with altitude on the downward and upward legs of the aeropass. It was felt that any predictors used in this limited set of runs would be unduly biased to the data set available. The guidance algorithm used a Standard-62 atmosphere for the internal guidance predictions. The guidance updates were based entirely on the sensed difference between the navigation state (position and velocity through perturbed atmosphere) and the state predicted using the Standard-62 atmosphere. As more

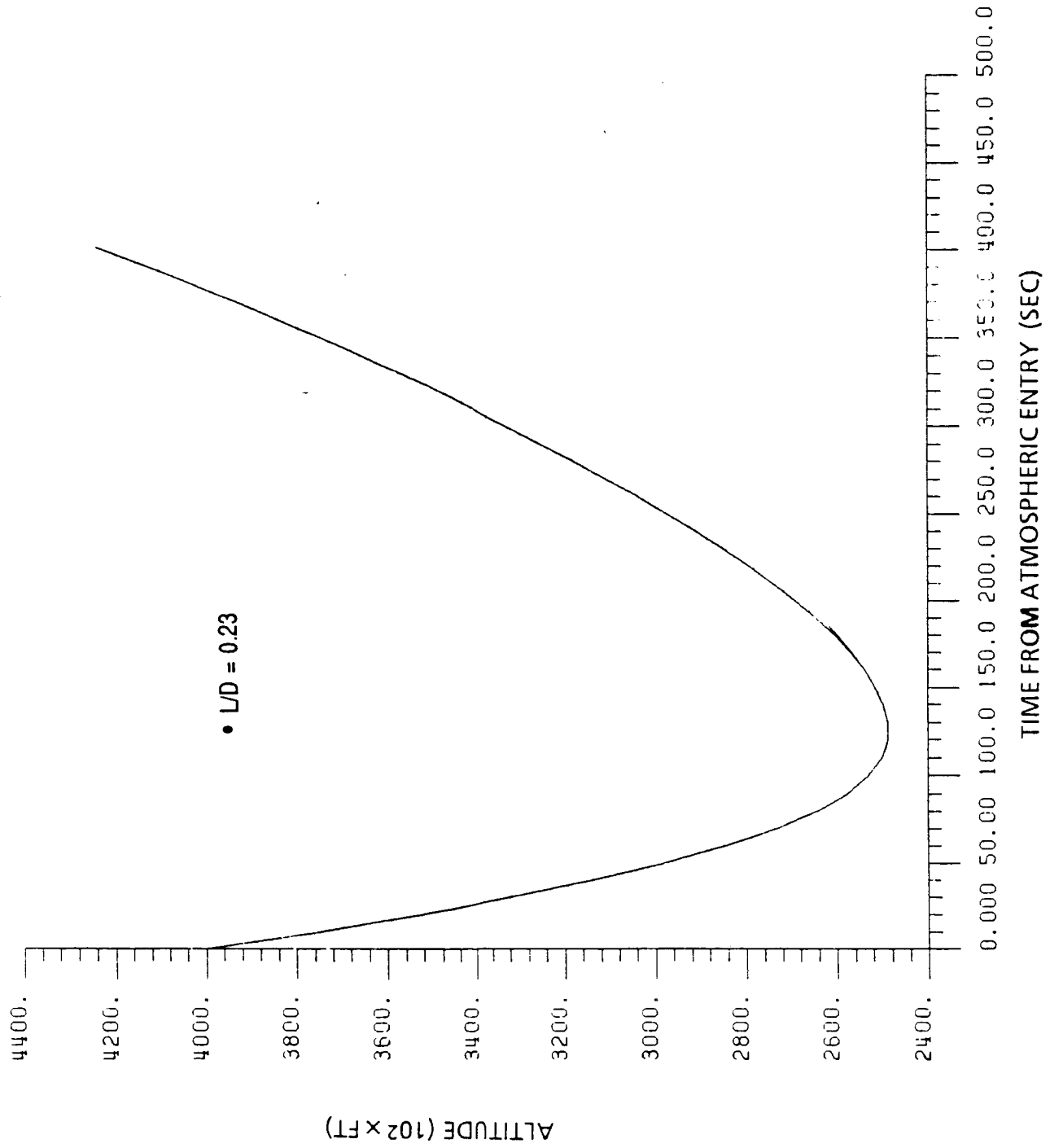


Figure 6.2.3.1-7. Altitude Profile for the Lifting Brake at $\alpha = 20^\circ$

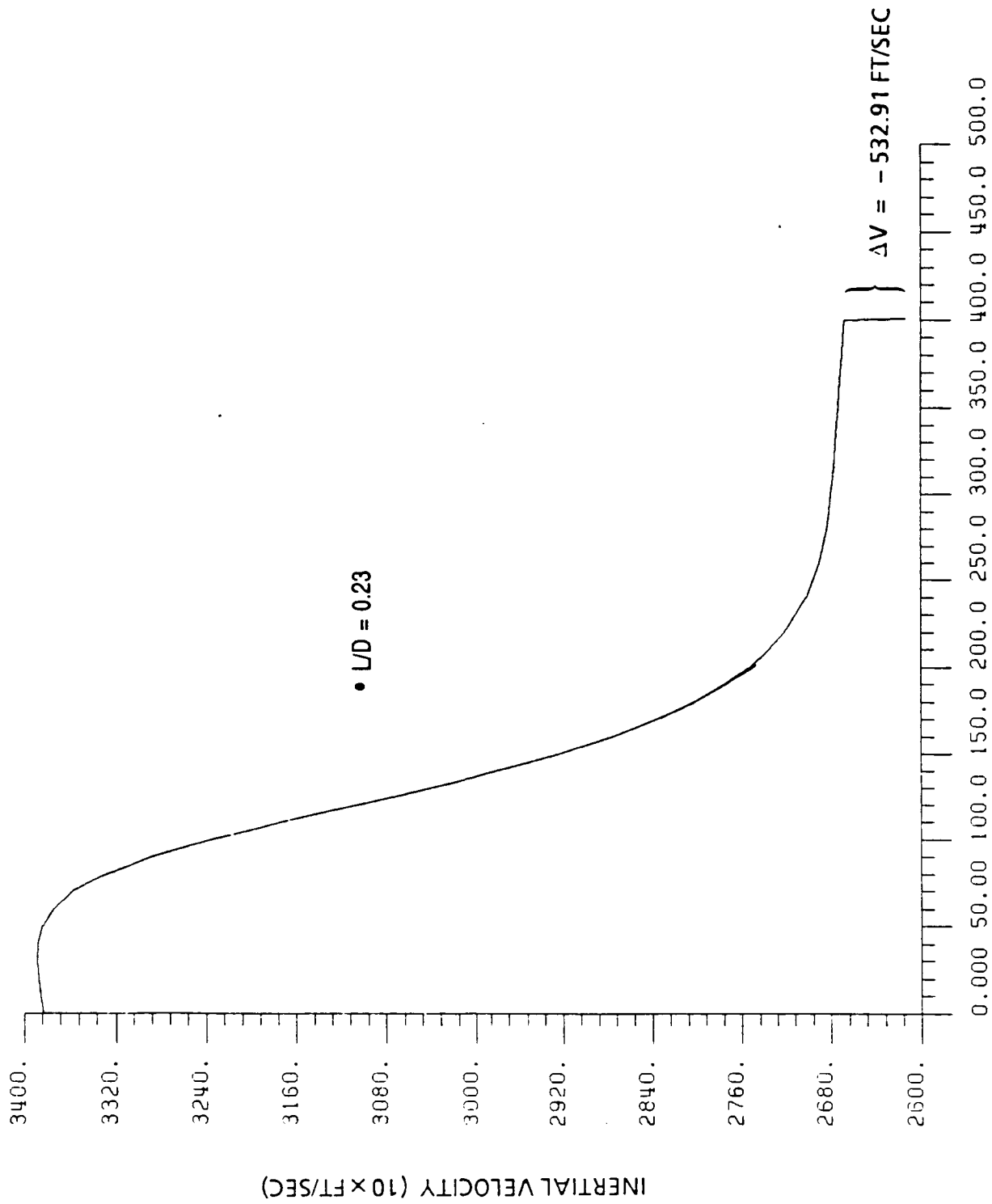


Figure 6.2.3.1-8. Velocity Profile for the Lifting Brake at $\alpha = 20^\circ$

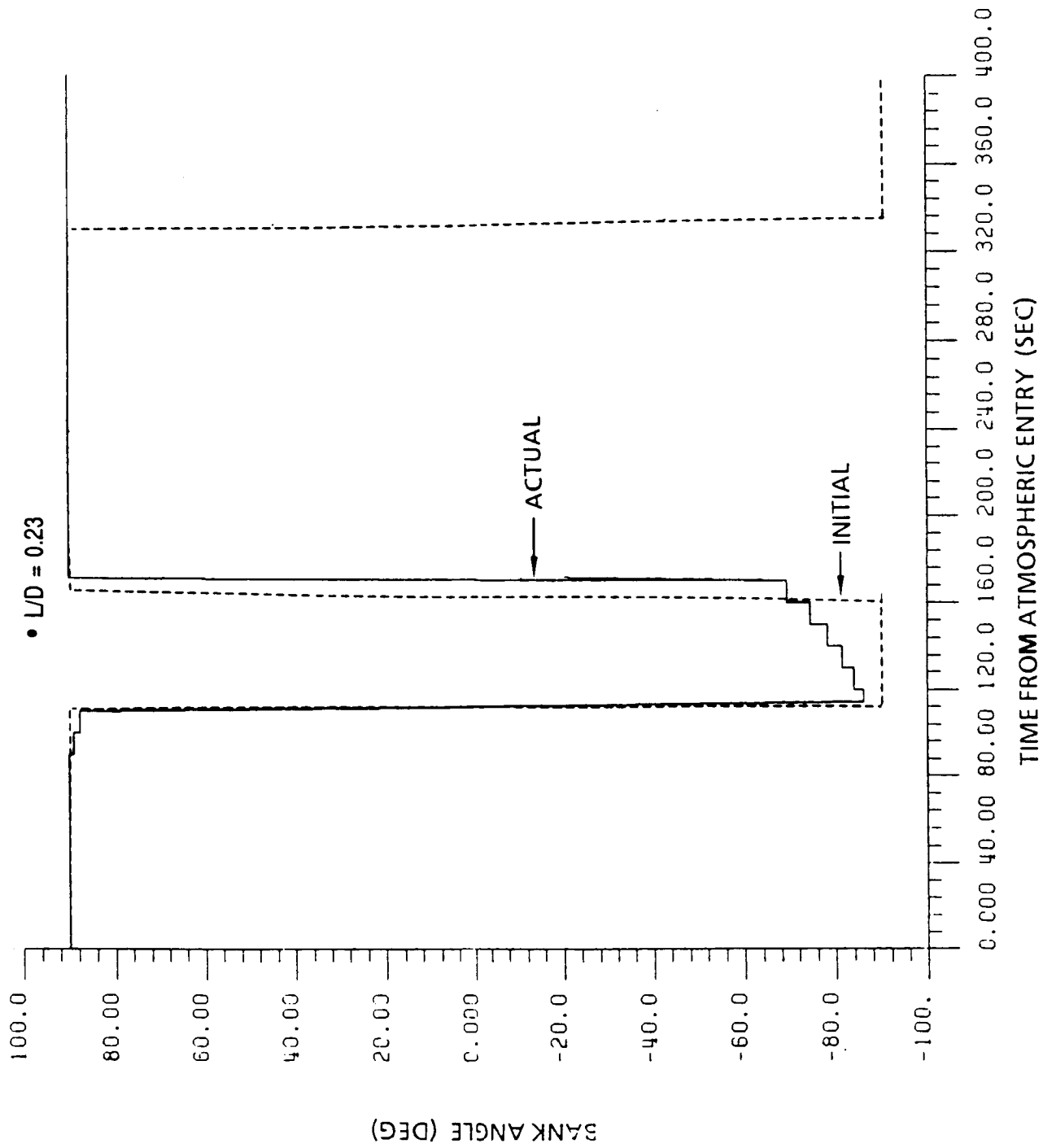
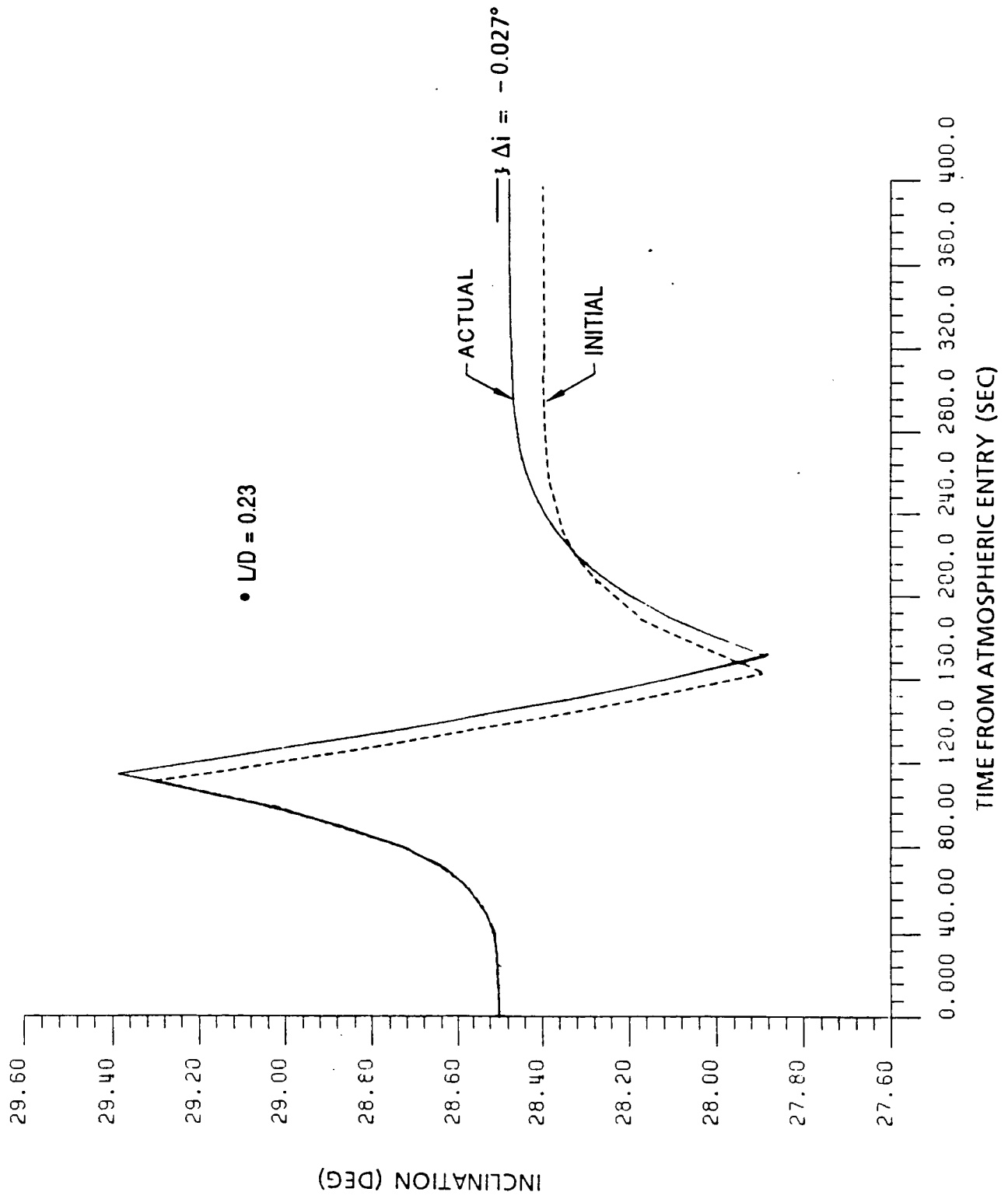


Figure 6.2.3.1-9. Initial Command and Actual Bank Angle Profile for the Lifting Brake at $\alpha = 20^\circ$

Figure 6.2.3.1-10. Inclination Profile for the Lifting Brake at $\alpha = 20^\circ$

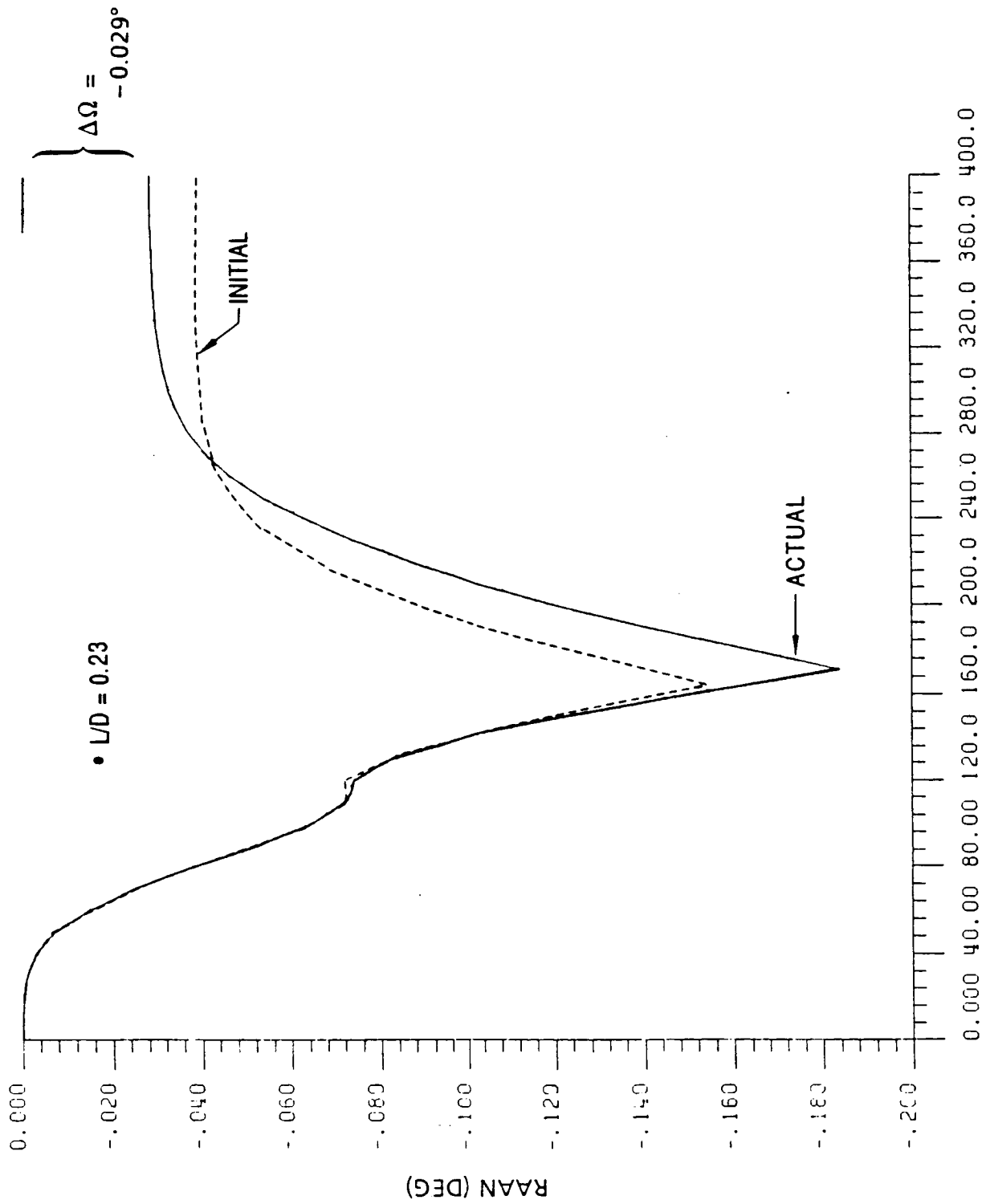


Figure 6.2.3.1-11. RAAN Profile for the Lifting Brake at $\alpha = 20^\circ$

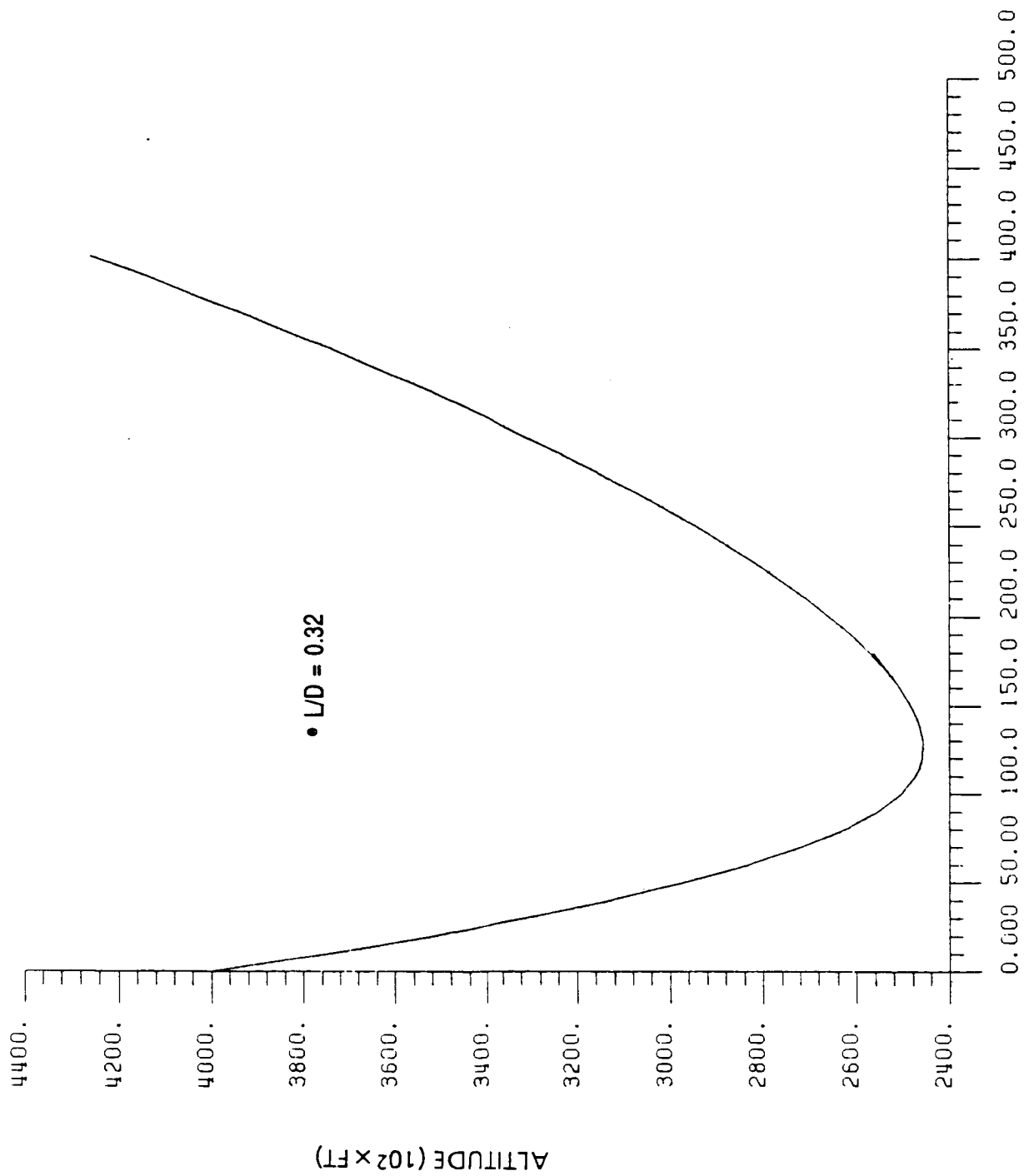


Figure 6.2.3.1-12. Altitude Profile for the Lifting Brake at $\alpha = 30^\circ$

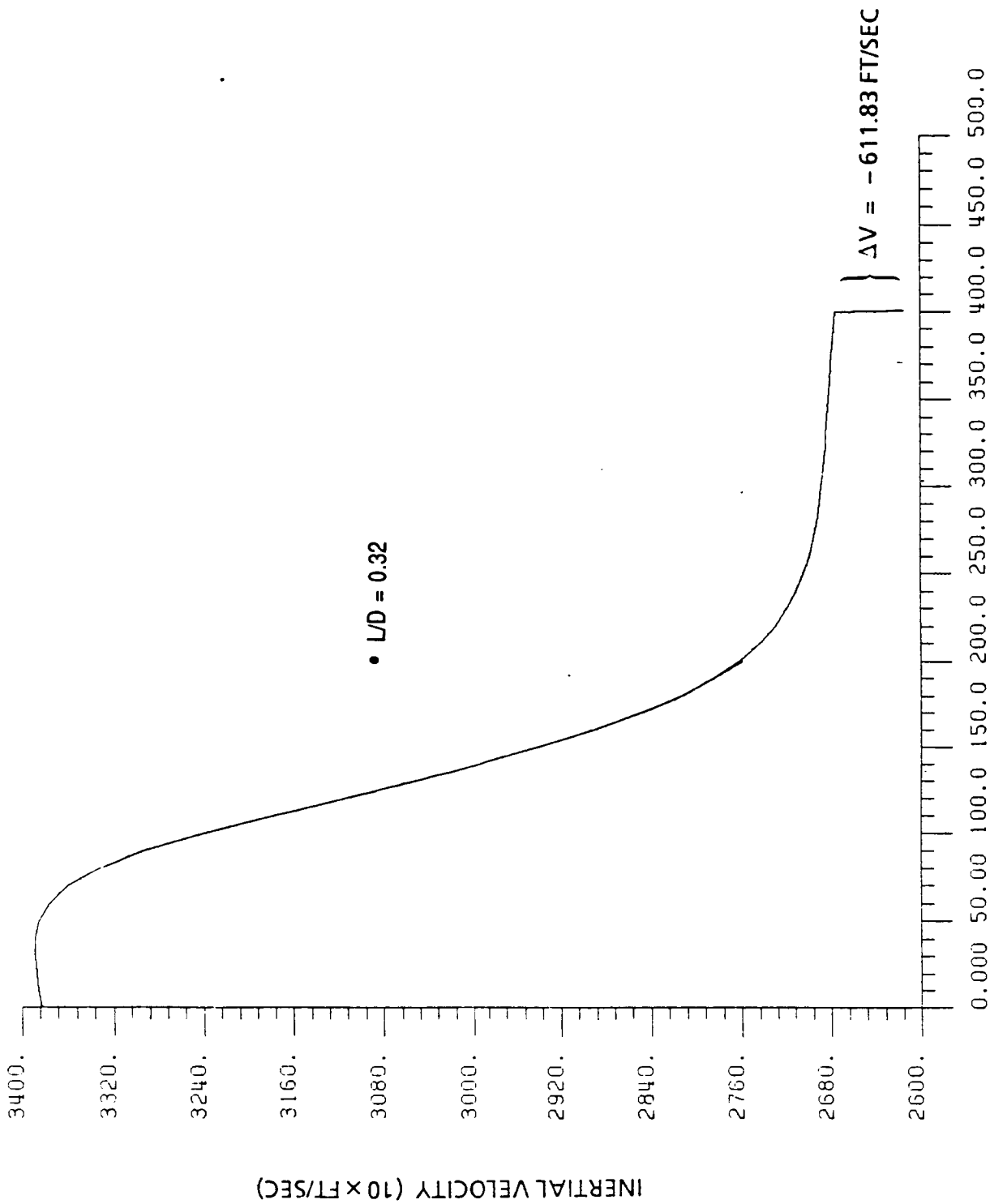


Figure 6.2.3.1-13. Velocity Profile for the Lifting Brake at $\alpha = 30^\circ$

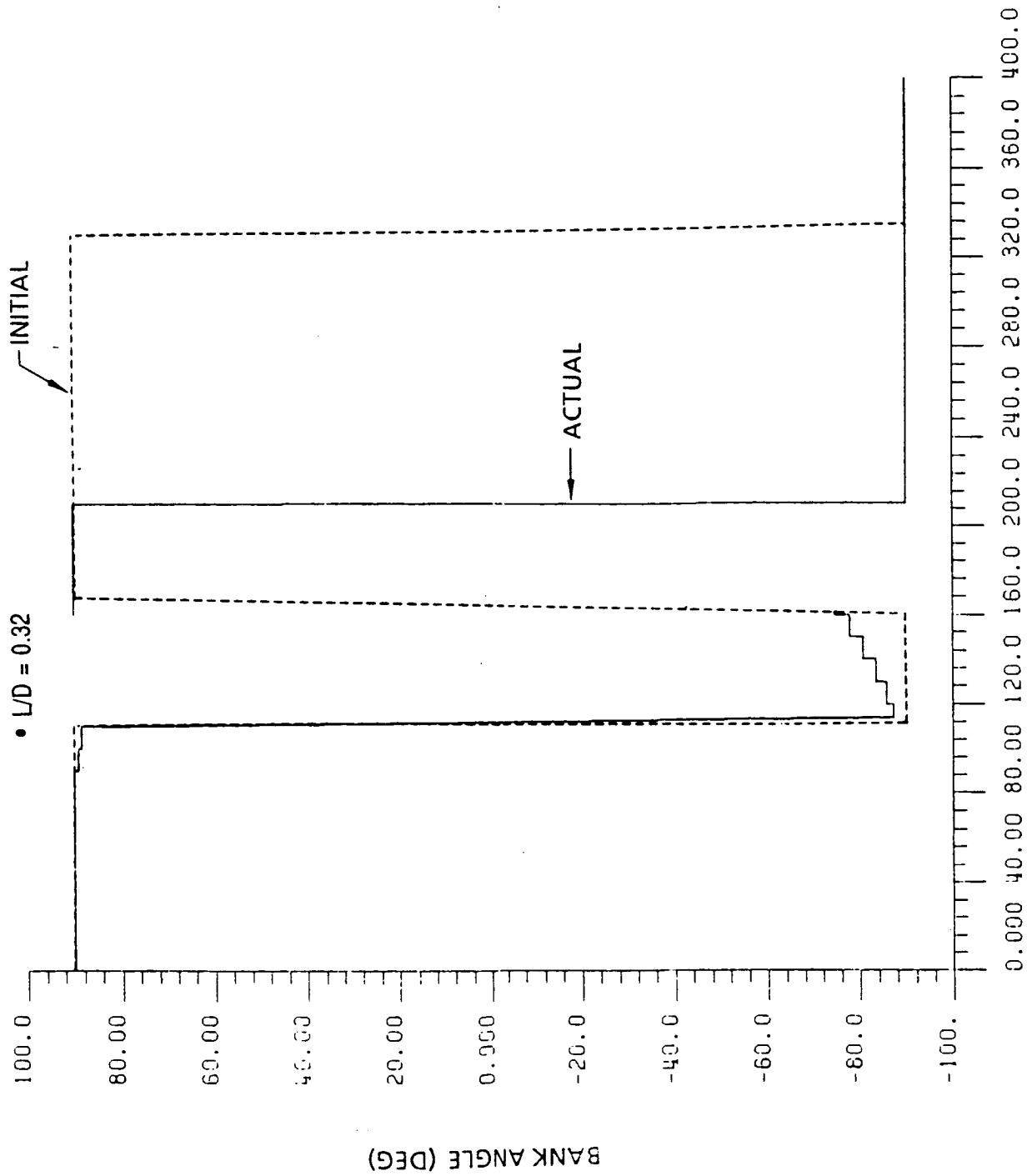


Figure 6.2.3.1-14. Initial Command and Actual Bank Angle Profile for the Lifting Brake at $\alpha = 30^\circ$

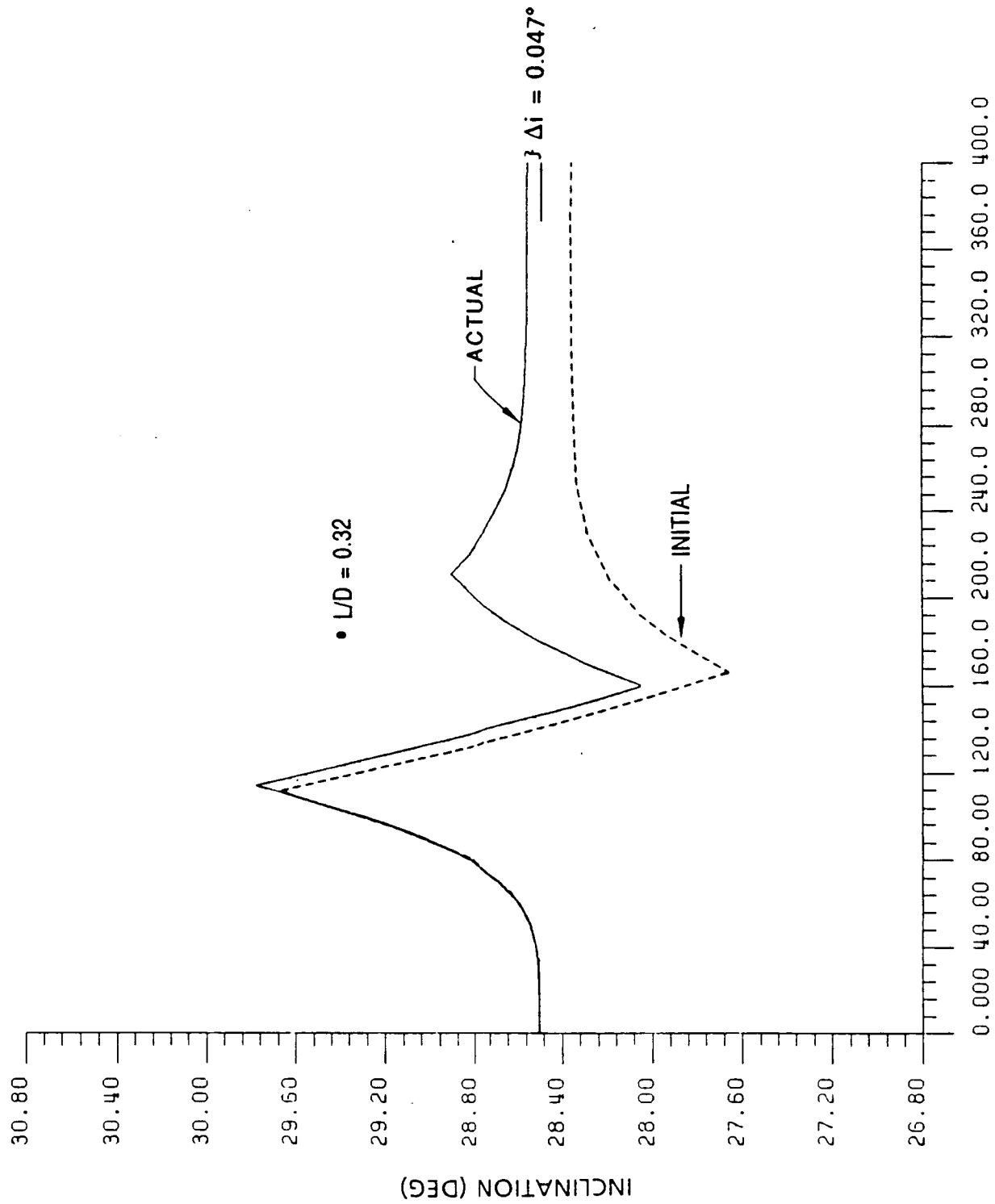


Figure 6.2.3.1-15. Inclination Profile for the Lifting Brake at $\alpha = 30^\circ$

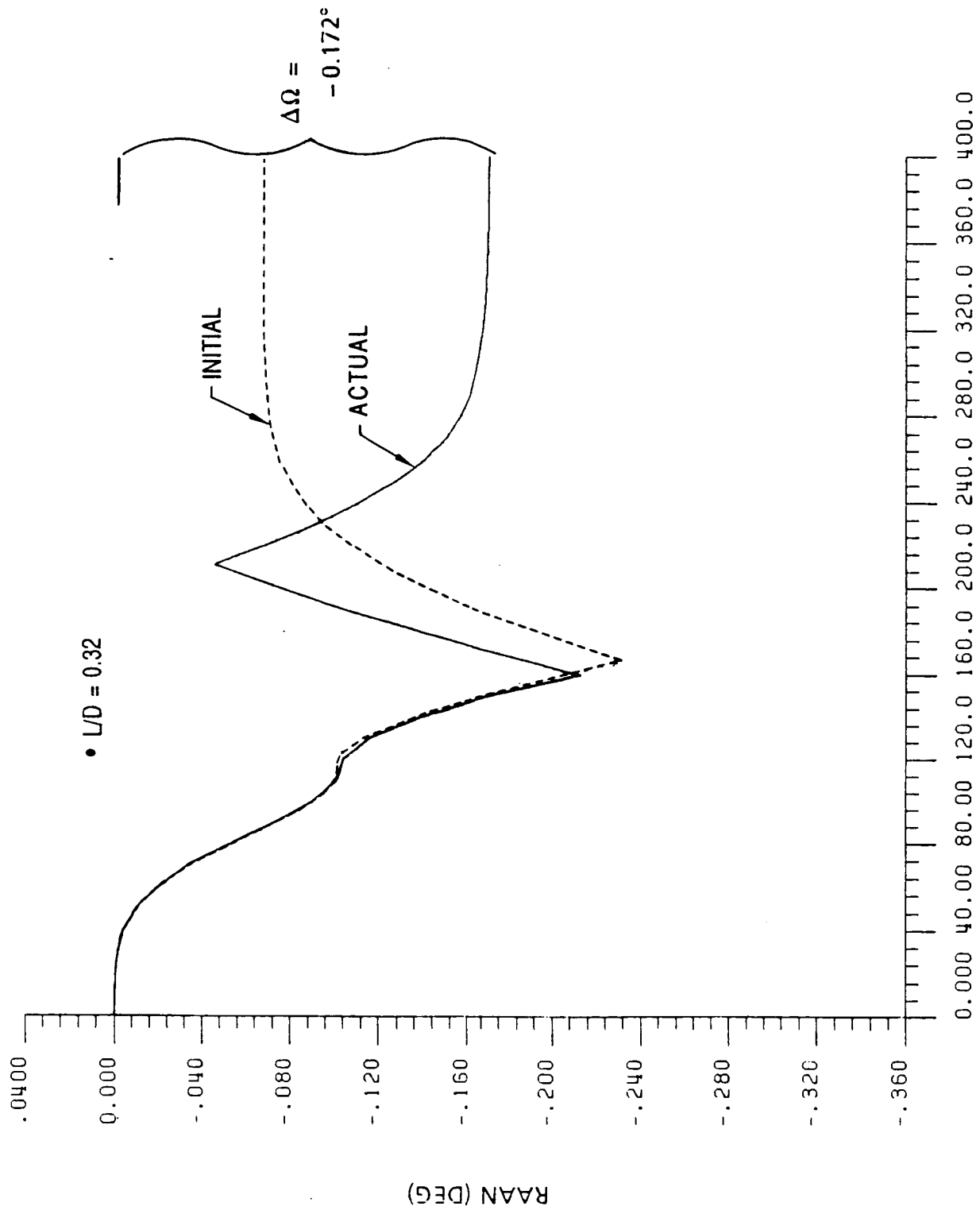


Figure 6.2.3.1-16. RAAN Profile for the Lifting Brake at $\alpha = 30^\circ$

- REENTRY WEIGHT = 22,417 LBS
- REFERENCE AREA = 1,256.6 FT²
- L/D = 0.203
- NOMINAL GEO-RETURN TRANSFER ORBIT
- PHASING ORBIT AT 260 NMI

REENTRY STATE

R = 400,000 FT
 V = 33,828.6 FT/SEC
 $\gamma = -4.427^\circ$
 LAT = 4.985°S
 LONG = 9.244°W
 AZIMUTH = 60.612°

TARGETED EXIT CONDITIONS

RADIUS-OF-APOGEE=260 NMI
 INCLINATION = 28.5°
 RAAN = 0°

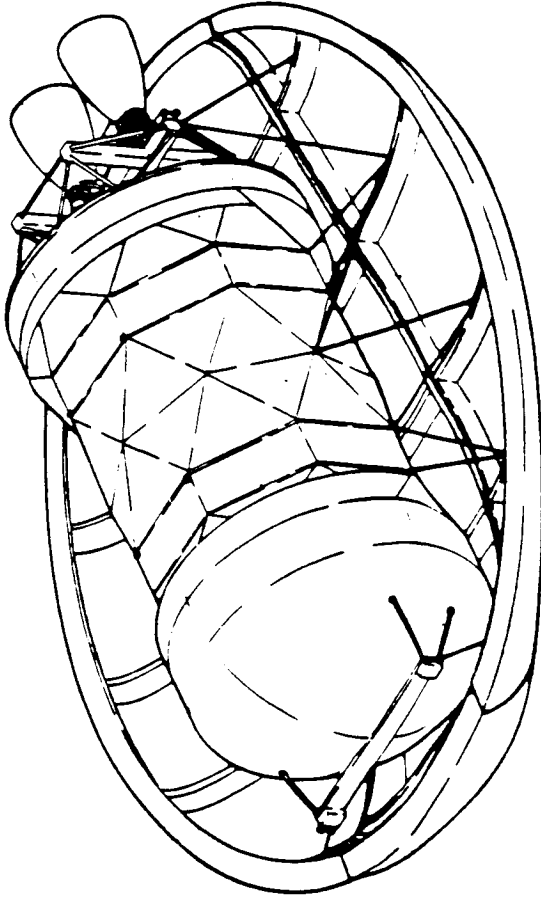


Figure 6.2.3.2-1. Shaped Brake Used in Guidance Analysis

SHAPED BRAKE, STS-2N

• $L/D = 0.203$

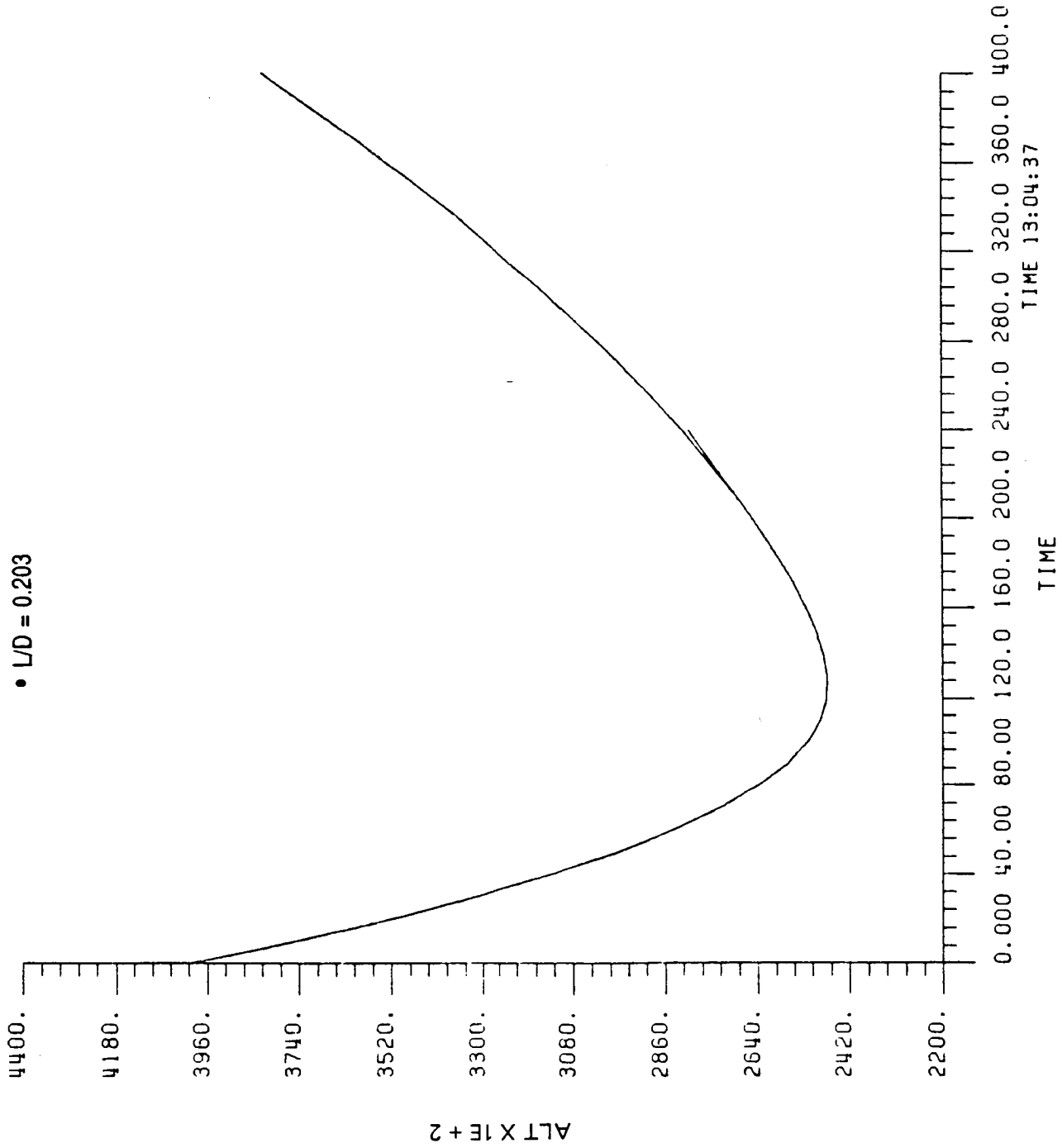
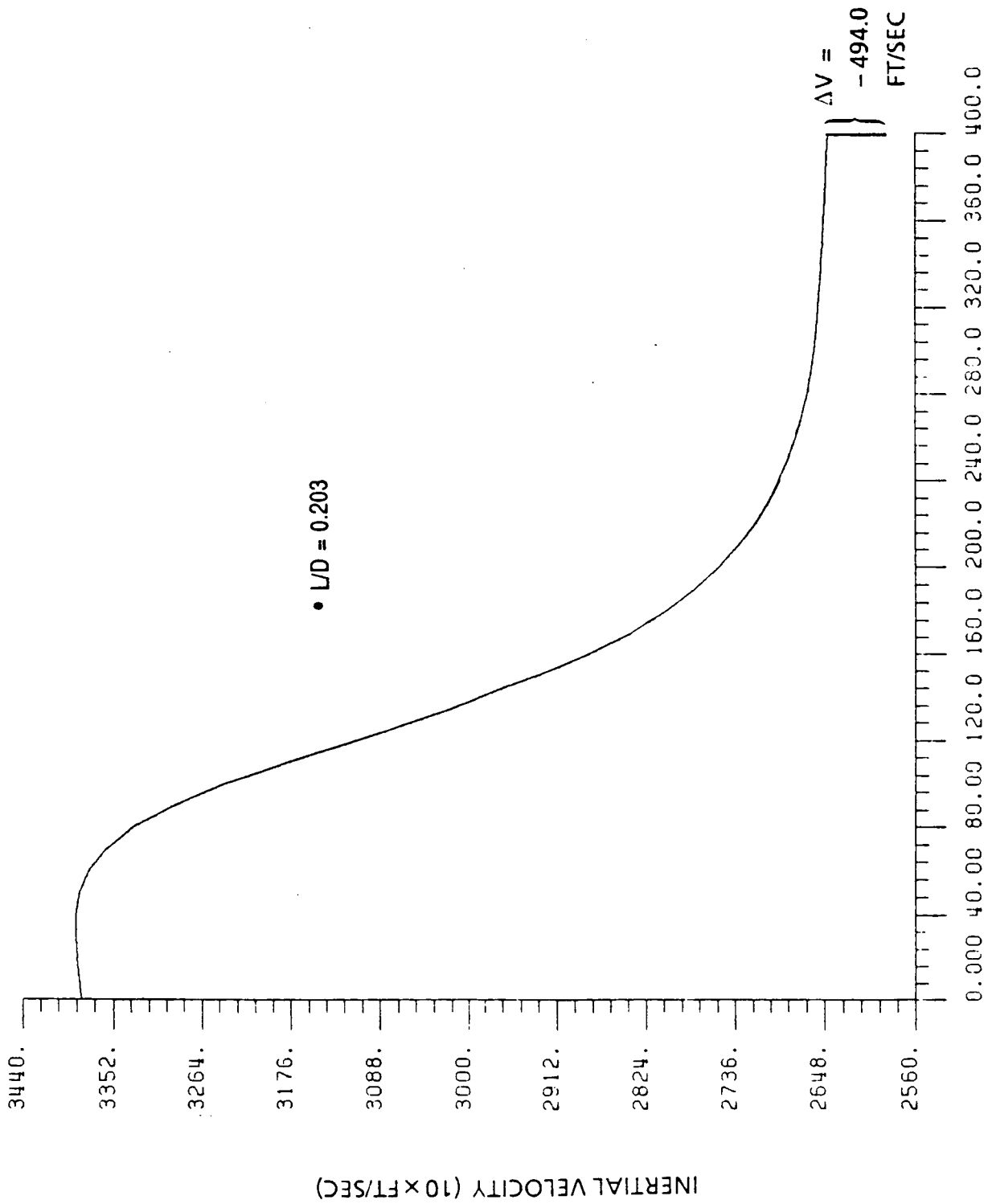


Figure 6.2.3.2-2. Altitude Profile for the Shaped Brake



TIME FROM ATMOSPHERIC ENTRY (SEC)

Figure 6.2.3.2-3. Velocity Profile for the Shaped Brake

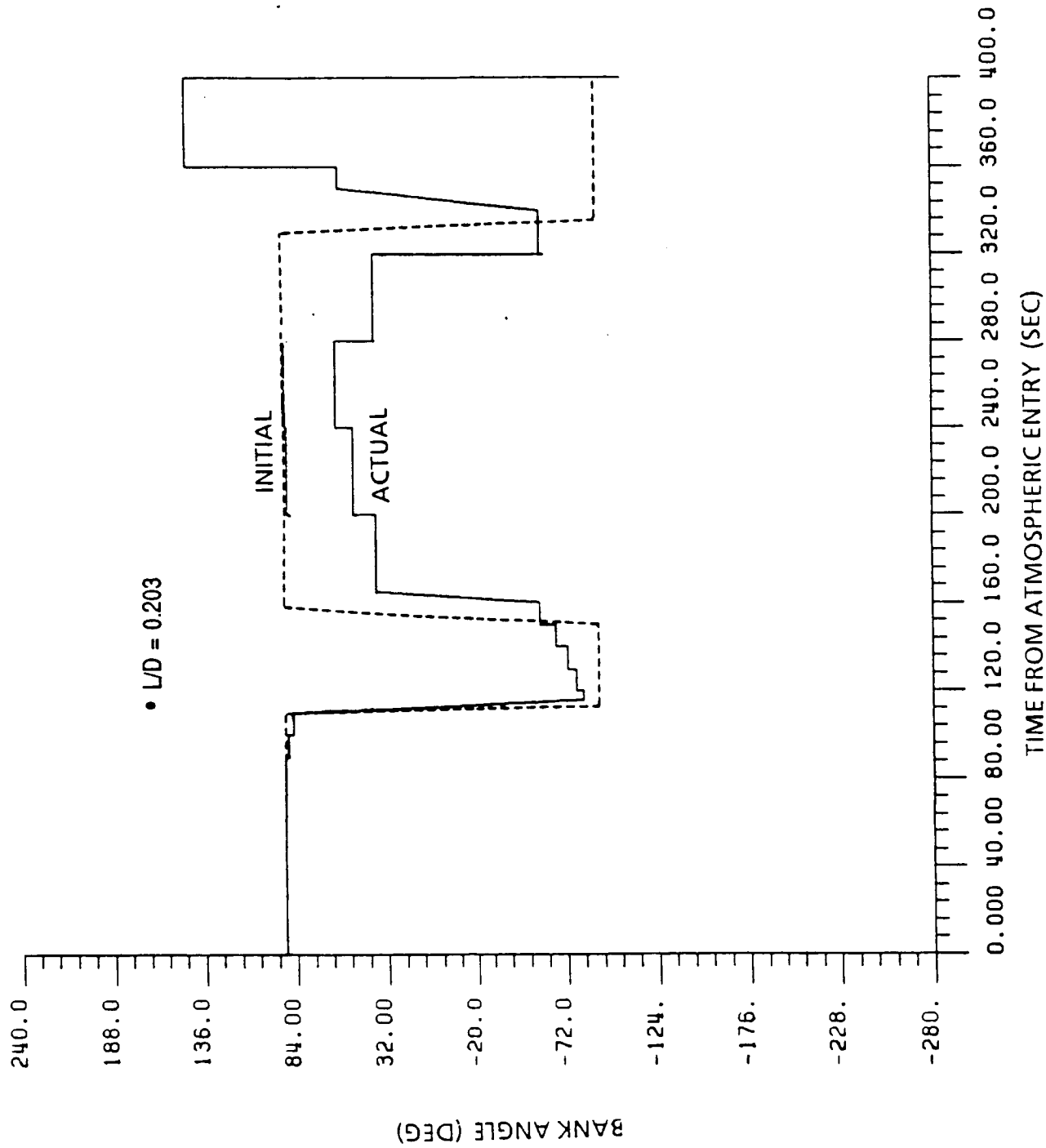


Figure 6.2.3.2-4. Initial Command and Actual Bank Angle Profile for the Shaped Brake

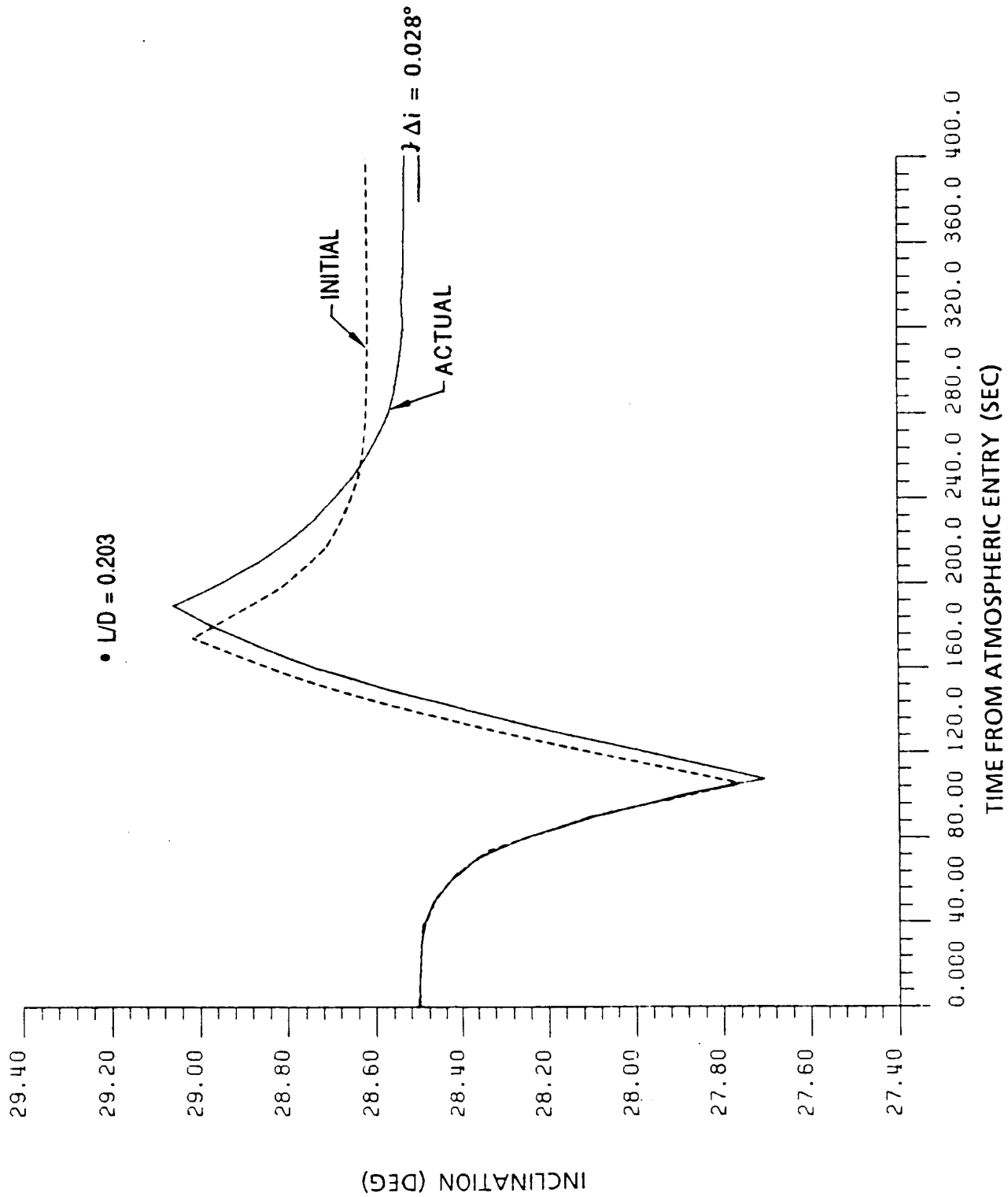


Figure 6.2.3.2-5. Inclination Profile for the Shaped Brake

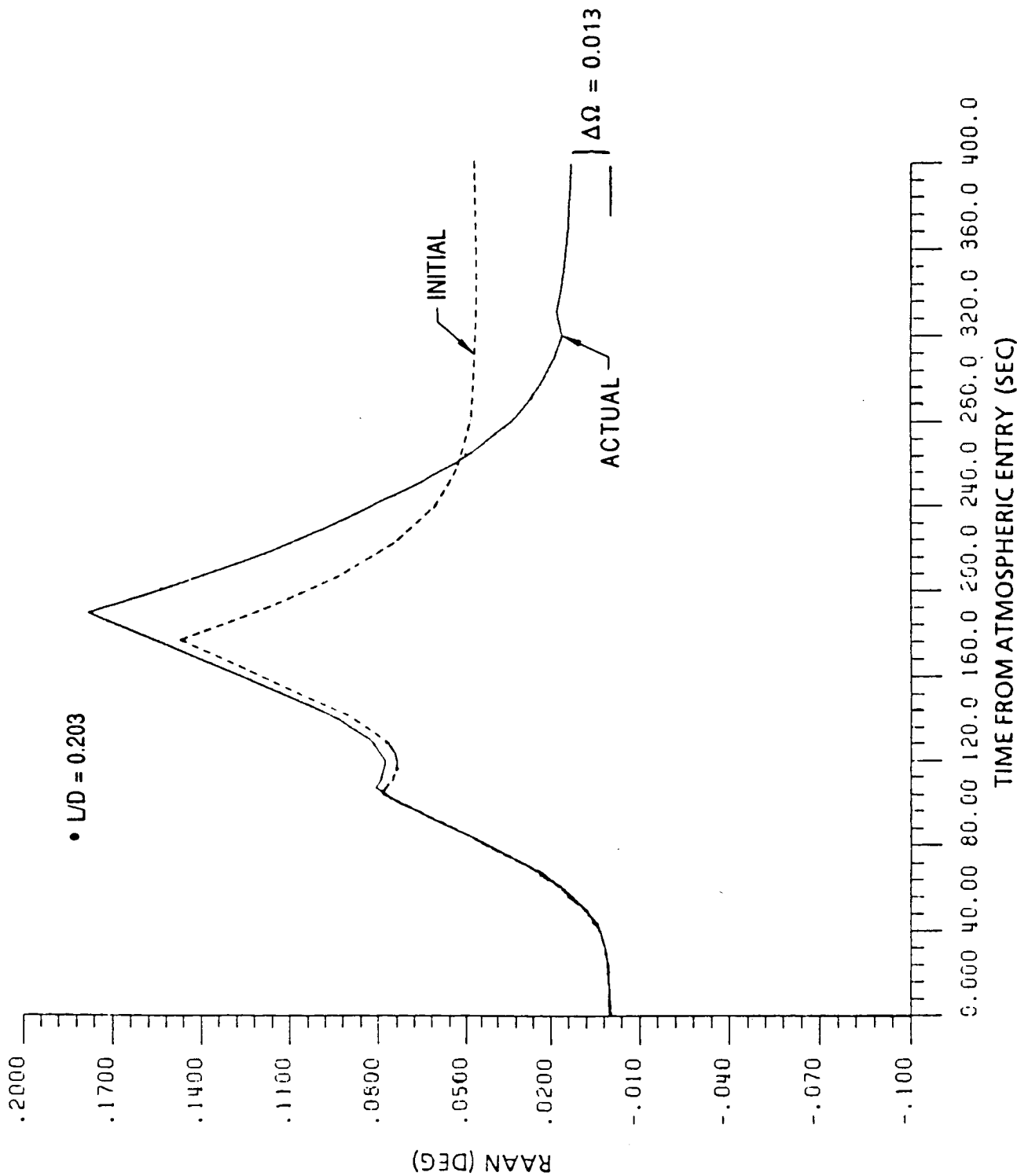


Figure 6.2.3.2-6. RAAN Profile for the Shaped Brake

knowledge of the atmosphere is obtained, a density predictor using knowledge of diurnal, seasonal, latitudinal, longitudinal, and vertical variability, as well as, horizontal and vertical correlation lengths can be developed to aid in the reduction of guidance error during an OTV aeromaneuver.

As the angle-of-attack of the vehicle increases, the L/D ratios increases. This enhances the capability of the vehicle to accomplish plane change maneuver, but as the angle-of-attack increases the C_D decreases. This reduces the capability of the vehicle to accomplish the primary task of reducing the energy of the OTV orbit. The results of the low L/D guidance analysis are shown in Figure 6.2.3.3-1. With no targeted plane change, the lower L/D vehicle has an advantage because it has more drag capability. However, if the plane change capability were utilized, there may be a small shift in the overall ΔV budget. The higher L/D vehicles have more plane change capability which could be used to reduce the plane change required at GEO. However, making use of this aerodynamic capability reduces the ability of the vehicle to make adjustments in the drag to respond to atmospheric perturbations. This may increase the guidance error in correcting for apogee. Further analysis is required to determine the optimum combination of L/D and targeted plane change.

- GUIDANCE PROBLEM SETUP
 - ATMOSPHERIC ENTRY TO 160 SEC.
 - CONTROL VARIABLES
 - BANK ANGLE MAGNITUDE
 - 3 BANK REVERSAL TIMES
 - CONSTRAINTS
 - RADIUS-OF-APOGEE
 - INCLINATION
 - RAAN
 - GUIDANCE UPDATE AT 80 SEC, THEN EVERY 10 SEC.
 - 160-SEC TO ATMOSPHERIC EXIT
 - CONTROL VARIABLES
 - BANK ANGLE
 - ΔV
 - CONSTRAINT
 - RADIUS-OF-APOGEE
 - GUIDANCE UPDATE EVERY 40 SEC.
 - VELOCITY ERROR AT ATMOSPHERIC EXIT IS THAT REQUIRED TO MEET TARGETED RADIUS-OF-APOGEE WITHIN 1000 FT.

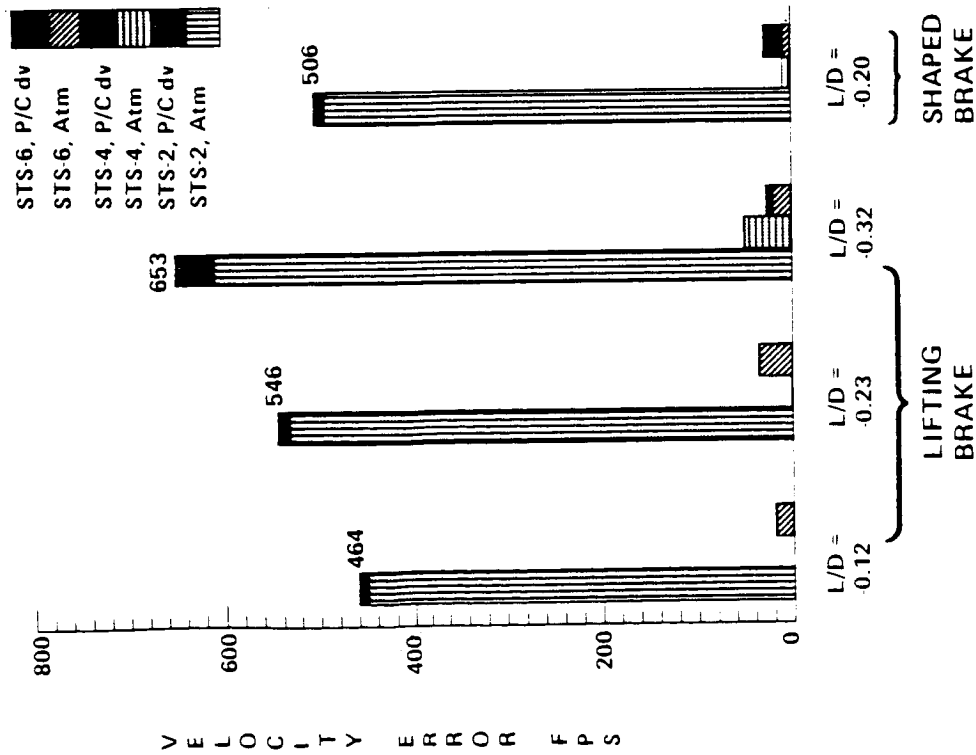


Figure 6.2.3.3-1. Low L/D Vehicle Response to Atmospheric Dispersions

7.0 DATA MANAGEMENT SUBSYSTEM TRADES

One of the primary objectives in the development of the OTV conceptual avionics design was to minimize life cycle costs. Additionally, the baseline avionics are designed for an unmanned vehicle, but allow for growth capability to a manned configuration.

The baseline configuration data management subsystem for OTV is based on distributed triple modular redundant computers utilizing a two out of three majority voting scheme. Hamming Error Detection and Correction is implemented in memory enabling single bit error correction and dual bit detection. Four computers will be required, with dual redundant I/O in each, expandable to triple redundant I/O for a manned configuration. Each computer will have a 64k word memory and a throughput of 600k operations per second. The data management subsystem will include built in test and fault tolerance as well as providing full redundancy management functions.

Data management subsystem trades were performed during the Ref. 5 study and in support of related Boeing space vehicle research and development. The trades were performed in four areas: system architecture, fault tolerance techniques, hardware and software. Following is a summary of the data management subsystem trades that are applicable to OTV.

7.1 SYSTEM ARCHITECTURE TRADE

Architecture trades were performed for distributed vs. centralized processing, system data bus, and bus protocols. The first architecture trade involved distributed versus centralized processing as presented in table 7.1-1. In a centralized processing system, system control is concentrated in the operating system of a single computing element. In a distributed system, system control is achieved through the cooperation of a number of autonomous operating systems. Distributed processing was chosen for the reasons of ease of expansion, and to facilitate software development.

A bus technology study compared parallel wire, serial twisted pair, and serial fiber optic buses. The serial fiber optic data bus was chosen due to its high throughput and low weight.

The bus protocol trade compared the following protocols: Token Bus, Token Ring, Carrier Sense Multiple Access, Carrier Sense Multiple Access with Collision Detection, Aloha, and MIL-STD-1553. The Token Passing Logical Bus was the preferred choice, due to fault tolerance implementation and flexibility.

Table 7.1-1 Centralized Versus Distributed Computer Functions

	CENTRALIZED COMPUTER							DISTRIBUTED COMPUTER						
	HARDWARE IMPACT	SOFTWARE IMPACT	SOFTWARE MODULE SIZE	EASE OF VALIDATION	REVALIDATION COSTS	THROUGHPUT	DESIGN COMPLEXITY	HARDWARE IMPACT	SOFTWARE IMPACT	SOFTWARE MODULE SIZE	EASE OF VALIDATION	REVALIDATION COSTS	THROUGHPUT	DESIGN COMPLEXITY
EASE OF EXPANSION	7	4	4	3	2	3	6	8	8	8	8	7	7	8
SOFTWARE DEVELOPMENT	---	3	3	2	---	6	8	---	7	8	8	---	7	8
SOFTWARE MODS	---	3	---	---	2	6	---	---	7	---	---	7	6	---
FAULT TOLERANCE OF P.E.'S	2	8	8	---	---	7	7	2	8	8	---	---	7	7
HARDWARE SIZE	7	---	---	---	---	5	6	5	---	---	---	---	7	4
SOFTWARE SIZE	---	---	6	2	---	---	---	---	---	8	8	---	---	---
RELIABILITY	4	7	7	5	---	5	6	4	7	8	4	---	6	6
WEIGHT	1.0	1.0	0.2	0.8	0.7	0.5	0.8	1.0	1.0	0.2	0.8	0.7	0.5	0.8
SCORE	35.0	35.0	7.8	16.8	9.8	18.6	37.0	26.6	51.8	11.2	39.2	34.3	23.3	37.0
TOTAL SCORE	160.0 OF 350							223.4 OF 350						

7.2 FAULT TOLERANCE TECHNIQUE TRADE

The fault tolerance trades included studies of various fault tolerance techniques, the use of dedicated spares versus pooled spares as shown in table 7.2-1, and the use of hot spares versus cold spares. Techniques of error detection and correction, error confinement, and fault masking and recovery are compared in table 7.2-2. The relative merits of each technique were compared in a high transient failure rate environment. The preferred techniques were shown to be N-modular redundancy (NMR) in the hardware, backup sparing, NMR with backup sparing, and adaptive NMR (also known as 'adaptive voting'). NMR with voting and backup sparing can be used for both the system data bus and the processors of the data management subsystem. Error detection and correction was selected, due to its effectiveness in reducing memory failures in a high failure rate environment.

7.3 HARDWARE TRADES

The hardware trades includes studies of processors and memory technologies. The processors considered were the microprocessor, the bit slice processor, and the custom design processor. The microprocessor was selected as the preferred option due to its small size, low risk and availability. Different microprocessors were also studied. Among the processors considered include the F9450 1750A CPU, the M68020, the N32032, and the Z8000. The F9450 was chosen, due to its MIL-STD-1750A instruction set architecture, its availability, and due to the fact it has been MIL-STD-883 qualified.

Memory trades addressed what devices should be used for random access memory (RAM) and for instruction memory. The random access memory trade compared the following devices: dynamic RAM, static RAM, EEPROM and ferrite core. The resulting choice was static RAM with its moderate density, moderate cost, and static-low power mode. The instruction memory trade considered read only memory (ROM) and EEPROM. EEPROM was the preferred choice since its contents can be modified should the software need reprogramming.

7.4 SOFTWARE TRADES

The software study considered the following high order languages (HOL's): Fortran-77, C, Pascal, Jovial, and Ada. The languages were compared considering the following characteristics: availability of compilers or translators, real time capabilities, data structures, standardization for portability purposes, and availability of development tools. Ada was the preferred choice, being the DoD's standard language

Table 7.2-1 Dedicated Versus Pooled Spares

	DEDICATED SPARES										POOLED SPARES									
	HARDWARE IMPACT	SOFTWARE IMPACT	SOFTWARE MODULE SIZE	EASE OF VALIDATION	EXTENT OF REVALIDATION	MODULE/SYSTEM LEVEL	PERFORMED IN HARDWARE/SOFTWARE	AFFECTS ONE/MANY MODULES	HARDWARE IMPACT	SOFTWARE IMPACT	SOFTWARE MODULE SIZE	EASE OF VALIDATION	EXTENT OF REVALIDATION	MODULE/SYSTEM LEVEL	PERFORMED IN HARDWARE/SOFTWARE	AFFECTS ONE/MANY MODULES	HARDWARE IMPACT	SOFTWARE IMPACT	SOFTWARE MODULE SIZE	EASE OF VALIDATION
EASE OF EXPANSION	8	8	8	8	7	---	---	8	7	3	6	2	1	---	---	2	---	---	---	2
SOFTWARE DEVELOPMENT	---	7	8	8	---	6	---	---	---	5	3	2	---	4	---	---	---	---	---	---
SOFTWARE MODS	---	7	---	---	7	8	---	8	---	2	---	---	2	3	---	2	---	---	---	2
FAULT TOLERANCE OF P.E.'S	2	8	8	---	---	8	6	8	8	2	2	---	---	2	4	3	---	---	---	3
USE OF NONCOMPATIBLE PROCESSOR IN A MODULE	8	8	---	8	8	8	---	8	8	2	---	3	2	4	---	3	---	---	---	---
HARDWARE SIZE	5	---	---	---	---	2	---	---	5	---	---	---	---	8	---	---	---	---	---	---
SOFTWARE SIZE	---	---	8	8	---	---	---	---	---	---	4	2	---	---	---	---	---	---	---	---
WEIGHT	1.0	1.0	0.2	0.8	0.7	0.1	0.1	0.4	1.0	1.0	0.2	0.8	0.7	0.1	0.1	0.1	0.1	0.1	0.1	0.4
SCORE	40.3	53.2	11.2	44.8	35.9	4.5	4.2	22.4	49.0	19.6	5.3	12.6	8.2	2.9	2.8	7.0				
TOTAL SCORE	216.5 OF 301										107.4 OF 301									

Table 7.2-2 Where Fault Tolerance Techniques are Applied

Boeing Aerospace Company		ECHOLOGY		COMPUTER FUNCTIONS		FAULT-DETECTION TECHNIQUES																																																																																																																																																																																																																																																																																																																																																																																																																																																																																																																																																																																																																																																																																																																																																																																																																																																																																																																																																																																																																																																																																																																																																																																																																																																																																																																																																																																																													
						DYNAMIC REDUNDANCY						MASKING REDUNDANCY				ERROR DETECT CODES																																																																																																																																																																																																																																																																																																																																																																																																																																																																																																																																																																																																																																																																																																																																																																																																																																																																																																																																																																																																																																																																																																																																																																																																																																																																																																																																																																																																			
						REC NMR	BACKUP SPARING	GRACEFUL DEG	MISC RECONFIG	RECOVERY	INTRWOVN L	CODED STATE	NMR	ECC	OTHER	HAMMING	PARITY	CHECKSUM	ARITHMETIC	CYCLIC	WATCHDOG	SELF CHECKING	CAPABILITY	WATER	WATER	WATER																																																																																																																																																																																																																																																																																																																																																																																																																																																																																																																																																																																																																																																																																																																																																																																																																																																																																																																																																																																																																																																																																																																																																																																																																																																																																																																																																																																									
POWER CONDITIONING																																																																																																																																																																																																																																																																																																																																																																																																																																																																																																																																																																																																																																																																																																																																																																																																																																																																																																																																																																																																																																																																																																																																																																																																																																																																																																																																																																																																																			</

Ø = COMMON USE

X = POSSIBLE USE

for embedded systems. Ada offers special modern constructs for real time programming, such as exception handling, tasking and low level bit manipulation.

8.0 ELECTRICAL POWER SUBSYSTEM

8.1 POWER SOURCE DEFINITION

The electrical power supply and distribution subsystem provides (1) power for vehicle equipment and spacecraft, (2) switching and distribution of electrical power to the vehicle and spacecraft, (3) interconnecting cabling for the avionics and other subsystems, and (4) the capability to use power supplied by the Orbiter, ground support equipment, or the Space Station when attached.

8.1.1 Top Level Requirements

The top level requirements for the electrical power subsystems are:

- a. Provide power to all vehicle subsystems.
- b. Provide capability to supply power to vehicle subsystems from the ground or Orbiter when in the launch configuration, from internal sources when deployed, and from the Space Station when attached.
- c. Provide redundancy of internal power sources.
- d. Control and distribute power to all vehicle subsystems.
- e. Provide interconnecting wiring for all vehicle subsystems except for instrumentation wiring and RF cabling.
- f. Provide 200 watts of power to a payload when attached.

The energy requirements for a nominal GEO delivery mission are summarized in table 8.1-1. Additional requirements, such as reliability, maintainability, and size are listed in table 8.1-2. A power requirement of 63.6Kwh has been assumed for sizing and evaluating possible power sources. During the first 36 hours, an average of 1700 watts will be required. This power level will supply enough energy to transport a payload from low-earth orbit to a higher earth orbit, and back. In the event of an emergency, enough power (100 watts) will be reserved to keep the OTV "alive" in low earth orbit for 24 hours until it can be retrieved at the space station (or Orbiter if a GB OTV) as shown in figure 8.1-1.

8.1.2 Baseline System Definition

The baseline power source selected for the OTV consists of three H₂-O₂ fuel cells. Each fuel cell can provide 2.0kW of power at a nominal voltage of 28 volts. During normal mission operations one, two, or all three fuel cells could be operating. However,

Table 8.1-1 OTV Reference Power Requirements

<u>SYSTEM</u>	<u>POWER</u>	<u>DURATION</u>	<u>ENERGY USAGE</u>
Payload	200 W	36.0 Hrs.	(7,200) WH
Avionics			(44,594)
G & N	189	51.231	9,683
Comm.	134	51.231	6,865
Data Mgt.	497	51.231	25,462
Instrumentation	50	50.767	2,538
	100	0.464	46
Propulsion			(1,861)
Engine	30	50.767	1,523
	168	0.464	78
TVC Actuators	560	0.464	260
Attitude Control			(1,916)
Thrusters	1.4	51.231	72
Heaters (Hydrazine opt.)	36	51.231	1,844
Power			(5,556)
Conversion/	104	20.744	2,157
Distribution Losses	68	30.487	2,073
	47	0.464	22
Heaters	32	20.744	664
	21	30.487	640
Emergency	100	24.000	(2,400)
Total			(63,527) WH

Table 8.1-2 Power System Requirements

- RELIABILITY
 - FAIL SAFE - ACHIEVED BY USE OF SIMPLE SYSTEMS WITH HIGH RELIABILITY AND/OR REDUNDANCY OF LESS RELIABLE SYSTEMS
- SAFETY
 - CAPABLE OF BECOMING MAN-RATED
- MAINTAINABILITY
 - MUST BE SPACE MAINTAINABLE
- COMPLEXITY - KEEP TO A MINIMUM
 - GREATER COMPLEXITY USUALLY LEADS TO LESS RELIABILITY AND MAINTAINABILITY
- AVAILABILITY
 - SYSTEMS MUST BE READILY AVAILABLE AND QUALIFIED FOR USE BY 1990
- LIFE
 - SHOULD BE GREATER THAN 5 YEARS
- SIZE
 - LOW WEIGHT AND VOLUME HIGHLY DESIRABLE
- COST
 - DEVELOPMENT AND PRODUCTION COSTS KEPT TO A MINIMUM

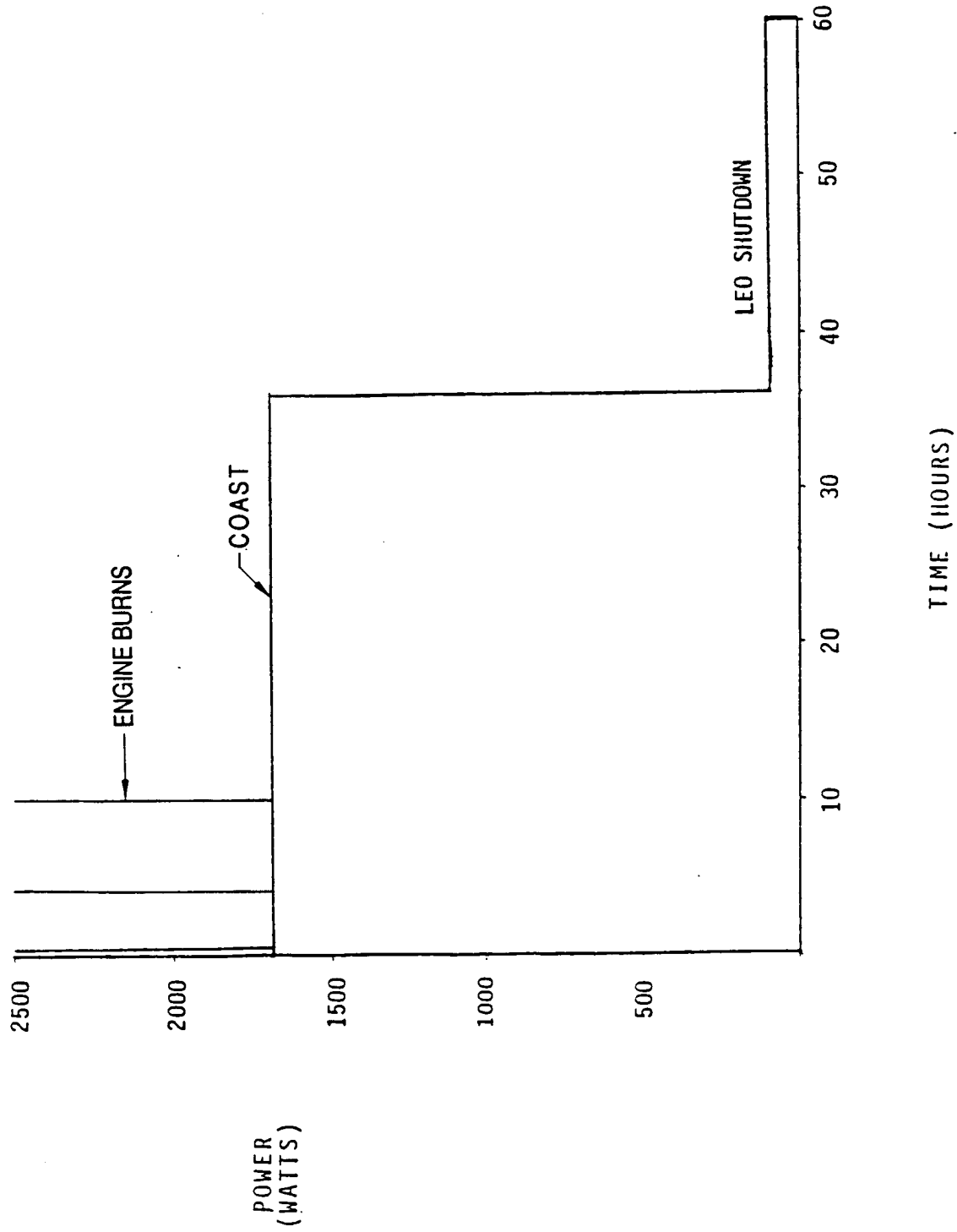


Figure 8.1-1 Electrical Power Requirements

two of the three could fail, and the remaining fuel cell could still sustain the total load. The design criteria is summarized in table 8.1-3. Redundant fuel and fuel tanks are not included.

Information used for sizing the fuel cell came from modifications of the Shuttle Orbiter hardware. Each fuel cell weighs approximately 80 lb. or 240 lb. for all three. The volume of each fuel cell is estimated at 2.12 cubic feet.

Hydrogen and oxygen are supplied on demand to the fuel cells at a nominal rate of 0.77lb/KWH as indicated in fig. 8.1-2. The fuel ratio of oxygen to hydrogen is approximately 8 to 1. The reactants can be stored either as pressurized gases in tanks, or at their supercritical state in cryogenic dewar-type vessels.

In the gaseous state, the fuels can be stored at 350 psi. The hydrogen tank would weigh approximately 40.5 times as much as the hydrogen fuel, and the oxygen tank would weigh approximately 2.5 times the weight of the oxygen fuel. Lower pressures could be used for the fuels to match the operating pressure of the fuel cell (60 psi) but the weight and volume of the tanks would increase significantly.

With cryogenic tanks the reactants would be maintained at supercritical pressures of 250 psi in the hydrogen tank and 900 psi in the oxygen tank during use by means of tank pressure controlled electric heaters. The weights and volumes of the tanks would be much smaller than those of the pressurized gas tanks shown in table 8.1-4. It might also be possible to use the fuels from the propulsion tanks. The savings in terms of size and weight would be minimal, however.

In either case, reactant preheaters and inlet regulators reduce the pressure of the fuels so that they can be accommodated by individual fuels cells. The reactant water product will be cooled and collected for return to the space station. There the water may either be converted back to hydrogen and oxygen or used as is in the space station.

8.2 TRADES AND ANALYSES

8.2.1 Power Source Trade

Electrical power sources being considered for OTV other than the primary fuel cell include primary batteries, solar array/battery combinations, RTG's, flywheels, turbo generators, reactors, and others. Of these choices, primary fuel cells, primary batteries, and solar array/battery combinations prove most economical and available for use by 1990.

The other systems are either still in the development stage or they are not suited to this application for other reasons. It is doubtful that the required time and money

H₂ - O₂ PRIMARY FUEL CELL

DESIGN CRITERIA:

- 1700 WATTS FOR 36 HOURS
100 WATTS FOR 24 HOURS
(63.6 KWH TOTAL)
- H₂ AND O₂ FUELS MAY BE STORED IN PRESSURIZED VESSELS, OR IN SEPARATE CRYOGENIC TANKS.
- 35% FUEL SURPLUS FOR ULLAGE, RESERVE, AND BOILOFF
- 2 OF 3 FUEL CELLS CAN FAIL AND STILL PROVIDE FULL POWER
- NO TANK REDUNDANCY
- SAVE H₂ O₂ BY-PRODUCT; RETURN TO SPACE STATION FOR ELECTROLYSIS

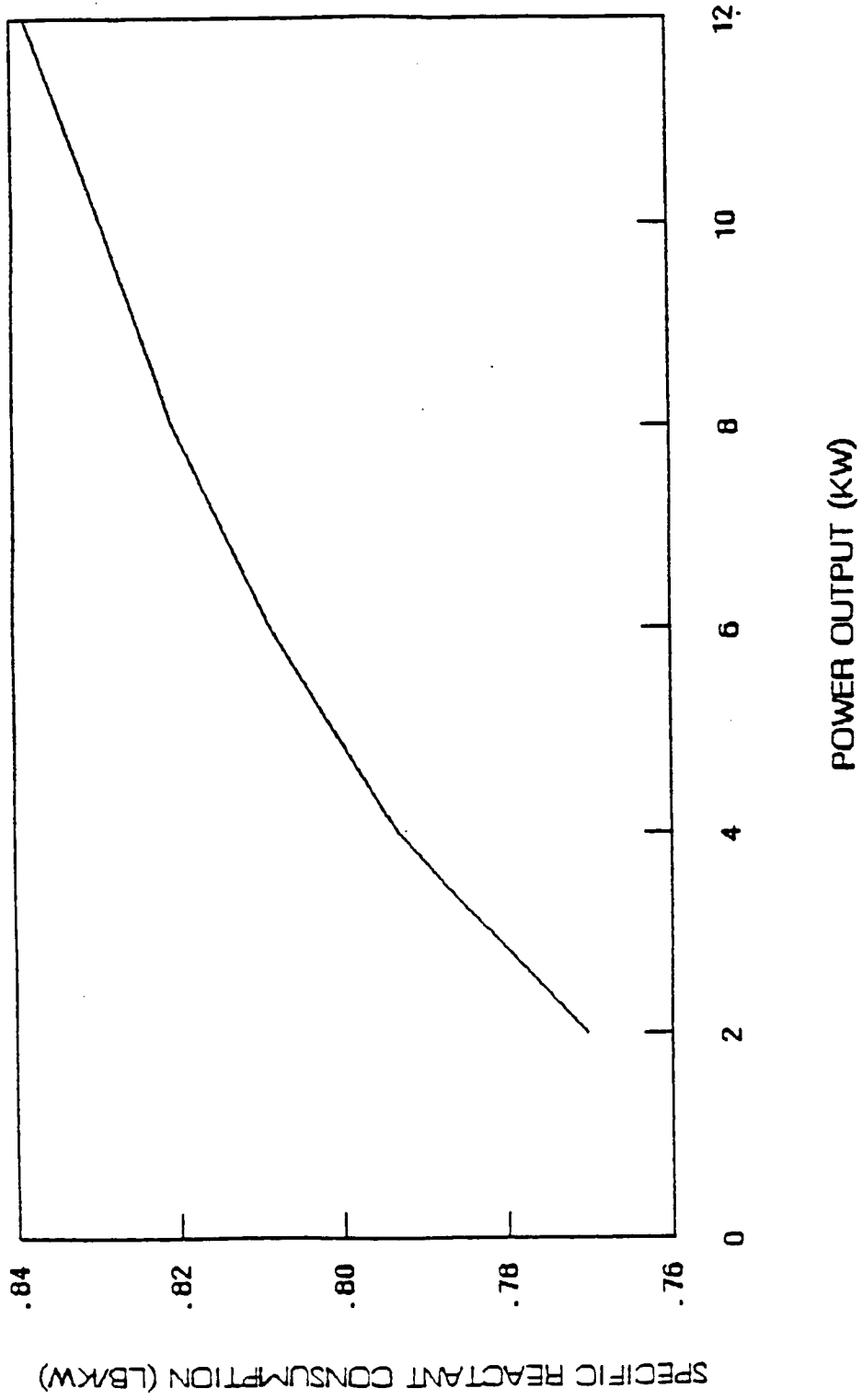


Figure 8.1-2 Fuel Cell Specific Reactant Consup Consumption

Table 8.1-4 H 2 - O 2 Fuel Cell Weight Determination, kg

ITEM	PRESSURIZED GAS TANKS - 60psi	PRESSURIZED GAS TANKS - 350psi	CRYOGENIC GAS- SEPARATE TANKS FROM PROPULSION TANKS
FUEL CELL UNITS (3 ea.)	244.7	244.7	244.7
HYDROGEN (H ₂) FUEL	7.3	7.3	7.0
OXYGEN (O ₂) FUEL	58.9	58.9	58.9
HYDROGEN TANK (VOLUME, ft ³)	1728 (387.4)	295 (66.4)	4.4
OXYGEN TANK (VOLUME, ft ³)	864 (193.5)	147.7 (34.3)	7.5
HEAT EXCHANGER	8.8	8.8	8.8
RADIATOR	24.3	24.3	24.3
WATER TANK	6.6	6.6	6.6
PIPES, VALVES, HEATERS, PUMPS	26.5	26.5	26.5
TOTALS	2970 lbm	820 lbm	390 lbm

would be spent for these systems to be ready by 1990. Flywheel development is presently being heavily funded, however, so it is possible that the flywheel could be an energy storage option for the OTV by the year 1990. Information used to compare the systems is shown in table 8.2-1.

In addition to sizing the primary fuel cells, weights for primary batteries and solar array/battery combinations were also determined. Of the two primary batteries considered, lithium thionyl chloride (Li/SOCl₂) and zinc silver oxide (Zn/AgO), the latter was more than two and one half times heavier than the former. The Li/SOCl₂ batteries do presently, however, pose more of a safety concern than the Zn/AgO batteries. Primary batteries also tend to be very costly and heavy, and they must be replaced after each mission. Weights represented in table 8.2-2 are for 6 batteries, where 2 of 6 may fail. Solar array/battery combinations were also sized to determine their ability to compete with the primary fuel cell and primary batteries. The design criteria is listed in table 8.2-3.

Several solar array panels configurations were considered. The simplest solar array would be a body-mounted configuration. Approximately 1120 ft² is available on the body of the OTV for solar panels. This configuration would satisfy many payloads, but not all. The solar array power capability would be a function of OTV attitude as indicated in figure 8.2-1.

If the solar arrays are at an angle perpendicular to the sun's light, the OTV may either be spinning or not spinning. If the OTV does not spin, the resultant operating temperature of 110°C would yield a power capability of approximately 7.6 W/ft². A slow spin would result in a temperature of approximately 20°C, and the power capability would be approximately 12.2 W/ft².

If a deployed solar array is considered, the temperature would probably not exceed 50°C, and the power capability would be approximately 10.7 W/ft² as shown in fig. 8.2-2.

Either primary or secondary batteries may accompany the solar array to provide power (5030 WH) during the eclipse periods. As can be seen in table 8.2-4, the primary batteries are lighter than the secondaries, but they must be replaced after each mission. Secondary batteries need only be recharged after each mission at the space station. The Li/SOCl₂ battery would be the logical primary battery choice for weight, provided the safety problems are resolved by 1990. Of the secondary batteries, the rechargeable lithiums are under development and could very well be the optimum choice by 1990. Nickel cadmiums are presently available but are very heavy. Nickel hydrogens are also a possibility since they are significantly lighter in weight than nickel cadmiums. Table

Table 8.2-1 Power System Trades

	TOTAL WEIGHT (lbm)	ADVANTAGES	DISADVANTAGES	CHOICES
<ul style="list-style-type: none"> PRIMARY FUEL CELL 		<ul style="list-style-type: none"> Space qualified, need to replace fuel only. 	<ul style="list-style-type: none"> Poor reliability due to many moving parts. 	
<ul style="list-style-type: none"> Pressurized Gas Tanks (60psi) 	2970	<ul style="list-style-type: none"> No need for pressure regulator between tanks & F.C. 	<ul style="list-style-type: none"> Tanks heavy & large. 	
<ul style="list-style-type: none"> Pressurized Gas Tanks (350psi) 	820	<ul style="list-style-type: none"> Much lighter & smaller than 60psi tanks. 	<ul style="list-style-type: none"> Needs pressure regulator, heavier than cryogenics. 	
<ul style="list-style-type: none"> Cryogenic Gas Tanks 	390	<ul style="list-style-type: none"> Lightest & smallest fuel tanks. 	<ul style="list-style-type: none"> Needs pressure regulator, cryogenics increase complexity. 	X
<ul style="list-style-type: none"> PRIMARY BATTERY 		<ul style="list-style-type: none"> Lightweight, Reliable. 	<ul style="list-style-type: none"> Must replace after each mission. 	
<ul style="list-style-type: none"> Li/SOCl₂ 	606	<ul style="list-style-type: none"> High energy density. 	<ul style="list-style-type: none"> Poor safety record. 	
<ul style="list-style-type: none"> Zn/AgO 	1559	<ul style="list-style-type: none"> Better safety record than Li/SOCl₂. 	<ul style="list-style-type: none"> Significantly heavier than Li/SOCl₂. 	X

Table 8.2-1. Power System Trades (Cont.)

TOTAL WEIGHT (lbm)	ADVANTAGES	DISADVANTAGES	CHOICES
● SOLAR ARRAY/BATTERY COMBINATIONS	● S.A. provides debris shielding.	● Must either replace primaries or recharge secondaries.	
● Body Mounted, Non-spinning/Primary		● S.A. gets hot on 1 side, loses efficiency, does not satisfy all payloads, more area for S.A. required.	
● Body Mounted, Non-spinning/Secondary	● OTV not required to spin.		
● Body Mounted, Spinning/Primary	● Solar array remains cooler which increases efficiency.	● OTV must spin to avoid "hot-spots" on S.A.; does not satisfy all payloads	
● Body Mounted, Spinning/Secondary		Solar panels must surround OTV.	
● Paddles, 1-sided/Primary	● Most lightweight system; accomodates all payloads	● Increased complexity due to deployable solar array.	
● Paddles, 1-sided/Secondary	Only one fourth the area required for solar cells.	● Pointing requirements	X

Table 8.2-1 Power System Trades (Cont.)

	TOTAL		ADVANTAGES	DISADVANTAGES	CHOICES
	WEIGHT	(lbm)			
• RTG			• Long life.	• Safety concerns for nuclear reasons; heavy.	
• TURBOGENERATORS			• High energy density, good shelf life.	• Still in development, used for short missions only (10-50 hrs).	
• • FLYWHEEL		823- 1668	• Efficient.	• Poor safety record due to material fatigue.	D180-29108-2-3

Table 8.2-2 Primary Battery

DESIGN CRITERIA (WORST CASE)

- 1700 W, 36 HRS; 100 W, 24 HRS
- TWO OF SIX MAY FAIL
- 90% DOD MAX

CANDIDATES

- Li/SOCl₂ ← CHOICE -- 6 BATTERIES @ 101 kg = 606 lbin
- Zn/AgO (HEAVY -- 6 @ 260 = 1558 lbm)

ASSESSMENT

- LITHIUM PRIMARY HAS SAFETY CONCERN, BUT THIS CAN BE MADE SAFE
- PRIMARY BATTERIES ARE HEAVY, COSTLY SPACE OPERATIONS TO REPLACE

Table 8.2-3 Basic Solar Array/Battery

DESIGN CRITERIA:

- FIRST 36 HOURS:
- 1700 WATTS
- 2 LEO ECLIPSES
- 1 GEO ECLIPSE
- LAST 24 HOURS
- 100 WATTS
- MAX OF 16 LEO ECLIPSES
- NOT NECESSARY TO RECHARGE SECONDARY BATTERIES UNTIL RETURNED TO SPACE STATION
- TWO OF SIX BATTERIES MAY FAIL AND FULL POWER WOULD STILL BE PROVIDED

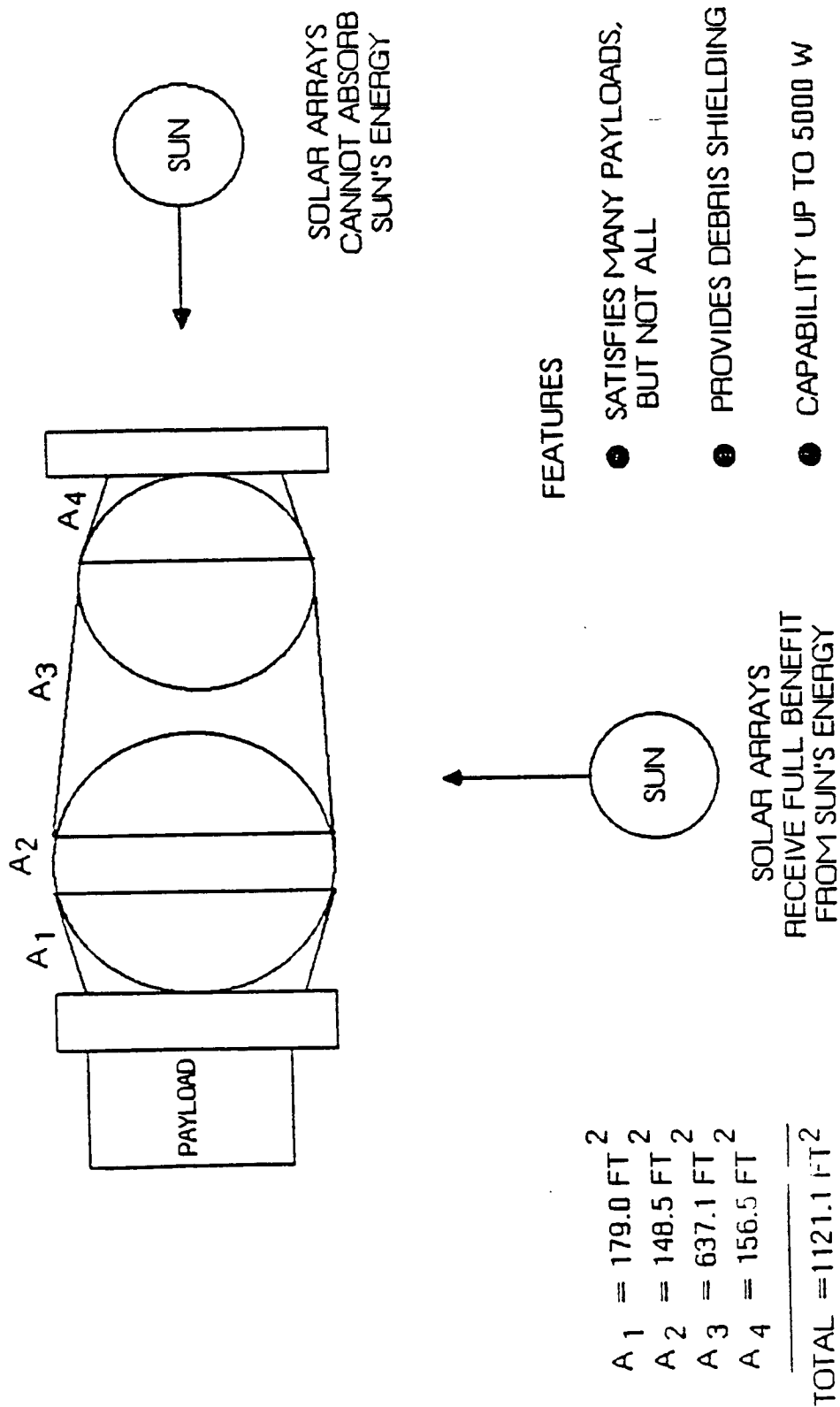
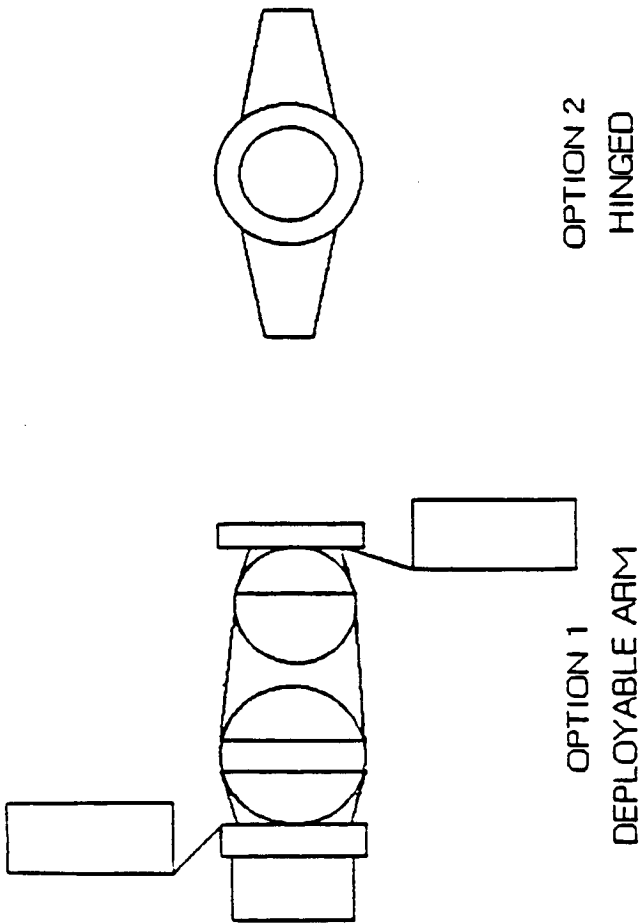


Figure 8.2-1 Solar Array, Body - Mounted



FEATURES -

- SOLAR ARRAY DEPLOYMENT ANGLE TAILORED TO MISSION
- MULTIPLE PANELS ARE PRACTICAL
- PANELS RETRACT FOR RETURN
- USEABLE FOR STATIONARY OR SPINNING VEHICLE
- ACCOMMODATES ALL PAYLOADS

Figure 8.2.2 Deployable Solar Array

Table 8.2-4 Battery Candidates for Solar-Powered Approaches

<u>PRIMARY BATTERIES</u>		REPLACE AFTER EACH MISSION
● Li/SOCl ₂	—	90% DOD (WORST CASE) 6 UNITS @ 8.0 ea. → 48 lbm
● Zn/AgO	—	90% DOD (WORST CASE) 6 UNITS @ 20.5 ea. → 123 lbm
<u>SECONDARY BATTERIES</u>		RECHARGE AFTER EACH MISSION
● Ni — Cd	—	60% DOD (WORST CASE) 6 UNITS @ 132 ea. → 791 lbm
MOST READILY AVAILABLE, MOST INEXPENSIVE SECONDARY BATTERY		
● Ni-H ₂	—	75% DOD (WORST CASE) 6 UNITS @ 84 ea. → 503 lbm
NEEDS FUNDING FOR MORE DEVELOPMENT		
● RECHARGEABLE LITHIUM	—	90% DOD (WORST CASE) 6 UNITS @ 34 ea. → 205 lbm
FASTEST DEVELOPING SYSTEM AND RAPIDLY DECREASING IN COST		

8.2-5 displays the weights for each of the solar array configurations with each of the battery candidates.

A summary of the weights of the most favorable power source candidates appears in table 8.2-6. The lightest overall system is the deployed solar array with a primary battery. Close behind in second place is the baseline primary fuel cell with cryogenic tanks. The deployed solar array/secondary battery combination comes in third.

8.2.2 Technology Assessment

A summary of the power systems technology assessment appears in table 8.2-7. The different categories include primary fuel cells, primary batteries, secondary batteries, solar arrays, flywheels, turbogenerators, RTG's Stirling engines, reactors, and solar Brayton.

The best overall choices for the OTV program appear to be a primary fuel cell or deployed solar array/battery system. These systems are lightest in weight and have the potential to grow significantly by the year 1990. Reliability is an important consideration for the fuel cell. However, with a triply redundant system where two of the three fuel cells may fail, the reliability of the system is considerably improved. Cost is also a major consideration with the fuel cell. The new electrolyte plate technology incorporated into a new 2 kW system will only increase the already high cost. With the solar array secondary battery system, there is a one time initial investment. The batteries need only be recharged at the Space Station after each mission. If primary batteries are used, however, they must be replaced after each mission. This will involve the transport of batteries from earth to the Space Station for each OTV mission in addition to the cost of the batteries themselves. Secondary rechargeables would probably be a more economical choice.

Newer, less developed systems such as turbogenerators, reactors, Stirling engines, and solar Brayton, would require large amounts of funding to make them qualified and available for use by 1990. Safety, reliability, and maintainability would also have to be proven.

8.2.3 Assessment

The primary fuel cell with cryogenic tanks or the deployed solar array/rechargeable lithium battery system provide the best features. The fuel cell system is selected as the baseline in part because of being easier to physically integrate into the vehicle. System characteristics of both concepts are shown in figures 8.2-3 and 8.2-4.

Table 8.2-5. Solar Array/Battery Combination Weights (lbm)

	PRIMARY BATTERY (5030 WH)		SECONDARY BATTERY (5030 WH)		
	Li/SOCl ₂	Zn/AgO	Ni-Cd	Ni-H ₂	Rechargeable Lithium
2000 W NOMINAL	49	123	791	505	205
SILICON PLANAR BODY-MOUNTED SOLAR ARRAY (NON-SPINNING) 1054	1102	1177	1845	1559	1259
SILICON PLANAR BODY-MOUNTED SOLAR ARRAY (SPINNING) 657	705	780	1448	1162	862
SILICON PLANAR DEPLOYED SOLAR ARRAY 207	256	1331	999	712	412

 INDICATES LIGHT WEIGHT COMBINATION

Table 8.2-6 Weight Comparison of Favorable Candidates

<u>CANDIDATES</u>	<u>WEIGHT (lbm)</u>
● PRIMARY FUEL CELL $H_2 - O_2$	
PRESSURIZED GAS TANKS (~ 60 psi)	2970
PRESSURIZED GAS TANKS (~ 350 psi)	820
CRYOGENIC GAS TANKS (SUPERCritical)	390
● PRIMARY BATTERY	
Li/SOCl ₂	606
Zn/AgO	1559
● SOLAR ARRAY/BATTERY COMBINATIONS	
BODY MOUNTED, NON SPINNING/PRIMARY	1102-1177
BODY MOUNTED, NON SPINNING/SECONDARY	1140-1845
BODY MOUNTED, SPINNING/PRIMARY	705-780
BODY MOUNTED, SPINNING/SECONDARY	862-1448
PADDLES, 1-SIDED/PRIMARY	256-331
PADDLES, 1-SIDED/SECONDARY	412-999

* INDICATES ALL PAYLOADS NOT SATISFIED

D180-29108-2-3

Table 8.2-7 Power Systems Technology Assessment

POWER SYSTEMS TECHNOLOGY ASSESSMENT

POWER OPTION	DEVELOPMENT PERIOD	TECHNOLOGY ADVANCEMENTS
PRIMARY FUEL CELL	SOA 1984	<ul style="list-style-type: none"> • Shuttle Orbiter Fuel Cell (3 Stacks Of Cells W 32 Cells/Stack; ~0.9V/Cell; 0.508 ft² Cell Area; 6-7 KW Fuel Cell); Space Qualified; \$2.5-3.0 Million.
	Normal Growth 1990	<ul style="list-style-type: none"> • Improved Reliability; 47% Reduction In Weight Due To New Electrolyte Reservoir Plate (ERP); 50% Reduction In Size With Same Output.
	Accelerated Growth 1990	<ul style="list-style-type: none"> • Reduce SOA To A Small, Efficient, Low-Power 2KW Fuel Cell; Integrated Anode Plate (IAP).

Table 8.2-7 (Cont.)

POWER OPTION	DEVELOPMENT PERIOD	TECHNOLOGY ADVANCEMENTS
TURBO- GENERATORS (APU)	SOA 1984	<ul style="list-style-type: none"> • High Power Density; Confined To Short Missions (10-15 Hrs.); Uses Cryogenic Fuels (H_2&O_2). Not Practical For Low Power Requirements.
	Normal Growth 1990	<ul style="list-style-type: none"> • None For Long Term, Low Power Requirements.
	Accelerated Growth 1990	<ul style="list-style-type: none"> • Huge Amounts Of Funding Could Result In A Longer Life Working System; But The Reliability Would Remain Low Due To Many Moving Parts & It Would Be Large.
RTG	SOA 1984	<ul style="list-style-type: none"> • 2.3-3.2 W/lb.; Space Qualified Through Snap Series; Very Heavy.
	Normal Growth 1990	<ul style="list-style-type: none"> • 4.5 W/lb.; Improved Efficiency.
	Accelerated Growth 1990	<ul style="list-style-type: none"> • Huge Funding Required For Any Significant Advancements.

Table 8.2-7 (Cont.)

POWER OPTION	DEVELOPMENT PERIOD	TECHNOLOGY ADVANCEMENTS
Ni-Cd SECONDARY BATTERY	SOA 1984	<ul style="list-style-type: none"> • 16 WH/lb.; 5-10 Yr Life; Readily Available; Least Expensive Secondary Battery; Space Qualified.
	Normal Growth 1990	<ul style="list-style-type: none"> • 20 WH/lb.; 8-14 Yr Life Due To Improved Separator Materials; Lighter Case.
	Accelerated Growth 1990	<ul style="list-style-type: none"> • Probably No More Than Can Be Expected During Normal Growth.
Ni-H ₂ SECONDARY BATTERY	SOA 1984	<ul style="list-style-type: none"> • 20 WH/lb.; 2-3 Yr Life; 50 AH Capacity; Space Qualified; 30 WH/lb. Has Been Bench Proven, But Not Flight Tested.
	Normal Growth 1990	<ul style="list-style-type: none"> • 32-36 WH/lb.; LEO—30,000 Cycles; 5 Yr Life; GEO—1,000 Cycles; 10 Yr Life; Bipolar Batteries Offer Advantage Of Less Volume With Same Power Output.
	Accelerated Growth 1990	<ul style="list-style-type: none"> • 36 WH/lb.; Reduced Weight & Volume.
RECHARGEABLE Li SECONDARY BATTERY	SOA 1984	<ul style="list-style-type: none"> • 41 WH/lb.; 500 Cycles; 20 AH Cell; "Beer Can Batteries."
	Normal Growth 1990	<ul style="list-style-type: none"> • 27 WH/lb.; 1,000 Cycles; 100-500 AH Cells; Fastest Improving System.
	Accelerated Growth 1990	<ul style="list-style-type: none"> • 34 WH/lb.; 5,000 Cycles; 2,000-20,000 AH Cells; Space Qualified.

Table 8.2-7 (Cont.)

POWER OPTION	DEVELOPMENT PERIOD	TECHNOLOGY ADVANCEMENTS
SOLAR ARRAY	SOA 1984	<ul style="list-style-type: none"> Planar Si Arrays: 13-17% Eff., 10-15 Yr Life, \$600-700/W; Si Concentrator Arrays, 20-22% Eff., 10-15 Yr Life, 2 to 4 Times More Expensive Than Planar Arrays; GaAs; 22-25% Eff. (Dev Stage).
	Normal Growth 1990	<ul style="list-style-type: none"> Adv. Si Concentrator Arrays @ 22-25% Eff.; GaAs Slow To Make Significant Advancements; Other Areas Of Investigation Include Polycrystalline Si Cells, Amorphous Si, Thin Layers, CdTe, CuIn Diselenide.
	Accelerated Growth 1990	<ul style="list-style-type: none"> High Concentration GaAs At 23-29% Efficiency; \$100-\$150/W; 30 Yr Life Expectancy, 15.2 W/ft², 13.6 W/lb.
FLYWHEEL	SOA 1984	<ul style="list-style-type: none"> 7-11 WH/lb.; 5,000 Hr. Expected Life; Safety Concern Due To Material Fatigue.
	Normal Growth 1990	<ul style="list-style-type: none"> Improvements In Materials To Improve Safety And Increase Life (10,000-50,000 Hr. Life).
	Accelerated Growth 1990	<ul style="list-style-type: none"> 150,000 Hr. Life, Space Qualified.

Table 8.2-7 (Cont.)

POWER OPTION	DEVELOPMENT PERIOD	TECHNOLOGY ADVANCEMENTS
Li/SOCl ₂ PRIMARY BATTERY	SOA 1984	<ul style="list-style-type: none"> 10,000 AH Cells, 3.4 Volt Operating, 34,000 WH/Cell; 0.05m²/Cell = Area; 175 WH/lb.; 3 Yr Life; Poor Safety Record.
	Normal Growth 1990	<ul style="list-style-type: none"> Improve Safety.
	Accelerated Growth 1990	<ul style="list-style-type: none"> Modify Chemistry To Increase Power Density (Up To 205 WH/lb.), And Rate Capability.
Zn/AgO PRIMARY BATTERY	SOA 1984	<ul style="list-style-type: none"> 600 AH Cells; 330 lbm; 64-68 WH/lb.; 90% Efficiency Of Theoretical Capacity.
	Normal Growth 1990	<ul style="list-style-type: none"> Increase WH/lb. By 10%; Investigate Methods To More Efficiently Cool The Battery.
	Accelerated Growth 1990	<ul style="list-style-type: none"> Decrease Weight Of Case Using Thinner Walls And Lighter Materials.

Table 8.2-7 (Cont.)

POWER OPTION	DEVELOPMENT PERIOD	TECHNOLOGY ADVANCEMENTS
STIRLING ENGINE REACTORS SOLAR BRAYTON	SOA 1984	<ul style="list-style-type: none"> • 5-10 Yr Life; Still In Development Stages; Not Space Qualified.
	Normal Growth 1990	<ul style="list-style-type: none"> • No Significant Advancements Towards Space Applications.
	Accelerated Growth 1990	<ul style="list-style-type: none"> • Huge Amounts Of Funding And Much Time Could Result In Some Space Qualified Models.

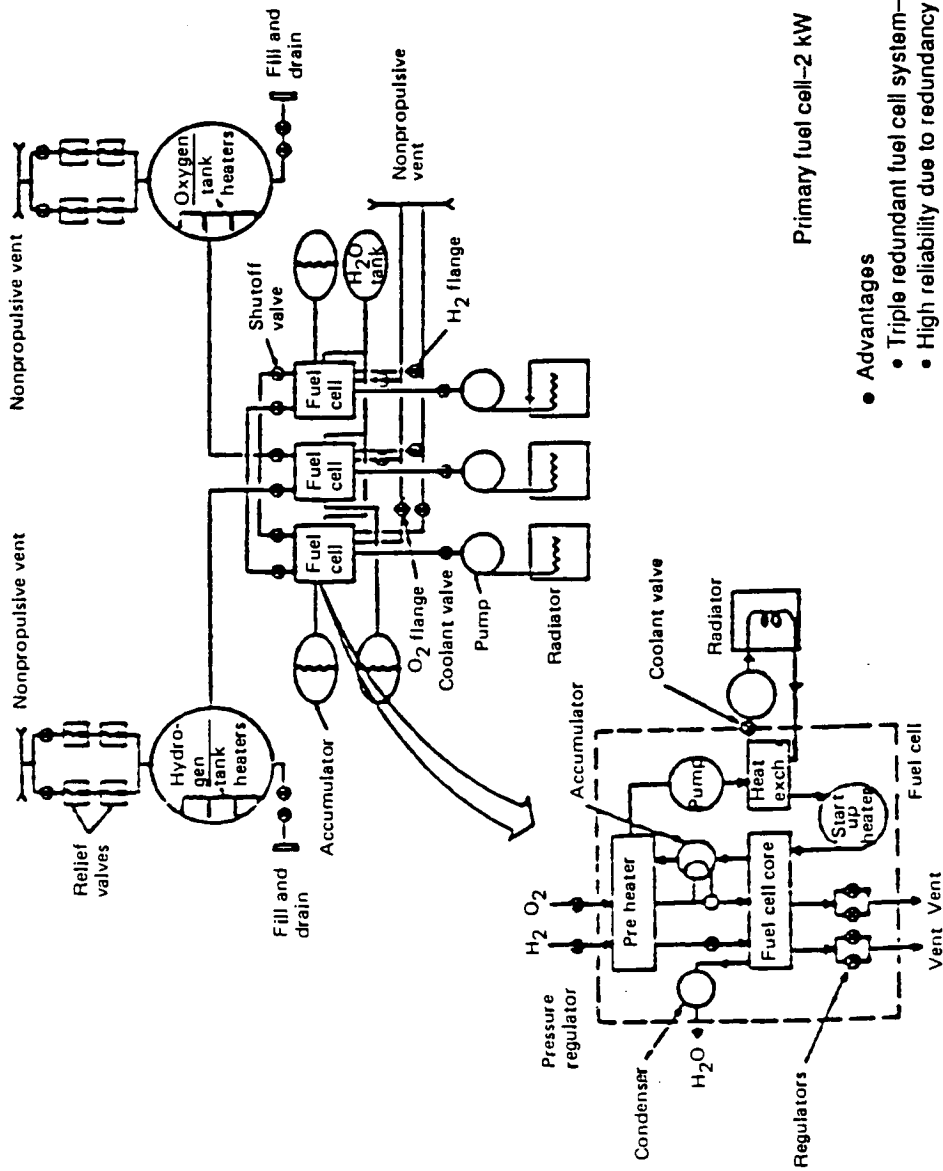
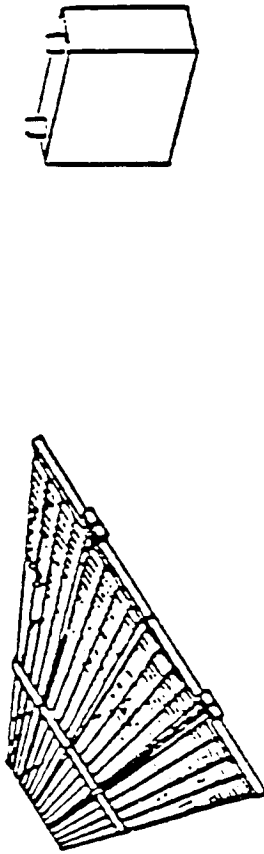


Figure 8.2-3. Baseline Power System



"PADDLE" SOLAR ARRAY / PRIMARY OR SECONDARY BATTERY

ADVANTAGES:

- System Accommodates All Payloads; OTV Not Required To Spin
- Solar Array Provides Debris Shielding
- Solar Array Deployment Angle Is Tailored To Mission Requirements
- Primary Batteries Are Small And Light
- Secondary Batteries Need Only Be Recharged At The Space Station

DISADVANTAGES:

- Deployable Solar Array Increases Complexity
- Primary Batteries Must Be Replaced After Each Mission
- Secondary Batteries Heavier Than Primaries

Figure 8.2.4 Alternate Choice Power System

9.0 PERFORMANCE

9.1 GROUND RULES AND ASSUMPTIONS

For the purposes of this study, several orbits were assumed in order to perform velocity and delta-velocity calculations. Significant orbital assumptions included:

<u>ORBIT</u>	<u>PERIGEE ALTITUDE</u>	<u>APOGEE ALTITUDE</u>	<u>INCLINATION</u>
LEO Space Station	270 nm.	270 nm.	28.5 deg.
GEO/GEO Space Station	19323	19323	0
Molniya	500	21300	63.4
Moon	207560	207560	28.5
LLO/Lunar space Station	70	70	0

For the ground based OTV, the capability of the Space Shuttle acted as the constraint for vehicle sizing and maximum payload considerations. Equations for the shuttle's deployment payload capability as a function of delivery altitude (nm) were assumed to be:

<u>DELIVERY INCLINATION</u>	<u>SHUTTLE DEPLOY PAYLOAD CAPABILITY</u>
28.5 DEG.	Payload = $87960 - 114 * (\text{delivery altitude})$
57.0	Payload = $69300 - 100 * (\text{delivery altitude})$

Gravity and steering losses experienced by the OTV were considered for only the initial perigee burns, and were approximated based on the equations detailed in Reference 47 for constant thrust and acceleration burns.

The reference vehicle's main propulsion system (MPS) consisted of 2 advanced engines with a specific impulse of 483.2 seconds and a total thrust of 10000 lbs. Start/Stop losses were assumed to be 25 lbs. for all MPS burns, and the MPS boiloff rate was assumed to be 3.7 lbs/hr. The attitude control system (ACS) had a specific impulse of 220 seconds. The electric power system (EPS) was assumed to expend 1.5 lbs/hr under normal operations, and 0 lbs/hr when docked to the Space Station. MPS, ACS, and

EPS reserves equalled 2%, 10%, and 20% of the nominal propellant required for the mission.

Certain generic delta-V's were assumed for the MPS and ACS for all mission classes. These were:

<u>ACTIVITY</u>	<u>SYSTEM</u>	<u>DELTA-V</u>
Pre-aeromaneuver correction	MPS	50 fps.
Coast for 1 orbit	ACS	20
Payload positioning	ACS	15
Unmanned Geo coast	ACS	50
Separation	ACS	10
Rendezvous	ACS	20
Docking	ACS	20

9.2 TRAJECTORY ANALYSIS

9.2.1 Impulsive Trajectories

9.2.1.1 Launch to Space Station

Certain ground based configurations start from a Shuttle delivered circular orbit, then proceed to the Space Station to mate with their payload, 2nd stage, or auxiliary MPS tanks. The impulsive delta-V's necessary to do this were:

<u>INITIAL CIRCULAR ORBIT</u>	<u>PERIGEE DELTA-V</u>	<u>APOGEE DELTA-V</u>
120 nm	261 fps	259 fps
140	225	223

9.2.1.2 GED Missions

The transfer from low Earth orbit (LEO) at 28.5 degrees inclination to geosynchronous orbit (GEO) was made either directly from the Space Shuttles or the Space Stations altitude. Impulsive delta-velocities corresponding to optimal inclination splits, delta inclinations, and transfer times are given below for the LEO to GEO transfers considered in this study:

DEPARTURE <u>ALTITUDE</u>	PERIGEE <u>DELTA-V</u>	APOGEE <u>DELTA-V</u>	PERIGEE <u>DELTA-I</u>	APOGEE <u>DELTA-I</u>	COAST <u>TIME</u>
120 nm	8108 fps	5865 fps	2.18 deg	28.32 deg	5.25 hrs
140	8074	5856	2.19	26.31	5.27
270	7856	5798	2.26	26.24	5.31

Deorbit from GEO to atmospheric entry for aeromaneuver involved lowering perigee altitude to 45 nm and 28.5 deg plane change. The impulsive delta-V for this maneuver is 6050 fps.

9.2.1.3 Lunar Missions

Delta-V's for the lunar missions were calculated based on a patched conic approach as outlined in reference 48. For the assumptions used, the required velocity increments for a transfer from a Low Earth Orbit (LEO) of 270 nm to a Low Lunar Orbit (LLO) of 70 nm. are dependent on the one-way transfer time:

LEO TO LLO <u>TRANSFER TIME</u>	LEO <u>DELTA-V</u>	LLO <u>DELTA-V</u>
62 hrs	10180 fps	3190 fps
68	10130	2973
80	10080	2750
120	10030	2536

The LLO escape burn was assumed equal to the injection burn, and 180 fps was allowed for plane change and midcourse correction.

9.2.1.4 Molniya Missions

The transfer from the Space Station (at 28.5 deg) to Molniya orbit was quite different from the ascent initialized from the Space Shuttle (at 57 deg). From the Space Station, a near optimal 3-burn ascent trajectory with a delta-V of 14685 fps compares favorably to a near optimal 2-burn ascent with a delta-V of 16080 fps. A near optimal 3-burn ascent to Molniya and return profile is covered in detail in Appendix A and summarized below:

-----ORBIT PRIOR TO BURN----- ---BURN---

PERIGEE <u>ALTITUDE</u>	APOGEE <u>ALTITUDE</u>	<u>INCLINATION</u>	<u>RAAN</u>	ARGUMENT <u>OF PERIGEE</u>	<u>DELTA-V</u>
270 nm	270 nm	28.5 deg	-15 deg	0 deg	7881 fps
270	19852	29.2	-11.6	246	4641
2345	26142	57.5	10.1	249	2163
500	21300	63.4	0	270	3383
2940	51856	57.9	6	235	2575
45	47069	28.5	-27.5	250	AEROBRAKE

From a Space Shuttle launched to 140 nm. orbit with an inclination of 57 degrees, a 3-burn ascent no longer offers a significant advantage over a 2-burn, and an ascent delta-V of 9507 fps is all that is required for the 2-burn transfer.

9.2.1.5 Planetary Missions

Transferring a payload from LEO to an interplanetary trajectory could be accomplished in one of three ways:

- (1) Using a reusable OTV that first attains the desired escape energy (C₃) - with the payload, then returns to an elliptical orbit, and finally deorbits for aerobraking,
- (2) The OTV is expended after attaining the escape energy (C₃) for the interplanetary trajectory, or
- (3) The payload includes a kick stage to accomplish the interplanetary trajectory thereby allowing the OTV to perform a less energetic return for the aerobraking maneuver.

Typical transfers from the Space Station orbit (270 mn) to an interplanetary trajectory and return to 270 nm requires the following:

ESCAPE ENERGY C ₃ (Km ² /sec ²)	ESCAPE DELTA-V (fps)	REDUCE APOGEE TO 4xGEO DELTA-V (fps)
20	13272	3712
28	14381	4821
50	17282	7723
98	22997	15222

To lower perigee from Space Station altitude (270 nm) to aerobraking altitude (45 nm) an additional 47 fps burn at apogee (4xGEO) is required.

9.2.1.6 Aerobraking Maneuvers

For the aerobraking maneuver, the assumed atmospheric entry and exit perigees values were based on those typically found on integrated trajectory runs (Section 9.2.3). The assumed entry perigee altitudes were 45 nm on entry, 30 nm on exit. For those missions returning to the Space Station, the delta-V required at apogee to go into a 260 nm by 270 nm orbit is 420 fps. For those missions which are retrieved by the Space Shuttle, the delta-V to go into a 150 nm circular orbit is 216 fps.

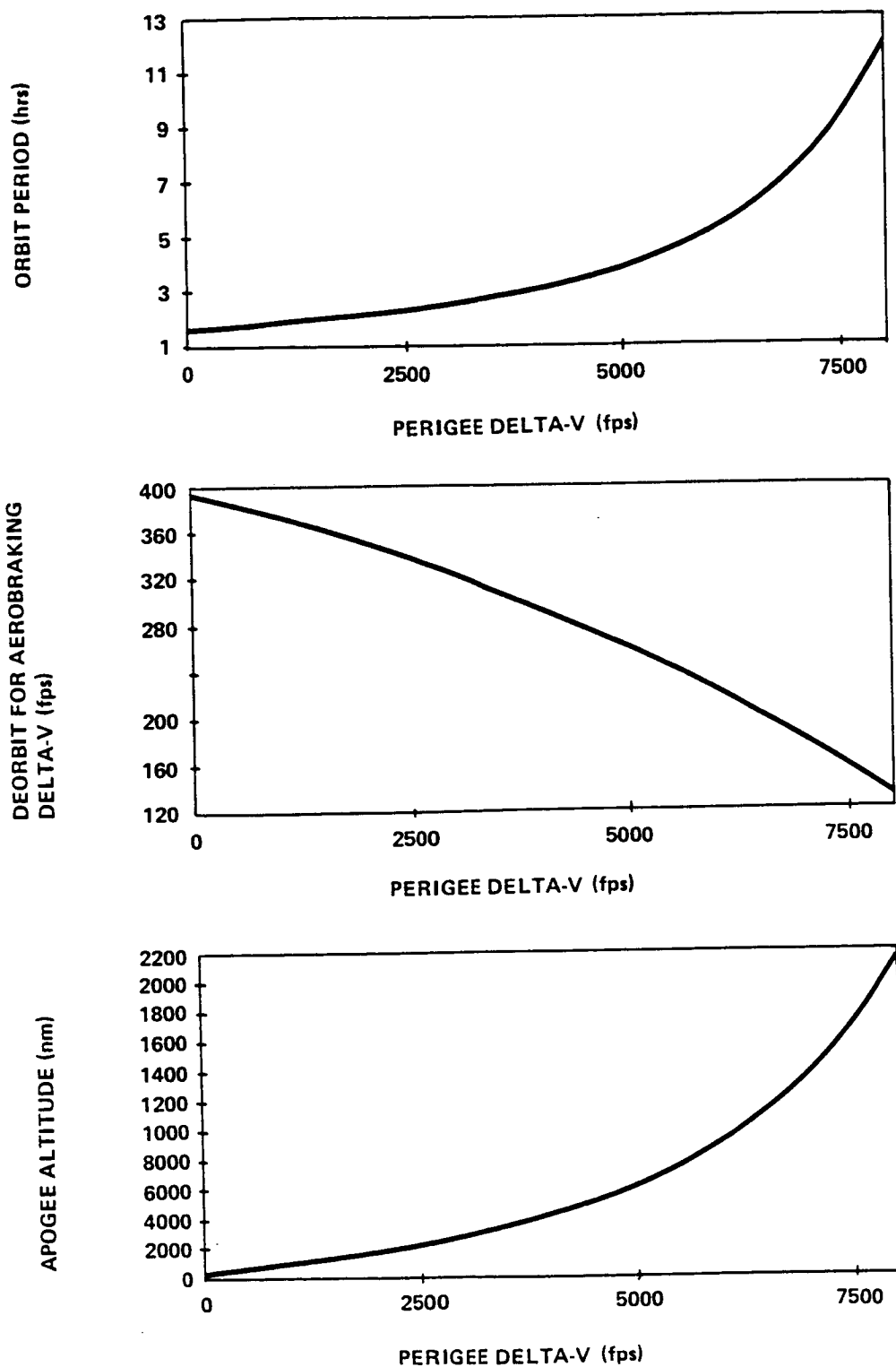
9.2.1.7 Multiple Perigee Burn Missions

Multiple perigee burns were employed to allow for phasing, reduce gravity and steering losses, and to allow time for the staging of multistage vehicles. Assuming an initial altitude of 270 nm and no plane change for initial burns, figure 9.2.1-1 shows the intermediate orbit period, apogee altitude, and apogee delta-V requirements to lower perigee to 45 nm for aerobraking, all as a function of the previously done perigee delta-V.

9.2.1.8 Space Station Rendezvous

Phasing the OTV with the Space Station at the conclusion of its mission has been handled in previous studies by having the OTV park in a phasing orbit until its line of nodes matches with the Stations, and a rendezvous made. In this study however, a trade between four methods of phasing from GEO were analyzed, and a different method was chosen for a baseline. The four methods analyzed were:

1. "Forward Phasing" The OTV exits from aerobraking and phases with the Space Station by moving into an orbit with a period smaller than that of the station. The OTV moves forwards with respect to the Station until their nodes are aligned.

*Figure 9.2.1-1 Intermediate Orbit Characteristics*

2. "Backwards Phasing" The OTV exits from aerobraking and phases with the Space Station by moving into an orbit with a period larger than that of the station. The OTV moves backwards with respect to the station until their nodes are aligned.

3. "Transfer Time Phasing" The OTV adjusts its transfer ellipse at GEO in order to adjust for the expected node misalignment at Space Station rendezvous.

4. "Double Aeropass Phasing" The OTV goes thru one aerobraking maneuver and exits into an orbit with a period which adjusts for the expected node misalignment and then goes thru a second aerobraking maneuver to reduce apogee.

A detailed comparison of return time and delta-V requirements for these various options from GEO to the Space Station may be found in Appendix B as a function of the expected node misalignment. Forward phasing has a minimal delta-V requirement but, for large misalignments, the phasing time becomes very long due to the period difference may never be very large without the perigee altitude entering the atmosphere. Backward phasing has the potential for shorter transfer times, but this also translates into a higher delta-V penalty. Double aeromaneuver offers low delta-V and short return time, but penalties associated with 2 aeromaneuvers prevent this from being viewed realistically. Transfer time phasing offers a very nice combination of short return times and small delta-V penalties. A worst case phasing was baselined, which represents an increase in return time of 55 minutes and a delta-V penalty of 195 fps over a Hohmann approach.

9.2.1.9 GEO Satellite Servicing Mission

In the GEO manned sortie mission, the OTV executes phasing maneuvers in GEO in order to meet four satellites with separation angles of 10 and 90 degrees. Phasing was accomplished by moving in and out of a phasing orbit with two burns of equal magnitude. Forward and backwards phasing were both analyzed, and a complete map of delta-V requirements versus phasing time is shown as a function of separation angle in figure 9.2.1-2. For the baseline mission, the following transfers were chosen:

ANGLE OF SEPARATION	PHASING ORBITS	PERIGEE ALTITUDE	APOGEE ALTITUDE	TOTAL DELTA-V	PHASING TIME
10 deg	2	19323 nm	19744 nm	92 fps	48.5 hrs
90	5	19323	20829	320	126

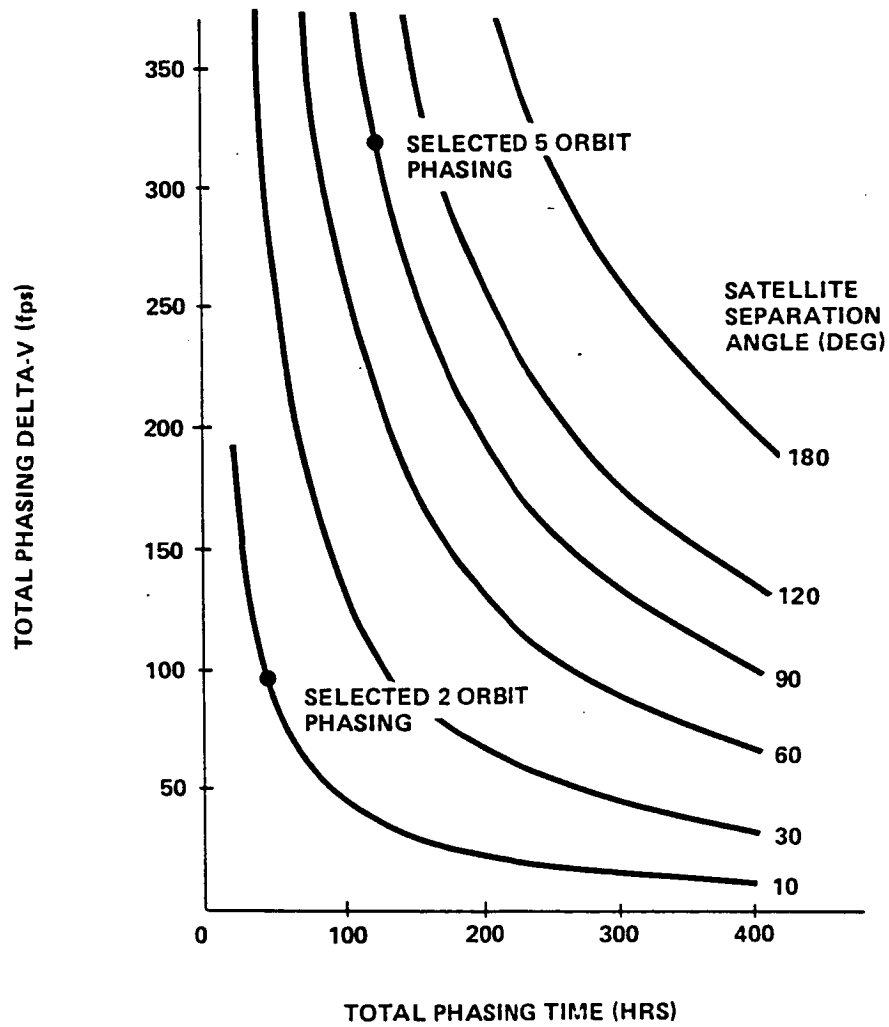


Figure 9.2.1-2 Phasing at GEO Between Satellites

9.2.2 Non-Impulsive Trajectories

For the performance analysis, gravity and steering losses were approximated based on the equations found in reference 47, and only considered for the initial perigee burns. The approximate velocity losses for constant acceleration and constant thrust for the baseline space-based vehicle LEO to GEO transfer are shown in figure 9.2.2-1 as a function of the initial thrust-to-weight (acceleration) and the number of perigee burns. The benefits of going from one perigee burn to two is a significant one, becoming less so as the number increases. Appendix C gives a more detailed explanation to the assumptions and equations used throughout the study.

The validity of the above approximate method for this study was checked using the Program to Optimize Simulated Trajectories (POST) and another integrated trajectory optimizer detailed in reference 47. A comparison between approximated losses and "exact" losses are shown in figure 9.2.2-2 for various initial thrust-to-weights, various number of perigee burns, constant thrust, and specific impulse of 483 seconds. The initial circular orbit had an altitude of 270 nm, inclined at 28.5 degrees, while the final circular orbit had an altitude of 19323 nm, at 0 degrees inclination. A comparison for an initial thrust-to-weight of 0.1 g's and two perigee burns is detailed below:

APPROXIMATE LEO TO GEO TRANSFER

-----ORBIT PRIOR TO BURN-----			-----BURN-----
<u>PERIGEE</u>	<u>APOGEE</u>		
<u>ALTITUDE</u>	<u>ALTITUDE</u>	<u>INCLINATION</u>	<u>DELTA-V</u>
270 nm	270 nm	28.50 deg	3522 fps
270	3332	27.37	4473
270	19323	26.24	5799

} 7995

EXACT LEO TO GEO TRANSFER

-----ORBIT PRIOR TO BURN-----			-----BURN-----
<u>PERIGEE</u>	<u>APOGEE</u>		
<u>ALTITUDE</u>	<u>ALTITUDE</u>	<u>INCLINATION</u>	<u>DELTA-VEE</u>
270 nm	270 nm	28.50 deg	3627 fps
316	3469	27.4	4388
362	19320	26.38	5774

} 8015

CONSTANT ACCELERATION OF 0.1 G's TRANSFER
 • OPTIMAL PERIGEE BURN SPLIT

NUMBER OF PERIGEE BURNS	VELOCITY LOSS (fps)
1	860
2	218
3	98
5	37

CONSTANT THRUST TRANSFER
 • OPTIMAL PERIGEE BURN SPLIT

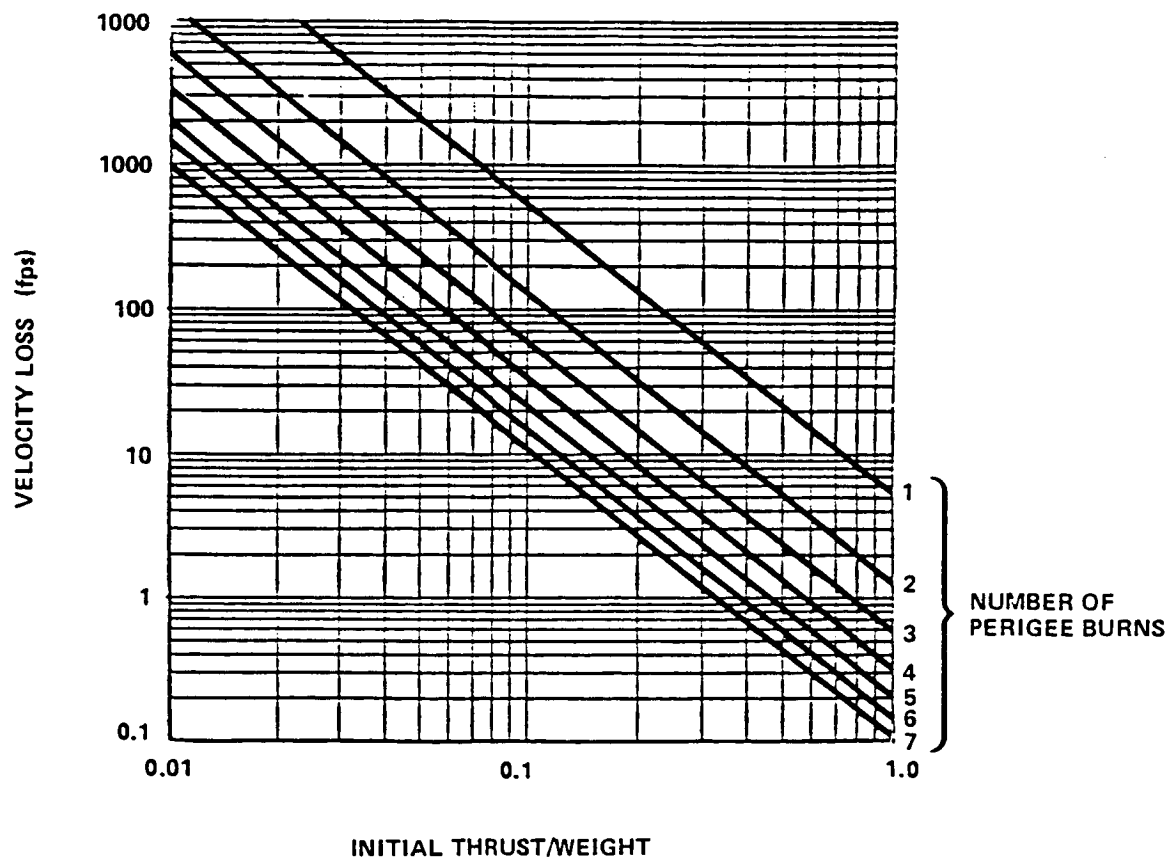


Figure 9.2.2-1 Approximate LEO to GEO Velocity Losses

NUMBER OF PERIGEE BURNS	INITIAL THRUST/WEIGHT	VELOCITY LOSS (fps) APPROXIMATE	EXACT	TRIP TIME (HRS) APPROXIMATE	EXACT
1	.50	21.1	21.0	5.31	5.39
1	.22	104.8	102.0	5.31	5.51
1	.10	553.6	484.1	5.31	5.84
1	.05	2215.	1433.	5.31	6.70
2	.22	26.3	26.2	8.03	8.15
2	.10	138.6	134.6	8.03	8.32
2	.05	554.9	496.6	8.03	8.66
3	.22	11.8	11.7	11.14	11.23
3	.10	62.0	61.3	11.14	11.26
3	.05	248.3	236.0	11.14	11.60

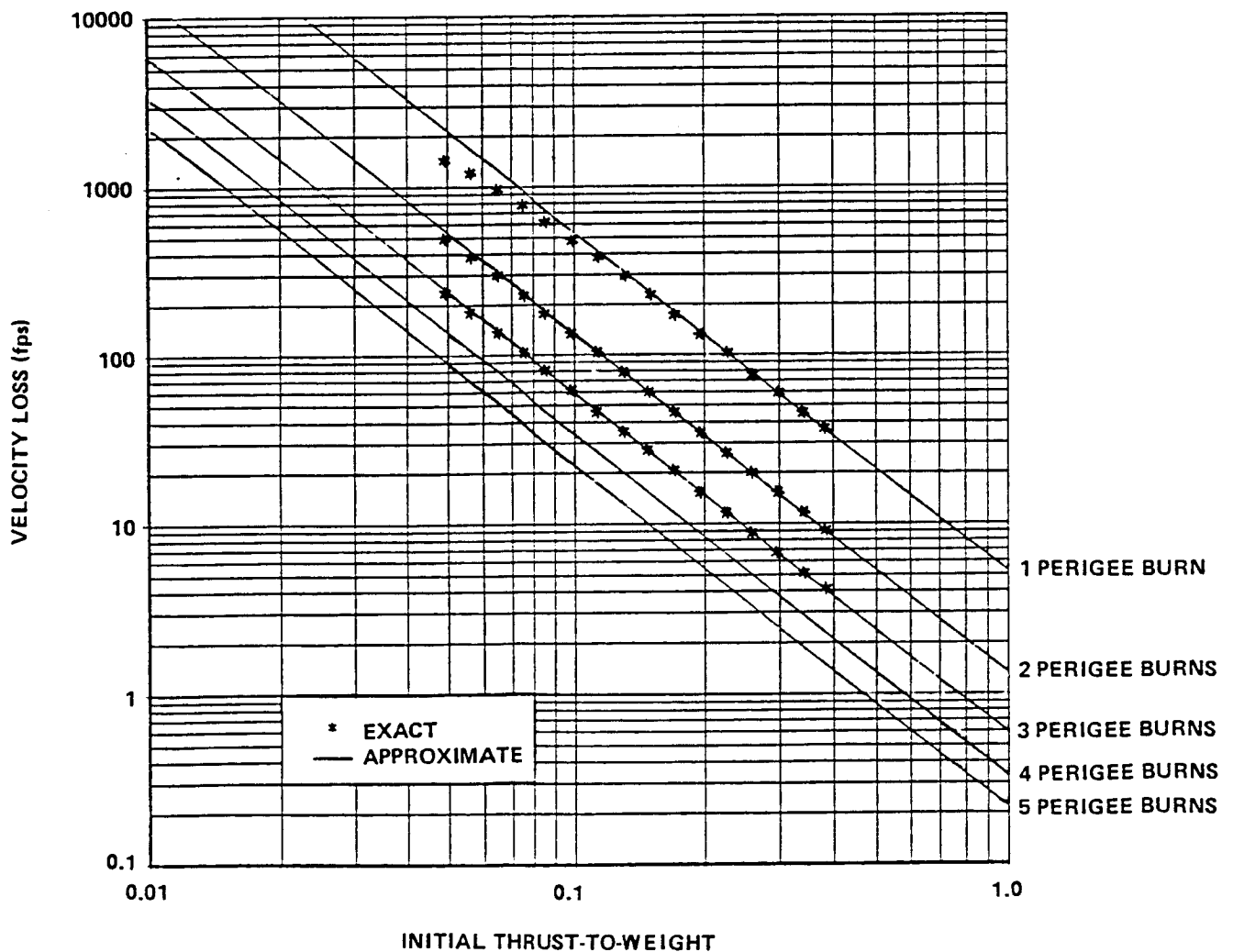


Figure 9.2.2-2 Comparison Between Approximate and Integration Velocity Losses

From above, it is seen that the approximation underestimates the perigee delta-V by 20 fps, but overestimates the apogee delta-V by 25 fps, tending to cancel out each other for the total loss difference of 5 fps. Therefore, this approximation may not be adequate in estimating losses for planetary escape missions, where this cancelling effect between perigee and apogee burns is never realized. However, for the thrust-to-weights being considered for OTV missions to GEO, this approximation is more than accurate enough for this phase of the study.

9.2.3 Aeromaneuver Trajectories

The characteristics of the aerobraking maneuver require that an integrated trajectory tool of some sort be used for the analyses. The Program to Optimize Simulated Trajectories (POST) was chosen for its simplicity and universal acceptance. Nominal trajectories were flown with fixed steering angles throughout the atmospheric pass. Atmospheric forces were considered below 400,000 ft and were modelled using the 1962 U.S. standard atmosphere. Entry and exit apogees were constrained to 19323 and 270 nm, respectively. Typical altitude vs. time and relative velocity are shown in figure 9.2.3-1 for a ballute vehicle with various ballistic coefficients. Angle of attack, bank, and sideslip were all fixed at 0 degrees for these runs. Values for the perigee altitude at an altitude of 400,000 ft for entry and exit were:

BALLISTIC COEFFICIENT	ENTRY PERIGEE	EXIT PERIGEE
2 lbs/ft**2	47.24 nm	32.00 nm
4	45.22	30.32
8	43.16	28.47
16	40.92	25.71
32	38.46	22.37

Trajectories for lifting devices were modelled in a similar manner, with the exception of the steering angles. Sideslip remained at 0 degrees, but angle of attack ranged from 0 to 60 degrees, and bank angle between 90 and 180 degrees.

9.3 PERFORMANCE ANALYSIS

In order to consistently trade among the various OTV concepts, a performance tool was developed which compiled inputs from the various disciplines, including: mission

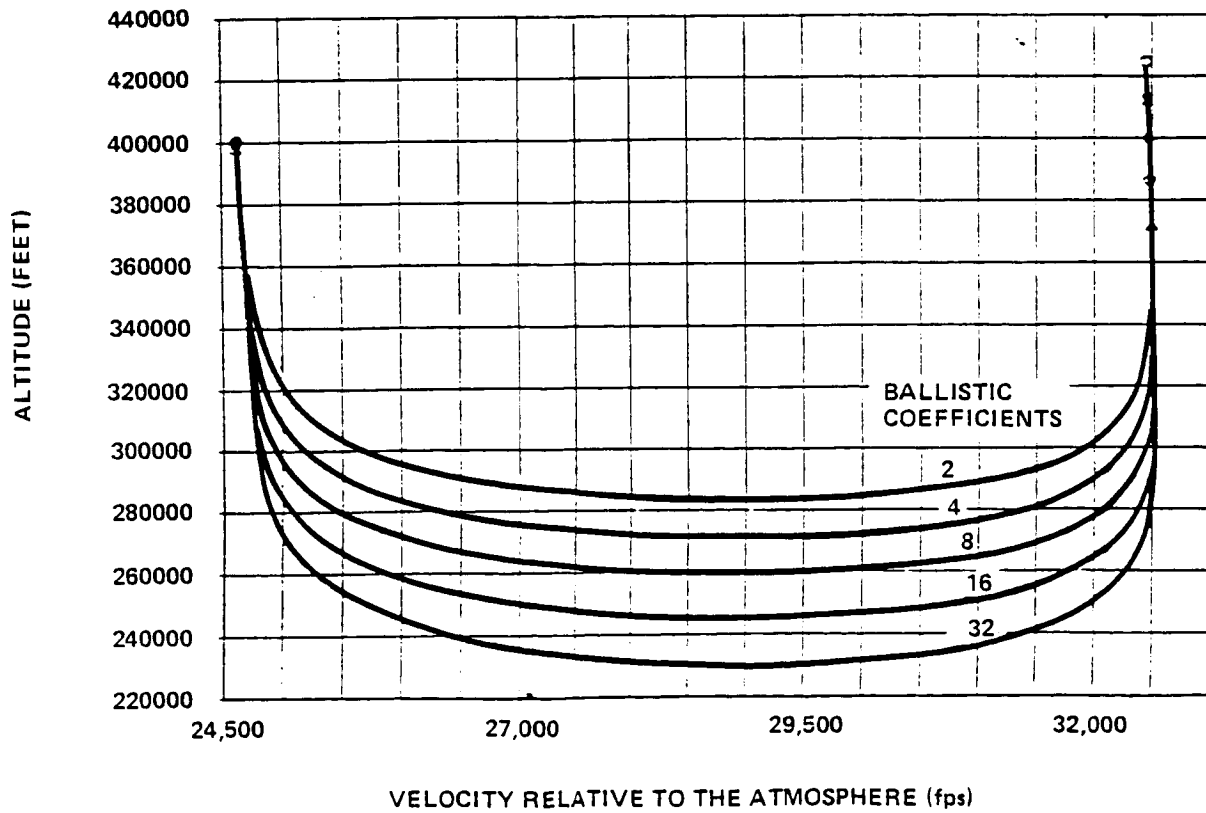
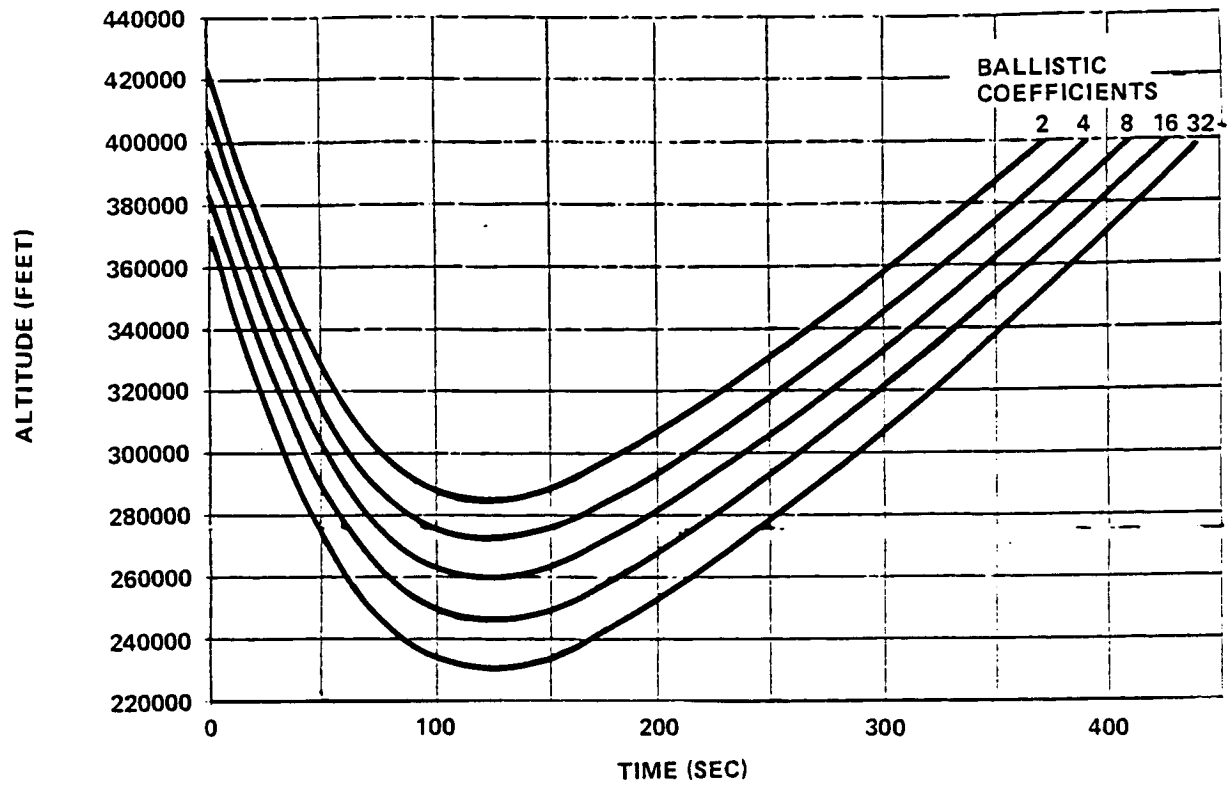


Figure 9.2.3-1 Nominal Aerobraking Profiles

analysis, trajectory analysis, weights, guidance, propulsion, and electric power. The necessary capabilities this tool had included are the ability to size or find offloaded performance based on payload, propellant, or start mission weight constraints. Inputs from the various disciplines were either assumed by the program or manually input. Mission timelines were run in reverse from the end of mission weights, and various parameters of interest were bookkept and totalled one event at a time. Vehicles were sized based on point-slope equations for the OTV and/or auxiliary MPS usable propellant jettisonable ballute weights as a function of MPS usable propellant necessary to accomplish the mission.

9.4 SPACE BASED VEHICLE TRADES

The space based vehicle trades were done against the low and nominal mission models. The sizing mission was chosen on the basis of the most demanding mission under a specific basing/vehicle/mission model rationale. The MPS propellant requirements for a space based vehicle with advanced engines sized specifically for several missions in the low mission model is shown pictorially in figure 9.4-1. This figure shows that the 7500 lb GEO manned sortie mission is the mission which requires the most MPS usable propellant, and therefore is the sizing mission under said rationale.

The vehicle sized for the 7500 lb GEO manned sortie mission has the heaviest end-of-mission and ballute weights, due to it needing larger MPS propellant tanks, a larger ballute to return a 7500 lb payload, and more equipment on board to satisfy the man-rating criterion. Use of this vehicle on the other "less demanding" missions significantly raises the propellant requirements for these missions, and has the potential to require even more propellant than that for which the tanks were originally sized. Figure 9.4-2 shows the propellant requirements for the vehicle previously sized for the 7500 lb GEO manned sortie mission, when required to do other missions in the low mission model. As this figure shows, the 20,000 lb GEO unmanned low g (acceleration) mission now requires more MPS usable propellant than the manned sortie mission, but when boiloff losses, start/stop losses, and residuals are accounted for, the manned sortie mission requires more MPS total propellant.

For the optimization of the space based vehicle, a consistent set of assumptions on the sizing rationale needed to be determined. The low mission model was chosen, since those missions were definite requirements which had to be fulfilled. The aerobrake was sized for a 7500 lb return payload, which represented the largest requirement in the mission model. The vehicle's MPS tank sizing mission was not as clear cut of an issue, as the previous paragraph may indicate. The 7500 lb GEO manned sortie mission

- VEHICLE SIZED FOR MISSIONS
- SPACE BASED 1 STAGE
- 2 ADVANCED ENGINES, $\epsilon=1000$, HYDRAZINE RCS
- EXPENDABLE BALLUTE-TURNDOWN 1.5, BACKWALL TEMP=600°F

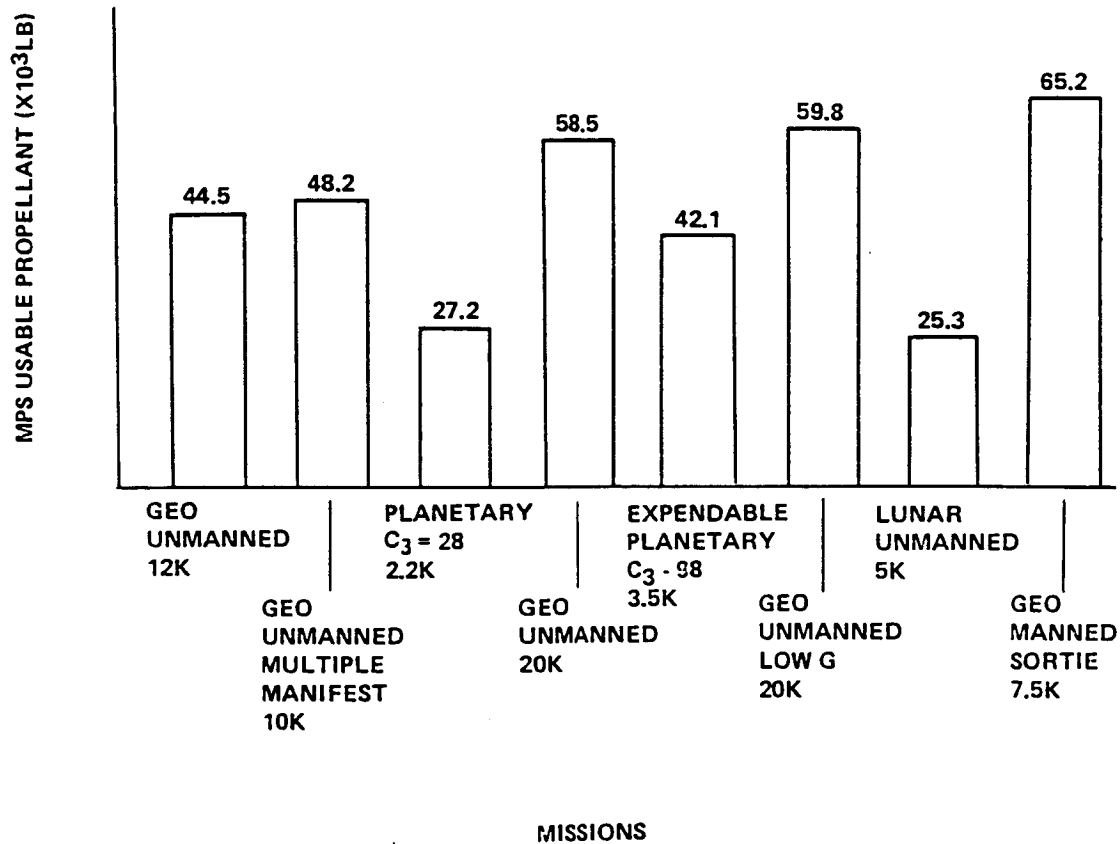


Figure 9.4-1 Sizing Missions Propellant Requirements

- VEHICLE SIZED FOR SPACE BASED MANNED GEO SORTIE
- 2 ADVANCED ENGINES, ϵ -1000, HYDRAZINE RCS
- EXPENDABLE BALLUTE-TURNDOWN 1.5, BACKWALL TEMP=600°F

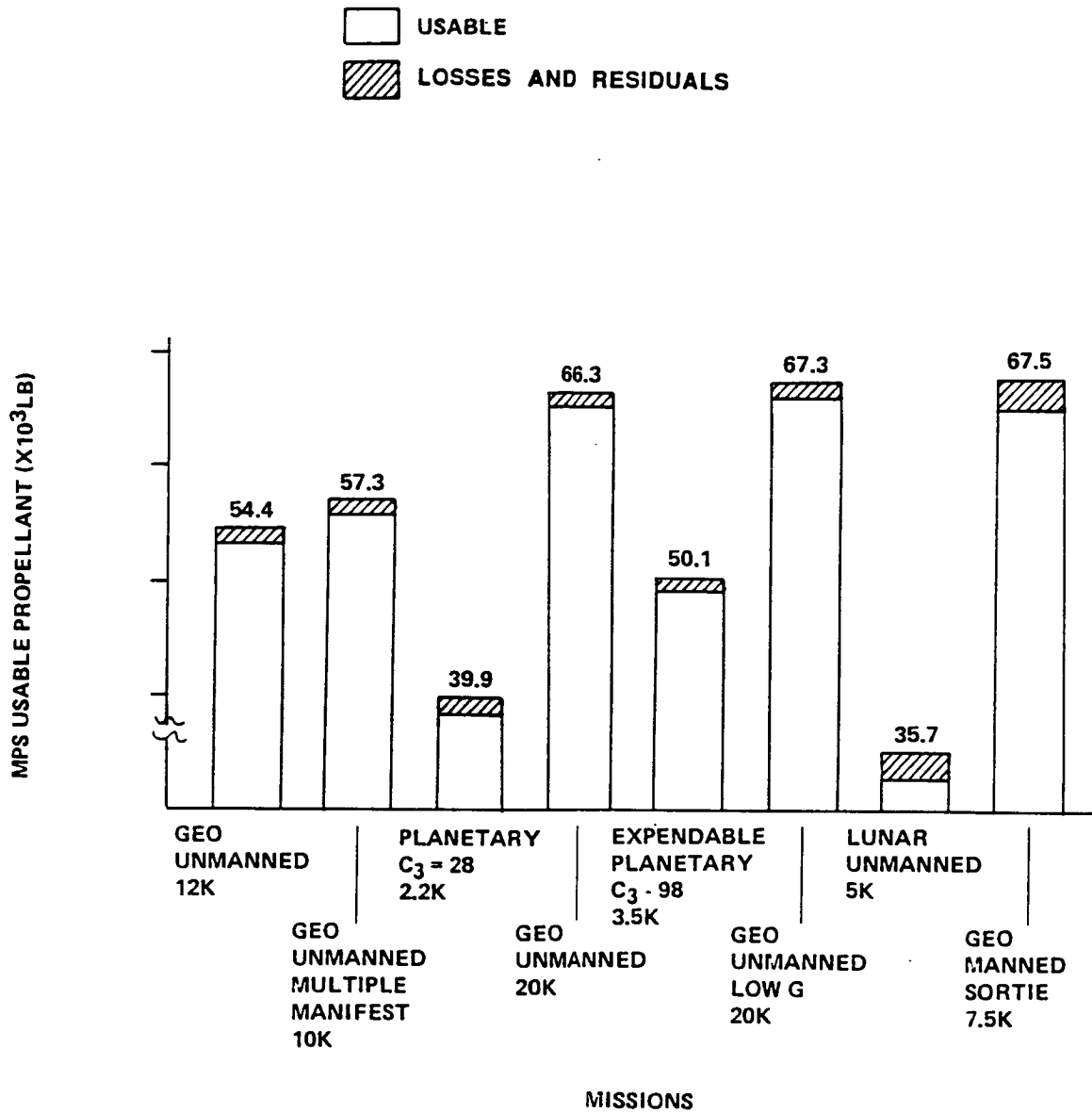


Figure 9.4-2 Offloaded Missions Propellant Requirements

required more total propellant for some concepts, and the 20,000 lb GEO unmanned low g mission required more total propellant for other sets. However, the differences between the two were usually less than 500 lbs with the 20,000 lb GEO low g mission usually requiring the most. Therefore, the 20,000 lb GEO low g mission was chosen to size the main propellant tanks for the space based optimization trades.

For the space based vehicle optimization, vehicles were individually sized in accordance with the above sizing assumptions, and then offload propellant requirements were determined for other mission classes as a function of the payload. For the GEO manned sortie mission, the payload was taken to be the manned module, and for the GEO unmanned multiple manifest mission, the payload was considered separate from the 2,000 lb payload carrier rack. In the following subsections, a summary of inputs and outputs will be given for each major trade. Weights inputs are given as weight as a linear function of MPS usable propellant in the form:

$$\text{OTV end of mission weight} = A + B * (\text{MPS usable propellant})$$

$$\text{Jettisonable ballute} = C + D * (\text{MPS usable propellant})$$

Similarly offloaded propellant requirements for various mission classes are given as a linear function of the payload:

$$\text{MPS total propellant} = A + B * (\text{Payload})$$

For the purposes of comparison, all trades were made against a reference vehicle. The reference vehicle performance characteristics are summarized in table 9.4-1. The actual performance sizing run computer output is shown in table 9.4-2. Sizing for the reference vehicle as well as for the vehicles involving the trade parameters was as follows: propellant capacity was dictated by the needs of the low g 20K lbm delivery mission; aerobrake sizing was established by the manned GEO roundtrip mission.

This vehicle was compared with several alternate concepts, in the form of the following 7 trades (the first option listed is that used by the reference vehicle).

1. Expansion ratio (1000, 900, 700, 500)
2. Main engine (Advanced, RL10-IIB, RL10-III)
3. Attitude control system propellant (Hydrazine, Oxygen-Hydrogen)
4. Ballute backwall temperature (600, 1500 deg F) and Drag control (Ballute turndown, Engine Modulation)
5. Lifting Brake L/D (-0.1, -0.2, -0.3)
6. Ballute turndown ratio (1.25, 1.5, 2.2)
7. Aeroassist device (Expendable Ballute, Lifting Brake, Shaped Brake)

Table 9.4-1 Reference Vehicle Summary

AEROBRAKE	expendable ballute, with backwall temperature of 600 deg F, turndown ratio of 1.5, and post aeromaneuver guidance correction of 251 fps.	
PROPULSION	MPS: 2 advanced engines, with an expansion ratio of 1000, thrust of 5000 lbs per engine, specific impulse of 483.2 sec, and throttled for low g mission specific impulse of 481.2 sec. ACS: Hydrazine, with a specific impulse of 220 sec.	
WEIGHT TRENDING		
	A	5852
	B	.0540
	C	1307
	D	.0264
SIZING		
	MPS Usable (lbs)	66682
	End of Mission (lbs)	9452
	Jettisonable Ballute (lbs)	3067
PROPELLANT REQUIREMENTS = A+B * Payload Wt.		
GEO unmanned multiple manifest	A	42599
	B	1.501
GEO unmanned	A	36755
	B	1.493
GEO manned sortie	A	44397
	B	3.150
Planetary, $C_3 = 28 \text{ km}^2/\text{sec}^2$	A	34868
	B	2.042
Geo unmanned Low g	A	37750
	B	1.498
Lunar unmanned	A	28598
	B	1.405

Table 9.4-2. Reference Vehicle Computer Sizing Output

OTV AND BALLUTE SIZING: A = 5852., B = .0540, C = 1307., D = .0264

MISSION/BASING: SPACE BASED GEO UNMANNED (LOW G)
 BRAKE: EXPENDABLE BALLUTE (600 DEG), BALLUTE TURNDOWN RATIO = 1.5
 ENGINE: ADVANCED (2), THROTTLED TO G LIMIT = 0.10
 PROPULSION: MPS ISP = 481.2, ACS ISP = 220.0
 STAGES: 1
 VEHICLE SIZING: SPACE BASED GEO UNMANNED (LOW G)
 BALLUTE SIZING: SPACE BASED GEO MANNED MGSS SORTIE

MISSION PROFILE	DELTA V (F/S)	DELTA T (HOURS)	DELTA W (LBS)	WEIGHT (LBS)
MAIN STAGE:				MAIN
1 DOCKED AT LEO STATION	0.	2.0	-7.	99194.
2 ACS SEPARATION	10.	0.0	-140.	99054.
3 ACS COAST	10.	0.8	-144.	98910.
4 MPS PERIGEE BURN 1 *	3928.	0.2	-22714.	76196.
5 ACS COAST	20.	3.0	-231.	75966.
6 MPS PERIGEE BURN 2 *	3928.	0.2	-17449.	58517.
7 ACS COAST	10.	5.3	-110.	58406.
8 MPS BURN	5798.	0.1	-18261.	40145.
9 ACS PAYLOAD POSITIONING	15.	1.0	-90.	40055.
10 DROP PAYLOAD	0.	0.0	-20000.	20055.
11 ACS COAST	50.	24.0	-265.	19790.
12 MPS DEORBIT BURN	6245.	0.1	-6586.	13204.
13 ACS COAST	10.	6.2	-51.	13153.
14 MPS PRE AERO CORRECT	50.	0.1	-67.	13086.
15 AEROMANEUVER	0.	0.1	-3067.	10019.
16 MPS POST AERO CORRECT	251.	0.1	-186.	9833.
17 ACS COAST	10.	0.8	-18.	9815.
18 MPS BURN	420.	0.1	-287.	9528.
19 ACS COAST	10.	0.8	-18.	9511.
20 ACS REND/DOCK	40.	1.0	-59.	9452.

* MAIN STAGE GRAVITY/STEERING LOSS (F/S) = 215.

OTV FLUIDS SUMMARY

MAIN STAGE				
MPS USABLE = 66682.	ACS USABLE = 992.	EPS USABLE = 77.		
NOMINAL = 65375.	NOMINAL = 902.	NOMINAL = 64.		
RESERVES = 1307.	RESERVES = 90.	RESERVES = 13.		
BOILOFF = 166.				
START/STOP = 175.				

These comparisons are discussed in the following subsections. It should be noted, however, the primary parameter for comparison relative to the reference vehicle is the quantity of MPS propellant. Values are also presented to calculate the propellant for other missions. The system level comparison involving costing of these trades is presented in Volume III.

9.4.1 Expansion Ratio Trade

The performance of vehicles with characteristics exactly that of the reference vehicle except using an MPS engine with lower expansion ratios of 900, 700, and 500 is shown in table 9.4-3.

9.4.2 Engine Trade

The performance of vehicles with characteristics exactly that of the reference vehicle except with two RL10-2B's and RL10-III's for main propulsion engines is shown in table 9.4-4.

9.4.3 Attitude Control System Trade

The performance of a vehicle with characteristics exactly that of the reference vehicle except that the attitude control system uses oxygen-hydrogen is shown in table 9.4-5.

9.4.4 Ballute Backwall Temperature and Drag Control Trade

The performance of vehicles with characteristics exactly that of the reference vehicle except that the backwall temperature is 1500 deg F, and also when the main engines are used for turndown with backwall temperatures of 600 and 1500 deg F is shown in table 9.4-6.

9.4.5 Lifting Brake L/D Trade

The performance of vehicles with different lift-to-drag ratios is shown in table 9.4-7.

9.4.6 Ballute Turndown Ratio Trade

The performance of vehicles with characteristics exactly that of the reference vehicle except that the turndown ratios are 1.25 and 2.2 is shown in table 9.4-8.

Table 9.4-3 Expansion Ratio Trade Summary

EXPANSION RATIO	900	700	500	1000 (Ref)
WEIGHT TRENDING				
A	5832	5791	5707	
B	.0540	.0540	.0540	
C	1308	1310	1313	
D	.0264	.0264	.0265	
PROPULSION				
Full thrust MPS Isp (sec)	482.5	481	479	
Throttled for low g Isp (sec)	480.5	479	477	
SIZING				
MPS Usable (lbs)	66682	67129	67456	66682
End of Mission (lbs)	9439	9415	9349	
Jettisonable Ballute (lbs)	3072	3082	3100	
PROPELLANT REQUIREMENTS = A + B * Payload Wt.				
GEO unmanned multiple manifest	A 42685	42881	43056	
	B 1.505	1.512	1.522	
GEO unmanned	A 36826	36988	37118	
	B 1.497	1.504	1.514	
GEO manned sortie	A 44483	44677	44849	
	B 3.158	3.177	3.203	
Planetary, $C_3 = 28 \text{ km}^2/\text{sec}^2$	A 34932	35079	35192	
	B 2.047	2.060	2.075	
Geo unmanned Low g	A 37824	37992	38130	
	B 1.501	1.508	1.518	
Lunar unmanned	A 28644	28748	28830	
	B 1.408	1.415	1.424	

Table 9.4-4. Main Engine Trade Summary

ENGINE	RL10-IIB	RL10-III	Adv. Eng.(Ref)
WEIGHT TRENDING			
	A	6561	6368
	B	.0540	.0540
	C	1269	1279
	D	.0261	.0262
PROPULSION			
thrust/engine (lbs)	15000	7500	
Full thrust MPS Isp (sec)	460	470	
Throttled for low g Isp (sec)	445	458	
SIZING			
MPS Usable (lbs)	82766	76575	66682
End of Mission (lbs)	11028	10501	
Jettisonable Ballute (lbs)	3428	3284	
PROPELLANT REQUIREMENTS = A+B * Payload Wt.			
GEO unmanned multiple manifest	A	52601	48588
	B	1.573	1.542
GEO unmanned	A	46244	42460
	B	1.572	1.537
GEO manned sortie	A	54990	50731
	B	3.337	3.253
Planetary, $C_3 = 28 \text{ km}^2/\text{sec}^2$	A	44191	40577
	B	1.763	1.885
Geo unmanned Low g	A	50149	45377
	B	1.689	1.615
Lunar unmanned	A	34849	32364
	B	1.534	1.477

Table 9.4-5 Trade Summary Attitude Control System

ATTITUDE CONTROL SYSTEM	Oxygen-Hydrogen	N ₂ H ₄ (Ref)
WEIGHT TRENDING		
	A 5894	
	B .0540	
	C 1310	
	D .0267	
PROPULSION		
Attitude control system Isp (sec)	410	
SIZING		
▶ MPS Usable (lbs)	66477	66682
End of Mission (lbs)	9483	
Jettisonable Ballute (lbs)	3084	
PROPELLANT REQUIREMENTS = A + B * Payload Wt.		
GEO unmanned multiple manifest	A 42403	
	B 1.498	
GEO unmanned	A 36610	
	B 1.490	
GEO manned sortie	A 44271	
	B 3.123	
Planetary, C ₃ = 28 km ² /sec ²	A 34803	
	B 2.036	
Geo unmanned Low g	A 37600	
	B 1.495	
Lunar unmanned	A 28534	
	B 1.402	

Table 9.4-6 Ballute Backwall Temperature and Drag Control Trade Summary

BACKWALL TEMPERATURE	1500	600	1500	600	(Ref)
DRAG CONTROL	Ballute	Engine	Engine	Ballute	
WEIGHT TRENDING					
	A	6013	5669	5806	
	B	.0573	.0540	.0578	
	C	788	1882	1014	
	D	.0143	.0066	.0032	
GUIDANCE					
Post aeromaneuver correction (fps)	251	285	285		
SIZING					
♦ MPS Usable (lbs)	63481	64646	62365	66682	
End of Mission (lbs)	9650	9232	9482		
Jettisonable Ballute (lbs)	1696	2536	1440		
PROPELLANT REQUIREMENTS = A + B * Payload Wt.					
GEO unmanned multiple manifest	A	39431	40602	38341	
	B	1.497	1.499	1.495	
GEO unmanned	A	33595	34746	32491	
	B	1.489	1.491	1.488	
GEO manned sortie	A	41099	42297	39944	
	B	3.140	3.153	3.146	
Planetary, $C_3 = 28 \text{ km}^2/\text{sec}^2$	A	31792	32909	30725	
	B	1.991	2.009	1.975	
Geo unmanned Low g	A	34521	35697	33392	
	B	1.498	1.498	1.498	
Lunar unmanned	A	26510	27272	25784	
	B	1.398	1.400	1.395	

Table 9.4-7 Lifting Brake L/D Trade Summary

L/D		- 0.117	- 0.226	- 0.324
WEIGHT TRENDING				
	A	7314	7314	7778
	B	.0723	.0723	.0651
GUIDANCE				
Post aeromaneuver correction (fps)		464	546	653
SIZING				
	MPS Usable (lbs)	67197	67534	67879
	End of Mission (lbs)	12172	12196	12197
PROPELLANT REQUIREMENTS = A+B * Payload Wt.				
GEO unmanned multiple manifest	A	43219	43595	43995
	B	1.502	1.502	1.503
GEO unmanned	A	37265	37597	37940
	B	1.494	1.494	1.494
GEO manned sortie	A	44903	45241	45589
	B	3.210	3.234	3.265
Planetary, $C_3 = 28 \text{ km}^2/\text{sec}^2$	A	35374	35701	36039
	B	2.045	2.049	2.053
Geo unmanned Low g	A	38258	38596	38946
	B	1.497	1.497	1.497
Lunar unmanned	A	29039	29284	29543
	B	1.405	1.406	1.407

Table 9.4-8 Ballute Turndown Ratio Trade Summary

Turndown Ratio	1.25	2.20	1.5 (Ref)
WEIGHT TRENDING			
A	5892	5854	
B	.0542	.0545	
C	1128	4900	
D	.0208	.0009	
GUIDANCE			
Post aeromaneuver correction (fps)	417	135	
SIZING			
MPS Usable (lbs)	65453	72698	66682
End of Mission (lbs)	9438	9814	
Jettisonable Ballute (lbs)	2489	4965	
PROPELLANT REQUIREMENTS = A + B * Payload Wt.			
GEO unmanned multiple manifest	A 41467	48510	
	B 1.500	1.511	
GEO unmanned	A 35541	42707	
	B 1.492	1.502	
GEO manned sortie	A 43115	50620	
	B 3.192	3.137	
Planetary, $C_3 = 28 \text{ km}^2/\text{sec}^2$	A 33685	40760	
	B 2.020	2.147	
Geo unmanned Low g	A 36498	43805	
	B 1.497	1.497	
Lunar unmanned	A 27911	32610	
	B 1.400	1.417	

9.4.7 Aeroassist Device Trade

The performance of 3 vehicles with characteristics exactly that of the reference vehicle except for the aeroassist devices used is shown in table 9.4-9. The key differences include:

1. an expendable ballute with backwall temperature of 1500 deg F and turndown ratio of 1.5.
2. a lifting brake with lift-to-drag ratio of -0.117.
3. a shaped brake with L/D of -0.324.

9.5 GROUND BASED VEHICLE TRADES

Results from the SB OTV optimization trades were used as a starting point for the GB OTV optimization trades. However, the vehicle sizing had an additional constraint which was not present in the space based trades. This constraint was that, for the more demanding missions, the combined weight of the payload and OTV would require one Shuttle flight to deliver auxiliary tanks and payload to the LEO Space Station, then another Shuttle flight would deliver the OTV main stage to the Station where total vehicle assembly would occur. The Shuttle deployment capability, airborne support equipment, and OTV maximum allowable total weight assumed for these missions were:

DEPLOYMENT

<u>ALTITUDE</u>	<u>PAYLOAD</u>	<u>ASE</u>	<u>OTV MAXIMUM</u>
120 nm	74280 lbs	6391 lbs	67889 lbs
140	72000	6391	65609

Payload goals which were attempted for the single stage vehicle were the 12,000 lb GEO delivery and the 10,000 lb GEO multiple manifest missions. From the space based optimization trades, an expendable ballute with backwall temperature of 1500 deg F and turndown ratio of 1.5 was used for aerobraking, two advanced engines with an expansion ratio of 1000 and thrust of 5000 lbs were used for main propulsion, and hydrazine was used for attitude control. The OTV was assumed to be picked up by the Space Shuttle in a 150 nm orbit at the conclusion of it's mission.

To meet the 12,000 lb GEO delivery constraint, a variation of Shuttle deploy altitude was investigated. To meet the 10,000 lb GEO multiple manifest constraint, a variation of payload rack weight was additionally investigated. A summary of these

Table 9.4-9 Aeroassist Device Trade Summary

AEROASSIST DEVICE	Expendable Ballute	Lifting Brake	Shaped Brake
WEIGHT TRENDING			
	A 6013	7314	6222
	B .0573	.0723	.0925
	C 788	0	0
	D .0143	0	0
GUIDANCE			
Post aeromaneuver correction (fps)	251	464	507
SIZING			
MPS Usable (lbs)	63481	67197	68489
End of Mission (lbs)	9650	12172	12555
Jettisonable Ballute (lbs)	1696	0	0
PROPELLANT REQUIREMENTS = A + B * Payload Wt.			
GEO unmanned multiple manifest	A 39431	43219	44522
	B 1.497	1.502	1.504
GEO unmanned	A 33595	37265	38543
	B 1.489	1.494	1.495
GEO manned sortie	A 41099	44903	46231
	B 3.140	3.210	3.226
Planetary, $C_3 = 28 \text{ km}^2/\text{sec}^2$	A 31792	35374	36629
	B 1.991	2.045	2.065
Geo unmanned Low g	A 34521	38258	39561
	B 1.498	1.497	1.497
Lunar unmanned	A 26510	29039	29906
	B 1.398	1.405	1.408

trades are shown in tables 9.5-1 and 9.5-2. To meet the 12,000 lb GEO delivery constraint, a shuttle deployment altitude of 120 nm was chosen. To meet the 10,000 lb GEO multiple manifest constraint, a 120 nm deployment altitude and a 1000 lb payload rack was chosen. Of the two, the multiple manifest required more propellant, and therefore became the sizing mission.

9.6 EVOLUTIONARY VEHICLE CONFIGURATION

During the course of the low mission model, three different eras may be defined where different sizing missions are of importance. These eras start with the following major sizing missions:

<u>YEAR</u>	<u>SIZING MISSION</u>
1994	10,000 lb GEO unmanned multiple manifest
2004	20,000 lb GEO unmanned low g
2008	7500 lb GEO manned sortie

Therefore, an OTV could be sized for either the worst case mission from the very start, and penalized throughout most of the mission model, or an attempt could be made to tailor the OTV to the sizing missions as they appear in the model. Three basic evolutionary approaches were analyzed in this study. Common sizing rationale between these were:

1. Size vehicles in the first two eras which are not man-rated, but easily modified to be so in the third era. This saves on some of the inert weight associated with the man-rating for all missions for which it is not needed.
2. Size three aerobrakes specifically for the three sizing missions, and use the smallest size brake possible for all missions.
3. Use a vehicle with these characteristics: two advanced MPS engines with an expansion ratio of 1000 and thrust of 5000 lbs each, hydrazine for attitude control, and an expendable ballute with a backwall temperature of 1500 deg F and turndown ratio of 1.5.

The three evolutionary approaches analyzed in this study were:

1. Size the main propellant tanks once for the worst case mission in the entire model, and fly all other missions offloaded. Due to shuttle limitations, this option is only available in the space based mode.

Table 9.5-1 Ground Based GEO Unmanned Delivery Summary

START ALTITUDE (NM)	140	120
WEIGHT TRENDING		
A	5565	5565
B	.0647	.0647
C	921	921
D	.0002	.0002
SIZING		
MPS Usable (lbs)	44764	44449
End of Mission (lbs)	8458	8438
Jettisonable Ballute (lbs)	928	928
▶ PAYLOAD CAPABILITY	11387	12064

Table 9.5-2 Ground Based GEO Unmanned Multiple Manifest Summary

START ALTITUDE (NM)	140	140	120
PAYLOAD RACK (LBS)	2000	1000	1000
WEIGHT TRENDING			
A	5611	5588	5588
B	.0641	.0644	.0644
C	923	922	922
D	.0021	.0002	.0002
SIZING			
MPS Usable (lbs)	45935	45349	46866
End of Mission (lbs)	8552	8505	8603
Jettisonable Ballute (lbs)	933	930	930
▶ PAYLOAD CAPABILITY	8107	9747	10427

2. Size the main propellant tanks for the sizing mission in the first era, then size auxiliary tanks for the more demanding missions in the second and third eras. This option was investigated for space based and ground based configurations.
3. Size the main propellant tanks as a perigee kickstage, using apogee kick motors for delivery missions, and a second stage to handle the more demanding missions. This option was investigated for the ground based configuration.

9.6.1 Space Based Evolution

In the space based vehicle evolution, a large single stage vehicle with main propellant tanks sized for the worst case 7500 lb GEO manned sortie was compared to a small single stage vehicle with main propellant tanks sized for the 10,000 lb GEO multiple manifest, and supplementary auxiliary tanks added for the more demanding missions. Figures 9.6.1-1 and 9.6.1-2 summarize vehicle sizes and propellant requirements for key missions for these two strategies and three sizing missions. Note from table 9.6.1-1 that the large single stage vehicles sized for the 10,000 lb GEO multiple manifest and 20,000 lb GEO unmanned low g missions have essentially the same end of mission and jettisonable ballute weights, so that only two vehicles are needed for the entire mission model. For the small single stage (table 9.6.1-2), the end of mission weights are essentially the same, but the ballute increases in size to accommodate the increase in atmospheric entry weight caused from returning the auxiliary tank. Performance sizing computer outputs for the manned sortie mission are shown in table 9.6.1-3 and 9.6.1-4 for the large and small space based vehicles.

9.6.2 Ground Based Evolution

In the ground based vehicle evolution, a small single stage with main propellant tanks sized for the 10,000 lb GEO multiple manifest and supplementary auxiliary tanks added for the more demanding missions was baselined. An even smaller reusable perigee kickstage (RPKS) was examined, which when used with a liquid propulsion module (LPM) was designed to deliver a 14,000 lb payload to GEO. More demanding missions would be handled using a two-stage configuration. Table 9.6.2-1 summarizes the vehicle sizings using the small stage and auxiliary tank option. The core vehicle is the same for the 10,000 lb GEO multiple manifest and 20,000 lb GEO unmanned low g, with man-rated systems added to this vehicle for the 7500 lb GEO manned sortie. The expendable ballute size increases as the return atmospheric entry weight increases, attributable to

Table 9.6.1-1 Large Space Based Vehicle Evolution Summary

-sizing MISSION		Multi - Manifest	Low G	Sortie
-sizing				
MPS Usable Capacity (lbs)		61582	61582	61582
▶ MPS Usable (lbs)		47199	60104	61582
End of Mission (lbs)		9229	9223	9494
Jettisonable Ballute (lbs)		932	932	1645
PROPELLANT REQUIREMENTS = A+B * Payload Wt.				
GEO unmanned	A	30289	30264	33002
	B	1.485	1.485	1.488
GEO unmanned multiple manifest	A	33201	33176	35917
	B	1.489	1.489	1.492
Planetary, $C_3 = 28 \text{ km}^2/\text{sec}^2$	A	28607	28582	31218
	B	1.943	1.943	1.983
Lunar unmanned	A	24318	24300	26115
	B	1.391	1.390	1.396
Geo unmanned Low g	A	31130	31104	33905
	B	1.497	1.497	1.497
GEO manned sortie	A	*****	*****	40480
	B	*****	*****	3.138

Table 9.6.1-2 Small Space Based Vehicle/Auxilliary Tank Evolution Summary

SIZING MISSION		Multi - Manifest	Low G	Sortie
SIZING				
OTV MPS Usable (lbs)		44267	44267	44267
OTV End of Mission (lbs)		8227	8218	8494
OTV Jettisonable Ballute (lbs)		930	1089	2336
Aux Tank MPS Usable (lbs)		*****	22437	27090
Aux Tank End of Mission (lbs)		*****	3090	3432
PROPELLANT REQUIREMENTS = A+B * Payload Wt.				
GEO unmanned	A	27369	36771	41983
	B	1.482	1.494	1.502
GEO unmanned multiple manifest	A	30278	39696	44914
	B	1.485	1.497	1.505
Planetary, $C_3 = 28 \text{ km}^2/\text{sec}^2$	A	25817	34890	40040
	B	1.903	2.041	2.130
Lunar unmanned	A	22374	28640	32106
	B	1.385	1.405	1.417
Geo unmanned Low g	A	*****	37759	43072
	B	*****	1.497	1.497
GEO manned sortie	A	*****	*****	49853
	B	*****	*****	3.166

Table 9.6.1-3 Large Space Based Vehicle Performance Output

STAGE TRENDING: END OF MISSION = 5948. + .0576 * MPS USABLE
 BALLUTE TRENDING: JETTISON = 832. + .0132 * MPS USABLE

MISSION/BASING: SPACE BASED GEO MANNED MGSS SORTIE
 BRAKE: EXPENDABLE BALLUTE (1500 DEG), BALLUTE TURNDOWN RATIO = 1.5
 ENGINE: ADVANCED (2), THRUST = 10000.
 PROPULSION: MPS ISP = 483.2, ACS ISP = 220.0, MGSS ISP = 220.0
 MAIN TANK SIZING: SPACE BASED GEO MANNED MGSS SORTIE
 BRAKE SIZING: SPACE BASED GEO MANNED MGSS SORTIE
 STAGES: 1

MISSION PROFILE	DELTA V (F/S)	DELTA T (HOURS)	DELTA W (LBS)	WEIGHT (LBS)
MAIN STAGE:				MAIN
1 DOCKED AT LEO STATION	0.	2.0	-7.	81611.
2 ACS SEPARATION	10.	0.0	-115.	81496.
3 ACS COAST	10.	0.8	-119.	81377.
4 MPS PERIGEE BURN 1 *	3600.	0.2	-17021.	64356.
5 ACS COAST	20.	3.0	-197.	64159.
6 MPS PERIGEE BURN 2 *	4256.	0.2	-15518.	48641.
7 ACS COAST	10.	5.3	-96.	48545.
8 MPS BURN	5798.	0.1	-15129.	33416.
9 ACS REND/DOCK	40.	1.0	-193.	33222.
10 ATTACH MGSS	0.	0.0	38159.	71381.
11 MGSS OPERATIONS	20.	24.0	-290.	71091.
12 DROP MGSS PAYLOAD	0.	0.0	-426.	70665.
13 MPS BURN	46.	0.1	-234.	70432.
14 MGSS COAST	10.	48.5	-279.	70153.
15 MPS BURN	46.	0.1	-232.	69921.
16 MGSS OPERATIONS	60.	24.0	-678.	69242.
17 DROP MGSS PAYLOAD	0.	0.0	-427.	68815.
18 MPS BURN	160.	0.1	-729.	68086.
19 MGSS COAST	10.	126.0	-562.	67524.
20 MPS BURN	160.	0.1	-716.	66808.
21 MGSS OPERATIONS	60.	24.0	-652.	66156.
22 DROP MGSS PAYLOAD	0.	0.0	-429.	65727.
23 MPS BURN	46.	0.1	-219.	65508.
24 MGSS COAST	10.	48.5	-272.	65237.
25 MPS BURN	46.	0.1	-218.	65019.
26 MGSS OPERATIONS	70.	48.0	-816.	64203.
27 DROP MGSS PAYLOAD	0.	0.0	-427.	63776.
28 MGSS COAST	10.	6.0	-112.	63664.
29 DETACH MGSS	0.	0.0	-34081.	29583.
30 ACS SEPARATION	10.	0.0	-42.	29541.
31 MPS DEORBIT BURN	6245.	0.1	-9789.	19752.
32 ACS COAST	10.	6.2	-60.	19692.
33 MPS BURN	50.	0.1	-88.	19604.
34 AEROMANEUVER	0.	0.1	-1645.	17959.
35 MPS POST AERO CORRECT	251.	0.1	-312.	17647.
36 ACS COAST	10.	0.8	-29.	17618.
37 MPS BURN	420.	0.1	-494.	17124.
38 ACS COAST	10.	0.8	-28.	17095.
39 ACS REND/DOCK	40.	1.0	-102.	16994.
40 DROP PAYLOAD	0.	0.0	-7500.	9494.

* MAIN STAGE GRAVITY/STEERING LOSS (F/S) = 86.

OTV FLUIDS SUMMARY

MAIN STAGE				
MPS USABLE	= 61582.	ACS USABLE	= 972.	EPS USABLE = 34.
NOMINAL	= 60375.	NOMINAL	= 884.	NOMINAL = 28.
RESERVES	= 1207.	RESERVES	= 88.	RESERVES = 6.
BOILOFF	= 1369.			
START/STOP	= 325.			

MGSS ACS NOMINAL = 2369.

Table 9.6.1-4 Small Space Based Vehicle and Auxilliary Tanks Performance Output

4:53 PM, 12-JUN-85

OTV MPS USABLE PROPELLANT FIXED AT 44267.
 STAGE TRENDING: END OF MISSION = 5948. + .0576 * MPS USABLE
 BALLUTE TRENDING: JETTISON = 1473. + .0319 * AUX TANK USABLE
 AUX TANK TRENDING: END OF MISSION = 1433. + .0739 * AUX TANK USABLE

MISSION/BASING: SPACE BASED GEO MANNED MGSS SORTIE
 BRAKE: EXPENDABLE BALLUTE (1500 DEG), BALLUTE TURNDOWN RATIO = 1.5
 ENGINE: ADVANCED (2), THRUST = 10000.
 PROPULSION: MPS ISP = 483.2, ACS ISP = 220.0, MGSS ISP = 220.0
 MAIN TANK SIZING: SPACE BASED GEO UNMANNED MULTIPLE MANIFEST
 BRAKE SIZING: SPACE BASED GEO MANNED MGSS SORTIE
 AUX TANK SIZING: SPACE BASED GEO UNMANNED (LOW G)
 STAGES: 1 WITH REUSABLE AUX TANKS

MISSION PROFILE	DELTA V (F/S)	DELTA T (HOURS)	DELTA W (LBS)	WEIGHT (LBS)
MAIN STAGE:				MAIN
1 DOCKED AT LEO STATION	0.	2.0	-7.	94435.
2 ACS SEPARATION	10.	0.0	-133.	94302.
3 ACS COAST	10.	0.8	-137.	94164.
4 AUX TANK PERIGEE BURN 1 *	5011.	0.2	-26583.	67581.
5 ACS COAST	20.	3.0	-206.	67374.
6 MPS PERIGEE BURN 2 *	2845.	0.2	-11342.	56032.
7 ACS COAST	10.	5.3	-107.	55926.
8 MPS BURN	5798.	0.1	-17427.	38499.
9 ACS REND/DOCK	40.	1.0	-222.	38277.
10 ATTACH MGSS	0.	0.0	38337.	76614.
11 MGSS OPERATIONS	20.	24.0	-305.	76309.
12 DROP MGSS PAYLOAD	0.	0.0	-426.	75883.
13 MPS BURN	46.	0.1	-249.	75634.
14 MGSS COAST	10.	48.5	-286.	75348.
15 MPS BURN	46.	0.1	-248.	75100.
16 MGSS OPERATIONS	60.	24.0	-722.	74378.
17 DROP MGSS PAYLOAD	0.	0.0	-427.	73951.
18 MPS BURN	160.	0.1	-782.	73169.
19 MGSS COAST	10.	126.0	-569.	72601.
20 MPS BURN	160.	0.1	-768.	71832.
21 MGSS OPERATIONS	60.	24.0	-694.	71138.
22 DROP MGSS PAYLOAD	0.	0.0	-429.	70709.
23 MPS BURN	46.	0.1	-234.	70475.
24 MGSS COAST	10.	48.5	-279.	70197.
25 MPS BURN	46.	0.1	-232.	69964.
26 MGSS OPERATIONS	70.	48.0	-864.	69100.
27 DROP MGSS PAYLOAD	0.	0.0	-427.	68673.
28 MGSS COAST	10.	6.0	-119.	68554.
29 DETACH MGSS	0.	0.0	-34081.	34473.
30 ACS SEPARATION	10.	0.0	-49.	34424.
31 MPS DEORBIT BURN	6245.	0.1	-11405.	23019.
32 ACS COAST	10.	6.2	-65.	22955.
33 MPS BURN	50.	0.1	-99.	22856.
34 AEROMANEUVER	0.	0.1	-2336.	20520.
35 MPS POST AERO CORRECT	251.	0.1	-353.	20167.
36 ACS COAST	10.	0.8	-33.	20134.
37 MPS BURN	420.	0.1	-561.	19573.
38 ACS COAST	10.	0.8	-32.	19541.
39 ACS REND/DOCK	40.	1.0	-115.	19426.
40 DROP PAYLOAD	0.	0.0	-7500.	11926.
41 DETACH AUX TANK	0.	0.0	-3432.	8494.

* MAIN STAGE GRAVITY/STEERING LOSS (F/S) = 157.

OTV FLUIDS SUMMARY

MAIN STAGE			
MPS USABLE = 44267.	ACS USABLE = 1100.	EPS USABLE = 34.	
NOMINAL = 43399.	NOMINAL = 1000.	NOMINAL = 28.	
RESERVES = 868.	RESERVES = 100.	RESERVES = 6.	
BOILOFF = 1369.			
START/STOP = 325.			

MAIN STAGE AUXILLIARY TANKS
 USABLE = 27090.
 NOMINAL = 26558.
 RESERVES = 531.
 BOILOFF = 0.

MGSS ACS NOMINAL = 2547.

Table 9.6.2-1 Ground Based Vehicle/ Auxilliary Tank Evolution Summary

SIZING MISSION		Multi - Manifest	Low G	Sortie
SIZING				
	OTV MPS Usable (lbs)	46867	46867	46867
	OTV End of Mission (lbs)	8604	8604	8874
OTV	Jettisonable Ballute (lbs)	930	1196	2509
	▶ Aux. Tank MPS Usable (lbs)	*****	23957	30677
	Aux. Tank End of Mission (lbs)	*****	3621	4155

the auxiliary tanks (4000 lbs) and the manned module (7500 lbs). The performance sizing computer output for the manned sortie mission is shown in table 9.6.2-2 for the ground based vehicle with auxiliary tanks.

Another concept investigated was the use of a cost-optimum, non man-rated reusable perigee kickstage (RPKS). This vehicle would be sized on the basis that it would be deployed from the Space Shuttle at an altitude of 140 nm, execute a single LEO to GEO perigee burn (no plane change), separate from the payload and it's liquid propulsion module (LPM), then deorbit to an aerobraking altitude of 45 nm, aerobrake, and circularize in a 140 nm orbit to await recovery. A 14,000 lb payload to GEO was used as a sizing mission. The LPM was a storable system with a specific impulse of 328 seconds and mass fraction of 0.92 and was used for the apogee circularization and 28.5 degrees plane change maneuver. More demanding unmanned delivery missions would be handled with use of two RPKS's, and the 7500 lb GEO manned sortie would use a man-rated second stage. A sizing summary of the cost-optimum stage, the man-rated stage, and the LPM is shown in table 9.6.2-3. The performance sizing computer output for both cases are shown in tables 9.6.2-4 and 9.6.2-5. Life cycle cost analysis was not performed on the RPKS concept.

9.7 VEHICLE SENSITIVITIES

Main propellant sensitivities to various performance parameters are given in section 9.7.1 for the selected space based vehicle. Payload sensitivities are given in section 9.7.2 for the selected ground based vehicle. For both cases, vehicle characteristics include: two advanced engines with an expansion ratio of 1000 and thrust of 5000 lbs each, expendable ballute with a backwall temperature of 1500 deg F and turndown ratio of 1.5, and a hydrazine attitude control system.

9.7.1 Space Based Sensitivities

MPS propellant sensitivities to various performance parameters are given in table 9.7.1-1, for a single stage space based vehicle with main propulsion tanks and aerobrake sized for the 7500 lb GEO manned sortie. Propellant sensitivities are given in table 9.7.1-2 for the same vehicle except non-man-rated and using an aerobrake sized for the 20,000 lb GEO unmanned low g mission. These sensitivities do not account for the change in tankage required for the change in propellant.

MPS propellant (W_p) and end of mission weight (W_{eom}) sensitivities to additional inert weight (W_{add}) for the small and large space based single stage are given in table

Table 9.6.2-2 Ground Based Vehicle Performance Output

2:15 PM, 12-JUN-85

OTV MPS USABLE PROPELLANT FIXED AT 46867.
 STAGE TRENDING: END OF MISSION = 5862. + .0643 • MPS USABLE
 BALLUTE TRENDING: JETTISON = 1534. + .0318 • AUX TANK USABLE
 AUX TANK TRENDING: END OF MISSION = 1715. + .0796 • AUX TANK USABLE

MISSION/BASING: GROUND BASED GEO MANNED MGSS SORTIE
 BRAKE: EXPENDABLE BALLUTE (1500 DEG), BALLUTE TURNDOWN RATIO = 1.5
 ENGINE: ADVANCED (2), THRUST = 10000.
 PROPULSION: MPS ISP = 483.2, ACS ISP = 220.0, MGSS ISP = 220.0
 MAIN TANK SIZING: GROUND BASED GEO UNMANNED MULTIPLE MANIFEST
 BRAKE SIZING: GROUND BASED GEO MANNED MGSS SORTIE
 STAGES: 1 WITH REUSABLE AUX TANKS

MISSION PROFILE	DELTA V (F/S)	DELTA T (HOURS)	DELTA W (LBS)	WEIGHT (LBS)
MAIN STAGE AUXILLIARY TANKS:				AUX TANK
1 DOCKED AT LEO STATION	0.	72.0	-180.	34256.
MAIN STAGE:				MAIN
2 MPS BURN FROM 120 NM. CIRC	261.	0.1	-1034.	59600.
3 ACS COAST	10.	0.8	-88.	59512.
4 MPS BURN TO 270 NM. CIRC	259.	0.1	-1008.	58504.
5 ACS REND/DOCK	40.	1.0	-335.	58169.
6 DOCKED AT LEO STATION	0.	24.0	-89.	58080.
7 ATTACH AUX TANK	0.	0.0	34256.	92336.
8 PICKUP PAYLOAD	0.	0.0	7500.	99836.
9 ACS SEPARATION	10.	0.0	-141.	99696.
10 ACS COAST	10.	0.8	-145.	99551.
11 AUX TANK PERIGEE BURN 1 •	5402.	0.2	-30101.	69450.
12 ACS COAST	20.	3.0	-212.	69238.
13 MPS PERIGEE BURN 2 •	2454.	0.2	-10174.	59065.
14 ACS COAST	10.	5.3	-111.	58954.
15 MPS BURN	5798.	0.1	-18369.	40584.
16 ACS REND/DOCK	40.	1.0	-234.	40351.
17 ATTACH MGSS	0.	0.0	38410.	78760.
18 MGSS OPERATIONS	20.	24.0	-311.	78450.
19 DROP MGSS PAYLOAD	0.	0.0	-426.	78024.
20 MPS BURN	46.	0.1	-255.	77768.
21 MGSS COAST	10.	48.5	-289.	77479.
22 MPS BURN	46.	0.1	-254.	77225.
23 MGSS OPERATIONS	60.	24.0	-740.	76485.
24 DROP MGSS PAYLOAD	0.	0.0	-427.	76058.
25 MPS BURN	160.	0.1	-804.	75255.
26 MGSS COAST	10.	126.0	-572.	74683.
27 MPS BURN	160.	0.1	-789.	73894.
28 MGSS OPERATIONS	60.	24.0	-712.	73182.
29 DROP MGSS PAYLOAD	0.	0.0	-429.	72753.
30 MPS BURN	46.	0.1	-240.	72513.
31 MGSS COAST	10.	48.5	-282.	72231.
32 MPS BURN	46.	0.1	-238.	71993.
33 MGSS OPERATIONS	70.	48.0	-884.	71109.
34 DROP MGSS PAYLOAD	0.	0.0	-427.	70682.
35 MGSS COAST	10.	6.0	-122.	70560.
36 DETACH MGSS	0.	0.0	-34081.	36479.
37 ACS SEPARATION	10.	0.0	-52.	36427.
38 MPS DEORBIT BURN	6245.	0.1	-12068.	24360.
39 ACS COAST	10.	6.2	-67.	24293.
40 MPS BURN	50.	0.1	-103.	24190.
41 AEROMANEUVER	0.	0.1	-2509.	21681.
42 MPS POST AERO CORRECT	251.	0.1	-372.	21310.
43 ACS COAST	10.	0.8	-34.	21275.
44 MPS BURN	420.	0.1	-591.	20684.
45 ACS COAST	10.	0.8	-33.	20651.
46 ACS REND/DOCK	40.	1.0	-122.	20529.
47 DROP PAYLOAD	0.	0.0	-7500.	13029.
48 DETACH AUX TANK	0.	0.0	-4155.	8874.

• MAIN STAGE GRAVITY/STEERING LOSS (F/S) = 203.

OTV FLUIDS SUMMARY

MAIN STAGE			
MPS USABLE = 46868.	ACS USABLE = 1611.	EPS USABLE = 37.	
NOMINAL = 45949.	NOMINAL = 1465.	NOMINAL = 31.	
RESERVES = 919.	RESERVES = 146.	RESERVES = 6.	
BOILOFF = 1457.			
START/STOP = 375.			

MAIN STAGE AUXILLIARY TANKS

USABLE = 30677.
 NOMINAL = 30076.
 RESERVES = 602.
 BOILOFF = 180.

MGSS ACS NOMINAL = 2620.

Table 9.6.2-3 Reusable Perigee Kickstage Summary

SIZING MISSION	14000 lb GEO Unmanned	7500 lb GEO Manned Sortie
-----	-----	-----
SECOND STAGE	LPM	RPKS
-----	-----	-----
INTERSTAGE WEIGHT (LBS)	0	634
-----	-----	-----
SIZING		

<u>STAGE 1</u>		
MPS Usable (lbs)	25064	25064
End of Mission (lbs)	6990	7624
Jettisonable Ballute (lbs)	924	924
<u>STAGE 2</u>		
MPS Usable (lbs)	11767	39160
End of Mission (lbs)	1023	8379
Jettisonable Ballute (lbs)	0	1357

Table 9.6.2-4 Reusable Perigee Kick Stage and Liquid Propellant Module Sized for 14000 lb GEO Delivery

10:56 AM, 10-JUL-85

BASING/MISSION: GROUND BASED GEO UNMANNED
 BRAKE: EXPENDABLE BALLUTE, B/W TEMP = 1500, T/D = 1.5
 ENGINE: 2 ADVANCED, THRUST = 10000.
 PROPULSION: MPS ISP STAGE 1 = 483.2, STAGE 2 = 328.0, ACS ISP = 220.0
 STAGES: 2

WEIGHTS INPUT

STAGE 1 END = 6990., JETT BALLUTE = 924.
 STAGE TRENDING: END OF MISSION = 5382. + .0642 * MPS USABLE
 BALLUTE TRENDING: JETTISON = 920. + .0002 * MPS USABLE

STAGE 2 END = 1023.
 STAGE TRENDING: END OF MISSION = 0. + .0870 * MPS USABLE

MISSION PROFILE	DELTA V (F/S)	DELTA T (HOURS)	DELTA W (LBS)	WEIGHT (LBS)
STAGE 1				
1 12 ACS COAST IN 140 NM	10.	0.8	-91.	59285.
2 12 MPS PERIGEE BURN	7997.	0.2	-24334.	34951.
3 1 ACS COAST TO GEO	10.	5.3	-39.	8328.
4 1 MPS DEORBIT BURN	61.	0.0	-58.	8271.
5 1 ACS COAST	10.	5.3	-39.	8232.
6 1 MPS PRE AERO BURN	50.	0.0	-51.	8180.
7 1 AEROMANEUVER	0.	0.0	-924.	7256.
8 1 MPS POST AERO CORRECT	251.	0.0	-141.	7115.
9 1 ACS COAST TO 140 NM	10.	0.0	-10.	7105.
10 1 MPS CIRCULARIZE BURN	199.	0.0	-115.	6990.
STAGE 2				
11 2 MPS BURN	6013.	0.0	-11561.	15023.
12 2 DROP PAYLOAD	0.	0.0	-14000.	1023.

GRAVITY/STEERING LOSS (FPS) STAGE 1 = 211., STAGE 2 = 0.

PROPELLANT SUMMARY

MPS TOTAL PROPELLANT = 37429.

STAGE 1

MPS USABLE = 25064.	ACS USABLE = 129.	EPS USABLE = 21.
NOMINAL = 24573.	NOMINAL = 117.	NOMINAL = 17.
RESERVES = 491.	RESERVES = 12.	RESERVES = 3.
BOILOFF = 42.		
START/STOP = 125.		

STAGE 2

MPS USABLE = 11767.	ACS USABLE = 0.	EPS USABLE = 0.
NOMINAL = 11536.	NOMINAL = 0.	NOMINAL = 0.
RESERVES = 231.	RESERVES = 0.	RESERVES = 0.
BOILOFF = 4.		
START/STOP = 25.		

PROPELLANT COEFFICIENTS: MPS TOTAL = A + B * PAYLOAD
 GROUND BASED GEO UNMANNED, A = 7961., B = 2.126

Table 9.6.2-5 Reusable Perigee Kickstage and Man Rated Stage Sized for 7500 lb GEO Sortie

8:04 AM, 10-JUL-85

OTV MPS USABLE PROPELLANT FIXED AT 25064.
 BASING/MISSION: GROUND BASED GEO WANNED SORTIE
 BRAKE: EXPENDABLE BALLUTE, B/W TEMP = 1500, T/D = 1.5
 ENGINE: 2 ADVANCED, THRUST = 10000.
 PROPULSION: MPS ISP STAGE 1 = 483.2, ACS ISP = 220.0, MGSS ISP = 220.0
 STAGES: 2

WEIGHTS INPUT

STAGE 1 END = 7624., JETT BALLUTE = 924.

STAGE 2 END = 8379., JETT BALLUTE = 1357.

STAGE TRENDING: END OF MISSION = 5862. + .0843 * MPS USABLE
 BALLUTE TRENDING: JETTISON = 833. + .0134 * MPS USABLE

MISSION PROFILE	DELTA V (F/S)	DELTA T (HOURS)	DELTA W (LBS)	WEIGHT (LBS)
STAGE 1				
1 1 MPS BURN FROM 140 NM.	225.	0.1	-513.	33464.
2 1 ACS COAST	10.	0.8	-51.	33412.
3 1 MPS BURN TO 270 NM.	223.	0.1	-500.	32912.
4 1 ACS REND/DOCK	40.	1.0	-191.	32721.
5 1 DOCKED AT LEO STATION	0.	24.0	-89.	32633.
STAGE 2				
6 2 MPS BURN FROM 140 NM.	225.	0.1	-755.	58077.
7 2 ACS COAST	10.	0.8	-75.	58002.
8 2 MPS BURN TO 270 NM.	223.	0.1	-737.	49265.
9 2 ACS REND/DOCK	40.	1.0	-283.	48982.
10 2 PICKUP PAYLOAD	0.	0.0	7500.	56482.
STAGE 1				
11 12 DOCKED AT LEO STATION	0.	2.0	-15.	89100.
12 12 ACS SEPARATION	10.	0.0	-126.	88974.
13 12 ACS COAST	10.	0.0	-133.	88842.
14 12 MPS PERIGEE BURN 1	4592.	0.2	-23212.	65630.
15 1 ACS COAST	10.	0.0	-23.	9135.
16 1 MPS DEORBIT BURN	276.	0.0	-185.	8950.
17 1 ACS COAST	10.	0.0	-23.	8927.
18 1 MPS BURN	50.	0.1	-54.	8873.
19 1 AEROMANEUVER	0.	0.1	-924.	7949.
20 1 MPS POST AERO CORRECT	251.	0.1	-152.	7798.
21 1 ACS COAST TO 140 NM.	10.	0.8	-15.	7782.
22 1 MPS BURN	216.	0.1	-132.	7650.
23 1 ACS COAST/AWAIT PICKUP	10.	3.0	-26.	7624.
STAGE 2				
24 2 ACS COAST	20.	3.0	-175.	56296.
25 2 MPS PERIGEE BURN 2	3182.	0.2	-10490.	45806.
26 2 ACS COAST	10.	5.3	-92.	45714.
27 2 MPS BURN	5964.	0.1	-14582.	31132.
28 2 ACS REND/DOCK	40.	1.0	-181.	30951.
29 2 ATTACH MGSS	0.	0.0	38079.	69030.
30 2 MGSS OPERATIONS	20.	24.0	-283.	68747.
31 2 DROP MGSS PAYLOAD	0.	0.0	-426.	68321.
32 2 MPS BURN	46.	0.1	-227.	68094.
33 2 MGSS COAST	10.	48.5	-275.	67818.
34 2 MPS BURN	46.	0.1	-225.	67593.
35 2 MGSS OPERATIONS	60.	24.0	-659.	66935.
36 2 DROP MGSS PAYLOAD	0.	0.0	-427.	66508.
37 2 MPS BURN	160.	0.1	-706.	65802.
38 2 MGSS COAST	10.	126.0	-558.	65243.
39 2 MPS BURN	160.	0.1	-693.	64551.
40 2 MGSS OPERATIONS	60.	24.0	-633.	63918.
41 2 DROP MGSS PAYLOAD	0.	0.0	-429.	63489.
42 2 MPS BURN	46.	0.1	-213.	63276.
43 2 MGSS COAST	10.	48.5	-269.	63008.
44 2 MPS BURN	46.	0.1	-211.	62797.
45 2 MGSS OPERATIONS	70.	48.0	-794.	62003.
46 2 DROP MGSS PAYLOAD	0.	0.0	-427.	61576.
47 2 MGSS COAST	10.	6.0	-109.	61467.
48 2 DETACH MGSS	0.	0.0	-34081.	27386.
49 2 ACS SEPARATION	10.	0.0	-39.	27347.
50 2 MPS DEORBIT BURN	6245.	0.1	-9064.	18283.
51 2 ACS COAST	10.	6.2	-58.	18225.
52 2 MPS BURN	50.	0.1	-83.	18142.
53 2 AEROMANEUVER	0.	0.1	-1357.	16785.
54 2 MPS POST AERO CORRECT	251.	0.1	-293.	16491.
55 2 ACS COAST TO 260 NM.	10.	0.8	-27.	16464.
56 2 MPS BURN	420.	0.1	-463.	16001.
57 2 ACS COAST TO 270 NM.	10.	0.8	-27.	15974.
58 2 ACS REND/DOCK	40.	1.0	-95.	15879.
59 2 DROP PAYLOAD	0.	0.0	-7500.	8379.

GRAVITY/STEERING LOSS (FPS) STAGE 1 = 112., STAGE 2 = 17.

PROPELLANT SUMMARY

MPS TOTAL PROPELLANT = 66895.

STAGE 1			
MPS USABLE = 25063.	ACS USABLE = 585.	EPS USABLE = 19.	
NOMINAL = 24372.	NOMINAL = 531.	NOMINAL = 16.	
RESERVES = 491.	RESERVES = 53.	RESERVES = 3.	
BOILOFF = 135.			
START/STOP = 175.			

STAGE 2			
MPS USABLE = 39160.	ACS USABLE = 1043.	EPS USABLE = 36.	
NOMINAL = 38392.	NOMINAL = 948.	NOMINAL = 30.	
RESERVES = 768.	RESERVES = 95.	RESERVES = 6.	
BOILOFF = 1376.			
START/STOP = 350.			

MGSS ACS NOMINAL = 2289.

Table 9.7.1-1 7500 lb GEO Manned Sortie MPS Propellant Sensitivities

<u>SENSITIVITY PARAMETER</u>	<u>CHANGE IN PROPELLANT/CHANGE IN PARAMETER</u>
MPS Isp	- 231. lbs/sec
ACS Isp	- 3.01 lbs/sec
End of Mission weight	+ 3.07 lbs/lb
Jettisoned ballute weight	+ 2.88 lbs/lb
Aeromaneuver correction delta-v	+ 4.50 lbs/fps
Payload	+ 3.01 lbs/lb

Table 9.7.1-2 20000 lb GEO Unmanned Low g MPS Propellant Sensitivities

<u>SENSITIVITY PARAMETER</u>	<u>CHANGE IN PROPELLANT/CHANGE IN PARAMETER</u>
MPS Isp	- 203. lbs/sec
ACS Isp	- 2.09 lbs/sec
End of Mission weight	+ 2.95 lbs/lb
Jettisoned ballute weight	+ 2.76 lbs/lb
Aeromaneuver correction delta-v	+ 2.39 lbs/fps
Payload	+ 1.49 lbs/lb

9.7.1-3. These sensitivities reflect the required change in tankage due to the change in propellant weight.

Table 9.7.1-3 MPS Propellant and End of Mission Sensitivities to Additional Inerts

<u>VEHICLE</u>	<u>dWeom/dWadd</u>	<u>dWp/dWadd</u>	<u>dWp/dWeom</u>
Small Space Based	1.20	3.51	2.92
Large Space Based	1.23	3.92	3.19

9.7.2 Ground Based Sensitivities

Payload sensitivities to certain performance variables for the single stage ground based vehicle sized for the 10,000 lb GEO unmanned multiple manifest mission (section 9.6.2) are given in table 9.7.2-1 for a GEO delivery mission. Shuttle deployment capability was assumed fixed for this analysis, and the maximum OTV weight was restrained to this value.

Table 9.7.2-1 Ground Based GEO Delivery Payload Sensitivities

<u>SENSITIVITY PARAMETER</u>	<u>CHANGE IN PAYLOAD/CHANGE IN PARAMETER</u>
MPS Isp	+ 64.2 lbs/sec
End of Mission Weight	- 1.56 lbs/lb
Jettisoned ballute weight	- 1.51 lbs/lb

10.0 AERODYNAMIC DATA DEVELOPMENT

The aerodynamic data and analysis techniques are described for the OTV's employing a ballute brake, symmetrical lifting brake, and shaped brake. Overall characteristics of these configurations are shown in figure 10-1. Flight test and/or wind tunnel data corrected to flight have been included in the data base whenever possible. Aerodynamic parameters for the shaped brake (no test data available) were based on the Aerodynamic Preliminary Analysis System (APAS) (which is described in ref. 49) with corrections for real gas effects. These data were scaled using the reference areas and length as required to complete performance trade studies.

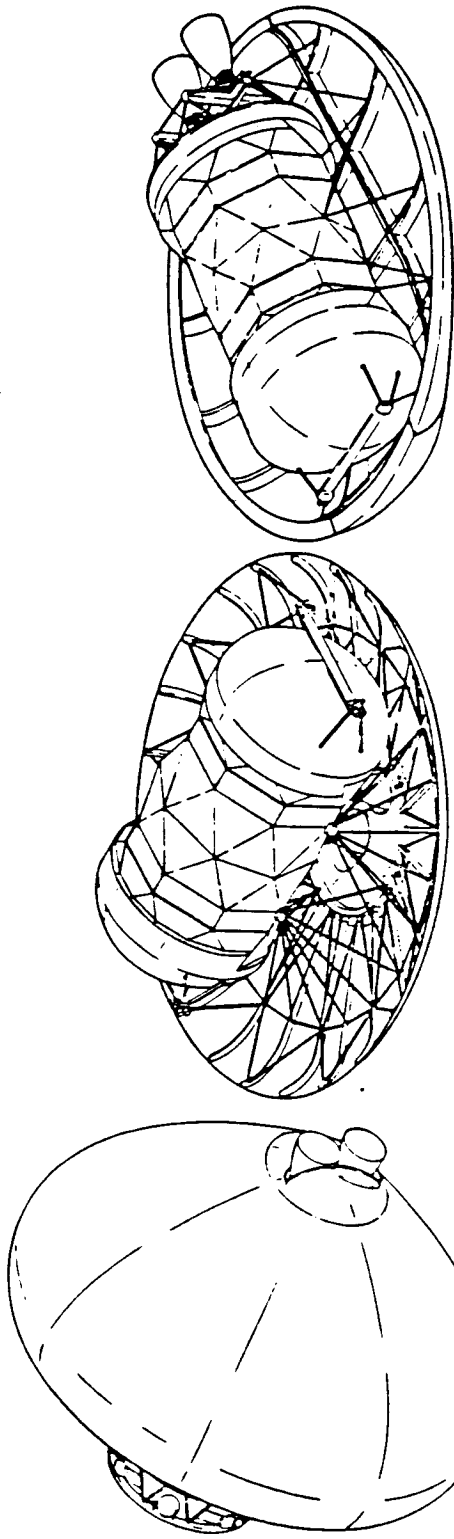
10.1 BALLUTE BRAKE OTV

Aerodynamic characteristics have been developed for the space based OTV using a 50 ft dia (max) ballute as shown in figure 10-2. For the baseline aerobrake concept which controls the internal ballute pressure to modulate drag, hypersonic aerodynamic characteristics were predicted for the 60 degree design ballute shape and the 48 degree turndown ballute shapes. The APAS model and lift, drag, and pitching moment trends are seen in figure 10-3. The impact method selected is modified Newtonian with $C_p(\max)$ of 1.95 ($\alpha=1.15$). The maximum drag coefficient (design shape) is 1.15 and the minimum drag coefficient (48° turndown) is 0.61. The turndown shape has the lower C_m values (referred to the nose) and determines the ballute static stability limits. The reference area and length are the respective maximum base area and diameter of the 60° design shape.

Similar analyses were completed by NASA LaRC for this configuration resulting in the variation in CDA and aerodynamic center versus ballute turndown angle shown in figure 10-4. Improvement in static stability (further downstream aerodynamic heating) can be achieved by increasing the initial design angle to 70 degrees.

The variation in ballute shape with internal pressure is shown in figure 10-5. The variation of CDA (units FT^2) with pressure ratio is shown in figure 10-6.

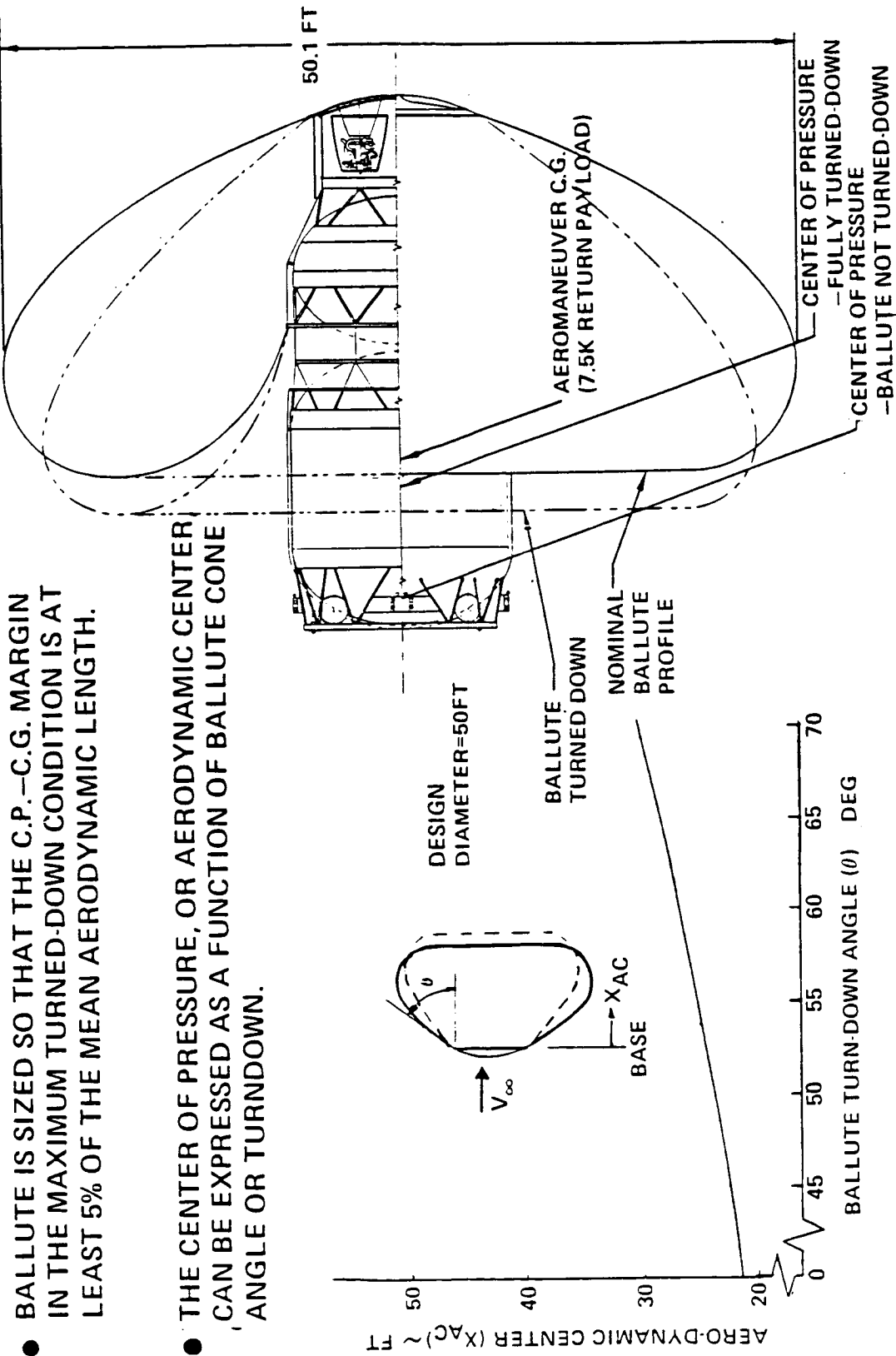
These ballute aerodynamic characteristics were scaled with reference area and length when trade studies involved different diameter ballutes. The scaling is recognized as a first approximation and the ballute actual characteristics are dependent on several parameters determined by its initial design point to be demonstrated in the Aeroassist Flight Experiment (AFE) Study. The key shape parameters include: ballute design angle, design internal-to-external pressure ratio, meridian stress, fabric stress, front and rear attach points, and maximum diameter.



● ALL SIZED FOR GEO MAN SORTIE (7.5 K LBS R.T.)

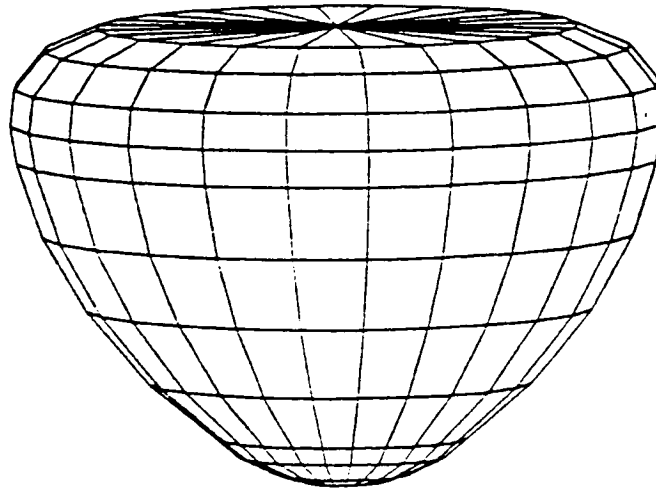
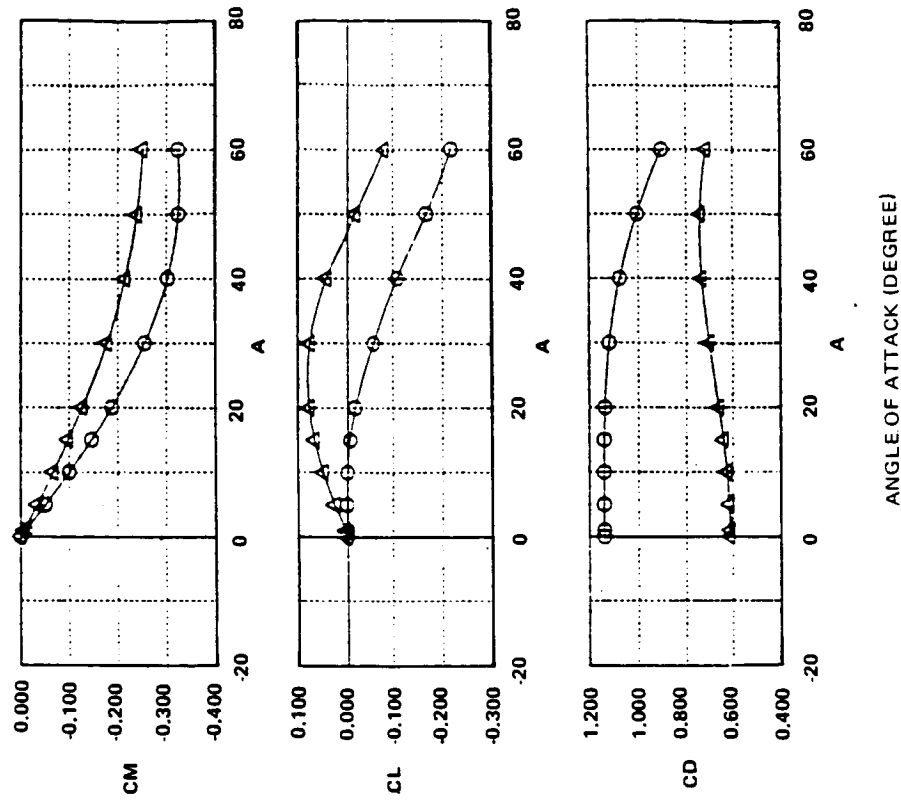
	<u>BALLUTE BRAKE</u>	<u>LIFTING BRAKE</u>	<u>SHAPED BRAKE</u>
● AEROMANEUVER FEATURES	T/D = 1.5 B/W = 1500 ⁰ F	L/D = .117	L/D = .234
● INITIAL ON- ORBIT ASSY.	NO	YES	YES
● VEHICLE SIZE (FT)	14.5 x 35.7 BALLUTE 50 FT. DIA.	42 DIA.	44 x 36
● BRAKE REPLACEMENT FREQ. (FLTS)	BALLUTE (1) HEAT SHIELD (20)	TPS FABRIC (5) HEAT SHIELD (20)	HEAT SHIELD (20)
● DRY WEIGHT (LBS) (BRAKE WT.)	9189 (2712)	9947 (3276)	10,314 (3608)
● PROP. WT. (LBS)	63,890	69,681	71,020

Figure 10-1 SB OTV Aeroassist Trade



- BALLUTE IS SIZED SO THAT THE C.P.-C.G. MARGIN IN THE MAXIMUM TURNED-DOWN CONDITION IS AT LEAST 5% OF THE MEAN AERODYNAMIC LENGTH.
- THE CENTER OF PRESSURE, OR AERODYNAMIC CENTER, CAN BE EXPRESSED AS A FUNCTION OF BALLUTE CONE ANGLE OR TURNDOWN.

Figure 10-2 Ballute Inflated and Modulated During Aeromaneuver



SYMBOL	RUN	M	θ
○	1	25,000	60°
△	2	25,000	48°

Figure 10-3 APAS Model and Aerodynamic Characteristics of Ballute

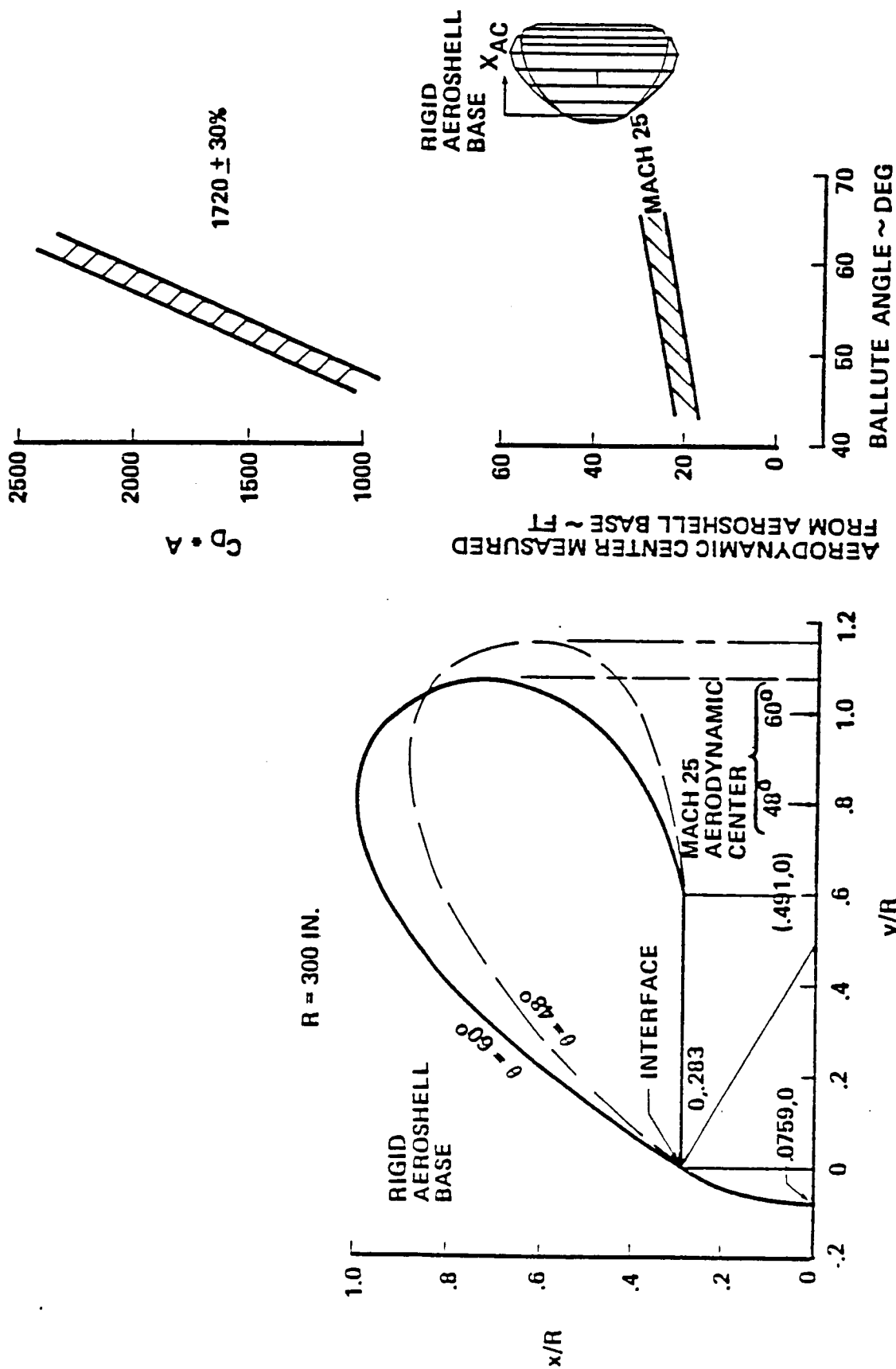


Figure 10-4 Baseline Aerobrake Aerodynamic Characteristics (Boeing)

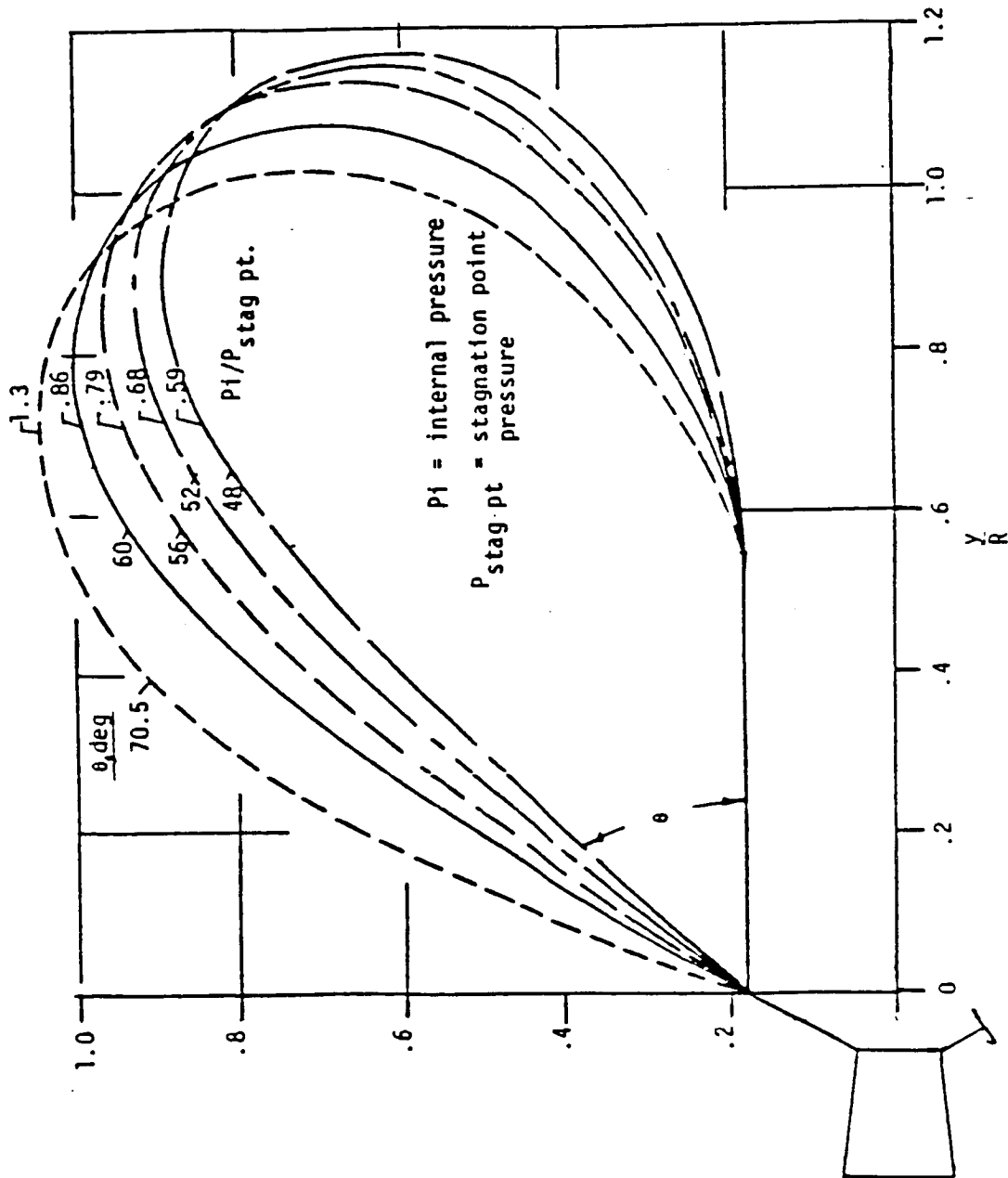


Figure 10-5 Pressure Controlled Ballute Shapes

OTV 1739

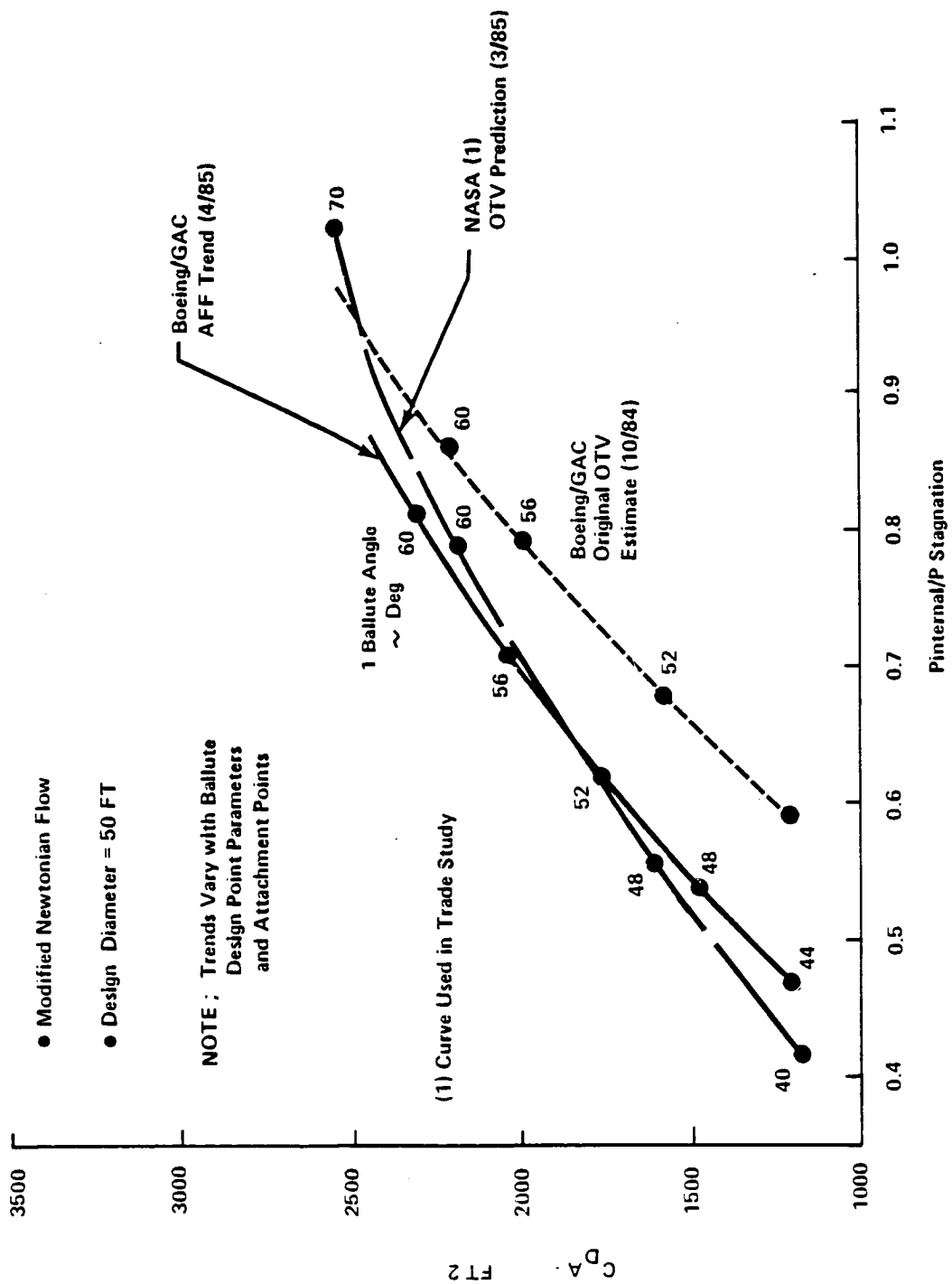


Figure 10-6 Variation of $C_D A$ With Pressure Ratio

For the trade studies, constraints were placed on the aerodynamic stability and turndown ratios. A positive static margin of 5% of the turndown length was imposed since the aerodynamic moments are large when compared to the RCS system capability. This static margin is typical for aerodynamically stabilized configurations. In addition, a minimum ballute diameter exists for which the desired turndown ratio can be achieved for given OTV vehicle attach points. This can only be determined by detailed analysis, but can be crudely approximated by bounding the turndown angles range as 70 to 48 degrees, by selecting the best information available from AFE analysis and examining the trends in C_{DA} versus ballute angle for different forward attach points. The minimum diameter for the OTV attach points is approximately 33 feet.

The ground based OTV employs ballute diameters of 33', 44' and 66' to accommodate different payloads. The first approximation of the design shape using isotenoid methods is shown in figure 10-7.

Another ballute concept investigated used main engine exhaust flow to modulate drag rather than change the ballute shape. The aerodynamic characteristics of this concept are based on wind tunnel test results as reported in references 10-2 and 10-3 and subsequent modified Newtonian aerodynamic analyses. Balance tests of ballute configurations with and without jet counterflow were conducted in the NASA/Langley 22 inch, Mach 20 helium tunnel. Results show that the ballute drag can be varied by an order of magnitude by modulating the ratio of the momentum flux of the engine exhaust to that of the ambient flow as shown in figure 10-8. Note that the drag coefficient shown in figure 10-8 represents only the drag on the ballute, and does not include the contribution of the center body. The concept for this test employed two 7500 lb thrust RL 10-3 engines, tank head idle with each providing about 25 lbs thrust resulting in a total momentum ratio of about 0.000057. Pumped idle can achieve up to about 10 percent thrust, or 1500 lbs which, by extrapolating the test results, indicates a reduction in drag by a factor of 10.

When the OTV returns from high energy orbits and uses the upper atmosphere for an aero-braking maneuver it passes through several different flow regions. The regions are free molecular, slip (or transitional) and continuum. The influence of these flow regimes on ballute drag coefficient are illustrated in figure 10-9. More than 95 percent of the ΔV , and more than 90 percent of the aerodynamic heating occurs at altitudes below 300,000 ft, where continuum flow can be considered.

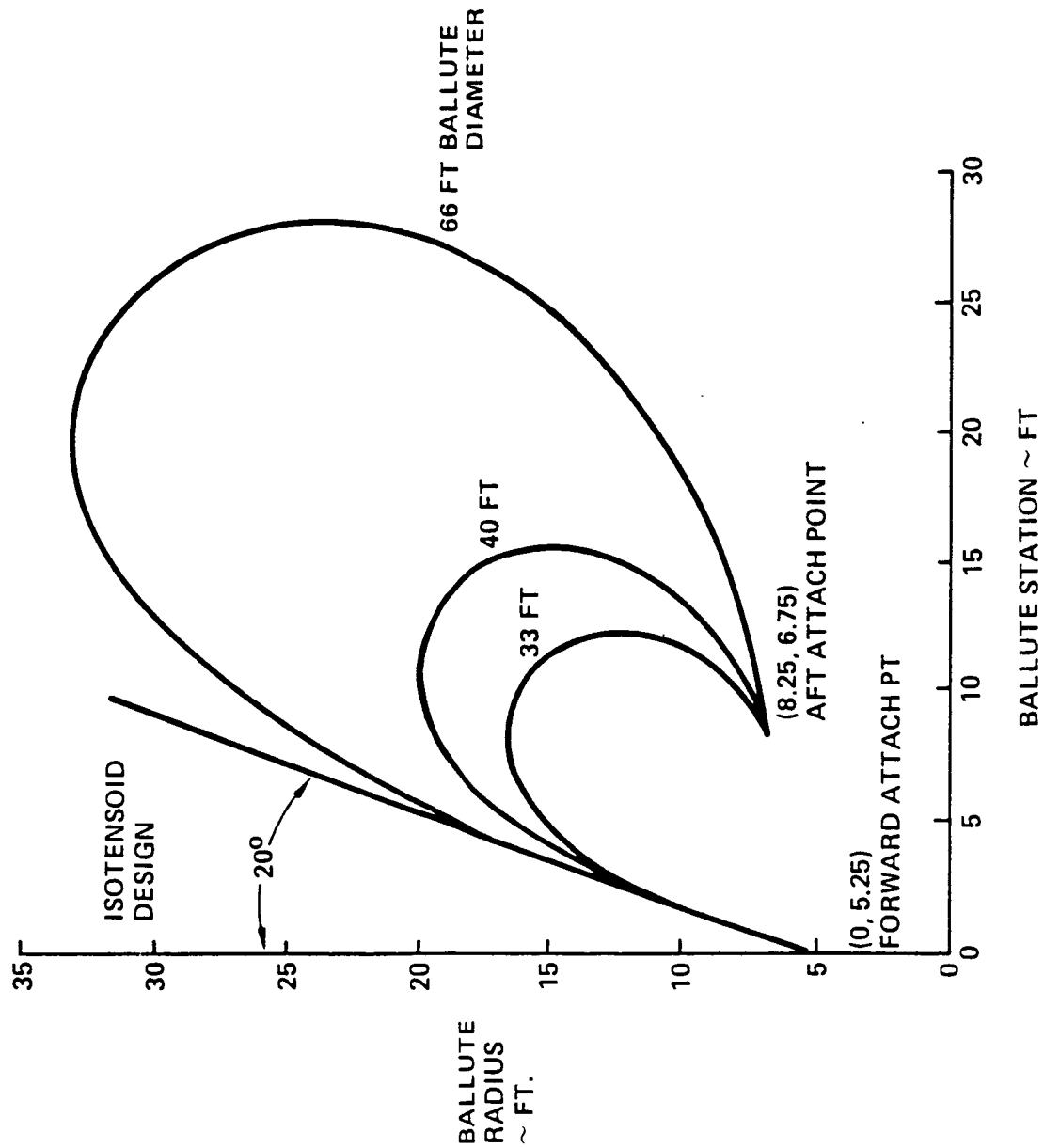


Figure 10-7. Ballute Shape Versus Diameter With Fixed Attach Points

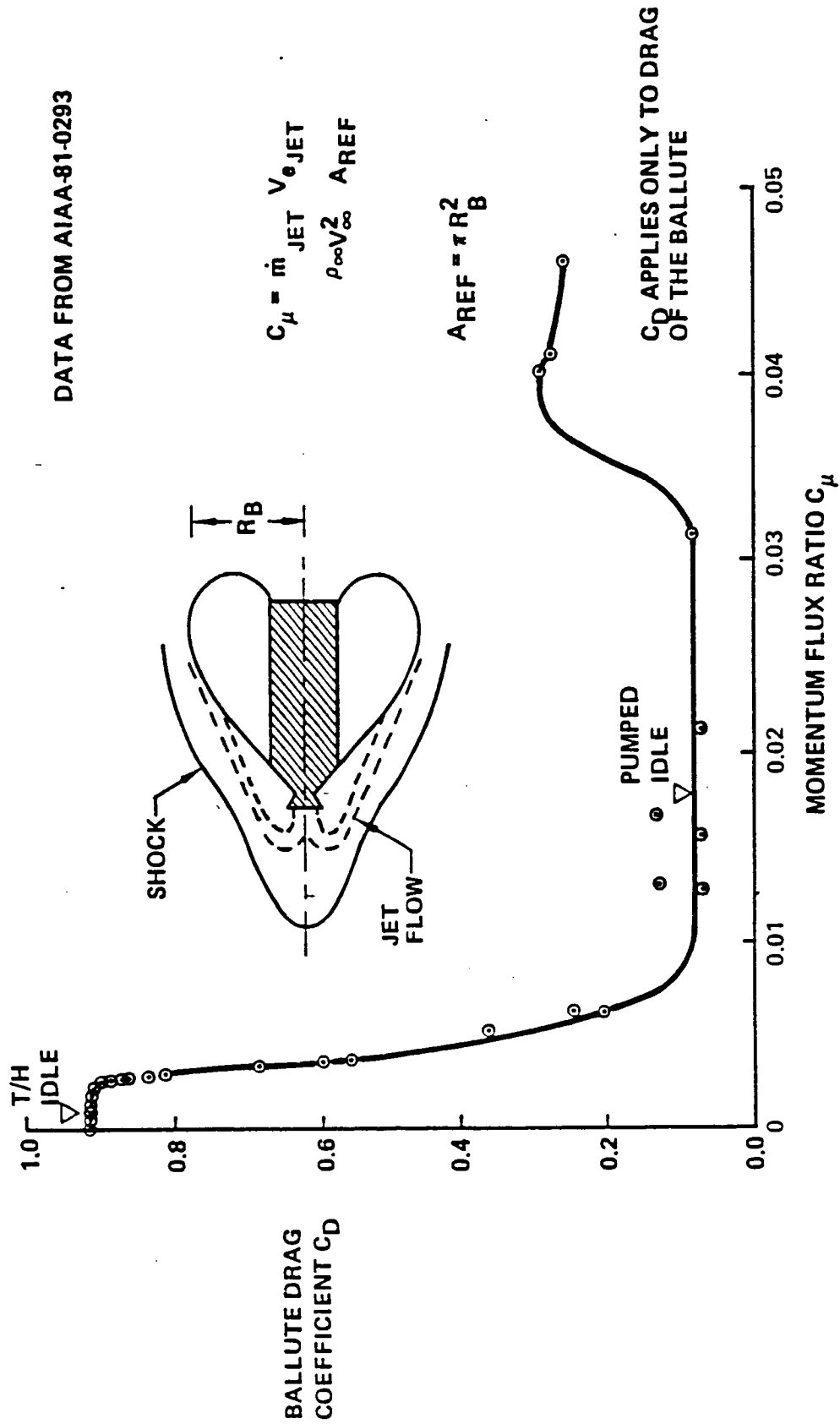


Figure 10-8 Effect of Engine Modulation on Ballute Drag

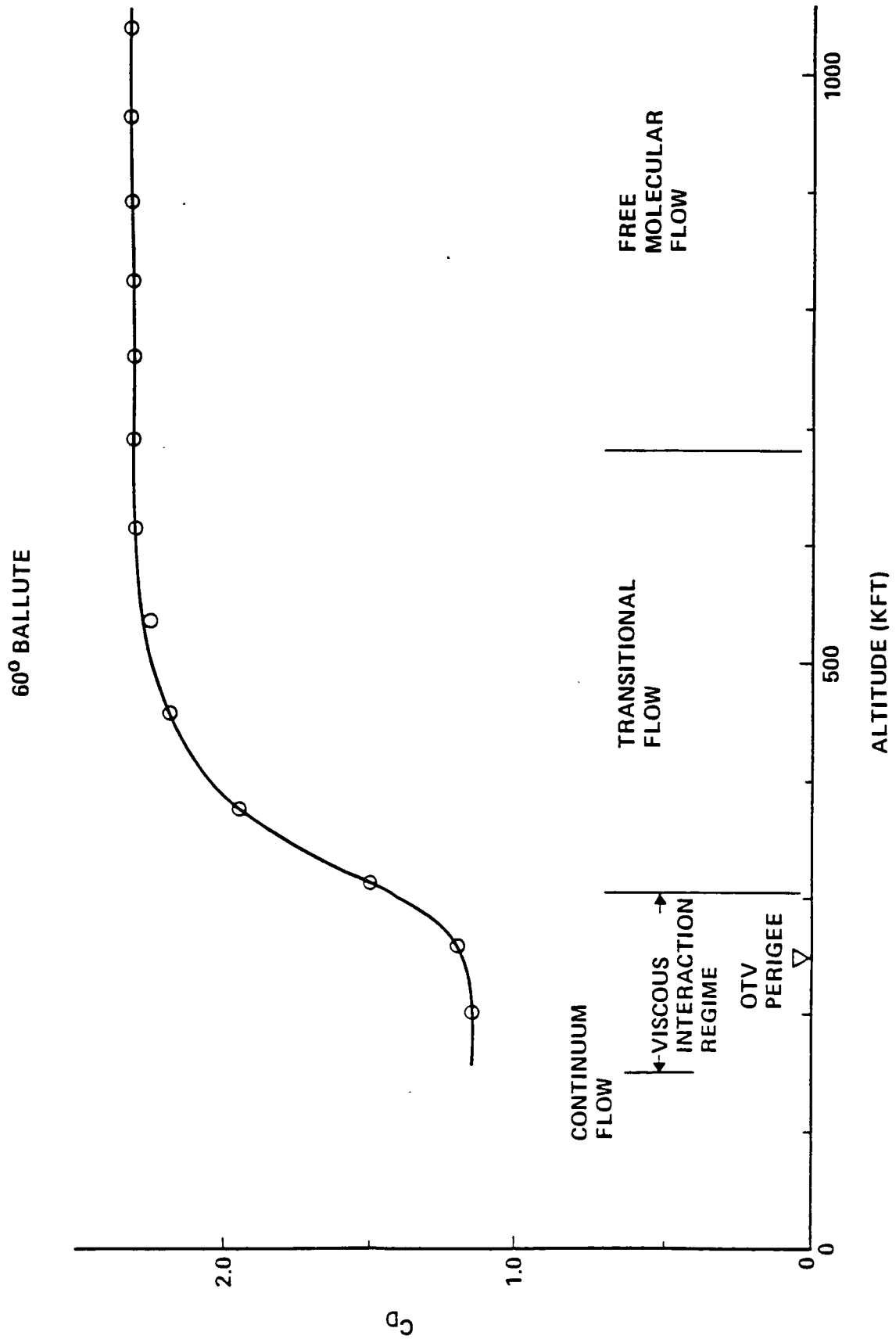


Figure 10-9 Rarefied low Effects

10.2 SYMMETRICAL LIFTING BRAKE CONFIGURATION

Hypersonic aerodynamic characteristics have been estimated for the symmetric brake configuration shown in figure 10-10 using APAS. The APAS model and lift, drag and pitching moment trends are seen in figure 10-11. The impact method is modified Newtonian with $C_p(\max)$ of 1.95 ($\alpha=1.15$). The aerodynamic stability characteristics are illustrated by the variation of pitching moment with center of gravity location. The lift-to-drag ratio is 0.25 at 20 degrees angle of attack and 0.30 at 30 degrees angle of attack. The reference area and length are the maximum area and radius, respectively. Viscous effects will vary L/D by less than 10% during the part of the trajectory which is important to guidance results (altitudes less than 280,000 ft).

APAS II results were used to investigate the lifting brake stability characteristics. The trim c.g. and aerodynamic center are shown for 0, 10, and 20 degree angle of attack in figure 10-12. The vehicle remains stable until the c.g. is aft of the nose by slightly over one brake radius. These data were used in the trade studies and scaled using the reference area and length.

10.3 SHAPED BRAKE

Similar hypersonic aerodynamic characteristic have been estimated for the shaped brake using APAS. The OTV shaped brake shown in figure 10-13 is a raked-off elliptical cone which has been blunted with an ellipsoid nose cap and faired into a 40 foot base skirt. The APAS model and the lift, drag, and pitching moments are shown in figure 10-14. The impact method selected is modified Newtonian with $C_p(\max)$ of 1.95 ($\alpha=1.15$). The design lift-to-drag ratio is 0.275 at zero degree angle of attack. The shape is a relatively stable configuration as seen from the pitching moment (referenced to the theoretical apex) slope. The lift and drag coefficients are 0.37 and 1.35, respectively. The reference area and length are the base area and diameter, respectively.

When compared to similar aerodynamic data for the equivalent raked-off elliptical cone, the effects of bluntness and the skirt are significant for the shaped brake with L/D being 10% lower. The skirt contributes more to this difference than does nose bluntness. Parametric data for trade studies is available from NASA TN D-2624 (ref 10-4) for the raked-off elliptical cones. The effect of c.g. position on pitching moment was investigated in order to determine the c.g. position to trim at zero angle of attack. The aerodynamic center and trim c.g. positions are presented in figure 10-15.

These data were used in trade studies and analyses which resulted in a modification of the basic concept for packaging. The base plane was modified to form a 44' X 36.4' ellipse and the overall depth normal to the base plane was increased 10

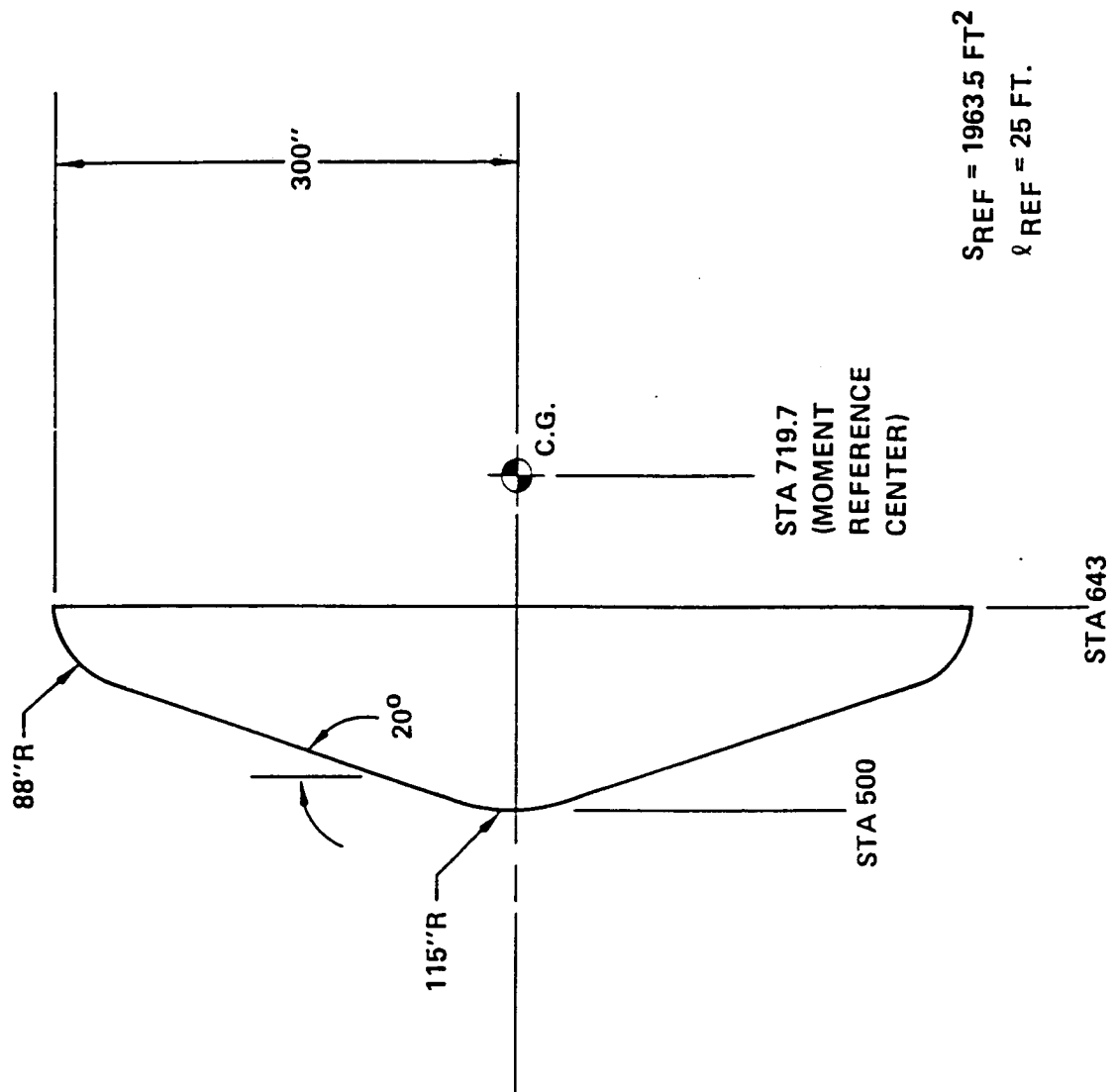
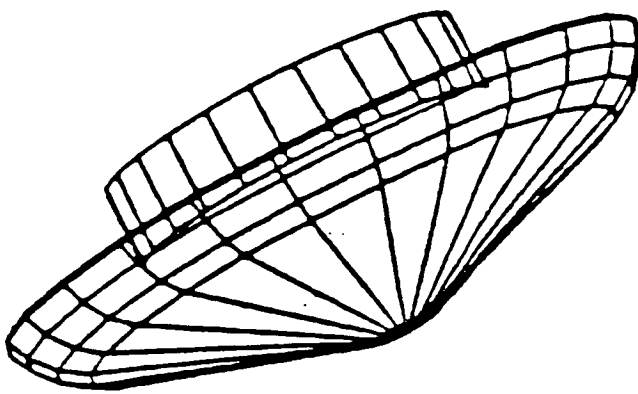
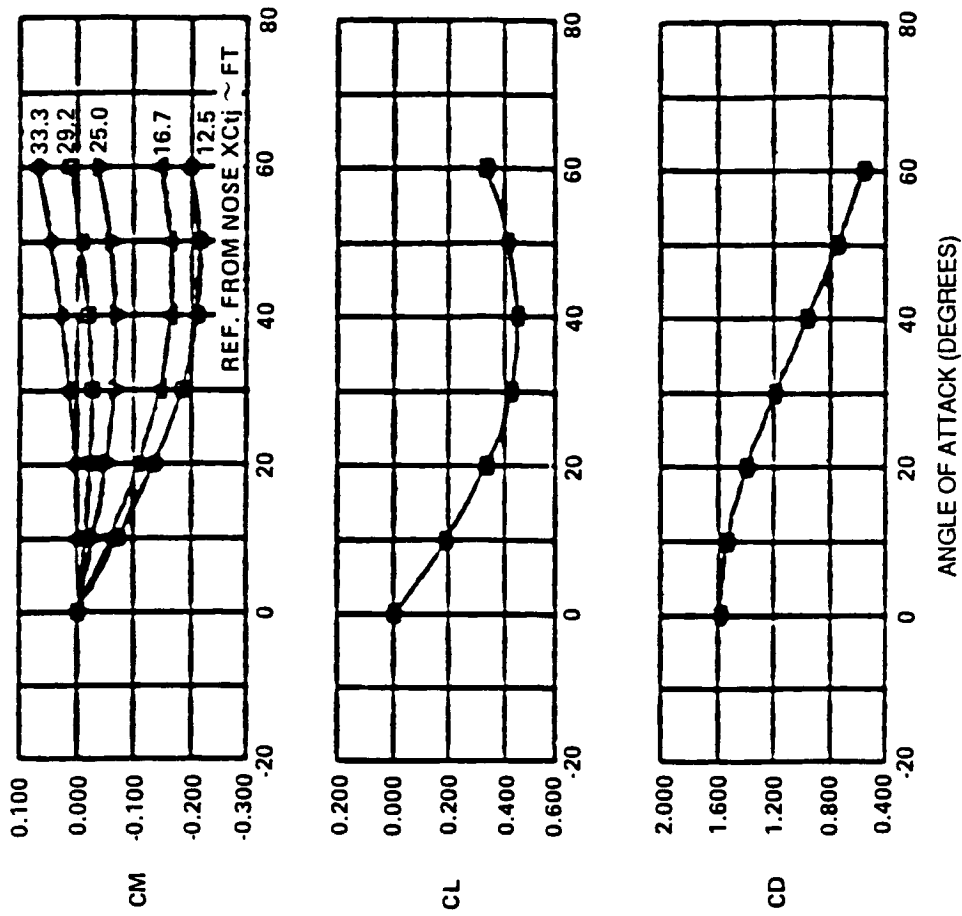


Figure 10-10. OTV Lifting Brake Aerodynamic Configuration



APAS II ANALYSIS SHOWS L/D = 0.25 AT 20 DEGREES
ANGLE OF ATTACK AND L/D = 0.30 AT 30 DEGREES

Figure 10-11. Lifting Brake Aerodynamics

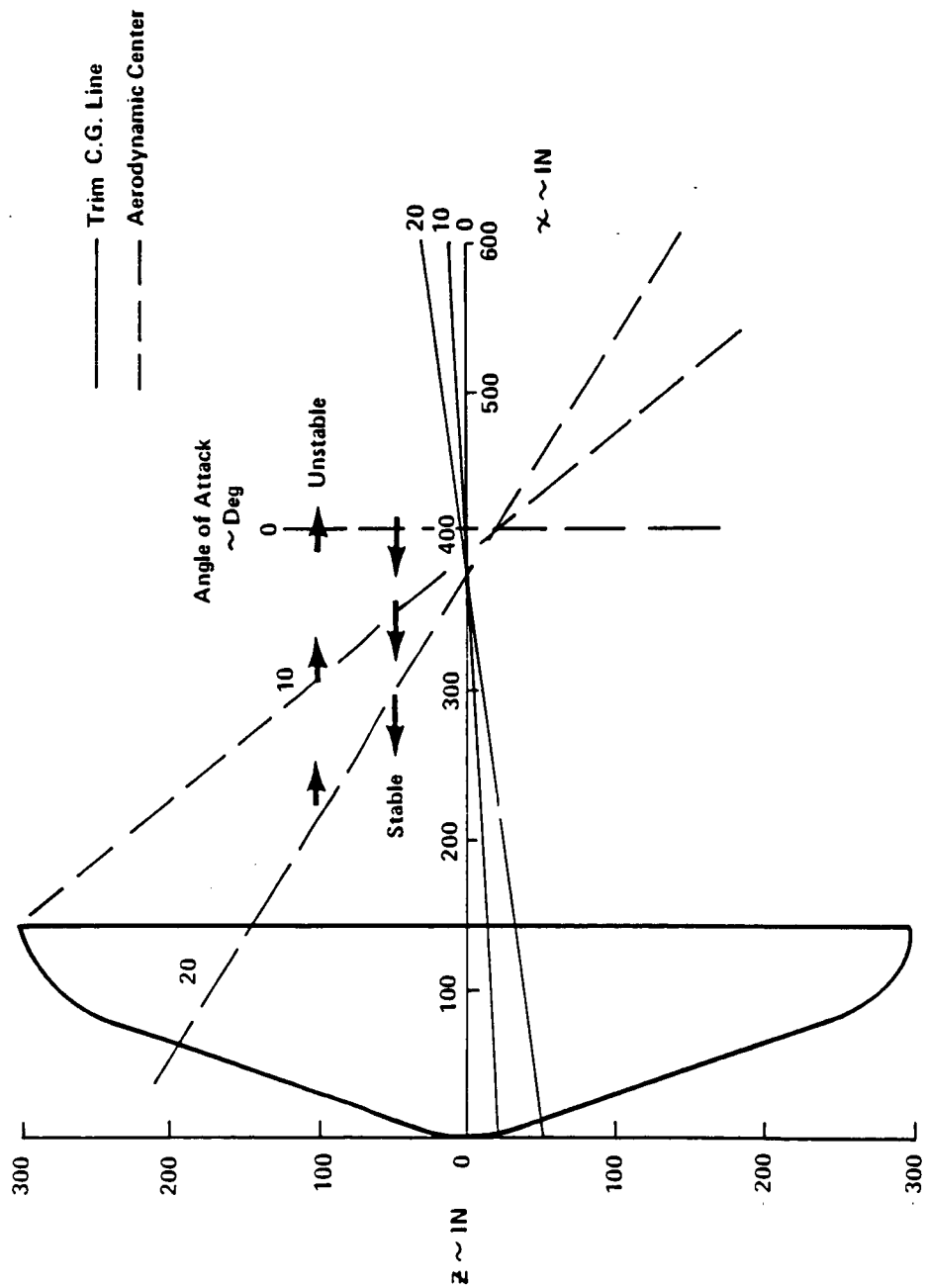


Figure 10-12 Symmetric Lifting Brake Trim C.G. and Aerodynamic Center

OTV 1742

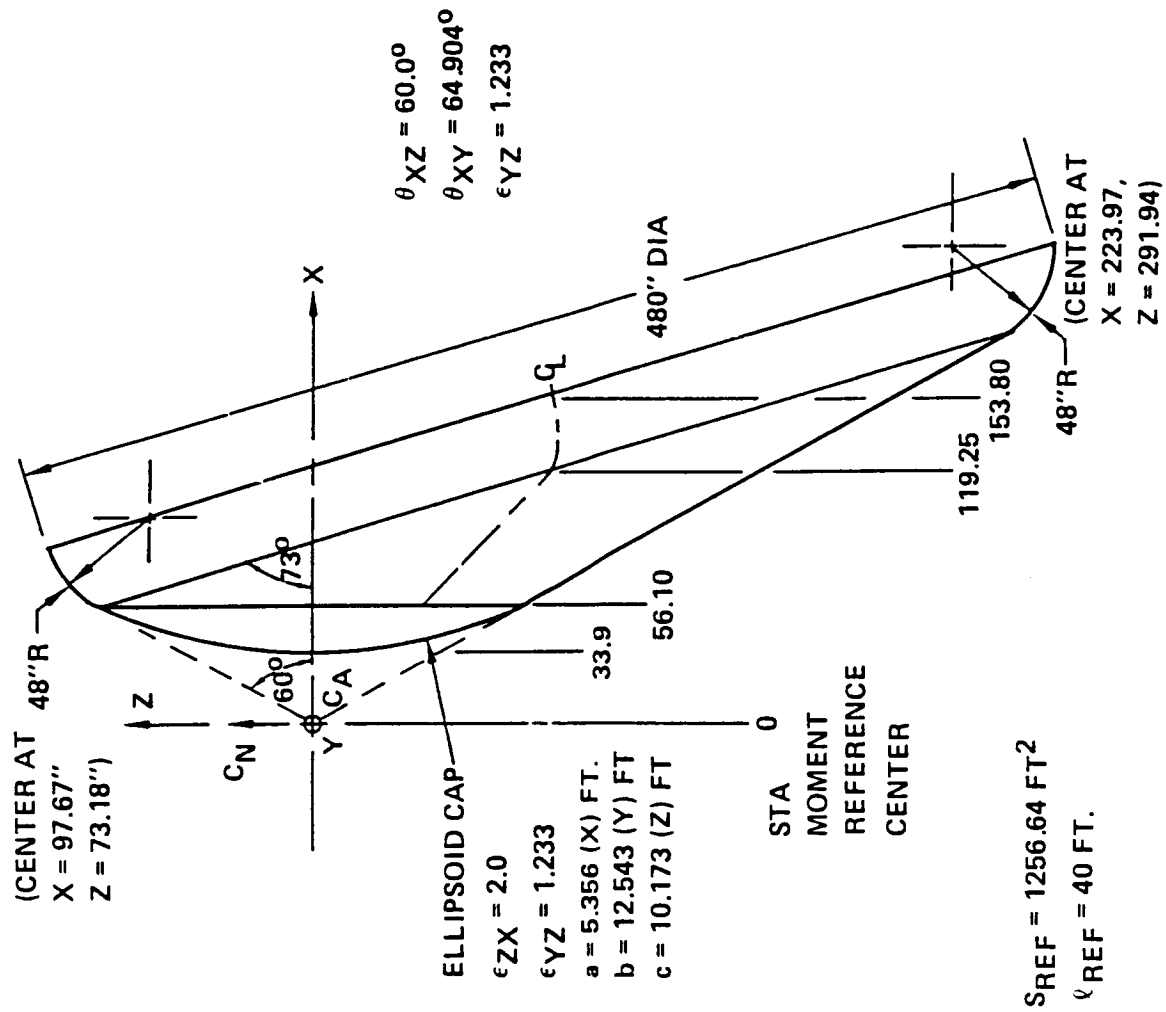


Figure 10-13. OTV Shaped Brake Aerodynamic Configuration

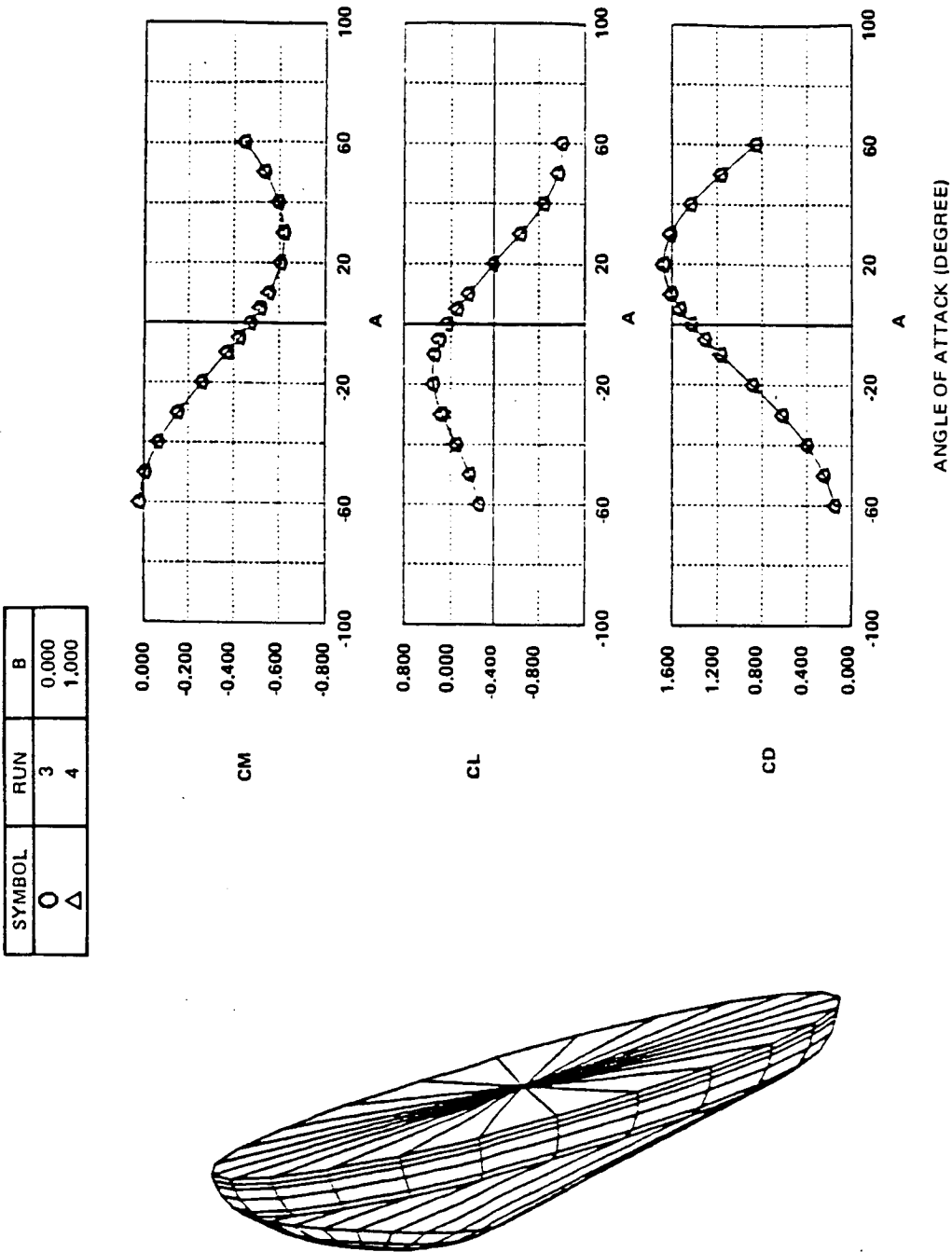


Figure 10-14 APAS Model and Aerodynamic Characteristics of Shaped Brake

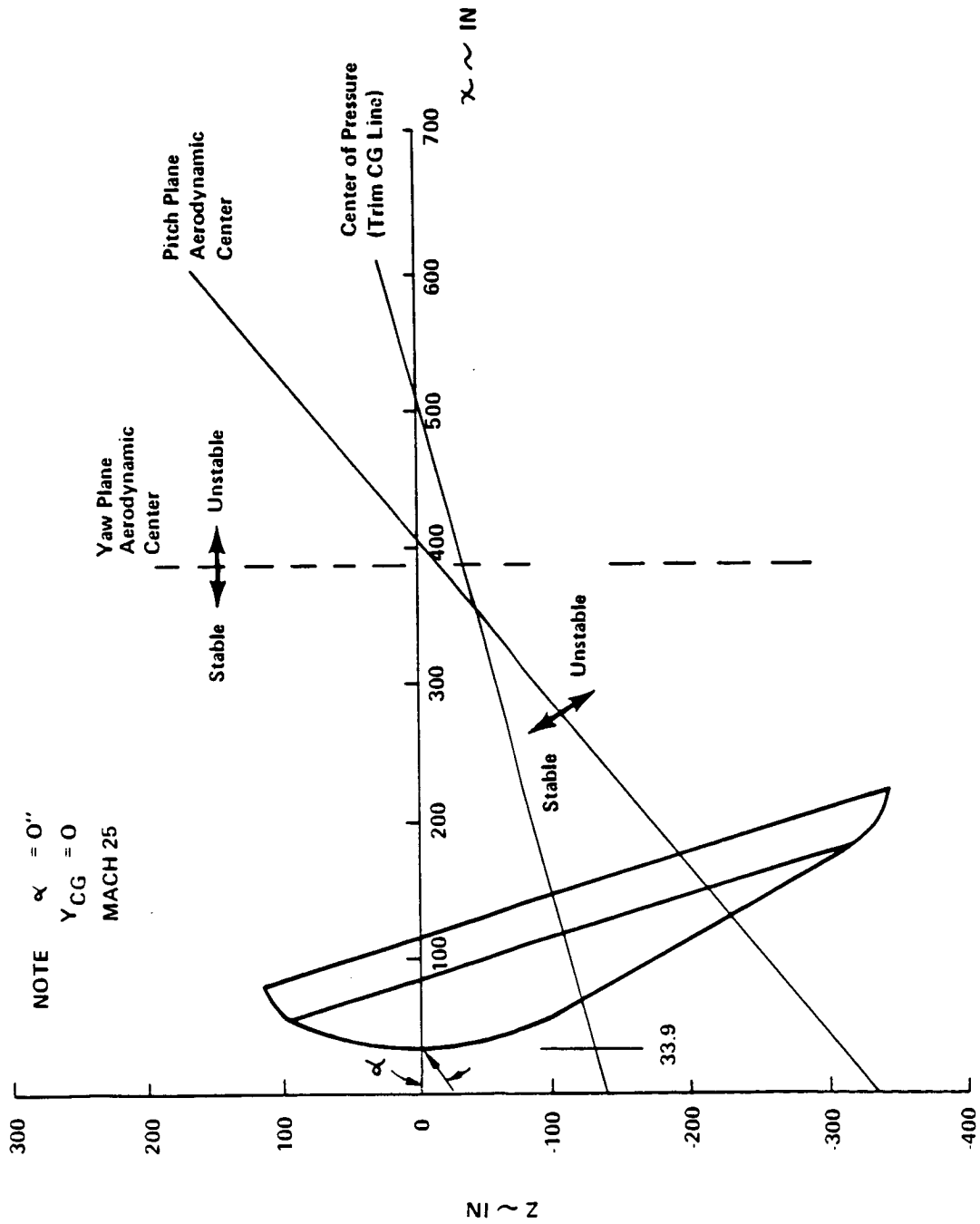
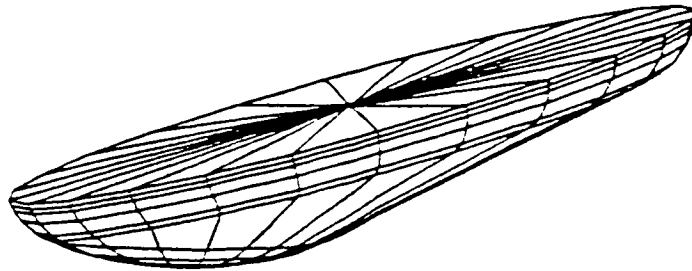
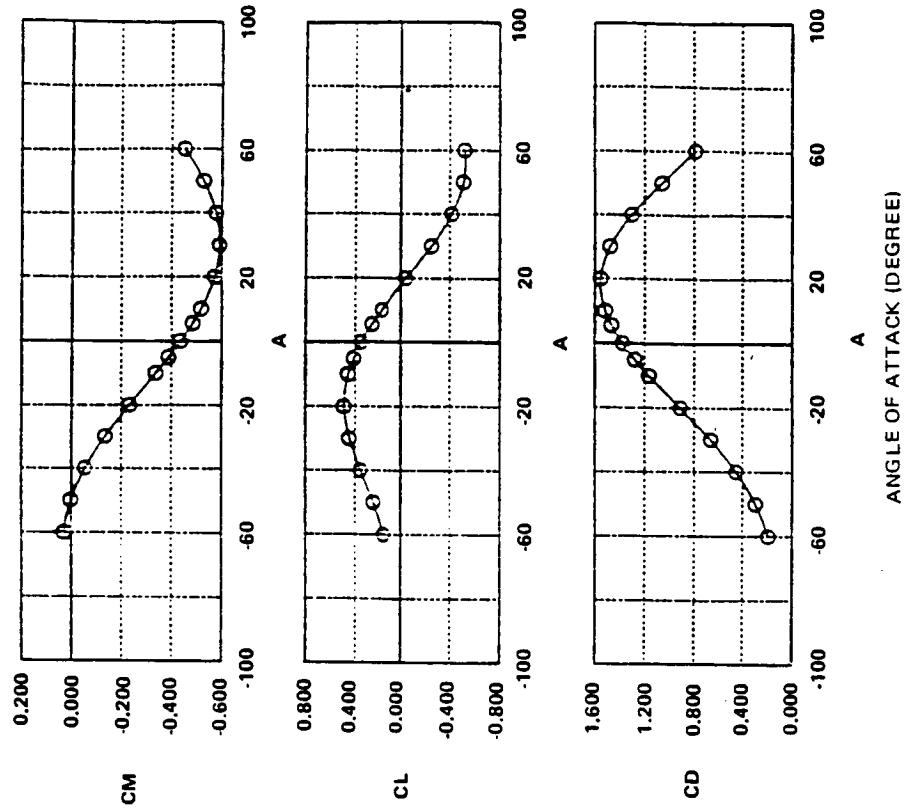


Figure 10-15 Shaped Brake Aerodynamic Center and C.G. Positions

percent. The APAS model of the modified shaped brake and its aerodynamic characteristic are shown in figure 10-16.



SYMBOL	RUN	M
O	1	25,000

Figure 10-16 APAS Model and Aerodynamic Characteristics of Modified Elliptical Shaped Brake

11.0 OTV RELIABILITY ANALYSIS

11.1 INTRODUCTION

The reliability analyses performed for the Phase A OTV study are the continuations of those earlier analyses performed during the FOTV and AOTV studies. The primary purpose of the OTV analyses was to determine an OTV hardware configuration optimized to meet anticipated mission requirements for an unmanned GEO delivery mission. Optimization was achieved via Life Cycle Cost (LCC) vs. Reliability (R) studies. In addition to the GEO delivery mission, preliminary reliability optimizations were performed for five other unmanned and manned missions which may be used in future OTV studies.

11.2 RELIABILITY MODEL

The OTV reliability block diagrams are shown in figures 11-1 through 11-6. Figure 11-1 shows the overall OTV system in terms of its subsystems. Subsequent figures detail the subsystems. (The Structure and Debris Protection subsystems are not detailed because they are structural in nature.) The configuration represented by these diagrams contains no redundancy; i.e., these are "single thread" diagrams and provide the starting point for subsequent analyses. All required OTV functions are satisfied by the components in these diagrams.

Each block is labelled with the component it represents and also contains the failure parts of that component during the boost and coast phases of the mission. The failure rates used in the later analyses described below are the averages of the boost and coast failure rates weighted by the amount of time spent in each of these phases for each mission analyzed. Numbers in parentheses under some blocks indicate the quantity of those components required to satisfy OTV functional requirements (see, for instance, fig.11-6).

The failure rates themselves are chiefly those which were used in prior FOTV and AOTV studies. These in turn were the failure rates obtained from similar IUS equipment and adapted for FOTV and AOTV use. A notable exception to the preceding is the failure rates used for the Data Management Units (DMU's) in the avionics subsystem. The DMU's, being of new design, required new failure rates. These failure rates were calculated in accordance with the parts count method of MIL HDBK 217D. Parts quality was assumed to be equivalent to class B.

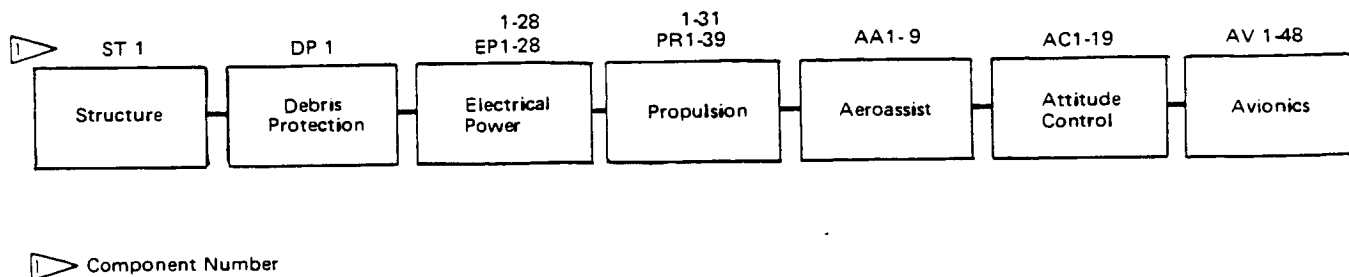


Figure 11-1 OTV System Single Thread Reliability Block Diagram

OTV-1585

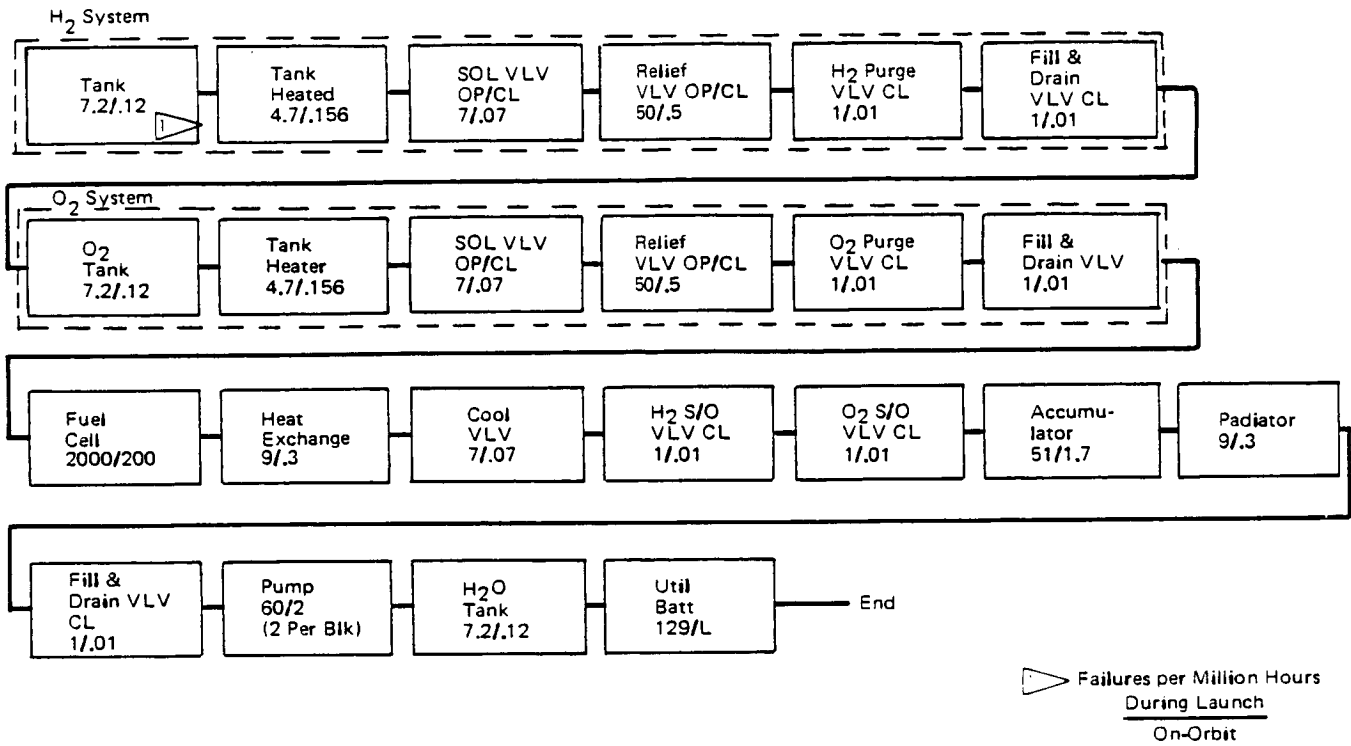
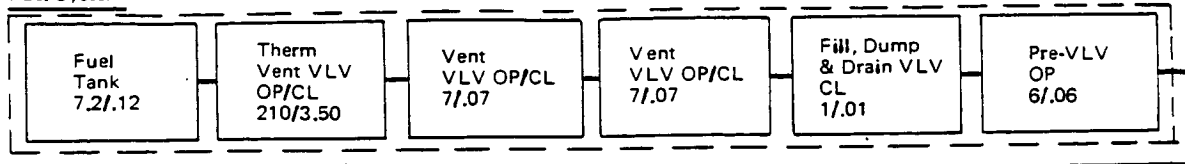


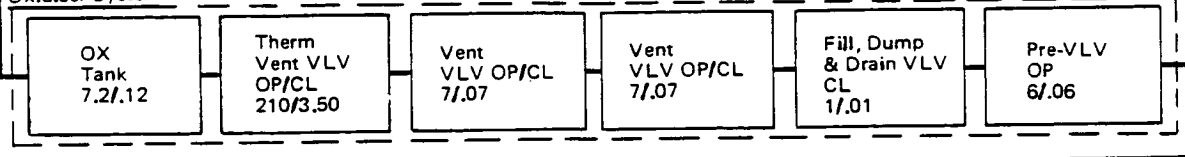
Figure 11-2 OTV EPS Reliability Block Diagram – Single Thread

OTV-1586

Fuel System



Oxidizer System



Engine System

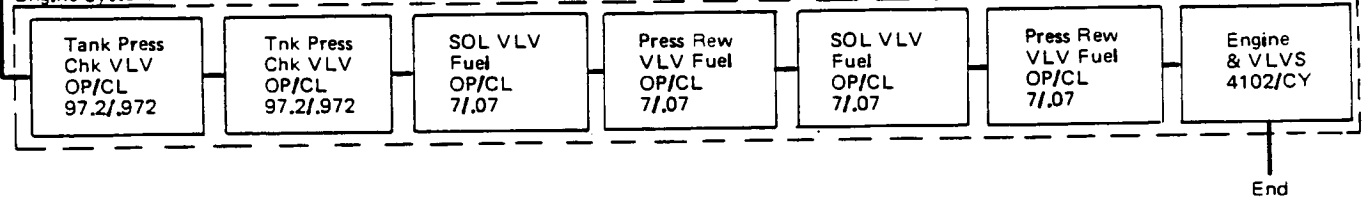


Figure 11-3 OTV Propulsion Reliability Block Diagram – Single Thread

OTV-1587

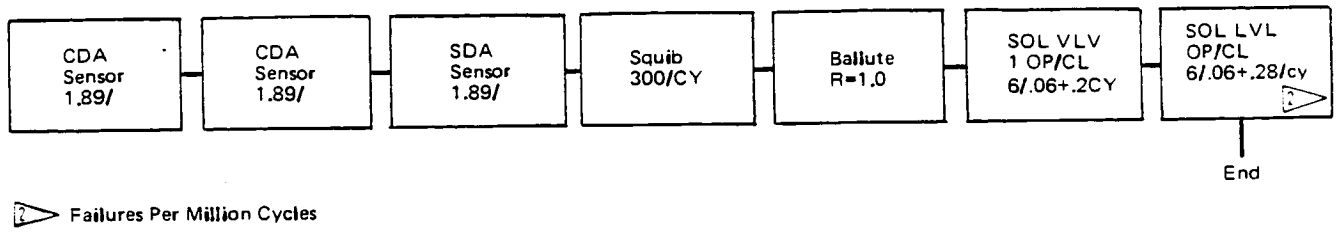


Figure 11-4 OTV Aero-Assist Reliability Block Diagram – Single Thread

OTV-1588



480

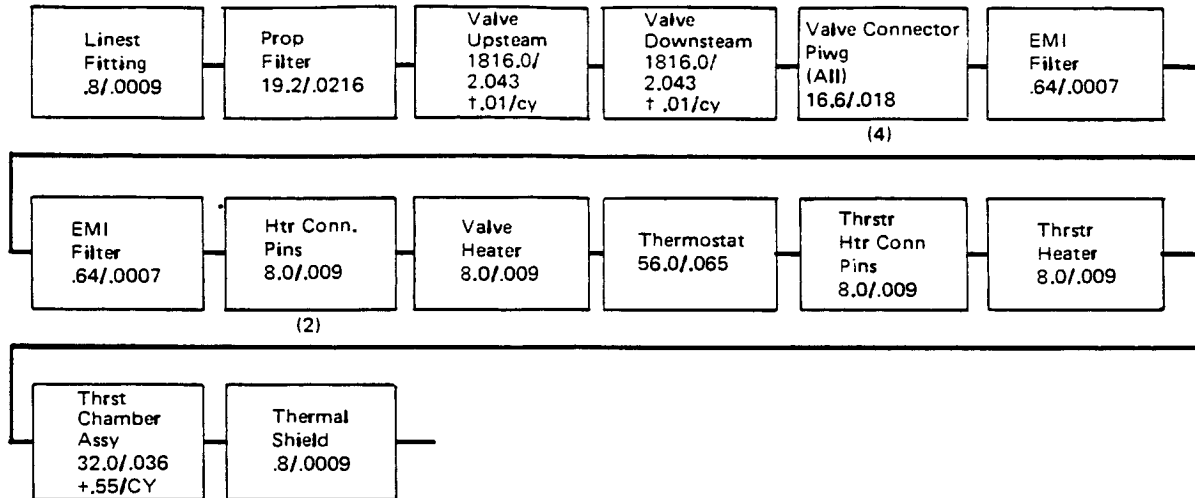


Figure 11-5 (Continued) REM Single Thread Reliability Block Diagram
(Derived from Rocket Research Co. Diagram)

OTV-1590

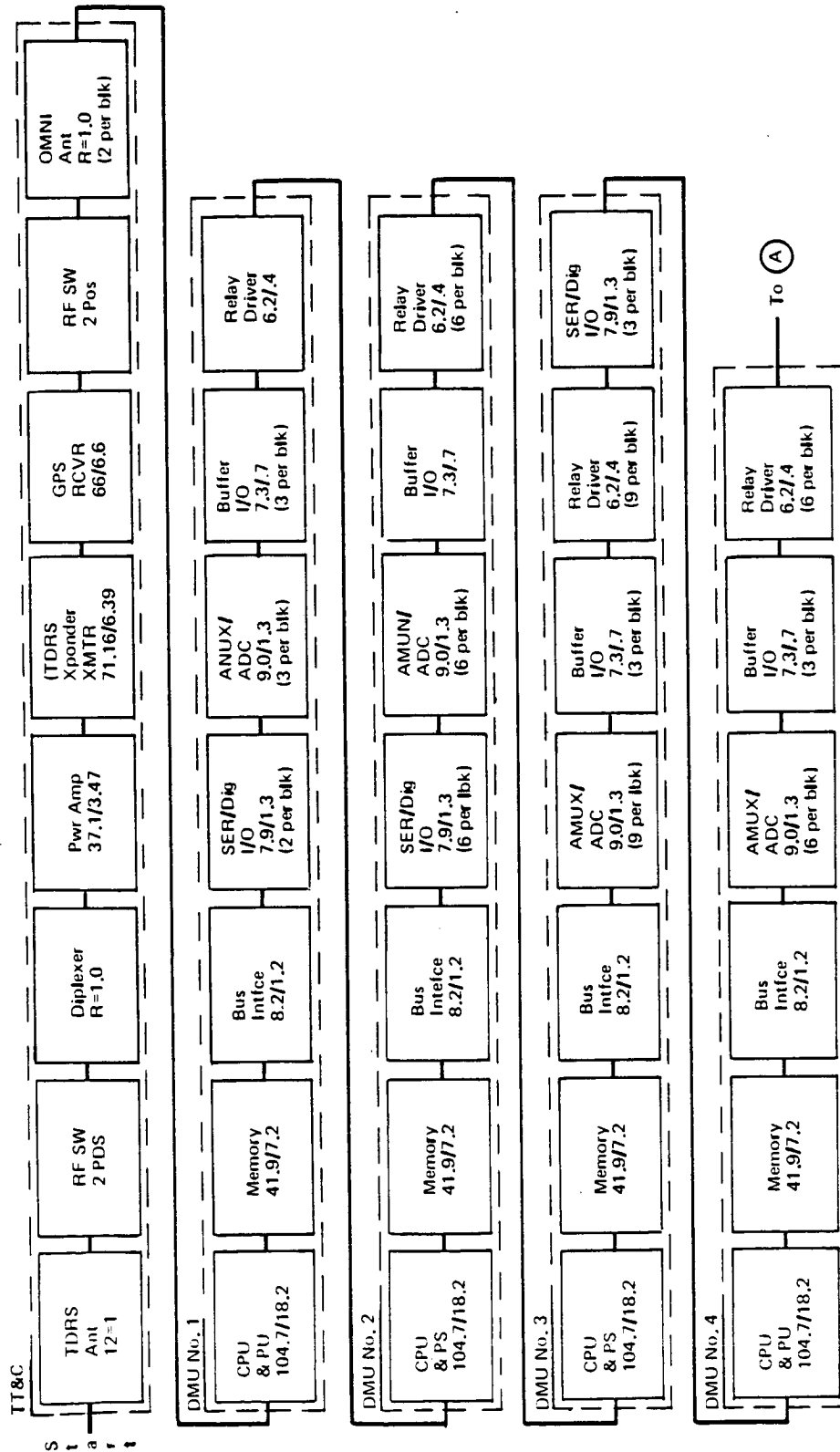


Figure 11-6 OTV Avionics Reliability Block Diagram – Single Thread

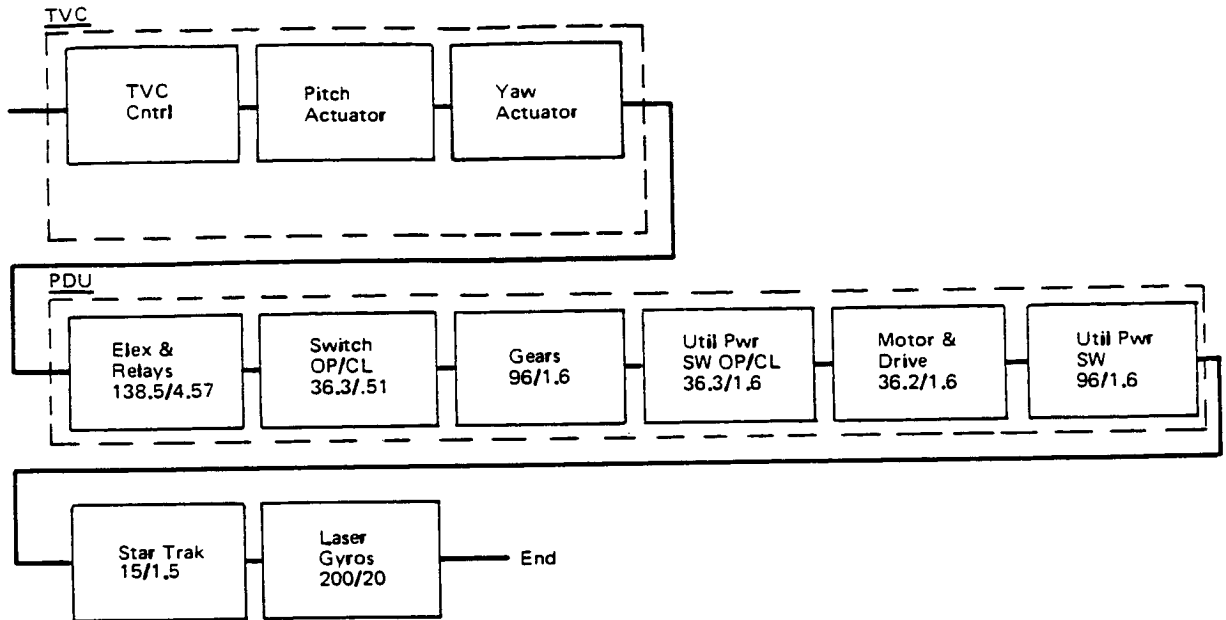


Figure 11-6 OTV Avionics Reliability Block Diagram – Single Thread (Continued)

OTV-1592

11.3 OTV MISSIONS

This paragraph contains a brief description of the missions which have been investigated and is divided into unmanned and manned missions. Analysis for the unmanned missions is comparatively straight forward as regards reliability. The manned missions require the consideration of survivability which adds a new dimension to these analyses. The following timelines relate to a SB OTV. GB OTV's would have a small time increment added to the beginning of the mission to account for launching into LEO.

11.3.1 Unmanned Missions

The timelines for the three unmanned OTV missions are shown in tables 11-1 through 11-3. For purposes of reliability and LCC analyses, two of the times during these missions are of importance: The time of payload separation (or rendezvous and docking) which determines the probability of successfully completing the purpose of the mission, and total mission times which determines the probability of recovering the OTV. As stated previously, analytical emphasis was placed upon the mission timeline in table 11-1.

11.3.2 Manned Missions

The timelines for projected manned missions are shown in table 11-4 through 11-6. For these missions reliability is the probability of successful payload delivery (or servicing) and survivability is the probability of successful return of the astronauts. These subjects are further described in paragraph 11.4.2.

11.4 REDUNDANCY OPTIMIZATION

The first step in the reliability/LCC optimization is the optimization of reliability starting with the single thread OTV configuration, with respect to cost and weight for a specific mission timeline. This amounts to adding redundant components to the single thread configuration in a specific sequence to increase reliability in the most cost effective manner. Redundancy optimization is performed by the Boeing-developed single thread reliability optimization program (STROP). STROP is a computer program for reliability vs "constraint" optimizations on single thread system configurations. OTV constraints are cost and weight. Optimization is based on redundancy additions sequentially selected in accordance with yielding the maximum ratio value of delta reliability/delta cost (or delta weight) for all possible options at each step. Reliability equations are based on Markovian formulations with the assumption of exponential

TABLE 11-1 UNMANNED GEO DELIVERY TIMELINE

EVENT	DURATION (Hrs)	ELAPSED (Hrs)
Start Mission	0.0	0.0
Pre-Launch Ops.	5.0	5.0
Separate/Coast	0.988	5.988
Transfer Burn 1	0.138	5.926
Coast	2.38	8.306
Transfer Burn 2	0.154	8.460
Coast	5.15	13.610
Circularize Burn	0.134	13.744
GEO Ops + Phasing	24.00	37.744 = T ₁
De-Orbit Burn	0.036	37.780
Coast	5.20	42.980
Aeromaneuver	0.05	43.030
Coast	0.05	43.080
Ballute Ejection	0.10	43.180
Coast	0.640	43.820 = T ₂
Perigee Raise Burn	0.001	43.821
Phase	12.409	56.230
LEO Circularization Burn	0.001	56.231
End Mission	0.0	56.231
OMV Retrieval	Not defined	

No. of Burns = 6
 Burn Time = 0.464 hrs
 Coast Time = 55.767 hrs
 Total Time = 56.231 hrs

TABLE 11-2 UNMANNED LUNAR DELIVERY TIMELINE

EVENT	DURATION (Hrs)	ELAPSED (Hrs)
Separate/Coast	0.788	0.788
Injection Burn	0.482	1.270
Coast W/Correction Burn	118.519	119.789
Lunar Insertion Burn	0.073	119.862
Rendezvous & Dock	3.000	122.862 = T ₁
Transfer Payload at LSS	2	124.862
Separate/Orientation	1.000	125.862
De-Orbit Burn	0.018	125.880
Coast W/Correction Burns (2)	119.520	245.400
Aeromaneuver	0.064	245.464 = T ₂
Coast	0.752	246.216
LEO Circularization	0.002	246.218

No. of Burns = 8

Burn Time = 0.583 hrs

Coast Time = 245.635 hrs

Total Time = 246.218 hrs

TABLE 11-3 UNMANNED PLANETARY

EVENT	DURATION (Hrs)	ELAPSED (Hrs)
Separate/Coast	0.788	0.788
Burn 1	0.227	1.015
Coast	6.135	7.150
Burn 2	0.170	7.320 = T ₁
Separate Payload		
Coast	0.111	7.431
Deceleration Burn	0.046	7.477
Coast/Correction	63.262	70.739
Aeromaneuver/Correction	0.027	70.766 = T ₂
Coast	0.755	71.521
Circularize at LEO	0.003	71.524

No. of Burns = 6
 Burn Time = 448 Hr
 Coast Time = 71.076 Hr
 Total Time = 71.524 Hr

TABLE 11-4 MGSS REFERENCE MISSION TIMELINE

EVENT	DURATION (Hrs)	ELAPSED (Hrs)
LEO Coast	0.788	
Perigee Burn 1	0.216	
Coast	2.530	
Perigee Burn 2	0.197	
Coast	5.213	
Geo Circ. Burn	0.192	
Servicing 1	24.	33.16 = T ₁₁
Transfer Burn 1	0.003	
Coast	48.024	
Phase Circ. Burn 1	0.003	
Servicing 2	24.	105.17 = T ₁₂
Transfer Burn 2	0.009	
Coast	115.019	
Phase Circ. Burn 2	0.009	
Servicing 3	24.	244.2 = T ₁₃
Transfer Burn 3	0.003	
Coast	48.024	
Phase Circ. Burn 3	0.003	
Servicing 4	48.	
GEO Phasing	6.	
Deorbit Burn	0.124	
Coast	6.109	
Coast	0.767	
LEO Circularize	0.006	
Contingency	48.	401.2 (Total)

TABLE 11-5 MANNED GEO MISSION (SELF-CONTAINED)

EVENT	DURATION (Hrs)	ELAPSED TIME (Hrs)
Separate/coast	0.788	0.788
Burn 1	0.315	1.103
Coast	2.237	3.340
Burn 2	0.350	3.690
Coast	5.055	8.745
GEO circularization burn	0.310	9.055
GEO ops 1	9.440	18.495 =T ₁₁
Phase burn (transfer) 1	0.011	18.506
Coast	77.779	96.285
Phase burn (circ.) 1	0.011	96.296
GEO ops 2	9.739	106.035 =T ₁₂
Phase burn (transfer) 2	0.011	106.046
Coast	77.779	183.825
Phase burn (circ.) 2	0.010	183.835
GEO ops 3	9.740	193.575 =T ₁₃
Phase burn (transfer) 3	0.010	193.585
Coast	77.780	271.365
Phase burn (circ.) 3	0.010	271.375
GEO ops 4	9.740	281.115 =T ₁₄
De-orbit burn	0.190	281.305
Coast to LEO w/correction	6.010	287.315
Aeromaneuver w/correction	0.066	287.381 =T ₂
Coast	0.735	288.116
LEO circularization	0.009	288.125

No. of Burns = 13
 Burn Time = 1.243 Hrs.
 Coast Time = 286.882 Hrs.
 Total Time = 288.125 Hrs.

TABLE 11-6 MANNED LUNAR MISSION

EVENT	DURATION (Hrs)	ELAPSED TIME (Hrs)
Pre-launch operations at space station	N.I.	
Separate from space station	N.I.	
Coast (1/2 orbit); orientation maneuvers	0.788	0.788
Burn to lunar transfer orbit	0.434	1.222
Coast to low lunar orbit (2 1/2 day transfer); midcourse correction	N.I.	
	61.566	62.788
Circularization burn at low lunar orbit	0.082	62.870
Rendezvous and dock with LSS	3.000	65.870=T ₁
Crew transfer to LSS habitat for lunar operations; OTV power down		
Crew transfer to OTV in preparation for return to Earth; OTV power up	N.I.	
OTV separation from LSS; orientation maneuver	N.I.	
	1.000	66.870
Burn to Earth transfer orbit	0.066	62.936
Coast to aeromaneuver (2 1/2 day transfer); midcourse correction	N.I.	
	61.933	124.869
Attitude correction	0.001	124.870
Aeromaneuver; correction burn	0.091	124.961=T ₂
Coast to LEO apogee (1/2 orbit); retract ballute	N.I.	
	0.718	125.679
Circularization burn at LEO	0.007	125.686
OMV retrieval and return to space station	N.I.	

N.I. = Not included

No. Of Burns = 8
 Total Burn Time = 0.602 Hr.
Total Coast Time = 125.084 Hr.

Total Mission Time = 125.686 Hr.

failure times for the single thread component blocks. A summary of the mission addressed and the types of redundancy optimizations performed is shown in tables 11-7.

11.4.1 Unmanned Mission Optimizations

Figures 11-7 through 11-10 show the results of the unmanned mission redundancy optimizations with respect to DDT&E and production costs (and component weight where applicable). Additions of major components are specified in these graphs. The small numbers associated with the various points on these curves refer to specific component additions delineated in the appropriate computer printouts. As a matter of practicality, the printouts are not included with this document, but are on file at BAC for customer inspection. Further, these graphs are plotted only to the region of $R=0.99$ to avoid the use of semi-log graph paper. The actual optimizations continued until $R=0.999$. Of course, these values are also contained in the aforementioned computer printouts and were used for the LCC/reliability trade studies.

Because of the emphasis on the GEO delivery mission, STROP optimization was performed for both cost and weight. The remaining two unmanned missions were optimized with respect to cost only. Should additional analyses be required for these missions at a later date, the necessary weight optimizations will be performed.

11.4.2 Manned Missions Optimizations

While redundancy optimization was performed for the manned missions, it was not pursued to the same depth as for the unmanned missions. The information in this paragraph is intended to provide a basis for future OTV manned mission LCC/reliability analyses.

NASA handbook NHB 5300.4 (1D-2), "Safety, Reliability, Maintainability and Quality Provisions for the Space Shuttle Program," was used to obtain guidance for reliability analysis in the absence of any other documentation more applicable for OTV manned missions. Information in this document provides the following two groundrules:

1. A manned vehicle shall have no single failure points (SFP's) for critical equipment.
2. Should failure(s) occur during a mission such as to result in an SFP in critical equipment anywhere in the system, the mission will be aborted. (All OTV components in the analyses herein are considered critical).

The first definition describes "survivability " (as distinct from reliability) and indicates that each component in the basic configuration will have at least one

Table 11-7 STROP Optimized OTV Missions

TYPE OF VEHICLE	MISSION	OPERATING TIME HOURS	OPTIMIZED WITH RESPECT TO	
			COST	WEIGHT
UNMANNED	BASELINE GEO DELIVERY	56.231	X	X
UNMANNED	LUNAR DELIVERY	246.218	X	X
UNMANNED	PLANETARY	71.524	X	
MANNED	MGSS	340.233*	X	X
MANNED	LUNAR	125.686	X	
MANNED	GEO	288.125	X	

* OPTIMIZED THOROUGH 4 TH ORBITAL OPERATION ONLY

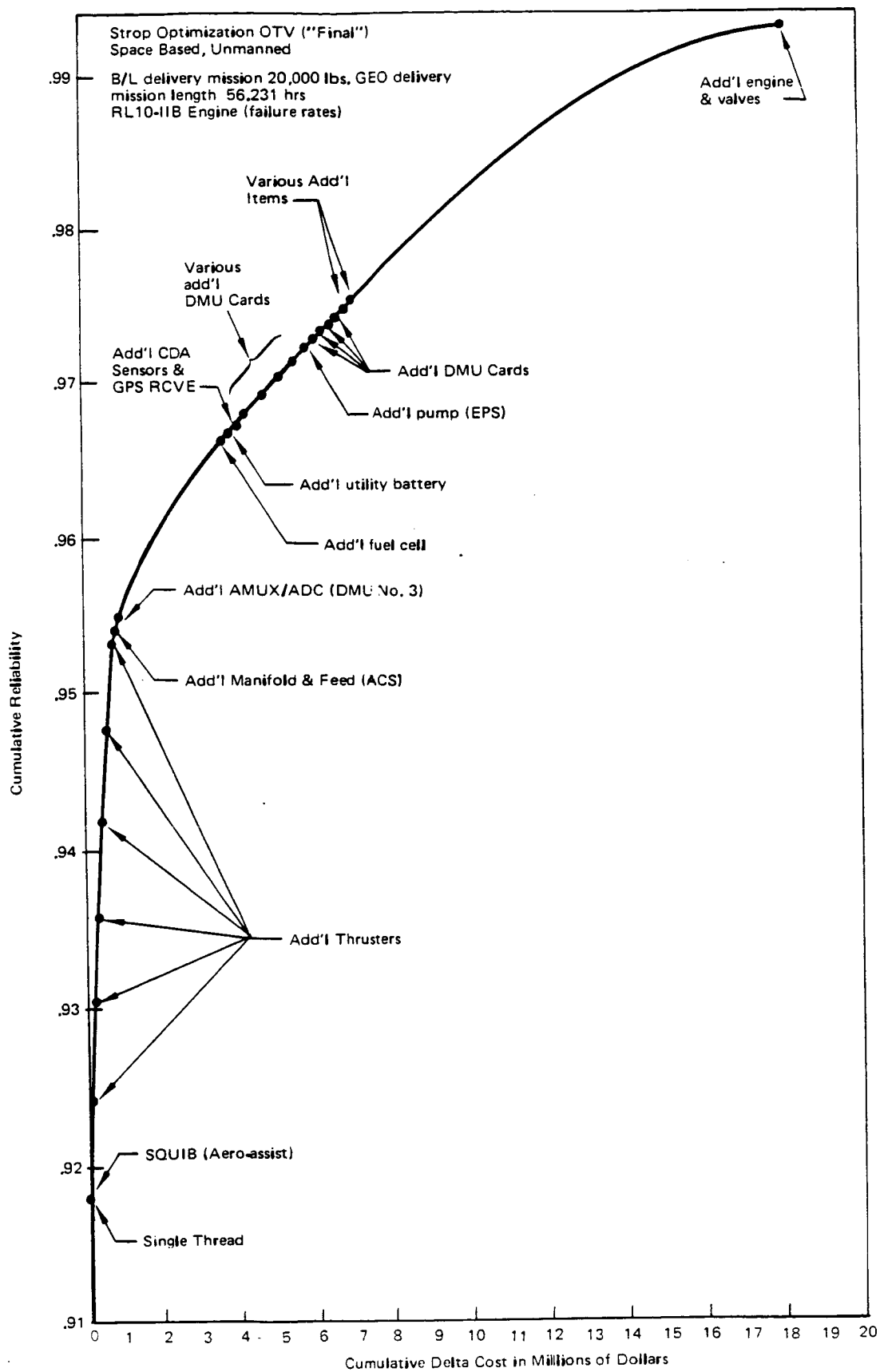


Figure 11-7 STROP Optimized by Cost – GEO Delivery

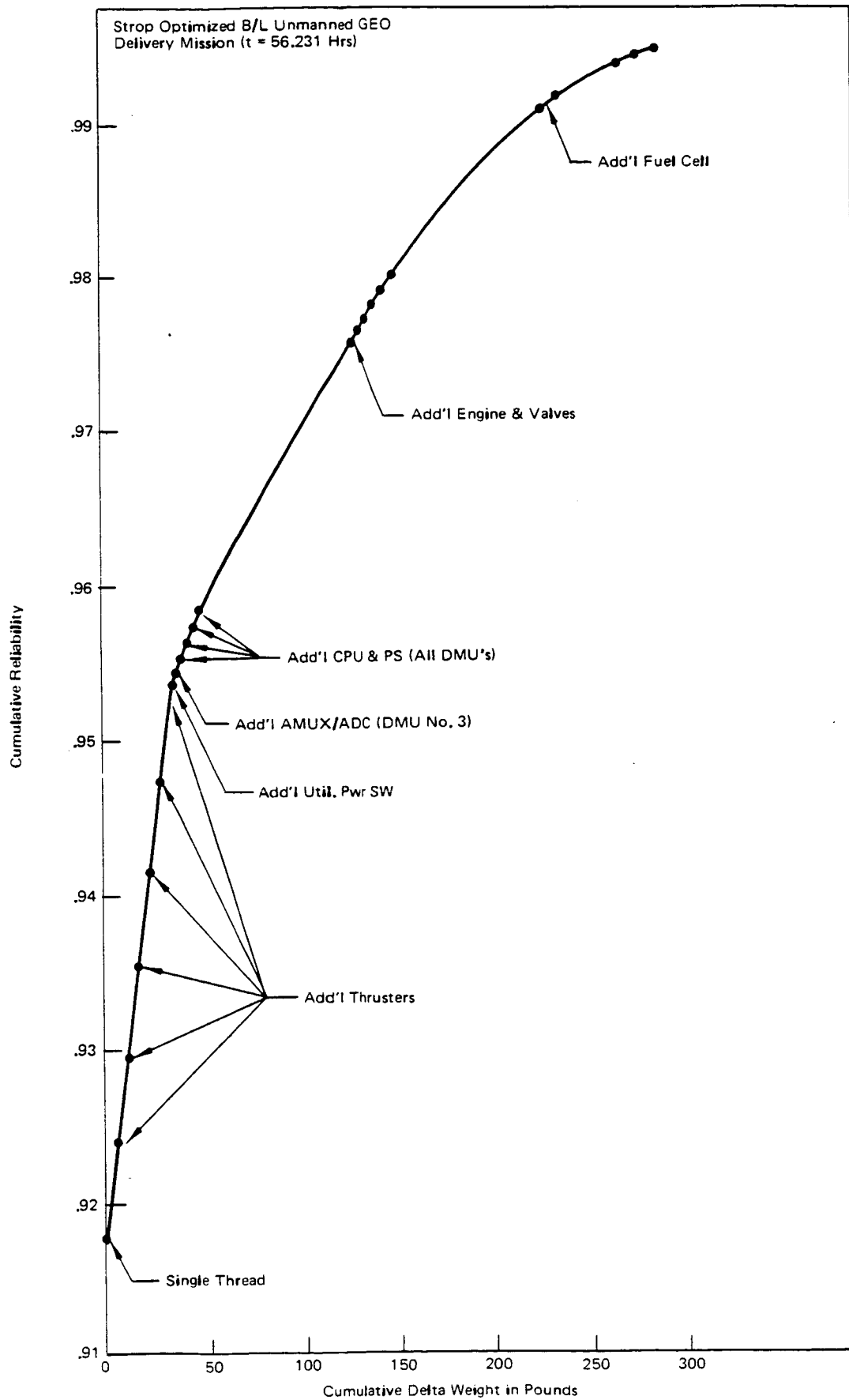


Figure 11-8 STROP Optimized by Weight – GEO Delivery

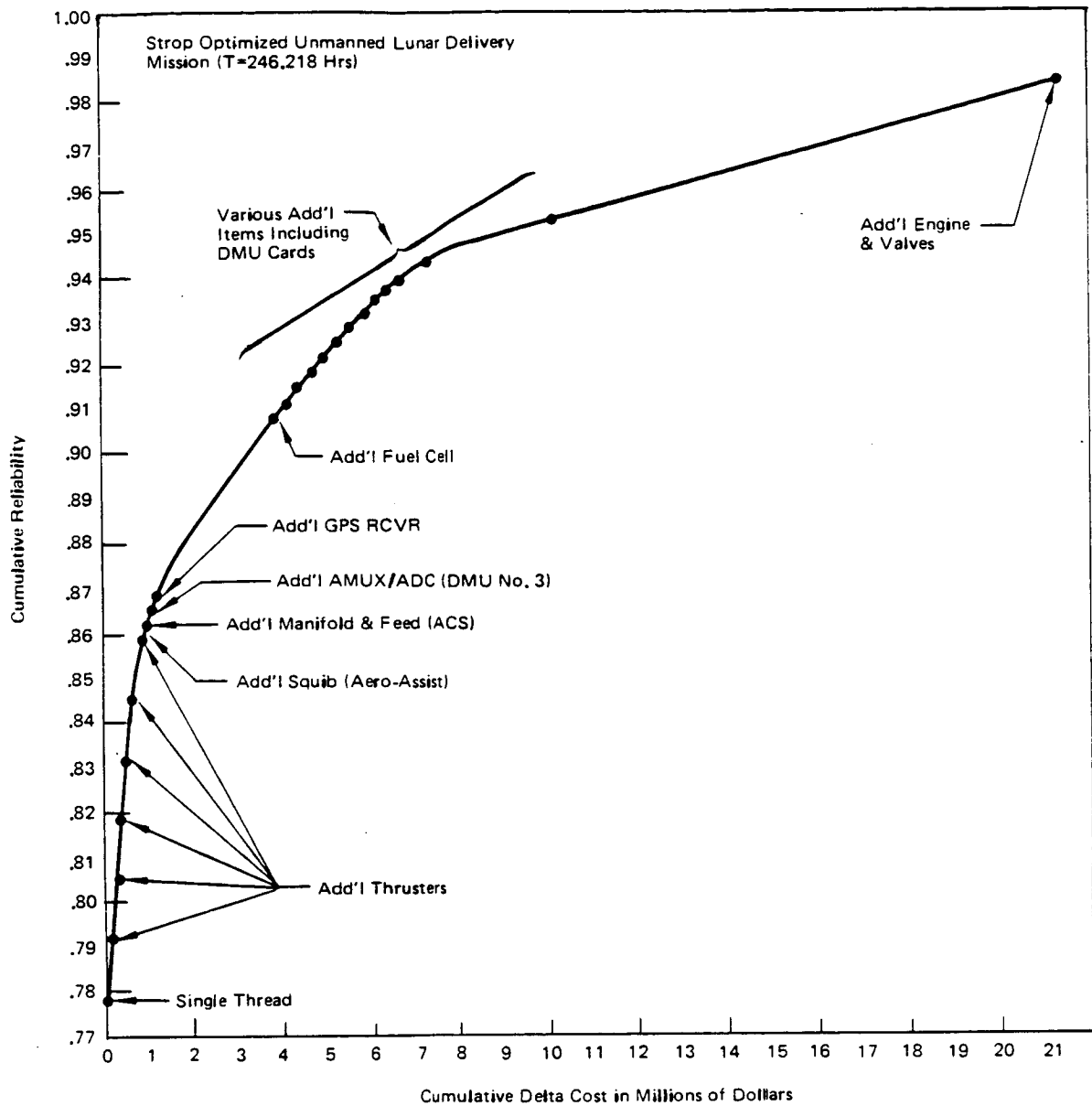


Figure 11-9 STROP Optimized by Cost – Lunar Delivery

OTV-1595

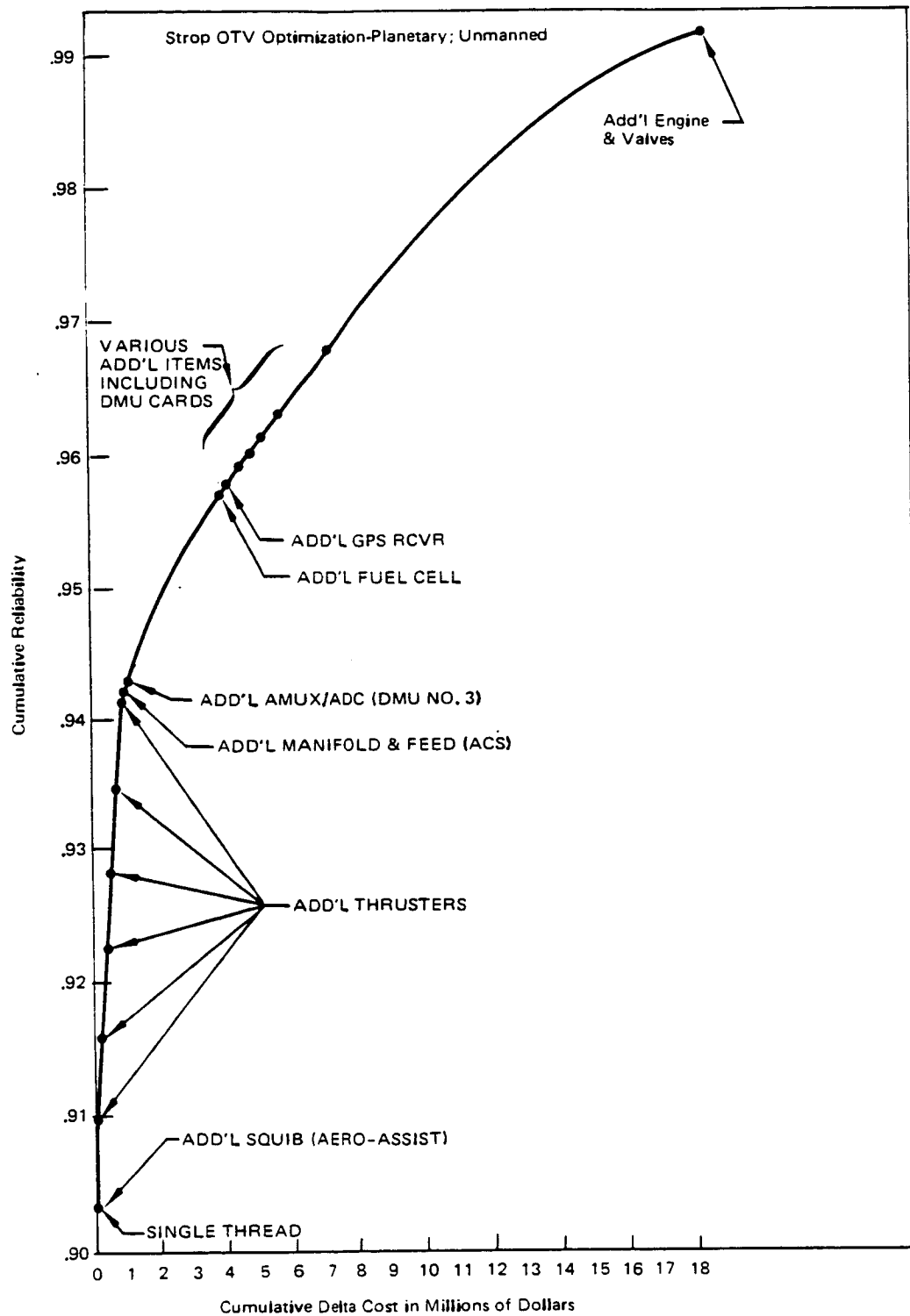


Figure 11-10 STROP Optimized by Cost - Planetary

redundant component; i.e., the basic configuration must be at least "Fail Safe." However, given that we have a Fail Safe configuration initially, the second definition says we will abort a mission should only one failure occur (because an SFP would then exist in the system). Thus, the second definition applies to reliability; i.e., probability of mission success where mission refers to placing or servicing a satellite in orbit, or making a human delivery. Survivability, on the other hand, refers to the probability of successful recovery of the astronauts.

Figure 11-11 illustrates the concepts described above. Survivability and reliability apply simultaneously depending on the point of view. Relative to the "mission," points A through E, reliability is of interest. At the completion of the mission, point E, the OTV returns to base and is in a "defacto" abort mode. Thus, from point E to point F survivability applies. In addition, should failure result in an SFP during the "mission," the mission would be aborted. Consequently, the diagrammed "mission survivability" applies at any time from point A through point F relative to safe return of the astronauts (and, incidentally, recovery of the OTV).

Redundancy optimization is performed relative to reliability. A true single thread configuration is used as the starting point. Even though the configuration is fully redundant for survivability, a single failure will cause mission abort which is equivalent to failure. It is to be remembered that redundant additions for reliability even further enhance survivability which, of course, is always greater than reliability.

Figure 11-12 and 11-13 show the results of the cost and weight optimizations for the MGSS mission. As described above, the optimization applies only through orbital operations (survivability must be calculated separately. MGSS "Mission Survivability" is 0.9993 for the configuration where mission reliability is 0.995). The remaining two manned missions were optimized using different groundrules than for the MGSS mission. Thus, their inclusion here would be inappropriate. These missions will be treated in future analyses.

11.5 MAINTENANCE IMPLICATIONS

A list of the top 20 failure items for the MGSS mission is shown in table 11-8. This list is based upon an assumed MGSS optimized reliability of 0.995 and is included for maintenance planning purposes. It will be updated when subsequent LCC/reliability analysis yields the true optimized reliability value.

A Poisson distribution was used to calculate the probability of exact numbers of failures for MGSS and is shown in table 11-9. The assumptions are the same as those in the preceding paragraph. This data will also be used for maintenance planning.

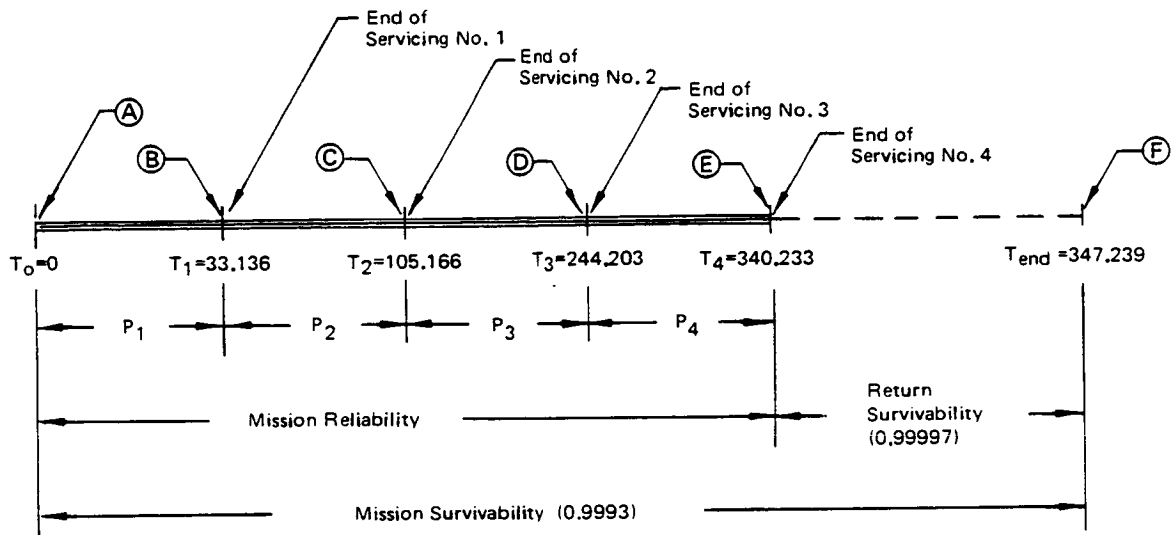


Figure 11-11 MGSS Mission Diagram for LCC/Reliability Analysis

OTV-1597

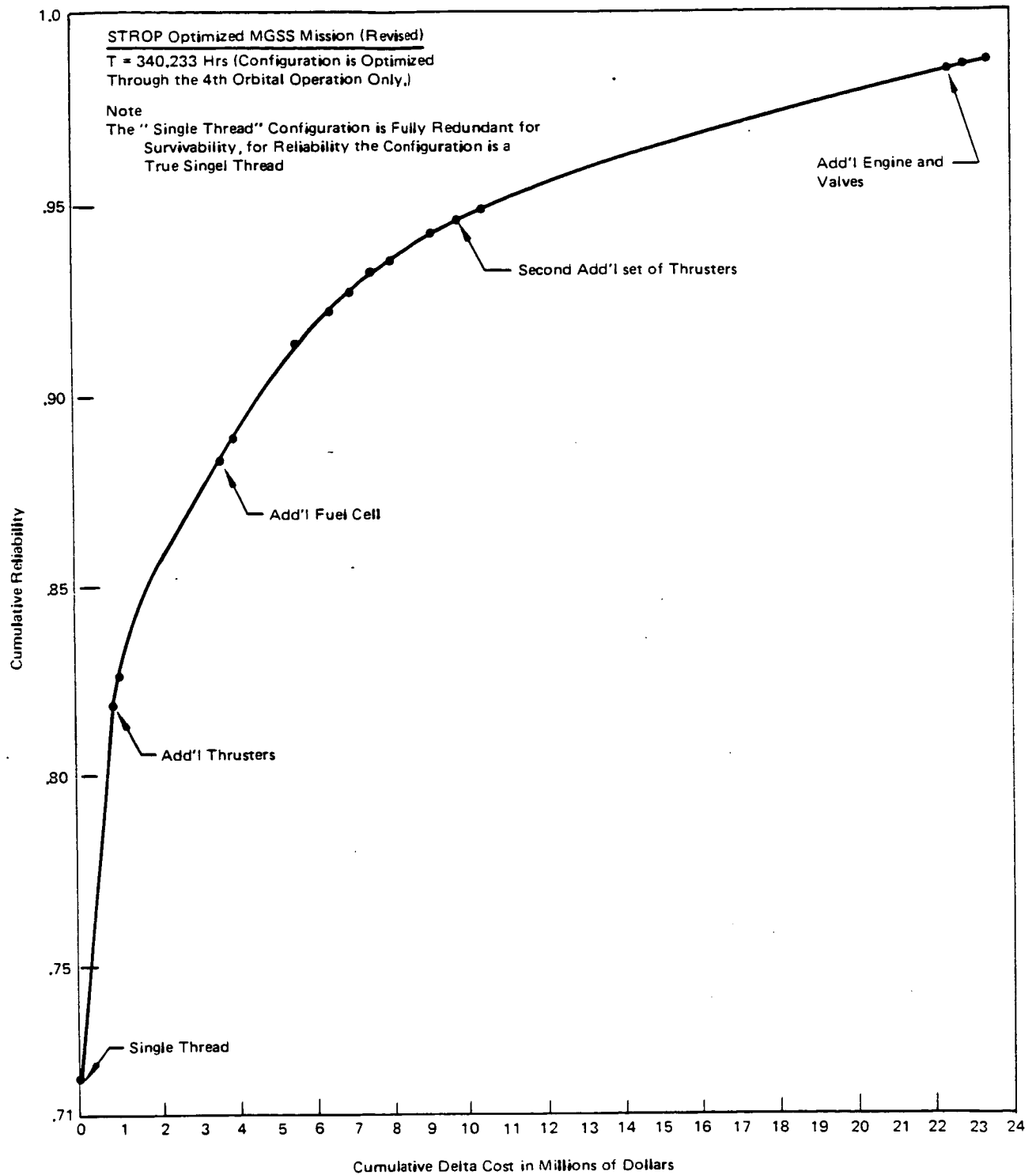


Figure 11-12 STROP Optimized by Cost – MGSS Mission

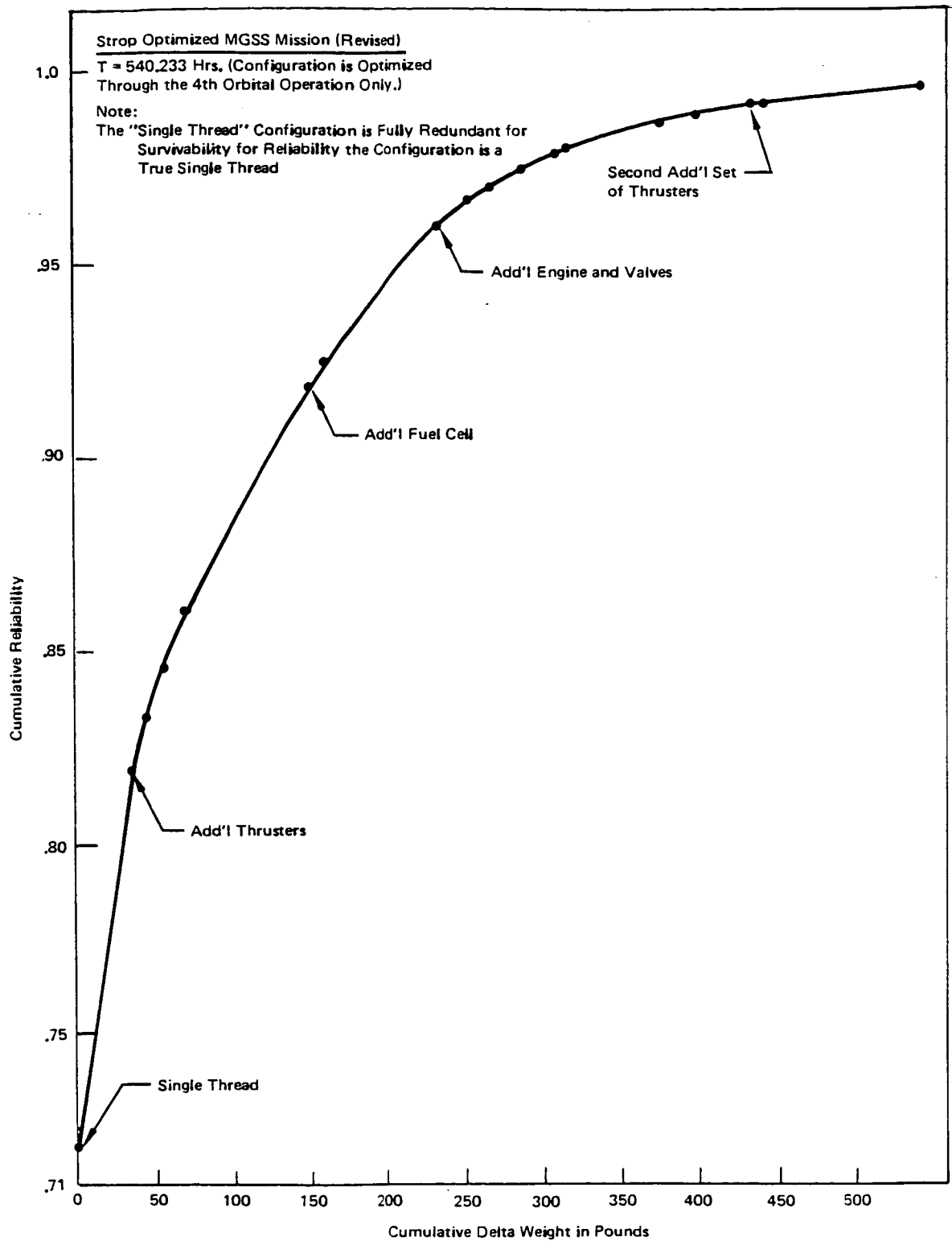


Figure 11-13 STROP Optimized by Weight – MGSS Mission

Table 11-8 OTV Leading Failure Contributors for MGSS Mission

RANK	COMPONENT	S/S	λ	N \triangle	QUANTITY PER SUBSYSTEM	N λ	MEAN MISSIONS TO REPAIR (MMTR)**
1	"2 REM"	ACS	* 64.660	24		1551.84	1.89
2	FUEL CELL	EPS	203.359	4		813.44	3.61
3	ENGINE & VALVES	PROP	*108.508	3		325.52	9.03
4	CPU & POWER SUPPLY CARDS	AV	18.361	13		238.69	12.31
5	MEMORY CARDS	AV	7.265	12		87.18	33.71
6	GYROS	AV	20.366	3 (SETS)		61.10	48.10
7	AMUX/ADC CARDS	AV	1.314	32		42.05	69.90
8	SER/DIG I/O CARDS	AV	1.312	17		22.30	131.80
9	GPS RECEIVER	AV	6.711	3		20.13	146.01
10	TRANSMITTER	AV	6.511	3		19.53	150.49
*CYCLIC FAILURE RATE EQUIVALENT							
**MMTR = $\frac{1}{N \lambda T}$							
\triangle N INCLUDES COMPONENTS FOR SURVIVABILITY							

MISSION: MGSS (T = 340.233 HRS)

Table 11-8 OTV Leading Failure Contributors for MGSS Mission (Continued)

RANK	COMPONENT	S/S	λ FAILURES PER 10 ⁶ HOURS	N QUANTITY PER SUBSYSTEM	$N \lambda$ FAILURES PER 10 ⁶ HOURS	MEAN MISSIONS TO REPAIR (MMTR)**
11	UTILITY BATTERY	EPS	6.230	3	18.69	157.3
12	BUFFER I/O CARDS	AV	0.712	26	18.51	158.8
13	MANIFOLD & FEED	ACX	5.162	3	15.49	189.7
14	ELECTRONICS & RELAYS (PDU)	AV	4.820	3	14.46	203.3
15	RELAY DRIVER CARDS	AV	0.411	32	13.15	223.5
16	THERM VENT VLV., FUEL	PROP	3.886	3	11.66	252.1
17	THERM. VENT VLV., OXIDIZER	PROP	3.886	3	11.66	252.1
18	POWER AMPLIFIER	AV	3.550	3	10.65	276.0
19	DUMP	EPS	2.108	4	8.43	348.7
20	ACCUMULATOR	EPS	1.792	3	5.38	546.3

VEHICLE CUM MMTR = 0.9

*CYCLIC FAILURE RATE EQUIVALENT

$$^{**}\text{MMTR} = \frac{1}{N \lambda T}$$

Table 11-9 Poission Failure Probabilities for Manned MGSS Mission

NUMBER OF FAILURES N		PROBABILITY OF EXACTLY N FAILURES
0		0.318
1		0.364
2		0.209
3		0.080
4		0.023
5		0.005

MGSS MISSION (T = 340.233 HRS) WHEN
R = 0.995 (OTV MTTR = 0.87)

Table 11-10 tabulates the beneficial effects of on-orbit maintenance. Starting with no on-orbit maintenance, the failure rates of those components judged to be maintainable in space are subtracted sequentially from the no-maintenance failure rate. The reciprocal of the product of each failure rate and this mission length result in an increasing Mean Mission to Earth Return (MMTER). This data indicates that for MGSS type missions if no maintenance provisions were available the vehicle would have to be returned essentially after each flight.

11.6 LCC/RELIABILITY OPTIMIZATION

LCC/Reliability analysis was performed for the baseline unmanned GEO delivery mission. Details of the LCC analysis are contained in another section of this document. The LCC/Reliability analysis is synopsized here for convenience.

Figure 11-14 illustrates the analytical concept. The various program costs are plotted relative to increasing reliability. Initially, the rising costs of increased reliability are more than offset by the decreasing re-flight costs resulting from increased reliability. However, there comes a point where the increasing cost overcomes the offsetting reflight costs and total program costs rise sharply as illustrated by graph 4 in figure 11-14. The lowest point on that curve, the so-called "bucket," represents the optimum reliability for the OTV mission, and the life cycle cost associated with that optimum value. The OTV configuration for that optimum reliability is found by referring to the appropriate computer printout of the redundancy optimization described above.

Figure 11-15 reiterates the results of the redundancy optimization for the unmanned GEO delivery mission. Figure 11-16 shows the actual costs associated with 100 flights of this OTV mission.

Figure 11-17 shows the results of the LCC/reliability optimization. The decreasing program costs resulting from increased reliability achieved by optimized redundant additions to the "single thread" system are evident, as is the sharp rise in program costs when the optimum point is exceeded. The optimum reliability, 0.995, is achieved by adding the 45 redundant components shown on the right side of figure 11-17. The cost savings of this redundancy rather than full fail safe redundancy is estimated at \$2 million per flight. Table 11-11 tabulates the OTV subsystem reliabilities when system reliability is 0.995. Table 11-12 shows the top 10 failure contributions for an unmanned OTV with system reliability of 0.995 and is intended as a guide to maintenance requirements.

Table 11-10 MMTER for MGSS Mission ($T = 340.233$ Hrs.) at $R = 0.995$

RANK	LEVEL OF SPACE MAINTENANCE	NON-SPACE MAINTAINABLE FAILURE RATE		MEAN MISSIONS TO EARTH RETURN (MMTER)
		FAILURES PER 10 ⁶ HRS		
0	NONE	3354.26	0.88	
1	RCS THRUSTERS	1802.42	1.63	
2	FUEL CELL	988.98	2.97	
3	CPU & PWR SPLY CARDS	424.59	6.92	
5	MEMORY CARDS	337.41	8.71	
6	GYROS	276.31	10.64	
7	AMUX/ADC CARDS	234.26	12.55	
8	SERIAL/DIGITAL I/O CARDS	211.96	13.87	
9	GPS RECEIVER	191.83	15.32	
10	TRANSMITTER	172.29	17.06	
11	UTILITY BATTERY	153.60	19.14	
12	BUFFER I/O CARDS	135.09	21.76	
13	ELEX & RELAYS (PDU)	120.63	24.37	
14	RELAY DRIVER CARDS	107.48	27.35	
15	POWER AMPLIFIER	96.83	30.35	
16	PUMP	88.40	33.25	
17	ACCUMULATOR	83.02	35.40	
18	UTILITY SWITCH	77.69	37.83	

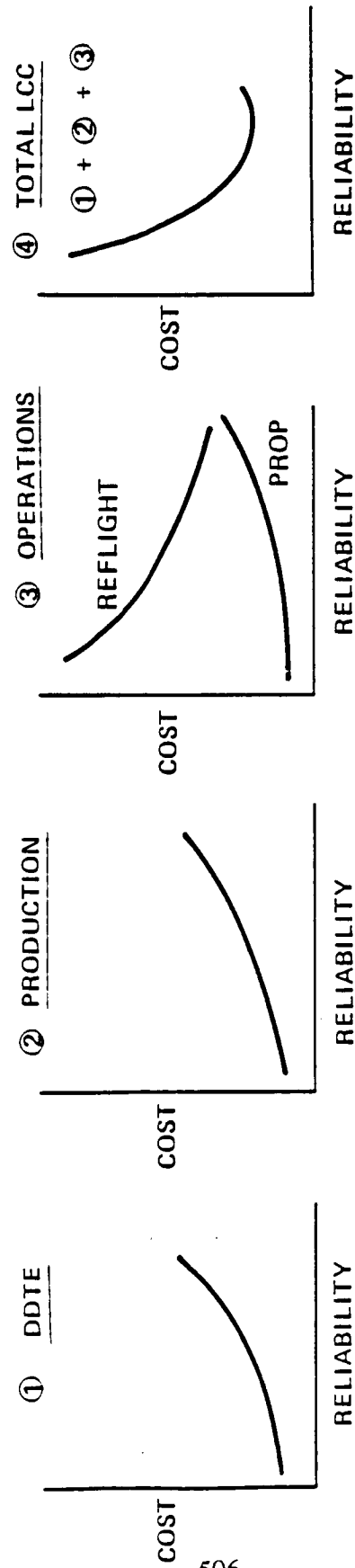


Figure 11-14 LCC/Reliability Optimization Concept

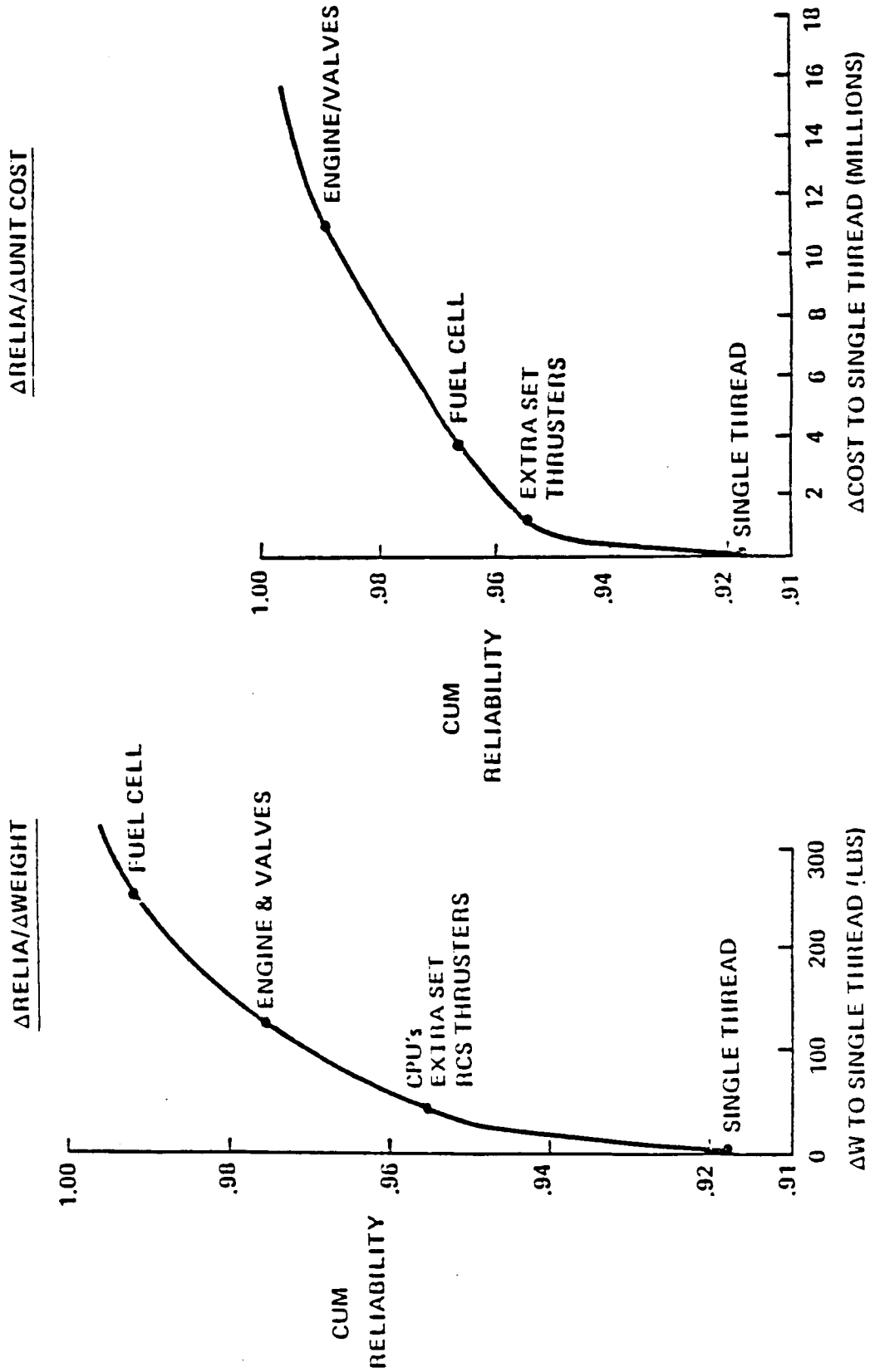


Figure 11-15 Optimized Addition of Redundant Components for the Unmanned GEO Delivery Mission

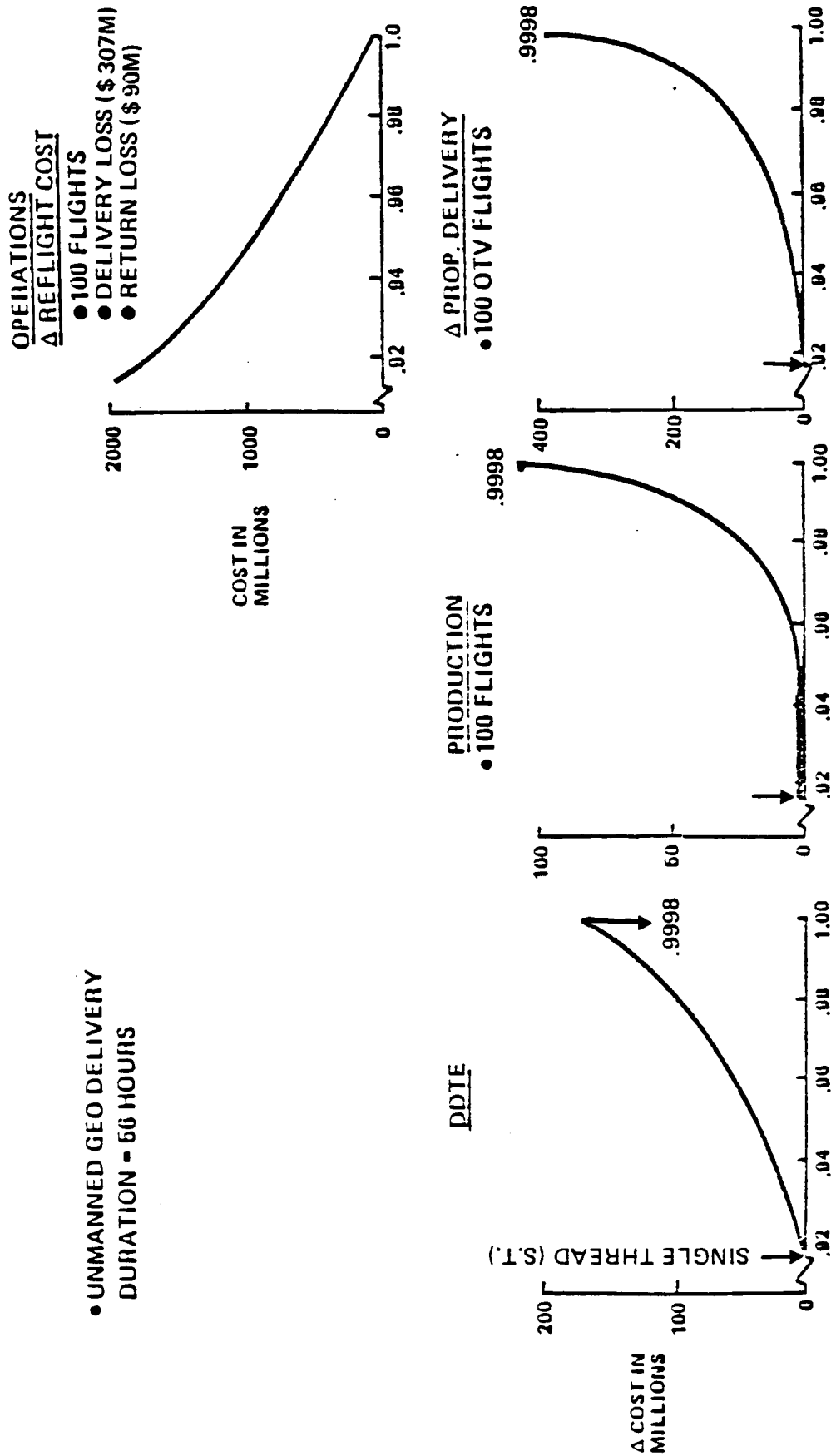


Figure 11-16 Cost Sensitivity to Reliability

REDUNDANT COMPONENTS (45)

- RCS THRUSTERS
- UTILITY POWER SWITCHES
- AMUX/ADC
- CPU & PS
- MAIN ENGINE AND VALVES
- BUFFER I/O's
- MEMORIES
- ELECTRICAL POWER PUMP
- SQUIB
- FUEL CELL
- RELAY DRIVERS
- LASER GYROS
- RCS TANK AND MANIFOLD HEATERS
- PDU SWITCH AND RELAY

COST COMPARISON

- 100 FLIGHTS
- INCLUDES DDTE PROD OPS

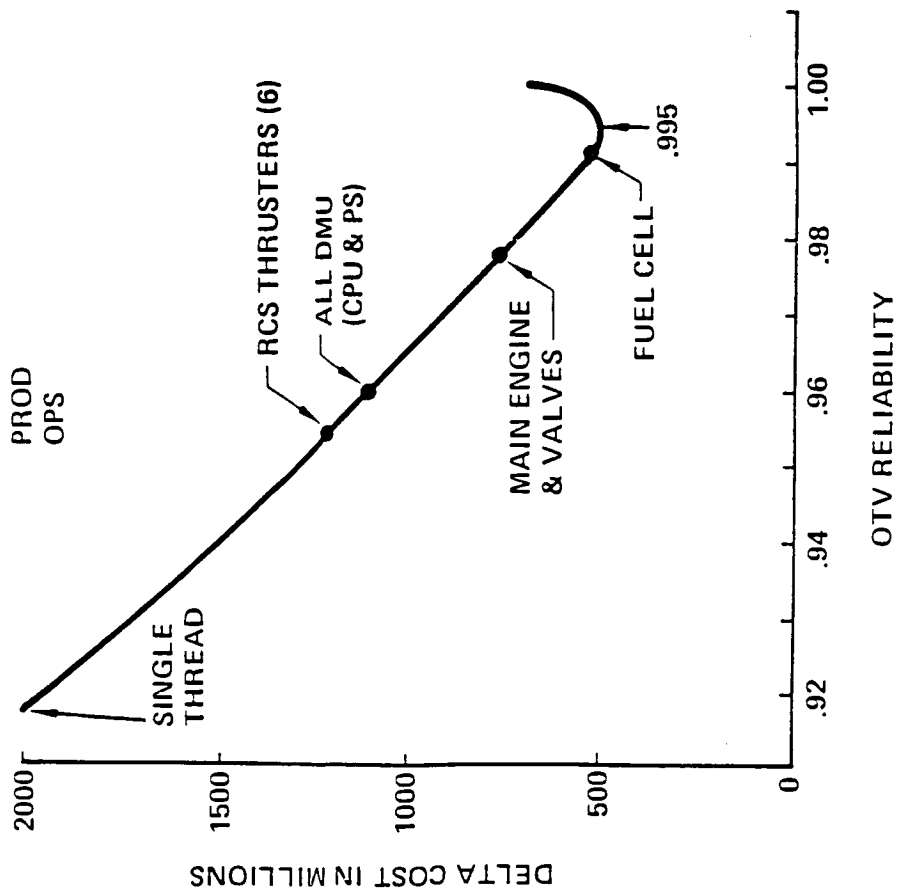


Figure 11-17 Cost Optimum Redundancy

Table 11-11 Subsystem Reliability for GEO Delivery Mission

SUBSYSTEM	RELIABILITY
STRUCTURE	*
DEBRIS SHIELD	*
ELECTRICAL POWER	.999,615
PROPULSION	.998,785
AERO-ASSIST	.999,985
ATTITUDE CONTROL	.999,594
AVIONICS	.996,744
SYSTEM	.995

* NOT INCLUDED IN OPTIMIZATION

Table 11-12 OTV Leading Failure Contributors for R=.995 - Unmanned GEO Delivery

RANK	COMPONENT	S/S	λ		N	$N \lambda$		MEAN MISSIONS TO REPAIR (MMTR)**
			FAILURES PER 10 ⁶ HOURS	FAILURES PER 10 ⁶ HOURS		FAILURES PER 10 ⁶ HOURS	FAILURES PER 10 ⁶ HOURS	
1	"2 REM"	AC	*113.024		12	1356.29		13.1
2	ENGINE & VALVES	PR	*330.993		2	661.99		26.9
3	FUEL CELL	EP	214.853		2	429.71		41.4
4	CPU & POWER SUPPLY	AV	18.914		8	151.31		117.5
5	MEMORY	AV	7.486		8	59.89		296.9
6	AMUX/ADC	AV	1.364		28	38.19		465.7
7	GYROS	AV	21.485		1 (SET)	21.49		827.5
8	SERIAL-DIGITAL I/O	AV	1.354		14	18.96		938.0
9	BUFFER I/O	AV	0.754		22	16.59		1072.0
10	GPS RECEIVER	AV	7.090		2	14.18		1254.1

VEHICLE CUM MMTR = 6

*CYCLIC FAILURE RATE EQUIVALENT

$$**MMTR = \frac{1}{N \lambda T}$$

The Poisson distribution was again used to estimate the probabilities of exact numbers of failures for the unmanned GEO delivery mission. These probabilities are based upon a full fail safe configuration, the reliability of which is somewhat greater than 0.995. However, the difference is not significant for this calculation. These calculations will aid in maintenance planning. The results are shown in table 11-13.

The Mean Missions to Earth Return (MMTER) for an unmanned OTV are tabulated in table 11-14. These MMTERs are much higher than those for the manned MGSS mission because less equipment is required in the absence of an initial fail safe configuration requirement for survivability. These results are used in volume III, System Trades to determine the optimum amount of on-orbit maintenance capability for a SB OTV.

11.7 CONCLUSIONS AND RECOMMENDATIONS

The LCC/reliability analysis described above results in a suggested OTV design configuration achieved in a logical manner. This approach is a considerable improvement over the hit-or-miss methods (fail-safe only, fail operational-fail safe only configurations, etc.) traditionally employed, and results in a design which is beneficial relative to national funding because it is an optimized approach.

It is recommended that this type of analysis be continued and refined for both manned and unmanned OTV missions. Further analysis will determine whether two OTV configurations-one for manned missions and one for unmanned missions-are cost effective.

Table 11-13 Poisson Failure Probabilities for Unmanned GEO Delivery Mission

NUMBER OF FAILURES		PROBABILITY OF EXACTLY N FAILURES
N		
0		0.846
1		0.141
2		0.012
3		0.0007

GEO DELIVERY MISSION (T = 56.231 HRS.)
MMTR = 5.98 FOR FULL FAIL SAFE CONFIGURATION

Table 11-14 MMTER for Unmanned GEO Delivery Mission (T=56,231 Hrs) Full Fail Safe Configuration

RANK	LEVEL OF SPACE MAINTENANCE	NON-SPACE MAINTAINABLE FAILURE RATE		MEAN MISSIONS TO EARTH RETURN (MMTER)
		FAILURES PER 10 ⁶ HRS		
0	NONE	2973.39	5.98	
1	RCS THRUSTERS	1617.10	11.00	
2	ENGINE & VALVES	955.11	18.62	
3	FUEL CELL	525.40	33.85	
4	CPU & PWR SPLY CARDS	374.09	47.54	
5	MEMORY CARDS	314.20	56.60	
6	GYROS	271.23	65.57	
7	AMUX/ADC CARDS	233.04	76.31	
8	SERIAL/DIGITAL I/O CARDS	214.08	83.07	
9	BUFFER I/O CARDS	197.49	90.05	
10	GPS RECEIVER	183.31	97.01	

12.0 REFERENCES

- 1 Report No. D180-26090-1, Orbital Transfer Vehicle Concept Definition Study, Boeing Aerospace Company, Contract NAS8-33532, 1980.
- 2 Report No. GDC-ASP-80-012, Orbital Transfer Vehicle Concept Definition Study, General Dynamics Convair Division, Contract NAS8-35333, February 1981.
- 3 NASA Contractor Reports 3535 and 3536, Future Orbital Transfer Vehicle Technology Study, Boeing Aerospace Company, Contract NAS1-16088, May 1982.
- 4 Report No. GDC-SP-83-052, Definition of Technology Development Missions for Early Space Station, General Dynamics Convair Division, Contract NAS8-35039, June 1983.
- 5 Report No. D180-27979, Systems Technology Analysis of Aeroassisted Orbital Transfer Vehicle Low Lift/Drag (0-0.75), Boeing Aerospace Company, Contract NAS8-35095, 1985.
- 6 Final Report, Orbital Transfer Vehicle Launch Operations Study, Boeing Aerospace Operations, Contract NAS10-11165, January 1986.
- 7 Report No. D524-10005-3A1, Space Transportation Architecture Study, Interim Report Set III Vol. I, Boeing Aerospace, Contract F04701-85-C-0156, June 1986.
- 8 MSFC-HDBK-505, "Structural Strength Program Requirements".
- 9 JSC 07700 Volume XIV Attachment 1 (ICD 2-19001) "Shuttle Orbiter/Cargo Standard Interfaces".
- 10 D290-10050-1, "IUS Structural Design Criteria".
- 11 NASA TM 82585, "Natural Environmental Design Criteria".
- 12 NASA TM 82478, "Space and Planetary Environment Criteria Guidelines for Use in Space Vehicle Development".
- 13 JSC-20001, "Orbital Debris Environment for Space Station".
- 14 Goldstein, Howard, "Advanced Fibrous Heat Shield Materials," presented at NASA/AIAA Fibrous Ceramic Materials Technology Seminar, NASA/Johnson Space Center, March, 1983.
- 15 Morita, W. H., "Direct-Bond RSI tile on GR/PI Structure, NASA Conference Publication 2315, December, 1983.
- 16 Savage, R. T., Love, W., and Bloetscher, F., "High Temperature Performance of Flexible Thermal Protection Materials," AIAA Paper 84-1770, June 1984.
- 17 Goldstein, H., Leiser, D., Larson, H., and Sawko, P., "Improved Thermal Protection System for the Space Shuttle Orbiter," AIAA Paper 82-0630-CP, May 1983.

- 18 Thomas, A. C., Perlbachs, A., and Nagel, A. L. "Advanced Reentry Systems Heat Transfer Manual for Hypersonic Flight," AFFDL-TR-65-195, 1966.
- 19 Fay, J. A. and Riddell, F. R., "Theory of Stagnation Point Heat Transfer in Dissociated Air," AIAA Journal, Vol. 25, No. 2, February 1958.
- 20 Tong, Henry, "User's Manual, Nonequilibrium Chemistry Boundary Layer Integral Matrix Procedure," Part 1, Aerotherm Report UM-73-37, July 1973.
- 21 Rakich, J.V., and Stewart, D.A., "Results of a Flight Experiment on the Catalytic Efficiency of the Space Shuttle Heat Shield," AIAA Paper 82-0944 June 1982.
- 22 Howe, J. T., "Introductory Aerothermodynamics of Advanced Space Transportation Systems," AIAA Paper 83-0406, January 1983.
- 23 Park, C., "Radiation Enhancement by Nonequilibrium in Earth's Atmosphere," AIAA Paper 83-0410, January 1983.
- 24 Sutton, K., "Air Radiation Revisited" AIAA Paper 84-1733, June 1984.
- 25 Scott, C. D., Ried, R. C., Maraia, R. J., Li, C. P., and Derry, S. M., "An AOTV Aeroheating and Thermal Protection Study, AIAA Paper 84-1710, June 1984.
- 26 Powell, R. W., Stone, H. W., and Naftel, J. C., "Performance Evaluation of the Atmospheric Phase of Aeromaneuvering Orbital Transfer Vehicles, AIAA Paper 84-0405, January 1984.
- 27 Ferri, A., Zakkay, V., and Ting, Lu, "Blunt Body Heat Transfer at Hypersonic Speed and Low Reynolds Numbers," J. Aero/Space Sci, Vol. 28, 1961.
- 28 "Investigation to Determine the Feasibility of Using Inflatable Balloon Type Drag Devices for Recovery Applications in the Transonic, Supersonic, and Hypersonic Flight Regime," ASD-TDR-62-702, Part II, October 1962.
- 29 Grenich, A. F., and Woods, W. C., "Flow Field Investigation of Atmospheric Braking for High Drag Vehicles with Forward Facing Jets," AIAA Paper 81- 0293, January 1981.
- 30 Gnoffo, P.A., "Complete Flowfields over Low and Wide Angle OTV Conceptual Configurations, AIAA Paper 84-1695, June 1984.
- 31 Heyman, R. J., Schmitt, D. A., Alexander, S. G., and Bienkowski, G. K., "Base Heating on a Voir Aerobraking Configuration in Rarefied Flow", AIAA Paper 82-0877, June 1982.
- 32 Little, H. R., "Heat-Transfer Tests on a 14-Percent-Scale Model of the NASA-MMC Viking Mars Entry Vehicle at Mach Number 16," AEDC AD-771 638, December 1973.
- 33 Lockman, W. K., "Base-Heating Measurements on Apollo Block II Command Module," J. Spacecraft, Vol. 7, No. 1, 1970.

- 34 Lee, D. B., and Goodrich, W. D., "The Aerothermodynamic Environment of the Apollo Command Module During Superorbital Entry", NASA TN D-6792, April 1972.
- 35 Bulmer, B. M., "Heat Transfer Measurements in a Separated Laminar Base Flow," J. Spacecraft, Vol. 14, No. 11, 1977.
- 36 "Boeing Engineering Thermal Analyzer Program (AS1917)", Boeing Document D180-10016-1, August 1970.
- 37 Hillberg, L. H., "The Improved Convective Heating and Ablation Program (CHAP)," Boeing Document D2-126104-1, June 1967.
- 38 Hair, L.M., and Engel, C. D., "Aerothermal Test Data of Low L/D Aerobraking Orbital Transfer Vehicle at Mach 10," Remtech Report RTR 069-1, April 1983.
- 39 Van Leehwen, A., Rosen, E., and Carrier, L., "The Global Positioning System and Its Application in Spacecraft Navigation," Navigation Journal of the Institute of Navigation, Vol. 26, No. 2, Summer 1979.
- 40 Jorgensen, P., "Autonomous Navigation of Geosynchronous Satellites Using the Navstar Global Positioning System," 1982 National Telesystems Conference, The Aerospace Corporation, November 1982.
- 41 Justus, C.G. et al., "The NASA/MSFC Global Reference Atmospheric Model- MOD 3, NASA Contractor Report 3256. Contract NA58-32897, March 1980.
- 42 Cole, A.E., and Kantor, A.J., "Air Force Reference Atmosphere, "AFGL-TR-78-0051, Air Force Surveys in Geophysics, No. 382, February 28, 1978.
- 43 Strickland, A.C., ed., COSPAR International Reference Atmosphere 1972, Akademie-Verlag, Berlin, 1972.
- 44 Findlay, J.T., et al., "Final Report Shuttle Derived Density Model," NASA Contract Report 171824, Contract NAS9-17158, December 1984.
- 45 Hauchecoine, A. and Chanin, M.L., "Mid-latitude LIDAR Observations of Planetary Waves in the Middle Atmosphere During the Winter of 1981-1982," Journal of Geophysical Research, Vol. 88, No. C6, April 20, 1983.
- 46 Hardtla, John W., "Gamma Guidance for the Inertial Upper Stage (IUS)," AIAA Guidance and Control Conference, August 1978.
- 47 Redding, D.C., "Optimal Low-Thrust Transfers to Geosynchronous Orbit," Stanford University Guidance and Control Laboratory, September 1983, SUDAAR 539.
- 48 Bate, R.R., et al., "Fundamentals of Astrodynamics," pp. 333-334, Dover, New York, 1971.
- 49 Divan, P., "Aerodynamic Preliminary Analysis System II", NASA CR 165618, Rockwell International, April 1980.
- 50 Andrews, D.G., and Bloetscher, F., "Optimization of Aerobraked Orbital Transfer Vehicles", AIAA-82-1126, June 1981.

- 51 Grenich, A.F., and Woods, W.C., "Flow Field Investigation of Atmospheric Braking for High Drag Vehicles with Forward Facing Jets", AIAA Paper No. AIAA-81-0293, January 1981.
- 52 Mayo, E.E., Lamb R.H., Romere, P.O., "Newtonian Aerodynamics for Blunted Raked-off Circular Cones and Raked-off Elliptical Cones", NASA TN D-2624, May 1965.

APPENDIX A

ASCENT TO A 12-HOUR MOLNIYA ORBIT

The purpose of this appendix is to describe the velocity requirements for OTV transfer from an initial orbit of 500 km (270 nmi) and 28.5° inclination (typical for a space station) to a mission orbit with a 12-hour period, 63.4° inclination, 270° argument of perigee and a 926 km (500 nmi) perigee altitude. Data is also shown for the return of the OTV to the space station orbit for an OTV that utilizes an aerobrake device.

Transfer to a highly elliptic orbit involves a trade off between argument of perigee, difference in the right ascension of the ascending node (RAAN) between the initial orbit and the mission orbit, and the difference in inclination between the two orbits. An optimization program is necessary in order to pick the burn locations that most efficiently meet the trajectory requirements. For this study both two-impulse and three-impulse transfers are examined. The three-impulse transfers result in very significant reductions in the velocity requirements for large inclination changes. The Multiple Impulse Trajectory Optimization Program (MITOP) was used to calculate the optimum trajectories. This program is designed for use with fixed impulse, staged vehicles; consequently it is not extremely efficient in this application. Modifications to the program are anticipated that will result in a more efficient code for finding single stage, minimum velocity transfers.

In this analysis the initial orbit is 500 km (270 nmi) circular, 28.5° inclined. The RAAN of this orbit is a key independent variable in determining the mission delta-V requirements. The spacecraft delivery orbit is a 12-hour Molniya orbit with a 926 km (500 nmi) perigee altitude. The elements of this orbit are: 26,565 km (14,344 nmi) semi-major axis, 0.725 eccentricity, 63.4° inclination, 0.0° RAAN and 270° argument of perigee. The mission orbit RAAN was kept fixed at 0° and the RAAN of the initial orbit was varied in determining the velocity requirements. The delta-V requirements for the optimum two-impulse transfer are shown in figure A-1. The velocity requirements for a three-impulse transfer to the mission orbit are shown in figure A-2. As can be seen from the two figures the three-impulse transfer offers a 10% reduction in total delta-V over the two-impulse case.

The transfer velocity requirements are symmetric about the 0° initial orbit RAAN line. This is due to the symmetry of the mission orbit for an argument of perigee of 270° . The minimum delta-V is at $\pm 25^\circ$ (figure A-1). The positive initial orbit RAAN uses a trajectory in which the second burn takes place on the downward leg of the

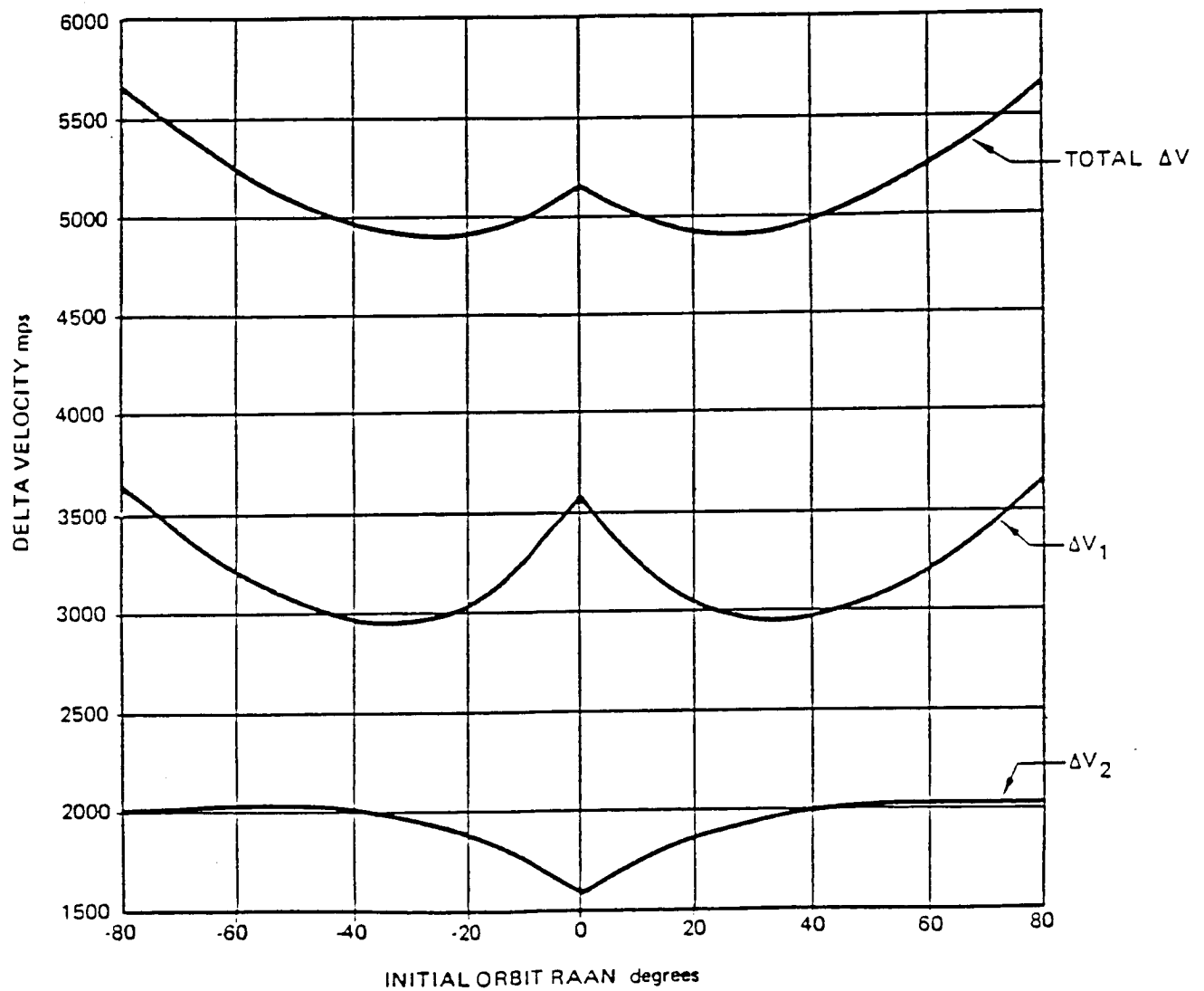


Figure A-1 Two-Impulse Transfer Velocity Requirements

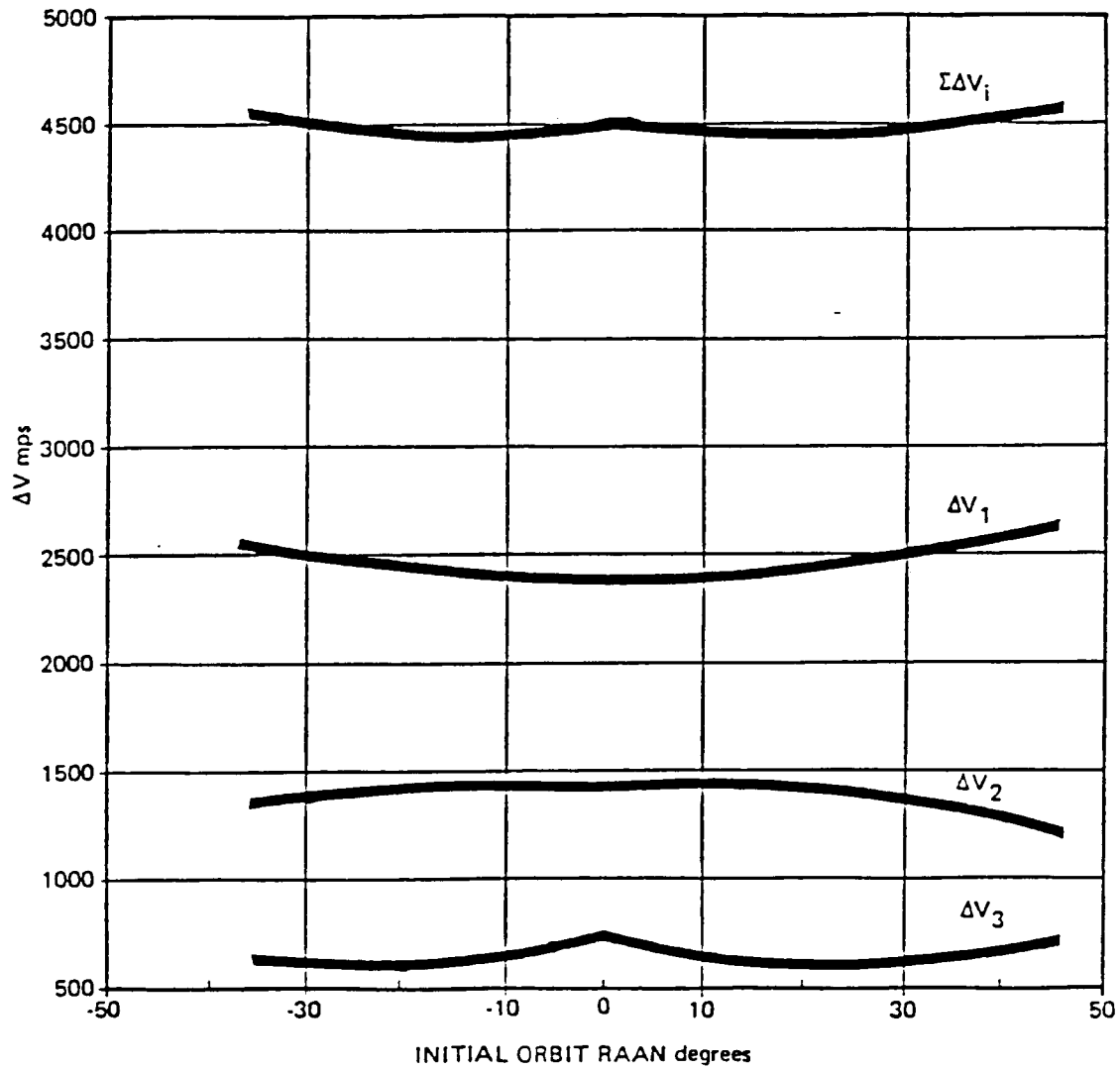


Figure A-2. Three Impulse Transfer Delta V Requirements

transfer orbit, while for the negative initial orbit RAAN the second burn occurs on the ascending leg.

The parking orbit drifts westerly (-) at a rate of -6.73° per day faster than the mission orbit. Consequently mission opportunities at the minimum delta-V occur initially at $+25^{\circ}$, then about 7.4 days later at -25° (referenced to the mission orbit). The next opportunity is again at $+25^{\circ}$, then about 7.4 days later at -25° (referenced to the mission orbit). The next opportunity is again at $+25^{\circ}$ which is now 46 days later. The number of revs and the manner in which one best utilizes this window is another matter and not the purpose of this memo. For the three-impulse transfer the minimum is flatter and occurs at $\pm 15^{\circ}$ RAAN.

The operational mode for a space-based OTV requires it to return to the space station using a combination of propulsive and aerobrake maneuvers. In calculating the optimum trajectory, the differential nodal regression between the initial orbit (Space Station orbit) and the trajectory flown by the OTV must be taken into account. The return transfer consists of two propulsive burns and one aerobrake maneuver. The goal in optimizing this return is to minimize the propulsive portion of the maneuver. This is done at the expense of increasing the velocity which must be shed during the aeromaneuver, and increasing the transfer time. This study presents only the propulsive results and does not attempt to make a trade between electrical power requirements, aerobrake size and propellant. For the purposes of this study the two propulsive burns take the OTV from the delivery orbit to an orbit with a semi-major axis of 50,000 km (26,998 nmi), eccentricity of 0.87077 (corresponding to an 83.3 km (45 nmi) perigee), 28.5° inclination, and a RAAN that corresponds to the nodal regression experienced by the Space Station orbit during the mission time. The RAAN shift of the Space Station orbit is shown in figure A-3. Argument of perigee is set at 250° for RAAN's that are less than 0 and at 290° for RAAN's greater than 0. In a more detailed study these values can be left free, however, there is not a significant penalty in using the fixed values.

The delta-V requirement to transfer from the delivery orbit to the aero-return orbit is shown in figure A-4. The time required to perform this maneuver is shown in figure A-5. Here the time is given from perigee of the delivery orbit to perigee of the aero-return orbit. Combining this data with the data from the transfer orbit trajectory analyses results in the data of figure A-6 and A-7. In figure A-6 is shown the total propulsive delta-V requirement for the mission. The minimum delta-V occurs for an initial orbit RAAN of -15° . It is broken into the transfer delta-V, during which the payload is attached, and the return delta-V, after deployment of the payload. The total

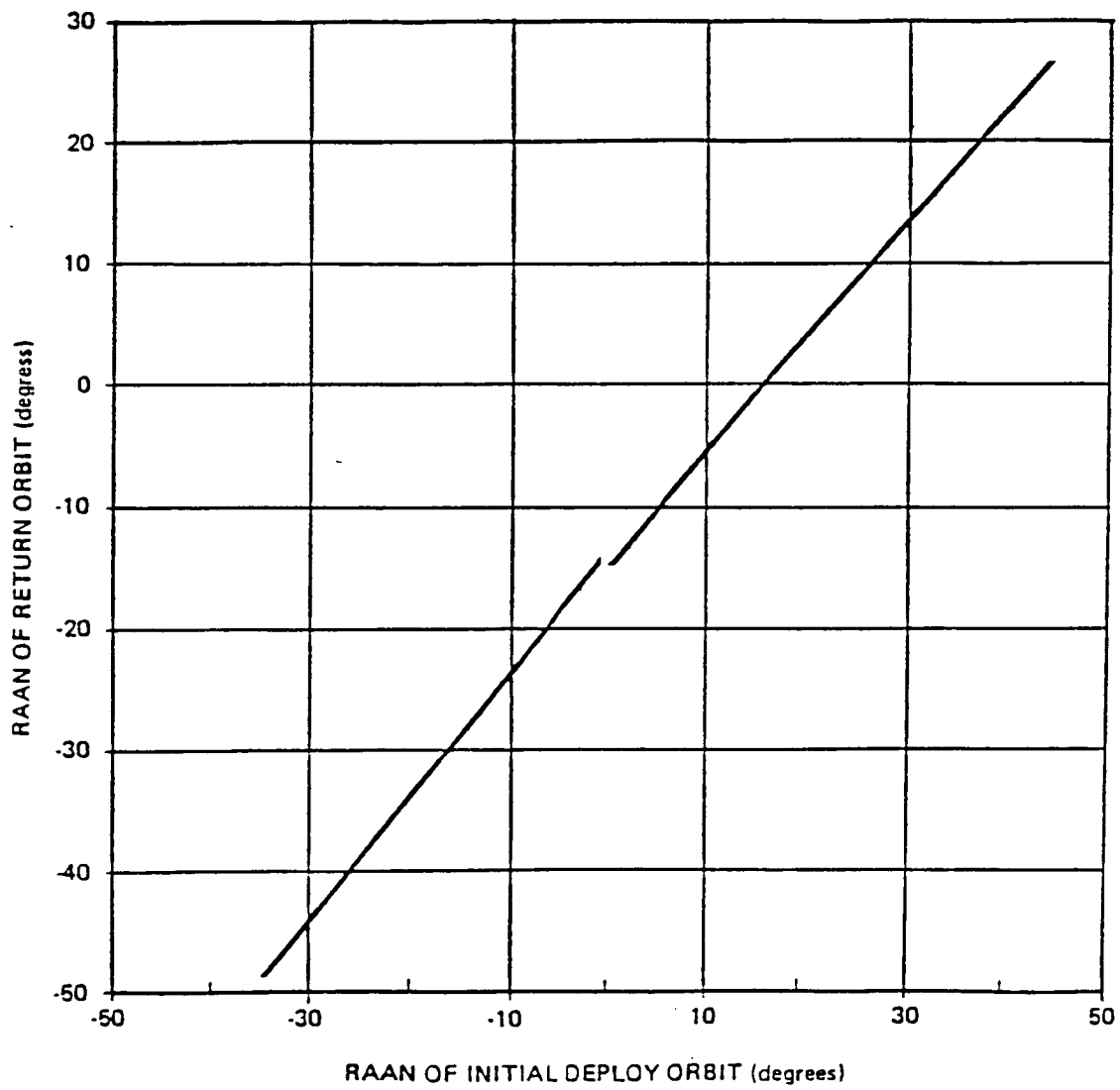


Figure A-3. RAAN Shift of the Space Station Orbit

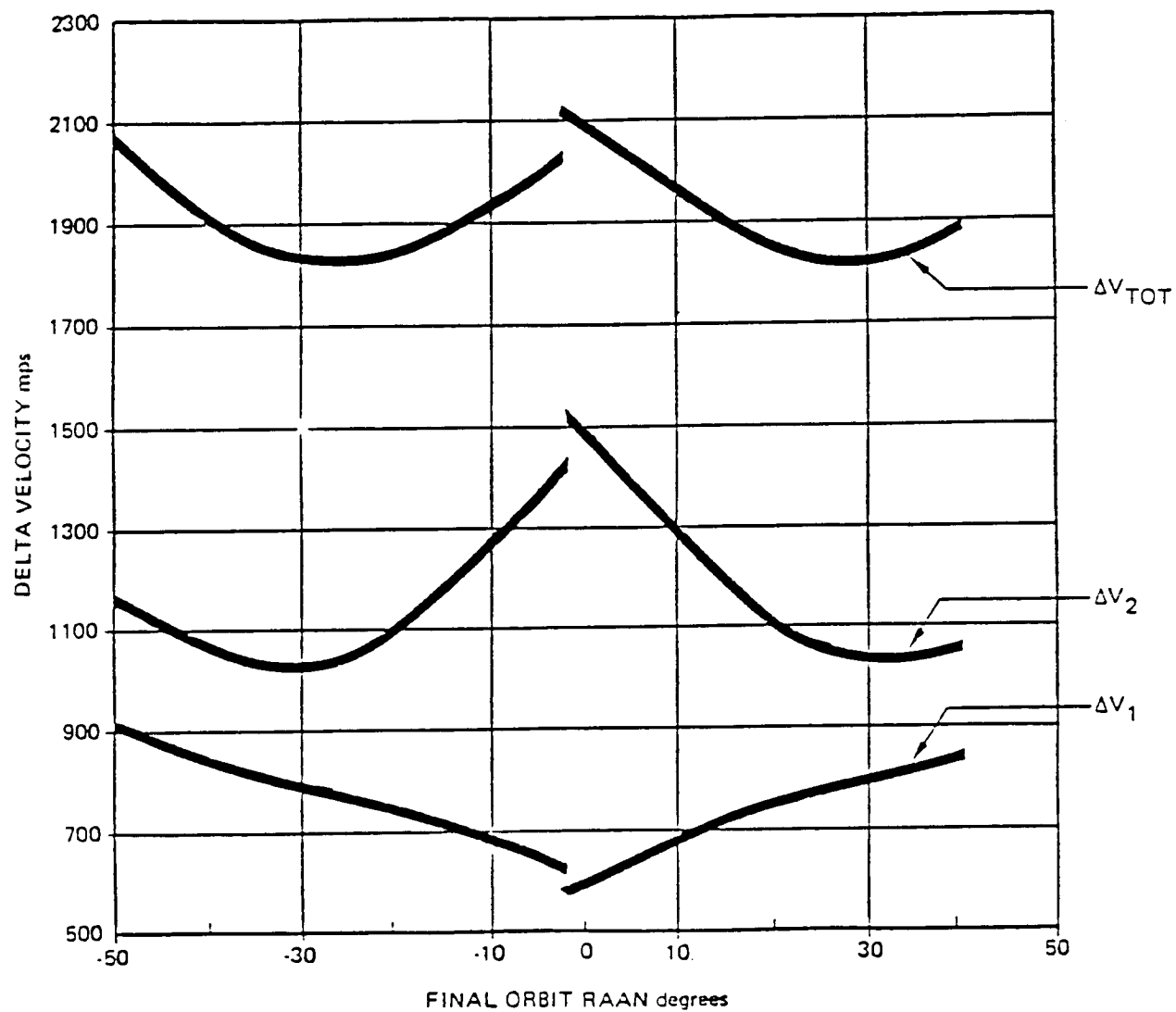
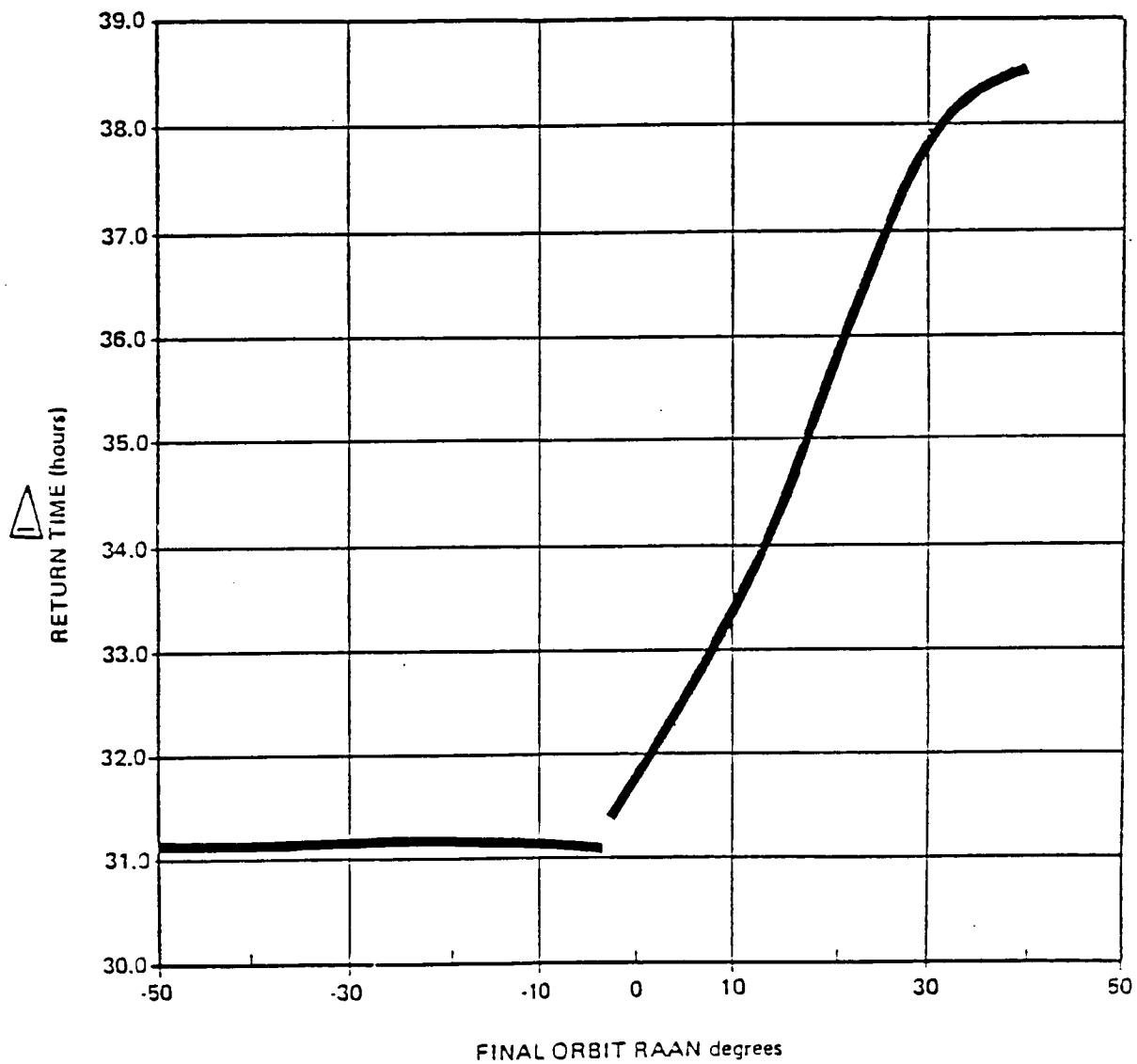


Figure A-4 Return Trajectory Velocity Requirements



▷ TIME FROM PERIGEE OF DELIVERY ORBIT
TO PERIGEE OF RETURN ORBIT

Figure A-5 Return Transfer Time

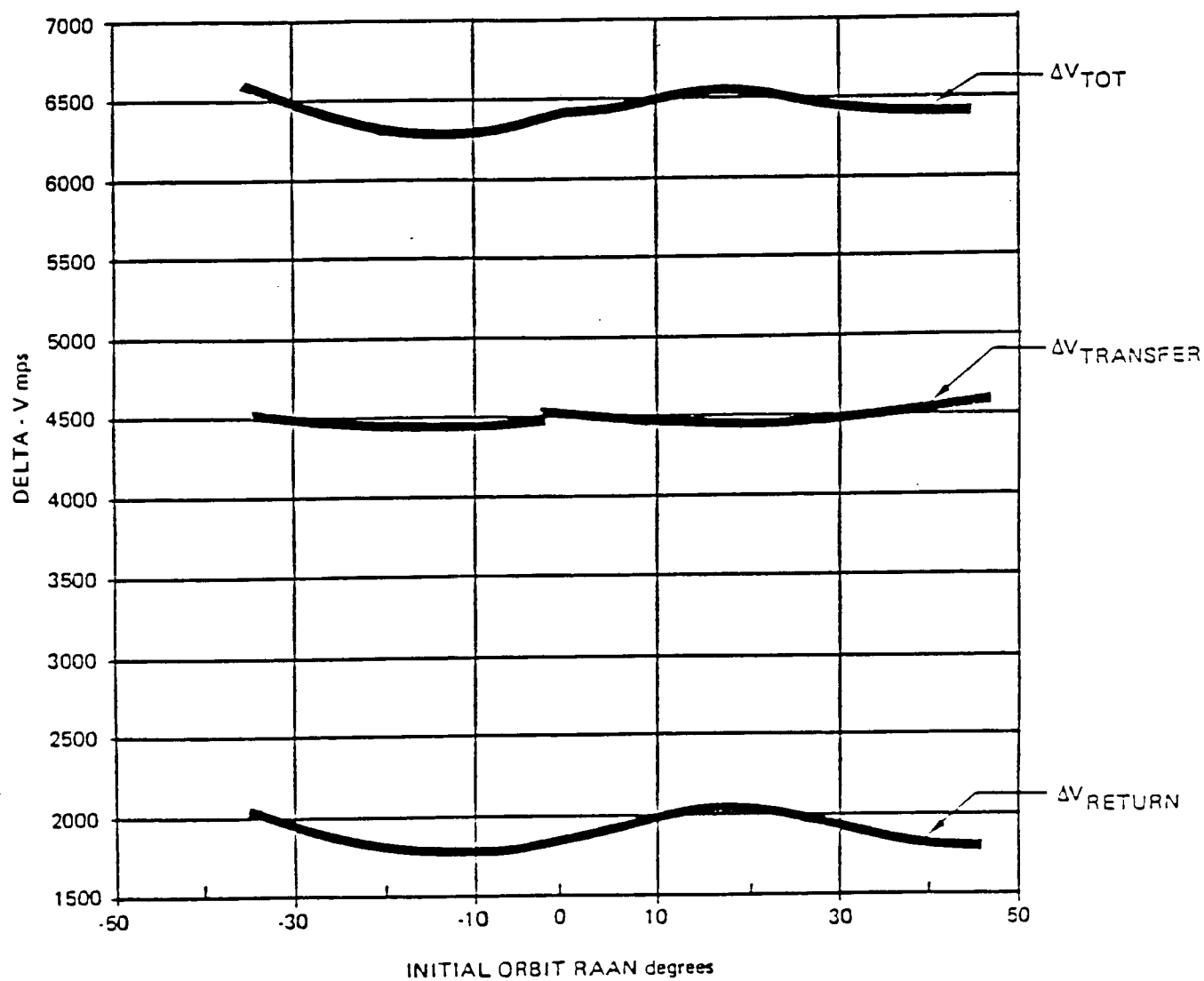
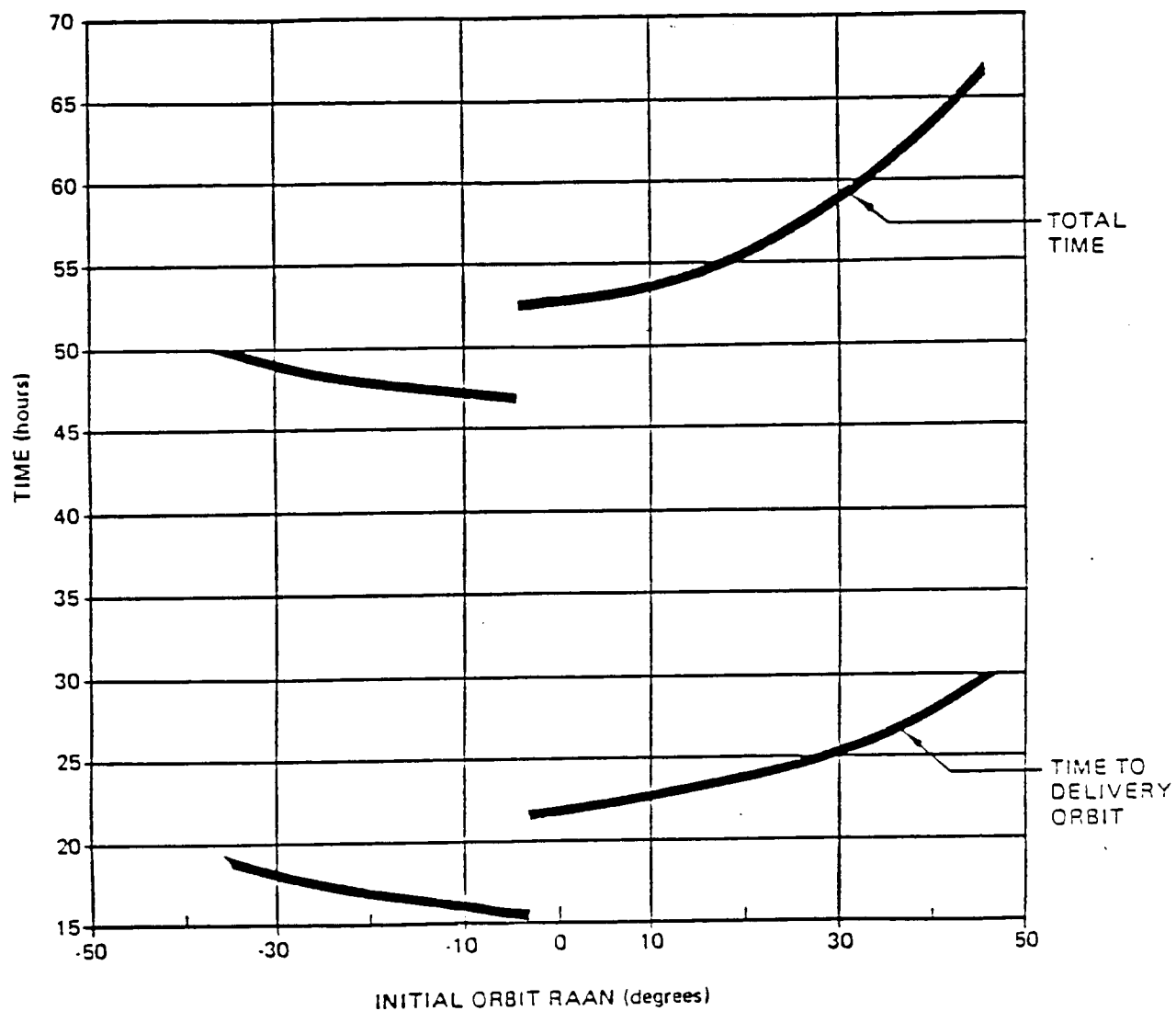


Figure A-6 Mission Delta-V Summary

*Figure A-7 Mission Time Summary*

mission time is shown in figure A-7. It is broken out into transfer time and total mission time. The total mission time is from the first propulsive burn in the initial orbit until arrival at perigee in the aero-return orbit.

It is also necessary for a returning vehicle is to have the proper time phasing with its service platform, in this case the Space Station. The Space Station orbit has a period of 1.58 hours, thus by varying the length of the mission by a total of 1.58 hours any arbitrary phasing difference can be accommodated. Operationally it would be most desirable to perform this phasing on the return trip so that the deployment of the spacecraft would not be impacted by any of these phasing maneuvers. This particular mission allows for a phasing maneuver that will actually decrease the total delta-V. The return transfer trajectory consists of transferring from the delivery orbit to the aero-return orbit which has been baselined to a semi-major axis of 50,000 km. This semi-major axis was arbitrarily chosen because it gives realistic trip times and delta-V's, not because it is optimum. The propulsive impulse required to transfer to the aero-return orbit goes down as the semi-major axis increases, while at the same time the trip time increases. This is illustrated in figures A-8 and A-9. Thus any phasing difference between the OTV return and the Space Station can be accommodated by slightly increasing the semi-major axis of the return orbit. There is no associated delta-V penalty that must be accounted for over the baseline. The aerobrake device, however, must be sized for this slightly higher return velocity, and the power requirements sized for the longer trip time.

The advantage of the three-burn transfer over the two-impulse transfer is shown in figure A-10. This shows the total delta-V for the two different cases as a function of the parking orbit inclination. The delta-V is for a $+10^\circ$ change in RAAN in all cases, so it does not give the minimum delta-V, but it is very close. The point that is being illustrated is that the three-impulse transfer does not offer any advantage if the parking orbit is greater than 52° . For a shuttle launch to the 12-hour orbit it is typical to specify a 57° parking orbit. This maximizes the payload capability to the 12-hour orbit while remaining within the range limitations of an ETR launch.

The relationships between the orbital maneuvers is shown graphically in figure A-11. The trajectory and the mission orbit are plotted to scale and the burn locations are indicated.

A table of the trajectory parameters for the selected three-impulse transfer and return is shown in figure A-12.

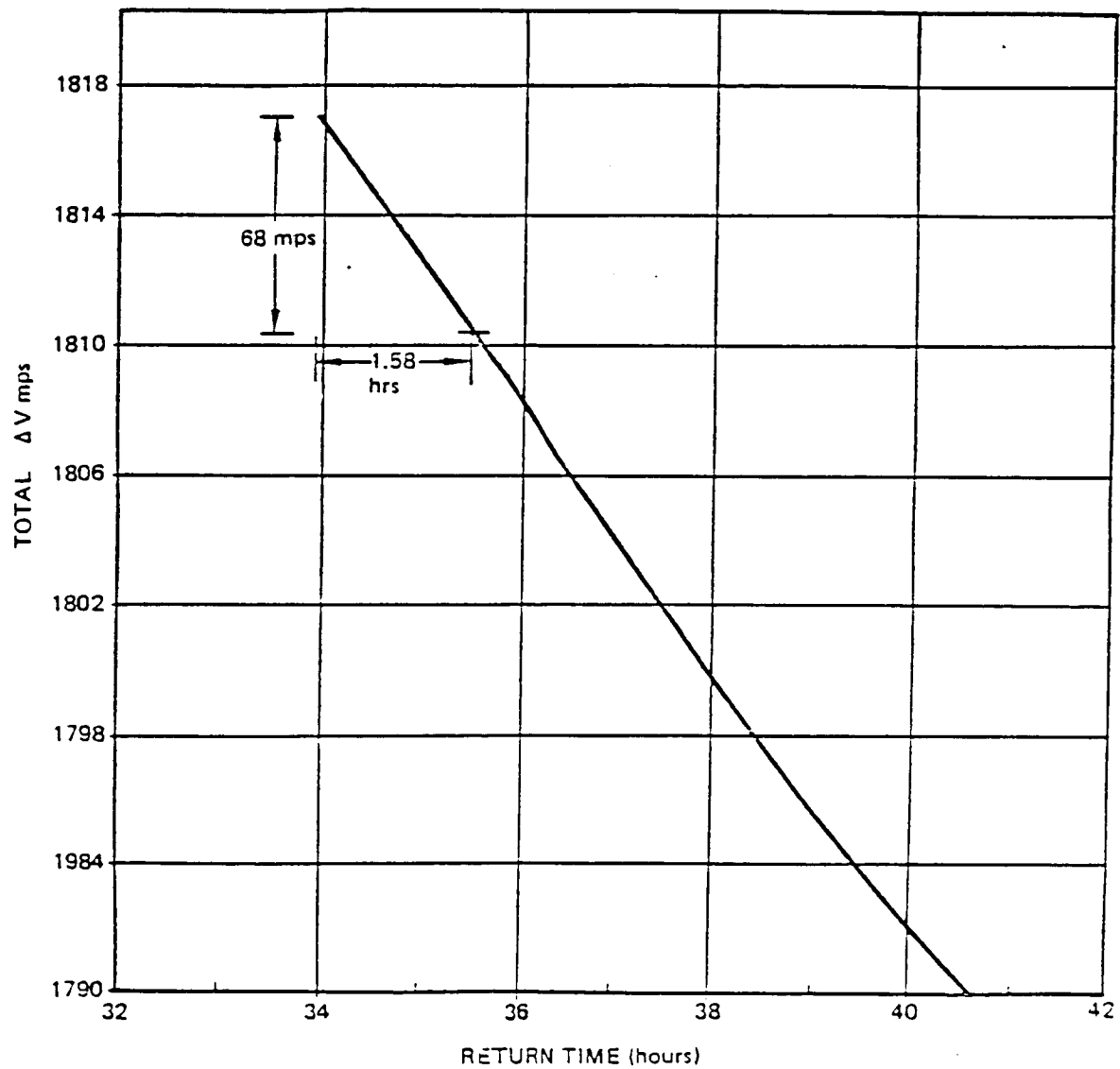


Figure A-8 Delta-V Requirement for Phasing Maneuver

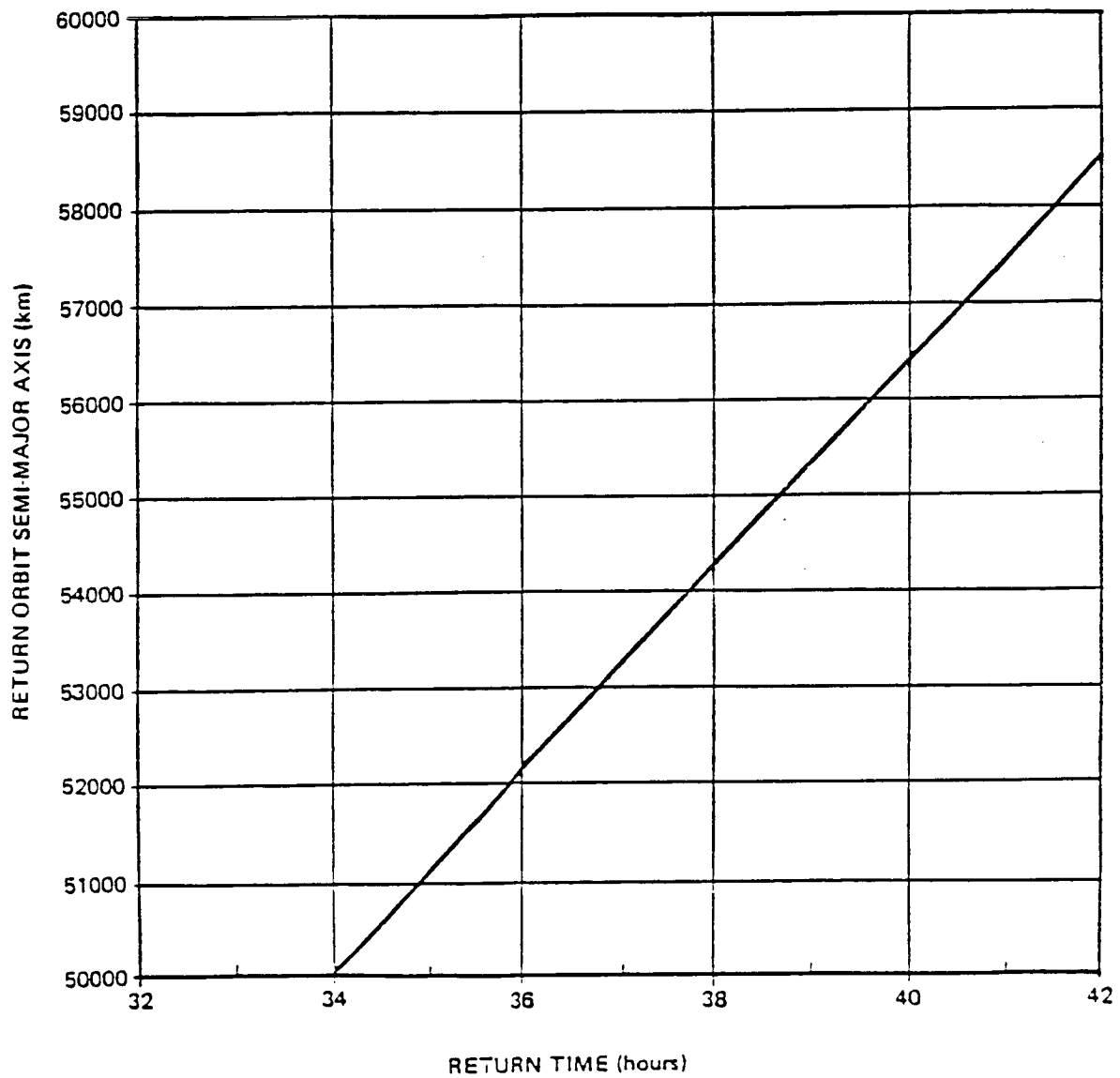


Figure A-9 Return Orbit Semi-Major Axis

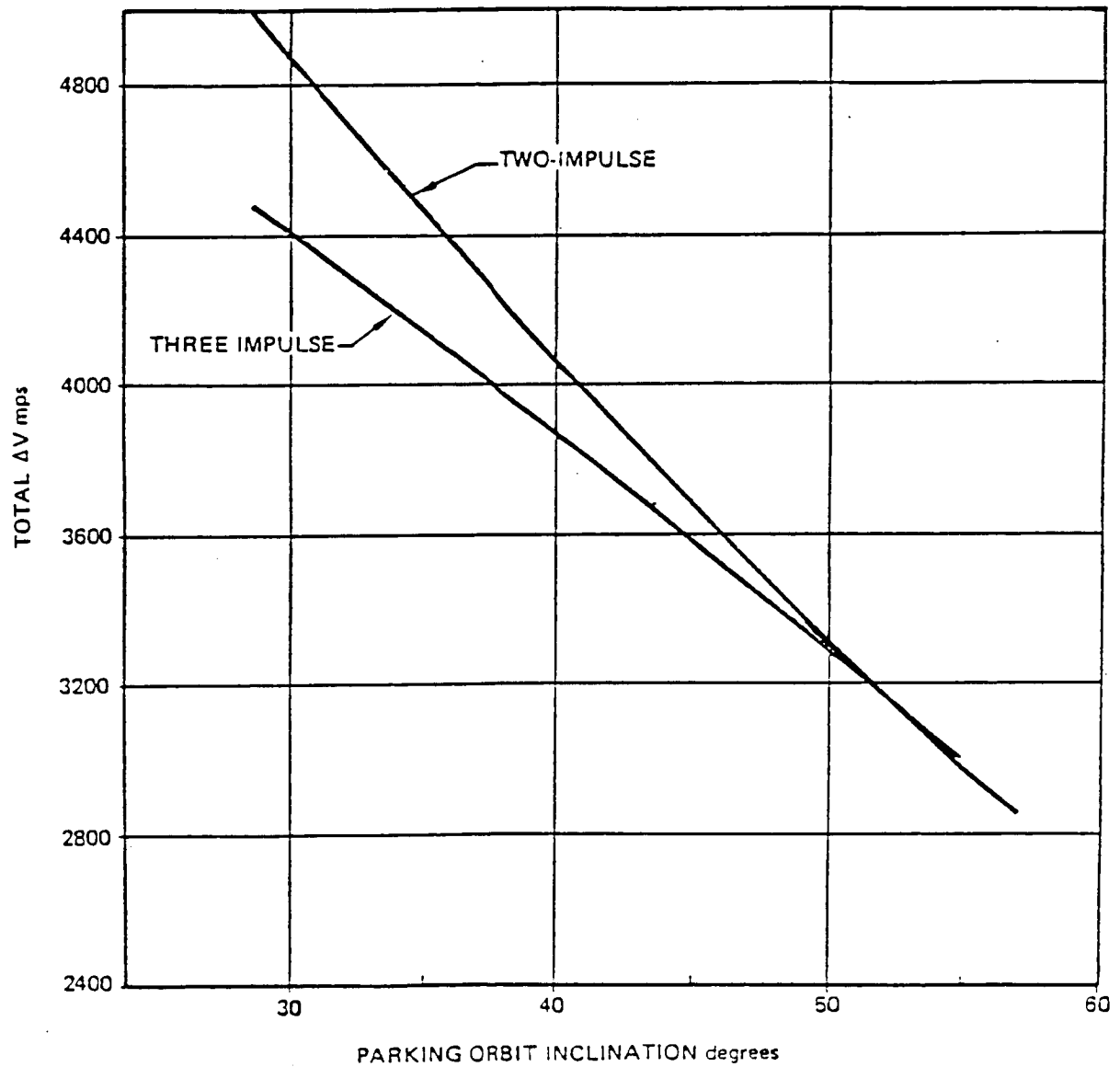


Figure A-10 Comparison of Two and Three Impulse Transfers

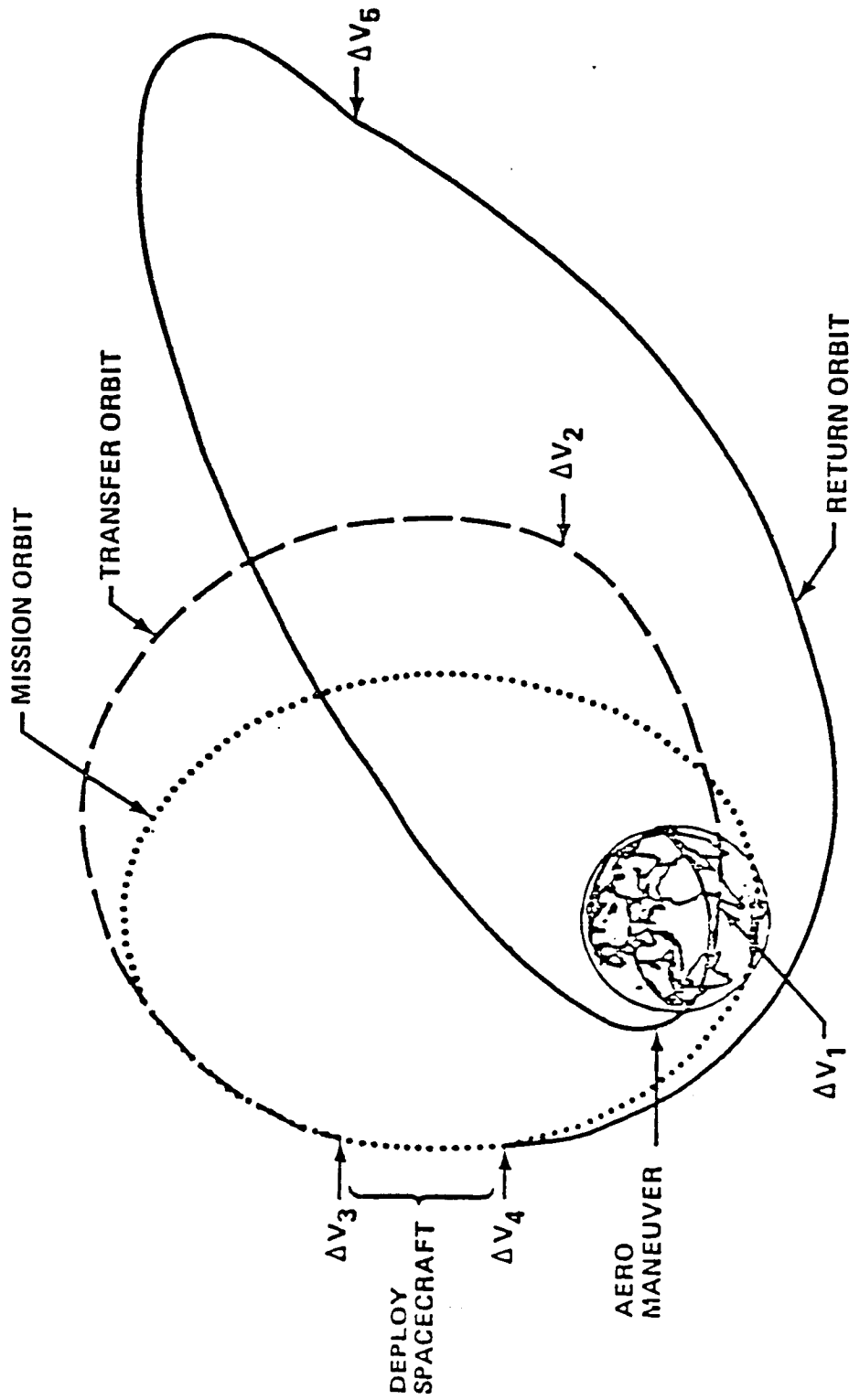


Figure A-11. Molniya Mission-Transfer and Return

1	Parking Orbit	[a, e, i, RAA, Arg. Perigee] [6878 km, 0.0, 28.5°, -15.0°, 0.0°] (270 nmi x 270 nmi)
	Burn 1	6878 km, RA = -129.8, Dec = -26.2 ΔV = 2402 mps (7881 fps)
2	Transfer Leg	[25011 km, .725, 29.2°, -11.6°, 246°] v_o = -8°, v_f = 150.8°; 2.30 hr coast (270 nmi x 19852 nmi)
	Burn 2	32315 km, RA = 21.3°, Dec = 16.9° ΔV = 1415 mps (4641 fps)
3	Transfer Leg	[32757 km, .6727, 57.5°, 10.1°, 249°] v_o = 131.4°, v_f = 232.4°; 12.02 hr coast (2345 nmi x 26142 nmi)
	Burn 3	30409 km, RA = 148.5°, Dec = 46.2° ΔV = 659 mps (2163 fps)
4	Mission Orbit (delivery)	[26565 km, .7250, 63.4°, 0.0°, 270°] v_o = 216.1°, v_f = 228.1°; 0.60 hr coast (500 nmi x 21300 nmi)
	Burn 4	24403 km, RA = 123.93°, Dec = 36.67° ΔV = 1031 mps (3383 fps)
5	Return Leg	[57120 km, .793, 57.9°, 6.0°, 235°] v_o = -99.6°, v_f = 151.6°; 7.91 hr coast (2940 nmi x 51856 nmi)
	Burn 5	70145 km, RA = -8.98°, Dec = 22.05° ΔV = 785 mps (2575 fps)
6	Return Leg	[50000 km, .871, 28.5°, -27.5°, 250°] v_o = 161.9, v_f = 360.0; 24.62 hr coast (45 nmi x 47069 nmi)

Figure A-12 Three-Impulse Trajectory Parameters

This Page
Intentionally
Left
Blank

APPENDIX B

OTV PHASING WITH THE SPACE STATION

ABSTRACT

At the conclusion of a mission in geosynchronous orbit (GEO), an orbital transfer vehicle (OTV) returns to the Space Station. This must be accomplished using a minimum amount of fuel, in order to maximize payload, and in a minimum amount of time lowering failure rates, fuel boil-off, and tracking costs. Two opportunities per day are available to commence a deorbit from GEO, these being the times when the line of nodes are aligned with the orbit of the Space Station. Various methods of achieving this return were analyzed, each with their own intuitive advantages and disadvantages. Illustration of these methods is presented in figure B-1.

INTRODUCTION

One method of transferring from GEO to the Space Station, forward phasing, is illustrated in method "a" in figure B-1. Employing three burns, the OTV executes an aeromaneuver and enters a phasing orbit which allows the OTV to "catch up" with the Space Station. The first burn occurs at GEO and places the OTV into a Hohmann transfer orbit (with an inclination equal to the Space Station) to the altitude of the aeromaneuver. The OTV exits the aeromaneuver with an orbit apogee equal to the radius of the Space Station orbit. Upon reaching apogee, the OTV executes a burn to raise its orbit perigee to an altitude high enough to free it from the effects of excessive atmospheric drag. This will be the intermediate phasing orbit in which the OTV will remain until it "catches up" with the Space Station at the time of apoapsis passage. A circularization burn at the apogee brings the OTV into an orbit which allows it to rendezvous with the Space Station.

A second method of reaching the Space Station, reverse phasing, is shown by method "b". Like forward phasing, this maneuver requires three burns and waiting in a phasing orbit. In this case, however, the phasing orbit allows the Space Station to "catch up" with the OTV. Following the Hohmann transfer and aeromaneuver, the OTV enters an orbit with an apogee higher than that of the Space Station. Upon reaching apogee, the OTV raises its perigee to the altitude of the Space Station. It then remains in this phasing orbit until the Space Station "catches up" with the OTV at the time of periapsis passage. The OTV circularizes at perigee, completing its mission.

A third method, which requires only two burns, is called transfer time phasing as shown by methods "c, d, e". At GEO, the OTV transfers into an orbit which will reach

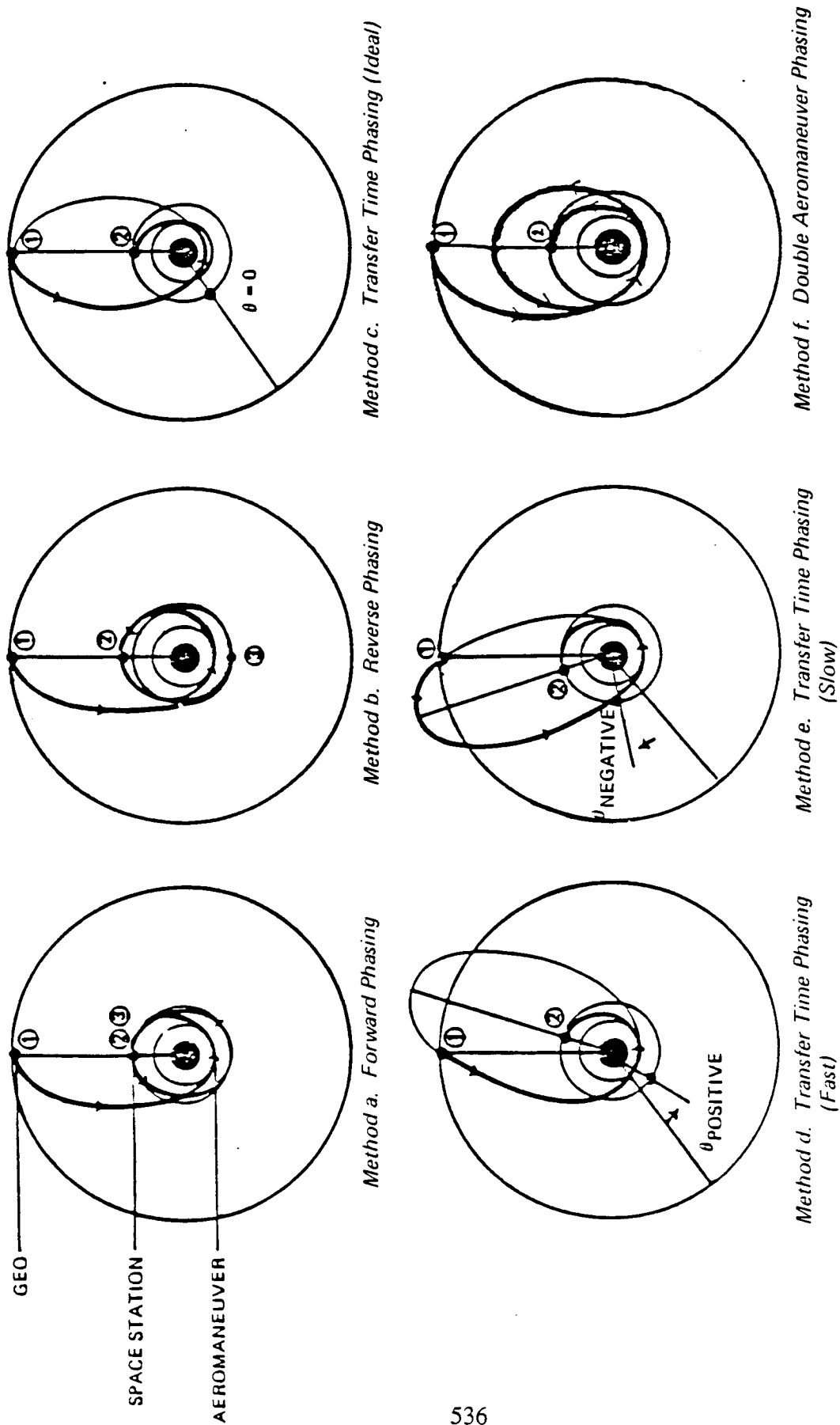


Figure B-1 OTV/Space Station Phasing Maneuvers

the aeromaneuver in such a time that allows it to coast to the Space Station without waiting in an intermediate phasing orbit. The first burn at GEO may or may not have a change in flight path angle, depending on the position of the Space Station at the time of deorbit. The OTV will reach the aeromaneuver altitude at the perigee of the transfer orbit. It exits the aeromaneuver into an orbit having an apogee equal to the altitude of the Space Station, and at apogee, its position is the same as the Space Station, due to the adjustment in transfer time made at the beginning of the deorbit. A final circularization burn completes the mission.

Another method, double aeromaneuver phasing is illustrated by method "f". This utilizes two aeromaneuver and two burns. The first burn at GEO puts the OTV into a Hohmann transfer orbit (with the same inclination as the Space Station) to the aeromaneuver altitude. Like reverse phasing, the exiting orbit is higher than the altitude of the Space Station. This orbit's difference in period with that of the Space Station is such that the OTV allows the Space Station to "catch up" with it in one intermediate phasing orbit. The second aeromaneuver brings the apogee of the OTV's orbit to the altitude of the Space Station, and at the time of apoapsis passage, the OTV circularizes and rendezvous with the Space Station.

COMPARISON OF TRANSFERS

Each of these returns has their own advantages and disadvantages, summarized in table B-1. Forward phasing has the benefits of utilizing the minimum delta-V, but the time spent waiting for the OTV to catch the station may be great, as the bounds of the atmosphere do not allow for large differences in period (semi-major axis) between the Space Station and phasing orbits. Transfer time phasing offers two advantages over the previous two methods: it eliminates one burn from the mission, and it requires no time "waiting" in an intermediate phasing orbit. The disadvantages of such a maneuver is that a non-ideal transfer is usually required at the time of the GEO deorbit, and it may impose more severe constraints on the guidance system. The double aeromaneuver transfer has the advantages of using two burns and minimum delta-V. The disadvantages of such a maneuver include the longer mission duration and the problems associated with the utilization of two aeromanuevers.

ANALYSIS

The assumptions for the following analysis include: the Space Station is in a circular orbit with an altitude of 270 nm and inclination of 28.5 degrees, the aeromaneuver takes place at an altitude of 45 nm, and the altitude where atmospheric

TABLE B-1 COMPARISON OF TRANSFERS

Concept	Advantages	Disadvantages
a. Forward Phasing	-Minimum delta-V	-Potentially very long mission time -3 burns
b. Reverse Phasing	-Mission time shorter than for forward phasing	-Potentially very large delta-V penalty -Mission time longer than transfer time phasing -3 burns
c-e. Transfer Time Phasing	-2 burns -Shortest mission time	-Modest delta-V penalty -Guidance system constraints
f. Double Aeromaneuver Phasing	-Minimum delta-V -Mission time shorter than for forward phasing	-Mission time longer than transfer time phasing -2 aeromaneuvers

drag becomes too great for maintaining Keplerian orbits is 75 nm. For the purposes of this study, these assumptions are good ones. The mission delta-V calculations exclude any losses due to gravity or boiloff.

In order to compare these three maneuvers, a variable which relates the relative position of the OTV to the Space Station is necessary. The variable chosen for this purpose is the angle theta, which is the angle the Space Station is away from a reference angle at the time of the OTVs deorbit from GEO. The reference angle (theta equals zero) is defined from the Hohmann case for transfer time phasing (method "c"), being the angle the Space Station would be positioned at the time of GEO deorbit to ensure such a transfer. This convention makes theta dependent on the mission itself, and not on any fixed reference frame.

A positive or negative value of theta determines which variation of transfer time phasing is utilized. For the case when theta is positive (method "d"), the OTV would need to reach the aeromaneuver altitude faster than it would for a Hohmann transfer. A non-ideal transfer at GEO would be required, which has the effect of shifting the transfer orbit's semimajor axis away from the Hohmann Case. Similarly, a negative value of theta (method "e") warrants the use of a longer transfer, and has the effect of shifting the semimajor axis from the Hohmann case in the opposite direction. This shift in axis changes the position where the OTV rendezvous with the Space Station.

In the case of forward and reverse phasing, the number of intermediate phasing orbits the OTV executes is a variable. When reverse phasing is employed, the number of phasing orbits determines the apogee altitude the OTV must target upon exiting the aeromaneuver. This apogee altitude corresponds to an orbit period (semimajor axis) which allows the Space Station to "catch up" with the OTV upon completion of the phasing orbits. Using fewer phasing orbits reduces the mission time, but it also requires a higher phasing orbit apogee, which creates a larger delta-V penalty at the circularization burn. When forward phasing is used, the phasing orbit has a perigee lower than the altitude of the Space Station. The restrictions the Earth and its atmosphere impose on a phasing perigee limit the number of phasing orbits which are allowed. In order to reduce the mission time, the lowest possible perigee altitude should be used, maximizing the period difference between the phasing orbit and the Space Station. Since the phasing orbit does not extend above the Space Station, there is no circularization delta-V penalty involved.

RESULTS

The total return delta-V and time of flight is illustrated in figures B-2 and B-3 as a function of theta for the four phasing maneuvers. For reverse phasing, the circularization delta-V penalty remains high until the number of phasing orbits becomes great, which involves very long mission times. Forward phasing offers consistently low delta-vee requirements, but the number of phasing orbits required due to the restrictions imposed by the atmosphere becomes great for large values of theta. Such a number of phasing orbits require a prohibitively high mission time.

The problems associated with the previous two maneuver types is not a consideration for transfer time phasing. It features the lowest mission time with only a modest (delta-V) penalty. It is advantageous to use a fast transfer from theta = 0 to 154 deg, both in terms of delta-V and transfer time. From theta = 154 to 360 deg (which corresponds to theta = -206 to 0 deg), a slow transfer yields a lower delta-V, with only a slight increase in the transfer time. For the worst case, (theta = 154 deg), the delta-vee penalty is 190 fps, which is insignificant when considering the time saved using this maneuver.

For transfer time phasing, a typical set of data would be:
 Angle which Space Station is away from ideal (theta) = 64 deg.
 Transfer orbit's semimajor axis = 13155 NM.
 Shift in transfer orbit's semimajor axis = 2.4 deg.
 Delta-vee required at GEO = 6079 fps.
 Circularization delta-V at the Space Station = 393 fps.
 Total return delta-V = 6472 fps.
 Total mission time from GEO to the Space Station = 5.65 hrs.

When double aeromaneuver phasing is used, there is no delta-V penalty, as the penalty associated with reverse phasing is handled with the second aeromaneuver. The total return time is also low, ranging from 2 to 3 hours longer than that for transfer time phasing.

For double aeromaneuver phasing, a typical set of data would be:
 Angle which Space Station is away from ideal (theta) = 62 deg.
 Delta-V required at GEO = 6050 fps.
 Circularization delta-V at the Space Station = 393 fps.
 Total return delta-V = 6443 fps.
 Total mission time from GEO to the Space Station = 8.87 hrs.

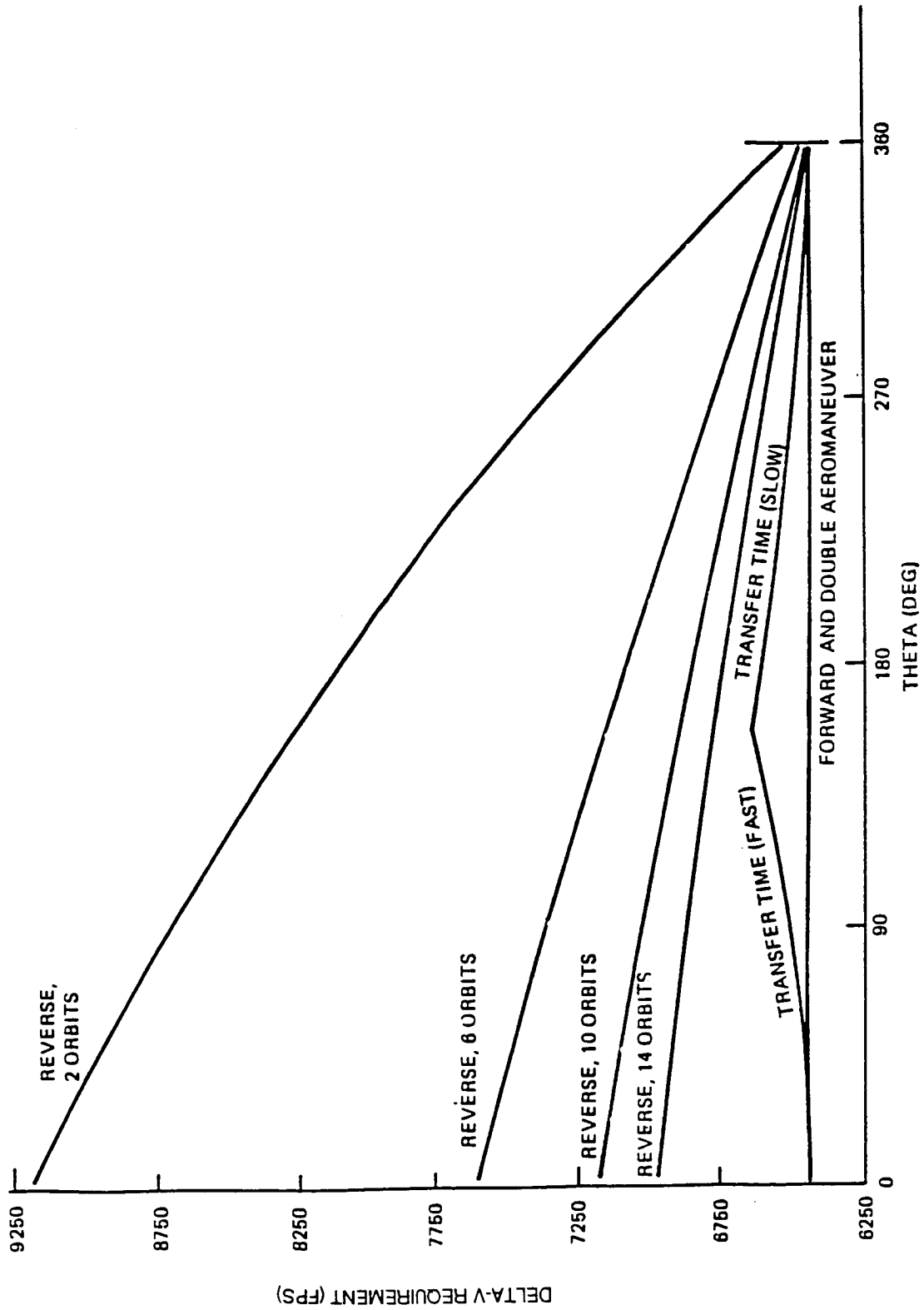


Figure B-2. Delta-V Requirements from GEO to the Space Station for Various Phasing Maneuvers

OTV-1850

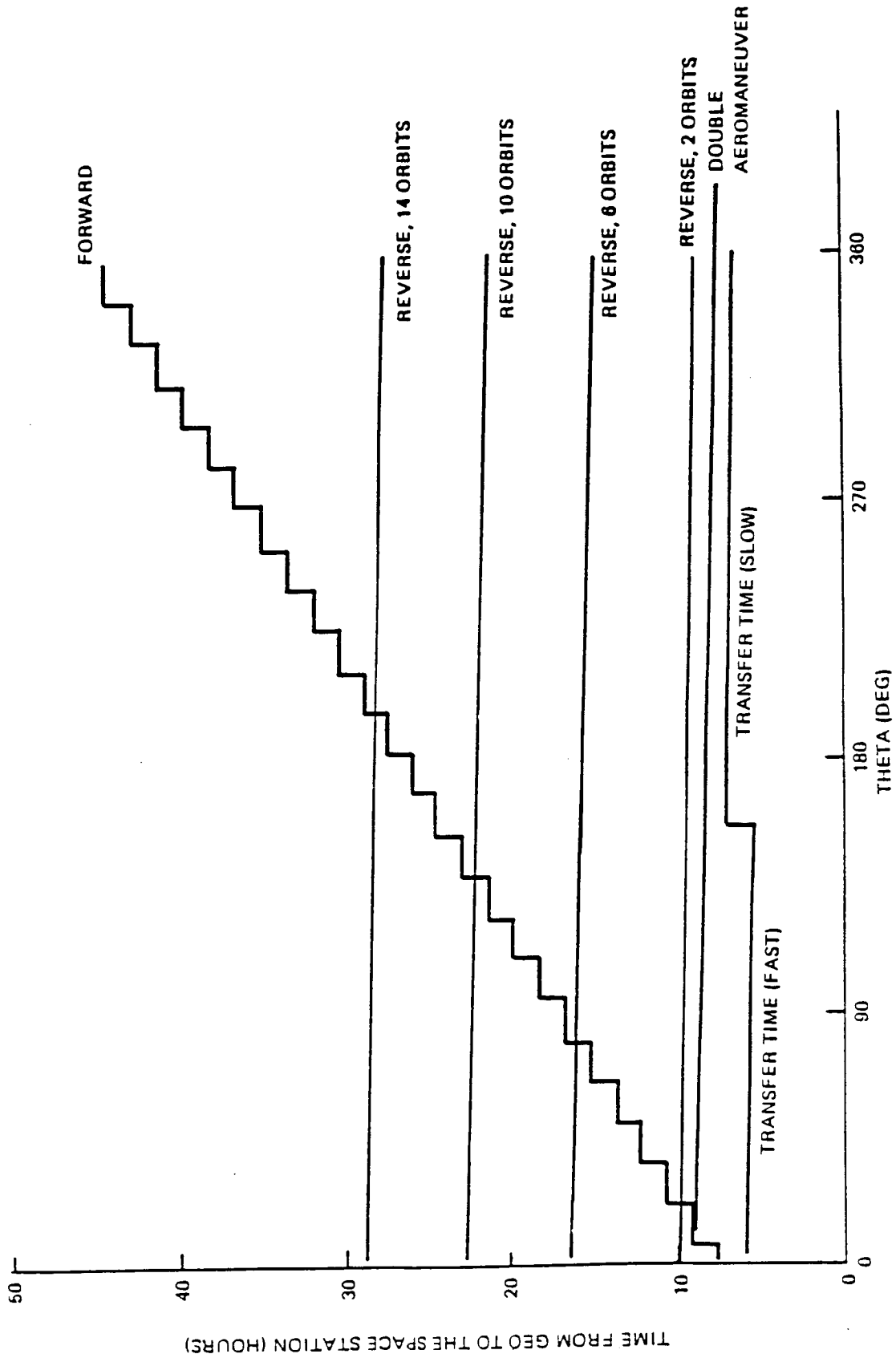


Figure B-3 Return Time from GEO to the Space Station for Various Phasing Maneuvers

CONCLUSIONS

From the phasing maneuvers studied, the transfer from GEO to the Space Station using an aerobraked OTV will be less costly in terms of return delta-V and time of flight using either a transfer time or double aeromaneuver phasing maneuver. The transfer time phasing maneuver has the fastest return time, with a minimal delta-V penalty. Use of double aeromaneuver phasing affords the minimum delta-V, with a slight increase in the return time. The total return delta-V requirement for transfer time phasing (excluding gravity losses) range from the Hohmann value of 6443 fps to a worst case of 190 fps over this minimum value, while the return time of flight ranges from 5.3 to 7 hours. Double aeromaneuver phasing uses the minimum delta-V of 6443 fps for all cases, with a return time of flight ranging between 7.45 and 9 hours. To determine which phasing maneuver is preferable, other criteria must be examined.

APPENDIX C

BURN LOSSES FOR THE OTV

REFERENCES

1. Redding, D. C., "Optimal Low-Thrust Transfers to Geosynchronous Orbit," Stanford University Guidance and Control Laboratory, September 1983, SUDAAR 539.
2. Robbins, H. M., "An Analytical Study of the Impulsive Approximation," AIAA Journal, Vol. 4, August 1966.

An approximate solution for fuel-optimal finite burn circle-to-circle transfers has been utilized to examine the velocity losses experienced by the OTV. The approximation has previously been shown to be quite accurate for relatively efficient transfers, becoming pessimistic as the acceleration is decreased. Examples of these approximate losses are included for current baseline OTV missions.

ROBBINS FORMULA

A derivation of Robbins formula for approximate finite burn losses can be found in references 1 and 2. The formula for an optimally steered circle-to-circle transfer with constant thrust as given in reference 1 is presented below.

The geometry of an impulsive circle-to-circle transfer with plane change is illustrated in figure C-1. For optimality, a certain ratio of the total plane change is accomplished in the first burn. From this change in inclination, an out of plane pointing angle β_1 may be defined, being the angle which the mean thrust direction is directed away from the plane of the transfer orbit. A similar pointing angle β_2 is defined for the second burn, and for an optimal transfer is given by:

$$\sin \beta_2 = \frac{1 + e}{1 - e} \sin \beta_1$$

here, e refers to the eccentricity of the transfer orbit.

When considering a finite burn, the direction with which the thrust is applied determines the amount of velocity losses incurred. For a circle-to-circle transfer, the optimal turn rate of the thrust direction at perigee and apogee are given to be:

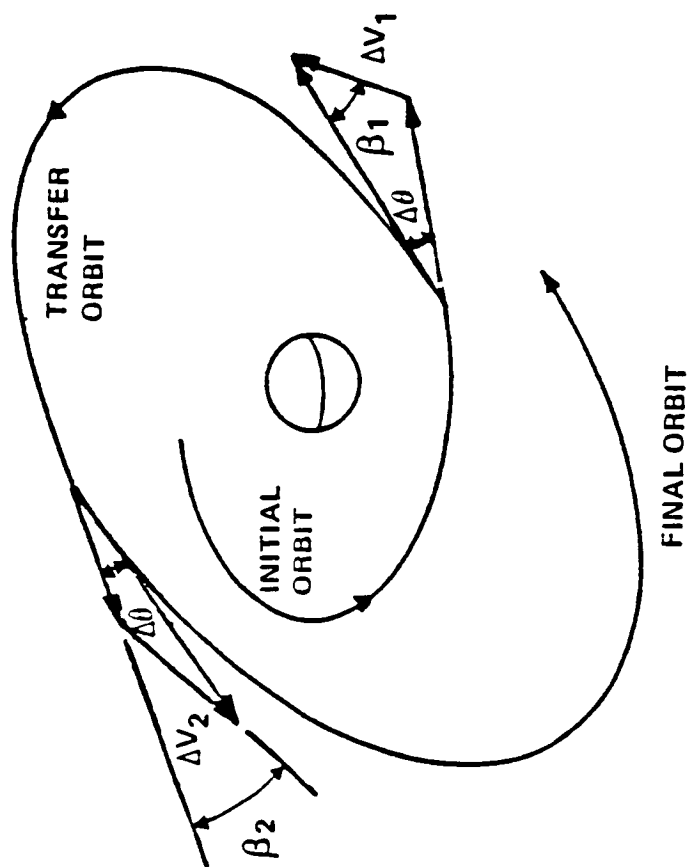


Figure C-1 Impulse Transfer Geometry

$$W_P = \frac{n}{4} \sqrt{\frac{1+e}{1-e} \left\{ \frac{3-e}{1-e} \cos \beta_1 + \sqrt{1 - \left(\frac{1+e}{1-e} \sin \beta_1 \right)^2} \right\}}$$

$$W_a = \left[\frac{(3+e)(1-e)}{(1+e)^2} W_P - \frac{2n \cos \beta_1}{(1+e) \sqrt{1-e^2}} \right]$$

here, n is the mean orbital motion of the transfer orbit.

Once the optimal turn rates are known, Robbins formula for constant thrust yields the approximate burn loss:

$$L = \frac{1}{(T/mo)^2} \left[(no^2 - W_{opt}^2) \frac{c^3}{2} \left[1 - \frac{m}{mo} \right]^2 \left\{ \frac{1}{1 - \frac{m}{mo}} - \frac{1}{2} + \frac{1}{1n \frac{m}{mo}} \right\} \right]$$

where,

- T/mo = initial thrust-to-mass ratio
- no = mean orbital motion of the initial orbit
- W_{opt} = optimal turn rates
- c = characteristic exhaust velocity = $g_0 * I_{sp}$
- $\frac{m}{mo}$ = impulsive mass ratio

Robbins approximation gives the burn loss to be nearly proportional to be the inverse of the square of the initial thrust-to-mass ratio.

A comparison between Robbins' approximation and an exact (integrated) solution as given in reference 1 shows that as the losses increase, the approximation becomes less accurate. The approximation is 5% high at 500 fps loss and 10% high at 800 fps loss. This level of accuracy is more than adequate for preliminary design work, and serves the purpose of indicating when burn losses become undesirably high.

OTV VELOCITY LOSSES

Current baseline OTV mission scenarios include transfers from the Space Station to geosynchronous orbit (GEO) and return. Assuming a Space Station at an altitude of 270 NM and an inclination of 28.5 deg, an optimal two-burn impulsive transfer to GEO

has a velocity increment of 7857 and 5798 fps at perigee and apogee, respectively. On the return from GEO, the OTV targets on a perigee altitude so that the OTV may execute an aeromaneuver, leaving the atmosphere with a new apogee and perigee. Using data from previous simulated trajectories (POST), the OTV is assumed to enter the atmosphere with a perigee altitude of 43 NM, and exit with a perigee and apogee altitudes of 29 and 270 NM, respectively. The impulsive GEO deorbit delta-V for an inclination change of 28.5 deg is 6051 fps, and a final circularization impulse of 422 fps allows the OTV to rendezvous with the Space Station.

Using Robbins approximation, the velocity losses for such maneuvers are given as a function of thrust-to-weight in figures C-2 through C-5. In figures C-2, C-3 and C-5 an Isp of 483 sec was assumed. In figure C-4, a variance of Isp's between 300 and 500 sec demonstrates the increase of velocity loss with an increase in Isp. For initial thrust-to-weights as low as 0.05, the velocity loss is negligible for all but the initial ascent to GEO. Losses in this portion may be effectively reduced by increasing the number of perigee burns, as figure C-2 shows. The negligibility of the remaining burn losses allows the flexibility to use a lower thrust propulsion system for these portions of the mission.

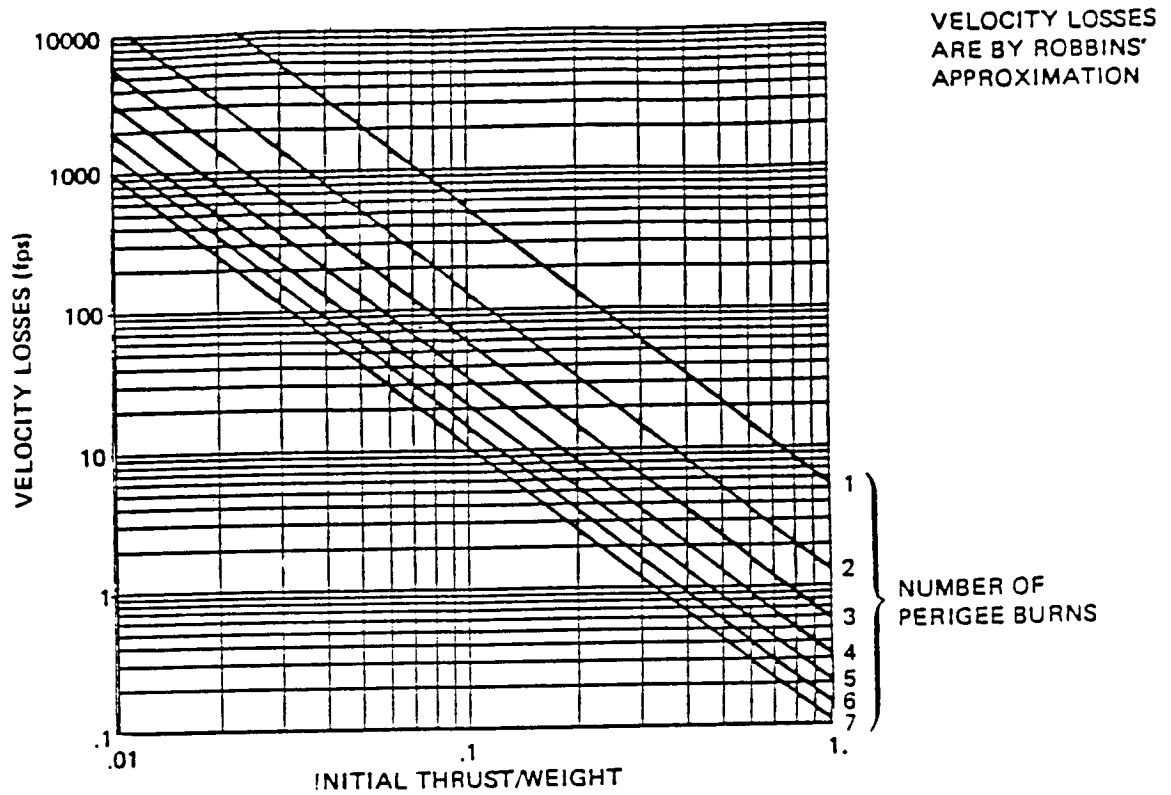


Figure C-2 LEO to GEO: Perigee Burn Losses

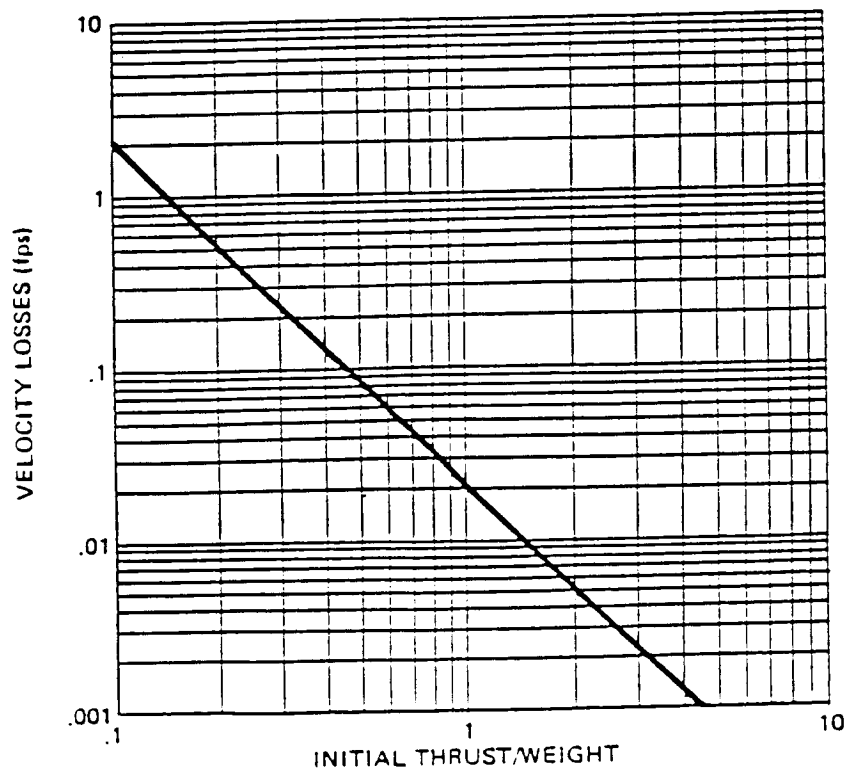


Figure C-3 LEO to GEO: Apogee Burn Losses

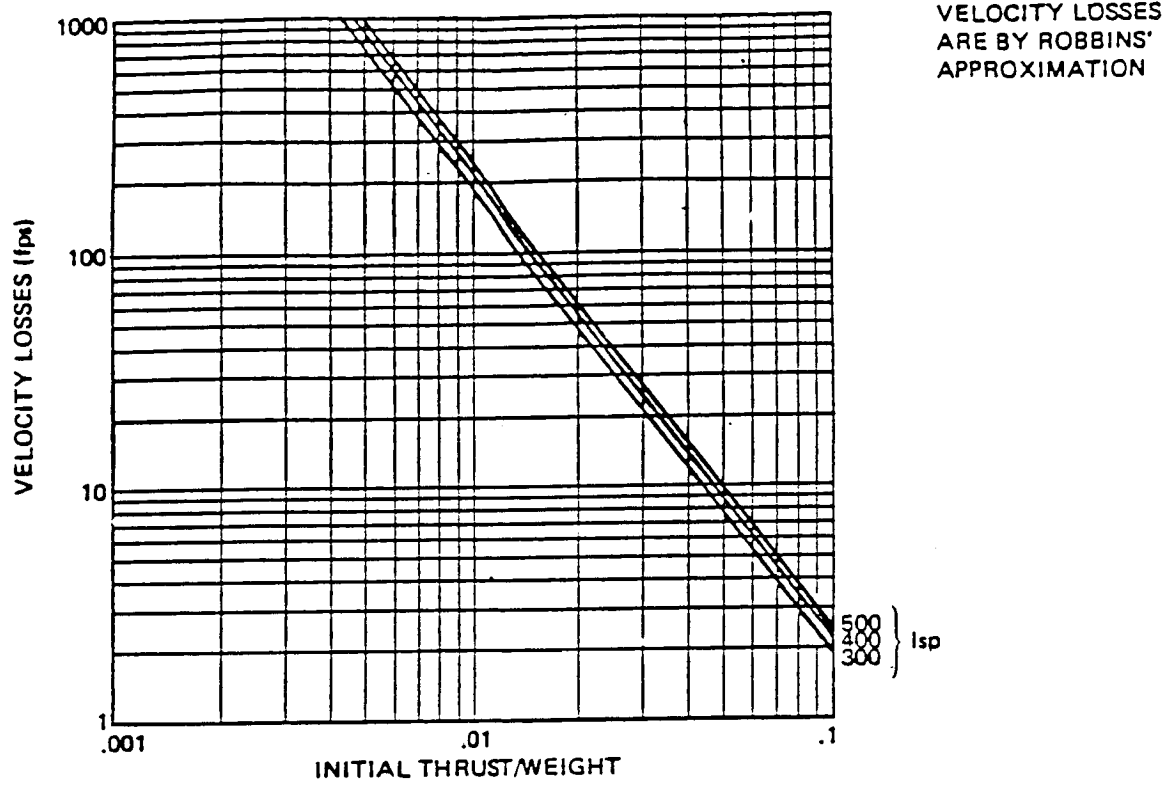


Figure C-4 GEO Deorbit Burn Losses

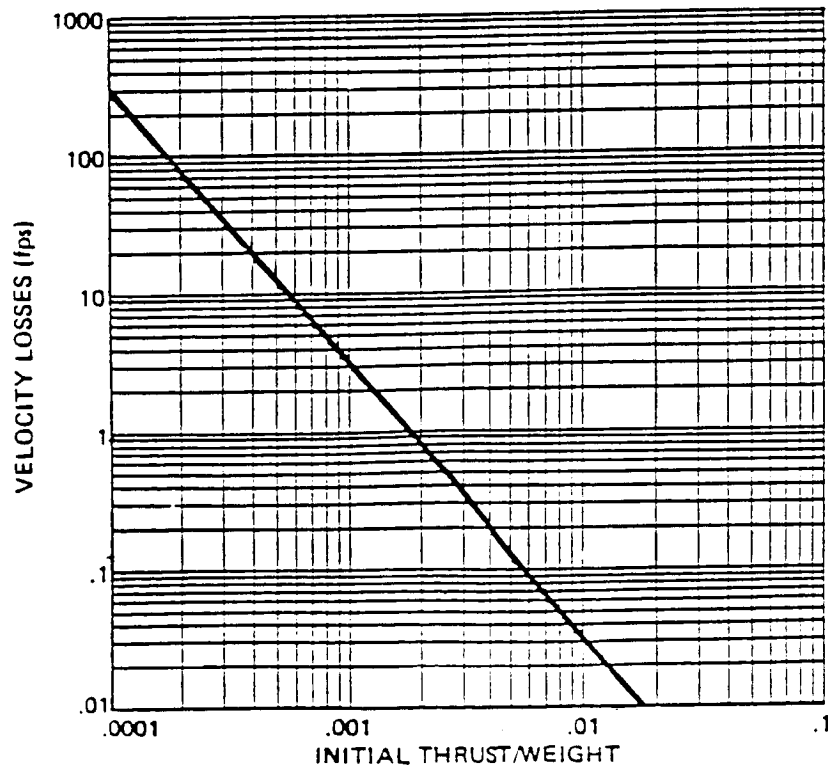


Figure C-5 LEO Circularization Burn Losses